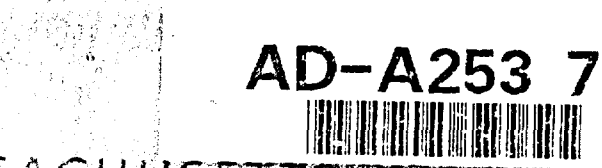
AD-A253 787



1

MASSACHUSETTS INSTITUTE OF TECHNOLOGY

The RESEARCH LABORATORY of ELECTRONICS

PROGRESS REPORT

NO. 134

JANUARY 1 - DECEMBER 31, 1991



DTIC
ELECTE
JUL 2 8 1992
S D
C

Approved for public release;
Distribution Unlimited

92-19874

RLE Progress Report

No. 134

January 1 - December 31, 1991

Submitted by

Professor Jonathan Allen
Professor Daniel Kleppner



DTIC QUALITY INSPECTED 5

Research Laboratory of Electronics
Massachusetts Institute of Technology
Cambridge, Massachusetts

Accession For	
NTIS GRA&I	☑
DTIC TAB	☐
Unannounced	☐
Justification	
By per AD-A244535	
Distribution/	
Availability Codes	
Dist	Avail and/or Special
A-1	

92 7 23 021

RLE Progress Report Number 134

Cover and title page:

This is an adaptation of an x-ray picture of the sun showing coronal holes, active regions, and coronal loops. The photograph from which this design was adapted was provided courtesy of Dr. Leon Golub (Ph.D. '72) of Harvard University's Center for Astrophysics; photo credit: IBM Corporation and the Smithsonian Astrophysical Observatory. This photograph follows from the research of Professor Bruno Coppi of RLE and the Department of Physics and reflects his research on the physics of the solar corona. A relevant paper is "Coronal Loops—Current-Based Heating Processes," by P. Beaufumé, B. Coppi, and L. Golub, which will be published in *Astrophysical Journal* 393: (1992).

Our special thanks to the following staff members of the RLE Communications Group: Mary J. Ziegler for her exceptional editing, formatting, and scanning; Mary S. Greene for proofreading and preparation of the publications and personnel chapters; and Rita C. McKinnon for proofreading. We also want to thank David W. Foss, Manager of the RLE Computer Facility, for his technical assistance.

We thank the faculty, staff, and students of RLE for their generous cooperation.

Editor:	Barbara Passero
Associate Editor:	Mary J. Ziegler
Design and Illustration:	Robert H. Priest
Photography:	John F. Cook
Printer:	InterCity Press, Rockland, Massachusetts
Typesetting:	This report was produced with IBM's BookMaster Software.

© Massachusetts Institute of Technology. 1992. All rights reserved.

ISSN 0163-9218

Table of Contents

Introduction 1

PART I SOLID STATE PHYSICS, ELECTRONICS AND OPTICS

Section 1 Materials and Fabrication 5

Chapter 1 Heterostructures for High Performance Devices 7

Professor Clifton J. Fonstad, Jr.

1.1 Introduction 7
• 1.2 Computer Controlled Growth of Lattice-Matched InGaAlAs Heterostructures on InP 7
• 1.3 Molecular Beam Epitaxy of InGaAlAs Strained-Layer Heterostructures on 111 GaAs and InP 8
1.4 Monolithic Fabrication of Strain-free GaAlAs Laser Diodes on Silicon Substrates 9
1.5 Integration of Vertical Cavity Surface Emitting Lasers on GaAs Integrated Circuits 9
1.6 Low Temperature Growth of GaAlAs Laser Diodes 10
1.7 MBE-Grown InGaAlAs/InP Long-Wavelength Laser Diodes for Narrow Linewidth Applications 11
1.8 New Three-Terminal Independently Addressable Asymmetric Laser Diodes (IAADQW-LD) with Dynamic Control of Gain and Refractive Index 11
• 1.9 Design and Fabrication of Distributed Feedback (DFB) InGaAlAs Laser Diodes Grown by Molecular Beam Epitaxy 12
1.10 Laser Diode Modeling and Design for Narrow Linewidth Operation 12
1.11 Growth and Processing of Improved InGaAlAs/InP Heterojunction Bipolar Transistors 13
1.12 Microwave Characterization, Analysis, and Modeling of Emitter-Down Heterojunction Bipolar Transistors 13
• 1.13 Analysis of Three-Terminal n-n-n Quantum Well Base, Tunnel-Barrier Transistors 14
• 1.14 Applications of AlAs Etch-Stop Layers in InGaAlAs/InP Heterostructure Electronics and Optoelectronics 14
• 1.15 Electrical Transport Studies in Directly Contacted InGaAs Quantum Wells 15
1.16 Investigation of Infrared Intersubband Emission from InGaAs/AlAs/InP Quantum Well Heterostructures 15
1.17 Investigation of Intersubband Relaxation Times in InGaAlAs Quantum Well Heterostructures 16
1.18 Infrared Characterization of InGaAs/AlAs/InP Quantum Well Heterostructures 16
1.19 Damage-Free In-Situ UHV Etching and Cleaning of III-V Heterostructures Using Molecular Beams 17
1.20 Publications 17

Chapter 2 High-Frequency InAlAs/InGaAs Metal-Insulator-Doped Semiconductor Field-Effect Transistors (MIDFETs) for Telecommunications 19

Professor Jesús A. del Alamo

• 2.1 Introduction 19
• 2.2 Quantum-channel InAlAs/n^+-InGaAs MIDFETs 20

Chapter 3 Novel Superconducting Tunneling Structures 29

Professor John M. Graybeal

• 3.1 Project Description 29

• Sponsored by the Joint Services Electronics Program

Chapter 4 Chemical Beam Epitaxy of Compound Semiconductors 33

Professor Leslie A. Kolodziejski

- 4.1 Facility for the Gas Source Epitaxy of Compound Semiconductors 33
- 4.2 Metalorganic Molecular Beam Epitaxy (MOMBE) of ZnSe 34
- 4.3 Photo-Assisted MOMBE of Wide Bandgap II-VI Compound Semiconductors 36
- 4.4 Publications 38

Chapter 5 Microstructural Evolution in Thin Films of Electronic Materials 39

Professor Carl V. Thompson

- 5.1 Electromigration and Microstructure 39
- 5.2 Microstructural Evolution in Polycrystalline Films 42
- 5.3 Magnetic Properties of Heteroepitaxial Thin Films 43
- 5.4 Interface Reactions in Multilayer Thin Films 43
- 5.5 Focused Ion Beam Induced Chemical Vapor Deposition 43
- 5.6 Publications 44

Chapter 6 Focused Ion Beam Microfabrication 47

Dr. John Melngailis

- 6.1 Introduction 47
- 6.2 Tunable Gunn Diodes—High Frequency Performance and Applications 47
- 6.3 Simulation of Tunable Gunn Diodes and MESFETs with Doping Gradients 48
- 6.4 Limited Lateral Straggle of Focused-Ion-Beam Implants 48
- 6.5 Focused Ion Beam Implantation of GaAs MMICs and Transistor Optimization 49
- 6.6 Ion Induced Deposition of Gold, Models and Microstructure 50
- 6.7 Focused Ion Beam Lithography for X-Ray Mask Making 50
- 6.8 Focused Ion Beams for the Repair of X-Ray Masks 51
- 6.9 Publications 51

Section 2 Quantum-Effect Devices 53

Chapter 1 Statistical Mechanics of Quantum Dots 55

Professor Boris L. Altshuler

- 1.1 Project Description 55

Chapter 2 Single Electron Transistors 57

Professor Marc A. Kastner

- 2.1 Project Description 57

Chapter 3 Transport Through a Quantum Dot 61

Professor Patrick A. Lee

- 3.1 Project Description 61

Chapter 4 Submicron and Nanometer Structures Technology and Research 63

Professor Henry I. Smith

- 4.1 Submicron Structures Laboratory 63
- 4.2 Microfabrication at Linewidths of 100 nm and Below 63
- 4.3 Improved Mask Technology for X-Ray Lithography 65
- 4.4 Study of Electron Transport in Si MOSFETs with Deep-Submicron Channel Lengths ... 66
- 4.5 Studies of Coulomb Charging in Ultrasmall Semiconductor Devices 66

4.6 Study of Quasi-One-Dimensional Wires and Superlattice Formation in GaAs/AlGaAs Modulation Doped Field-Effect Transistors 68
4.7 GaAs Electron Waveguide Devices Fabricated by X-Ray Lithography 70
● 4.8 Arrays of Field-Effect-Induced Quantum Dots 71
4.9 Planar-Resonant-Tunneling Field-Effect Transistors (PRESTFET) 72
● 4.10 Fabrication of Distributed-Feedback Lasers and Channel-Dropping Filters 72
● 4.11 Novel Superconducting Tunneling Structures 73
● 4.12 Submicrometer-Period Transmission Gratings for X-Ray and Atom-Beam Spectroscopy and Interferometry 74
4.13 High-Dispersion, High Efficiency Transmission Gratings for Astrophysical X-Ray Spectroscopy 74
4.14 Submicron-Thickness X-Ray Window Technology 75
4.15 Epitaxy via Surface-Energy-Driven Grain Growth 75
● 4.16 GaAs Epitaxy on Sawtooth-patterned Si 76
4.17 Publications 76

Section 3 Optics and Devices 79

Chapter 1 Optics and Quantum Electronics 81

Professor Hermann A. Haus, Professor Erich P. Ippen, Professor James G. Fujimoto, Professor Peter L. Hagelstein, Dr. Lucio H. Acioli, Dr. Santanu Basu, Dr. Guiseppe Gabetta, Dr. Yuzo Hirayama, Dr. Joseph A. Izatt, Dr. Franz X. Kärtner, Dr. Antonio Mecozzi, Dr. Kazunori Naganuma

● 1.1 Additive Pulse Modelocking 81
● 1.2 Ultrashort Pulse Fiber Laser 82
1.3 Long Distance Fiber Communications 82
1.4 Squeezing 83
1.5 Integrated Optics Components 83
1.6 Tunable Lasers 84
● 1.7 Gain Dynamics in Semiconductor Amplifiers 85
1.8 Ultrafast Optical Kerr Effect in Active Waveguides 86
● 1.9 Coherent Phonons in Electronic Materials 86
● 1.10 Femtosecond Studies of Superconductivity 87
● 1.11 Femtosecond Pulse Generation in Solid State Lasers 88
● 1.12 Studies of Ultrafast Phenomena in Optoelectronic Materials 91
● 1.13 Time Domain Diagnostics of Waveguide Devices 95
1.14 Laser Medicine and Surgery 97
1.15 Overview of the EUV Laser Effort 100
1.16 Nd:glass Amplifier Development 100
1.17 Spectral Measurements of a Ni-like Mo Plasma 101
1.18 Progress in EUV Laser Kinetics Modeling 102
1.19 Laser Cavities in the Soft X-Ray Region 103
1.20 Boltzmann Equation Studies 104
1.21 Coherent Fusion Studies 105

Chapter 2 Optical Propagation and Communication 109

Professor Jeffrey H. Shapiro, Dr. Robert H. Rediker, Dr. Ngai C. Wong

2.1 Introduction 109
2.2 Squeezed States of Light 109
2.3 Optical Frequency Division 111
2.4 Laser Radar System Theory 112
2.5 Fiber-Coupled External-Cavity Semiconductor High Power Laser 114
2.6 Analog Processing of Optical Wavefronts Using Integrated Guided-Wave Optics 114

Chapter 3 High-Frequency (> 100 GHz) Electronic Devices 117

Professor Qing Hu

3.1 Millimeter Wave and Infrared Superconducting Focal-plane Receiver Arrays 117
3.2 Photon-assisted Quantum Transport in Quantum Point Contacts 118
3.3 High-Tc Superconducting Josephson Devices 119
3.4 Far-infrared (THz) Lasers Using Multiple Quantum Wells 120
3.5 Research Facility 121
3.6 Publications 121

Section 4 Surfaces and Interfaces 123

Chapter 1 Statistical Mechanics of Surface Systems and Quantum-Correlated Systems 125

Professor A. Nihat Berker

- 1.1 Introduction 125
- 1.2 Renormalization-Group Approach to Electronic Systems 125
- 1.3 Phase Diagrams of Semiconductor Alloys 126
- 1.4 Quantum Spin Systems 126
- 1.5 Publications 127

Chapter 2 Synchrotron X-Ray Studies of Surface Disordering 129

Professor Robert J. Birgeneau

- 2.1 Introduction 129
- 2.2 Metal Surface Studies 129
- 2.3 Semiconductor Surface Studies 130
- 2.4 Publications 130

Chapter 3 Chemical Reaction Dynamics at Surfaces 133

Professor Sylvia T. Ceyer

- 3.1 Dynamics of the Reaction of F_2 with Si(100) 133
- 3.2 Dynamics of the Reaction of F_2 with Fluorinated Si(100) 133
3.3 New Mechanisms for Surface Processes 134

Chapter 4 Semiconductor Surface Studies 137

Professor John D. Joannopoulos

- 4.1 Introduction 137
- 4.2 Heteroepitaxial Growth 137
- 4.3 Molecules 140
- 4.4 Publications 142

Chapter 5 Epitaxy and Step Structures on Semiconductor Surfaces 143

Professor Simon G.J. Mochrie

- 5.1 Structure and Phase Behavior of the Si(113) Surface 143

PART II APPLIED PHYSICS

Section 1 Atomic, Molecular and Optical Physics 149

Chapter 1 Quantum Optics and Photonics 151

Professor Shaoul Ezekiel

1.1 Error Sources in a Fiber Optic Resonator Gyroscope 151
1.2 Stimulated Brillouin Fiber Laser Gyroscope 153
1.3 Applications of Stimulated Brillouin Fiber Lasers 155
1.4 First Observation of Deflection and Cooling of Three-level Atoms in Raman Resonant Standing Wave Optical Fields 157
1.5 Origin of the Optical Force on the Raman Dark State in Two Standing Waves 158
1.6 Optical Data Storage with Raman Excited Microwave Spin Echoes 160

Chapter 2 Basic Atomic Physics 163

Professor Daniel Kleppner, Professor David E. Pritchard

2.1 The Diamagnetic Rydberg Atom 163
• 2.2 Millimeter-Wave Frequency Measurement of the Rydberg Constant 167
• 2.3 Atom Interferometry 170
• 2.4 Cooling and Trapping Neutral Atoms 172
• 2.5 Precision Mass Spectroscopy of Ions 174

Section 2 Plasma Physics 177

Chapter 1 Plasma Dynamics 179

Professor George Bekefi, Professor Abraham Bers, Professor Bruno Coppi, Professor Miklos Porkolab, Professor Jonathan S. Wurtele, Dr. Ronald C. Englade, Dr. Stefano Migliuolo, Dr. Abhay K. Ram, Dr. Barrett Rogers, Dr. Linda E. Sugiyama

1.1 Relativistic Electron Beams 179
1.2 Plasma Wave Interactions—RF Heating and Current Generation 183
1.3 Physics of Thermonuclear Plasmas 190
1.4 Versator II Tokamak Research Program 204

Section 3 Electromagnetics 209

Chapter 1 Electromagnetic Wave Theory and Applications 211

Professor Jin Au Kong, Dr. Sami M. Ali, Dr. Robert T. Shin, Dr. Ying-Ching E. Yang

1.1 ILS/MLS Frequency Management Assessment 211
1.2 Future Aircraft Landing System: Global Positioning System (GPS) and Synthetic Vision Sensors (SVS) 213
• 1.3 Multilayer Media and Superconducting Electronics 214
1.4 Remote Sensing of Earth Terrain 217
1.5 SAR Image Interpretation and Simulation 219

Section 4 Radio Astronomy 223

Chapter 1 Radio Astronomy 225

Professor Bernard F. Burke, Professor David H. Staelin, Professor Jacqueline N. Hewitt, Dr. Philip W. Rosenkranz

1.1 Extragalactic Radio Source Studies 225
1.2 Studies of Gravitational Lenses 229
1.3 Radio Interferometry of Nearby dMe Stars 229

1.4 Tiros-N Satellite Microwave Sounder 230
1.5 Earth Observing System: Advanced Microwave Sounding Unit 231
1.6 High-Resolution Passive Microwave Imaging of Atmospheric Structure 232
1.7 Characterization of Dolphin Whistles 232
1.8 Rapid Precision Net-Form Manufacturing 232
1.9 Conformal Experiment Design 232

PART III SYSTEMS AND SIGNALS

Section 1 Computer-Aided Design 237

Chapter 1 Custom Integrated Circuits 239

Professor Jonathan Allen, Professor John L. Wyatt, Jr., Professor Jacob White, Professor Srinivas Devadas

1.1 Custom Integrated Circuits 239
1.2 Analog VLSI Systems for Integrated Image Acquisition and Early Vision Processing 241
1.3 Mixed Circuit/Device Simulation 250
1.4 Simulation Algorithms for Clocked Analog Circuits 251
1.5 Numerical Simulation of Short Channel MOS Devices 251
1.6 Efficient Three-Dimensional Interconnect Analysis 252
1.7 Parallel Numerical Algorithms 253
1.8 Microelectromechanical Computer-Aided Design 254
1.9 Techniques for Logic Synthesis, Formal Verification and Testing 254

Chapter 2 Computer-Aided Fabrication System Structure 261

Professor Donald E. Troxel

2.1 CAFE - The MIT Computer-Aided Fabrication Environment 261

Section 2 Digital Signal Processing 263

Chapter 1 Digital Signal Processing Research Program 265

Professor Alan V. Oppenheim, Professor Arthur B. Baggeroer, Professor Gregory W. Wornell

1.1 Introduction 265
1.2 Oceanographic Signal Processing 265
1.3 Fault-Tolerant Algorithms and Architectures for Digital Signal Processing 267
1.4 Imaging Ice-cracks Using Diffraction Tomography 267
1.5 Implementation and Evaluation of a Dual-Sensor Time-Adaptive EM Algorithm for Signal Enhancement 268
1.6 Quantitative Comparisons of Dolphin Signature Whistles 268
1.7 Applications of Synchronization in Chaotic Systems 269
1.8 Signal Processing Applications of Chaotic Dynamical Systems 269
1.9 High-Resolution Direction Finding for Multidimensional Scenarios 270
1.10 Wavelet-Based Representation and Algorithms for Generalized Fractal Signals 270
1.11 Signal Processing for Ocean Acoustic Tomography 271
1.12 Chaotic Signaling in Binary Data Transmission and Detection 271
1.13 Adaptive Matched Field Processing in an Uncertain Propagation Environment 272
1.14 State and Parameter Estimation with Chaotic Systems 272
1.15 Causal Filters with Negative Group Delay 273
1.16 Codebook Prediction: A Nonlinear Signal Modeling Paradigm 274
1.17 Synthesis, Analysis, and Processing of Fractal Signals 274
1.18 Active Noise Cancellation 275

Chapter 2 Advanced Television and Signal Processing Program 277

Professor Jae S. Lim

2.1 Introduction 277
2.2 ATRP Facilities 277
2.3 Coding of the Motion-Compensated Residual for an All-Digital HDTV System 278
2.4 Motion-Compensated Vertico-Temporal and Spatial Interpolation 278
2.5 Design of a Channel-Compatible HDTV System 279
2.6 Multirate Systems and Structures for Image and Video 279
2.7 Development of a 1.5 Kbps Speech Vocoder 280
2.8 A New Method for Representing Speech Spectrograms 280
2.9 Transform Coding for High-Definition Television 281
2.10 A Dual Excitation Speech Model 281
2.11 Design of an HDTV Display System 282
2.12 Signal Processing for Advanced Television Systems 282
2.13 Relative Importance of Encoded Data Types in an All-Digital HDTV System 282
2.14 Transmission of HDTV Signals in a Terrestrial Broadcast Environment 283
2.15 Hybrid Analog/Digital Representation of Analog Signals 283
2.16 An Iterative Method for Designing Separable Wiener Filter 284

Chapter 3 Combined Source and Channel Coding for High-Definition Television 285

Professor William F. Schreiber

3.1 Project Description 285

PART IV LANGUAGE, SPEECH AND HEARING

Section 1 Speech Communication 289

Chapter 1 Speech Communication 291

Professor Kenneth N. Stevens, Dr. Joseph S. Perkell, Dr. Stefanie Shattuck-Hufnagel

1.1 Introduction 292
1.2 Studies of the Acoustics, Perception, and Modeling of Speech Sounds 292
1.3 Speech Synthesis 295
1.4 Studies of Speech Production 296
1.5 Speech Production Planning 297
1.6 Speech Research Relating to Special Populations 298
1.7 Models for Lexical Representation and Lexical Access 299
1.8 Speech Analysis and Synthesis Facilities 300
1.9 Publications 300

Section 2 Sensory Communication 303

Chapter 1 Sensory Communication 305

Professor Louis D. Braida, Nathaniel I. Durlach, Dr. William M. Rabinowitz, Dr. Charlotte M. Reed, Dr. Mandayam A. Srinivasan, Dr. Patrick M. Zurek

1.1 Introduction 305
1.2 Hearing Aid Research 305
1.3 Multimicrophone Hearing Aids 307
1.4 Cochlear Prostheses 308
1.5 Binaural Hearing 309
1.6 Clinical Applications of Binaural Hearing 310
1.7 Tactile Communication of Speech 311

1.8 Super Auditory Localization for Improved Human-Machine Interfaces 312
1.9 Research on Reduced-Capability Human Hands 313
1.10 Mechanistic Modeling of Primate Fingerpad 314
1.11 Biomechanics of Skin-Object Contact 316
1.12 Publications 317

Section 3 Auditory Physiology 319

Chapter 1 Signal Transmission in the Auditory System 321

Professor Lawrence S. Frishkopf, Professor Nelson Y.S. Kiang, Professor William T. Peake, Professor William M. Siebert, Professor Thomas F. Weiss, Dr. Bertrand Delgutte, Dr. Donald K. Eddington, Dr. Dennis M. Freeman, Dr. John J. Guinan, Jr., Dr. John J. Rosowski

1.1 Introduction 321
1.2 Signal Transmission in the External and Middle Ear 321
1.3 Basic and Clinical Studies of the Auditory System 322
1.4 Cochlear Mechanisms 323
1.5 Electrical Stimulation of the Auditory Nerve 325
1.6 Middle-Ear Muscle Reflex 326
1.7 Cochlear Efferent System 326
1.8 Cochlear Implants 327

Section 4 Linguistics 329

Chapter 1 Linguistics 331

Professor Noam Chomsky, Professor Morris Halle

1.1 Introduction 331
1.2 Abstracts of Doctoral Dissertations 331

APPENDICES

Appendix A RLE Publications and Papers Presented 341

A.1 Meeting Papers 341
A.2 Journal Articles 353
A.3 Books/Chapters in Books 364
A.4 RLE Publications 365
A.5 RLE Theses 366
A.6 Miscellaneous 368

Appendix B Current RLE Personnel 369

Appendix C Milestones 375

C.1 New Faculty and Staff 375
C.2 Retirements 375
C.3 Promotions 375
C.4 Chair Appointments 375
C.5 Awards and Honors 375

Appendix D RLE Research Support Index 377

Project Staff and Subject Index 381

Introduction

The Research Laboratory of Electronics

The Research Laboratory of Electronics (RLE) was established in 1946 as the Institute's first interdepartmental laboratory. Originally organized under the joint sponsorship of the Departments of Physics and Electrical Engineering, RLE has broadened its interests to cover a wide range of research.

The RLE environment provides both the freedom of action essential in an academic institution and the availability of large-scale laboratory facilities and services required by researchers. RLE's interdisciplinary setting offers many opportunities for creative and collaborative research. By fostering this powerful combination of research and education, RLE effectively penetrates beyond the horizon of new ideas and information.

RLE Progress Report

RLE Progress Report Number 134 describes research programs at RLE for the period January 1 through December 31, 1991. Each chapter of the *Progress Report* contains both a statement of research objectives and a summary of research efforts for research projects listed. Faculty, research staff, students and others who participated in these projects are identified at the beginning of each project, along with sources of funding.

There are four appendices at the end of the report: Appendix A is a bibliography of RLE publications and papers presented by RLE staff during 1991; Appendix B is a roster of current RLE staff; Appendix C is a list of RLE faculty and staff milestones and honors received during 1991; and Appendix D is an index of RLE sponsors. In addition, the Project Staff and Subject Index provides access to the information in this report.

RLE Progress Report Number 134 was produced by the RLE Communications Office. Further inquiries may be addressed to:

Research Laboratory of Electronics
Communications Office
Room 36-412
Massachusetts Institute of Technology
Cambridge, Massachusetts 02139-4307
Tel. (617) 253-2566
Fax (617) 258-7864

Part I Solid State Physics, Electronics and Optics

Section 1 Materials and Fabrication

Section 2 Quantum-Effect Devices

Section 3 Optics and Devices

Section 4 Surfaces and Interfaces

Section 1 Materials and Fabrication

Chapter 1 Heterostructures for High Performance Devices

Chapter 2 High-Frequency InAlAs/InGaAs Metal-Insulator-Doped Semiconductor Field-Effect Transistors (MIDFETs) for Telecommunications

Chapter 3 Novel Superconducting Tunneling Structures

Chapter 4 Chemical Beam Epitaxy of Compound Semiconductors

Chapter 5 Microstructural Evolution in Thin Films of Electronic Materials

Chapter 6 Focused Ion Beam Fabrication

Chapter 1. Heterostructures for High Performance Devices

Academic and Research Staff

Professor Clifton G. Fonstad, Jr.

Visiting Scientists and Research Affiliates

Anton Failla,[1] Sheila Prasad,[2] Jae-Jin Lee,[3] Jong Tae Park[4]

Graduate Students

Rajni J. Aggarwal, Thomas P.E. Broekaert, Geoffrey F. Burns, Woo-Young Choi, Isako Hoshino, Paul S. Martin, Lung-Han Peng, Yakov Royter, Krishna V. Shenoy, Richard A. Singer, Jurgen H. Smet, James C. Vlcek

Technical and Support Staff

Kelley S. Donovan, Angela R. Odoardi, Richard R. Perilli

1.1 Introduction

The broad objective of our research effort is to develop III-V quantum heterostructures for high performance electronic, optoelectronic, and photonic devices for applications in high speed optical communications and signal processing. To this end, we are developing: (1) new, higher performance materials systems including InP-based InGaAlAs heterostructures and <111> oriented strained layer superlattices; (2) novel approaches to integrate laser diodes on VLSI-level electronic integrated circuits; (3) a new family of quantum-well-base, tunnel-barrier n-n-n transistors and near- and far-infrared optoelectronic devices; and (4) new damage-free in situ processing techniques for fabricating advanced quantum structure and embedded heterostructures.

The following sections describe our progress during the past year in the above research areas. Our group works closely with Professors Hermann A. Haus, James G. Fujimoto, and Erich P. Ippen to develop the optical device application, characterization, and modeling aspects of this program, and with Professor Sylvia T. Ceyer to develop new in situ processing techniques.

1.2 Computer Controlled Growth of Lattice-Matched InGaAlAs Heterostructures on InP

Sponsors

Charles S. Draper Laboratories
Contract DL-H-418483
DARPA/NCIPT
Joint Services Electronics Program
Contract DAAL03-89-C-0001
Contract DAAL03-92-C-0001

Project Staff

James C. Vlcek, Professor Clifton G. Fonstad, Jr.

In electronic and optical semiconductor devices, the need for both graded-composition and hyper-abrupt metallurgical junctions frequently arises. The use of graded-composition junctions allows for precise control of the confinement of charge carriers and optical fields through spatially varying bandgaps and refractive indices, respectively. On the other hand, hyper-abrupt junctions may be

---

[1] Centro Studi e Laboratori Telecomunicazoni, Torino, Italy.

[2] Northeastern University, Boston, Massachusetts.

[3] Electronics and Telecommunications Research Institute (ETRI), Daejeon, Korea.

[4] Incheon Unversity of Korea, Incheon, Korea.

desired in some devices, most notably quantum effect devices, where a sharp interface is desired to reduce fluctuations in the confinement energy which might arise from graded interfaces due to shutter transients.

In this work, we have grown the quaternary $In_xGa_yAl_{1-y}As_{1-x}$, lattice-matched to InP substrates. The need to lattice-match, such as to an InP substrate, further constrains the ratio of constituent fluxes.

We have implemented a computer-automated MBE control system whose aim is to provide precise control of the constituent and dopant fluxes such as is necessary to achieve graded-composition lattice-matched alloys and maintain uniform lattice-matched compositions in the presence of shutter events. Key to this system are accurate models of the characteristics of the effusion cells, including not only the static flux versus temperature relationship, but also the time-dependent behavior of the cell in the presence of changes in either setpoint and/or shutter status. These models approximate the temporal response of the effusion cells to a setpoint change with a single-pole system function, with the location of the pole being determined by a direct measurement of the flux profile generated by a step change in the cell setpoint temperature.

In the case of graded-composition layers, the thermal lag time of the cell requires modification of the time-dependent effusion cell setpoint temperature profile, most notably to eliminate the over- and undershoot effects at the endpoints of the graded layer which would result if the effects of cell response time were neglected. With such modifications, we have achieved linearly graded flux profiles whose deviation from the desired profile can be held within one percent.

To remove flux transients which arise from the operation of the cell shutters, we have structured the control system so that it seeks to maintain the flux in the effusion cell at a constant value, irrespective of the shutter status. In practice, this entails maintaining the setpoint temperature of the cell at a lower value with the shutter closed than with it open and performing an exponential ramp sequence upon change of shutter status. Using this technique, we have reduced cell shutter transients from as high as 30 percent to one percent or less.

1.3 Molecular Beam Epitaxy of InGaAlAs Strained-Layer Heterostructures on 111 GaAs and InP

Sponsors

DARPA/NCIPT
Joint Services Electronics Program
Contract DAAL03-89-C-0001
Contract DAAL03-92-C-0001

Project Staff

Richard A. Singer, Professor Clifton G. Fonstad, Jr.

The issues associated with the molecular beam epitaxial (MBE) deposition of $In_x(Ga_yAl_{1-y})_{1-x}As$ upon (111)B InP have been extensively explored. As a result, a reproducible growth algorithm has been developed whose execution has resulted in bulk n and p-type InGaAs and InGaAlAs of comparable crystallinity to simultaneously grown (100) oriented epilayers.

When epitaxial layers are pseudomorphically deposited upon a (111) zincblende substrate, a piezoelectric field is generated due to the ionic character of the chemical bond between the constituent elements and the lack of inversion symmetry in the (111) orientation. Recently, this strain-generated electric field has been demonstrated in a GaAs based p-i-n modulator whose absorption edge was in the vicinity of 0.9 μm.

Growth on (111) InP is especially difficult because of the volatility of the InP surface and the problems attendant to (111) surface chemistry. Not surprisingly, initial attempts to grow epitaxial layer of InGaAs on (111)B InP according to the proven methods of (100) orientations were unsuccessful. Moreover, reflection high-energy electron diffraction (RHEED) patterns, which usually provide essential in situ information about the condition of a growing surface, are unclear in this material system. As a result, the most critical step in the MBE growth process—the synchronization of the desorption of the substrate's native oxide layer with the initiation of growth—is performed "in the dark."

To address these issues, an alternative growth algorithm, called quasi-migration enhanced epitaxy, was developed and named for the unusually low intensity of As overpressure, low substrate temperature, and slow growth rate which comprise its parameter set. It was learned that an intense group III overpressure, expressed in a rapid rate of growth, is needed to stabilize the (111) growth front: a $\sqrt{19} \times \sqrt{19}$ surface reconstruction that is rich in group III atoms. This is quite different from

the case of (100) materials whose c(2x8) surface reconstructions are As stabilized. Another important modification was the elimination of the traditional 5: 1: 1 $H_2SO_4H_2O_2$-H_2O etching step in the pre-growth substrate preparation procedure. As a result, the thickness of the residual oxide layer was reduced which, in turn, allowed growth to be successfully initiated without the need of a risky high temperature desorption cycle.

1.4 Monolithic Fabrication of Strain-free GaAlAs Laser Diodes on Silicon Substrates

Sponsors

DARPA/NCIPT
IBM Corporation Fellowship

Project Staff

Geoffrey F. Burns, Anton Failla, Professor Clifton G. Fonstad, Jr.

Prospects for monolithic integration of III-V electrical and optical devices with Si circuits have fueled vigorous research in direct heteroepitaxial growth of these compounds on Si substrates. Developing III-V optical sources useful for VLSI optical interconnects is one goal which has been pursued by several groups. Along these lines we have focused upon the laser diode due to its capacity for high speed modulation and efficient electrical to optical power conversion.

In this work molecular beam epitaxy of (Al,Ga)As heterostructures directly on silicon substrates has been investigated for use in fabricating semiconductor lasers for monolithic optoelectronic integration. A base laser process was developed and evaluated using homoepitaxy of (Al,Ga)As on GaAs substrates, incorporating a graded-index separate confinement heterostructure (GRINSCH) quantum well active region. Etched ridge waveguide lasers were fabricated from these layers, achieving continuous wave threshold currents of 19 mA and differential quantum efficiency of 66%. This same laser process was adopted to GaAs-on-Si growth initiation layers to produce monolithic (Al,Ga)As laser on silicon substrates. High dislocation density and residual thermal tension in the laser epitaxial layer degraded threshold currents and slightly degraded external quantum efficiency, with threshold currents as low as 40 mA and differential efficiencies as high as 60 percent. In addition, the same problems precluded continuous wave operation for these devices.

To address residual thermal tension, a technique for monolithic epitaxial separation and reattachment was developed to produce strain-free GaAs-on-Si. Rapid thermal annealing of these layers was also investigated for alleviating defect density imposed by the heteroepitaxial growth process. Photoluminescence studies demonstrated that epitaxial separation, along with rapid thermal annealing 600°C, produced strain-free material. In addition, these layers could be annealed at temperatures up to 800°C without reintroducing thermal stress and demonstrated further material improvement as indicated by photoluminescence intensity. Epitaxial separation and annealing was also applied to (Al,Ga)As laser epitaxy layers to produce the first strain-free lasers fabricated monolithically on Si substrates, an important achievement for advancing heteroepitaxy as a viable optoelectronic integration strategy.

1.5 Integration of Vertical Cavity Surface Emitting Lasers on GaAs Integrated Circuits

Sponsors

DARPA/NCIPT
IBM Corporation Fellowship
National Science Foundation Fellowship
Vitesse Semiconductor

Project Staff

Krishna V. Shenoy, Geoffrey F. Burns, Professor Clifton G. Fonstad, Jr. in collaboration with J. Mikkelson[5]

There exists a long history of interest in the integration of high performance optoelectronic devices, particularly lasers and detectors, on high density electronic integrated circuits, and considerable attention has been focused on GaAs-on-Si processes because silicon has traditionally been the only source of VLSI circuitry. However, with the recent availability of GaAs-based VLSI, realized using refractory-metal gate processes, we feel that this picture has changed significantly. It is the purpose of this program to demonstrate that the growth of optoelectronic heterostructures on partially processed GaAs-VLSI wafers is a viable alternative to GaAs-on-Si for applications requiring the

[5] Vitesse Semiconductor, Camarillo, California.

integration of high density electronic circuitry and optoelectronic devices. Such applications include in-plane (on-chip and chip-to-chip) and plane-to-plane optical communication, computation, and signal distribution.

In this research, the integration of high-density laser diodes on production GaAs electronics (Vitesse Semiconductor) is being investigated. Thermal studies have been conducted on refractory metal gate enhancement and depletion mode MESFETs and their tolerance to extended periods of time at molecular beam epitaxy (MBE) growth temperatures has been determined. While device performance is observed to decrease for anneal temperatures greater than 550°C, performance is modestly enhanced for anneal temperatures between 400°C and 550°C. Thus, the electronic thermal constraint is that lasers must be grown on the GaAs circuitry at a temperature less than 550°C. Work on lasers compatible with this constraint is described in the next section.

Surface emitting lasers, or lasers with radiation emitted normal to the wafer plane, will be fabricated by etching a total internal reflection mirror using ion beam assisted etching (IBAE) (MIT Lincoln Laboratory) and standard III-V processing techniques. Growth of lasers, compatible with the underlying GaAs VLSI circuitry, directly on the partially processed circuitry will then be conducted. We are currently determining the optimal step in the electronic fabrication sequence for lasers to be grown as well as the optimal shape of the sidewalls etched through the electronics down to the GaAs substrate. This project will culminate by demonstrating an interconnected optoelectronic system.

1.6 Low Temperature Growth of GaAlAs Laser Diodes

Sponsors

DARPA/NCIPT
GTE Laboratories
IBM Corporation Fellowship
National Science Foundation Fellowship
Vitesse Semiconductor

Project Staff

Krishna V. Shenoy, Professor Clifton G. Fonstad, Jr. in collaboration with J. Mikkelson[6] and B. Elman[6]

Reducing the temperature at which laser diodes are grown is of interest for several reasons. The first reason is our interest in growing lasers on GaAs MESFET wafers (see preceding section). A laser diode heterostructure, compatible with the electronic thermal constraint, has been designed and grown using conventional MBE techniques. The laser incorporates a 60Å strained layer $In_{0.2}Ga_{0.8}As$ single quantum well active region, a GaAs waveguide, low aluminum fraction $Al_{0.22}Ga_{0.78}As$ cladding layers, and an AlAs etch-stop layer. The strained layer quantum well active region yields lower threshold currents than unstrained quantum wells because compressively strained InGaAs decreases the effective mass in the parallel direction, thus reducing the density of states and the number of carriers required to reach population inversion. A GaAs waveguide, GaAs on either side of the InGaAs, confines the optical mode and by varying the thickness of this material, the proximity of the AlGaAs cladding layers to the active region can be altered, thus AlGaAs dependent laser characteristics may be studied. The effect of low temperature AlGaAs epitaxial quality on laser performance is currently under investigation (GTE Laboratories) and is central to this research because conventional AlGaAs is grown at 700°C, which violates the electronic thermal constraint. Low aluminum fraction AlGaAs can be grown at temperatures as low as 600°C without significant degradation. Exotic growth techniques such as migration enhanced epitaxy (MEE), variable duty cycle As cell shuttering, and precisely controlled low As overpressure are all being pursued to achieve high quality, low temperature ($\leq$ 600°C) AlGaAs. An AlAs etch-stop layer is placed 1400Å above the top GaAs waveguide to provide a selective etch barrier. This increases the reproducibility of the ridge etch depth.

Lasers grown between 600°C and 530°C have been fabricated as ridge lasers. Preliminary optical and electrical characterization of the higher temperature material has demonstrated close to state-of-the-art lasers while the lower temperature material (grown conventionally) appears promising.

[6] GTE Laboratories, Waltham, Massachusetts.

1.7 MBE-Grown InGaAlAs/InP Long-Wavelength Laser Diodes for Narrow Linewidth Applications

Sponsor

Charles S. Draper Laboratories
Contract DL-H-418483

Project Staff

Woo-Young Choi, Yakov Royter, Professor Clifton G. Fonstad, Jr.

Semiconductor lasers emitting at the wavelength of 1.3 to 1.55 mm are a key element of low-loss optical fiber communication systems. The material system most often used for such laser diodes is the quaternary alloy InGaAsP lattice-matched to InP substrates. Liquid phase epitaxy (LPE) and metal-organic chemical vapor deposition (MOCVD) are the usual growth techniques for this material system.

The InGaAlAs material system, grown by conventional solid-source molecular beam epitaxy (MBE), is another promising candidate for laser diodes emitting in the 1.3 to 1.55 mm range. Significantly, the InGaAs/InAlAs heterojunction has a larger conduction band discontinuity than the InGaAs/InP heterojunction (approximately, 0.5 eV versus 0.22 eV). This enhances quantum confinement of electrons and results in the stronger optical transitions which, in turn, can result in better laser diode device performance.

To achieve this goal, we first did an extensive MBE growth study in which the optical quality of InGaAlAs materials were optimized. We then investigated, theoretically and experimentally, various device structures that were suitable for our MBE growth. From these studies, we were able to demonstrate 1.55 mm InGaAlAs graded-index separate confinement (GRIN-SCH) multiple quantum well (MQW) laser diodes whose device performances are comparable to those of the best-reported InGaAsP laser diodes.

Currently, we are working on strained quantum well devices in the hope of achieving further device improvements as well as obtaining a deeper understanding of strained quantum well laser diodes.

1.8 New Three-Terminal Independently Addressable Asymmetric Laser Diodes (IAADQW-LD) with Dynamic Control of Gain and Refractive Index

Sponsor

DARPA/NCIPT

Project Staff

Paul S. Martin, Professor Clifton G. Fonstad, Jr. in collaboration with Professor Hermann A. Haus

We are investigating a new class of devices in which the active region consists of two quantum wells with different widths and therefore different optical gain profiles. By designing structures in which the current injection into these two quantum wells can be independently controlled, we gain a new, as yet unutilized, degree of freedom in controlling light output from the device. The immediate goal of this program is to use this new degree of freedom to design a ridge-type laser diode with reduced alpha-parameter; the ratio of refractive index change to gain change associated with an injected current density change. We expect narrow-linewidth lasers incorporating this scheme to find application in many optical communications systems where linewidth of the signal laser limits the transmission bit rate-distance product. New systems based on Er-doped fiber are particularly sensitive to signal laser linewidth because optical signals are amplified but not regenerated or retimed. The recent explosion of interest in Er-doped fiber communications systems makes this application especially timely.

Wavelength division multiplexing (WDM) is another area in which we believe this new class of devices can have an important impact. As modulation frequencies for individual laser diodes move into the multi-gigabit per second range, dramatic increases in data rates become increasingly more difficult to achieve through increases in modulation frequency. An alternative approach is to use many slower and, thus, simpler, less expensive and more reliable laser diodes all transmitting down the same fiber but at slightly different wavelengths. Two devices that are essential for realizing practical WDM systems are (1) dynamically tunable laser diodes for adjusting the wavelength of each signal channel, and (2) narrow linewidth channel dropping filters for routing of individual channels to their respective detection circuits. Both of these devices can be much improved over existing designs by exploiting the advantages of the IAADQW-LD.

Other applications for these devices include pure FM laser diodes with reduced AM noise, two wavelength integrated but independently controlled laser diodes and other non-laser devices like tunable narrow bandwidth filters and light modulators.

1.9 Design and Fabrication of Distributed Feedback (DFB) InGaAlAs Laser Diodes Grown by Molecular Beam Epitaxy

Sponsors

DARPA/NCIPT
Joint Services Electronics Program
Contract DAAL03-89-C-0001
Contract DAAL03-92-C-0001

Project Staff

Woo-Young Choi, Professor Clifton G. Fonstad, Jr.

It is essential that laser diodes for optical fiber communication applications operate with a single oscillation frequency. Typically, schemes of distributed feedback (DFB) or distributed Bragg reflector (DBR) are used in which gratings above or below the active layer (DFB) or outside the active layer (DBR) perform the act of frequency selection. To make such a device structure, either epitaxial growth is initiated on a corrugated substrate, or regrowth is performed on the epitaxial material onto which gratings have been formed.

In this project, we are in the pursuit of a DFB device structure in which gratings are formed entirely after the complete epitaxial growth. Our motivation for this approach stems from the fact that we are working on laser diodes grown by the conventional solid-source Molecular Beam Epitaxy technology and, due to its growth kinetics, successful MBE growth on the corrugated surface is very difficult to achieve.

We have proposed a ridge stripe structure in which gratings are made on the side walls of the ridge as well as on the bottom channels next to the ridge. According to our initial calculation, there is enough coupling between the optical wave and gratings to result in single mode selection.

To realize such a device structure, we are collaborating with Professor Henry I. Smith's group at MIT and utilizing their x-ray lithography technology. Currently, we are in the process of combining x-ray lithography technology with the ridge-stripe laser diode fabrication technology.

1.10 Laser Diode Modeling and Design for Narrow Linewidth Operation

Sponsor

Charles S. Draper Laboratories

Project Staff

Yakov Royter, Professor Clifton G. Fonstad, Jr. in collaboration with J.H. Hopps[7]

Many of the current laser applications require narrow linewidth output characteristics. Unfortunately, semiconductor lasers, possessing such advantages as small size, direct modulation capability, and integrability with other optical and electronic devices, have broad linewidths in comparison to most other kinds of lasers. The relatively broad linewidths are due to the low Q of the cavity and to the intrinsic effects specific to the semiconductor gain medium. Since most of the linewidth reduction methods have involved the increase of the cavity Q, our goal is to investigate and to help in the reduction of the intrinsic linewidth broadening effects. Reduction of these effects, in conjunction with the increase of the cavity Q, would produce semiconductor lasers with narrowest possible linewidths.

The first step in our research is to investigate theoretically the intrinsic linewidth broadening effects. In particular, we concentrate on the linewidth broadening parameter, α, the largest intrinsic linewidth broadening factor, which describes the coupling of gain and refractive index fluctuations in the gain medium via carrier density fluctuations. Also, due to their apparent promise over conventional diode lasers, we consider only quantum-well semiconductor lasers. We begin the investigation of the α parameter by first calculating the carrier energy bands of the active region semiconductor material, using both parabolic band and $k \cdot p$ approximations. From the energy bands, we can obtain gain and refractive index profiles and the linewidth broadening parameter. Thus, the energy band calculations are the first major task in our investigation.

To test our models, we plan to compare the calculated laser characteristics, such as threshold current, gain, refractive index and linewidth, with

[7] Charles S. Draper Laboratories, Cambridge, Massachusetts.

experimental results obtained from measurements done in our laboratory, as well as the ones quoted in the literature. Moreover, we will work on establishing systematic ways of obtaining parameters for our models. Finally, we hope to be able to use our modeling to help in the fabrication of narrow linewidth semiconductor lasers.

As an extension of our modeling efforts, we will also investigate strain layer quantum-well lasers. Furthermore, we intend to improve our models by including calculations of energy dependent carrier lifetimes, different loss mechanisms, and other sources of linewidth broadening.

1.11 Growth and Processing of Improved InGaAlAs/InP Heterojunction Bipolar Transistors

Sponsor

Electronics and Telecommunications Research Institute (ETRI) Fellowship

Project Staff

Jae-Jin Lee, Woo-Young Choi, James C. Vlcek, Professor Clifton G. Fonstad, Jr.

HBTs fabricated in the $In_xGa_yAl_{1-x-y}As$ alloy system, lattice matched to semi-insulating InP substrates, are emerging as promising candidates for microwave applications. By utilizing the advantageous material properties of this alloy system, in particular the properties of ternary alloy InGaAs, HBT device performance superior to that of GaAlAs HBTs may be realized. The $In_xGa_yAl_{1-x-y}As$ system is also better suited to the solid-source molecular beam epitaxial (MBE) growth techniques typically employed in HBT fabrication than the $In_{1-x}Ga_xAs_yP_{1-y}$ system, which also lattice matched to InP.

While, in its simplest form, an HBT need only have an emitter of a wider bandgap material than the base, such single heterojunction devices suffer from a number of drawbacks. Most notably, the base-collector junction of such a device will have a lower turn-on voltage than the base-emitter junction, resulting in an "offset" voltage in the output characteristics. A single heterojunction HBT which uses the ternary InGaAs for both base and collector will also suffer from a high output conductance and low collector-emitter breakdown voltage due to the narrow gap collector material. Finally, the use of abrupt heterojunctions, at either of the two pn junctions in the device, introduces "spikes" in the band edges at the junctions which could lead to carrier trapping and degraded device performance. For these reasons, an HBT fabricated in the $In_xGa_yAl_{1-x-y}As$ alloy system is best achieved with graded base-emitter and base-collector junctions.

Using advanced computer-controlled MBE growth techniques, we have successfully fabricated and characterized an $In_xGa_yAl_{1-x-y}As$/InP emitter-up, doubly-graded heterojunction bipolar transistor. By using parabolic compositional gradings in the pn junctions devices have been realized with dc characteristics much improved over abrupt single-heterojunction devices fabricated in this same material system. We are continuing this work with the objective of now optimizing microwave, as well as dc performance.

1.12 Microwave Characterization, Analysis, and Modeling of Emitter-Down Heterojunction Bipolar Transistors

Sponsors

National Science Foundation/Northeastern University
TRW Systems

Project Staff

Sheila Prasad, Professor Clifton G. Fonstad, Jr. in collaboration with B. Meskoob[8] and M. Kim[9]

Emitter-down InGaAs/InAlAs/InP heterojunction bipolar transistors have been characterized at microwave frequencies. Small-signal equivalent circuit models were obtained using the commercial Touchstone software. The simulated annealing (SA) algorithm, which does not depend on good initial conditions, has been applied to the modeling problem. The results obtained with SA and Touchstone were consistent. However, continuous human intervention was required to obtain the results with Touchstone, whereas SA yielded the results automatically. SA was therefore proved to

[8] Northeastern University, Boston, Massachusetts.

[9] TRW Systems, Redondo Beach, California.

be the superior method for optimization because of its speed and convenience.

Small-signal S parameter measurements were made by on-wafer probing of the devices using the Hewlett-Packard 8510B automatic network analyzer and the Cascade Microtech microwave probe station for 39 different bias points. The bias dependence of elements of the small-signal equivalent circuit was determined and it was found that five of the elements of the circuit were highly bias dependent. These results are being used for the large-signal modeling of the HBT which is in progress. Measurements are also in progress to determine the third-order intermodulation product (IP3). The optimized model for high IP3 which is related to device linearity is to be determined.

1.13 Analysis of Three-Terminal n-n-n Quantum Well Base, Tunnel-Barrier Transistors

Sponsor

Joint Services Electronics Program
Contract DAAL03-89-C-0001
Contract DAAL03-92-C-0001

Project Staff

Thomas P.E. Broekaert, Professor Clifton G. Fonstad, Jr.

Three-terminal n-n-n quantum-well base, tunnel barrier transistors, consisting of a resonant tunneling structure with an ohmic contact to the quantum well have been fabricated. Although an ohmic contact to the quantum well was successfully achieved by heavily doping the quantum well, it was found that all such structures exhibit strong leakage currents from base to emitter.

The conductance of surface quantum wells in such transistor structures has been measured successfully, and the dependence of sheet carrier concentration, sheet conductance, and carrier mobility as a function of temperature has been measured. No transistor action was seen for the tested temperature range of 10 to 300 K. The lack of transistor action is tentatively attributed to fast hot carrier relaxation, resulting in large base currents and small collector currents. Possible mechanisms for the hot carrier relaxation are impurity scattering, polar optical phonon scattering, and electron-electron scattering.

Several non-idealities that hamper the active behavior of the resonant tunneling transistor have been analyzed. First, electron-polar optical phonon and electron-electron scattering from second to first subband in the quantum well are believed to be the dominant mechanisms at low temperatures that limit the ultimate gain of the resonant tunneling transistor. Second, due to the fact that this device only has a single dipole layer, it follows that the emitter accumulation region is not completely shielded from the collector potential, which results in a low output impedance and a low voltage gain.

A novel device structure is introduced, in which the hot carrier relaxation, which is prevalent in InGaAlAs resonant tunneling structures, is reduced. This reduction in hot carrier relaxation rate is obtained by having a quantum well in which the quantum-well level for base potential modulation and the quantum-well level for emitter to collector tunneling are located at different points in the Brillouin zone, e.g., direct vs. indirect valley quantum well. A possible material system for this novel device structure would be GaAs/AlAs/Ge/AlAs/GaAs for emitter/barrier/base/barrier/collector respectively. This material system would also improve the performance of the bipolar quantum-well resonant tunneling transistor and the hot electron transistor.

1.14 Applications of AlAs Etch-Stop Layers in InGaAlAs/InP Heterostructure Electronics and Optoelectronics

Sponsor

Joint Services Electronics Program
Contract DAAL03-89-C-0001
Contract DAAL03-92-C-0001

Project Staff

Thomas P.E. Broekaert, Woo-Young Choi, Professor Clifton G. Fonstad, Jr.

We have used wet chemical etching solutions that allow the selective etching of InP lattice-matched InGaAlAs quaternary compounds using thin pseudomorphic AlAs layers as etch stops to explore new device concepts.

We developed the etchants used here last year, and they typically consist of succinic acid (or other dicarboxylic acids), ammonia, and hydrogen peroxide. The etchant is well buffered and can be used over a wide pH range including from 4.2 to 7.0 by varying the amount of ammonia added. In addition, the etchant is compatible with Cr/Au contact metallization and standard positive photoresists. Typically, the InGaAs etch rate is about 100 nm/min. At a pH of 4.2, the etch rate of InGaAs is found to be over 1000 times the etch

rate of AlAs, while the etch rate of InAlAs is over 500 times that of the AlAs. A typical AlAs stop layer is about 10 monolayers (m.l.) thick (2.73 nm). Buffered HF can be used to remove the AlAs stop layer without etching InGaAlAs to any significant degree.

These selective etchants have enabled us, for the first time, to measure the conductance and mobility of a directly contacted quantum well in a resonant tunneling structure, and they open up the possibility of fabricating a whole new set of novel quantum devices.

Also, we utilized the selective etchants in fabricating ridge-stripe InGaAlAs/InP GRIN-SCH MQW laser diodes. By inserting a thin pseudomorphic AlAs layer at a desired location during the epitaxial growth and then selectively etching away InGaAlAs materials up to the etch stop layer, we were able to fabricate laser devices with ridges whose heights are precisely and reliably controlled.

1.15 Electrical Transport Studies in Directly Contacted InGaAs Quantum Wells

Sponsors

Joint Services Electronics Program
Contract DAAL03-89-C-0001
Contract DAAL03-92-C-0001
National Science Foundation Fellowship
U.S. Army Research Office

Project Staff

Rajni J. Aggarwal, Thomas P.E. Broekaert, Professor Clifton G. Fonstad, Jr.

Using a recently developed selective etch, we have been able to demonstrate direct electrical contact to the quantum well of an AlAs/InAs/InGaAs resonant tunneling structure. This contact serves as the base contact in our three-terminal, unipolar resonant tunneling transistor (RTT). Our devices incorporate high indium content materials in the quantum well. In addition to their favorable transport properties, these compounds have low Schottky barrier heights, enhancing our ability to make ohmic contact to them. We are limited in the indium fraction that we can use by the lattice mismatch of such compounds with the InP based lattice constant of the device.

We believe that the performance of our device is limited by two factors: (1) doping within the quantum well and (2) depletion of the well due to surface exposure. Neither of these problems has been overcome by the inclusion of high indium content materials alone. We feel that it is necessary to study the nature of the contact itself in order to engineer around the present limitations. Specifically, we are interested in elucidating the effect, if any, of quantization on Schottky barrier height. In addition, we would like to experimentally determine any potential barriers that may exist in electron transport from quasi-confined (contact) regions to confined (intrinsic base) regions within the device.

We are measuring the Schottky barrier height of a variety of quantum well contacts and comparing them to those obtained for comparable bulk materials. Among the experimental variables are quantum well and barrier thickness and well indium content. In addition, we are performing photoluminescence studies in hopes of experimentally observing the shift in energy of the n=1 quantum state within the well as one barrier is removed.

1.16 Investigation of Infrared Intersubband Emission from InGaAs/AlAs/InP Quantum Well Heterostructures

Sponsor

National Science Foundation Fellowship

Project Staff

Jurgen H. Smet, Professor Clifton G. Fonstad, Jr. in collaboration with Professor Qing Hu

Subbands in quasi-two-dimensional semiconductor structures exhibit a large electric dipole matrix element, making them attractive as the active medium in an infrared source. Triple quantum-well structures are proposed in which electrons are selectively injected into the second subband of a wide center quantum well. After relaxation to the first subband, electrons are selectively removed. Two important issues need to be addressed: the achievement of population inversion and the confinement of the emitted radiation.

To avoid fast relaxation through electron/LO-phonon scattering, it is desirable to design a structure for a lasing frequency smaller than the LO-phonon frequency. This requires a subband separation of less than 30 meV. This requirement fixes the center well width and the width of the side wells. The balancing of gain and losses determines the required population inversion. The threshold current density is then, in essence, this population inversion divided by the intersubband relaxation time, provided that popu-

lation of the second subband and depopulation of the first subband do not limit the current density. Calculations indicate that for reported intersubband relaxation times in the regime below the LO-phonon threshold and for the necessary population inversion to balance the losses, the structure is not feasible unless coherent tunneling, giving rise to larger transmission coefficients than sequential tunneling, is invoked and thin barriers are used. We are in the process of measuring the I-V characteristics at low temperature of triple quantum-well structures with varying barrier thickness to verify that the current density at low applied bias voltages is not a strong function of the barrier thickness. That would support the hypothesis that injection and removal of the electrons is not the current limiting factor and thus that population inversion might be achieved.

The traditional confinement of the generated radiation in a dielectric waveguide is not practical because of the long wavelength. Highly doped regions, with a plasma frequency higher than the light frequency will be used to confine the light.

1.17 Investigation of Intersubband Relaxation Times in InGaAlAs Quantum Well Heterostructures

Sponsor

National Science Foundation

Project Staff

Jurgen H. Smet, Professor Clifton G. Fonstad, Jr.

The carrier dynamics in systems of reduced dimensionality is of great interest because of its implications on both electronic and optical quantum-well heterostructure devices. Intersubband transitions in multiple quantum-well structures with energy level separations larger than the LO-phonon energy have attracted considerable attention because of their large optical nonlinearities and fast relaxation times.

At the same time, three terminal unipolar quantum well base, tunnel barrier transistors (11.0), in which the subband separation is larger than the LO-phonon threshold, have been hampered by excessive base current due to fast electron relaxation from the second to the first subband in the quantum well.

Structures in which the energy separation between the fourth and first subband corresponds to a wavelength of 1.55 μm were designed taking the non-parabolicity of the bandstructure into account. Similarly resonant tunneling transistor structures were modified to make them suitable for pump and probe time resolved measurements. Both structures consist of pseudomorphic AlAs barriers and strained InGaAs wells on InP.

Wide quantum-well structures with energy separations smaller than the energy of an optical phonon are of interest to test the feasibility of far infrared emitting devices (14.0). Fast relaxation is undesirable since it prevents the achievement of population inversion. By going to subband separations smaller than the LO-phonon threshold energy one avoids fast relaxation by LO-phonon emission. However, so far, the intersubband relaxation times reported by different authors in this regime show considerable discrepancies. Therefore, pump probe measurements on these structures will be carried out and compared with existing data in the literature.

1.18 Infrared Characterization of InGaAs/AlAs/InP Quantum Well Heterostructures

Sponsor

National Science Foundation

Project Staff

Lung-Han Peng, Professor Clifton G. Fonstad, Jr. in collaboration with R. Victor Jones and Victor Ehrenrich[10]

We have been successfully measuring the long wavelength infrared quantum well (LWIR) intersubband absorption in 2 to 5 μm wavelength region based on InAs/InGaAs/AlAs resonnant tunneling diode structures for the IR detectors application. Over 40 percent intersubband absorption can be achieved from a doped single quantum well through our dedicated designed waveguiding system, where IR is focused upon the sample edge and makes 20 times total internal reflection while it propagates along the samples and dramatically increases the aborption strength. We also demonstrate both theoretically and experimentally that TE as well as TM modes can excite the intersubband absorption. We also pointed out that the interface Fe interband absorption at 0.3 eV could seriously

[10] Harvard University, Cambridge, Massachusetts.

obscure the IR absorption spectra and have shown how they can be avoided. These results, applied in concert with recently developed selective etches that allow us to make electrical contact to the quantum well directly, open the way to realizing high performance LWIR detectors.

1.19 Damage-Free In-Situ UHV Etching and Cleaning of III-V Heterostructures Using Molecular Beams

Sponsors

AT&T Bell Laboratories Fellowship
DARPA/NCIPT
National Science Foundation
Grant ECS 90-07745

Project Staff

Isako Hoshino, Professor Clifton G. Fonstad, Jr. in collaboration with Professor Sylvia T. Ceyer and Professor Herbert H. Sawin

The development of damage-free ultra-high vacuum (UHV) etching, cleaning, and regrowth techniques compatible with molecular beam epitaxy (MBE) and ex situ processing of III-V heterostructures is a major challenge facing device researchers. The ability to selectively pattern, etch, and overgrow quantum heterostructures is crucial to the effective realization of integrated optical circuitry and quantum effect electronic structures. Present techniques involve relatively high energy (100eV and above) ion beams which cause substantial sub-surface damage, much of which is impossible to remove.

As a solution to the problem of process-induced damage, we have begun a program investigating the use of UHV kinetic molecular beam techniques (widely used to study atomic surface interactions) to etch and clean III-V substrates and heterostructures with a minimum of surface damage and maximum flexibility. Depending on the etchant gas mixture established, it is anticipated that low energy (0.5 to 2 eV) kinetic beams can be used to (1) anisotropically etch-pattern III-V heterostructure wafers with no damage; (2) clean surfaces allowing epitaxial growth on wafers that have been removed from the UHV environment for external processing; and (3) selectively remove masking materials and clean surfaces suitable for subsequent overgrowth.

This program benefits from collaboration with Professor Sylvia Ceyer, an expert on using supersonic beams to probe surface reactions and to etch silicon, and with Professor Herb Sawin, an expert on the design of molecular beam and RF plasma sources and reactors as well as plasma reaction dynamics. Funding has been obtained to assemble a UHV chamber for kinetic beam processing which will be connected through a transfer mechanism of special design to the present Riber 2300 solid source MBE system. An etch chamber designed to use a methane-hydrogen gas mixture in a supersonic beam source is currently being assembled.

1.20 Publications

Journal Articles

Broekaert, T.P.E., and C.G. Fonstad. "AlAs Etch-Stop Layers for InGaAlAs/InP Heterostructure Devices and Circuits." *IEEE Trans. Electron. Dev.* Forthcoming.

Burns, G.F., and C.G. Fonstad. "Monolithic Fabrication of Strain-Free (Al,Ga)As Heterostructure Lasers on Silicon Substrates." *IEEE Photonics Tech. Lett.* Forthcoming.

Chiu, T.H., T.Y. Kuo, and C.G. Fonstad. "Growth and Metallization of AlGaAs/GaAs Carbon-Doped HBT's Using Trimethylamine Alane by CBE." *IEEE Electron Dev. Lett.* EDL-12: 287-289 (1991).

Eugster, C.C., T.P.E. Broekaert, J.A. del Alamo, and C.G. Fonstad. "An InAlAs/InAs MODFET." *IEEE Electron Dev. Lett.* EDL-12: 707-709 (1991).

Goossen, K.W., J.E. Cunningham, T.Y. Kuo, W.Y. Jan, and C.G. Fonstad. "Monolayer d-doped Heterojunction Bipolar Transistor Characteristics from 10 to 350 K." *Appl. Phys. Lett.* 59: 682-684 (1991).

Kuo, T.Y., J.E. Cunningham, K.W. Goosen, A. Ourmazd, W. Jan, C.G. Fonstad, and F. Ren. "Planarized Be δ-doped Heterostructure Bipolar Transistor Fabricated Using Doping Selective Contact and Selective Hole Epitaxy." *Jpn. J. Appl. Phys.* 30: L262-L265 (1991).

McCann, P.J., and C.G. Fonstad. "Auger Electron Spectroscopic Analysis of Barium Fluoride Surfaces Exposed to Selenium Vapor." *J. Electron. Mat.* 20(11): 915-920 (1991).

McCann, P.J., and C.G. Fonstad. "Liquid Phase Epitaxial Growth of PbSe on (111) and (100) BaF_2." *J. Cryst. Growth* 114: 687-692 (1991).

Meskoob, B., S. Prasad, M-K Vai, J.Vlcek, H. Sato, and C.G. Fonstad. "Microwave Model of Inverted InGaAs/InAlAs/InP Heterojunction Bipolar Transistor." *Proceedings of the 1991 International Semiconductor Device Research Symposium.* Forthcoming.

Meskoob, B., S. Prasad, M-K Vai, J.C. Vlcek, H. Sato, and C.G. Fonstad. "Bias-dependence of the Intrinsic Element Values of InGaAs/InAlAs/InP Inverted Heterojunction Bipolar Transistor." *IEEE Trans. Microwave Theory Tech.* Forthcoming.

Peng, L.-H., T.P.E. Broekaert, W-Y. Choi, C.G. Fonstad, and V. Jones. "Defect Activated Infrared Multiphonon Excitation in Iron-doped Semi-Insulating Indium Phosphide." *Appl. Phys Lett.* 59: 564-566 (1991).

Smet, J.H., T.P.E. Broekaert, and C.G. Fonstad. "Peak-to-valley Current Ratios As High as 50:1 At Room Temperature in Pseudomorphic $In_{0.53}Ga_{0.47}As$/AlAs/InAs Resonant Tunneling Diodes." *J. Appl. Phys.* Forthcoming.

Vlcek, J.C., and C.G. Fonstad. "Multiply-graded InGaAlAs Heterojunction Bipolar Transistors." *Electron. Lett.* 27: 1213-1215 (1991).

Vlcek, J.C., and C.G. Fonstad. "Precise Computer Control of the MBE Process—Application of Graded InGaAlAs/InP Alloys." *J. Cryst. Growth* 111: 56-60 (1991).

Theses

Burns, G. *Growth of (Ga,Al)As On Silicon Substrates by Molecular Beam Epitaxy.* Ph.D. diss. Dept. of Electr. Eng. and Comput. Sci., MIT, 1992.

Kuo, T.Y. *Delta-Doped Heterojunction Bipolar Transistors.* Ph.D. diss. Dept. of Electr. Eng. and Comput. Sci., MIT, 1991.

Royter, Y. *Modeling and Design of Narrow Linewidth Quantum Well Semiconductor Lasers.* S.M. theses. Dept. of Electr. Eng. and Comput. Sci., MIT, 1992.

Vlcek, J.C. *Molecular Beam Epitaxial Growth and Applications of Graded Bandgap in GaAlAs Semiconducting Alloys.* Ph.D. diss. Dept. of Electr. Eng. and Comput. Sci., MIT, 1991.

Chapter 2. High-Frequency InAlAs/InGaAs Metal-Insulator-Doped Semiconductor Field-Effect Transistors (MIDFETs) for Telecommunications

Academic and Research Staff

Professor Jesús A. del Alamo

Visiting Scientists and Research Affiliates

Dr. Yuji Awano[1]

Graduate Students

Sandeep R. Bahl, Brian R. Bennett

Undergraduate Students

Michael H. Leary, Akbar A. Moolji

Technical and Support Staff

Kelley S. Donovan, Angela R. Odoardi

2.1 Introduction

Sponsors

Charles S. Draper Laboratories, Inc.
Contract DL-H-418488
Fujitsu Laboratories
Joint Services Electronics Program
Contract DAAL03-89-C-0001
Contract DAAL03-92-C-0001
Texas Instruments

The goal of this project is to investigate InAlAs/n$^+$-InGaAs Metal-Insulator Doped channel Field-Effect Transistors (MIDFETs) on InP. These devices are of great interest for applications in long-wavelength lightwave communication systems and ultra-high frequency high-power microwave telecommunications.

InAlAs/InGaAs Modulation-Doped Field-Effect Transistors (MODFETs) on InP have recently emerged as an optimum choice for a variety of microwave and photonics applications. This is because the outstanding transport properties of InGaAs have yielded devices with very low-noise and high-frequency characteristics. Unfortunately, the low breakdown voltage of InAlAs/InGaAs MODFETs on InP (typically less than 5 V) severely restricts their use in high-power applications, such as large-signal microwave amplification and laser driving. It also forces the use of a separate high voltage supply to operate the Metal-Semiconductor-Metal (MSM) photodetectors in InP photonics receivers.

A device strategy with great potential for power handling is the InAlAs/n$^+$-InGaAs MIDFET featuring an undoped insulator and a thin, heavily-doped channel. In this structure, the breakdown voltage, V_B, is large and can be engineered using pseudomorphic insulators[2] and channel quantization (shown below). Drain current, I_D, can also be considerably improved with InAs-rich channels.[3] The attainment of high power, however, demands a large $I_D \times V_B$ product. InAs-rich channel devices unfortunately suffer from a low breakdown voltage due to: (1) the reduced channel bandgap, and (2)

---

[1] Fujitsu Laboratories, Atsugi, Japan.

[2] S.R. Bahl, W.J. Azzam, and J.A. del Alamo, "Strained-Insulator $In_xAl_{1-x}As/n^+$-$In_{0.53}Ga_{0.47}As$ Heterostructure Field-Effect Transistors," *IEEE Trans. Electron Dev.* 38(9): 1986-1992 (1991).

[3] S.R. Bahl and J.A. del Alamo, "An $In_{0.52}Al_{0.48}As/n^+$-$In_xGa_{1-x}As$ Heterostructure Field-Effect Transistor with an In-Enriched Channel," *Proceedings of the Second International Conference on InP and Related Compounds,* Denver, Colorado, April 23-25, 1990, p. 100.

severe gate leakage at the sidewall of the mesa, where the gate comes in contact with the heavily-doped channel.[4]

Towards solving this severe problem in this period of performance, we have studied the effect of quantizing the InGaAs channel. This has resulted in a drastically improved breakdown voltage through a quantum mechanically engineered enlargement of the effective bandgap of the channel. We have also solved the isolation problem through a selective chemical recessing of the edge of the channel on the mesa sidewall. We have finally integrated all our understanding developed over the last three years into a device with a strained (InAs-rich) channel, strained (AlAs-rich) insulator, quantized channel, optimized channel doping, and edge isolated device which has displayed unprecedented power and frequency performance. A detailed description of these experiments is presented in this report.

2.2 Quantum-channel InAlAs/n⁺-InGaAs MIDFETs

In previous work, we have shown that enriching the InAs mole fraction of $In_{0.53}Ga_{0.47}As$ channel results in MIDFETs with superior transport properties. However this comes at the cost of a severely reduced breakdown voltage, V_B, presumably through the decrease in the energy gap, E_g.[3] A method of increasing the effective energy gap in the channel is to introduce energy quantization by reducing the channel thickness to dimensions comparable to the electron wavelength (figure 1). In fact, it has been shown that in $In_{0.53}Ga_{0.47}As/In_{0.52}Al_{0.48}As$ quantum wells the photoluminescence emission wavelength decreases[5] with a reduction in well thickness.

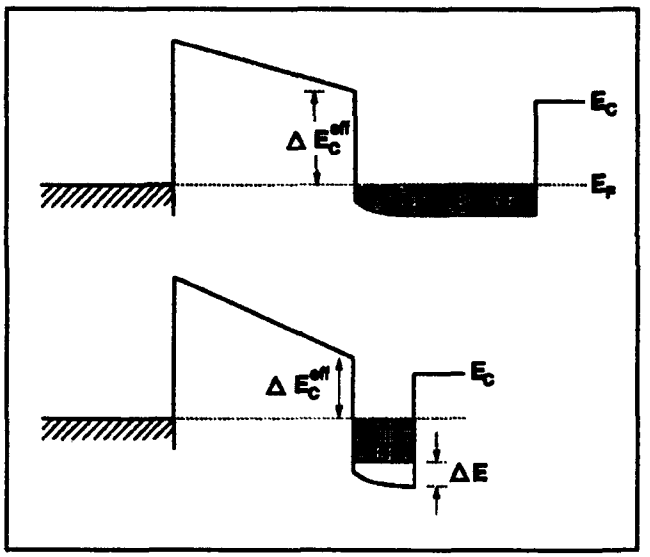


Figure 1. Schematic conduction band diagrams in equilibrium of InAlAs/n⁺-InGaAs HFETs for thick and thin channels, showing the increase in effective energy gap in the thinner channel.

In this work, we exploit this effect to enhance the breakdown voltage of $In_{0.52}Al_{0.48}As/n^+$-$In_{0.53}Ga_{0.47}As$ MIDFETs on InP. We have doubled V_B by shrinking the $In_{0.53}Ga_{0.47}As$ channel thickness from 350Å to 100Å, keeping other physical parameters constant. The principle behind our work should allow one to better exploit the excellent transport properties of InAs-rich InGaAs and other promising narrow gap semiconductors like InAs[6] and InSb.

A cross section of the device structure is shown in figure 2. The wafers were grown on SI-InP by MBE in MIT's Riber 2300 system. In an effort to keep the channel charge constant, the thickness of its undoped portion was varied while the thickness of its heavily doped portion was kept constant at 100Å. Four wafers were subsequently grown with subchannel thicknesses of 250Å, 100Å, 50Å, and 0Å, i.e., total channel thicknesses of 350Å, 200Å, 150Å, and 100Å. Devices were fabricated with nominal gate lengths of 1 μm and widths of 30

[4] S.R. Bahl and J.A. del Alamo, "An $In_{0.52}Al_{0.48}As/n^+$-$In_xGa_{1-x}As$ Heterostructure Field-Effect Transistor with an In-Enriched Channel," *Proceedings of the Second International Conference on InP and Related Compounds,* Denver, Colorado, April 23-25, 1990, p. 100.

[5] D.F. Welch, G.W. Wicks, and L.F. Eastman, "Optical Properties of GaInAs/AlInAs Single Quantum Wells," *Appl. Phys. Lett.* 43(8): 762-764 (1983); W. Stolz, K. Fujiwara, L. Tapfer, H. Oppolzer, and K. Ploog, "Luminescence of $In_{0.53}Ga_{0.47}As/In_{0.52}Al_{0.48}As$ Quantum Well Heterostructures Grown by Molecular Beam Epitaxy," *Inst. Phys. Conf. Ser.* 74(3): 139-144 (1985).

[6] C.C. Eugster, T.P. Broekaert, J.A. del Alamo, and C.G. Fonstad, "An InAlAs/InAs MODFET," *IEEE Electron Dev. Lett.* 12(12): 707-709 (1992).

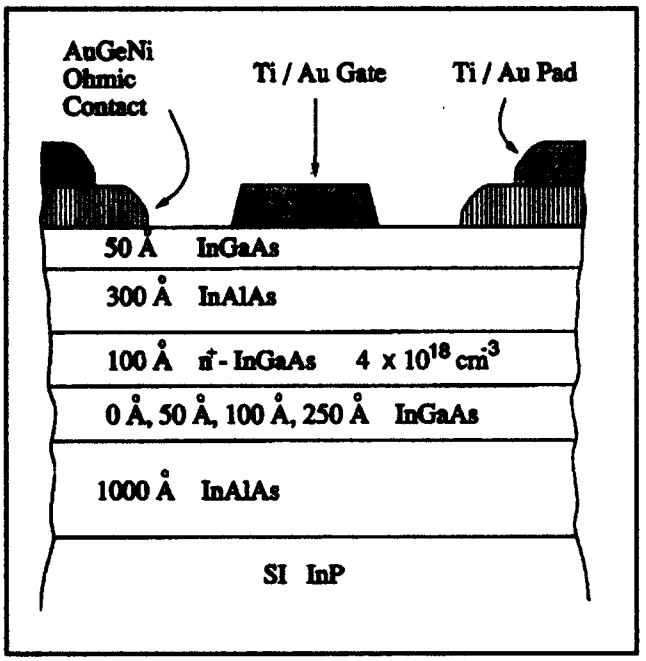


Figure 2. Cross-section of grown device structures in quantum-channel experiment.

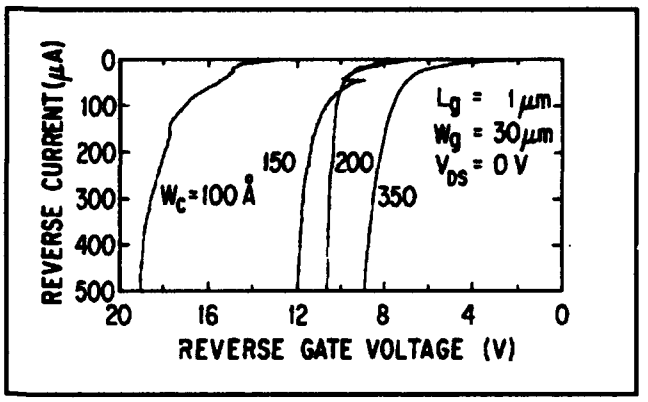


Figure 3. Breakdown voltage, V_B, for typical HFETs with channel thicknesses of 100Å, 150Å, 200Å, and 350Å.

μm. Fabrication is similar to that used in Bahl, Azzam, and del Alamo (1991).[7]

Our baseline device, 200Å channel thickness, had a peak transconductance, $g_{m(peak)}$, of 202 mS/mm and a maximum drain current, $I_{d(max)}$, of 312 mA/mm. The output conductance, g_d, was 5.73 mS/mm, resulting in a voltage gain, A_V, of 35. These are average values over five devices. $g_{m(peak)}$ and $I_{d(max)}$ were measured at $V_{ds} = 4$ V, and g_d at $V_{ds} = 4$ V and $V_{gs} = 0$ V. The contact and channel sheet resistances, measured by TLM, are 0.37 $\Omega \cdot$ mm and 625 $\Omega/\square$, respectively.

The reverse gate breakdown voltage, V_B, was measured with the source and drain grounded, and was defined at a reverse gate current of 500 μA, corresponding to about 5% of the peak drain current of our baseline device.[8] Here we focus on our main result: the increased breakdown voltage in devices with thinner channels and the experimental confirmation of the energy quantization therein.

Figure 3 shows typical reverse gate I-V characteristics of HFETs as a function of channel thickness. As shown, V_B increases gradually from 9 V at a channel thickness of 350Å to 10.6 V at 200Å, 11.9 V at 150Å, and to 19.1 V at 100Å. Average V_B measurements over several devices are within 1 V of the typical values shown in figure 3. V_B for the 200Å channel is also similar to what we have previously measured in identical devices grown and processed separately.[8] The drastic improvement in breakdown voltage of our quantized-channel HFETs is a significant merit for high-power applications. This is particularly so in this material system because typical InAlAs/InGaAs MODFET breakdown voltages are on the order of 5 V.[9]

In order to verify the bandgap enhancement in the channel as a result of carrier quantization, we have carried out photoluminescence (PL) measurements on unprocessed portions of the device samples at 77 K. The results are shown in figure 4. The energy of the peak PL intensity increases from 0.83 eV for the 350Å channel, to 0.86 for 200Å, to 0.88 for 150Å, and to 0.92 eV for the 100Å channel. The literature reports a temperature-independent PL energy shift of about 60 meV over

---

[7] S.R. Bahl, W.J. Azzam, and J.A. del Alamo, "Strained-Insulator $In_xAl_{1-x}As/n^+$-$In_{0.53}Ga_{0.47}As$ Heterostructure Field-Effect Transistors," *IEEE Trans. Electron Dev.* 38(9): 1986-1992 (1991).

[8] S.R. Bahl and J.A. del Alamo, "An $In_{0.52}Al_{0.48}As/n^+$-$In_xGa_{1-x}As$ Heterostructure Field-Effect Transistor with an In-Enriched Channel," *Proceedings of the Second International Conference on InP and Related Compounds,* Denver, Colorado, April 23-25, 1990, p. 100.

[9] P.C. Chao, A.J. Tessmer, K.-H.G. Duh, P. Ho, M.-Y. Kao, P.M. Smith, J.M. Ballingall, S.-M. Liu, and A.A. Jabra, "W-band Low-Noise InAlAs/InGaAs Lattice-Matched HEMT's," *IEEE Electron Dev. Lett.* 11(1): 59-62 (1990); Y.-C. Pao, C.K. Nishimoto, R. Majidi-Ahy, J. Archer, N.G. Bechtel, and J.S. Harris, Jr., "Characterization of Surface-Undoped $In_{0.52}Al_{0.48}As/In_{0.53}Ga_{0.47}As$/InP High Electron Mobility Transistors," *IEEE Trans. Electron. Dev.* 37(10): 2165-2170 (1990).

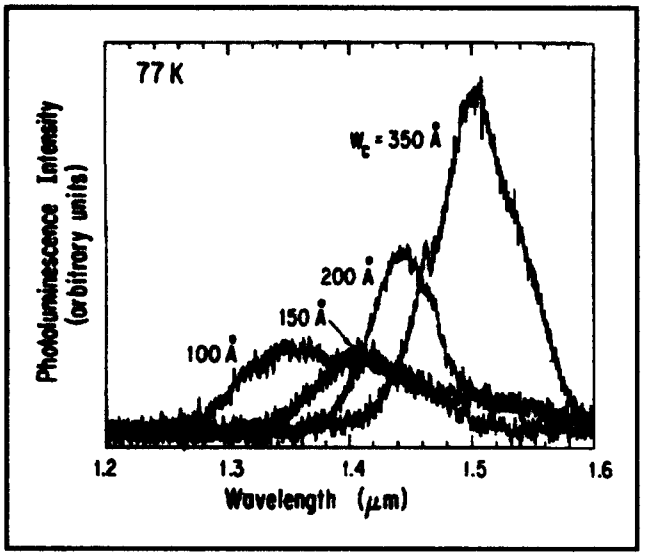


Figure 4. Photoluminescence spectra of the device heterostructures, showing an increase in photoluminescence energy with decreasing channel thickness.

the $In_{0.53}Ga_{0.47}As$ bulk value for 100Å thick $In_{0.52}Al_{0.48}As/In_{0.53}Ga_{0.47}As$ quantum wells.[10] This value of 60 meV is also consistent with simple calculations for a finite square well of thickness 100Å. Our slightly larger shift of 90 meV in the 100Å channel might be due to depletion at the top and possibly bottom interfaces, causing a reduced effective well thickness. Additionally, band bending in the insulator results in an effective stronger potential than a square well (figure 1). Both effects will tend to enhance the strength of carrier quantization over a simple quantum well.

Electron quantization, as schematically shown in figure 1, also implies a reduction of the effective conduction band discontinuity between channel and metal gate. This, in return, is expected to result in enhanced forward gate leakage current. We have experimentally found this to be the case at 300 K and 77 K,[11] providing us in this manner with an independent confirmation of the presence of quantization in the channel.

Unfortunately, we have found that a reduction in the channel thickness results in the degradation of transconductance and peak drain current.[11] $g_{m(peak)}$ decreases from 262 mS/mm to 138 mS/mm, and $I_{d(max)}$ from 451 mA/mm to 208 mA/mm in going from a channel thickness of 350Å to 100Å. However, the output conductance g_d, improves due to the enhanced channel aspect ratio, decreasing from 10.8 mS/mm to 1.84 mS/mm. This results in an enhancement in the voltage gain, A_V, from 24 to 75. The degradation in $g_{m(peak)}$ and $I_{d(max)}$ results from an increased source resistance R_s, a reduced channel sheet charge concentration n_s, and degraded mobility, μ. From 350Å to 100 Å, R_s increases from 1.4 Ω • mm to 2.7 Ω • mm, n_s drops from 2.38×10^{12} cm^{-2} to 1.77×10^{12} cm^{-2}, and μ decreases from 4318 $cm^2/V\text{-}s$ to 3591 $cm^2/V\text{-}s$. n_s and μ were measured by the Hall-effect. The acknowledged poor quality of the reverse InGaAs/InAlAs interface at the back of the channel can be held responsible for the mobility reduction.[12] As the undoped subchannel is thinned down, the reverse interface has a larger impact on carrier mobility since the channel electrons travel closer to the reverse InAlAs/InGaAs interface. There are, however, techniques that could mitigate this degradation: superlattice buffers to improve mobility[13] and the Migration-Enhanced Epitaxy (MEE) growth technique to reduce interface roughness.[14]

---

[10] D.F. Welch, G.W. Wicks, and L.F. Eastman, "Optical Properties of GaInAs/AlInAs Single Quantum Wells," *Appl. Phys. Lett.* 43(8): 762-764 (1983); W. Stolz, K. Fujiwara, L. Tapfer, H. Oppolzer, and K. Ploog, "Luminescence of $In_{0.53}Ga_{0.47}As/In_{0.52}Al_{0.48}As$ Quantum Well Heterostructures Grown by Molecular Beam Epitaxy," *Inst. Phys. Conf. Ser.* 74(3): 139-144 (1985).

[11] S.R. Bahl and J.A. del Alamo, "A Quantized-channel $In_{0.52}Al_{0.48}As/n^+\text{-}In_{0.53}Ga_{0.47}As$ HFET with High Breakdown Voltage," Extended Abstracts of the Materials Research Society 1990 Fall Meeting, Boston, Massachusetts, no. EA-21, p. 117.

[12] A.S. Brown, J.A. Henige, and M.J. Delaney, "Photoluminescence Broadening Mechanisms in High Quality GaInAs-AlInAs Quantum Well Structures," *Appl. Phys. Lett.* 52(14): 1142-1143 (1988); T. Sajoto, M. Santos, J.J. Heremans, M. Shayegan, M. Heiblum, M.V. Weckwerth, and U. Meirav, "Use of Superlattices to Realize Inverted GaAs/AlGaAs Heterojunctions with Low-temperature Mobility of 2×10^6 $cm^2/V\,s$," *Appl. Phys. Lett.* 54(9): 840-842 (1989).

[13] T. Sajoto, M. Santos, J.J. Heremans, M. Shayegan, M. Heiblum, M.V. Weckwerth, and U. Meirav, "Use of Superlattices to Realize Inverted GaAs/AlGaAs Heterojunctions with Low-temperature Mobility of 2×10^6 $cm^2/V\,s$," *Appl. Phys. Lett.* 54(9): 840-842 (1989).

[14] Y.C. Chen, P. Bhattacharya, and J. Singh, "Strained Layer Epitaxy of InGaAs (on GaAs) by MBE and Migration Enhanced Epitaxy - Comparison of Growth Modes and Surface Quality," *J. Cryst. Growth* 111(1-4): 228-232 (1991).

Thinning down the subchannel reduces the sheet carrier concentration, possibly from backside depletion. A reduced channel doping can also result in an improvement of breakdown voltage. In a separate experiment on similar devices (with 200 Å channel thickness), we examined the impact of channel doping on V_B. This experiment indicated that a reduction in sheet charge concentration from 2.38×10^{12} cm^{-2} to 1.77×10^{12} cm^{-2} should result in an improvement of V_B by 5 V. Our experimental observation of a 10 V improvement in going from a 350Å to 100Å channel is evidence that quantization is instrumental in drastically enhancing the breakdown characteristics of our HFETs.

In conclusion, $In_{0.52}Al_{0.48}As/n^+$-$In_{0.53}Ga_{0.47}As$ HFETs have been fabricated with channel thicknesses of 100Å, 150Å, 200Å, and 350Å. For devices with channel thicknesses of 100Å, the breakdown voltage improved twofold over the 350 Å devices. This is postulated to arise partially from an enlargement of the effective energy gap caused by energy quantization introduced from electron confinement, as observed by PL.

2.2.1 Elimination of Mesa-Sidewall Gate-Leakage Current by Selective Sidewall Recessing

We have shown in previous work[15] that fabrication of InAlAs/n^+-InGaAs MIDFETs by conventional mesa isolation results in sidewalls where the InGaAs channel is exposed and comes in contact with the gate metallization running up the mesa (figure 5). The low Schottky barrier height of metals on InGaAs[16] potentially results in a sidewall leakage path from the gate to the channel. Sidewall-leakage in InAlAs/InGaAs HFETs results in excessive gate-leakage current,[15] reduced breakdown voltage,[15] and increased sidegating.[17] In HFETs, sidewall-leakage was also found, by the present authors, to worsen with high doping, an increased channel thickness, and increased x ($x > 0.53$) in the $In_xGa_{1-x}As$ channel.[18] This latest trend is particularly consequential, since HFETs with InAs enriched channels have shown excellent electron transport properties.[19]

Airbridging and ion implantation have been utilized in InGaAs HFET isolation. Airbridging is complex, and implantation demands capital-intensive tools. In this paper, we propose and demonstrate a new, simpler technique by which we selectively recess the exposed InGaAs channel into the sidewall. The subsequently e-beamed gate metallization does not enter this cavity and remains isolated from the channel edge. This one-step technique is self aligned to the mesa, requires no additional masks, gate-length insensitive, and works for mesas in all crystallographic directions on the (100) surface.

The MBE grown heterostructure, lattice-matched to S.I. InP, consists of (bottom to top) a 1000Å undoped $In_{0.52}Al_{0.48}As$ buffer layer, an $In_{0.53}Ga_{0.47}As$ channel consisting of a 100Å undoped subchannel and a 80Å heavily Si doped ($N_D = 6\times 10^{18}$ cm^{-3}) transport layer, a 300Å undoped $In_{0.52}Al_{0.48}As$ gate insulator layer, and an undoped 50Å $In_{0.53}Ga_{0.47}As$ cap. For clarity in SEM imaging, an additional heterostructure with a thicker $In_{0.53}Ga_{0.47}As$ channel (120Å doped and 300Å undoped) was processed along with the device sample.

Devices were fabricated by first chemically etching a mesa down to the InP substrate using a H_2SO_4:H_2O_2:H_2O 1:10:220 etch. Then, before removing the mesa-level photoresist mask, the wafer was dipped for 45 seconds into a SA:H_2O_2

---

[15] S.R. Bahl and J.A. del Alamo, "An $In_{0.52}Al_{0.48}As/n^+$-$In_xGa_{1-x}As$ Heterostructure Field-Effect Transistor with an In-Enriched Channel," *Proceedings of the Second International Conference on InP and Related Compounds,* Denver, Colorado, April 23-25, 1990, p. 100.

[16] H.H. Wieder, "Fermi Level and Surface Barrier of $Ga_xIn_{1-x}As$ Alloys," *Appl. Phys. Lett.* 38(3): 170-171 (1981).

[17] Y-J. Chan, D. Pavlidis, and G-I. Ng, "The Influence of Gate-Feeder/Mesa-Edge Contacting on Sidegating Effects in $In_{0.52}Al_{0.48}As/n^+$-$In_{0.53}Ga_{0.47}As$ Heterostructure FET's," *IEEE Electron Dev. Lett.* 12 (7): 360-362 (1991).

[18] S.R. Bahl and J.A. del Alamo, "An $In_{0.52}Al_{0.48}As/n^+$-$In_xGa_{1-x}As$ Heterostructure Field-Effect Transistor with an In-Enriched Channel," *Proceedings of the Second International Conference on InP and Related Compounds,* Denver, Colorado, April 23-25, 1990, p. 100; S.R. Bahl, M.H. Leary, and J.A. del Alamo, "Mesa-Sidewall Gate-Leakage in InAlAs/InGaAs Heterostructure Field-Effect Transistors," submitted for publication.

[19] S.R. Bahl and J.A. del Alamo, "An $In_{0.52}Al_{0.48}As/n^+$-$In_xGa_{1-x}As$ Heterostructure Field-Effect Transistor with an In-Enriched Channel," *Proceedings of the Second International Conference on InP and Related Compounds,* Denver, Colorado, April 23-25, 1990, p. 100; U.K. Mishra, A.S. Brown, and S.E. Rosenbaum, "DC and RF Performance of 0.1 μm Gate Length $Al_{0.48}In_{0.52}As$-$Ga_{0.38}In_{0.62}As$ Pseudomorphic HEMT's," *Proceedings of the International Electron Device Meeting,* 1988. pp. 180-183.

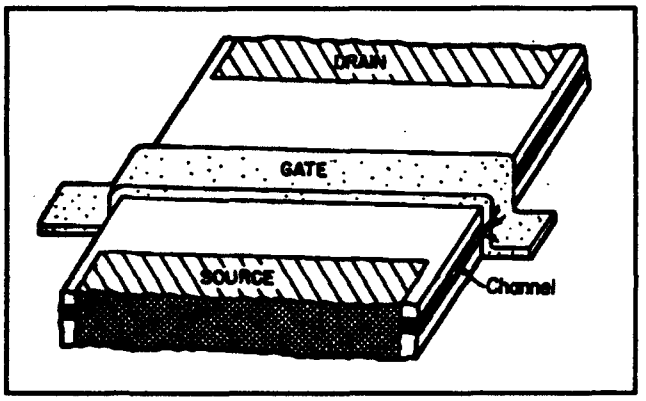


Figure 5. Three-dimensional perspective of an HFET showing the mesa-sidewall gate-leakage path.

6:1 solution[20] to selectively etch the exposed portion of the $In_{0.53}Ga_{0.47}As$ channel in a self-aligned manner. The SA solution was prepared by adding 1 liter H_2O to 200 g. succinic acid with the addition of ammonium hydroxide until the pH was 5.5. A planar selectivity of 23:1 was measured, with the $In_{0.52}Al_{0.48}As$ etching at 25Å/min. For reference, a portion of the wafer was masked during this etch by coating with photoresist using a paintbrush. In this portion, mesa etching was performed, but no selective sidewall-recessing was carried out. For the ohmic contacts, 2000Å of AuGe and 600Å of Ni were evaporated, lifted off, and RTA alloyed at 360° C. For the gate and pad, 300Å of Ti, 300Å of Pt, and 2000 Å of Au were e-beam evaporated and lifted off. This process should be compatible with recessed-gate devices. If the same etchant is used for gate-recessing, then sidewall-recessing could be performed simultaneously.

To study sidewall-leakage, we fabricated special-purpose heterojunction diodes with an active Schottky area of 10,000 μm^2. Gate-metal/mesa-sidewall overlaps were created by etching grooves through the active diode during mesa formation, and then depositing gate metal on top. The ohmic contact surrounds the gate region. Twelve diodes were fabricated in each die, with sidewall-overlap lengths, L_s, of 0, 200, 400, and 600 μm, running in each of [011], [001] and [011] crystallographic directions. Figure 6 shows a photograph of the diode test structure with various sidewall-overlap lengths along one selected crystallographic direction.

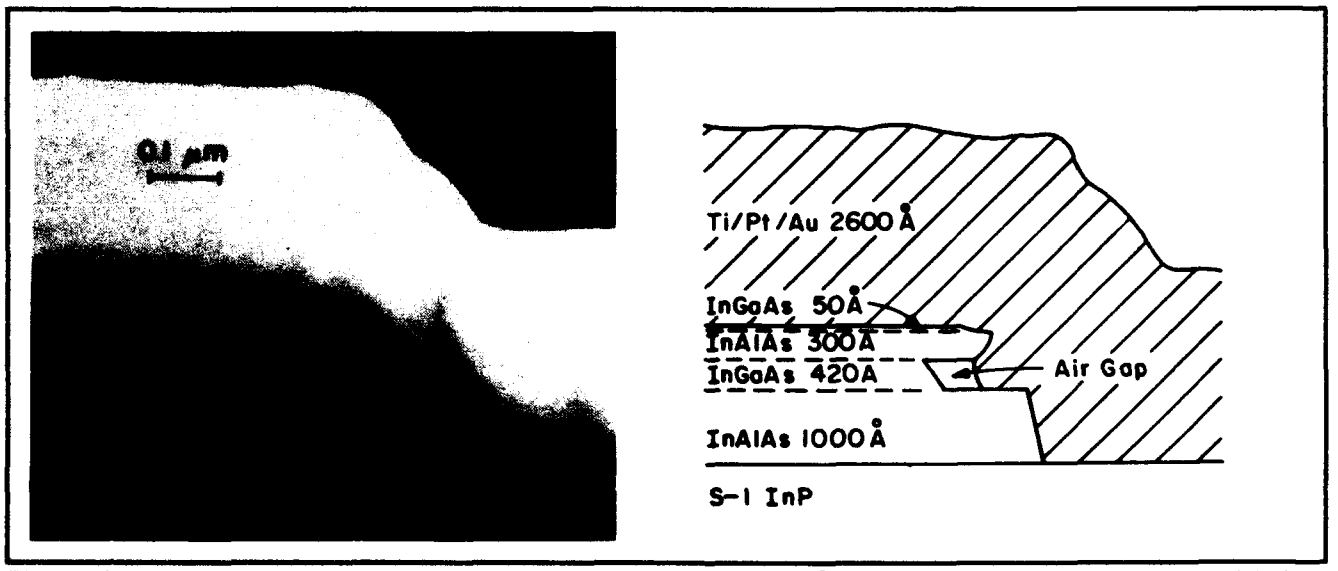


Figure 6. Photograph of sidewall-leakage test diodes with 10,000 μm^2 area and sidewall overlap lengths of (left to right) 600, 400, 200, and 0 μm.

[20] T.P.E. Broekaert and C.G. Fonstad, "AlAs Etch-Stop Layers for InGaAsAs/InP Heterostructure Devices and Circuits," *IEEE Trans. Electron Dev.*, forthcoming (1992).

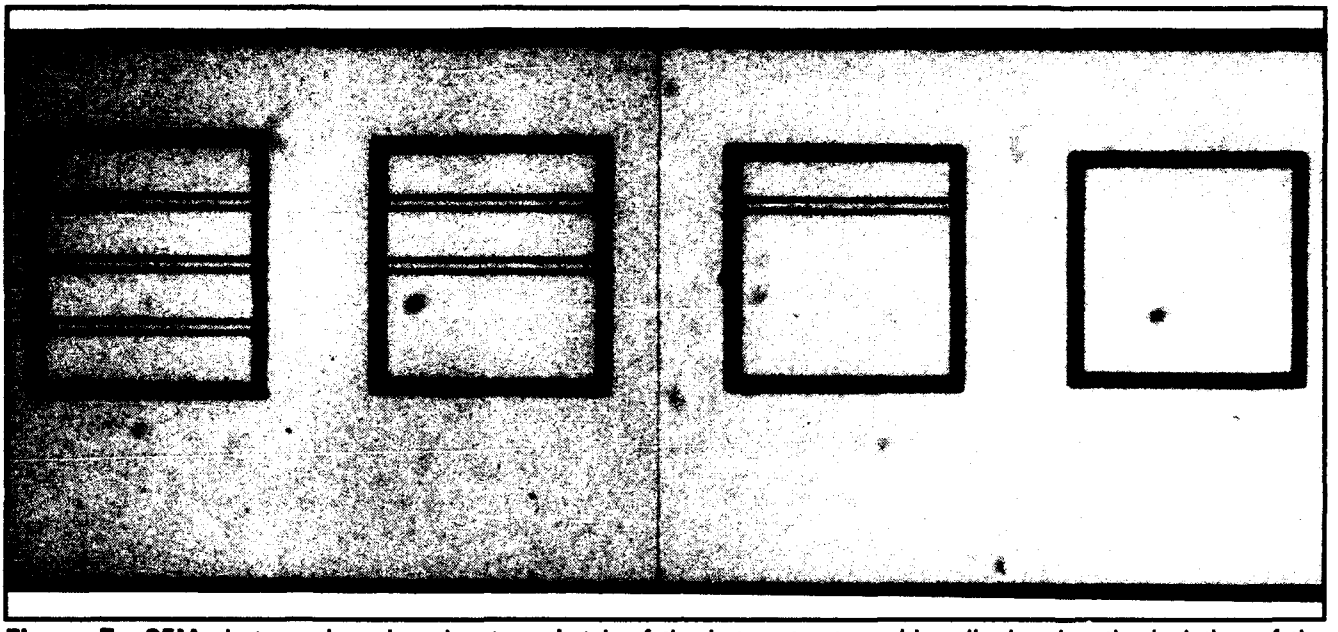


Figure 7. SEM photograph and explanatory sketch of the heterostructure sidewall, showing the isolation of the gate metal from the channel.

Figure 7 shows an SEM photograph and a sketch of the finished heterostructure with 420 Å $In_{0.53}Ga_{0.47}As$ channel processed with the other device samples. The presence of a sidewall cavity is clearly revealed. This confirms the successful action of the selective etchant. The overhang formed by the InAlAs insulator prevents the gate from contacting the channel edge.

Figure 8 shows the I-V characteristics of typical heterojunction diodes from the non-sidewall-recessed portion of the wafer with grooves along the [0$\bar{1}$1] direction. Both forward and reverse diode currents increase with sidewall-overlap length, as expected from the increase in contact area. This unmistakably proves the existence of a significant sidewall-leakage path. The figure shows that sidewall-leakage plays a major role from forward-bias till threshold (-0.82 V), when the channel is depleted. We also find (not shown) that sidewall-leakage depends on crystallographic orientation as $I[0\bar{1}1] > I[001] > I[011]$. For typical diodes with $L_e = 200$ μm, I increases by 38% from [011] to [0$\bar{1}$1] at $V = -2$ V.

In the sidewall-recessed portion of the wafer, both sidewall-length and orientation dependence of the diode current have disappeared. This is shown in figure 9, a plot of the I-V characteristics of twelve diodes (one of each stripe and orientation) from the sidewall isolated portion of the wafer. All reverse characteristics are tightly clustered and randomly distributed around the baseline area leakage characteristic observed for zero overlap length in figure 8. The absence of orientation and overlap length dependence confirms that sidewall-leakage has been completely eliminated for all crystallographic orientations.

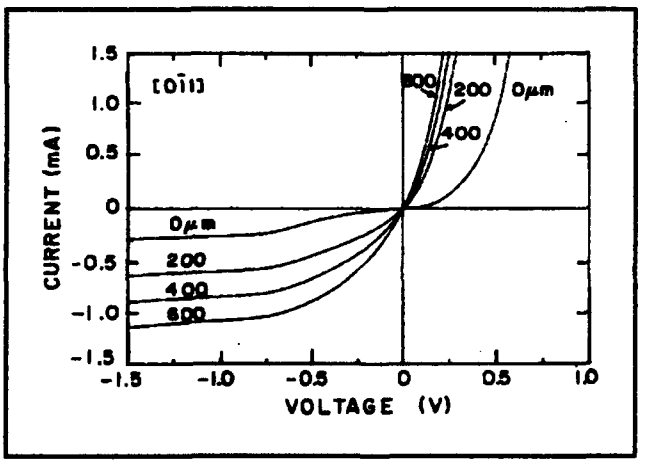


Figure 8. I-V characteristics of test diodes without sidewall recessing, as a function of sidewall overlap length along the [0$\bar{1}$1] direction on the wafer surface.

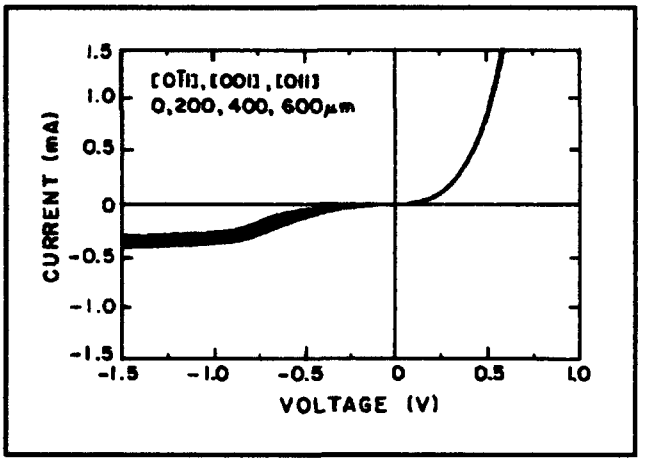


Figure 9. I-V characteristics of test diodes with sidewall recessing, for different orientations and sidewall overlap lengths.

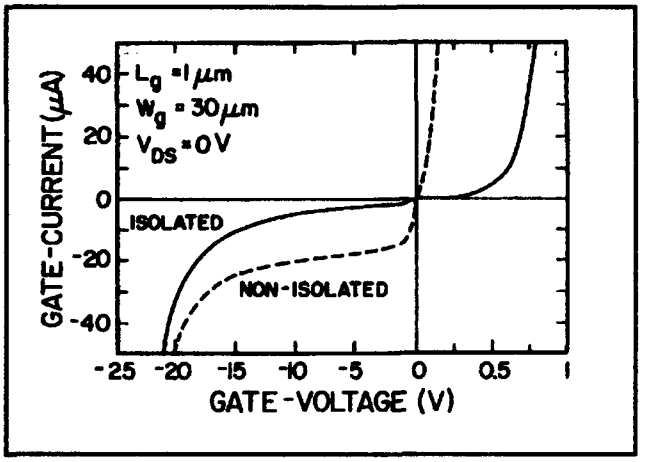


Figure 10. Gate-diode characteristics of HFETs, with and without sidewall isolation, for $L_g = 1$ μm and mesa sidewall along [0$\bar{1}$1].

On the same wafer, we have also fabricated HFETs with nominal gate length, L_g, and width, W_g, of 1 μm and 30 μm respectively. Figure 10 shows the impact of sidewall isolation on the gate characteristics. Sidewall isolation results in lower gate-leakage current, a larger gate turn-on voltage, and an increased breakdown voltage. The complete elimination of sidewall-leakage in HFETs was confirmed by the disappearance in orientation dependence of the subthreshold current (not shown) at several gate-lengths.

In conclusion, a simple self-aligned technique for eliminating mesa-sidewall gate-leakage has been developed. This technique uses selective etching to etch the exposed part of the InGaAs channel into the mesa-sidewall, creating a cavity to isolate the channel from the gate. Measurements on specially designed diodes have shown complete elimination of sidewall-leakage. This process should be useful for any kind of heterostructure in the InAlAs/InGaAs system.

2.2.2 Doubly Strained InAlAs/n⁺-InGaAs HFET

In this section, we pull together all the knowledge developed over the last three years on InAlAs/n⁺-InGaAs MIDFETs and present an original device design that features for the first time: (1) complete elimination of sidewall leakage, (2) an optimized channel doping level, and (3) high electron confinement by using a strained (AlAs-rich) insulator and a quantized and strained (InAs-rich) channel. The resulting device, though moderate in L_g, displays unprecedented power handling capabilities.

The MBE grown HFET (figure 11) on S.I. InP consists of (bottom to top), a 1000Å $In_{0.52}Al_{0.48}As$ buffer, a 75Å $In_{0.53}Ga_{0.47}As$ subchannel, a 100 Å n^+-$In_xGa_{1-x}As$ channel, a 300Å $In_{0.41}Al_{0.59}As$ strained insulator, and a 50Å $In_{0.53}Ga_{0.47}As$ cap. The insulator thickness and mole fraction were chosen to avoid misfit dislocations while providing maximum conduction band discontinuity. The subchannel thickness was chosen to introduce electron quantization and increase E_g in the channel without significantly degrading current driving capability. The impact of channel doping was examined by growing three wafers with lattice matched (x = 0.53) channels nominally doped to 4, 6, and 8 $\times 10^{18}$ cm^{-3}. From power considerations, as indicated below, an optimum doping level of 6 $\times 10^{18}$ cm^{-3} was selected. This is the doping at which the InAs-rich channel (x=0.65) device was grown.

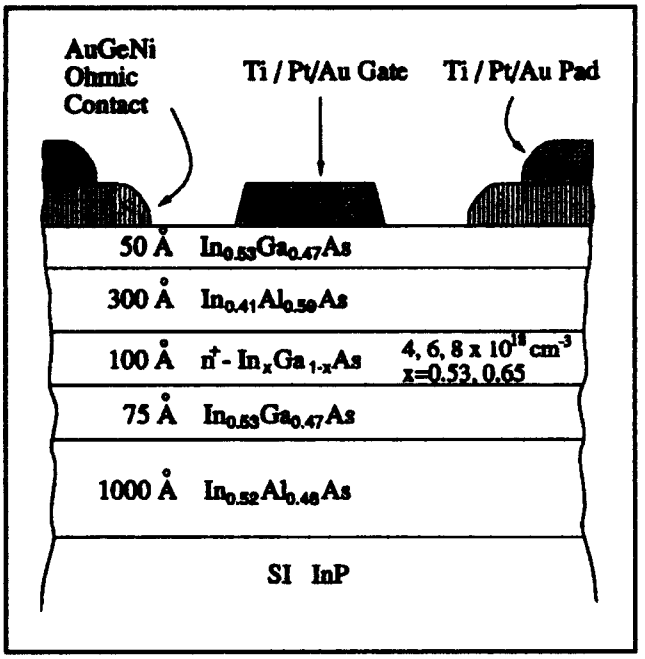


Figure 11. Cross-section of doubly-strained device structure.

Devices (see sketch in figure 11) were processed by mesa etching, sidewall isolation etching, RTA alloying of lifted-off Ge/Au/Ni ohmic contacts, and lifting-off Ti/Pt/Au gates and pads. Sidewall isolation was done by selectively etching the InGaAs channel edge into the sidewall to create a cavity. Gate-metal running up the mesa sidewall does not enter the cavity, and therefore does not contact the channel edge. Measurements are reported for 1.9 μm gate length (L_g) HFETs. All DC measurements are averaged over several devices.

In our x=0.53 channel devices, higher channel doping results in higher $I_{D(max)}$, but lower V_B. $I_{D(max)}$ for dopings of 4, 6, and 8 $\times 10^{18}$ cm^{-3} is respectively 117, 220, and 371 mA/mm. V_B is 21.1, 15.6, and 5.3 V, giving an $I_{D(max)} \times V_B$ product of 2.5, 3.4, and 2.0 W/mm respectively. f_t and f_{max} also increase with doping. f_t is 9.2, 11.3, and 12.8 GHz, and f_{max} is 34, 42, and 68 GHz, respectively.

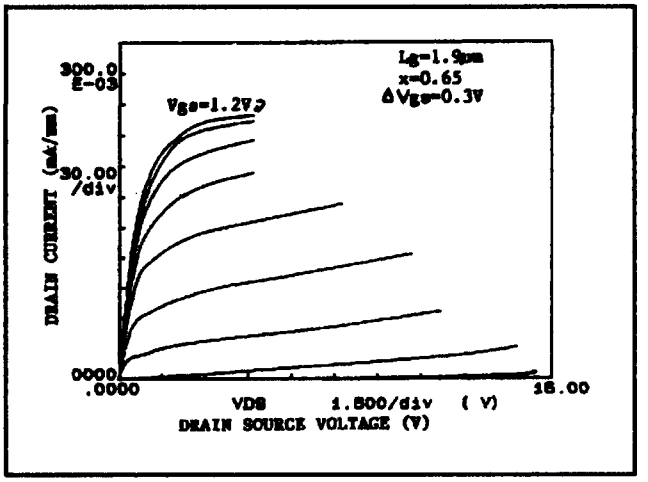


Figure 12. I-V characteristics of x=0.65 HFET.

For our doubly-strained InAs-rich (x=0.65) channel device, we found $g_{m(peak)}$ = 201 mS/mm, and $I_{D(max)}$ = 276 mA/mm (figure 12). f_t was 14.9 GHz and f_{max} 101 GHz (figure 13). This gives an effective electron velocity of 1.8 $\times 10^7$ cm/sec for our 1.9 μm L_g, comparable to values obtained in MODFETs of similar L_g 's. The high f_{max} is a consequence of low g_d (0.9 mS/mm at peak f_t) as this device is now able to enter accumulation at $V_{gs} \geq 0$ V. The voltage gain at peak f_t is 150. The average V_B was 12.8 V (figure 14). This results in an average $I_D \times V_B$ product of 3.5 W/mm. Devices capable of handling as much as $I_D \times V_B$ = 4 W/mm were obtained. These values represent an improvement over similar gate length MODFETs of 2 to 3 times. High electron confinement and reduced gate leakage in these HFETs are instrumental in obtaining these values.

In conclusion, in the pursuit of high-power InAlAs/InGaAs HFETs, we have combined for the first time in a single device, an optimized heavily-doped channel, an AlAs enriched insulator, an InAs enriched channel, channel quantization, and mesa-sidewall leakage elimination. We have thereby been able to fabricate a high-voltage, high-current device with excellent microwave characteristics. Scaled down versions of this device are very promising for high-power microwave and photonics applications.

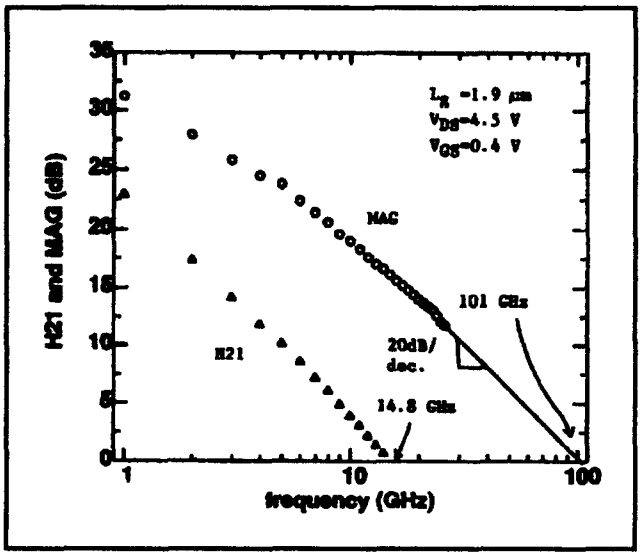


Figure 13. H_{21} and MAG vs. frequency for x=0.65.

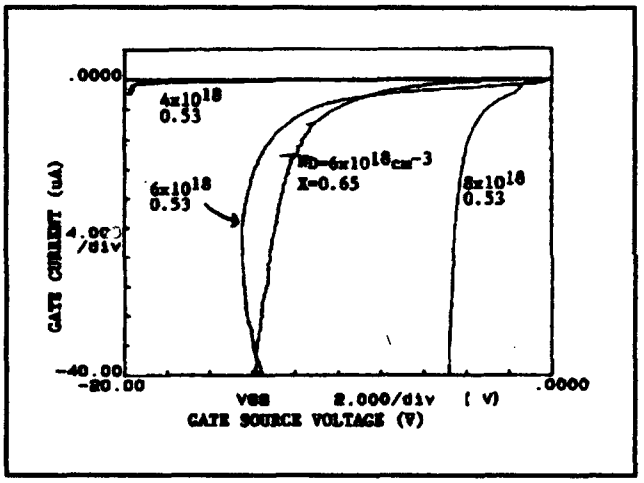


Figure 14. Reverse I_g vs. V_{gs} characteristics for typical HFETs showing that our improvements have mitigated the degradation in V_B for x=0.65 ($W_g = 30\mu m$).

2.2.3 Publications and Meeting Papers

Bahl, S.R., and J.A. del Alamo. "InAlAs/n$^+$-InGaAs HFETs: Impact of Dislocations and Channel Quantization." Paper presented at the Workshop on Compound Semiconductors Materials and Devices (WOCSEMMAD), Ft. Lauderdale, Florida, February 18-20, 1991.

Bahl, S.R., W.J. Azzam, and J.A. del Alamo. "Orientation Dependence of Mismatched $In_xAl_{1-x}As/In_{0.53}Ga_{0.47}As$ HFETs." *J. Crystal Growth* 111(1-4): 479-483 (1991).

Bahl, S.R., W.J. Azzam, and J.A. del Alamo. "Strained-Insulator $In_xAl_{1-x}As/n^+$-$In_{0.53}Ga_{0.47}As$ Heterostructure Field-Effect Transistors." *IEEE Trans. Electron Dev.* 38(9): 1986-1992 (1991).

Bahl, S.R., and J.A. del Alamo. "Elimination of Mesa-Sidewall Gate Leakage in InAlAs/InGaAs HFETs by Selective Sidewall Recessing." *Proceedings of the 18th International Symposium on Gallium Arsenide and Related Compounds,* Seattle, Washington, September 9-12, 1991.

Chapter 3. Novel Superconducting Tunneling Structures

Academic and Research Staff

Professor John M. Graybeal, Professor Henry I. Smith

Visiting Scientists and Research Affiliates

Dr. Bernard S. Meyerson[1]

Graduate Students

George E. Rittenhouse

3.1 Project Description

Sponsor

Joint Services Electronics Program
Contract DAAL03-89-C-0001
Contract DAAL03-92-C-0001

Project Staff

Professor John M. Graybeal, Professor Henry I. Smith, Dr. Bernard S. Meyerson, George E. Rittenhouse

In this program we seek to examine the superconducting Josephson behavior in short-channel electronic structures where interference effects can take place. Additionally, our hybrid superconducting-semiconducting structure represents the first attempt at Josephson coupling via resonant tunneling. A significant consequence of this approach is that the energy scale for modulating the Josephson coupling is set by the quantum confinement levels and not the intrinsic semiconducting gap voltage.

Our device uses a thin vertical Si membrane (< 1000Å) as a degenerate semi-conducting weak link between the superconducting source and drain electrodes which lie on either side. This structure is in many ways an electrical analogue of a Fabry-Perot interferometer. The membrane defines a vertical quantum well in which the charge carriers can interfere with each other (either constructively or destructively), thus creating a resonant tunneling structure between the source and drain for both the Cooper pairs (i.e., the Josephson channel) and the normal quasiparticle (i.e., electron) channel. A separately applied gate voltage biases the levels within the semiconducting well, and ideally will modulate the Josephson current by varying the wavelength of the tunneling particles. Previous efforts on such hybrid Josephson devices have not utilized either resonant tunneling or quantum confinement, and their lack of gain arises from the significant mismatch between the semiconducting and superconducting gap energy scales.[2] A key motivation for our devices is that the energy scale is set by quantum confinement, and can be tuned separately from either of the gap energies. For Si well widths in the range of 500-1000Å, the energy levels separation in the well can be more comparable to the superconducting gap energy, i.e., many times smaller than the semiconducting gap.

Recent progress has now validated our basic device geometry in uniformly doped low-mobility Si:P. We are now progressing to fabricate the devices on doped high-mobility epitaxial layers grown on Si wafers at IBM. Higher mobilities will increase the characteristic lengths for the carriers in the semiconducting well, thereby better enabling internal interferences.

A schematic of the device geometry is shown in figure 1. More details of the fabrication process and progress will be published elsewhere.[3] The primary aspects of the fabrication are described here. The originating wafer is $< 110 >$ Si, phosphorous-doped via ion implantation to yield

---

[1] IBM Corporation, Thomas J. Watson Research Center, Yorktown Heights, New York.

[2] A.W. Kleinsasser, T.N. Jackson, G.D. Pettit, H. Schmid, J.M. Woodall, and D.P. Kern, *IEEE Trans. Mag.* MAG-25(2): 1274 (1989), and references within.

[3] K. Early, G.E. Rittenhouse, J.M. Graybeal, and Henry I. Smith, "Sub-100 and sub 10-nm-thick Membranes Aniso-

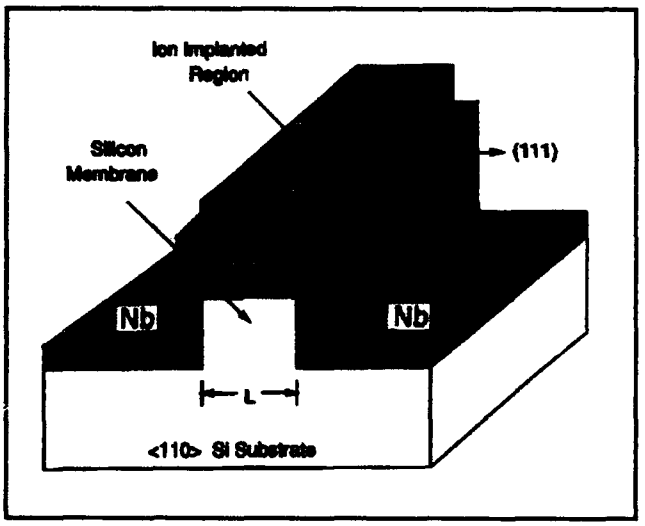


Figure 1. Schematic of the planar device structure. The vertical membrane consists of two etch pits separated by a length $L \leq 1000$Å. The typical height for the vertical membrane is ≈3000Å.

1×10^{19} cm^{-3} carriers at low temperature. A 300Å Si_3N_4 layer is used as an etchant mask, with the membrane defined by aligning a mask stripe along either the [1$\bar{1}$2] or [112] crystalline axis. The membrane fabrication is done via wet etching, using a potassium hydroxide/isopropyl alcohol solution which is well known for its highly anisotropic etching of Si. Because of the wafers' crystallographic orientation, the resultant terminating (111) planes are perpendicular to the wafer surface and form the walls of the vertical membrane structure. Such processing yields atomically-smooth surfaces which possess a significantly higher degree of parallelism and a significantly lower surface defect density than could be obtained by reactive-ion-etching (RIE) or other energetic processes. The niobium counterelectrodes are subsequently deposited, and source-drain isolation is obtained by planarization followed by a chlorine RIE etch.

The electrical results of such devices fall into two categories. Those with wall thicknesses (denoted L in figure 1) greater than roughly 1000Å displayed no Josephson currents, and showed current-voltage (I-V) characteristics consistent with superconducting-insulator-normal (SIN) metal behavior. The thin "insulating" layer is presumably a Schottky barrier at the Nb/Si interface, whereas the lack of a Josephson current reflects the fact that the device thickness L is significantly greater than the proximity-induced superconducting coherence length ξ_N in the Si ($\xi_N \approx 65$-100Å at 4.2K for these low-mobility devices). However, devices with membrane thicknesses comparable to 600Å displayed finite Josephson currents, and fine I-V behavior consistent with SNS behavior. The I-Vs are shown as a function of temperature for one device in figure 2. The product of the critical current and the high-bias device resistance I_cR_n was as high as 0.4 meV at low temperatures, consistent with the best previous results on Nb/Si/Nb devices. Careful examination of the device characteristics plus imaging with a high-resolution STEM ruled out the existence of any Nb shorts over the top of the membrane. Additionally, modulation of the critical current versus applied magnetic flux was entirely consistent with the device geometry.

The next step for this work is to fabricate these devices using high-mobility Si. Note that conventional uniformly doped Si cannot provide the necessary characteristic lengths as its mobility is too low. Therefore, we are turning to chemical-vapor deposited epitaxial layers of Si/Si:B grown on (110) oriented wafers which can have mobilities approaching 10^4 cm^2/V-sec. This work is presently underway.

tropically Etched in (110) Silicon," submitted for publication; G.E. Rittenhouse, Henry I. Smith, and J.M. Graybeal, "A Silicon Weak-Link Josephson Junction Using a Vertical Membrane Structure," forthcoming.

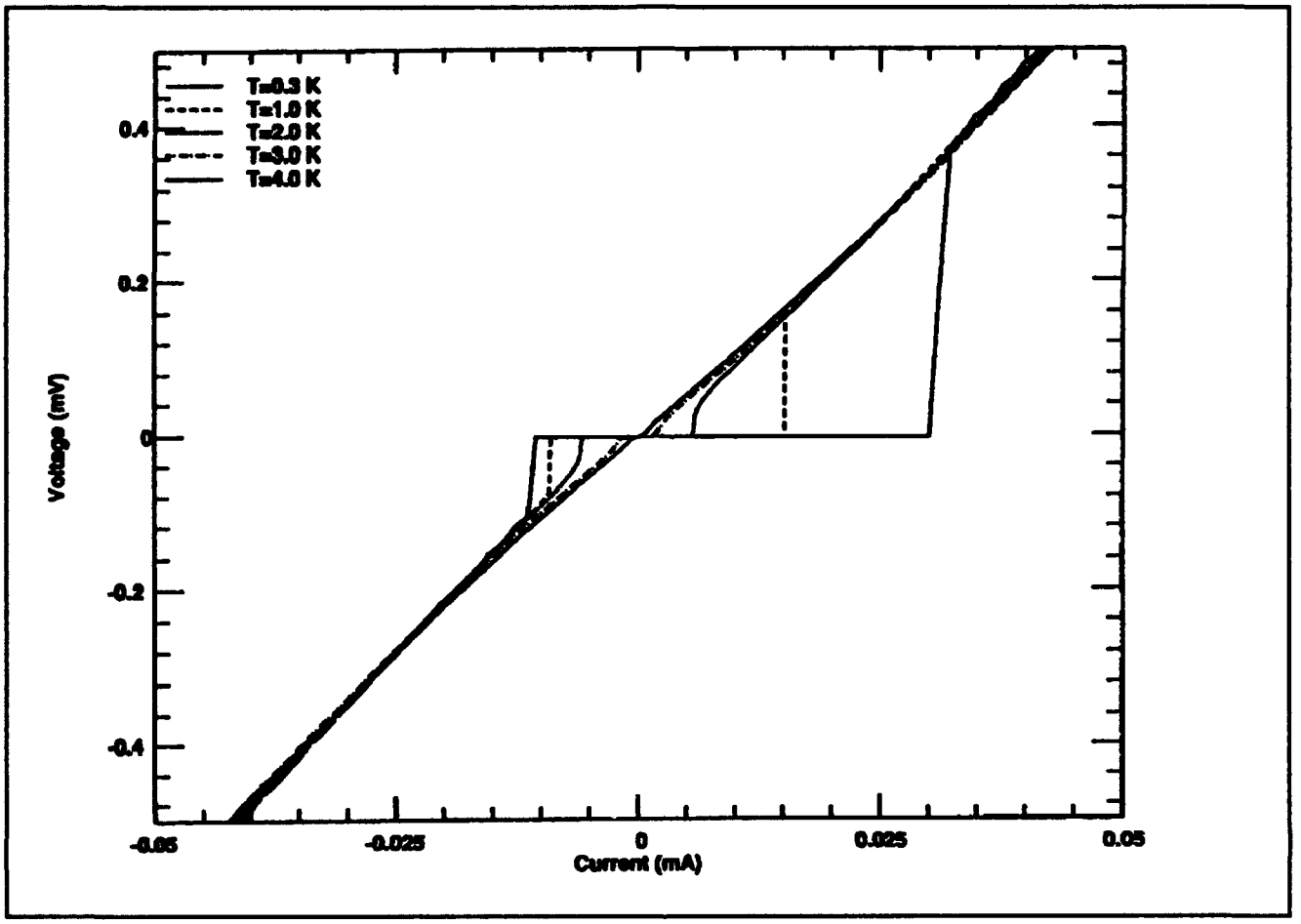


Figure 2. Current-voltage characteristics of one device versus temperature. Note presence of a finite Josephson current.



Professor Leslie A. Kolodziejski

Chapter 4. Chemical Beam Epitaxy of Compound Semiconductors

Academic and Research Staff

Professor Leslie A. Kolodziejski

Visiting Scientists and Research Affiliates

Dr. Carmen Huber[1]

Graduate Students

Ziad Azzam, Christopher A. Coronado, Jay N. Damask, Easen Ho

Undergraduate Students

George C. Chen, Sang H. Park, Chung-Hao Shue, Ayca Yuksel

Technical and Support Staff

Kelley S. Donovan, David S. Lee, Angela R. Odoardi

4.1 Facility for the Gas Source Epitaxy of Compound Semiconductors

Sponsors

3M Company Faculty Development Grant
AT&T Research Foundation
Special Purpose Grant
Charles S. Draper Laboratories
Contract DL-H-418484
Defense Advanced Research Projects Agency
Subcontract 216-25013 and 542383
Joint Services Electronics Program
Contract DAAL03-89-C-0001
Contract DAAL03-92-C-0001
National Science Foundation
Grant ECS 88-46919
Grant ECS 89-05909

The new laboratory for the growth of both II-VI and III-V compound semiconductor heterostructures, using gas source epitaxy techniques, has received all hardware necessary to complete the multichamber system. The epitaxy system consists of six interconnected ultrahigh vacuum chambers: two introduction chambers, a transfer chamber, a II-VI-dedicated reactor, a III-V-dedicated reactor, and an analytical/metalization chamber. The analytical/metalization chamber is now attached to the transfer chamber; figure 1 shows a photograph of the new chamber. In situ analytical tools which are available include Auger electron spectroscopy, reflection high energy electron diffraction (RHEED), additional ports for laser illumination of the sample, and a three-source electron beam evaporator for metals. The ultrahigh vacuum interconnection to both of the growth systems allows surface analysis of the many II-VI, III-V, and II-VI/III-V heterostructures which are envisioned, immediately following fabrication, without concern of contamination from atmospheric gases. The analysis chamber is expected to provide additional insight into the effect of both electron and photon beams on the surface of films grown using metalorganic molecular beam epitaxy. Metal evaporators will enable us to probe the initial stages of ohmic contact formation specifically with regard to the difficulties experienced in forming an ohmic contact to p-type ZnSe. The presence or absence of mixed interfacial layers in multilayered II-VI/III-V heterostructures may also be detected (in some instances) in the analytical chamber.

The final addition was the connection of a gas source molecular beam epitaxy (GSMBE) reactor to a small buffer chamber attached to the transfer chamber. The new reactor, shown in figure 2, was purchased from Instruments S.A., Riber Division, and is now in the final stages of installation. The gas source reactor has solid elemental sources of Ga, In, Al, Si, and Be, and gaseous hydride sources of arsenic and phosphorus. The purpose

[1] Physics Department, University of Puerto Rico, Rio Piedras, Puerto Rico.

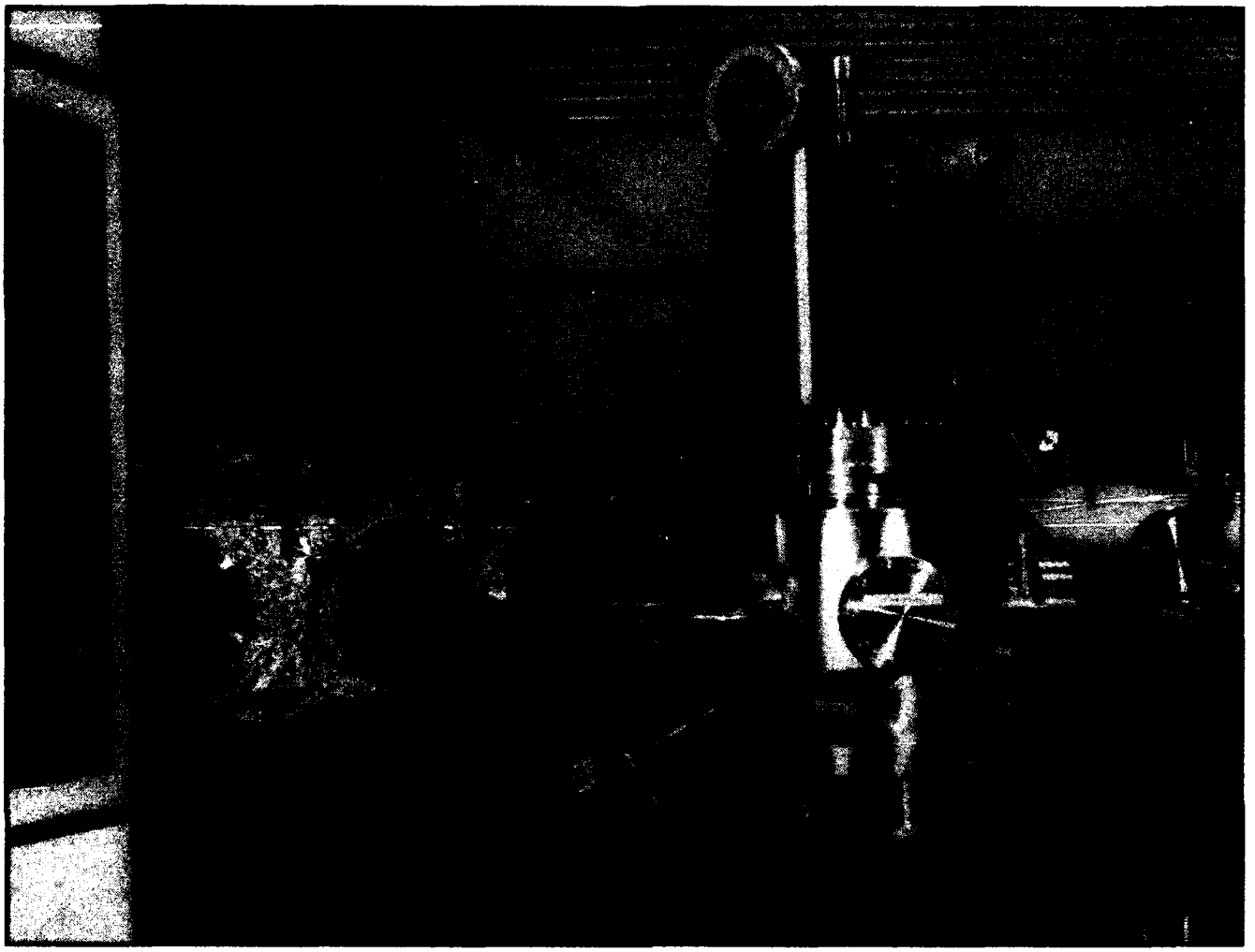


Figure 1. Photograph of the analytical/metalization chamber. Connection to the ultrahigh vacuum transfer chamber is yet to be completed.

of the III-V chamber is two-fold: (1) layers containing P and As will be crucial for utilizing lattice-matched buffer layers for the II-VI-based quantum well structures which are under investigation, and (2) III-V-based optical and electronic devices will be explored including quantum-effect electronic devices (in collaboration with Professors Dimitri A. Antoniadis and Henry I. Smith), and channel dropping filters and waveguide structures (in collaboration with Professor Hermann A. Haus). In addition, the III-V chamber will be employed for fabrication of II-VI/III-V multilayered heterostructures which contain III-V layers having substantial thickness. The II-VI reactor, which has gaseous sources for In, Ga, and As, will only be used for the growth of very thin III-V layers on the order of hundreds of angstroms or less.

4.2 Metalorganic Molecular Beam Epitaxy (MOMBE) of ZnSe

Sponsors

Charles S. Draper Laboratories
Contract DL-H-418484
Defense Advanced Research Projects Agency
Subcontract 542383 and 5300716-07
Joint Services Electronics Program
Contract DAAL03-89-C-0001
Contract DAAL03-92-C-0001
National Science Foundation
Grant ECS 88-46919
U.S. Navy - Office of Naval Research
Contract N00014-88-K-0564

Optical sources operating in the blue portion of the visible light spectrum have many potential commercial and military applications in, for example, optical information storage systems,

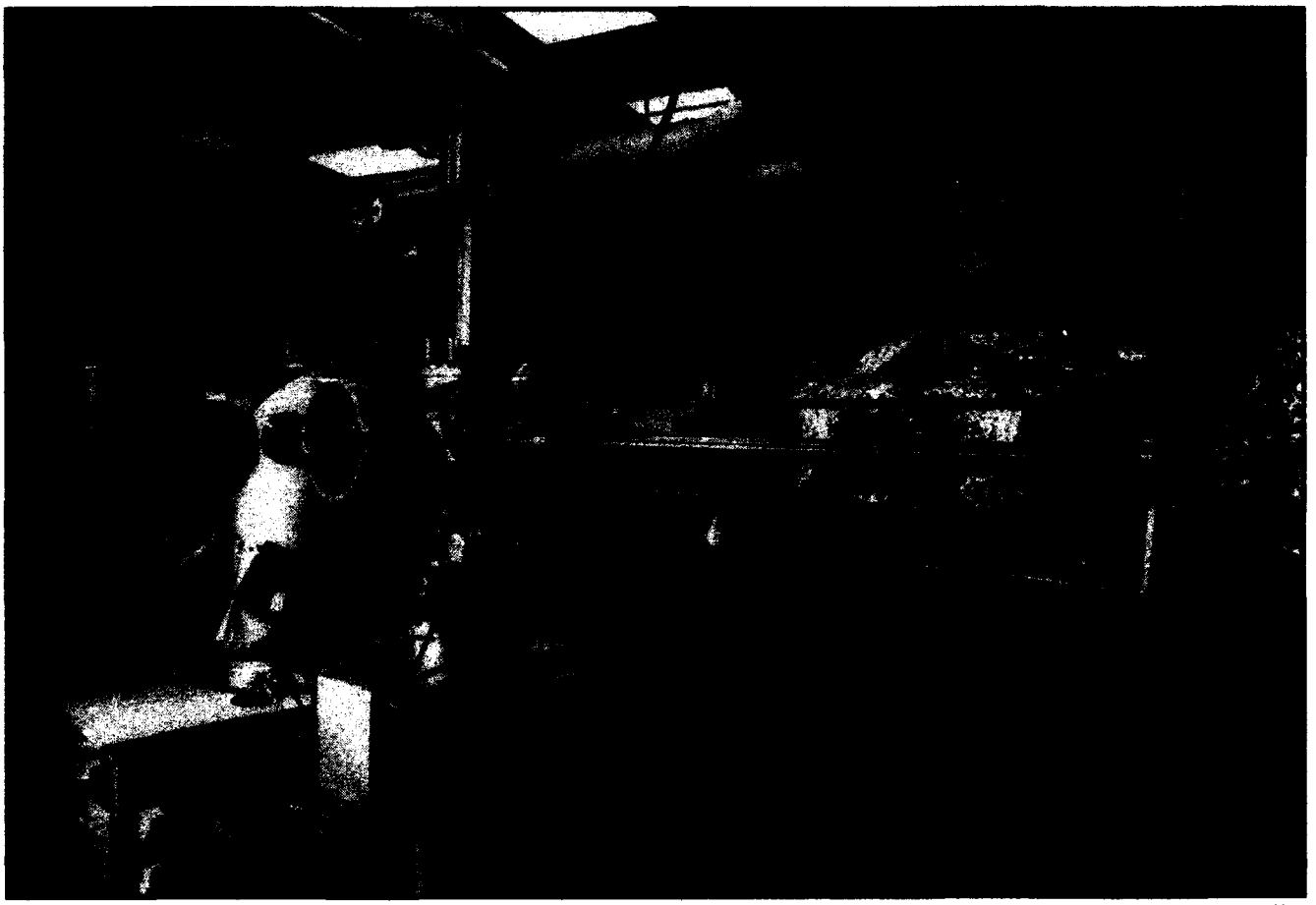


Figure 2. Photograph of the new III-V-dedicated GSMBE (which is attached to the small loadlock/buffer chamber). Final connection to the hemispherical ultrahigh vacuum transfer chamber can be seen.

medical imaging systems, electroluminescent flat panel displays, and color laser printers.

Although there are a variety of material systems, such as SiC, frequency doubled III-V-based lasers, and GaN, which can potentially offer a source of blue light, each of these systems has some limitations relative to integration and/or fabrication. The II-VI family of semiconductors (specifically the Zn chalcogenides) offers a solution to the problem of integration, and impressive recent gains have been achieved in fabrication technology. II-VI-based quantum well structures exhibiting excellent crystal quality are routinely fabricated on technologically important III-V substrates, suggesting that future integration needs will be straightforward. However, some substantial problems still remain to be solved.

In order to meet the requirements for room temperature, blue optical sources, the II-VI materials will require greater concentrations of sulfur to increase the bandgap. However, the alloying of ZnSe with sulfur results in a contraction of the lattice parameter and, therefore, an increase in the lattice mismatch with binary compounds such as GaAs. This problem is eliminated by utilizing lattice-matched alloy buffer layers such as InGaP and GaAsP. The attached III-V gas source molecular beam epitaxy reactor will be the source of any III-V-based lattice-matched buffer layer. Although the lattice mismatch difficulty is circumvented here, we are also fabricating "epilayer-on-epilayer" structures. These epilayer-on-epilayer structures are necessary to provide the minimum possible number of defects created at the heterovalent interface and ultimately within the active region of the II-VI optical device. In addition, a key advantage offered by gas source epitaxy techniques is the ability to control, via mass flow controllers, the flux of species which exhibit very high vapor pressures as a function of temperature. Sulfur and phosphorus containing materials are excellent candidates for fabrication utilizing gas source epitaxy techniques with impressive successes reported.

The objectives of the research described here revolve around the growth of various II-VI-based heterostructures using gaseous source epitaxy including metalorganic molecular beam epitaxy (MOMBE), chemical beam epitaxy (CBE), and gas source molecular beam epitaxy (GSMBE). The various techniques utilize combinations of gaseous

sources such as metalorganics and hydrides, as well as solid elemental sources. Thus far we have explored the MOMBE of ZnSe using diethylzinc and diethylselenium.

A large number of films have been grown with the details of the growth parameters described below. ZnSe epilayers were normally grown on carbon-controlled semi-insulating (001) GaAs wafers, although n-type, p-type and 2°-off n-type GaAs were also used. Typical growth temperatures ranged from 250°C to 425°C, with the majority of the film growths performed near 320°C. The VI/II flow ratio was varied from 0.2 to 5.0, with diethylzinc (DEZn) and diethylselenium (DESe) gas flows ranging from 0.5 to 2.5 sccm. Reactor pressure during growth was typically $1x10^{-4}$ Torr. In nearly all cases the DEZn cracker was set at 50°C, and the DESe was thermally decomposed at 800°C. Cracking experiments with the quadrupole mass spectrometer (QMS) indicated that DESe decomposed at 800°C, while DEZn thermally dissociated at temperatures above 300°C.

Preliminary microstructural and optical characterization of the ZnSe suggests that the thin films are of good quality. A typical RHEED pattern observed following growth shows the presence of narrow streaks and readily apparent Kikuchi bands suggesting the existence of single crystalline films with smooth surface morphology. Secondary ion mass spectroscopy (SIMS) results indicate very low levels of carbon incorporation which is near the detectability limit of our instrument (VG-Fisons Instruments Model IX70S SIMSLAB). X-ray diffraction rocking curve analysis confirms the pseudomorphic nature of thin 1000Å films of ZnSe on GaAs. Typical full width at half maximum measurements for the (400) reflection is around 220 arc seconds. Optical characterization from photoluminescence measurements indicates the presence of bandedge excitonic features which are shifted to higher energy reflecting the presence of strain, in addition to features originating from deep level defects. We speculate that the presence of these particular deep level features is due to stoichiometry such as Zn vacancies, and we are therefore investigating growth with various flux ratios.

The growth rate using DEZn and DESe has continued to be very low. Although the actual species at the surface front are not known, we expect to find ethyl species of Zn and Se, in addition to dimers of Se from the thermal decomposition of the metalorganic. The growth temperatures investigated and the cracking data suggest that there is sufficient thermal energy to decompose the Zn molecules. (The RHEED patterns exhibit reconstructions of a Zn-stabilized surface.) In addition, the nearly constant growth rate observed for a wide variety of growth conditions (flow ratio and rate, substrate temperature, and with and without hydrogen) suggests that the growth is surface kinetics limited. Similar to metalorganic vapor phase epitaxy (MOVPE), although lacking the gas phase reactions, the MOMBE growth technique is expected to exhibit complex surface chemical reactions. We speculate that at the necessary low growth temperatures employed here, lattice sites for incorporation of Zn and Se are being blocked by alkyl radicals. The alkyl radicals are a copious byproduct of the surface pyrolysis of DEZn and thermal decomposition of the DESe. At higher growth temperatures (≥425°C), where one might expect the alkyl radicals to desorb, competing desorption of Zn and Se limits the growth rate. Previous work[2] reported using these metalorganic sources show growth rates approximately an order of magnitude greater under similar growth conditions. Differences which may exist include (1) pressure during growth, (2) use of hydrogen carrier gas, or (3) the actual design of the gas crackers.

4.3 Photo-Assisted MOMBE of Wide Bandgap II-VI Compound Semiconductors

Sponsors

Defense Advanced Research Projects Agency
Subcontract 530-0716-07
Joint Services Electronics Program
Contract DAAL03-89-C-0001
Contract DAAL03-92-C-0001
National Science Foundation
Subcontract DMR 90-07890

Photo-assisted heteroepitaxial growth of ZnSe on GaAs by MOMBE is currently under intense investigation. MOMBE has several potential advantages when compared to other epitaxial growth techniques such as metalorganic vapor phase epitaxy (MOVPE) and molecular beam epitaxy (MBE). The advantages include: (1) The flux ratio of gaseous metalorganics can be precisely controlled using mass flow controllers; (2) in-situ analysis techniques such as reflection high-energy electron diffraction (RHEED) and quadrupole mass

[2] H. Ando, A. Taike, R. Kimura, M. Konagai, and K. Takahashi, "Metalorganic Molecular Beam Epitaxial Growth of ZnSe Using Diethylzinc and Diethylselenide," *Japanese J. Appl. Phys.* 25(4): L279-L281 (1986).

spectroscopy (QMS) are available; and (3) surface chemistry allows for fine tuning of the growth conditions. Photo-assisted MOMBE adds an extra degree of versatility because both selective deposition of material and modification of the surface chemistry are possible.

Photo-assisted growth was performed by selectively illuminating a portion of the wafer's surface. Radiation from a 5 Watt Ar ion laser (Spectra-Physics, Model 2025) was introduced at a 45° angle to the substrate normal. The laser spot on the wafer was typically an ellipse with major and minor axes of 1.4 and 1.0 cm. The effect of wavelength on growth has been studied by using laser radiation ranging from 780 nm to 350 nm. To produce the 780 nm line, a Ti:sapphire crystal was pumped with all lines of the argon ion laser. The power density was kept low at approximately 180 mW/cm^2, thus allowing thermal heating effects to be neglected.

As mentioned in Section 4.2, under the growth conditions described here, the growth rate during MOMBE of ZnSe has consistently remained very low. The growth rate without laser illumination is typically 250 to 375Å/hour. As a function of calibrated growth temperature, the unilluminated growth rate shows a remarkable temperature insensitivity over the temperature range of 250-425°C. This is quite unexpected since MOMBE has typically demonstrated a strong temperature dependence.[3] Laser illumination, however, has been found to ameliorate the low growth rate. For the portion of the film grown with photo-assistance, a significant temperature dependence is observed which is more typical of MOMBE growth.

Figure 3 shows the ratio of illuminated to unilluminated growth rates (enhancement ratio) as a function of laser wavelength. At a growth temperature of 320°C the bandgap energy of ZnSe corresponds to a photon energy of ~520 nm.[4] The 780 nm radiation was found to produce no growth rate enhancement, while the higher energy photons produced significant growth rate enhancement. Furthermore, the growth rate enhancement was found to be directly proportional to the laser intensity (see insert of figure 3). When the TEM$_{00}$ mode of the argon ion laser was used, the

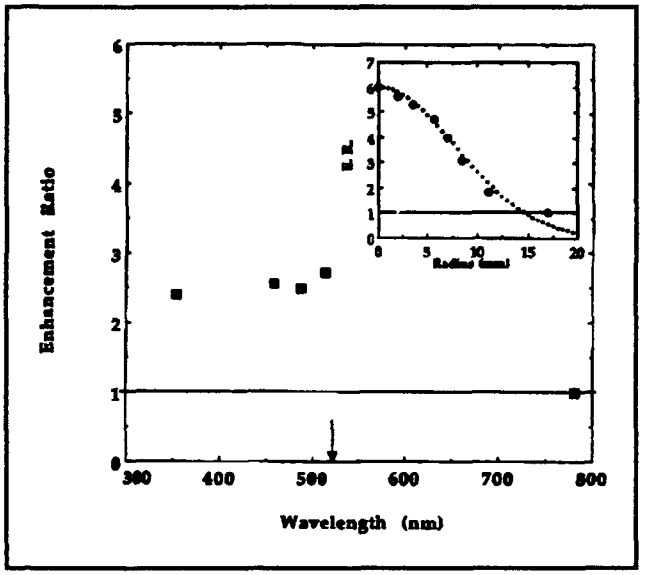


Figure 3. Growth rate enhancement ratio (ER) as a function of laser wavelength. The DESe and DEZn flow rates are both 0.5 sccm, and the substrate temperature is ~320°C (arrow indicates ZnSe bandgap). The insert shows the growth rate enhancement ratio of the illuminated region (457.9 nm laser line) as a function of spot radius (mm). The dotted curve is a Gaussian fit to the data suggesting a direct correlation between growth rate enhancement and power density.

enhancement ratio (solid circles) across the illuminated growth region was found to correlate well with the Gaussian intensity profile of the laser. The largest enhancement in the growth rate has been a factor of 9, although we have not yet attempted to optimize the various growth parameters to maximize the growth rate.

Thus far our data suggest that the creation of electron/hole pairs are required for the growth rate to be enhanced during photo-assisted growth. Photons having energies above the bandgap of ZnSe (at the growth temperature) resulted in growth rate enhancement, while photons with longer wavelengths do not increase the growth rate. Similar dependencies have been observed by Yoshikawa et al[4] for growth of ZnSe by photo-assisted MOVPE. For the metalorganic molecules utilized here, gas phase absorption[5] is expected to occur at wavelengths much shorter (248 nm for DEZn) than investigated here. Although a more

---

[3] H. Ando, A. Taike, R. Kimura, M. Konagai, and K. Takahashi, "Metalorganic Molecular Beam Epitaxial Growth of ZnSe Using Diethylzinc and Diethylselenide," *Japanese J. Appl. Phys.* 25(4): L279-L281 (1986).

[4] A. Yoshikawa, T. Okamoto, T. Fujimoto, K. Onoue, S. Yamaga, and H. Kasai, "Ar-Ion Laser-Assisted MOVPE of ZnSe Using DMZn and DMSe as Reactants," *Japanese J. Appl. Phys.* 29(2): L225-L228 (1990).

[5] H. Hou, Z. Zhang, U. Ray, and M. Vernon, "A Crossed-Laser Beam Study of the Photodissociation Dynamics of $Zn(C_2H_5)_2$ and $(Zn(C_2H_5)_2)_2$ at 248 nm and 193 nm," *J. Chem. Phys.* 92(3): 1728-1746 (1990).

detailed investigation is required, we speculate that a potential mechanism is that a photo-generated carrier (we suspect holes) eliminates an ethyl-metal bond at the surface leading to a higher growth rate. Preliminary data (not shown here) provide evidence that there is a dependence of the growth rate enhancement on the gas flow ratio; this suggests that the growth rate enhancement is not due to liberation of surface alkyls which are blocking lattice sites by photo-generated carriers. The photo-assisted growth experiments currently underway are expected to aid our understanding of the dominant surface chemistry and growth mechanisms. By adjusting conditions such that growth will only occur in regions irradiated by the laser, selective area epitaxy of ZnSe will be possible.

4.4 Publications

Coronado, C.A., E. Ho, L.A. Kolodziejski, and C.A. Huber. "Photo-Assisted Molecular Beam Epitaxy of ZnSe." Submitted to *Appl. Phys. Lett.*

Kolodziejski, L.A. "Chemical Beam Epitaxy of II-VI Semiconductors." Invited paper presented at the American Vacuum Society Meeting, Seattle, Washington, November, 1991.

Chapter 5. Microstructural Evolution in Thin Films of Electronic Materials

Academic and Research Staff

Professor Carl V. Thompson, Dr. Craig Ballentine, Dr. Paul D. Bristowe, Dr. En Ma,[1] Dr. John Melngailis, Dr. Robert C. O'Handley

Visiting Scientists and Research Affiliates

Dr. Sergei Bogomolov,[2] Dr. Harold J. Frost,[3] Hideo Miura,[4] Takauki Uda,[4] Dr. A. Wagner,[5] Derek T. Walton[6]

Graduate Students

Roland Carel, Steven S. Cooperman, Anthony D. Della Ratta, Andrew D. Dubner, Jerrold A. Floro, Heather E. Inglefield, Young-Chang Joo, Harold Kahn, Brett D. Knowlton, Ya-Chin Liu, Hai P. Longworth, Jaesang Ro

Technical and Support Staff

Peter C. Heron

5.1 Electromigration and Microstructure

Electric-current-induced atomic self-diffusion, or electromigration, causes open and short circuit interconnect failures in integrated circuits. Electromigration occurs primarily by diffusion along grain boundaries, and interconnect failure initiates at grain boundaries, so that interconnect reliability is strongly dependent on the grain sizes and orientations in polycrystalline interconnects. The relationships between these microstructural characteristics and interconnect reliability have become more complex as interconnect dimensions (widths and thicknesses) have become comparable to grain sizes. We have studied the effects of microstructure on the reliability of submicron and larger interconnects as well as vias and contacts. We have done this by using a variety of techniques for controlling grain sizes and grain size distributions in thin films. We are also developing models for microstructural evolution in order to develop accurate models for electromigration in submicron interconnects.

5.1.1 Control of Microstructures in Aluminum Films

Sponsor

Joint Services Electronics Program
Contract DAAL03-89-C-0001

Project Staff

Hai P. Longworth, Professor Carl V. Thompson

In previous years, we reported the use of precipitate-induced abnormal grain growth to produce grains as large as 1 mm in 1 μm thick films. In the past year, we completed an extensive study in which we have established the requirements for precipitate-induced abnormal grain growth in thin films and have demonstrated similar

---

[1] Presently at the University of Michigan, Ann Arbor, Michigan.

[2] Ural Polytechnical Institute, Sverdlovsk, Russia.

[3] Dartmouth College, Hanover, New Hampshire.

[4] Hitachi Limited, Tokyo, Japan.

[5] IBM Corporation, Yorktown Heights, New York.

[6] Formerly of Dartmouth College, currently with Digital Equipment Corporation, Hudson, Massachusetts.

phenomena in Al-Cu-Cr, Al-Ag-Cr, Al-Mn-Cr, and Al-W alloys. We have found that to optimize the precipitate-induced abnormal grain growth process, the alloy additions should initially be present as pure layers in the middle of the Al film. In alloys containing Cr, the Cr serves to aid in the nucleation of precipitates, leading to localization of the precipitates in the middle of the film, and leading to a larger number of smaller, more closely spaced precipitates. Through controlled abnormal grain growth, the microstructure of thin films can be controllably varied over broad ranges.

5.1.2 Reliability of Vias

Sponsor

Semiconductor Research Corporation

Project Staff

Harold Kahn, Professor Carl V. Thompson

Over the past year, we have developed a via test structure that allows statistical characterization of via reliability by stressing multiple vias in *parallel*. We have used this process to characterize the reliability of vias with W plugs and have shown that under normal test conditions, joule heating of the plugs contributes to accelerated open failures of Al interconnects. We are developing simple thermal models to evaluate the effect of joule heating at service conditions. We have also demonstrated that the grain size in the Al interconnect greatly affects via reliabilities and also the statistics of failure. Large grains lead to bimodal failure distributions. We are developing tools for statistical analysis of via reliability.

5.1.3 Modeling of Microstructures in Interconnects

Sponsors

Semiconductor Research Corporation
National Science Foundation

Project Staff

Derek T. Walton, Dr. Harold J. Frost, Professor Carl V. Thompson

Over the years, we have developed and tested models for crystal nucleation and growth to form continuous polycrystalline films. We have also modeled grain growth in continuous polycrystalline films. In the past year we have modified these models to investigate the evolution of the microstructures of polycrystalline interconnects to "bamboo" structures, as illustrated in figure 1. We find that the approach to a fully bamboo structure is exponential in time and that the rate of transformation is inversely proportional to the square of the strip width. When the simulation is extended to model grain boundary pinning due to grooving at grain boundary-free surface intersections, we find that there exists a maximum strip width-to-thickness ratio (approximately 3) beyond which the transformation to the bamboo structure does not proceed to completion. In earlier work, we have shown that reliability of nearly-bamboo and fully-bamboo lines is greatly different. Our modeling work is now allowing us to identify the conditions under which it is reasonable to expect to obtain only fully-bamboo lines.

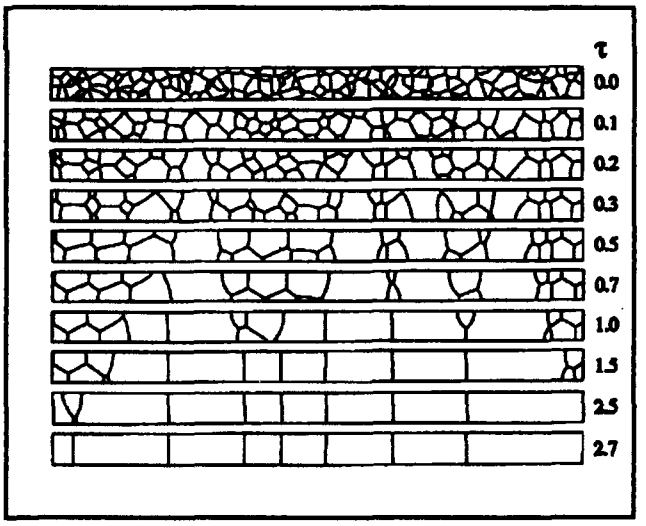


Figure 1. Evolution of the grain structure within a strip. The transformation to a "bamboo" structure is dominated by the growth of bamboo sections into regions of grain clusters. The rate of this transformation depends strongly on the strip width.

5.1.4 Electromigration in Bicrystals

Sponsors

Joint Services Electronics Program
Contract DAAL03-89-C-0001
Semiconductor Research Corporation

Project Staff

Hai P. Longworth, Young-Chang Joo, Brett D. Knowlton, Professor Carl V. Thompson

In previous work we have shown that individual grain boundaries greatly affect the reliability of an interconnect line. In order to understand the reliability of interconnects, it is therefore important to understand the reliability of individual grain boundaries. To do this we have developed a new technique that allows us to characterize the reliability of populations of lines with single, identical grain boundaries with controlled types, locations, and orientations. The technique is schematically shown in figure 2. We start by making NaCl bicrystals of the desired type, on which we grow epitaxial bicrystal Al films which are transferred and sintered to oxidized silicon wafers. We then use conventional lithographic techniques to pattern multiline test structures with the same controlled Al grain boundary running through all the lines. We can then investigate, as an example, the effect of the boundary orientation on the reliability of the line, as illustrated in figure 3.

We have shown that (1) failure times of lines containing single identical boundaries are lognormally distributed, (2) the medium time to failure depends more strongly on the boundary orientations than the types of grain boundaries, (3) the deviation in the time to failure has a large component not dependent on microstructure, and (4) both interfacial diffusion and grain boundary diffusion appear to contribute to failure in bicrystal lines and probably in bamboo and near-bamboo lines as well.

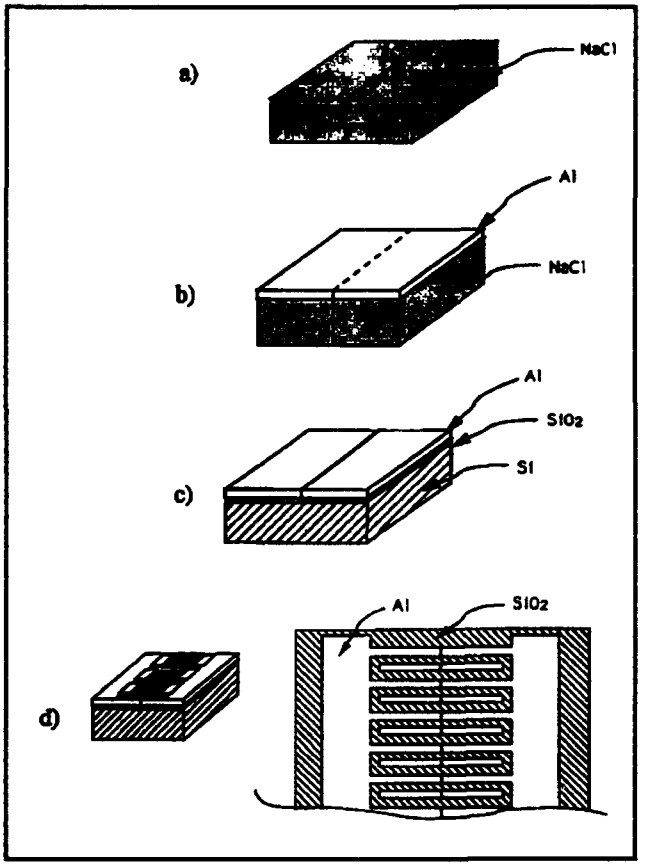


Figure 2. The fabrication process of bicrystal test patterns. (a) NaCl bicrystal substrate made from two NaCl single crystals; (b) Al bicrystal thin film epitaxially deposited on the NaCl substrate; (c) Al film transferred to an oxidized Si wafer; and (d) patterning.

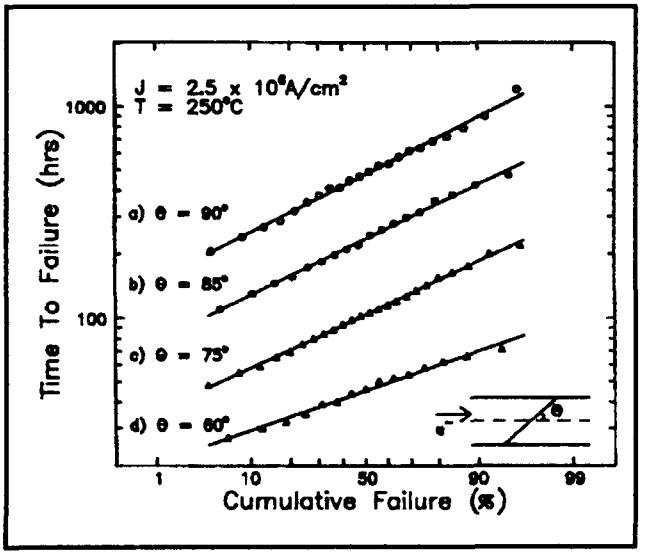


Figure 3. Failure distributions of Σ13[100] bicrystal lines as a function of θ, the angle between the current direction and the grain boundary plane.

5.2 Microstructural Evolution in Polycrystalline Films

Polycrystalline thin films are used in a wide variety of applications, especially in electronics. In these applications the properties and performance of polycrystalline films depend strongly on the average grain size, the distribution of grain sizes, and the distribution of grain orientations. These are controlled by the deposition conditions and the conditions for post-deposition processing. In the past, we have carried out modeling and experiments on the effects of crystal nucleation and growth and grain growth on the microstructure of thin films. This has included work on semiconductors as well as metals, and has explored the effects of dopants, ion bombardment, and rapid thermal annealing, as well as other processing conditions. Our current activity is focused on modeling of grain growth in continuous and patterned films and experiments on epitaxial grain growth.

5.2.1 Modeling of Grain Growth in Thin Films

Sponsor

National Science Foundation

Project Staff

Jerrold A. Floro, Derek T. Walton, Roland Carel, Dr. Harold J. Frost, Professor Carl V. Thompson

We have developed a mean field model for grain growth in thin films which accounts for the effects of the energies of the free surfaces and the film/substrate interfaces of the films. Anistropies of these energies affect the evolution of the distribution of grain orientations, as well as grain sizes. With our analysis we can predict the differences in the rate of grain growth and film texture evolution that result from different specific interface or surface energy versus orientation relationships. These predictions are being compared with experimental results.

In collaboration with Dr. H.J. Frost of Dartmouth College, we have also developed computer simulations of grain growth in thin films. We have included in our simulations the effects of grain boundary drag due to surface grooving. This leads to stagnation of normal grain growth at a point where the grain sizes are lognormally distributed and the average grain diameter is about three times the film thickness. This simulation result closely matches experimental results in a wide variety of systems. We can also include the effects of surface and interface energy anisotropy and determine the conditions which lead to surface-energy-driven abnormal or secondary grain growth. These simulations allow investigation of the effect of the surface and interface energy anisotropy on the evolution of texture in thin films. Our mean field models allow us to model and predict the behavior of large populations of grains, while our computer simulations allow us to investigate the behavior of smaller populations of grains as well as specific grain configurations. We have also recently modified our computer simulations to model grain growth in patterned films, as described in Section 5.1.3.

5.2.2 Epitaxial Grain Growth

Sponsor

National Science Foundation

Project Staff

Jerrold A. Floro, Roland Carel, Dr. Paul D. Bristowe, Professor Carl V. Thompson

When polycrystalline films on single crystal substrates undergo grain growth, interface-energy-anisotropy leads to the preferred growth of epitaxially oriented grains. We have demonstrated this phenomenon in metallic films deposited on single crystals of NaCl, mica, and MgO. We have also demonstrated epitaxial grain growth in polycrystalline Ag films on single crystals of Ni. We have chosen to study the latter experimental system because calculations of the structure and energies of Ag/Ni interfaces for a number of different Ag/Ni relative crystallographic orientations exist. These calculations have been shown to be consistent with results from rotating sphere experiments in which very small single crystal Ag spheres rotate into low energy orientations when annealed on single crystal Ni substrates. As-deposited epitaxial films of Ag on Ni are also readily attainable. We have found that the epitaxial orientations obtained are different in each of these three types of experiments (as-deposited epitaxy, rotating spheres, and epitaxial grain growth). These results suggest that the orientation obtained by conventional epitaxy may be metastable once a film is continuous. In exploring this issue, we are using embedded atom calculations to calculate interface and surface energies and using the results from these calculations in our grain growth models and simulations.

5.3 Magnetic Properties of Heteroepitaxial Thin Films

Sponsors

National Science Foundation
U.S. Army Research Office

Project Staff

Heather E. Inglefield, Dr. Sergei Bogomolov, Dr. Craig Ballentine, Dr. Robert C. O'Handley, Professor Carl V. Thompson

In this new program we are investigating the effect of strain and misfit dislocations on the magnetic properties of very thin ($\lesssim$10 nm) heteroepitaxial metallic films. In particular, we are studying Ni films deposited on Ni-Cu alloy films. In this and related systems, when overlayers are very thin, they will grow pseudomorphically, adopting the lattice parameter of the substrate. However, as the overlayer thickens, the strain energy will become sufficient to drive deformation and the formation of misfit dislocations. Grids of perpendicular arrays of misfit dislocations often result. These structural changes are expected to have profound effects on the magnetic properties of the films. We are preparing to use measurements of the magneto-optic Kerr effect (MOKE) and low energy electron spin polarization analysis (LEESPA) to analyze changes in magnetic properties *during* film deposition. We will correlate changes in magnetic properties with changes in structure as determined using *in situ* reflection high energy electron diffraction (RHEED), as well as *ex situ* x-ray diffraction analysis and transmission electron microscopy.

In addition to using *in situ* magnetic characterization of films to probe and monitor structural changes, we will also investigate the effects of misfit dislocations on the large-scale and small-scale magnetic properties of films. As part of this analysis we will use scanning electron microscopy and polarization analysis (SEMPA) to image magnetic domains with a spatial resolution smaller than the dimensions of the misfit dislocation grid.

5.4 Interface Reactions in Multilayer Thin Films

Sponsors

Hitachi Limited
IBM Corporation

Project Staff

Dr. En Ma, Hideo Miura, Takauki Uda, Professor Carl V. Thompson

When two materials are brought into contact and heated, interdiffusion will lead to compound formation. This phenomena is important throughout technology, but is especially important in electronics in understanding unwanted reactions between films and substrates, as well as desired reactions that form silicides and diffusion barriers. Despite the importance of interface reactions, the initial processes that control which compound phase will form during a reaction (phase selection) is not well understood. We have investigated phase selection during interface reactions by using multilayer films in which we have alternately deposited pure layers with layer thicknesses as low as a few nanometers. By using multilayer films, we can focus on the earliest stages of interface reactions because these early reactions consume all or most of the volume of the overall films. This allows the use of tools such as transmission electron microscopy, x-ray analysis, and differential scanning calorimetry (DSC) to study formation of compound layers that are only a few nanometers thick. DSC is especially useful in studying the kinetics as well as the thermodynamics of these processes. We have used these techniques to study reactions in Ni/Si, Ti/Si, V/Si, Co/Si, and Ni/Al multilayer films. We have shown that interdiffusion always precedes nucleation of a compound and have argued that interdiffusion is in fact a necessary precursor to compound formation. Phase selection is therefore constrained by the rates of self-diffusion and interdiffusion. This insight has allowed us to explain our frequent observations that the initial phase to form is often metastable. We are also now able to make predictions about phase selection sequences in interface reactions.

5.5 Focused Ion Beam Induced Chemical Vapor Deposition

Sponsor

U.S. Army Research Office

Project Staff

Anthony D. Della Ratta, Jaesang Ro, Andrew D. Dubner, Dr. A. Wagner, Dr. John Melngailis, Professor Carl V. Thompson

A focused ion beam (FIB) can be used to cause local deposition of a film to write lines for x-ray mask repair or circuit restructuring. Ions are accelerated to the substrate where each ion can cause tens of decomposition events in a chemical vapor

deposition process. We have carried out experiments focused on understanding the energy transfer mechanism which leads to FIB-induced chemical vapor deposition. The process is substrate mediated and scales with the ion energy and ion mass in such a way as to strongly suggest that decomposition is caused by collisions between knock-on substrate atoms and adsorbed monolayers of unreacted molecules. It also appears that removal of the reactant product can be rate limiting. It is found that film purities are improved when films are deposited at lower rates or higher temperatures. These insights will help in the development of processes for deposition of high purity lines with controlled widths and aspect ratios.

5.6 Publications

Dubner, A.D., A. Wagner, J. Melngailis, and C.V. Thompson. "The Role of the Ion/Solid Interaction in Ion Beam Induced Deposition of Gold." *J. Appl. Phys.* 70: 665 (1991).

Evans, P.V., D.A. Smith, and C.V. Thompson. "Absence of Electrical Activity at High Angle Grain Boundaries in Zone-Melt-Recrystallised Silicon-on-Insulator Films." *Appl. Phys. Lett.* 60: 439 (1992).

Floro, J.A., and C.V. Thompson. "Epitaxial Grain Growth and Orientation Metastability in Heteroepitaxial Thin Films." *Materials Research Society Symposium Proceedings* 187: 274 (1991).

Frost, H.J., C.V. Thompson, and D.T. Walton. "Simulation of Thin Film Grain Structures: II. Abnormal Grain Growth." *Acta Metall. Mat.* Forthcoming.

Frost, H.J., C.V. Thompson, and D.T. Walton. "Abnormal Grain Growth in Thin Films Due to Anisotropy of Free-Surface Energies." Proceedings of the First International Conference on Grain Growth in Polycrystalline Materials, Rome, 1991. Forthcoming.

Jiran, E., and C.V. Thompson. "Capillary Instabilities in Thin Continuous Films." *Thin Solid Films.* Forthcoming.

Kahn, H., and C.V. Thompson. "A Statistical Characterization of Electromigration-Induced Open Failures in 2-Level Metal Structures." *Materials Research Society Symposium Proceedings* 225: 15 (1991).

Kahn, H., and C.V. Thompson. "The Effect of Applied Mechanical Stress on the Electromigration Failure Times of Aluminum Interconnects." *Appl. Phys. Lett.* 56: 1308 (1991).

Longworth, H.P., and C.V. Thompson. "Abnormal Grain Growth in Aluminum Alloy Thin Films." *J. Appl. Phys.* 69: 3929 (1991).

Longworth, H.P., and C.V. Thompson. "An Experimental Study of Electromigration in Bicrystal Al Lines." *Appl. Phys. Lett.* Forthcoming.

Ma, E., and C.V. Thompson. "Nucleation and Growth During Reactions in Multilayer Al/Ni Films: The Early Stages of Al_3Ni Formation." *J. Appl. Phys.* 69: 2211 (1991).

Ma, E., L.A. Clevenger, C.V. Thompson, and K.N. Tu. "Kinetic and Thermodynamic Aspects of Phase Evolution." *Materials Research Society Symposium Proceedings* 187: 83 (1991).

Ma, E., C.V. Thompson, and L.A. Clevenger. "A Calorimetric Study of the Kinetics of Al_3Ni Nucleation and Growth During Reactions in Al/Ni Thin Films." *Materials Research Society Symposium Proceedings* 157: 455 (1991).

Miura, H., E. Ma, and C.V. Thompson. "Initial Sequence and Kinetics of Silicide Formation in the Cobalt/Amorphous-Silicon Multilayer Thin Films." *J. Appl. Phys.* 70: 4287 (1991).

Thompson, C.V., J.Y. Tsao, and D.J. Srolovitz, editors. "Evolution of Thin Film and Surface Microstructure." *Materials Research Society Symposium Proceedings* 202 (1991).

Thompson, C.V. "On the Role of Diffusion in Phase Selection During Reactions at Interfaces." *J. Mater. Res.* 7: 367 (1992).

Thompson, C.V., L.A. Clevenger, R. DeAvillez, E. Ma, and H. Miura. "Kinetics and Thermodynamics of Amorphous Silicide Formation in Metal/Amorphous Multilayer Thin Films." (Invited Paper) *Materials Research Society Symposium Proceedings* 187: 61 (1991).

Thompson, C.V. "Experimental and Theoretical Aspects of Grain Growth in Thin Films." (Invited Paper) Proceedings of the First International Conference on Grain Growth in Polycrystalline Materials, Rome, 1991. Forthcoming.

Walton, D.T., H.J. Frost, and C.V. Thompson. "The Development of Bamboo and Near-Bamboo Microstructures in Thin Film Strips." *Appl. Phys. Lett.* Forthcoming.

Walton, D.T., H.J. Frost, and C.V. Thompson. "Computer Simulation of Grain Growth in Thin-Film Interconnect Lines." *Materials Research Society Symposium Proceedings* 225: 219 (1991).

Walton, D.T., H.J. Frost, and C.V. Thompson. "Modeling of Grain Growth in Thin Film Strips." Proceedings of the First International Conference on Grain Growth in Polycrystalline Materials, Rome, 1991. Forthcoming.

5.7 Theses

Cooperman, S. *Electromigration in Submicron-Wide Interconnects.* S.M thesis. Dept. of Mater. Sci. and Eng., MIT, 1992.

Liu, Y. *Coplanar-Spherical-Particle Coarsening in Discontinuous Ultrathin Polycrystalline Gold Films on Amorphous Silicon-Nitride Substrates.* Ph.D. diss. Dept. of Mater. Sci. and Eng., MIT, 1991.

Longworth, H. *Electromigration in Aluminum and Aluminum Alloy Thin Films with Controlled Microstructures.* Ph.D. diss. Dept. of Mater. Sci. and Eng., MIT, 1992.

Ro, J. *Microstructural Evolution During Focused Ion Beam Induced Deposition.* Ph.D. diss. Co-supervised with Dr. J. Melngailis. Dept. of Mater. Sci. and Eng., MIT, 1991.



From left: Senior Research Scientist Dr. John Melngailis with Research Engineer Sergey Etchin of MIT's Microsystems Technology Laboratories, and Research Assistants Christian R. Musil and Henri J. Lezec

Chapter 6. Focused Ion Beam Microfabrication

Academic and Research Staff

Dr. John Melngailis, Professor Dimitri A. Antoniadis, Professor Carl V. Thompson, Dr. Xin Xu, Sergey Etchin, Mark I. Shepard

Visiting Scientists and Research Affiliates

Dr. Dominique Vignaud, Akira Shimase, Jane Sosonkina

Graduate Students

Tony P. Chiang, William Chu, Anthony D. Della Ratta, Henri J. Lezec, Kenneth S. Liao, Christian R. Musil, Jaesang Ro

Technical and Support Staff

Donna R. Martinez

6.1 Introduction

The focused ion beam research program at MIT can be divided into two areas. The first, served by a 150 kV system, is the high energy regime and includes implantation and lithography. The second is the lower energy regime and is aimed at developing repair processes for masks and integrated circuits.

The high energy system includes automated patterning capability over wafers up to six inches in diameter. Alignment of the focused ion beam writing to within $\pm 0.1 \mu m$ of existing features on a wafer has been demonstrated. Software has been developed which permits patterns to be transferred from the layout system used in the Microsystems Technologies Laboratory to the focused ion beam machine. Accordingly, this permits flexible, mixed fabrication where standard steps have been carried out in the integrated circuits laboratory at MIT, and special implantation or lithography steps have been carried out on the focused ion beam system. Similar mixed fabrication has also been carried out on Si wafers partly fabricated at Ford Aerospace and on GaAs wafers fabricated at Raytheon Research Laboratory. The ion species available for implantation include the principal dopants of GaAs and of Si. The minimum beam diameter available is on the order of 0.1 μm at an ion current of 20 pA. In many of the implantation projects where the minimum diameter is not needed, a higher beam current can be used.

In the lower energy regime our work has mainly focused on the development of ion induced deposition. This technique uses a local ambient of a precursor gas, usually organometallic or metal halide, to permit deposition to be carried out with minimum linewidth of 0.1 μm. The local patterned deposition complements material removal by ion milling and is used to add missing absorber material in the repair of photomasks and x-ray lithography masks or to rewire local connections in integrated circuits. Our efforts have focused on gold and platinum deposition, on understanding the fundamentals of the process, and on deposition at non-normal incidence. Mainly Ga^+ ions in the range of 10-50 kV are used.

Our work in this area will be greatly enhanced by the recent donation of an FEI 500D focused ion beam system to MIT. This system is more convenient and flexible and compliments our existing, largely home-built machine. The FEI machine delivers Ga^+ ions at energies of 5 to 25 kV and beam diameters down to 0.05 μm.

6.2 Tunable Gunn Diodes—High Frequency Performance and Applications

Sponsor

Defense Advanced Research Projects Agency/
U.S. Army Research Office
Contract DAAL03-88-K-0108

Project Staff

Henri J. Lezec, Christian R. Musil, Leonard J. Mahoney,[1] Dr. Alex Chu,[2] Larry Chu,[3] Professor Dimitri A. Antoniadis, Dr. John Melngailis

Gunn diodes have been fabricated by focused-ion-beam implanting Si in the GaAs surface area between two contacts. This planar fabrication is easily incorporated into GaAs microwave integrated circuits. To achieve tunability the focused ion beam is programmed to implant a gradient of doping in the direction of current flow. This means that the frequency of oscillation of the Gunn diode depends on the bias resulting, in effect, in a voltage controlled oscillator (VCO). The maximum frequency of oscillation observed so far is 42 GHz with a tuning range of 20 GHz. The performance of two of these devices is shown in figure 1. These VCOs are expected to have numerous applications in high performance GaAs monolithic microwave integrated circuits (MMICs). The most immediate application is a built-in test where a swept frequency Gunn diode is coupled to the input, and a planar diode detector is coupled to the output of the device under test. This permits the RF performance to be tested by means of D.C. probes.

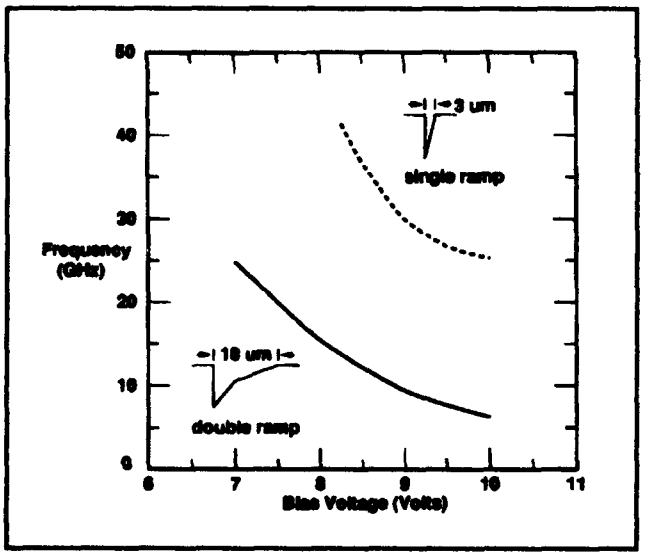


Figure 1. Measured frequency versus bias voltage for two Gunn diodes. The inserts show schematically the doping profiles, which are generated by ramping the implanted dose of Si ions from 0.5 to 1.5×10^{13} ions/cm^2.

6.3 Simulation of Tunable Gunn Diodes and MESFETs with Doping Gradients

Sponsor

Defense Advanced Research Projects Agency/
U.S. Army Research Office
Contract DAAL03-88-K-0108

Project Staff

Christian R. Musil, Henri J. Lezec, Professor Dimitri A. Antoniadis, Dr. John Melngailis

The tunable Gunn diodes and MESFETs we have fabricated with focused ion beam gradients have complex carrier dynamics. The properties of these devices have been simulated on the Cray computer using a non-stationary hydrodynamic solution of the Boltzmann transport equation. In the MESFETs this permits visualization of the effects of doping gradients and the formation of stationary Gunn domains. In the case of the tunable Gunn diodes the bias-dependent domain propagation length, which in effect produces the tunability, is simulated. As shown in figure 2, a non-equilibrium carrier concentration is associated with the propagating Gunn domain. Each domain travels up the implanted carrier concentration gradient until a new domain is nucleated at the low carrier concentration end.

6.4 Limited Lateral Straggle of Focused-Ion-Beam Implants

Sponsor

Defense Advanced Research Projects Agency/
U.S. Army Research Office
Contract DAAL03-88-K-0108

Project Staff

Dr. Dominique Vignaud, Kenneth S. Liao, Christian R. Musil, Akira Shimase, Professor James Chung, Sergey Etchin, Professor Dimitri A. Antoniadis, Dr. John Melngailis

The minimum lateral dimensions of focused ion beam implanted doping profiles is ultimately

[1] MIT Lincoln Laboratories.

[2] Mitre Corporation, Bedford, Massachusetts.

[3] M/A Com Corporation, Burlington, Massachusetts.

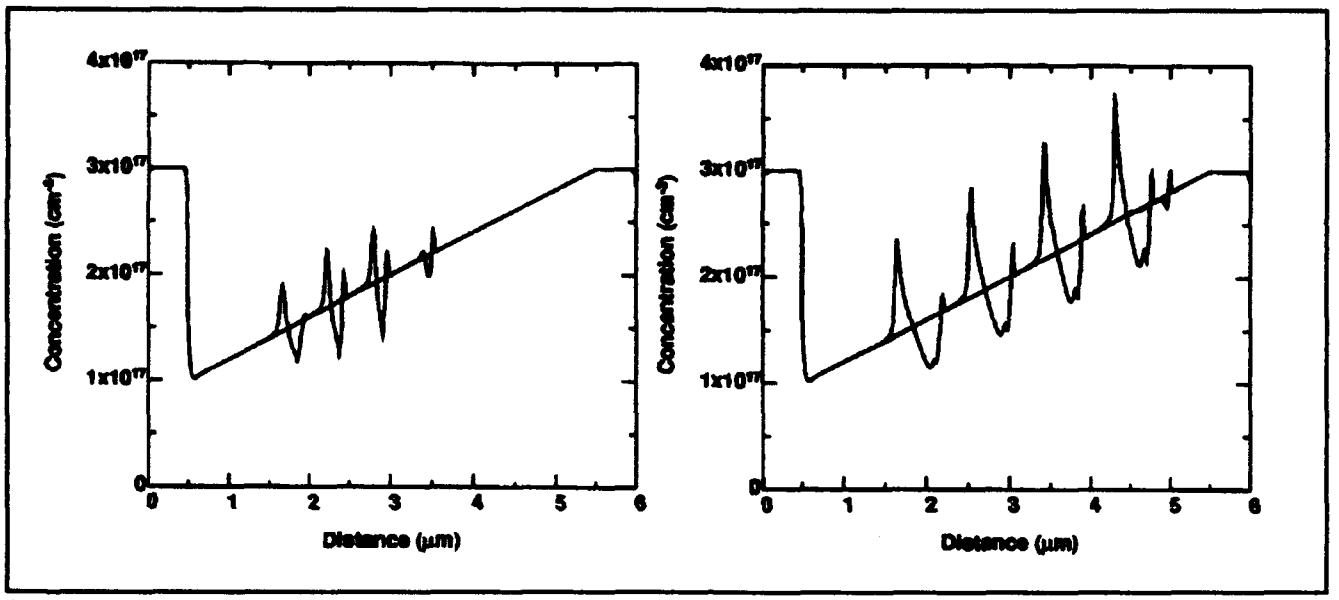


Figure 2. Simulated electron concentration profiles versus lateral position at successive time intervals during domain propagation. Left: bias = 2 V, frequency = 40 GHz, Δt = 6 psec. Right: bias = 6 V, frequency = 25 GHz, Δt = 12 psec.

limited by the lateral straggle of the ions as they penetrate into the crystal lattice. This is particularly true for light ions. One way to minimize the lateral straggle is to exploit channeling by implanting along a crystal axis. To verify this we have implanted Be in GaAs and B in Si both on-axis and off-axis. The focused ion beam was used to implant gratings of various periods. The extent of overlap between the grating lines was measured electrically. In GaAs two types of experiments were carried out. In the first a grating was implanted with lines parallel to the direction of current flow in an n-type mesa structure situated between two contacts. Since the implant was not annealed, insulating stripes were produced. As the period of the grating decreased the conduction was cut off. The results for 230 keV Be ions show that the lines begin to overlap at a period of 0.3 to 0.4 μm, but there is still a modulation of the conductivity down to below 0.1 μm for on-axis implants. In the second experiment, gratings were implanted in semiinsulating GaAs between two p-type contacts with the grating lines perpendicular to the current flow. These implants were rapid-thermal-annealed, and the conductivity sharply increased as the period decreased and the lines began to touch. Various doses were used between 3×10^{12} and 1×10^{14} ions/cm^2, and a clear difference was observed between on-axis and off-axis implants. The standard deviation of the lateral spread of the carriers was deduced from a one-dimensional model. The minimum half-width of an implanted line was found to be 140 nm in on-axis material. In off-axis material the width was 50 to 90 nm larger depending on dose. In all cases the width is smaller than the 450 nm straggle predicted by Monte-Carlo simulations in amorphous material. Similar structures have also been made by implants in Si, but results are not yet available.

6.5 Focused Ion Beam Implantation of GaAs MMICs and Transistor Optimization

Sponsor

National Science Foundation
Grant ECS 89-21728

Project Staff

Sergey Etchin, Dr. John Melngailis in collaboration with Dr. Thomas Kazior[4]

Some GaAs monolithic microwave integrated circuits (MMICs) require as many as five implantation steps in order to produce highly optimized transistors for various functions. Yet the area implanted in each step is small. The focused ion beam provides a potentially cost effective means of carrying out all five implants in a single fabrication step, thereby eliminating a large number of con-

[4] Raytheon Corporation, Lexington, Massachusetts.

ventional steps: resist spinning, lithography, development, blanket implantation, and resist stripping, each repeated five times. Device patterns have been transferred from Raytheon to MIT and aligned local implants of MMICs have been carried out to verify that the performance of the focused ion beam implanted devices is equivalent to the the conventionally fabricated devices.

In addition, the capability of the focused ion beam to implant devices side by side each with a different dose or at a different ion energy has been used to optimize the performance of buried p-layer, n-channel MESFETs. In one experiment, for example, devices were implanted with Be ions at energies of 70, 90, and 110 keV and doses from 4×10^{11} to 1.5×10^{12} in order to find the optimum set of parameters. In another experiment, the Si-channel implant was also carried out with the focused ion beam, and the dose was varied from device to device. These successful experiments demonstrate the utility of the focused ion beam for device optimization. Similar optimization by conventional broad beam implantation would require many more wafers and would introduce complications due to wafer-to-wafer variations.

6.6 Ion Induced Deposition of Gold, Models and Microstructure

Sponsor

U.S. Army Research Office
Contract DAAL03-87-K-0126
U.S. Navy - Naval Research Laboratory/Micrion
Agreement M08774

Project Staff

Jaesang Ro, Professor Carl V. Thompson, Dr. John Melngailis

When a local gas ambient of, for example, an organometallic gas is created on a substrate, incident energetic ions can cause the adsorbed gas molecules to dissociate, creating a metallic deposit. With a focused ion beam, this technique can be used to write patterns of minimum dimensions down to 0.1 μm. The technique is being used commercially for the local repair of integrated circuits. First, the ion beam is used to mill vias through the passivation, and then gas is introduced locally with a capillary gas feed and a metal "jumper" is connected between the vias. Deposition of metals, particularly high Z metals such as Au and W, is also being developed for the repair of x-ray lithography masks.

We have studied the microstructure of the gold film and the correlation between its microstructure and deposition conditions. Some carbon is always incorporated into the gold films. Three types of microstructures have been identified: (1) granules of gold in a carbon background produced at high ion current densities at room temperature, (2) columns of gold in a carbon background produced at lower current densities or at higher current densities on substrates at 100° C, and (3) polycrystaline gold with minimal carbon content produced at lower current densities in substrates at 100° C. For x-ray mask repair the granular or columnar structures are not desirable.

The deposition yield was also measured for all of the noble gas ions at energies of 50 and 100 keV. The deposition yield varied from 3 to 29 and was highest for the highest mass ion, Xe. A model of the process based on the Monte Carlo calculation of collision cascades fits the data. The collision cascades that terminate on the surface transfer energy to the adsorbed monolayer of organometallic gas molecules and cause dissociation.

6.7 Focused Ion Beam Lithography for X-Ray Mask Making

Sponsor

SEMATECH

Project Staff

Tony P. Chiang, Sergey Etchin, W. Chu, Professor Henry I. Smith, Dr. John Melngailis, in collaboration with Mark A. Hartney[6] and D.C. Shaver[6]

One of the main challenges in the application of x-ray lithography is the making of the mask. The absorber material on the thin mask membrane must be fabricated of high Z material (e.g., Au or W) with high aspect ratio, (e.g., 0.25 to 0.5 μm thick at minimum dimensions down to 0.1 μm). Two techniques for writing the original pattern of the mask in resist are electron beam lithography and focused ion beam lithography. While electron beams have been extensively developed and applied, ion beams have been used to write patterns down to 0.015 μm minimum linewidth and show no proximity effects even for resists over

[6] MIT Lincoln Laboratory.

high Z material. The resist exposure times for the two techniques are comparable. Previously we have fabricated x-ray masks at MIT with minimum linewidth of 0.05 μm. The goal of this program is to fabricate x-ray masks for use at the Center for X-Ray Lithography at the University of Wisconsin. Masks will be made initially by exposing PMMA and plating up the gold absorber. An alternate process which may be preferable for the making of x-ray masks with a tungsten absorber is focused ion beam exposure followed by resist silylation. We have demonstrated this silylation process in collaboration with Lincoln Laboratory and have achieved minimum dimensions of 0.08 μm in 1 μm thick resist. The writing in this process is as fast as the fastest e-beam. In addition, the resist used is compatible with reactive ion etching. Thus, we will pursue making x-ray masks using reactive ion etching to define the high aspect ratio patterns in tungsten.

6.8 Focused Ion Beams for the Repair of X-Ray Masks

Sponsor

U.S. Navy - Naval Research Laboratory/Micrion Agreement M08774

Project Staff

Dr. Xin Xu, Anthony D. Della Ratta, Jane Sosonkina, Dr. John Melngailis

X-ray lithography is being developed for the fabrication of integrated circuits with minimum dimensions of 0.25 mm and below. The masks needed for this lithography will have over 10^9 features. Thus it is unlikely that they will be fabricated free of defects. The focused ion beam is the logical tool for the local repair of mask defects and is being developed for this purpose. Local ion milling can be used to remove unwanted absorber and ion induced deposition can be used to add missing absorber. The challenge is that these structures must be refabricated with high aspect ratios often in the proximity of existing high aspect ratio structures. Thus, ion milling and ion induced depositions at non-normal incidence is unavoidable. We have measured the ion induced deposition of gold as a function of the angle of incidence. The precursor gas used was dimethyl-gold hexafluoro-acetylacetonate. The deposition yield was found to rise rapidly as the angle of incidence approaches a grazing angle. In addition, at angles above about 50° (0° is normal, 90° is grazing) the deposited structure takes on a ripply, irregular aspect which develops into an almost periodic array of protrusions at grazing incidence. We are also measuring the milling yield as function of the angle of incidence. Both of these aspects of the repair process need to be taken into account if high aspect ratio mask structures are to be accurately refabricated.

6.9 Publications

Chu, A., L. Chi, W. Macropoulos, K. Khair, R. Patel, M. Cordaro, H.J. Lezec, J. Melngailis, and L.J. Mahoney. "Performance and Applications of Novel Oscillators Utilizing Focused Ion Beam Implanted Gunn-Effect Devices." Paper presented at the 1991 IEEE MTT-S International Microwave Symposium, Boston, June 11-14, 1991. Published in *IEEE MTT-S Digest* 1179 (1991).

Dubner, A.D., A. Wagner, J. Melngailis, and C.V. Thompson. "The Role of the Ion/Solid Interaction in Ion Beam Induced Deposition of Gold." *J. Appl. Phys.* 70: 665 (1991).

Ehrlich, D.J., and J. Melngailis. "Fast Room-Temperature Growth of SiO2 Films by Molecular-Layer Dosing." *Appl. Phys. Lett.* 58: 2675-2677 (1991).

Hartney, M.A., D.C. Shaver, M.I. Shepard, J. Melngailis, V. Medvedev, and W.P. Robinson. "Surface Imaging of Focused Ion Beam Exposed Resists." Presented at the 35th International Symposium on Electron, Ion and Photon Beams, Seattle May 28-June 1, 1991; *J. Vac. Sci. Technol. B* 9: 3432 (1991).

Hartney, M.A., D.C. Shaver, M.I. Shepard, J.S. Huh, and J. Melngailis. "Silylation of Focused Ion Beam Exposed Resists." *Appl. Phys. Lett.* 59: 485-487 (1991).

Huh, J.S., M.I. Shepard, and J. Melngailis. "Focused Ion Beam Lithography." *J. Vac. Sci. Technol. B* 9: 173 (1991).

Kunz, R., D.J. Ehrlich, J. Melngailis, and M.W. Horn. "Selective Area Growth of Metal Oxide Films Induced by Patterned Excimer Laser Surface Photolysis." Presented MRS Meeting, Boston, December 1991. MRS Symposium Proceedings. Forthcoming.

Lattes, A.L., S.C. Munroe, M.M. Seaver, J.E Murguia, and J. Melngailis. "Improved Drift in Two-Phase, Long-Channel, Shallow-Buried-Channel CCDs with Longitudinally Nonuniform Storage-Gate Implants." Submitted to *IEEE Trans. Electron Devices.*

Lezec, H.J., C.R. Musil, J. Melngailis, L.J. Mahoney, and J. Woodhouse. "Dose-Rate Effects in Focused-Ion-Beam Implantation of Si into GaAs." Presented at the US/Japan Technology Seminar on FIB, Portland, Oregon. *J. Vac. Sci. Technol. B* 9: 2709 (1991).

Melngailis, J. "Focused Ion Beam Induced Deposition - A Review." *SPIE Proc.* 1465 (1991).

Melngailis, J. "Ion Lithography and Focused Ion Beam Implantation." In *Handbook of VLSI Lithography.* Eds. W.B. Glendinning and J.N. Helbert. Noyes Publications, 1991.

Melngailis, J., P.G. Blauner, A.D. Dubner, J.S. Ro, T. Tao, and C.V. Thompson. "Focused Ion Beam Induced Deposition." *Proceedings of the Second International Symposium on Process Physics and Modeling in Semiconductors* 91-4: 653 (ECS 1991).

Murguia, J.E., M.I. Shepard, J. Melngailis, A.L. Lattes, and S.C. Munroe. "Increase in Silicon CCD Speed with Focused Ion Beam Implanted Channels." Presented at the US/Japan Technology Seminar on FIB, Portland, Oregon. *J. Vac. Sci. Technol. B* 9: 2714 (1991).

Tao, T., W. Wilkinson, and J. Melngailis. "Focused Ion Beam Induced Deposition of Platinum for Repair Processes." *J. Vac. Sci. Technol. B* 9: 162 (1991).

Theses

Murguia, J.E. *The Application of Focused Ion Beam Implantation to the Design and Fabrication of MOS Devices.* Ph.D. diss. Dept. of Electr. Eng. and Comput. Sci., MIT, 1991.

Ro, J.S. *Microstructure and Mechanism of Gold Films Grown by Ion Induced Deposition.* Ph.D. diss. Dept. of Mater. Sci. and Eng., MIT, 1991.

Section 2 Quantum-Effect Devices

Chapter 1 Statistical Mechanics of Quantum Dots

Chapter 2 Single Electron Transistors

Chapter 3 Transport Through a Quantum Dot

Chapter 4 Submicron and Nanometer Structures Technology and Research

Chapter 1. Statistical Mechanics of Quantum Dots

Academic and Research Staff

Professor Boris L. Altshuler, Dr. Richard Berkovits, Dr. Aaron Szafer

Graduate Students

Michael Faas

Technical and Support Staff

Imadiel Ariel

1.1 Project Description

Sponsor

Joint Services Electronics Program
Contract DAAL03-92-C-0001

We are investigating equilibrium properties of quantum dots (isolated metallic systems with sizes smaller than the typical length of an electron dephasing). Until recently, we concentrated on such properties of an individual dot as capacitance and electric and magnetic susceptibility. The most dramatic manifestation of the quantum nature of the magnetic polarizability takes place for a multiply connected geometry, e.g., for a ring, and is known as a persistent current. This current is a metallic system response to the magnetic flux through the hole. It can exist even when there is no field in the material, and it does not dissipate.

Due to the impurity or surface scattering of the conductivity electrons, there is certain dispersion of the properties in the ensemble of macroscopically equivalent samples. Therefore, we must consider the sample to sample (mesoscopic) fluctuations as well as ensemble averaged properties such as persistent current.

Earlier[1] we developed a theory on the persistent current neglecting the interaction between the electrons. This problem involves two energy scales: (1) the mean energy spacing between the exact one electron states in a random potential Δ, and (2) the inverse typical time of an electron diffusion around the sample $h/t = E_c$, also known as the Thouless shift. The dimensionless ratio E_c/Δ is the sample conductance in natural units e^2/h. We found that the mean root square of the mesoscopic fluctuations of the persistent current is of the order of $E_c e/h$, while the averaged persistent current, although nonzero, is much smaller and determined by Δ.

The persistent current was recently observed[2] and found to be orders of magnitude larger than the theoretical predictions *in the absence of the interaction between electrons.* Also, superconductive-like fluctuations cannot explain why the effect is so large. On the other hand, the magnitude of the observed persistent current is more or less consistent with the charging energy e^2/R, where R is the radius of a ring. This was one of the motivations for us to study dielectric properties of mesoscopic systems.

We have developed a technique to investigate the local charge fluctuations and local electric fields within a mesoscopic system. We have found that, due to quantum interference, there are long range correlations in these local fluctuations (similar to the well-known Friedel oscillations). These correlations determine the additional energy caused by the Coulomb interaction between the fluctuations, and, therefore, their contribution to the thermodynamics.

We have calculated the distribution of electric fields outside a disordered, neutral quantum dot as well as the quantum correction to its polarizability. Although both of the effects are small, they are very important ideologically from the point of view of the scaling theory of metal-insulator transition, which we believe are observable.

---

[1] B.L. Altshuler, Y. Gefen, and Y. Imry, *Phys. Rev. Lett.* 66: 88 (1991); B.L. Altshuler and B.Z. Spivak, *Zh. Eksp Teo.* 92: 607 (1987).

[2] L.P. Levy, G. Doland, J. Dunsmuir, and H. Bouchiat, *Phys. Rev. Lett.* 64: 2074 (1990); V. Chandrasekhar, R.A. Webb, M.Y. Brady, M.D. Ketchen, W.J. Gallagher, and A. Kleinsasser, *Phys. Rev. Lett.* 67: 3578 (1991).

These small effects are caused by the screening of the Coulomb interaction. Due to this screening, additional energy is determined only by the charge distribution in a layer near the sample surface of a width of the screening length. As a result, interaction between the charge fluctuations is not sufficient to account for the persistent current. On the other hand, there is another magnetic flux dependent contribution to the Coulomb energy: the interaction between the charge fluctuations and the confining potential in a quantum dot (e.g., a finite work function of a metallic grain is determined by a dipole layer on the surface). The energy of the local charge fluctuations in the field of this layer apparently depends on the magnetic field and explains the observed persistent current. This interaction can have a number of important and observable consequences such as substantial mesoscopic fluctuations of the work function and its dependence on the external parameters such as low magnetic field.

Publications

Altshuler, B.L. "Thermodynamics of Mesoscopic Systems." Paper presented at the International Symposium on Nanostructures and Mesoscopic Systems, Santa Fe, New Mexico, May, 1991.

Chapter 2. Single Electron Transistors

Academic and Research Staff

Professor Marc A. Kastner, Professor Dimitri A. Antoniadis, Professor Henry I. Smith, Paul L. McEuen

Visiting Scientists and Research Affiliates

Shalom Wind[1]

Graduate Students

Paul A. Belk, Ethan B. Foxman

2.1 Project Description

Sponsors

Joint Services Electronics Program
Contract DAAL03-89-C-0001
Contract DAAL03-92-C-0001
National Science Foundation
Grant ECS 88-13250

Several years ago, we discovered, completely unexpectedly, new behavior in very small Si MOSFETs. Whereas conventional transistors turn from the off state to the on state only once as the gate voltage increases, these small transistors turn on and off periodically, in some cases as many as one hundred times. We have since learned how to control the period of these oscillations in GaAs field effect devices and have shown that a nm-size transistor turns on and off once for every electron added to it. Because of this, we call such a device a Single Electron Transistor.

Having established that each cycle corresponds to the addition of one electron, the period in gate voltage provides a very precise measure of the capacitance of our devices. Because it is very small, $\sim 10^{-16}$ F, such transistors may eventually find application in ultra-sensitive charge detection. Furthermore, capacitive coupling may make possible arrays of single-electron transistors with unique properties. Unfortunately, the single electron behavior has only been observed, so far, below about 1 K. Whether this behavior can be observed at higher temperatures in the future depends on the details of the mechanism that causes it. Our objective is, therefore, to better understand that mechanism.

Our initial discovery was made[2] with inversion layers in Si which were about 30 nm wide and several mm long. These were dual gate MOSFETs with a narrow slot, ~600 nm wide, in the lower gate, fashioned with X-ray lithography. This lower gate was made of refractory metals allowing a high temperature anneal after all unconventional lithography was complete. In the end, these devices were the narrowest transistors ever made, but whereas most previous narrow devices had low mobility, these had mobilities comparable to wide devices. The successful fabrication of these ultra-narrow devices was the result of a close collaboration between Professor Henry I. Smith, Professor Dimitri A. Antoniadis, and Professor Marc A. Kastner and their students.

Soon after these devices were first fabricated, it was discovered that their conductance oscillated periodically as a function of the density of electrons in the conducting channel, proportional to the gate voltage, V_g. To prove that the period of the oscillations corresponded to the addition of a single electron, new devices had to be made.

The first step was to produce devices close in their operation to a MOSFET but in GaAs where the influence of interface charges is much weaker.[3] This was accomplished through a remarkably suc-

---

[1] IBM Thomas J. Watson Research Center, Yorktown Heights, New York.

[2] J.H.F. Scott-Thomas, S.B. Field, M.A. Kastner, H.I. Smith, and D.A. Antoniadis, "Conductance Oscillations Periodic in the Density of a One-Dimensional Electron Gas," *Phys. Rev. Lett.* 62: 583 (1989); S.B. Field, M.A. Kastner, U. Meirav, J.H.F. Scott-Thomas, D.A. Antoniadis, H.I. Smith, and S.J. Wind, "Conductance Oscillations Periodic in the Density of One-Dimensional Electron Gases," *Phys. Rev. B* 42: 3523 (1990).

[3] U. Meirav, M.A. Kastner, M. Heiblum, and S.J. Wind, "One-Dimensional Electron Gas in GaAs: Periodic Conductance Oscillations as a Function of Density," *Phys. Rev. B* (Rapid Comm.) 40: 5871 (1989).

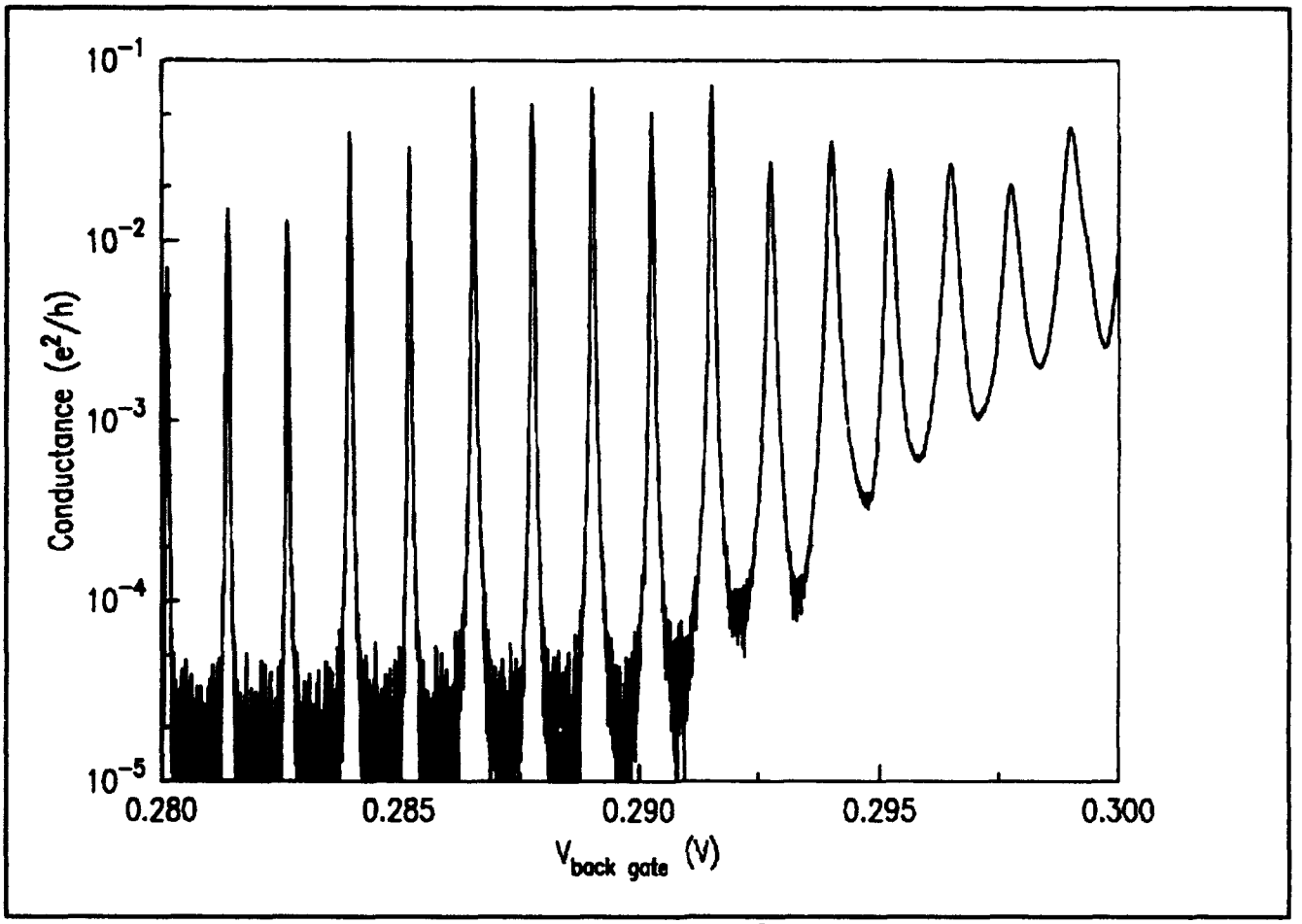


Figure 1. Conductance in units of the quantum of conductance e^2/h versus voltage on the n^+GaAs substrate, the "back gate." On the logarithmic plot it is clear that the transistor has an on-to-off conductance ratio that exceeds 10^3 for the lowest gate voltages. The measurements were made at 30 mK with a source-drain voltage of only 2.5 μV.

cessful collaboration with M. Heiblum of IBM. The new structure was created by growing AlGaAs on a conductive substrate, followed by a layer of undoped GaAs. The electron density at the GaAs/AlGaAs interface, inverted from the usual configuration, was varied by applying a voltage to the substrate. Heiblum was able to grow such inverted heterojunctions with mobilities of $\sim 500{,}000 cm^2/V\text{-}s$.

Next, the conducting channel is defined by depositing a metal gate on top of the GaAs, and a gap is patterned in the gate by electron beam lithography. Because a depletion region is created under the gate, the electrons accumulate only under the gap. In order to emulate the effect of two charged impurities, two constrictions are patterned in the gap. The electron beam lithography was done at IBM with the help of Shalom Wind.

Devices of this kind worked exactly as we hoped they would.[4] Periodic oscillations of the conductance were seen again, but now they were controlled: The period was the same for different devices with the same spacing between constrictions and was larger when the spacing was shorter, consistent with the idea that the same number of electrons is added for one period in all devices. Calculations of the capacitance of such devices are only consistent with each period corresponding to one electron added per oscillation.

This is an amazing result: Figure 1 shows that the conductance consists of periodic, narrow, well-separated resonances. The conductance rises and falls by a factor ~1000 with a variation of gate voltage that corresponds to only ~1/3 of an electron.

[4] U. Meirav, M.A. Kastner, and S.J. Wind, "Single Electron Charging and Periodic Conductance Resonances in GaAs Nanostructures," *Phys. Rev. Lett.* 65: 771 (1990).

We now understand quite well why the Single Electron Transistor works the way it does. The conductance results from resonant tunneling, and Professor Patrick Lee and his collaborators have shown that the states arise from single particle quantum states (the Fabry-Perot states induced by the two barriers, the same as expected for any "quantum dot"), but that the energies of the levels are dominated by the Coulomb interaction between the electrons in the isolated segment.

Experiments in the quantum Hall regime[5] at first seemed to indicate that the nature of the quantum states was very simple. By measuring the position in gate voltage of a series of conductance resonances, we were able to measure the energies for adding a series of electrons as a function of magnetic field. Figure 2 shows (top panel) how the peak positions oscillated with magnetic field. Subtracting a constant V_g difference from each pair of curves we emulated the effect of subtracting a constant Coulomb energy. We thereby obtained the level spectrum shown in the lower panel.

The level spectrum looks remarkably similar to that for non-interacting electrons in a magnetic field and a confining electrostatic potential. We thought, therefore, that the simple Coulomb blockade model, with a constant Coulomb interaction between any two electrons in the isolated region, was adequate. However, more careful analysis of data like that in figure 2 shows that this simple picture is inadequate. In particular, the difference in energies for electron spin parallel and antiparallel to the magnetic field are much too large in the experiment.

Recently, a density functional model for the isolated region has been developed in collaboration with Professor Lee's group. The good agreement between the model and the experimental results shows that electrons in different spatial and even spin states have very different Coulomb interactions. This is a major step in deepening our understanding of the physics of single electron transistors.

Publications

McEuen, P.L., E.B. Foxman, U. Meirav, M.A. Kastner, Y. Meir, N.S. Wingreen, and S.J. Wind. "Transport Spectroscopy of a Coulomb Island in the Quantum Hall Regime." *Phys. Rev. Lett.* 66: 1926 (1991).

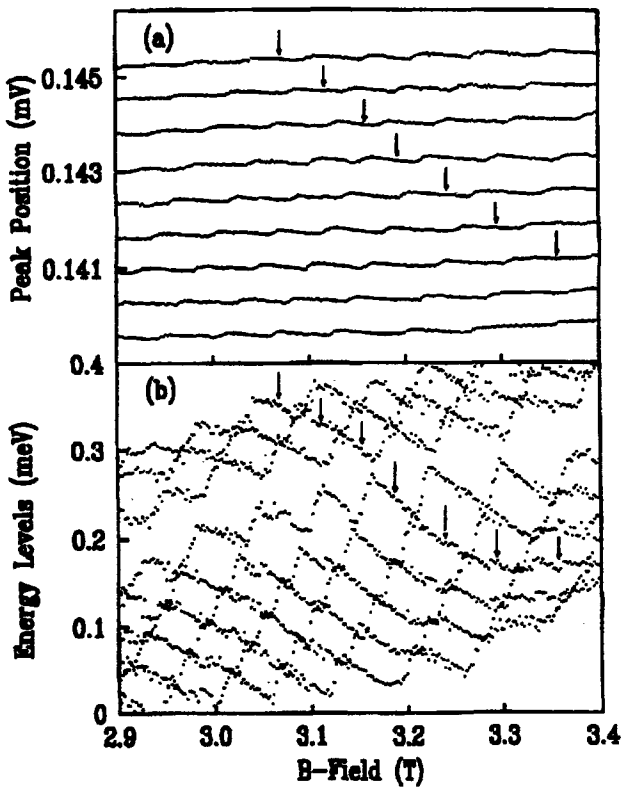


Figure 2. (a) The gate voltages corresponding to a series of consecutive conductance peaks like those in figure 1, as a function of magnetic field. (b) Result of subtracting a constant voltage from each successive peak in (a). This gives the energy for adding the next electron as a function of field with the average Coulomb interaction subtracted. The arrows follow a particular level as it moves through successive peaks.

[5] P.L. McEuen, E.B. Foxman, U. Meirav, M.A. Kastner, Y. Meir, N.S. Wingreen and S.J. Wind, "Transport Spectroscopy of a Coulomb Island in the Quantum Hall Regime," *Phys. Rev. Lett.* 66: 1926 (1991).



Professor Patrick A. Lee

Chapter 3. Transport Through a Quantum Dot

Academic and Research Staff

Professor Patrick A. Lee, Dr. Yigal Meir, Dr. Ned S. Wingreen

Graduate Students

Jari M. Kinaret

Technical and Support Staff

Imadiel Ariel

3.1 Project Description

Sponsor

Joint Services Electronics Program
Contract DAAL03-89-C-0001
Contract DAAL03-92-C-0001

We continue the study of electron transport through a quantum dot. It is now well established both experimentally[1] and theoretically[2] that Coulomb blockade plays a key role in this problem and is responsible for the conductance peaks which have been observed to be periodic as a function of gate voltage. Each of these conductance peaks occurs at a gate voltage where the energy of N and N+1 electron state are degenerate and each peak corresponds to the addition of a single electron to the quantum dot. In the past year, the general formalism developed by Meir et al.[2] has been extended and applied to the case where a strong magnetic field is applied to the system. The field is strong enough so that only the lowest two Landau levels are occupied, i.e., the system would be in the integer quantum Hall regime in the bulk. The advantage of this system is that the single particle states are well known to be edge states, and the energy of these states are well understood as a function of magnetic field. Thus, the successful application of the theory to explain the experimental data[3] provides strong support for the general theory[2] of Coulomb blockade in resonant tunneling.

Experimentally it was found that in the presence of a strong magnetic field, the location in gate voltage of each conductance peak exhibits small periodic fluctuation. At the same time, the magnitude of each conductance peak goes through deep minima. This can be explained based on a model where the low lying states are the edge states of the first and second Landau levels. For a given conductance peak, the number of electrons on the quantum fluctuates between N and N+1. However, as the magnetic field is increased, the N electrons are distributed between the two Landau levels in a different way, and electrons are transferred from the second Landau level to the first. The transfer occurs when the edge state of the first Landau level crosses the edge state of the second Landau level. Thus, as a function as of a magnetic field, we are watching the transfer of electrons from the second to the first Landau level, one electron at a time. Furthermore, since the dependence of the energy of the edge state on magnetic field is understood, the periodic fluctuation of the resonant energy with magnetic field can be understood. The dips in the magnitude of the conductance peak can also be explained as being due to the fact that the edge state of the second Landau level is more tightly bound, and its coupling to the leads is much smaller so that a dip occurs every time the second Landau level moves through the chemical potential of the leads. Based on this picture, quantitative calculation of the temperature dependence of the peak position was made and successfully compared with the experiment. Indeed, we now have sufficient confidence in the model that the problem can be turned around, and we can use the experiment as a spectroscopy of the single particle level, i.e., we can

---

1 U. Meirav, M.A. Kastner, and S.J. Wind, *Phys. Rev. Lett.* 65: 771 (1990).

2 Y. Meir, N.S. Wingreen, and P.A. Lee, "Transport through a Strongly Interacting Electron System: Theory of Periodic Conductance Oscillations," *Phys. Rev. Lett.* 66: 3048 (1991).

3 P.L. McEuen, E.B. Foxman, U. Meirav, M.A. Kastner, Y. Meir, N.S. Wingreen, and S.J. Wind, "Transport Spectroscopy of a Coulomb Island in the Quantum Hall Regime," *Phys. Rev. Lett.* 66: 1926 (1991).

extract the dependence of the edge state energy level as a function of magnetic field.

Publications

Feng, S., and P.A. Lee. "Mesoscopic Conductors and Correlations in Laser Speckle Patterns." *Sci.* 251: 633 (1991).

Kinaret, J., and P.A. Lee. "Conductance of a Disordered Narrow Wire in a Strong Magnetic Field." *Phys. Rev. B.* Forthcoming.

Lee, P.A. "Small Structures: A Laboratory for Studying Strongly Interacting Systems," *Proceedings of the Taniguchi Symposium on Mesoscopic Physics* 1991. Shima, Japan. Forthcoming.

McEuen, P.L., E.B. Foxman, U. Meirav, M.A. Kastner, Y. Meir, N.S. Wingreen, and S.J. Wind. "Transport Spectroscopy of a Coulomb Island in the Quantum Hall Regime." *Phys. Rev. Lett.* 66: 1926 (1991).

Meir, Y., N. Wingreen, and P.A. Lee. "Transport Through a Strongly Interacting Electron System: Theory of Periodic Conductance Oscillations." *Phys. Rev. Lett.* 66: 3048 (1991).

Chapter 4. Submicron and Nanometer Structures Technology and Research

Academic and Research Staff

Professor Henry I. Smith, Professor Dimitri A. Antoniadis, James M. Carter, Robert C. Fleming Jr., Dr. Mark L. Schattenburg

Visiting Scientists and Research Affiliates

Dr. Khalid Ismail,[1] Seppo Nenonen,[2] Yang Zhao[3]

Graduate Students

Martin Burkhardt, Mike T. Chou, William Chu, Steven S. Cooperman, Kathleen R. Early, Cristopher C. Eugster, Jerrold A. Floro, Reza A. Ghanbari, Scott D. Hector, Hang Hu, Harold Kahn, Yao-Ching Ku, Arvind Kumar, Ady Levy, Ya-Chin Liu, Hai P. Longworth, Alberto M. Moel, George E. Rittenhouse, Lisa T-F. Su, Vincent V. Wong, Kenneth Yee, Anthony Yen

Undergraduate Students

Juan Ferrera, Michael H.Y. Lim, Euclid E. Moon, Pablo Munguia, Lee-Peng Ng, Daniel B. Olster, Flora S. Tsai, Sabah Yunus

Technical and Support Staff

Donna R. Martinez, Mark K. Mondol, Jeanne M. Porter

4.1 Submicron Structures Laboratory

The Submicron Structures Laboratory at MIT develops techniques for fabricating surface structures with feature sizes in the range from nanometers to micrometers and uses these structures in a variety of research projects. These projects, which are described briefly below, fall into four major categories: (1) development of submicron and nanometer fabrication technology; (2) nanometer and quantum-effect electronics; (3) crystalline films on non-lattice-matching substrates; and (4) periodic structures for x-ray optics, spectroscopy and atomic interferometry.

4.2 Microfabrication at Linewidths of 100 nm and Below

Sponsors

Joint Services Electronics Program
Contract DAAL03-89-C-0001
Contract DAAL03-92-C-0001
National Science Foundation
Grant ECS 90-16437

Project Staff

Martin Burkhardt, James M. Carter, William Chu, Kathleen R. Early, Reza A. Ghanbari, Scott D. Hector, Yao-Ching Ku, Alberto M. Moel, George E. Rittenhouse, Dr. Mark L. Schattenburg, Professor Henry I. Smith, Vincent V. Wong, Anthony Yen

A variety of techniques for fabricating structures with characteristic dimensions of 100 nm (0.1 μm)

---

[1] University of Cairo, Giza, Egypt, and IBM Corporation, Thomas J. Watson Research Center, Yorktown Heights, New York.

[2] Outokumpu Electronics, Espoo, Finland.

[3] Princeton University, Princeton, New Jersey.

and below are investigated. These include: x-ray nanolithography, holographic lithography, achromatic holographic lithography, electron-beam lithography, focused-ion-beam lithography, reactive-ion etching, electroplating, and liftoff. Development of such techniques is essential if we are to explore the rich field of research applications in the deep-submicron and nanometer domains. X-ray nanolithography is of special interest because it can provide high throughput and broad process latitude at linewidths of 100 nm and below. As discussed in section 4.3, we have established a reliable mask technology, based on 1 μm-thick SiN_x membranes, as shown schematically in figure 1. Mask blanks are patterned by several techniques including electron-beam lithography, focused-ion-beam lithography, holographic lithography, and transfer from other x-ray masks.

For high-quality x-ray lithography, the mask-to-sample gap, G, must be precisely controlled. The mesa-rim architecture of figure 1 yields optically flat membranes enabling us to control gap down to about 2 microns by means of spacer studs. For 100 nm features a gap of 10 microns is suitable. However, for 50 nm features a gap of 2.5 microns is required. Figure 2 shows the replication of a planar-resonant-tunneling field-effect transistor pattern having 50 nm minimum features. The gap in this case was 2.7 microns. This gap is significantly larger than predicted by simple Fresnel diffraction formulae which neglect diffraction inside the mask absorber. Taking this into account, using vector electromagnetic calculations and accounting for the finite source size, we have developed a simulation that predicts image contrast as a function of feature size and gap. In order to increase the allowable gap for features of 70 nm and below, we are investigating the feasibility of near-field in-line x-ray holography.

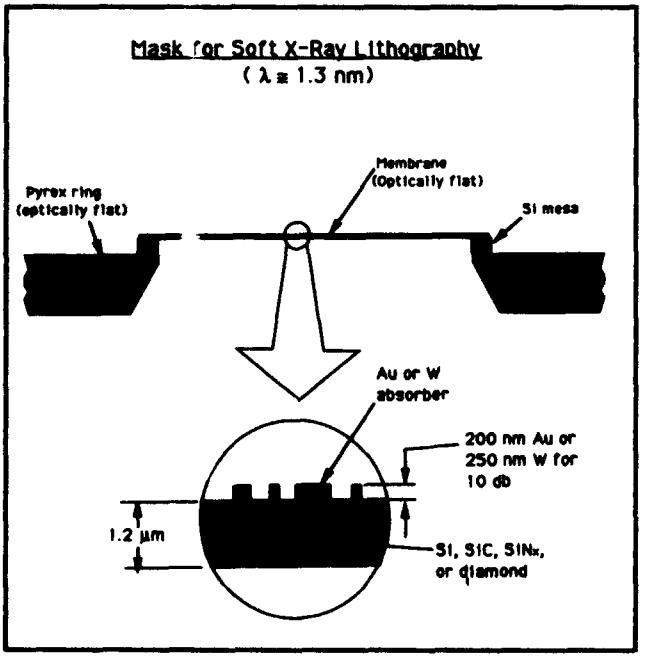


Figure 1. Structure of the new standard, 31 mm diameter, mesa-rim, x-ray mask suitable for lithography from 1000 to 20 nm feature sizes. Membranes are flat to < 0.25 μm.

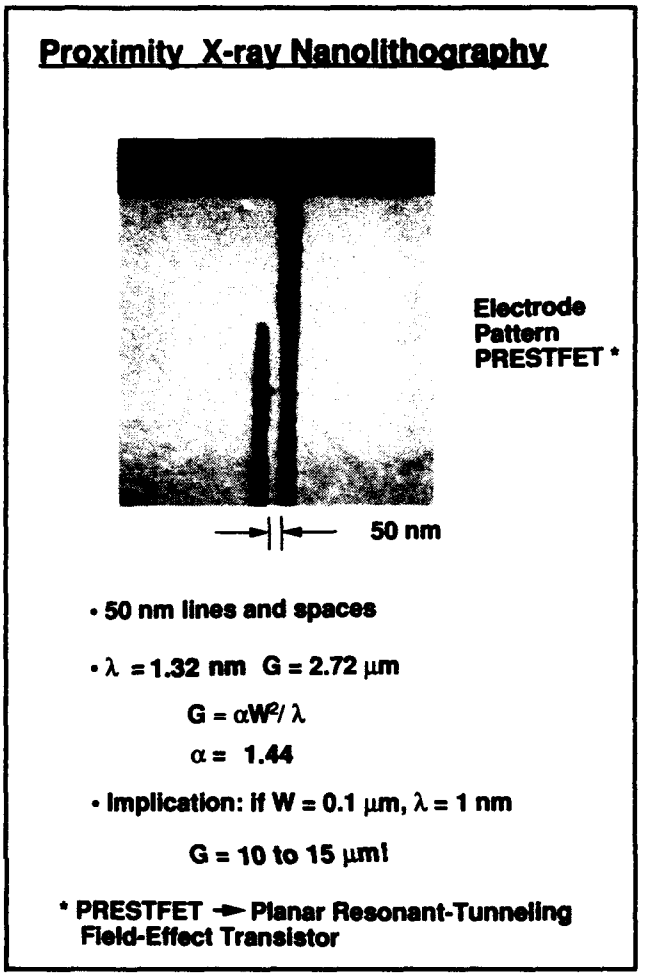


Figure 2. Replication, using the Cu_L x-ray (1.3 nm) and a mask-substrate gap of 2.7 microns, of 50 nm line and space pattern.

Using the figure 1 mask architecture, patterns are readily transferred onto standard Si wafers. However, in research on GaAs or other III-V devices, substrates are often much smaller than the 31 mm-diameter mask membrane. We have developed an apparatus that allows us to bring the membrane into contact with such substrates during exposure, without risk of mask damage. Resolution down to 10-20 nm is feasible under such exposure conditions.

Alignment of x-ray masks to patterns pre-existing on a substrate is currently done with an optical imaging system equipped with a video camera. We are investigating electronically enhanced moiré imaging methods in order to achieve sub-10 nm alignment precision. In this approach the gap is

set at ~4 microns and the mask translated piezoelectrically.

The achromatic holographic lithography system in conjunction with an anti-reflection coating (ARC) specially formulated for the 193 nm wavelength is now producing high quality images, as shown in figure 3. The ARC consists of PMMA and a bis-azide, 4, 4'-diazidodiphenyl sulfone.

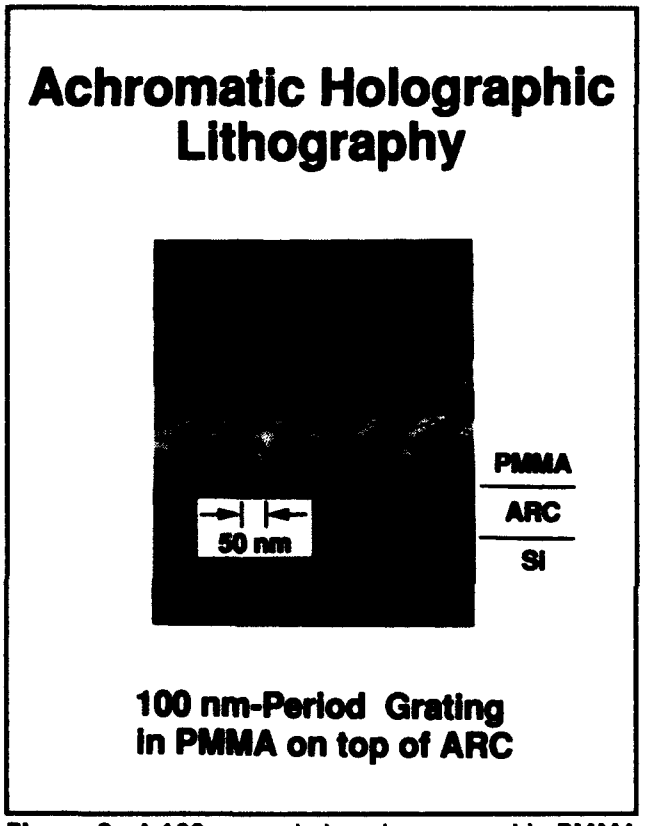


Figure 3. A 100 nm-period grating exposed in PMMA on top of an anti-reflection coating (ARC) by achromatic holographic lithography using the ArF laser at 193 nm.

4.3 Improved Mask Technology for X-Ray Lithography

Sponsors

National Science Foundation
Grant ECS 90-16437
Semiconductor Research Corporation
Contract 90-SP-080
U.S. Navy - Naval Research Laboratory
Contract N00014-90-K-2018

Project Staff

Juan Ferrera, Yao-Ching Ku, Mark K. Mondol, Lee-Peng Ng, Dr. Mark L. Schattenburg, Professor Henry I. Smith, Flora S. Tsai, Sabah Yunus

The x-ray mask architecture shown in figure 1 is compatible with both our research in the sub-100 *nm* domain and the commercial fabrication of submicron integrated electronics. For the latter application especially, distortion in the mask must be eliminated. Distortion can arise from stress in the absorber, which is usually gold (Au) or tungsten (W). We have developed means of sputtering W so that the stress is below 5 E 7 dynes/cm^2, and the distortion induced by stress is below the level of detectability in a Linnik interferometer. The corresponding in-plane pattern distortion is calculated to be less than 1 nm. We are currently developing an interferometer to directly measure in-plane distortion.

Membranes of SiN_x are preferred at the present time because they can be made by conventional LPCVD methods and are extremely rugged and resistant to breakage. (SiN_x membranes only 1 micron thick can even be used as vacuum windows, 20 mm in diameter.) Membranes are characterized by their optical transmission, resonant frequency and bulge under pressure. From these measurements we extract index of refraction, optical attenuation, thickness, stress, and Young's modulus. We have also made radiation hardness measurements on membranes by subjecting them to the equivalent of one million exposures on the University of Wisconsin synchrotron. Effects of x radiation on membrane stress are extremely small, and we believe this can be eliminated by reducing the oxygen content of the SiN_x. To this end a special purpose LPCVD reactor for low-stress SiN_x will be set up within the Integrated Circuit Laboratory at MIT.

We are collaborating with the Naval Research Laboratory (NRL) in using their JEOL JBX5D11 e-beam lithography system to pattern x-ray masks. The patterns are generated using the CAD tools at MIT, converted to an acceptable binary intermediate format, transferred to NRL via ARPA Internet, converted there to the JEOL format, and written onto mask blanks that we send in advance to NRL (by express mail). Once the masks are written, they are shipped back to MIT for further processing. This collaboration has been fruitful for a number of projects including short-channel MOSFETs (section 4.4), multiple-parallel one-dimensional conductors (section 4.6), and the electron waveguide device (section 4.7).

4.4 Study of Electron Transport in Si MOSFETs with Deep-Submicron Channel Lengths

Sponsors

IBM Corporation
Joint Services Electronics Program
Contract DAAL03-89-C-0001
Contract DAAL03-92-C-0001
Semiconductor Research Corporation
Contract 90-SP-080

Project Staff

Professor Dimitri A. Antoniadis, Professor James Chung, Dr. Hao Fang, Hang Hu, Professor Henry I. Smith, Lisa T-F. Su

We have continued using x-ray lithography to fabricate both N and P channel MOSFET devices with effective channel length down to 80 nm. As channel lengths decrease below about 150 nm, electron velocity overshoot, and thus an increase of device transconductance has been observed both at room temperature and liquid nitrogen temperature. It appears that the necessary conditions for this phenomenon are high carrier mobility close to the Si/SiO_2 interface, and low parasitic resistance. The former is achieved in both our NMOSFET and PMOSFET devices by utilizing a super steep retrograde doping of the channel. In the NMOSFET case, indium, by virtue of its heavier mass and desirable doping profile in silicon, has been used to give retrograde threshold control doping with low surface concentration and yet high peak concentration. In the PMOSFET case, arsenic has been used to achieve the same goals.

Record saturation transconductance of over 1S/mm in deep submicron NMOSFET with channel length down to 100 nm was obtained with the indium doping technique. This underscores the achievement of increased surface mobility with the steeper retrograde channel doping. A transconductance of 0.23 S/mm was achieved in deep-submicron PMOSFET.

As shown in figure 4 we have developed a technology for self-aligned silicide N/PMOSFET device fabrication for the purpose of significantly reducing parasitic resistance. We have used cobalt deposition on the exposed silicon of source/drain and the exposed polysilicon of the gate electrode with a subsequent two-step rapid thermal annealing to form cobalt silicide ($CoSi_2$). Thin oxide spacers around the gate electrode have been used to prevent shorts between gate and source/drain. These process improvements were

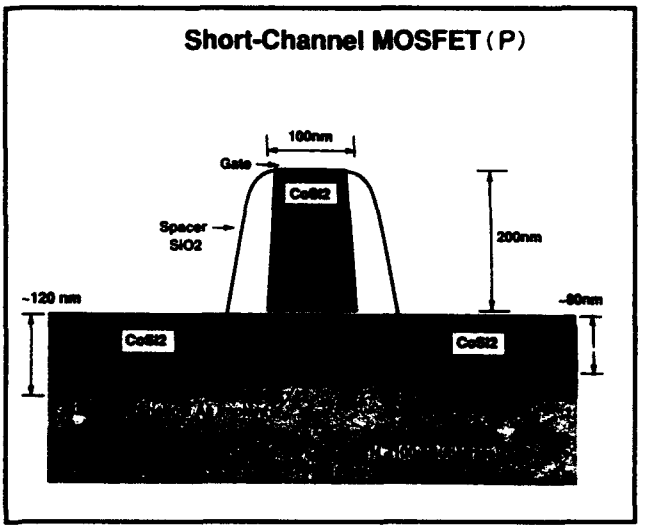


Figure 4. Configuration of self-aligned, 100 nm-channel-length, P-MOSFET.

tested first with conventional lithography where the submicron gate was achieved by resist erosion in an O_2 plasma after resist exposure and development. The first ultrashort channel self-aligned silicide MOSFET devices with channel length down to 0.12 μm for PMOS and 0.15 μm for NMOS and parasitic resistance down to 400 ohms per micron width have been successfully fabricated.

More recently, SiN_x-membrane x-ray mask technology has allowed us to use x-ray lithography for the definition of the gates. X-ray masks were patterned by electron-beam lithography at the Naval Research Laboratory, as shown in figure 5. Fabrication of both NMOSFET and PMOSFET devices with the new lithography technology and new cobalt silicide shallow junction source/drain technology should give us 100 nm channel length CMOS circuits compatible with commercial mass production.

4.5 Studies of Coulomb Charging in Ultrasmall Semiconductor Devices

Sponsor

Joint Services Electronics Program
Contract DAAL03-89-C-0001
Contract DAAL03-92-C-0001
U.S. Air Force - Office of Scientific Research
Grant F49620-92-J-0064

Project Staff

Professor Dimitri A. Antoniadis, Professor Marc A. Kastner, Arvind Kumar, Professor Terry P. Orlando, Professor Henry I. Smith

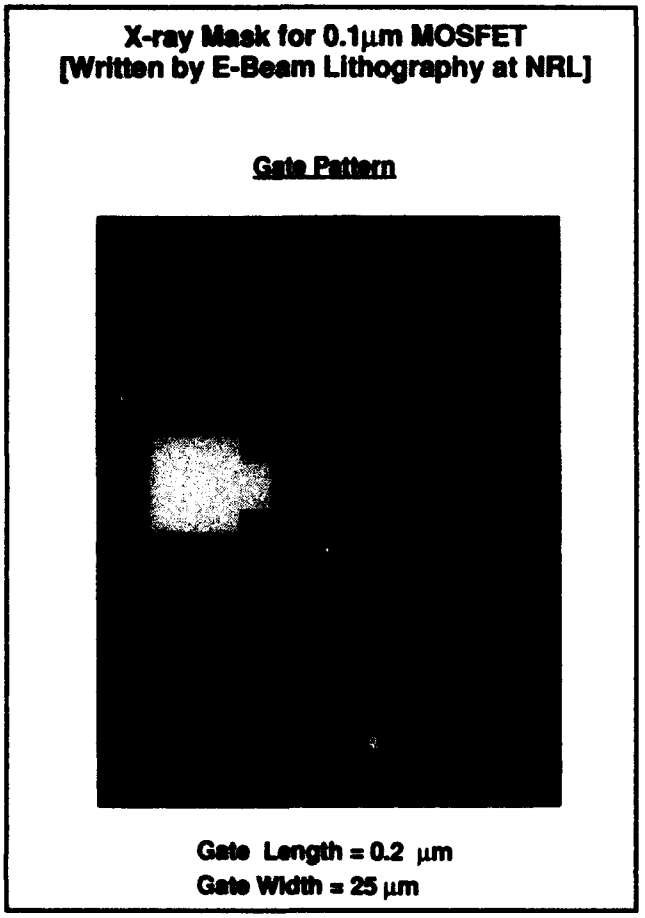


Figure 5. Scanning electron micrograph of x-ray mask for the 100 nm channel-length MOSFET. The e-beam patterning was done at the Naval Research Laboratory, the plating and x-ray lithography was done at MIT.

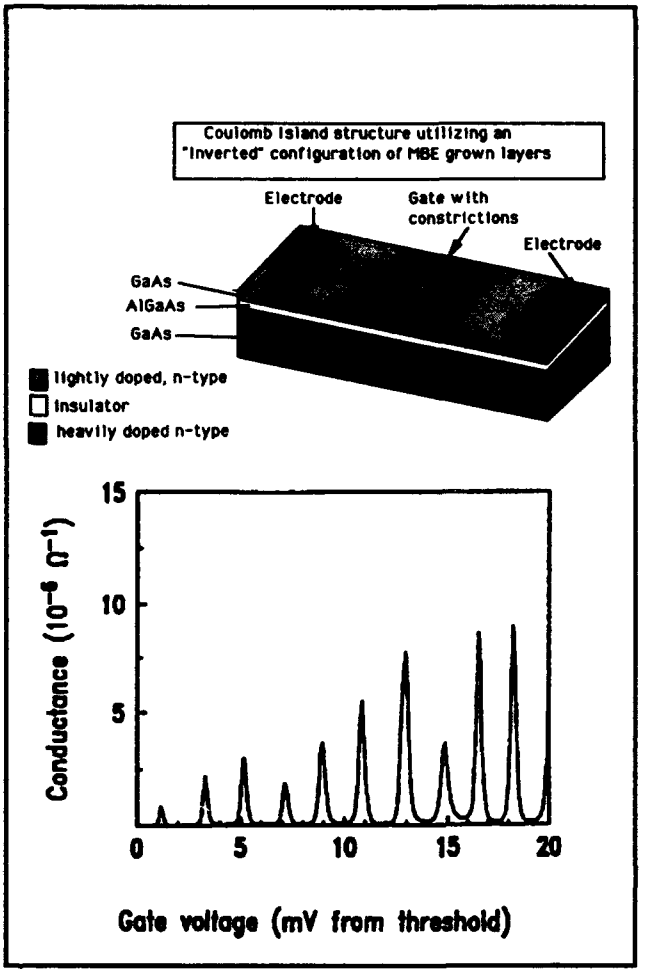


Figure 6. (a) Device structure used to study Coulomb blockade effects. A negative voltage on the two Schottky gates on the top depletes the electron gas at the lower GaAs/AlGaAs interface below, forming a narrow electron channel interrupted by two potential barriers at the constrictions. The n+ GaAs substrate serves as a bottom gate to modulate the channel electron density. (b) Periodic oscillations in the conductance as a function of bottom gate voltage for the device shown in (a).

In previous studies on very narrow silicon MOSFETs fabricated using x-ray lithography a fundamentally different mechanism to modulate the low-temperature electrical conduction was found. When the devices were cooled to the milli-Kelvin range, the electrical conductance exhibited a series of sharp oscillations which were almost perfectly periodic in the voltage of the gate used to control the electron density. This periodic modulation of the conductance was thought to be caused by presence of two dominant impurities in the electron channel which resulted in an isolated segment of the electron gas. In order to test the two-impurity hypothesis, the structure illustrated in figure 6(a) was fabricated using electron beam lithography and liftoff. The structure, fabricated on an inverted GaAs/AlGaAs heterostructure, consists of two Schottky gates used to squeeze the electron gas laterally, while the n+ substrate serves as a bottom gate to independently modulate the channel electron density. The two sets of constrictions were intended to emulate the potential due to the two impurities in the MOSFET device, while the mobility was sufficiently high to reduce the probability of unwanted accidental impurities.

When cooled to milli-Kelvin temperatures, conductance oscillations periodic in the bottom gate voltage were again observed, as shown in figure 6(b). Moreover, the voltage separation between successive conductance peaks was found to depend on the separation between the two potential barriers. To better understand these structures, we performed semi-classical calculations of potential profiles and electron densities for the structure in figure 6(a). Equipotential contours near the AlGaAs/GaAs interface are shown in figure 7 for a typical bias point with the shaded regions indicating areas occupied by inversion electrons.

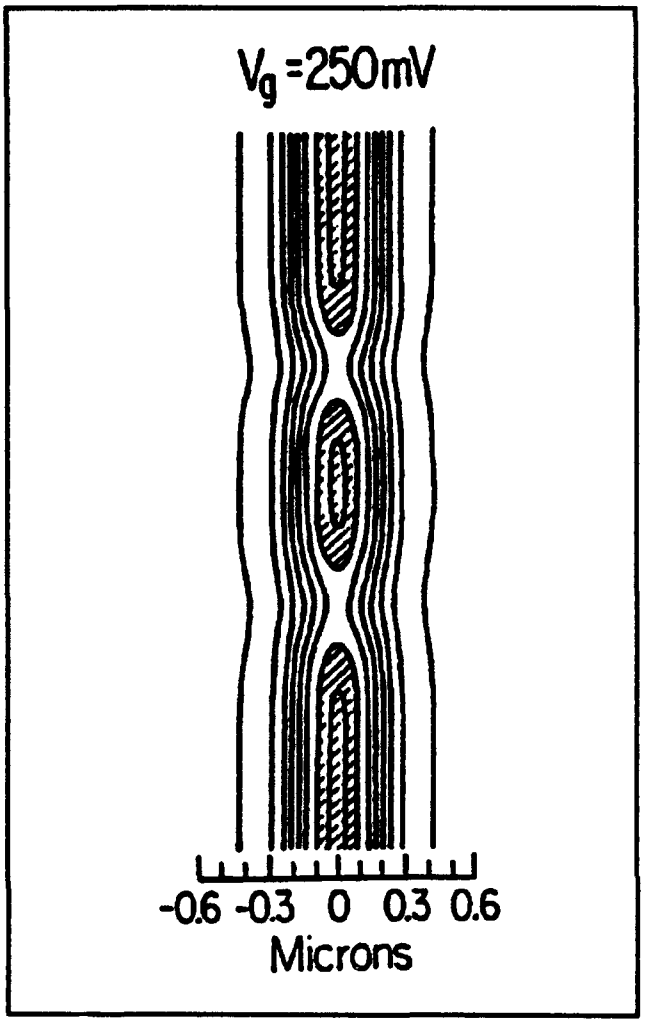


Figure 7. Equipotential contours for the device in figure 6(a) near the lower GaAs/AlGaAs interface at a typical bias point. The shaded regions indicate areas occupied by electrons. The two sets of constrictions result in an isolated electron segment, or "island," through which transport can be thermally activated.

We calculated the integrated electron charge in the isolated electron segment, or "island," between the sets of constrictions as a function of bottom gate voltage and found that it is approximately linear in bottom gate voltage, and that the voltage required to add one electron to the island is very nearly the spacing between successive conductance peaks. Thus, each conductance peak corresponds to the addition of a single electron to the island. This modulation of the conductance by changing the charge by a single electron can be understood in terms of a theory known as Coulomb blockage. According to the Coulomb blockade theory, a conductance valley corresponds to the electrostatic energy of the island being minimized by an integer number of electrons, so that addition of another electron costs some finite charging energy and transport is thermally activated. A conductance peak, on the other hand, corresponds to a state of the island where the electrostatic energy is minimized by a half-integer number of electrons, so that there is no energy barrier to adding another electron. These two states repeat cyclically in bottom gate voltage, resulting in the observed periodic modulation of the conductance.

We are presently enhancing our understanding of Coulomb blockade effects both experimentally and theoretically. We first plan to reproduce the effect in a conventional modulation-doped GaAs/AlGaAs heterostructure, which is much more widely available than the inverted heterostructure. Secondly, we are working to understand all the capacitance components to the island in addition to the bottom gate capacitance described above. This is important because the observability temperature for Coulomb effects depends inversely on the total capacitance of the island, so that reducing the island capacitance is key to observing these effects at temperatures above the milli-Kelvin regime. Finally, we plan to study experimentally transport through more than one dot as well as the coupling of dots in parallel.

Because the modulation of the conductance is so strong, Coulomb blockade is among the most promising of novel effects in ultrasmall structures for long-term applications.

4.6 Study of Quasi-One-Dimensional Wires and Superlattice Formation in GaAs/AlGaAs Modulation Doped Field-Effect Transistors

Sponsor

U.S. Air Force - Office of Scientific Research
Grant F49620-92-J-0064

Project Staff

Professor Dimitri A. Antoniadis, Martin Burkhardt, William Chu, Professor Jesús A. del Alamo, Reza A. Ghanbari, Professor Terry P. Orlando, Professor Henry I. Smith

We have continued to use the modulation-doped field-effect transistor (MODFET) to explore electron back diffraction effects and reduced dimensionality effects in the GaAs/AlGaAs system. Because such devices have critical dimensions on the order of 100 nm, the use of x-ray lithography for fine feature definition has been central to our strategy. Recent results in our laboratory indicate that there may be a significant advantage in using x-ray lithography over direct-write e-beam lithography to fabricate quantum-effect electronic

devices because of significantly less mobility degradation in x-ray exposed samples.

Quasi-one-dimensional (Q1D) wires are defined on modulation-doped GaAs/AlGaAs material by first aligning the substrate and x-ray mask optically and then exposing. The region between the resist lines is then etched away chemically. After etching, the areas under the etched regions are depleted of electrons, leaving behind many parallel quasi-one-dimensional channels between source and drain. A continuous Schottky gate is then deposited over the wires, as depicted in Figure 8, to allow control of the electron density in the wires. A scanning-electron micrograph of a typical device is shown in Figure 9.

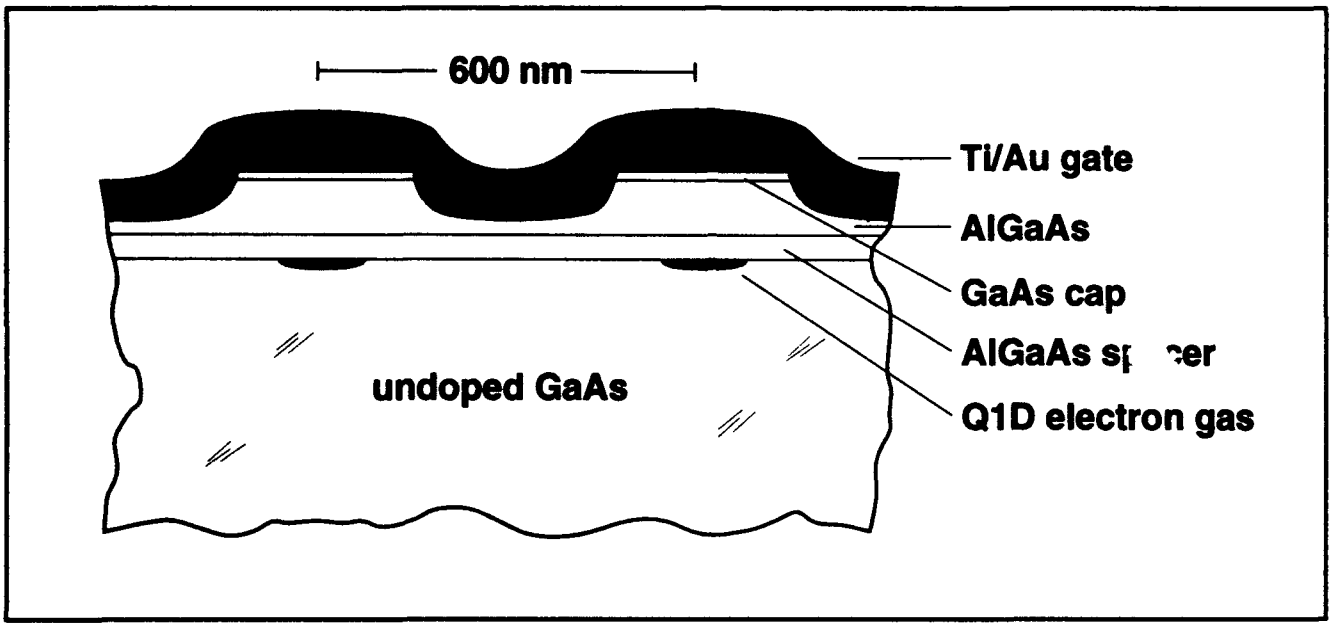


Figure 8. Cross-sectional schematic of device for studying conduction in multiple parallel quasi-one-dimensional quantum wires.

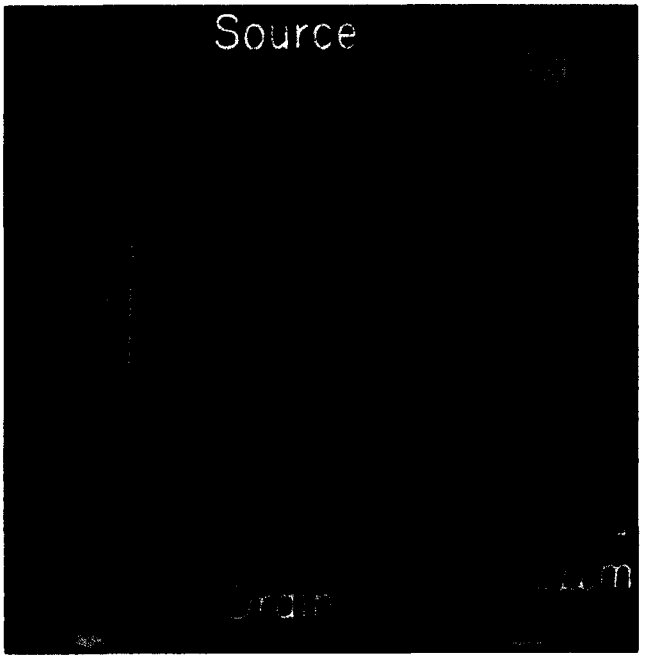


Figure 9. Scanning electron micrograph of device depicted in figure 8.

We have also fabricated MODFETs in which rather than having a large continuous gate over the channel, we have a grid gate (periodicity of 200 nm) as shown schematically in Figure 10. As a negative bias is applied to the gate, the regions immediately under the metal lines deplete more quickly than the the regions under the open areas of the gate. Thus, electrons travelling between source and drain see a periodic potential. When the electron wave-length matches the periodic pctential, coherent back diffraction occurs. Such back diffraction manifests itself as a drop in conductance between source and drain. The stronger the potential modulation, the more pronounced the back diffraction ought to be. We are in the process of optimizing our device design to increase the strength of the potential modulation.

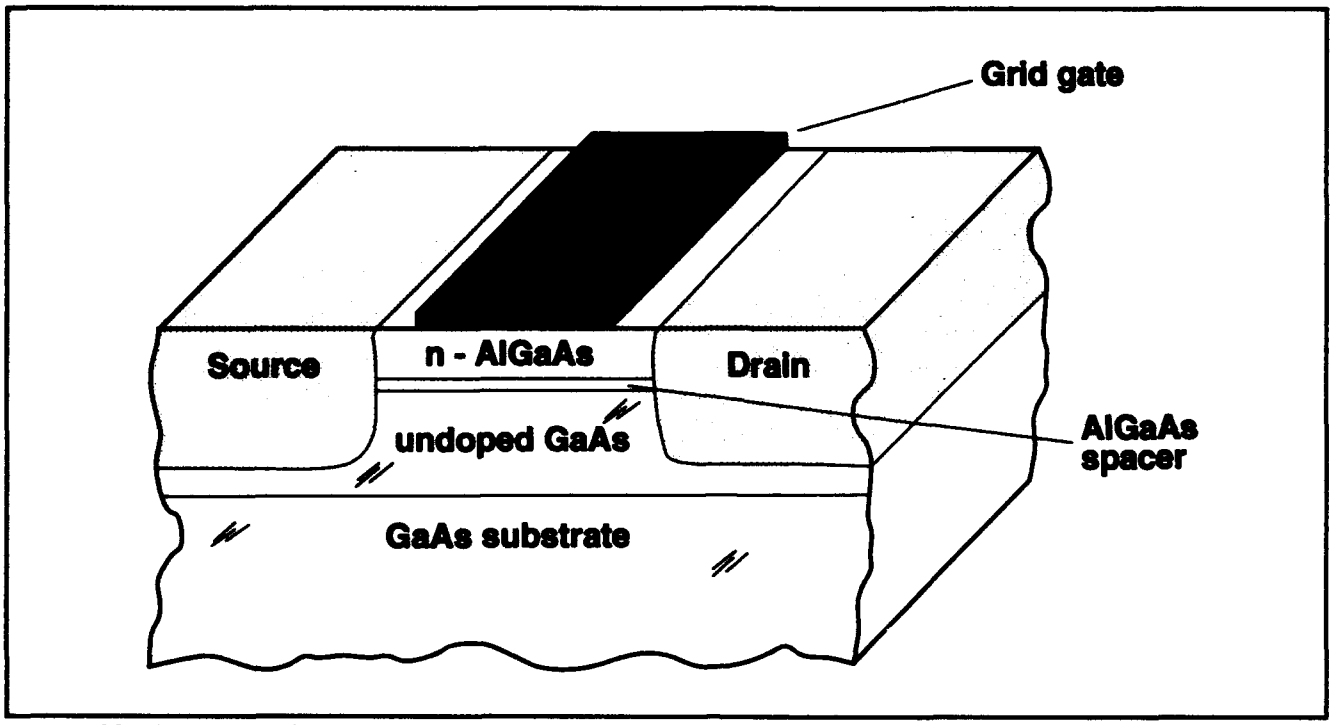


Figure 10. Schematic of grid-gate MODFET for study of surface superlattice formation.

4.7 GaAs Electron Waveguide Devices Fabricated by X-Ray Lithography

Sponsor

National Science Foundation
Grant DMR 87-19217
Grant DMR 90-22933

Project Staff

Professor Jesús A. del Alamo, William Chu, Cristopher C. Eugster, Alberto M. Moel, Euclid E. Moon, Dr. Mark L. Schattenburg, Professor Henry I. Smith.

We have successfully fabricated electron waveguide devices using x-ray lithography. As shown in figure 11, a split-gate structure constricts the electron gas of a high-mobility AlGaAs/GaAs heterostructure in the region between the gate fingers (length L and width W). If electron wavefunctions are coherent over the length of the device, then transport through this region is considered ballistic, and the structure can be considered an electron waveguide. A clear signature of ballistic transport is quantized conductance as a function of the electron density in this constricted region. Thus, the quality of conductance steps serves as a measure of the quality of the material and the ability of the processing steps to maintain this quality. The longer the length of devices in which this effect can be observed, the higher the quality of the material.

We have fabricated electron waveguides of length 0.1 μm up to 2 μm using x-ray lithography. An x-ray mask (parent mask) is fabricated by using e-beam lithography to define the split-gate pattern on a PMMA-coated silicon-nitride (SiN_x) membrane. After development, the absorbers are formed by electroplating 200 nm of Au. A scanning-electron micrograph of the parent mask is shown in figure 12. In order to reverse the mask polarity, the parent mask is replicated by proximity x-ray lithography (λ = 1.3 nm) to generate a replica (daughter) mask. The daughter mask is then aligned to a PMMA-coated AlGaAs/GaAs sample and x-ray exposed.

The finished devices are bonded and then tested at liquid-helium temperatures. Using standard lock-in techniques, the conductance of the electron waveguides is measured as a function of the split-gate bias which controls the electron density in the waveguide Sharp $2e^2/h$ conductance steps were observed in a 0.75 μm-long device at T=2K, as shown in figure 13. The features in the conductance remain visible up to temperatures of 15K. Conductance features were observed in devices as long as 2 μm.

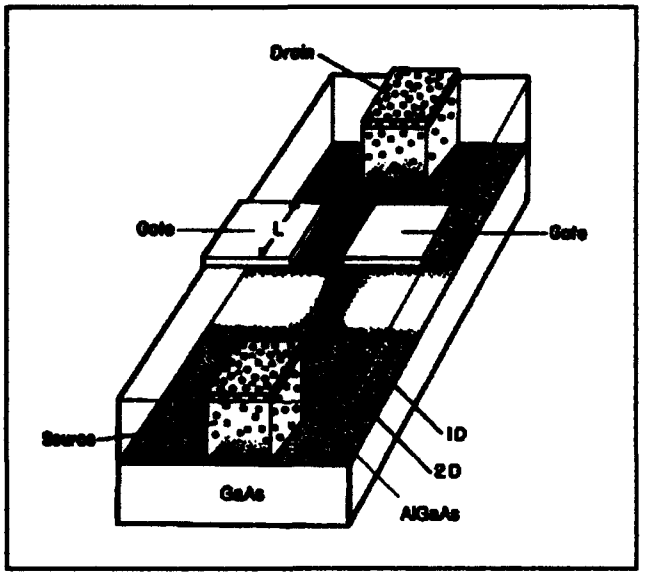


Figure 11. Schematic of an electron waveguide device defined by the split-gate configuration. The shaded region represents the electron concentration at the AlGaAs/GaAs interface.

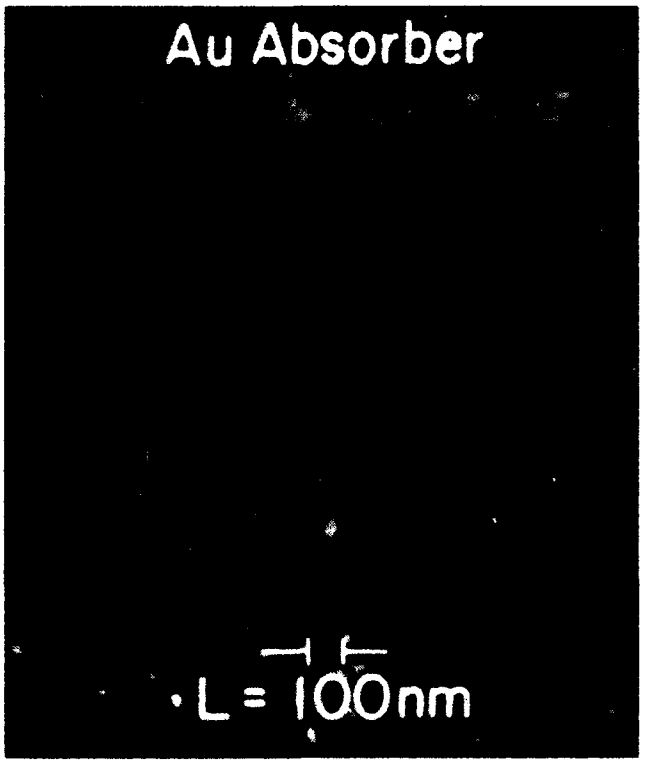


Figure 12. Top view of a parent x-ray mask showing the pattern for a 0.1 μm-long waveguide device.

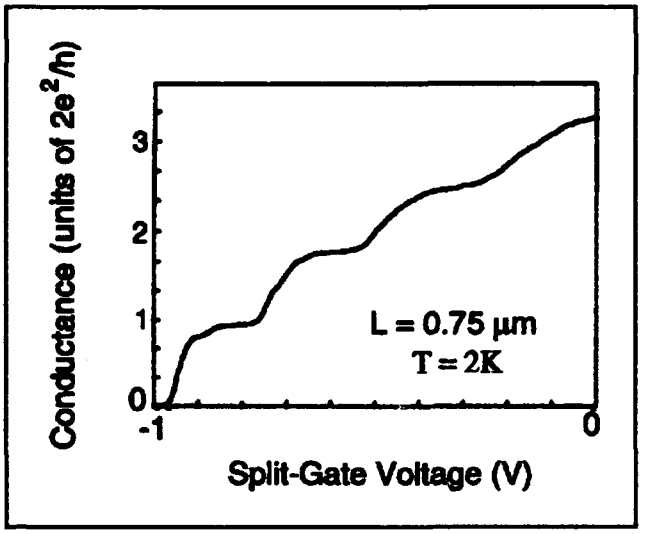


Figure 13. Conductance of a L = 0.75 μm electron waveguide device as a function of split-gate voltage.

4.8 Arrays of Field-Effect-Induced Quantum Dots

Sponsors

Joint Services Electronics Program
Contract DAAL03-89-C-001
Contract DAAL03-92-C-001
U.S. Air Force - Office of Scientific Research
Grant F49620-92-J-0064

Project Staff

Professor Dimitri A. Antoniadis, Martin Burkhardt, Reza A. Ghanbari, Professor Terry P. Orlando, Professor Henry I. Smith, Professor M. Shayegan,[4] Professor Daniel Tsui,[4] Yang Zhao[4]

A metal grid on a modulation-doped AlGaAs/GaAs substrate (depicted in figure 14a) produces a two-dimensional periodic potential modulation at the AlGaAs/GaAs interface via the Schottky effect. If a gate electrode is attached to the grid, the potential can be further modified with an external voltage source. By changing the gate voltage from positive to negative values, the potential seen by the electrons located at the AlGaAs/GaAs interface can be varied from uniform (in which case the electrons behave as a 2-D electron gas), to weakly coupled zero-D quantum wells (figure 14b), to isolated zero-D quantum dots (figure 14c). We have made such structures with spatial periods of 200 nm in both orthogonal directions and covering

[4] Princeton University, Princeton, New Jersey.

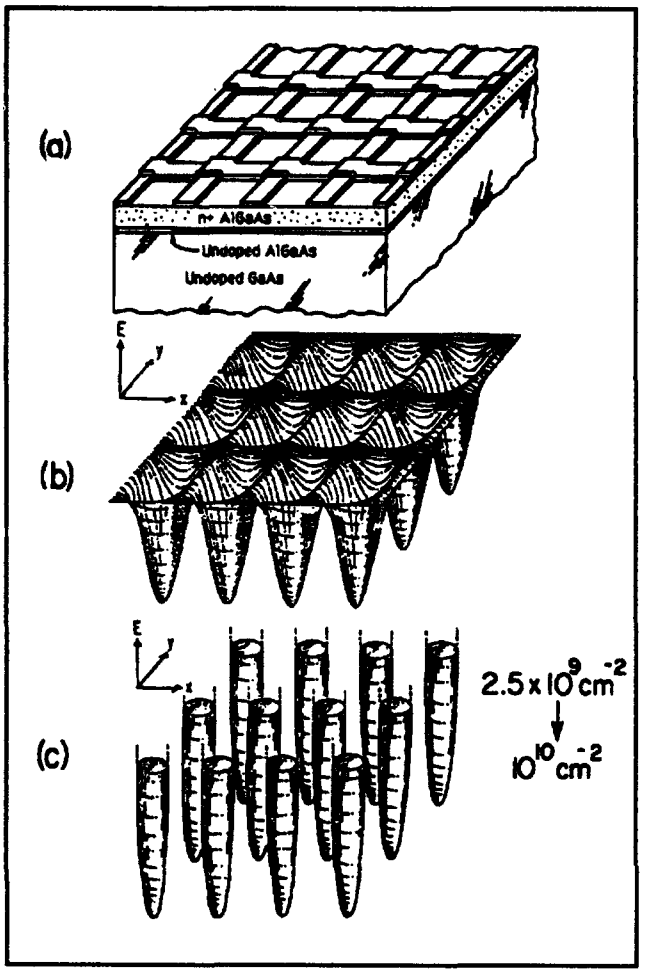


Figure 14. (a) Metal grid gate on a modulation-doped AlGaAs/GaAs substrate; (b) Depiction of potential seen by electrons at the AlGaAs/GaAs interface for weakly coupled quantum dots; (c) Potential for the case of isolated quantum dots.

areas of several square millimeters. The isolated quantum dots and the attendant zero-dimensional electronic sub-bands were examined in collaboration with D. Tsui at Princeton University using far-infrared (FIR) cyclotron resonance. Transitions between the discrete energy levels in the quantum dots were observed as a function of magnetic filed. Results were in agreement with a theoretical model.

Currently, we are continuing our study using extremely high quality samples prepared by M. Shayegan's group at Princeton. With mobilities typically greater than 10^6 cm^2/Vsec, the resolution of the experiments should improve dramatically.

4.9 Planar-Resonant-Tunneling Field-Effect Transistors (PRESTFET)

Sponsor

U.S. Air Force - Office of Scientific Research
Grant F49620-92-J-0064

Project Staff

Professor Dimitri A. Antoniadis, Mike T. Chou, William Chu, Professor Henry I. Smith

Previously, we reported on the performance of a planar-resonant-tunneling field-effect transistor (PRESTFET) depicted in figure 15, in which the gate electrodes were 60 nm long and separated by 60 nm. Clear evidence of resonant tunneling through the bound states in the well between electrodes was observed, as shown in figure 15(b).

In order to reduce the electrode separation while retaining a large process latitude, we have chosen to pursue a new technology for making the PRESTFET. In collaboration with S. Rishton of IBM, a high-performance e-beam nanolithography system was used to write PRESTFET patterns on SiN_x x-ray mask membranes, 1 μm thick. Reduced backscattering from the thin membrane has permitted us to achieve 50 nm lines and spaces. We hope to get even finer features in the future. The written masks are processed at MIT, replicated using the Cu_L x-ray (1.3 nm), and Schottky electrodes formed by liftoff. Masks are aligned to GaAs substrate using a specially built alignment and exposure station.

4.10 Fabrication of Distributed-Feedback Lasers and Channel-Dropping Filters

Sponsor

Joint Services Electronics Program
Contract DAAL03-89-C-0001
Contract DAAL03-92-C-0001

Project Staff

James M. Carter, Woo-Young Choi, Jay N. Damask, Professor Clifton G. Fonstad, Jr., Professor Herman Haus, Professor Leslie A. Kolodziejski, Professor Henry I. Smith, Vincent V. Wong

We are developing techniques to fabricate large area, spatially-coherent gratings for both quarter-wave-shifted distributed-feedback (DFB) lasers

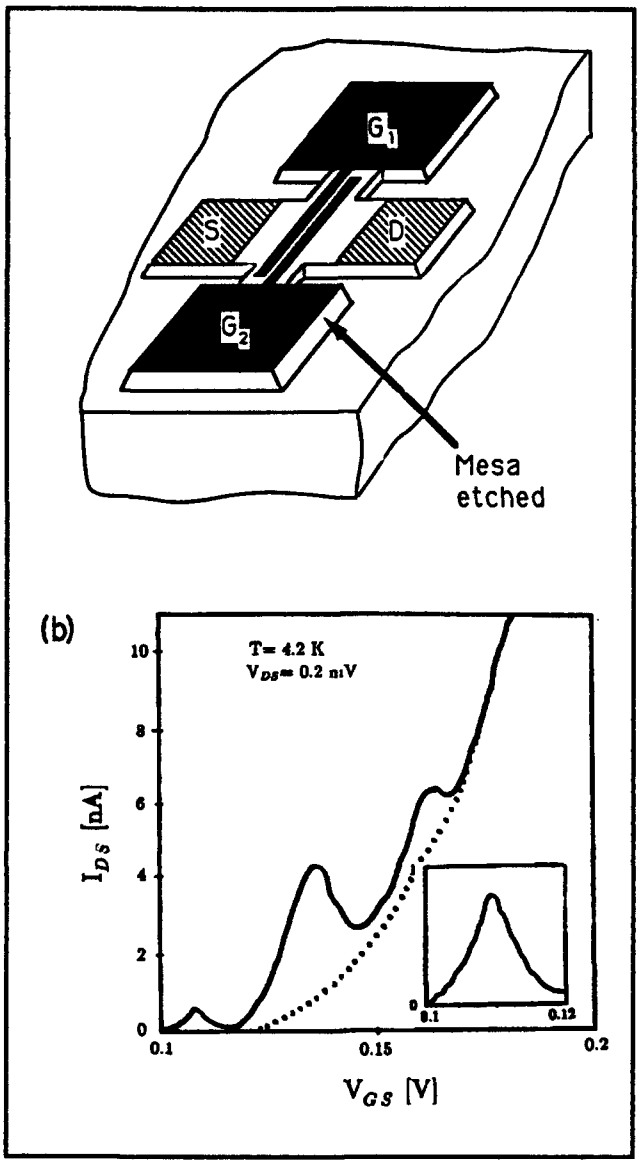


Figure 15. (a) Layout of a 4-terminal double-barrier planar-resonant-tunneling field-effect transistor (PRESTFET). (b) Plot of source-drain current versus gate voltage for a PRESTFET with 60 nm well width.

and channel-dropping filters (CDFs) on InP-based materials. The quality of these gratings is the most important factor determining the performance of these devices. Typical grating periods will be ~200 nm, and grating lengths will range from ~500 μm to several millimeters. Much of the nanofabrication technology developed in our lab over the years is directly applicable to the fabrication of these devices. SiN_x x-ray masks will be patterned using both holographic lithography and e-beam lithography, as described below. X-ray lithography will then be used to define the device patterns on the InP-based material.

Through the use of holographic lithography, large-area, spatially-coherent grating patterns can be defined. Fine control of the grating period is also possible. However, the incorporation of the quarter-wave shift into the grating structure is not easily accomplished by holographic means. We are pursuing a technique that takes advantage of a unique aspect of x-ray lithography: the phase of a segment of a grating can be shifted by pi-radians by transferring it onto the back surface of the mask membrane. Grating structures containing single and multiple quarter-wave shifts, which are necessary for both DFB lasers and CDFs, will be fabricated using this technique.

The incorporation of quarter-wave shifts into a grating structure is straightforward with e-beam lithography. However, precise control of the grating period, and large-area, spatially-coherent grating patterns are not easily obtained with e-beam lithography. For precise control of the grating period, a continuously-variable field size is necessary. To achieve spatial coherence in the written gratings one must eliminate the stitching errors, which occur when writing adjacent fields. We are pursuing a technique based on a global-fiducial grid scheme which potentially can solve both of these problems. Once developed, this technique will be incorporated into the e-beam lithography process to define the appropriate DFB laser and CDF grating patterns onto a SiN_x x-ray mask.

4.11 Novel Superconducting Tunneling Structures

Sponsor

Joint Services Electronics Program
Contract DAAL03-89-C-0001
Contract DAAL03-92-C-0001

Project Staff

Professor John M. Graybeal, Dr. Bernard S. Meyerson,[5] George E. Rittenhouse, Professor Henry I. Smith

In this program we seek to examine the behavior of short-channel hybrid Josephson devices, whose geometry is designed to display quantum electronic interference behavior. These devices represent the first attempt to observe Josephson

[5] IBM Corporation.

coupling via resonant tunneling. The characteristic energy scale for such a device would be set by quantum confinement, and consequently may provide a new avenue for obtaining finite gains in Josephson three-terminal devices.

These novel structures consist of an ultrathin vertical Si membrane (the quantum well) sandwiched between two superconducting Nb counterelectrodes. These structures are fabricated using a combination of x-ray and optical lithography, anisotropic wet chemical etching, planarization and reactive dry etching techniques. The basic geometry of these new structures has now been fully validated using low-mobility uniformly doped Si wafers, where we find Josephson behavior consistent with the best published work on "conventional" Nb/Si/Nb junctions. However, no resonant tunneling effects were expected or observed in these devices due to their low mobility. Present work now centers on the fabrication of similar structures in high-mobility modulation-doped epitaxial layers grown on Si, where we expect resonant tunneling effects to appear.

4.12 Submicrometer-Period Transmission Gratings for X-Ray and Atom-Beam Spectroscopy and Interferometry

Sponsor

Joint Services Electronics Program
Contract DAAL03-89-C-0001
Contract DAAL03-92-C-0001

Project Staff

James M. Carter, Daniel B. Olster, Dr. Mark L. Schattenburg, Professor Henry I. Smith

Transmission gratings with periods of 100-1000 nm are finding increasing utility in applications such as x-ray, vacuum-ultraviolet, and atom- beam spectroscopy and interferometry. Over 20 laboratories around the world depend on MIT-supplied gratings in their work. For x-ray and UV spectroscopy, gratings are made of gold and have periods of 100-1000 nm, and thicknesses ranging from 100-1000 nm. They are most commonly used for spectroscopy of the x-ray emission from high-temperature plasmas. Transmission gratings are supported on thin (1 μm) polyimide membranes or made self supporting ("free standing") by the addition of crossing struts (mesh). (For short x-ray wavelengths membrane support is desired, while for the long wavelengths a mesh support is preferred in order to increase efficiency.) Fabrication is generally performed by holographic lithography, x-ray lithography and electroplating. Progress in this area tends to focus on improving the yield and flexibility of the fabrication procedures.

Another application is the diffraction of neutral sodium beams (de Broglie-wavelength ~17 pm) by mesh-supported gratings. Professor Pritchard's group at MIT has clearly demonstrated atomic diffraction and interference. Because good spatial coherence (low distortion) of the grating is critical to ensure measurable interference of the beams, efforts are concentrated on the use of holographic lithography and the reactive-ion etching of free-standing gratings in low stress and high stiffness materials such as silicon nitride. Results are shown in figure 16.

4.13 High-Dispersion, High Efficiency Transmission Gratings for Astrophysical X-Ray Spectroscopy

Sponsor

National Aeronautics and Space Administration
Contract NAS8-36748

Project Staff

Professor Claude R. Canizares, Robert C. Fleming, Dr. Mark L. Schattenburg, Professor Henry I. Smith

This work involves a collaboration between the Center for Space Research and the Submicron Structures Laboratory (SSL), providing transmission gratings for the Advanced X-ray Astrophysics Facility (AXAF) x-ray telescope, currently scheduled for launch in 1998. Many hundreds of low-distortion, large area transmission gratings of 200 nm period (gold) and 600 nm period (silver) are required. These will provide high resolution x-ray spectroscopy of astrophysical sources in the 100 eV to 10 keV band.

Because of the requirements of low distortion, high yield, and manufacturability, a fabrication procedure involving the replication of x-ray masks has been selected. Masks are made of high-stiffness silicon nitride membranes to eliminate distortion, and patterned using a process involving holographic lithography, reactive-ion etching, and electroplating. The masks are then replicated using soft x-rays (1-1.5 nm) and the resulting patterns electroplated with gold or silver. An etching step then yields membrane-supported gratings suitable for space use. Flight prototype gratings have been fabricated and continue to undergo space-worthiness tests. Progress in this area tends

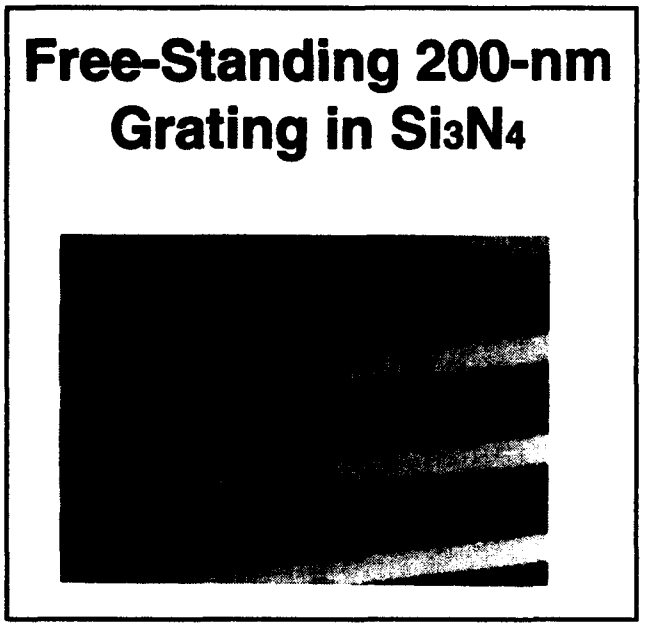


Figure 16. Scanning electron micrograph of free-standing Si_3N_4 grating fabricated for use in an atom inteferometer.

to focus on increasing the yield and flexibility of the fabrication procedures, and the perfection of various mask and grating evaluation tests.

4.14 Submicron-Thickness X-Ray Window Technology

Sponsor

National Aeronautics and Space Administration
Grant NAGW-2003
Contract NAS8-36748

Project Staff

Robert C. Fleming, Seppo Nenonen, Dr. Mark L. Schattenburg, Professor Henry I. Smith

We have been investigating various schemes for fabricating leak-free, large-area, ultrathin membranes to serve as vacuum isolation windows for the transmission of x-rays. Applications include gas-filled x-ray detector windows and high-vacuum isolation windows for x-ray lithography. Current window technology uses relatively thick beryllium windows which are opaque to x-ray with wavelengths in the 0.5 - 1.5 nm band. However, this band is very useful for x-ray detector and x-ray lithography applications. Current efforts seek to perfect large-area polyimide windows which have a 1.0 micron thickness. When combined with tungsten or nickel meshes, these have been made leak free to the limit of He leak detector technology. Woven tungsten support meshes are used, and also advanced nickel meshes made by deep-etch x-ray lithography (so-called LIGA process), in collaboration with the MicroParts company in Germany. Future efforts will seek to reduce the membrane thickness still further and also experiment with silicon nitride membranes which promise to be leak free and also bakeable for high vacuum applications. A silicon nitride isolation window of preliminary design is already being used as a vacuum isolation window in our laboratory x-ray aligner.

4.15 Epitaxy via Surface-Energy-Driven Grain Growth

Sponsor

National Science Foundation
Grant DMR 90-01698

Project Staff

Dr. Paul D. Bristowe, Roland Carel, Jerrold A. Floro, Professor Henry I. Smith, Professor Carl V. Thompson

Epitaxial grain growth (EGG) in polycrystalline thin films on single crystal substrates is being investigated as an alternative process for obtaining and studying epitaxy. EGG can produce smoother ultrathin epitaxial films than those produced in conventional epitaxy and may yield lower defect densities as well. Compared to conventional epitaxy, EGG is a near-equilibrium transformation process that can probe the true energy-minimizing orientation of an overlayer on a single crystal substrate. In film/substrate systems that are weakly interacting or have large lattice mismatch the minimum energy orientation is often *not* that which is obtained during conventional epitaxy.

The mechanism of epitaxial grain growth is simple. The anisotropic film/single crystal substrate interfacial energy selects one film crystallographic orientation as having lowest total free energy. Grains in this orientation have the largest driving force for growth and will predominate as the system coarsens.

We are studying EGG in polycrystalline Ag films on single crystal Ni substrates (or vice-versa). This system is useful for fundamental study because the variation in interfacial energy with Ag/Ni crystallographic orientation can be calculated computationally using well-established embedded atom potentials. Thus, special low energy orientations can be predicted and then searched for in epitaxial grain growth experiments.

Extensive numerical analysis of EGG using mean field coarsening theory has been performed. We have examined model interface energy functions (interface energy versus orientation) and shown which of the specific aspects of the interface energy function are important in promoting bimodal secondary or epitaxial grain growth, i.e., grain growth which is strongly orientation selective.

4.16 GaAs Epitaxy on Sawtooth-patterned Si

Sponsor

Joint Services Electronics Program
Contract DAAL03-89-C-0001
Contract DAAL03-92-C-0001
Spire Corporation

Project Staff

Professor Henry I. Smith, Kenneth Yee, Dr. Khalid Ismail, Nasser Karam[6]

The growth of GaAs on Si offers the possibility of combining high-speed and optoelectronic GaAs devices with Si integrated-circuit technology. Oriented gratings of 200 nm period are fabricated in Si_3N_4 on (100) Si substrates. Anistrotropic etching in KOH is then used to produce sawtooth-profile gratings in the Si. These then serve as substrates for GaAs growth by MOCVD. The dislocation density in the grown GaAs films is orders of magnitude lower than the density in films formed on planar Si substrates.

4.17 Publications

4.17.1 Journal Articles

Anderson, E.H., V. Boegli, M.L. Schattenburg, D.P. Kern, and H.I. Smith. "Metrology of Electron Beam Lithography Systems Using Holographically Produced Reference Samples." *J. Vac. Sci. Technol.* B9: 3606-3611 (1991).

Bagwell, P.F., A. Yen, S.L. Park, D.A. Antoniadis, H.I. Smith, T.P. Orlando, and M.A. Kastner. "Magnetotransport in Multiple Narrow Silicon Inversion Channels Opened Electrostatically into a Two-Dimensional Electron Gas." *Phys. Rev.* B 45: April 1992.

Bagwell, P.F., and A. Kumar. "Comment on Effects of Channel Opening and Disorder on the Conductance of Narrow Wires." Submitted to *Phys. Rev. B*.

Chu, W., H.I. Smith, and M.L. Schattenburg. "Replication of 50nm Linewidth Device Patterns using Proximity X-ray Lithography at Large Gaps." *Appl. Phys. Lett.* 59: 1641-1643 (1991).

Chu, W., S.A. Rishton, M.L. Schattenburg, D.P. Kern, and H.I. Smith. "Fabrication of 50 nm Line-and-Space X-ray Masks in Thick Au Using a 50 keV Electron Beam System." *J. Vac. Sci. Technol.* B 10: 118-121(1992).

Early, K., G.E. Rittenhouse, J.M. Graybeal, and H.I. Smith. "Sub-100- and Sub-10-nm-thick Membranes Anisotropically Etched in (110) Silicon." Submitted to *Appl. Phys. Lett.*

Geis, M.W., H.I. Smith, A. Argoitia, J. Angus, G.H.M. Ma, J.T. Glass, J. Butler, C.J. Robinson, and R. Pryor. "Large-Area Mosaic Diamond Films Approaching Single-Crystal Quality." *Appl. Phys. Lett.* 58: 2485 (1991).

Ismail, K., M. Burkhardt, H.I. Smith, N.H. Karam, and P.A. Sekula-Moise. "Patterning and Characterization of Large-Area Quantum-Wire Arrays." *Appl. Phys. Lett.* 58: 1539-1541 (1991).

Ismail, K., P.F. Bagwell, T.P. Orlando, D.A. Antoniadis, and H.I. Smith. "Quantum Phenonema in Field-Effect-Controlled Semiconductor Nanostructures." *Proc. IEEE* 79: 1106-1116 (1991).

Ismail, K., F. Legoues, N.H. Karam, J. Carter, and H.I. Smith. "High Quality GaAs on Sawtooth-Patterned Si Substrates." *Appl. Phys. Lett.* 59: 2418-2420 (1991).

Karam, N.H., A. Mastrovita, V. Haven, K. Ismail, S. Pennycock, and H.I. Smith. "Patterning and Overgrowth of Nanostructure Quantum Well Wire Arrays by LP-MOVPE." *J. Crystal Growth* 107: 591-597, (1991)

Ku, Y.C., Lee-Peng Ng, R. Carpenter, K. Lu, H.I. Smith, L.E. Haas, and I. Plotnik. "In-Situ Stress Monitoring and Deposition of Zero Stress W for

[6] Spire Corporation.

X-ray Masks." *J. Vac. Sci. Technol.* B9: 3297-3300 (1991).

Kumar, A., and P.F. Bagwell. "Resonant Tunneling in a Quasi-One-Dimensional Wire: Influence of Evanescent Modes." *Phys. Rev. B* 43: 9012-9020 (1991).

Kumar, A., P.F. Bagwell. "Evolution of the Quantized Ballistic Conductance with Increasing Disorder in Narrow Wire Arrays." *J. Phys. Rev.* B 44: 1747-1753 (1991).

Liu, C.T., D.C. Tsui, M. Shayegan, K. Ismail, D.A. Antoniadis, and H.I. Smith. "Guiding-Center-Drift Resonance of Two-Dimensional Electrons in a Grid-Gate Superlattice Potential." *Appl. Phys. Lett.* 58: 2945-2947 (1991).

Moel, A., W. Chu, K. Early, Y.C. Ku, E.E. Moon, M.L. Schattenburg, J.M. Bauer, F. Tsai, F.W. Griffith, L.E. Haas, and H.I. Smith. "Fabrication and Characterization of High-Flatness Mesa-Etched Silicon Nitride X-ray Masks." *J. Vac. Sci. Technol. B* 9: 3287-3291 (1991).

Schattenburg, M.L., C.R. Canizares, D. Dewey, K.A. Flanagan, M.A. Hamnett, A.M. Levine, K.S.K. Lum, R. Manikkalingam, T.H. Markert, and H.I. Smith. "Transmission Grating Spectroscopy and the Advanced X-ray Astrophysics Facility." *Opt. Eng.* 30: 1590-1600 (1991).

Schattenburg, M.L., K. Li, R.T. Shin, J.A. Kong, and H.I. Smith. "Electromagnetic Calculation of Soft-X-ray Diffraction from 0.1 from 0.1 μm Gold Structures." *J. Vac. Sci. Technol. B* 9: 3232-3236 1991.

Smith, H.I., S.D. Hector, M.L. Schattenburg, and E.H. Anderson. "A New Approach to High Fidelity E-Beam Lithography Based on an In-Situ, Global Fiducial Grid." *J. Vac. Sci. Technol. B* 9: 2992-2995 (1991).

Yen, A., H.I. Smith, M.L. Schattenburg, and G.N. Taylor. "An Anti-Reflection Coating for use with PMMA at 193 nm." *J. Electrochem. Scc.* (Feb. 1992).

Yen, A., E.H. Anderson, R.A. Ghanbari, M.L. Schattenburg, and H.I. Smith. "An Achromatic Holographic Configuration for 100 nm Period Lithography." *Appl. Opt.* Forthcoming.

Yen, A., M.L. Schattenburg, and H.I. Smith. "A Proposed Method for Fabricating 50 nm-period Gratings by Achromatic Holographic Lithography." *Appl. Opt.* Forthcoming.

Zhao, Y., D.C. Tsui, M. Santos, M. Shayegan, R.A. Ghanbari, D.A. Antoniadis, and H.I. Smith. "Magneto-optical Absorption In A Two Dimensional Electron Grid." *Appl. Phys. Lett.* Forthcoming.

4.17.2 Conference Papers

Bagwell, P.F., and A. Kumar. "Evolution of the Quantized Ballistic Conductance with Increasing Disorder in Narrow Wire Arrays." *Bull. Am. Phys. Soc.* 36: 359 (1991).

Chu, W., M.L. Schattenburg, and H.I. Smith. "Low-Stress Gold Electroplating for X-ray Masks." Microcircuit Engineering '91 Conference, Rome, Italy, September 17-19, 1991.

Early, K., M.L. Schattenburg, D.B. Olster, M.I. Shepard, and H.I. Smith. "Diffraction in X-ray Proximity Printing: Comparing Theory and Experiment for Gratings, Lines, and Spaces." Microcircuit Engineering '91 Conference, Rome, Italy, September 17-19, 1991.

Eugster, C.C., J.A. del Alamo, and M.J. Rooks. "Planar Field-Effect Coupled Quantum Wires." Device Research Conference, Boulder, Colorado, June 1991.

Karam, N.H., V. Haven, K. Ismail, F. Legoues, J. Carter, and H.I. Smith. "A New Approach for Low Defect Density GaAs on Patterned Si Substrates by MOCVD." Materials Research Society Spring Meeting, Anaheim, California, April 1991.

Kumar, A. "Self-Consistent Calculations on Confined Electrons in Three- Dimensional Geometries." Ninth Electronic Properties of 2-D Systems Conference, Nara, Japan, July 8-12, 1991, to be published in *Surf. Sci.*

Liu, C.T., D.C. Tsui, M. Shayegan, K. Ismail, D.A. Antoniadis, and H.I. Smith. "Observation of Landau Level Splitting in Two-Dimensional Lateral Surface Superlattices." 20th International Conference on the Physics of Semiconductors, Thessaloniki, Greece, August 6-10, 1990.

Markert, T., M.L. Schattenburg, T. Isobe, J. Bauer, C. Canizares, J. O'Connor, J. Porter, and H.I. Smith. "Investigations of Materials for Ultra-Thin Window X-ray Detectors." Presented at the 177th Meeting of the American Astronomical Society, Philadelphia, Pennsylvania, January 13-17, 1991.

Markert, T.H., J.M. Bauer, C.R. Canizares, T. Isobe, S. Nenonen, O'Connor, J., M.L. Schattenburg, K.A. Flanagan, M.V. Zombeck. "Proportional Counter Windows for the Bragg Crystal Spectrometer on AXAF." SPIE Conference on EUV, X-ray and Gamma Instruments for Astronomy II, July 24-26, 1991.

Park, S.L., P.F. Bagwell, A. Yen, D.A. Antoniadis, H.I. Smith, T.P. Orlando, and M.A. Kastner. "Magnetotransport in Multiple Narrow Si Inversion Channels Opened Electrostatically Into a Two-Dimensional Electron Gas." *Bull. Am. Phys. Soc.* 36: 360 (1991).

Rittenhouse, G., H.I. Smith, J.M. Graybeal, B. Meyerson. "A Novel Structure for a Three-Terminal Superconducting Resonant Tunneling Device." Presented at the March Meeting of the American Physical Society. *Bull. Am. Phys. Soc.* (1991).

Schattenburg, M.L., and H.I. Smith. "X-ray Nanolithography—the Clearest Path to 0.1 and sub-0.1 μm ULSI." Presented at the 1991 International MicroProcess Conference, Kanazawa, Japan, July 15-18, 1991

Schattenburg, M.L., K. Li, R.T. Shin, J.A. Kong, and H.I. Smith. "Calculation of Soft X-ray Diffraction from Nanometer-Scale Gold Structures Using a Finite-Element Time-Domain Method." Progress in Electromagnetics Research Symposium, Boston, Massachusetts, July 1991.

Smith, H.I., and M.L. Schattenburg. "Lithography for Manufacturing at 0.25 Micrometer and Below." Presented at International School of Materials Science and Technology, A NATO Advanced Study Institute, Erice-Sicily, July 1-13, 1991. *Semiconductor Materials and Processing Technology.* Ed. J.M. Poate. Dordrecht, The Netherlands: Kluwer Academic Publishers, 1992.

Smith, H.I., and M.L. Schattenburg. "Proximity X-ray Nanolithography." Optical Society Meeting, Monterey, California, Optical Society of America, *OSA Proceedings on Soft X-ray Projection Lithography* 12: 148-149 (1991).

Toriumi, A., K. Ismail, M. Burkhardt, D.A. Antoniadis, and H.I. Smith. "Resonant Magneto-Conductance in a Two-Dimensional Lateral-Surface-Superlattice." 20th International Conference on the Physics of Semiconductors, Thessaloniki, Greece, August 6-10, 1990.

Yen, A., R.A. Ghanbari, Y.-C. Ku, W. Chu, M.L. Schattenburg, J.M. Carter, and H.I. Smith. "X-ray Masks with Large-Area 100 nm Period Gratings for Quantum-Effect Device Applications." *Microelectronic Eng.* 13: 271-274 (1991).

Zhao, Y., D.C. Tsui, S.J. Allen, K. Ismail, H.I. Smith, and D.A. Antoniadis. "Spectroscopy of 2-Deg in a Grid Gate Patterned Heterostructure." Presented at the March Meeting of the American Physical Society, *Bull. Am. Phys. Soc.* (1991).

4.17.3 Theses

Early, K.R. *Experimental Characterization and Physical Modeling of Resolution Limits in Proximity Printing X-ray Lithography.* Ph.D. diss., Dept. of Electr. Eng. and Comput. Sci., MIT, 1991.

Ku, Y.-C. *Fabrication of Distortion Free X-ray Masks using Low Stress Tungsten.* Ph.D. diss., Dept. of Electr. Eng. and Comput. Sci., MIT, 1991.

Yen, A. *Fabrication of Large-Area 100 nm-Period Gratings using Achromatic Holographic Lithography.* Ph.D. diss., Dept. of Electr. Eng. and Comput. Sci., MIT, 1991.

Section 3 Optics and Devices

Chapter 1 Optics and Quantum Electronics

Chapter 2 Optical Propagation and Communication

Chapter 3 High Frequency (> 100 GHz) Electronic Devices

Chapter 1. Optics and Quantum Electronics

Academic and Research Staff

Professor Hermann A. Haus, Professor Erich P. Ippen, Professor James G. Fujimoto, Professor Peter L. Hagelstein, Dr. Santanu Basu, Dr. Joseph A. Izatt

Visiting Scientists and Research Affiliates

Dr. Lucio H. Acioli, Dr. Guiseppe Gabetta, Dr. Yuzo Hirayama, Dr. Franz X. Kärtner, Dr. Charles P. Lin, Dr. Antonio Mecozzi, Dr. Kazunori Naganuma, Dr. Masataka Shirasaki

Graduate Students

Keren Bergman, John Paul Braud, Jerry C. Chen, Isaac L. Chuang, Jay N. Damask, Christopher R. Doerr, David J. Dougherty, James G. Goodberlet, Katherine L. Hall, Michael R. Hee, David Huang, Charles T. Hultgren, Janice M. Huxley, Sumanth Kaushik, Farzana I. Khatri, Joseph M. Jacobson, Yinchieh Lai, Gadi Lenz, John D. Moores, Ann W. Morgenthaler, Martin H. Muendel, Lynn E. Nelson, Janet L. Pan, Malini Ramaswamy, Kohichi R. Tamura, Morrison Ulman

Undergraduate Students

Michele M. Bierbaum, Irfan U. Chaudhary, Stephen Y. Hon

Technical and Support Staff

Mary C. Aldridge, Donna L. Gale, Cynthia Y. Kopf, Lisbeth N. Lauritzen

1.1 Additive Pulse Modelocking

Sponsors

Joint Services Electronics Program
Contract DAAL03-89-C-0001
Contract DAAL03-92-C-0001
U.S. Air Force - Office of Scientific Research
Contract F49620-91-C-0091

Project Staff

Professor Hermann A. Haus, Professor Erich P. Ippen, Dr. Antonio Mecozzi, Jerry C. Chen, Farzana I. Khatri, John D. Moores, Stephen Y. Hon

Additive Pulse Modelocking (APM) is a technique of mode locking that simulates a fast saturable absorber via nonlinear interferometric action using a Kerr medium. Often this medium is a fiber placed in an auxiliary cavity, but the Kerr effect may be produced in the components internal to the main cavity of the laser. The Kerr Lens Modelocking pioneered by Coherent, produces equivalent saturable absorber action by self focusing. A general theory has been developed for both kinds of systems.[1] Its main results are:

1. An analytic treatment of the modelocking process in the presence of self-phase modulation and group velocity dispersion;
2. Criteria for the stability of the modelocked pulses;
3. The condition for self starting of the pulses and the explanation of a power threshold for mode locking.[2]

The theory is helpful in pointing the way to the generation of shorter pulses with lower fluctuations.

In conjunction with this theory, an analysis of noise in modelocked systems has been carried out.[3] This analysis provides an explanation of the observed spectra of the detector current illumi-

---

[1] H.A. Haus, J.G. Fujimoto, and E.P. Ippen, "Structures for Additive Pulse Modelocking," *J. Opt. Soc. Am. B* 8: 2068-2076 (1991).

[2] H.A. Haus and E.P. Ippen, "Self Starting of Passively Modelocked Lasers," *Opt. Lett.* 16: 1331-1333 (1991).

[3] S. Hon, K. Bergman, A. Mecozzi, and H.A. Haus, "Noise Spectra of Modelocked Laser Pulses," submitted for presentation at CLEO '92, Anaheim, CA (1992).

nated by modelocked pulses observed by many researchers. Stephen Hon has performed extensive measurements of three different laser systems (actively modelocked Nd:YAG, soliton laser, APM Ti:Sapphire laser). We have shown theoretically that the current spectrum reveals not only the amplitude and timing jitter, as heretofore assumed, but also gives information on the correlation between the two. These experiments have been an important guide to the theory. Conversely, the newly developed theory is now being applied to extract full information from the detector current spectra. The fluctuations that are not observable from the current spectrum of direct detection are the phase fluctuations (that give rise to the well-known Schawlow-Townes linewidth) and the carrier frequency fluctuations.

The analysis has also been extended to allow for the inclusion of slow, as well as fast, absorber effects. Such a combination may be used to advantage in lasers where pulse initiation is a problem. There is a trade-off in the range of gain and dispersion over which steady-state stability can be achieved.

1.2 Ultrashort Pulse Fiber Laser

Sponsors

Charles S. Draper Laboratories
Contract DL-H-441629
Joint Services Electronics Program
Contract DAAL03-89-C-0001
Contract DAAL03-92-C-0001
U.S. Air Force - Office of Scientific Research
Contract F49620-91-C-0091

Project Staff

Professor Hermann A. Haus, Professor Erich P. Ippen, Janice M. Huxley, Lynn E. Nelson, Kohichi R. Tamura

High bit-rate optical communication networks and ultrafast optical signal processing systems will require compact, chirp-free picosecond pulse sources. Erbium-doped fiber lasers are prime candidates because of their compatibility with transmission fibers, their operation at 1.5 μm, and their amenability to diode pumping. The nonlinear refractive index effects in these fibers also make them attractive lasers for additive pulse modelocking (APM). We have therefore constructed an erbium fiber laser with intent to study how APM may be implemented in an all-fiber device and to optimize ultrashort pulse generation.

In a fiber, the nonlinear interferometric action necessary for APM is most easily achieved through intensity dependent polarization rotation. Thus our laser uses fiber polarizers and polarization controllers in a fiber ring with an erbium amplifying section. Fiber couplers to the ring facilitate pumping (with a Ti:sapphire laser for the time being) and output coupling. Short pulse operation has already been obtained and studied under several operating conditions. Pulse spectra indicate durations as short as 300 fs. Autocorrelation measurements and variations with pumping level indicate that the output consists of strings of pulses quantized by soliton effects. A computer model has been developed that extends our APM theory to cases like this in which pulse shaping effects per round trip are large and cannot be treated perturbationally. This model is now being used to map regions of stability and single pulse operation.

1.3 Long Distance Fiber Communications

Sponsor

MIT Lincoln Laboratory

Project Staff

Professor Hermann A. Haus, Dr. Antonio Mecozzi, Yinchieh Lai, John D. Moores

In 1986, J.P. Gordon and Professor Hermann A. Haus published a paper[4] pointing out that transatlantic transmission using solitons would suffer from timing jitter of the pulses caused by frequency jitter induced by the spontaneous emission of the amplifier stages. This effect, now called the Gordon-Haus effect, has had an important influence on the planning of the next transatlantic cable of AT&T which will be laid in 1995. This cable will not use solitons, but will operate at (or near) the zero dispersion wavelength of the fiber. It is designed for 5 Gbit transmission and so that future Wavelength Division Multiplexing will not be permitted, at least not when using similar channels shifted in frequency. The reason for this design is that the dynamic range of the input pulse stream of the soliton version of the system is limited by two effects. On one hand, the pulses have to be energetic enough

[4] J.P. Gordon and H.A. Haus, "Random Walk of Coherently Amplified Solitons in Optical Fiber Transmission," *Opt. Lett.* 11: 665-667 (1986).

to overcome detector shot noise. On the other hand, if too powerful, the Gordon-Haus effect produces excessive timing jitter.

We have come up with a means of combatting the Gordon-Haus effect using periodically spaced filters.[5] Kodama and Hasegawa at AT&T Bell Laboratories have proposed this scheme independently, and Mollenhauer has tested it. Because the information was company confidential, we were not aware of it until recently. As of this date (12/19/91), their paper had not been published. The scheme permits wavelength multiplexing because the filter to be used could be a Fabry-Perot with a characteristic period in frequency.

1.4 Squeezing

Sponsors

Charles S. Draper Laboratories, Inc.
Contract DL-H-418478
Fujitsu Laboratories
National Science Foundation
Grant ECS 90-12787

Project Staff

Professor Hermann A. Haus, Keren Bergman, Christopher R. Doerr, Dr. Masataka Shirasaki, Dr. Franz X. Kärtner

The successful squeezing experiments of last year have been continued. It should be reemphasized that our squeezing scheme in a fiber ring[6] can save, in principle, all the pump power for local oscillator power, and hence is superior to schemes that "waste" the pump (such as those using parametric amplification).

Figure 1 shows the experimental setup that has been used to observe both reduced and increased shot noise as a function of phase between local oscillator (derived from the pulse used for squeezing) and the squeezed radiation. The upper trace in figure 2 shows the calibrated shot noise level, the lower trace shows the noise as a function of mirror position that changes the phase between the L.O. and the squeezed light. The center frequency is 40 kHz, the bandwidth is 2 kHz. Although this may not be the best way to determine the degree of squeezing (5 dB below shot noise), it is a rather spectacular display of squeezing and antisqueezing.

We have measured the noise of the laser oscillator (part of the motivation for the study of mode-locked laser noise described above was motivated by this investigation) and found that the mode locked Nd:YAG laser produces noise only 20 dB above shot noise at frequencies of 40 kHz and higher (and away from the line spectrum of pulse repetition periodicity). Our balanced detector is designed to suppress 30 dB or more of the local oscillator noise.

We have also initiated a thorough study of the Guided Acoustic Wave (GAWBs) noise observed by the IBM group. We have found that the contributions of GAWBS are not large enough to have affected our noise spectra in the low frequency regime (40-80 kHz).

We have succeeded in stabilizing the phase between the local oscillator and the squeezed radiation to achieve a constant noise reduction of 5 dB below shot noise. In a future experiment, this system will be employed to demonstrate sub shot noise interferometric detection in a future experiment.

We envisage that squeezing will eventually be used in fiber gyros that would operate below the shot noise level. We have studied the problem of the nonlinearity of the Sagnac fiber and found that, to take advantage of the squeezed radiation noise reduction, the Sagnac loop must have reduced nonlinearity.[7]

1.5 Integrated Optics Components

Sponsors

National Science Foundation
Grant ECS 90-12787
National Center for Integrated Photonics

---

[5] A. Mecozzi, J.D. Moores, H.A. Haus, and Y. Lai, "Soliton Transmission Control," *Opt. Lett.* 16: 1841-1843 (1991).

[6] M. Shirasaki and H.A. Haus, "Squeezing of Pulses in a Nonlinear Interferometer," *J. Opt. Soc. Am. B* 7: 30-34 (1990).

[7] H.A. Haus, K. Bergman, and Y. Lai, "Fiber Gyro With Squeezed Radiation," *J. Opt. Soc. Am. B* 8: 1952-1957 (1991).

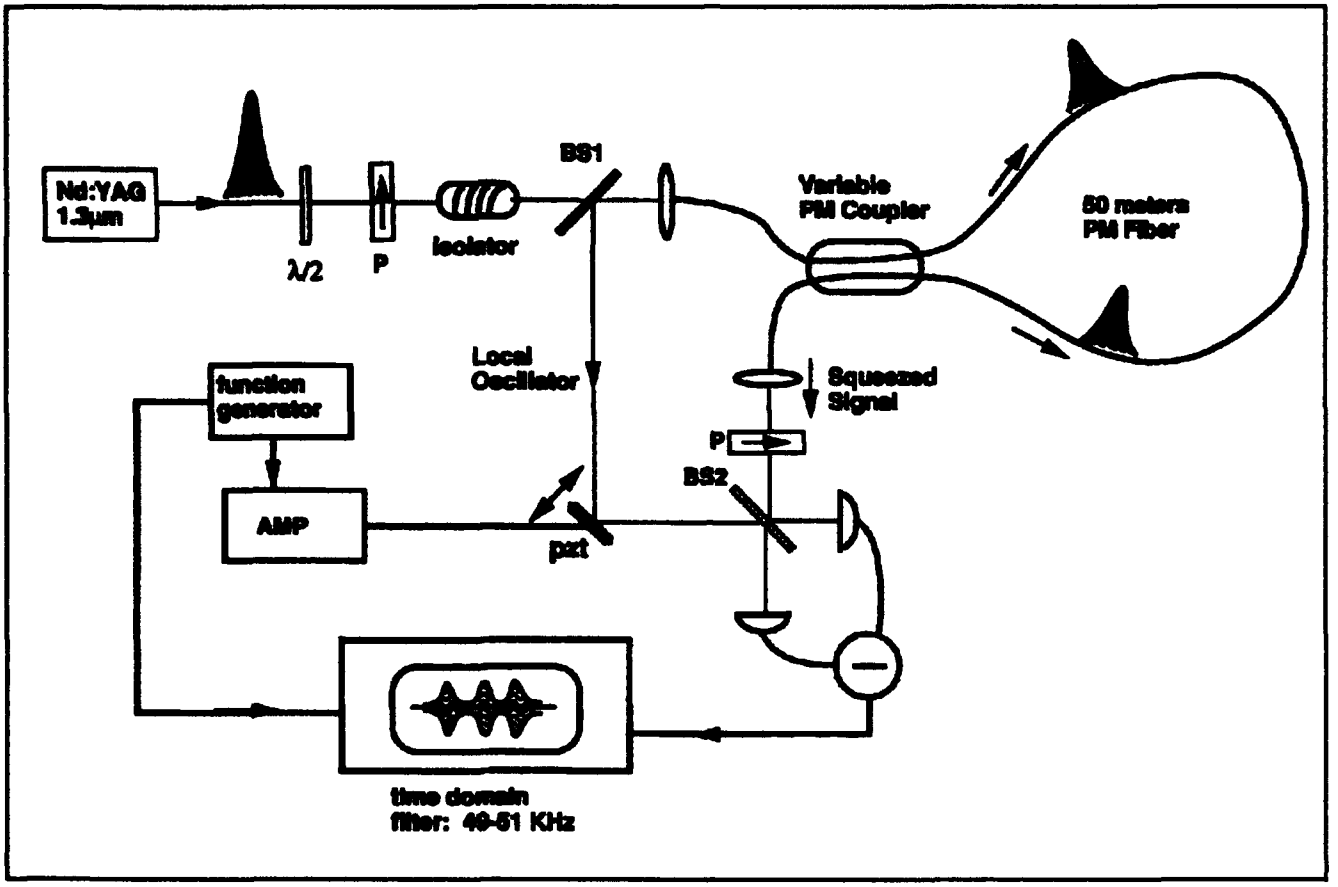


Figure 1.

Project Staff

Professor Hermann A. Haus, Jay N. Damask, Professor Henry I. Smith, Vincent V. Wong

Fiber communications using wavelength division multiplexing requires channel dropping filters to avoid the power loss due to "broadcasting" of all channels. No proposal existed for a cascadable channel dropping filter that would be narrow-band enough to accommodate channels of bandwidth corresponding to Gbit transmission rates. We have proposed a channel dropping filter of a new design,[8] based on the quarter wave shifted Distributed Feedback Structure patented by H.A. Haus and C.V Shank in 1976. The structure is already in wide use for frequency stable DFB lasers. In this novel application, the structure is side-coupled to the "transmission bus" to affect only the channel to be dropped. Various forms of the design have been laid out, one of which employs an active layer for amplification and reinjects the dropped signal so that it can be detected "downstream."

We have begun the fabrication of a prototype device in collaboration with Professor Henry I. Smith of the MIT Submicron Structures Laboratory. In conjunction with the tuning scheme pursued in collaboration with Professor Clifton G. Fonstad described below, the channel dropping filters could be made tunable.

1.6 Tunable Lasers

Sponsor

National Center for Integrated Photonics

Project Staff

Professor Hermann A. Haus, Professor Clifton G. Fonstad, Paul S. Martin

Tunable lasers have been constructed successfully with Bragg Reflectors whose optical index is changed by current injection. The laser section of the structure itself is maintained at constant gain

[8] H.A. Haus and Y. Lai, "Narrow-band Optical Channel Dropping Filter," *IEEE J. Lightwave Technol.* 10: 57-62 (1992).

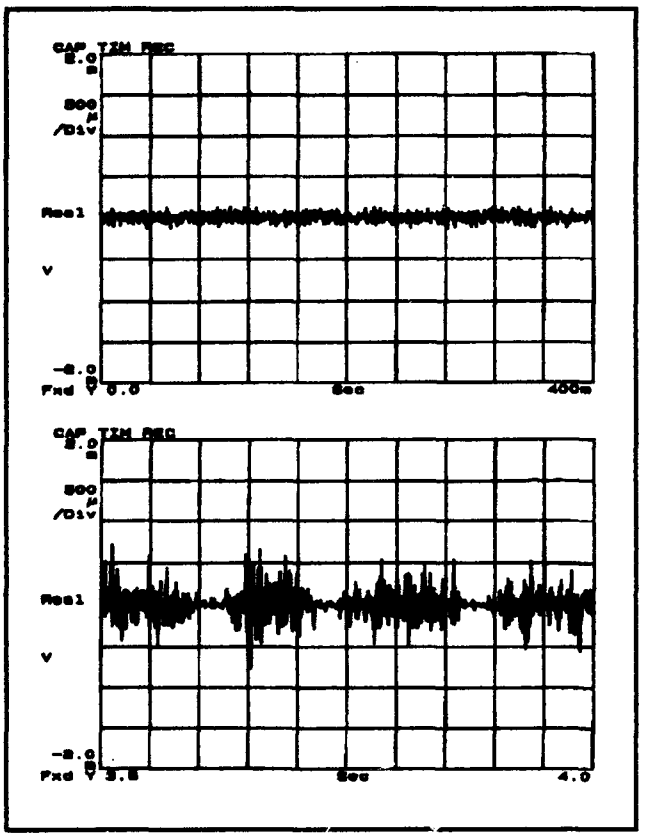


Figure 2.

by keeping its injection current relatively constant. Such structures have achieved wide tuning ranges, but not in a continuous manner.

We are pursuing an alternate approach that relies on the ability of controlling the injection currents into two quantum wells, one on top of the other, by contacts properly fabricated by ion implantation. The two quantum wells are different and have transitions at different frequencies. The respective gain peaks are displaced in frequency, and, along with them, the index characteristics. By controlling the currents injected into the two quantum wells separately, one can control the gain and index independently. Such structures would be ideal for tuning of monolythic resonators at constant gain.

1.7 Gain Dynamics in Semiconductor Amplifiers

Sponsors

Joint Services Electronics Program
Contract DAAL03-89-C-0001
Contract DAAL03-92-C-0001
National Science Foundation
Grant EET 88-15834
U.S. Air Force - Office of Scientific Research
Contract F49620-91-C-0091

Project Staff

Professor Erich P. Ippen, Katherine L. Hall, Gadi Lenz, Dr. Kazunori Naganuma

The potential application of semiconductor amplifiers to wideband communication networks and integrated photonic circuits motivates our studies of these devices. We use femtosecond optical pulses to probe propagation effects in amplifier structures, characterize optical nonlinearities in the gain, and observe fundamental ultrafast carrier dynamics in the semiconductor active layers.

During the past year we have performed the first femtosecond time-domain measurements of group velocity dispersion (GVD) in diode lasers at 1.5 μm.[9] The effects of GVD are two-fold: (1) it can distort pulses being transmitted and amplified, and (2) it limits the temporal resolution, or frequency bandwidth, of nonlinear optical interactions. Our measurements, in both bulk and multiple-quantum-well (MQW) samples yield values for $\lambda d^2 n_{eff}/d\lambda^2$ in the range -0.63 to $0.95\ \mu m^{-1}$ and indicate that intrinsic material dispersion is the dominant factor. In addition, we discovered differences in group velocity between TE and TM modes on the order of 200 fs/mm. These must be accounted for in studies of anisotropic nonlinearities.

We have also demonstrated a new technique for femtosecond pump-probe measurement that makes it possible to use parallel-polarized pump and probe beams even in strictly collinear geometries.[10] The method makes use of acousto-optic frequency shifting and relies on heterodyne detection to distinguish between pump and probe pulses. In experiments with bulk (V-groove) diode amplifiers, we have demonstrated the obser-

[9] K.L. Hall, G. Lenz, and E.P Ippen, "Femtosecond Time Domain Measurements of Group Velocity Dispersion in Diode Lasers at 1.5 μm," *J. Lightwave Tech.*, forthcoming, May 1992.

[10] K.L. Hall, G. Lenz, E.P. Ippen, and G. Raybon, "Heterodyne Pump-Probe Technique for Time-Domain Studies of Optical Nonlinearities in Waveguides," submitted to *Opt. Lett.*

vation of differences due to nonlinear as well as linear anisotropy. Preliminary results have been obtained on strained-layer quantum-well devices which have highly anisotropic gain.

1.8 Ultrafast Optical Kerr Effect in Active Waveguides

Sponsors

National Center for Integrated Photonics
National Science Foundation
Grant EET 88-15834
U.S. Air Force - Office of Scientific Research
Contract F49620-91-C-0091

Project Staff

Professor Erich P. Ippen, David J. Dougherty, Charles T. Hultgren

Active optical waveguides offer interesting possibilities for performing nonlinear functions in photonic circuits. By varying the injected carrier density one can change not only the linear components of gain and index of refraction but also the nonlinear ones. A particularly interesting regime of operation is that near the point of nonlinear transparency. At that point, an optical pulse traveling through the waveguide neither creates carriers by absorption nor removes carriers by stimulated emission. There is no long-lived change. Yet the optical wavelength is above bandgap and the density of carriers in the medium is high.

In previous studies of gain dynamics in AlGaAs lasers near this point, we discovered a large transient gain nonlinearity which we identified with nonequilibrium carrier heating. The initial purpose of the work described here was to investigate the index of refraction dynamic associated with this gain nonlinearity. We have done so,[11] using a time-division interferometric technique originally demonstrated by Professor Fujimoto's group in passive guides. With this technique we have observed the predicted index dynamic in channeled-substrate planar (CSP) AlGaAs diode lasers (Hitachi HLP 1400) biased just below threshold. The dynamic is identified by its approximately 1.7 ps recovery time and positive sign that is consistent with a theoretical calculation for nonequilibrium heating. To our surprise, however, these experiments have also uncovered a faster and even larger index change. We attribute this new component to an above-band optical Stark shift.[12]

Our experiments were performed with orthogonally polarized pump and probe, so that what we measure is $n_{2\perp}$. The ultrafast Stark-like component has a negative sign, as do below-bandgap values, but an enhanced value of about -5×10^{-12}cm^2/W. We believe that the resonant enhancement in the active region has contributions from filled states below the laser photon energy as well as from filled states above. A theoretical description of this possibility has now been put forward by Sheik-Bahai.[13] Such an effect may have application to ultrafast optical switching. It can also provide a new means for studying femtosecond carrier relaxation phenomena in semiconductors.

1.9 Coherent Phonons in Electronic Materials

Sponsors

Joint Services Electronics Program
Contract DAAL03-89-C-0001
Contract DAAL03-92-C-0001
U.S. Air Force - Office of Scientific Research
Contract F49620-91-C-0091

Project Staff

Professor Erich P. Ippen, Tak K. Cheng, Siegfried B. Fleischer

With optical pulses shorter than 100 fs it has become possible to excite and observe in the time domain the coherent oscillation of optical phonons with frequencies up to 10 THz (333 cm^{-1}). In collaboration with Professor Dresselhaus' group we have been investigating the application of this possibility to electronic materials. Recently, we have reported that excitation of such phonons is

---

[11] C.T. Hultgren and E.P. Ippen, "Ultrafast Refractive Index Dynamics in AlGaAs Diode Laser Amplifiers," *Appl. Phys. Lett.* 59: 635 (1991).

[12] C.T. Hultgren and E.P. Ippen, "Ultrafast Optical Kerr Effect in Active Semiconductor Waveguides," *Proceedings of the O.S.A. Topical Meeting on Nonlinear Guided-Wave Phenomena,* paper TuB2, Cambridge, England, September 1991.

[13] M. Sheik-Bahai and E.W. Van Stryland, "Theory of Ultrafast Nonlinear Refraction in Semiconductor Lasers," *Proceedings of the O.S.A. Annual Meeting,* San Jose, California, November 1991, paper TuB4, post-deadline paper.

particularly efficient in certain semimetals and semiconductors (e.g., Bi, Sb, Te and Ti_2O_3).[14]

For our experiments we used pulses from a dispersion-balanced colliding-pulse-modelocked (CPM) dye laser, focused to a 2 μm spot. Reflectivity oscillations were observed in these materials with amplitudes of several percent. That is several orders of magnitude larger than can be expected from impulsive stimulated Raman scattering. In each material only one oscillation frequency was observed, the one corresponding to the A_{1g} mode; and the phase of the amplitude was cosinusoidal with respect to excitation at t=0. All of these facts are inconsistent with a stimulated Raman mechanism. To explain them, we have proposed a new theory, dubbed displacive excitation of coherent phonons (DECP).[15] It attributes behavior to a rapid displacement of the ion equilibrium coordinates by the electronic excitation.

The temperature dependence of this effect in Ti_2O_3 is particularly interesting. In the range 300 K-570 K dramatic changes take place in Ti_2O_3 with respect to both its lattice and electronic properties, turning it from a semiconductor to a metal. In our femtosecond experiments, we have observed temperature dependent changes in the optical phonon frequency and electronic relaxation rate that are consistent with this transition. On a dynamic basis this may mean that the bandgap and conductivity of the material are being modulated at the 6 THz phonon frequency. Work in progress will test this hypothesis. Higher excitation levels may also make it possible to observe anharmonic lattice dynamics. In recent preliminary experiments with an amplified CPM system we have measured refractive index modulations at the phonon frequency of as much as 15 percent.

1.10 Femtosecond Studies of Superconductivity

Sponsors

Joint Services Electronics Program
Contract DAAL03-89-C-0001
Contract DAAL03-92-C-0001
U.S. Air Force - Office of Scientific Research
Contract F49620-91-C-0091

Project Staff

Professor Erich P. Ippen, Tak K. Cheng, Siegfried B. Fleischer

Femtosecond optical experiments that monitor the rate of hot electron cooling in materials provide an estimate of the strength of the electron-phonon interaction. If one is dealing with BCS-like superconductors, and one knows the electron-phonon spectral density, femtosecond data on the cooling rate can be related directly to T_c . We have been successful in making such determinations in a range of metallic superconductors and in some high-T_c materials.[16] Recently, we have performed the first femtosecond pump-probe experiments on C_{60} and two of its intercalants.

Most of the properties of C_{60} and its intercalants can be explained by treating them as rolled up sheets of graphite. For this reason it is surprising that K_3C_{60} has a superconducting transition temperature (18 K) more than an order of magnitude higher than that of the other graphite intercalation compounds. Determining the reason for this difference may help develop a better understanding of the mechanisms leading to high-T_c.

For our experiments, thin films (1000Å) of C_{60}, K_3C_{60}, and K_6C_{60} were deposited on quartz substrates and encapsulated to prevent contamination. Femtosecond dynamics were induced and observed, in reflectivity and transmission at $\lambda = 630$ nm, using pulses from a colliding-pulse-modelocked (CPM) dye laser. We believe we are monitoring carrier cooling rates and have deduced time constants of 9 ps, 0.2 ps and 0.7 ps for the

---

[14] T.K. Cheng, J. Vidal, H.J. Zeiger, G. Dresselhaus, M.S. Dresselhaus, and E.P. Ippen, "Mechanism for Displacive Excitation of Coherent Phonons in Sb, Bi, Te, and Ti_2O_3," *Appl. Phys. Lett.* 59: 1923 (1991).

[15] H.J. Zeiger, J. Vidal, T.K. Cheng, E.P. Ippen, G. Dresselhaus, and M.S. Dresselhaus, "Theory for Displacive Excitation of Coherent Phonons," *Phys. Rev. B* 45: 768 (1992).

[16] S.D. Brorson, A. Kazeroonian, J.S. Moodera, D.W. Face, T.K. Cheng, E.P. Ippen, M.S. Dresselhaus, and G. Dresselhaus, "Femtosecond Room-temperature Measurement of the Electron-phonon Coupling Constant λ in Metallic Superconductors," *Phys. Rev. Lett.* 64: 2172 (1990); S.D. Brorson, A. Kazeroonian, D.W. Face, G.L. Doll, T.K. Cheng, M.S. Dresselhaus, G. Dresselhaus, E.P. Ippen, T. Venkatesan, X.D. Wu, and A. Inam. "Femtosecond Thermomodulation Study of high-T_c," *Solid. State Commun.* 74: 1305 (1990).

three samples, respectively. As might be expected, the superconducting sample has the shortest time constant. But the absolute value of the rate, in the context of the material's phonon spectral density, is surprisingly low for a T_c of 18 K. One possible explanation is that electron-phonon coupling is specific to certain types of phonons. This will be investigated by experiments with different material compositions as well as by more detailed studies of these particular intercalants.

1.11 Femtosecond Pulse Generation in Solid State Lasers

Sponsors

Joint Services Electronics Program
Contract DAAL03-89-C-0001
Contract DAAL03-92-C-0001
National Science Foundation
Grant ECS 85-52701
U.S. Air Force - Office of Scientific Research
Contract F49620-88-C-0089
U.S. Navy - Office of Naval Research
Contract N00014-91-C-0084

Project Staff

Dr. Guiseppe Gabetta, Joseph M. Jacobson, David Huang, Malini Ramaswamy, Professor Hermann A. Haus, Professor Erich P. Ippen, Professor James G. Fujimoto

1.11.1 Introduction

Ultrashort pulse laser technology is of primary importance for the development of high speed optical communication and measurement techniques and for studies of ultrafast phenomena. The principle objectives of our research program are the investigation and development of new ultrashort laser pulse generation and measurement techniques. Special emphasis is placed on studies of solid state ultrashort pulse laser technology. Solid state lasers represent a third generation technology that has several advantages over existing dye-laser technology. Solid state lasers feature lower cost, greater compactness, higher power, and broader tunability. The large gain bandwidths of solid state laser media can support pulse durations in the femtosecond range with wavelength tunability. These features make solid state laser technology a versatile tool for engineering and research applications in ultrafast phenomena.

One of the most promising solid state laser materials that has emerged to date is Ti:Al_2O_3.[17] The Ti:Al_2O_3 laser operates at room temperature, has a high energy storage suitable for high power operation, and a broad gain bandwidth with an extremely wide tuning range from 670 to 1000 nm. These features make it an ideal system for femtosecond pulse generation and spectroscopy.

Recently, we have developed and demonstrated a new ultrashort pulse generation technique known as Additive Pulse Modelocking (APM).[18] Self starting, passive modelocking was demonstrated in Ti:Al_2O_3 and pulse durations of 200 fs were achieved.[19] An APM laser utilizes an external cavity containing a nonlinear element such as an optical fiber to produce a pulse shortening mechanism similar to saturable absorber action. A saturable absorber is a nonlinear element that exhibits greater transmittivity or reflectivity for higher intensities. This nonlinearity produces pulse shortening by enhancing the peak of the pulse compared to the wings.

Our research in modelocked Ti:Al_2O_3 represented the first demonstration of self starting passive Additive Pulse Modelocking. The self-starting APM system represented a significant advancement because it eliminated the need for a high frequency loss modulation element and thus reduced system complexity and cost. We have extended the self-starting APM technique to modelock diode pumped laser systems and have generated 1.7 ps pulses in a Nd:YAG system and 2 ps pulses in a Nd:YLF system.[20]

---

[17] P.F. Moulton, "Spectroscopic and Laser Characteristics of Ti:Al_2O_3," *J. Opt. Soc. Am. B* 3: 125 (1986).

[18] E.P. Ippen, "Additive Pulse Modelocking," *J. Opt. Soc. Am. B* 6: 1736-1745 (1989); J. Goodberlet, J. Wang, J.G. Fujimoto, and P.A. Schulz, "Femtosecond Passive Modelocked Ti:Al_2O_3 Laser with a Nonlinear External Cavity," *Opt. Lett.* 14: 1125 (1989).

[19] J. Goodberlet, J. Wang, J.G. Fujimoto, and P.A. Schulz, "Femtosecond Passive Modelocked Ti:Al_2O_3 Laser with a Nonlinear External Cavity," *Opt. Lett.* 14: 1125 (1989).

[20] J. Goodberlet, J. Jacobson, J.G. Fujimoto, P.A. Schulz, and T.Y. Fan, "Self-starting Additive-pulse Mode-locked Diode-pumped Nd:YAG Laser," *Opt. Lett.* 15: 504-506 (1990).

1.11.2 Femtosecond Generation Using Nonlinear Intracavity Elements

Studies by other investigators have recently demonstrated that a single cavity Ti:Al_2O_3 system can be modelocked without an active modulator, saturable absorber, or nonlinear external cavity.[21] This phenomena was termed self-modelocking. Although these investigations did not elucidate the short pulse generation mechanisms, they demonstrated that a solid state laser could be modelocked solely by intracavity optical nonlinearities.

Solid state femtosecond lasers such as Ti:Al_2O_3 can achieve peak intracavity intensities of 0.5 MW when they are modelocked. These high peak intensities make possible a wide range of new modelocking techniques which utilize intracavity nonlinearities. Saturable absorber action based on all-optical solid state refractive index nonlinearities is of particular interest because of its extremely fast response and recovery times. Our group has pursued this approach further and demonstrated two different types of passive modelocking schemes in Ti:Al_2O_3 using all solid state nonlinear intracavity modulators.[22] These modelocking techniques permit the generation of femtosecond pulse durations and can be extended to a wide range of solid state lasers at different wavelengths. In addition, they represent a significant reduction in cost and system complexity over previous modelocking techniques.

One approach for modelocking uses a nonlinear intracavity element which functions by nonlinear polarization rotation. This device is called a Kerr Polarization Modulator (KPM)[23] and consists of a quarter-wave plate, a focusing lens, an SF11 glass plate, a second quarter-wave plate, and a curved end mirror. The KPM works by generating an elliptical polarization state which undergoes a nonlinear rotation due to the intensity dependent refractive index of the SF11 glass plate. The linear and nonlinear transmission functions of the KPM can be controlled by setting the retardations of the quarter-wave plates. Thus the KPM can be made to have an increasing transmission with increasing intensity and function as a saturable absorber. We have demonstrated this technique for modelocking Ti:Al_2O_3 and achieved pulse durations of 230 fs.

Another approach for modelocking relies on the use of intracavity self focusing. This technique has been termed Kerr Lens Modelocking (KLM),[24] and pulse durations in the 100 fs range have been demonstrated in Ti:Al_2O_3. KLM produces a fast saturable-like action by using self focusing in the laser rod combined with intracavity aperaturing. Research in our group has emphasized developing both a fundamental understanding of the underlying nonlinear processes as well as an approach for engineering these systems. We have introduced a significant simplification in the design of KLM lasers by developing a modular nonlinear intracavity element called a micro-dot mirror.[25]

The end mirror of the laser is substituted with a focusing lens and a mirror with small diameter micro-dots. The mirror is antireflection (AR) coated on the first surface (i.e., the surface that laser beam first encounters) and high reflection (HR) coated on the second surface. The second surface is patterned into an array of HR spots (micro-dots) with varying diameter using microelectronic techniques. Fast saturable absorber action is produced by nonlinear self focusing which produces a smaller spot size for higher intensities. When a pulse is reflected from the micro-dot mirror, the higher intensity peaks of the pulse are reflected more than the lower intensity

---

[21] D.E. Spence, P.N. Kean, and W. Sibbett, "60-fsec Pulse Generation from a Self-mode-locked Ti:sapphire Laser," *Opt. Lett.* 16: 42 (1991).

[22] G. Gabetta, D. Huang, J. Jacobson, M. Ramaswamy, H.A. Haus, E.P. Ippen, and J.G. Fujimoto, "Femtosecond Pulse Generation in Ti:Al_2O_3 Using Nonlinear Intracavity Elements," CLEO 1991, Baltimore, Maryland, 1991; G. Gabetta, D. Huang, J. Jacobson, M. Ramaswamy, H.A. Haus, E.P. Ippen, and J.G. Fujimoto, "Femtosecond Pulse Generation in Ti:Al_2O_3 Using a Microdot Mirror Modelocker," *Opt. Lett.* 16: 1756 (1991).

[23] G. Gabetta, D. Huang, J. Jacobson, M. Ramaswamy, H.A. Haus, E.P. Ippen, and J.G. Fujimoto, "Femtosecond Pulse Generation in Ti:Al_2O_3 Using Nonlinear Intracavity Elements," CLEO 1991, Baltimore, Maryland, 1991.

[24] D.K. Negus, L. Spinelli, N. Goldblatt, and G. Feugnet, "Sub-100 Femtosecond Pulse Generation by Kerr Lens Modelocking in Ti:Al_2O_3," OSA Meeting on Advanced Solid State Lasers, Hilton Head, South Carolina, March 18-20, 1991, postdeadline paper.

[25] G. Gabetta, D. Huang, J. Jacobson, M. Ramaswamy, H.A. Haus, E.P. Ippen, and J.G. Fujimoto, "Femtosecond Pulse Generation in Ti:Al_2O_3 Using a Microdot Mirror Modelocker," *Opt. Lett.* 16: 1756 (1991); D. Huang, M. Ulman, L. Acioli, H.A. Haus, and J.G. Fujimoto, "Self-focusing Induced Saturable Absorber Loss for Laser Mode Locking," *Opt. Lett.*, forthcoming.

wings of the pulse. Thus the micro-dot mirror effectively acts as a fast saturable absorber. We have demonstrated the micro-dot mirror for modelocking the Ti:Al_2O_3 laser and achieved pulse durations of 190 fs.

The modelocking techniques described above have led to a better understanding of passive modelocking mechanisms in solid state laser systems. In the case of self-focusing modelocking, we developed a new theoretical framework which is applicable to the majority of single cavity passively modelocked Ti:Al_2O_3 systems.[26] Theoretical studies are important not only for understanding pulse shortening mechanisms but also for investigating factors which limit pulse duration.

We have developed an analytical description of modelocking which includes fast saturable absorption, self phase modulation, gain bandwidth limiting, and dispersion. A pulse in a modelocked laser can be mathematically described by a single equation similar to the nonlinear Schrodinger equation. We have studied the behavior of pulse characteristics such as pulse duration, chirp, bandwidth, and stability.[26] Our primary findings show that there are two basic operating regimes where stable short pulse generation may be achieved. A laser may be constructed either with positive (normal) or negative (anomalous) dispersion. The pulse shaping mechanisms for these two regimes are different and a laser that has anomalous dispersion will in general produce dramatically shorter pulses than one with normal dispersion. These results suggest design criteria for a wide range of modelocked solid state lasers.

1.11.3 Reduction of Pulse Duration by Dispersion Compensation

One of the key topics of investigation in ultrashort pulse generation is the development of approaches for generating the shortest possible pulse durations. The fundamental limit to pulse duration is determined by the energy-time uncertainty principle which implies that the pulse duration is inversely related to the laser gain bandwidth. The gain bandwidth in Ti:Al_2O_3 is in excess of 100-200 nm[27] and thus pulse durations of a few femtoseconds are theoretically possible. Pulse compression techniques using amplified femtosecond pulses have been demonstrated to achieve pulses as short as 6 fs.[28] However, pulses in the 10 fs range have not as yet been generated directly from a laser. The broad bandwidths associated with these pulse durations allow the use of frequency synthesis techniques to control pulse shape or generate multiple pulse, multiple wavelength pulse trains.[29] Thus, the development of new sources with pulse durations in the 10 fs range would have a major impact on the study of ultrafast phenomena.

One area of investigation in our program is the exploration of the factors which limit the short pulse duration that can be generated. The theoretical considerations discussed above are valid only in systems where the pulses are long enough that dispersive terms higher than those of second order can be neglected. Previous pulse compression studies have demonstrated that higher order dispersion presents an important limitation to pulse duration as pulses become very short and their corresponding frequency bandwidths become broad.[30]

In order to explore and extend the limits of short pulse generation, we have developed and demonstrated a solid state laser with independently adjustable second and third order dispersion. Compensation of dispersion is achieved using a pair of intracavity prisms which are set to produce a net negative second order dispersion in the

---

[26] H.A. Haus, J.G. Fujimoto, and E.P. Ippen, "Structures for Additive Pulse Modelocking," *J. Opt. Soc. Am. B* 8: 2068 (1991).

[27] P.F. Moulton, "Spectroscopic and Laser Characteristics of Ti:Al_2O_3," *J. Opt. Soc. Am. B* 3: 125 (1986).

[28] R.L. Fork, C.H. Brito Cruz, P.C. Becker, and C.V. Shank, "Compression of Optical Pulses to Six Femtoseconds by Using Cubic Phase Compensation," *Opt. Lett.* 12: 483 (1987).

[29] A.M. Weiner, J.P. Heritage, and E.M. Kirschner, "High-resolution Femtosecond Pulse Shaping," *J. Opt. Soc. Am. B* 5: 1563 (1988).

[30] W.J. Tomlinson and W.H. Knox, "Limits of Fiber-grating Optical Pulse Compression," *J. Opt. Soc. Am. B* 4: 1404 (1987); C.H. Brito Cruz, P.C. Becker, R.L. Fork, and C.V. Shank, "Phase Correction of Femtosecond Optical Pulses Using a Combination of Prisms and Gratings," *Opt. Lett.* 13: 123 (1988).

cavity. Intracavity prisms are a standard technique for dispersion compensation which have been applied to a number of solid state and dye lasers. An undesirable consequence of this prism arrangement, however, is that it also introduces a significant negative third order dispersive term which produces pulse distortion effects.[30] In order to explicitly compensate for third order dispersion, we have developed an intracavity thin film element which has positive third order dispersion but zero second order dispersion. Working in collaboration with investigators at CVI Incorporated, we designed and fabricated a thin film Gires-Tourneau Interferometer (GTI) on a mirror substrate. The amount of third order compensation introduced in the laser cavity can be varied by adjustment of the number of times the pulse bounces off each GTI surface during each round trip. This is the first laser that has directly adjustable second and third order dispersion. Using this technique we have generated pulse durations as short as 28 fs directly from a modelocked Ti:Al_2O_3 laser. These pulses are the shortest pulses which have been directly generated from a Ti:Al_2O_3 laser without using pulse compression techniques.[31]

1.12 Studies of Ultrafast Phenomena in Optoelectronic Materials

Sponsors

Joint Services Electronics Program
Contract DAAL03-89-C-0001
Contract DAAL03-92-C-0001
National Science Foundation
Grant ECS 85-52701
U.S. Air Force - Office of Scientific Research
Contract F49620-88-C-0089
U.S. Navy - Office of Naval Research
Grant N00014-91-J-1956

Project Staff

Dr. Lucio H. Acioli, Morrison Ulman, David Huang, Professor Erich P. Ippen, Professor James G. Fujimoto

1.12.1 Four Wave Mixing and Temporal Encoding in Barium Titanate

The idea of optically encoding information in photosensitive materials is relevant to applications in optical signal processing, image processing, and optical logic. Holography is an example of a technique in which three-dimensional spatial information can be recorded in a suitable matrix such as film or photorefractive material. In addition to spatial information, temporal information may also be encoded. The search for systems to record information in the temporal domain have usually been based on the concept of encoding information using inhomogeneously broadening transitions in atomic systems. The techniques most often applied for temporal storage have been variations of photon echo like schemes. Working in collaboration with investigators from Tufts University, we have performed the first studies of femtosecond wave-mixing in $BaTiO_3$ and demonstrated the possibility of using volume holography for recording temporal information.[32]

Photorefractive materials such as $BaTiO_3$, or SBN, have been demonstrated for a wide range of optical phase conjugation and signal processing experiments using continuous wave lasers.[33] These materials exhibit extremely large nonlinearities, and studies can be performed without the need for high laser intensities. However, the response and relaxation times of the photorefractive materials are extremely slow, and thus only recently has the use of such materials under pulsed laser excitation been considered. In order to circumvent the slow material response, our technique records temporal information in the spatial domain using four wave mixing and modulated volume photorefractive gratings.

Experiments were performed using a colliding pulse modelocked, CPM, dye laser source which generated 40 fs pulse durations. Temporal information was encoded using a signal and a reference beam. When the signal and reference beams interact in the photorefractive crystal, they form a

---

[31] J.M. Jacobson, A.G. Jacobson, K. Naganuma, and J.G. Fujimoto, "Generation of 28 fs Pulses from a $TiAl_2O_3$ Laser Using Second and Third Order Intracavity Dispersion Compensation," paper to be presented at CLEO 1992, Anaheim, California.

[32] L.H. Acioli, M. Ulman, E.P. Ippen, J.G. Fujimoto, H. Kong, B.S. Chen, and M. Cronin-Golomb, "Femtosecond Temporal Encoding in Barium Titanate," *Opt. Lett.* 16: 1984 (1991).

[33] M. Cronin-Golomb, B. Fischer, J.O. White, and A. Yariv, "Theory and Applications of Four-wave Mixing in Photorefractive Media," *IEEE J. Quant. Electron.* QE-20: 12 (1984).

standing wave interference pattern where they geometrically overlap. This in turn induces a photorefractive diffraction grating. If the signal beam contains a femtosecond temporal waveform, and the reference beam consists of a single femtosecond pulse, a spatially varying interference pattern will be formed according to the geometrical overlap of the signal and the reference optical waveforms. The temporal information on the signal beam is recorded as a volume grating in the $BaTiO_3$ crystal. The photorefractive gratings have a long persistence time and can be used to store the temporal information. The femtosecond waveform can subsequently be reconstructed by diffracting a femtosecond reference pulse from the stored volume grating.[34] This process is analogous to image reconstruction in holography.

Different phase conjugation geometries were examined including the ring resonator and the two beam coupling geometry. A surprising discovery was that temporal signals are influenced only by material dispersion effects and that pulse durations of 40 fs could be preserved. We have determined that the factors that influence the temporal resolution of the temporal encoding and reconstruction process and developed a simple geometrical model to predict resolution and information storage capacity. Our experiments are closely related to femtosecond holography which uses holographic recording to store transient femtosecond images,[35] except that our results demonstrate an extension of this technique to both the storage and reconstruction of temporal information. Variations of our approach using acousto-optic modulators or other programmable volume diffraction devices could make possible the generation of programmable optical pulses at THz repetition rates.

1.12.2 Self-Focusing and Nonlinear Propagation

Nonlinear optical media with Kerr-like refractive index nonlinearities are relevant to a wide range of applications including all-optical switching, optical modulation, short pulse generation, and short pulse propagation in optical fibers. Self-focusing is a classic nonlinear optical process which has been the subject of investigation for many years. This process has been of interest in previous studies because it poses a limitation to high power laser generation. Recently, however, self-focusing has become technologically important for applications which involve high speed all-optical modulation and short pulse generation. A new technique for modelocking solid state lasers, called Kerr lens modelocking has been developed which uses self focusing to achieve fast saturable absorber action.[36] Pulse durations of less than 100 fs have been achieved in the $Ti:Al_2O_3$ laser. Self-focusing also plays a major role in other short pulse generation techniques such as high power femtosecond pulse compression and continuum generation.[37]

Self-focusing is produced by the intensity dependent nonlinear index of refraction of the material and the spatial intensity variation of the laser beam. The transverse spatial intensity variation of the beam induces a graded index lens in the nonlinear material which, in turn, produces a geometric focusing of the beam. Several researchers have studied this problem in the past, and, with the advent of high intensity femtosecond lasers, a description of the temporal as well as the spatial behavior of self-focusing has become of interest. There is no theory yet that fully describes the problem of nonlinear femtosecond pulse propagation in bulk nonlinear media.

Our investigations of self-focusing are directed toward applications in laser modelocking and short pulse generation. Self-focusing has recently been used to achieve fast saturable absorber mode-

---

[34] L.H. Acioli, M. Ulman, E.P. Ippen, J.G. Fujimoto, H. Kong, B.S. Chen, and M. Cronin-Golomb, "Femtosecond Temporal Encoding in Barium Titanate," *Opt. Lett.* 16: 1984 (1991).

[35] J.A. Valdmanis, H. Chen, E.N. Leith, Y. Chen, and J.L. Lopez, "Three Dimensional Imaging with Femtosecond Optical Pulses," *CLEO Technical Digest* paper CTUA1, 1990, p. 54.

[36] D.K. Negus, L. Spinelli, N. Goldblatt, and G. Feugnet, "Sub-100 Femtosecond Pulse Generation by Kerr Lens Modelocking in $Ti:Al_2O_3$," OSA Meeting on Advanced Solid State Lasers, Hilton Head, South Carolina, March 18-20, 1991, postdeadline paper.

[37] C. Rolland and P.B. Corkum, "Compression of High-power Optical Pulses," *J. Opt. Soc. Am. B* 5: 641 (1988); D.H. Reitze, A.M. Weiner, and D.E. Leaird, "High-power Femtosecond Optical Pulse Compression by Using Spatial Solitons," *Opt. Lett.* 16: 1409 (1991); R.L. Fork, C.V. Shank, C. Hirlimann, R. Yen, and W.J. Tomlinson, "Femtosecond White-light Continuum Pulses," *Opt. Lett.* 8: 1 (1983).

locking in $Ti:Al_2O_3$. This process has been termed Kerr Lens Modelocking and can form the basis for ultrashort pulse generation in a wide range of solid state lasers.[38] As discussed previously, we have developed a modular device called a micro-dot mirror which uses self-focusing to modelock the $Ti:Al_2O_3$ laser.[39] In addition, self-focusing in bulk materials can also be used for short pulse generation and nonlinear measurement. High power pulse compression has been demonstrated using self phase modulation in bulk nonlinear materials.[40] It has also been shown that self-focusing plays a fundamental role in the process of continuum generation with femtosecond pulses and can be used to generate spatial optical solitons for pulse compression.[41] An experimental technique, based on the self-focusing effect and referred to as "z-scan,"[42] has been introduced as a sensitive probe of the magnitude of the nonlinear refractive index.

In order to investigate the use of self-focusing for modelocking and ultrashort pulse propagation, we have developed a new approach to describe the effects of self-focusing in thick (compared to the confocal parameter of the beam) nonlinear media.[43] This method is based on a complex scaling operation applied to the q parameter of a gaussian beam. Self-focusing can be described in the perturbative limit using a compact formulation that is compatible with the *ABCD* matrix description of gaussian beam propagation. Experimental "z-scan" measurements of self-focusing were performed using a femtosecond CPM (colliding pulse modelocked) dye laser and high repetition rate copper vapor laser pumped amplifier.[44] Excellent agreement between the theoretical predictions and the experimental results have been obtained for thick optical glasses (BK7 and fused silica). These theoretical and experimental studies provide a basis for designing and developing Kerr lens modelocking techniques in a wide range of solid state lasers.

We have also studied the effects of self-focusing in continuum generation. Our investigations use variations of the "z-scan" technique[45] in order to quantify the continuum generation process by varying the nonlinear propagation parameters of the beam. Our current studies focus on describing energy transfer to wavelengths different from that of the input beam, the amplitude stability, and the divergence properties of the output beam. An increased understanding of these processes can form the basis for developing new short pulse generation techniques based on nonlinear propagation.

1.12.3 Femtosecond Carrier Dynamics in Semiconductors

The efficient design of high speed electronic and photonic devices requires a detailed understanding of transient carrier dynamics in semiconductor materials. The dynamics of electrons and holes determine fundamental limitations to device speed. For example, intervalley scattering processes affect

---

[38] D.K. Negus, L. Spinelli, N. Goldblatt, and G. Feugnet, "Sub-100 Femtosecond Pulse Generation by Kerr Lens Modelocking in $Ti:Al_2O_3$," OSA Meeting on Advanced Solid State Lasers, Hilton Head, South Carolina, March 18-20, 1991, postdeadline paper.

[39] G. Gabetta, D. Huang, J.M. Jacobson, M. Ramaswamy, E.P. Ippen, and J.G. Fujimoto, "Femtosecond Pulse Generation in $Ti:Al_2O_3$ Using a Microdot Mirror Mode Locker," *Opt. Lett.* 16: 1756 (1991).

[40] C. Rolland and P.B. Corkum, "Compression of High-power Optical Pulses," *J. Opt. Soc. Am. B* 5: 641 (1988); D.H. Reitze, A.M. Weiner, and D.E. Leaird, "High-power Femtosecond Optical Pulse Compression by Using Spatial Solitons," *Opt. Lett.* 16: 1409 (1991).

[41] D.H. Reitze, A.M. Weiner, and D.E. Leaird, "High-power Femtosecond Optical Pulse Compression by Using Spatial Solitons," *Opt. Lett.* 16: 1409 (1991); R.L. Fork, C.V. Shank, C. Hirlimann, R. Yen, and W.J. Tomlinson, "Femtosecond White-light Continuum Pulses," *Opt. Lett.* 8: 1 (1983).

[42] M. Sheik-Bahae, A.A. Said, T. Wei, D.J. Hagan, and E.W. Van Stryland, "Sensitive Measurement of Optical Nonlinearities Using a Single Beam," *IEEE J. Quant. Electron.* 26: 760 (1990).

[43] D. Huang, M. Ulman, L. Acioli, H.A. Haus, and J.G. Fujimoto, "Self-focusing Induced Saturable Absorber Loss for Laser Mode Locking," *Opt. Lett.*, forthcoming.

[44] R.L. Fork, C.V. Shank, C. Hirlimann, R. Yen, and W.J. Tomlinson, "Femtosecond White-light Continuum Pulses," *Opt. Lett.* 8: 1 (1983).

[45] M. Sheik-Bahae, A.A. Said, T. Wei, D.J. Hagan, and E.W. Van Stryland, "Sensitive Measurement of Optical Nonlinearities Using a Single Beam," *IEEE J. Quant. Electron.* 26: 760 (1990).

the high field transport behavior of GaAs devices.[46] Carrier dynamics have been studied with a number of techniques including luminescence spectroscopy and femtosecond absorption saturation.[47] Our research program combines state-of-the-art experimental and theoretical approaches to develop an accurate model for carrier dynamics on an ultrashort timescale. The ultrahigh temporal resolution of femtosecond lasers permits direct measurement of electronic scattering processes that occur in less than 100 femtoseconds. Carrier scattering events may be examined both experimentally and by supercomputer simulation. As a result of these investigations, transient electronic behavior in a variety of important semiconductor materials and quantum structures may be predicted. Recently, we have focused our efforts on intervalley scattering in AlGaAs as a paradigm for investigating femtosecond carrier dynamics.

Our research program is a collaborative effort with Professor C.J. Stanton's solid state theory group at the University of Florida. The objective of the theoretical component of the program is to develop both numerical simulation and analytical methods which establish a correspondence between experimental femtosecond transient absorption saturation results and theoretical models. The problem of investigating transient carrier dynamics in III-V semiconductors is extremely complicated because of the large number of scattering processes. Thus, advanced theoretical techniques such as Ensemble Monte Carlo theory are necessary to accurately interpret experimental results. A full zone, 30 band, empirical k • p procedure is used to determine the relevant electronic bandstructure. A Monte Carlo simulation of 40,000 electrons and holes tracks the time development of the electron and hole distribution functions. Finally, the differential transmission is calculated and compared directly to the results of femtosecond pump-probe experiments.[48] In this way, fundamental material parameters such as deformation potential constants and carrier-carrier scattering rates may be determined. An analytic discretization of the Boltzmann equation combined with a rate equation approach has also been developed to provide intuitive insight into the transient carrier relaxation process. This interdisciplinary approach has already shown that collisional broadening and femtosecond hole redistribution must be included in the theory in order to match the experimental results. We are now investigating the role of carrier diffusion and coulomb enhancement on the differential transmission data.

In the past year, work at MIT has been directed toward femtosecond pump-probe absorption saturation studies of the GaAs and AlGaAs semiconductor systems. Femtosecond intervalley scattering in AlGaAs is investigated using a tunable wavelength technique. Systematic variation of the wavelength and spectral content of ultrashort laser pulses permits a selective study of different scattering channels, such as scattering to the L satellite valley. An amplified colliding pulse modelocked (CPM) ring dye laser system provides the source for our experiments. Femtosecond optical pulses from the CPM are amplified by a copper vapor laser pumped dye amplifier to microjoule energies. The amplified pulses are focused on a jet of ethylene glycol to generate a femtosecond white light continuum using nonlinear self phase modulation. A Fourier synthesis scheme selects variable wavelengths and pulse durations for use in pump-probe experiments.[49] This approach has the advantage that it permits studies using wavelength tunable pulses with durations as short as 30 fs. The samples used in our studies are grown by molecular beam epitaxy at MIT Lincoln Laboratory. The mole fraction of Al in the $Al_xGa_{1-x}As$ system is chosen to vary the bandstructure and isolate optical transitions of interest. Scattering to the L valley in $Al_{0.1}Ga_{0.9}As$ is only allowed for photoexcited carriers with energy greater than 1.8 eV. The possibility of scattering by this channel affects the behavior of the transient in femtosecond absorption saturation.

---

[46] M.A. Littlejohn, J.R. Hauser, T.H. Glisson, D.K. Ferry, and J.W. Harrison, "Alloy Scattering and High Field Transport in Ternary and Quaternary III-V Semiconductors," *Solid State Electron.* 21: 107 (1978).

[47] S.A. Lyon, "Spectroscopy of Hot Carrier in Semiconductors," *J. Lumines.* 35: 121-154 (1986); J. Shah, B. Deveaud, T.C. Damen, and W.T. Tsang, "Determination of Intervalley Scattering Rates in GaAs by Subpicosecond Luminescence Spectroscopy," *Phys. Rev. Lett.* 59: 2222-2225 (1987); R.G. Ulbrich, J.A. Kash, and J.C. Tsang, "Hot-electron Recombination at Neutral Acceptors in GaAs: A cw Probe of Femtosecond Intervalley Scattering," *Phys. Rev. Lett.* 62: 949-952 (1989); P.C. Becker, H.L. Fragnito, C.H. Brito Cruz, R.L. Fork, J.E. Cunningham, J.E. Henry, and C.V. Shank, "Femtosecond Intervalley Scattering in GaAs," *Appl. Phys. Lett.* 53: 2089-2090 (1988).

[48] C.J. Stanton and D.W. Bailey, "Evaluating Photoexitation Experiments Using Monte Carlo Simulations," in *Monte Carlo Simulations of Semiconductors and Semiconductor Devices,* ed. K. Hess (Boston: Klunker Academic, 1991).

[49] A.M. Weiner, J.P. Heritage, and E.M. Kirschner, "High Resolution Femtosecond Pulse Synthesis," *J. Opt. Soc. Am. B* 5: 1563 (1988).

Thus, a wavelength tunable study discerns salient features of the data in both the time and energy dimensions.

The results already obtained will be extended to new materials systems and to quantum confined structures. Device design in the future will depend on thorough knowledge of the transient electronic properties of semiconductor materials. The combination of advanced femtosecond laser technology with sophisticated theoretical methods provides a potent tool for discovery of fundamental information on ultrafast carrier dynamics.

1.13 Time Domain Diagnostics of Waveguide Devices

Sponsors

Joint Services Electronics Program
Contract DAAL03-89-C-0001
Contract DAAL03-92-C-0001
National Science Foundation
Grant ECS 85-52701
U.S. Air Force - Office of Scientific Research
Contract F49620-88-C-0089

Project Staff

Claudio D.C. Chamon, Chi-Kuang Sun, Professor Hermann A. Haus, Professor James G. Fujimoto

1.13.1 Time Domain Interferometry

Investigations of nonlinear processes such as measurements of the nonlinear index of refraction in waveguide devices are key to the development of high speed all-optical switching devices. In particular, the magnitude of the nonlinear index is an important parameter for all-optical switching and modulation, since it determines the laser pulse energy which is necessary to achieve switching behavior. Time domain measurements permit both the magnitude as well as the dynamics of the nonlinear index of refraction to be characterized. Previous investigators have used a number of time or frequency domain techniques to measure nonlinear index including four wave mixing,[50] nonlinear waveguide couplers,[51] nonlinear Fabry-Perots,[52] fringe shift interferometry,[53] and Mach-Zehnder interferometry.[54] In general, direct measurements of index nonlinearities are complicated because measurement techniques are sensitive to thermal or acoustical parasitic signals, have low sensitivity, or require deconvolution.

Recently, we have developed a new technique, femtosecond time division interferometry (TDI), that permits high sensitivity, direct measurements of the nonlinear index n_2 in waveguide devices with reduced interference from thermal or acoustical parasitic signals.[55] In this technique, pump and probe pulses are coupled into a waveguide device and the nonlinear phase shift which is induced on the probe by the pump is measured by interfering it with a reference pulse. TDI was previously limited to measurements of $n_{2\perp}$, i.e., index changes induced on a probe pulse by an orthogonally polarized pump. However, new materials such as quantum wells, quantum wires, organic polymers as well as other anisotropic systems are

---

[50] W.K. Burns and N. Bloembergen, "Third-harmonic Generation in Absorbing Media of Cubic or Isotropic Symmetry," *Phys. Rev. B* 4: 3437 (1971).

[51] P. Li, K. Wa, J.E. Sitch, N.J. Mason, J.S. Roberts, and P.N. Robson, "All Optical Multiple-quantum-well Waveguide Switch," *Electron. Lett.* 21: 27 (1985).

[52] Y.H. Lee, A. Chavez-Pirson, S.W. Koch, H.M. Gibbs, S.H. Park, J. Morhange, A. Jeffrey, N. Peyghambarian, L. Banyai, A.C. Gossard, and W. Wiegmann, "Room Temperature Optical Nonlinearities in GaAs," *Phys. Rev. Lett.* 57: 2446 (1986).

[53] G.R. Olbright and N. Peyghambarian, "Interferometric Measurement of the Nonlinear Index of Refraction, n_2, of CdS_xSe_{1-x}-doped Glasses," *Appl. Phys. Lett.* 48: 1184 (1986).

[54] D. Cotter, C.N. Ironside, B.J. Ailslie, and H.P. Girdlestone, "Picosecond Pump Probe Interferometric Measurement of Optical Nonlinearity in Semiconductor Doped Fibers," *Opt. Lett.* 14: 317 (1989).

[55] M.J. LaGasse, K.K. Anderson, H.A. Haus, and J.G. Fujimoto, "Femtosecond All-optical Switching in AlGaAs Waveguides Using a Single Arm Interferometer," *Appl. Phys. Lett.* 54: 2068 (1989); M.J. LaGasse, K.K. Anderson, C.A. Wang, H.A. Haus, and J.G. Fujimoto, "Femtosecond Measurements of the Nonresonant Nonlinear Index in AlGaAs," *Appl. Phys. Lett.* 56: 417 (1990).

becoming increasingly important candidates for all optical switching devices. A complete characterization of n_2 requires the measurement of n_{2I}.

During the past year, we have developed a new variation of our original time division interferometry, TDI, technique which permits the complete characterization of the nonlinear index.[56] By using a novel phase modulation technique which breaks the degeneracy between the pump and probe and actively stabilizes the interferometer, the magnitude and femtosecond transient response of n_{2I} can be measured. Experiments have been performed to measure $n_{2\perp}$ and n_{2I} in an optical fiber to demonstrate this new measurement technique. High sensitivities have also been achieved and phase shifts as small as 5 milirad can easily be detected. Thus, TDI can be applied to studies of nonlinear index and all-optical switching in a wide range of waveguide devices.

1.13.2 Time Domain Diagnostics of Strained Layer Devices

Strained layer quantum well devices represent one of the most active and technologically promising areas of current optoelectronics device research. Strained layer materials greatly extend the available wavelength range of optoelectronic devices by permitting the growth of non-lattice materials. In addition, strained layer materials represent a bandgap engineering approach to achieve superior device performance. By modifying the valence band structure, lower threshold current density, higher efficiency, smaller chirp, wider modulation bandwidth, and improved high temperature performance[57] can be achieved over conventional devices.[58] High power, high efficiency, long lifetime, and low threshold current density[59] semiconductor lasers have been achieved in InGaAs strained layer devices. With their extended wavelength range and high output power, InGaAs/GaAs strained layer lasers are important for applications such as coherent optical communications, pumping erbium doped fiber amplifier and solid state lasers, and high speed optical signal processing.

With the development of new tunable femtosecond laser source of wavelengths between 900 and 1000 nm, time domain diagnostics can become a powerful tool for characterizing dispersion, gain dynamics, nonlinear index change, and transient nonlinearities. We have recently begun a program in collaboration with Groups 67 and 83 at Lincoln Laboratory to develop frequency and time domain diagnostics of strained layer diode lasers. The objective of our program is twofold: To develop and demonstrate new time and frequency domain diagnostics of diode lasers, and to examine fundamental processes and device design issues which limit high power single frequency performance in strained layer diodes.

Studies will involve InGaAs/GaAs graded-index separate-confinement heterostructure strained layer single quantum well laser diodes.[60] Femtosecond pump probe measurements of gain dynamics, nonlinear index, and dispersion are being performed. Continous wave measurements such as linewidth, spectral character, self heterodyne four wave mixing, and injection locking are being performed at Lincoln Laboratory. These two approaches represent complementary techniques which, taken together, can permit a more comprehensive characterization of device and materials properties. When completed, this study should establish new approaches for performing time domain diagnostics on a wide range of devices as well as provide

---

[56] C. de C. Chamon, C. K. Sun, H.A. Haus, and J.G. Fujimoto, "Femtosecond Time Division Interferometry Technique for Measuring the Tensor Components of $\chi^{(3)}$," *Appl. Phys. Lett.*, forthcoming.

[57] N.K. Dutta, J. Lopata, D.L. Sivco, and A.Y. Cho, "Temperature Dependence of Threshold of Strained Quantum Well Lasers," *Appl. Phys. Lett.* 58: 1125 (1991).

[58] E. Yablonovitch and E.O. Kane, "Reduction of Lasing Threshold Current Density by the Lowering of Valence Band Effective Mass," *J. Lightwave Technol.* LT-4: 504 (1986); A.R. Adams, "Band-structure Engineering for Low-threshold High-efficiency Semiconductor Lasers," *Electron. Lett.* 22: 249 (1986); I. Suemune, L.A. Coldren, M. Yamanishi, and Y. Kan, "Extremely Wide Modulation Bandwidth in a Low Threshold Current Strained Quantum Well Laser," *Appl. Phys. Lett.* 53: 1378 (1988).

[59] H.K. Choi and C.A. Wang, "InGaAs/AlGaAs Strained Single-quantum-well Diode Lasers with Extremely Low Threshold Current Density and High Efficiency," *Appl. Phys. Lett.* 57: 321 (1990); R.L. Williams, M. Dion, F. Chatenoud, and K. Dzurko, "Extremely Low Threshold Current Strained InGaAs/AlGaAs Lasers by Molecular Beam Epitaxy," *Appl. Phys. Lett.* 58: 1816 (1991).

[60] H.K. Choi and C.A. Wang, "InGaAs/AlGaAs Strained Single-quantum-well Diode Lasers with Extremely Low Threshold Current Density and High Efficiency," *Appl. Phys. Lett.* 57: 321 (1990).

information relevant to optimizing high power device performance in the InGaAs/GaAs system.

1.14 Laser Medicine and Surgery

Sponsors

Johnson and Johnson Research Grant
National Institutes of Health
Contract 2-R01-GM35459
U.S. Navy - Office of Naval Research
Contract N00014-91-C-0084

Project Staff

Dr. Joseph A. Izatt, Dr. Charles P. Lin, David Huang, Michael R. Hee, Professor James G. Fujimoto

1.14.1 The Ultrashort Pulse Laser Scalpel

In recent years, the use of short optical pulses has enhanced the degree of control and localizability of intraocular laser surgery.[61] Laser induced optical breakdown is a nonlinear laser tissue interaction which permits the photodisruption or cutting of transparent structures within the eye without the need for intervening surgical incision. The objective of our program is to develop an optimized ultrashort pulse laser scalpel which can be used to perform surgical incisions of intraocular structures even in close proximity to sensitive ocular structures such as the retina and cornea. These studies are part of an onging collaboration between investigators at MIT, the New England Eye Center of New England Medical Center Hospitals, and the Wellman Laboratories of Photomedicine at Massachusetts General Hospital.

The physical processes which occur in laser induced breakdown include plasma formation, acoustic wave generation, and cavitation. These processes produce the laser tissue surgical effects as well as collateral damage. To date, the majority of clinical applications of laser induced optical breakdown have utilized nanosecond duration pulses in the millijoule energy range and single pulse exposures. We have studied and compared the mechanisms, scaling behavior, and tissue effects of single pulses in the nanosecond and picosecond ranges.[62] In general, nanosecond and picosecond optical breakdown results in comparable damage zones if the same amount of energy is deposited; however, since the threshold energy for breakdown is much lower for picosecond pulses, near-threshold picosecond pulses produce greatly reduced collateral damage zones. For example, we have demonstrated collateral damage ranges in a corneal endothelial cell model of only 100 μm with 40 picosecond duration pulses at 8 microjoules pulse energy. We have also studied tissue effects (corneal excisions) into the femtosecond domain.[63] Ultrashort pulses with high peak intensities can produce a plasma mediated ablation of transparent tissues such as the cornea. Picosecond and femtosecond pulse durations have been demonstrated to produce much smoother excision edges and less damage to the adjacent tissue than nanosecond pulses.

We have demonstrated that clinically viable surgical incisions can be made using multiple pulse, high repetition rate picosecond pulses. Each pulse produces minimal collateral damage while multiple exposures produce a cumulative incision effect. In order to study the effect of repetition rate, we have developed a new Nd:YAG laser system which produces 100 picosecond duration pulses with a maximum energy of 140 μJ and a repetition rate variable from 3 to 1000 Hz. This laser has been used to demonstrate in vitro cutting of a monolayer of cultured fibroblast cells suspended over corneal endothelium in saline as a model for vitreous membrane surgery. Membrane cutting in the deep vitreous in close proximity to the retina remains one of the most challenging problems for

---

[61] F. Fankhauser, P. Roussel, J. Steffen, E. Van der Zypen, and A. Cherenkova, "Clinical Studies on the Efficiency of High Power Laser Radiation Upon Some Structures of the Anterior Segment of the Eye," *Int. Ophthalmol.* 3: 129 (1981).

[62] J.G. Fujimoto, W.Z. Lin, E.P. Ippen, C.A. Puliafito, and R.F. Steinert, "Time Resolved Studies of Nd:YAG Laser Induced Breakdown," *Invest. Ophthal. Vis. Sci.* 26: 1771 (1985); B. Zysset, J.G. Fujimoto, and T.F. Deutsch, "Time Resolved Measurements of Picosecond Optical Breakdown," *Appl. Phys. B* 48: 139 (1989); B. Zysset, J.G. Fujimoto, C.A. Puliafito, R. Birngruber, and T.F. Deutsch, "Picosecond Optical Breakdown: Tissue Effects and Reduction of Collateral Damage," *Lasers Surg. Med.* 9: 193 (1989); D. Stern, R. Schoenlein, C.A. Puliafito, E.T. Dobi, R. Birngruber, and J.G. Fujimoto, "Corneal Ablations by Nanosecond, Picosecond, and Femtosecond Lasers at 532 and 625 nm," *Arch. Ophthalmol.* 107: 587 (1989).

[63] D. Stern, R. Schoenlein, C.A. Puliafito, E.T. Dobi, R. Birngruber, and J.G. Fujimoto, "Corneal Ablations by Nanosecond, Picosecond, and Femtosecond Lasers at 532 and 625 nm," *Arch. Ophthalmol.* 107: 587 (1989).

vitreoretinal surgeons, despite advances in mechanical vitrectomy. In our experiments, efficient cutting of fibroblast cell membranes was observed by applying repetitive, 50-80 μJ pulses at 50-200 Hz while translating the membranes across the laser focus. Incision widths were as narrow as 5 cell diameters, or 50 μm, while membranes suspended as close as 200 μm over corneal endothelium could be incised without detectable damage to the endothelial cells. These experiments were followed up by in vivo incision of induced vitreous membranes in rabbit eyes. In these experiments, vitreous strands were cut at distances as close as 100 μm to the retina using 60-100 μJ pulses at 200 Hz. No retinal hemorrhages were observed, and histological examination of the underlying retina revealed only minor cell disruption. These results comprise considerable advances over the capabilities of nanosecond pulse duration photodisrupters in current clinical use.

1.14.2 Optical Coherence Domain Reflectometry in Biological Systems

Optical coherence domain reflectometry (OCDR) is a new noninvasive, noncontact ranging technique able to profile optical reflectivity versus depth in both transparent and scattering media.[64] OCDR employs a short coherence length light source and interferometric detection to determine the time-of-flight delay of light reflected from different points in a sample. The technique is the optical analog of ultrasound, but offers higher spatial resolution and noncontact measurement. OCDR uses heterodyne signal detection techniques common in high performance optical communication systems to achieve superior sensitivity and noise rejection. Unlike time-domain optical ranging techniques, OCDR only requires a small, low-power, superluminescent laser diode source and may be engineered into a safe, compact, clinically useful fiber optic device. We believe that OCDR has important clinical applications in laser microsurgery and medical diagnostics.

Working in collaboration with the Optical Communications Group 67 at Lincoln Laboratories, we have developed a new fiber optic OCDR system optimized for high speed and high detection sensitivity.[65] The device features a high speed translation device for fast data acquisition, optimized analog detection and signal processing electronics, and a modular probe which may be easily coupled to a slit-lamp biomicroscope. Low-coherence 830 nm light from a broad bandwidth superluminescent laser diode is launched into a fiber optic Michelson interferometer and split into reference and sample arms at a fiber coupler. Backscattered and retroreflected light from the biological sample is recombined with light returning from a scanning reference mirror. Coherent interference occurs at the detector only when the reference and sample arm optical path lengths match to within the source coherence length (17 μm FWHM). The reference mirror translates at a velocity of 38 mm/s which Doppler shift modulates the coherent interference signal at 93 kHz, a modulation frequency above the predominant optical and mechanical noise in the system. Detection and demodulation produce a profile of sample reflectivity versus depth. This heterodyne detection technique achieves quantum limited sensitivity and is able to resolve reflected signals as small as $\sim 10^{-10}$ of the incident optical power (> 90 dB dynamic range).

OCDR has many potential applications as a noninvasive medical diagnostic, especially in the transparent tissues of the eye. In collaboration with investigators at the New England Eye Center of Tufts University Medical Center and the Wellman Laboratories of Massachusetts General Hospital, we have examined medical applications which require the high-ranging resolution and high sensitivity possible with OCDR. We have used OCDR to demonstrate in vitro measurements of corneal thickness and excimer laser corneal excision depth, which are directly relevant to micron-precision monitoring of keratorefractive surgeries.[66] Our high speed OCDR system has allowed us to perform similar in vivo measurements in the anterior chamber of a rabbit eye, with no reduction in sen-

---

[64] R.C. Youngquist, S. Carr, and D.E.N. Davies, "Optical Coherence-domain Reflectometry: a New Optical Evaluation Technique," *Opt. Lett.* 12: 158 (1987); K. Takada, I. Yokohama, K. Chida, and J. Noda, "New Measurement System for Fault Location in Optical Waveguide Devices Based on an Interferometric Technique," *Appl. Opt.* 26: 1603 (1987).

[65] E.A. Swanson, D. Huang, M.R. Hee, J.G. Fujimoto, C.P. Lin, and C.A. Puliafito, "High-speed Optical Coherence Domain Reflectometry," *Opt. Lett.* 17: 151 (1992).

[66] D. Huang, J. Wang, C.P. Lin, C.A. Puliafito, and J.G. Fujimoto, "Micron-resolution Ranging of Cornea Anterior Chamber by Optical Reflectometry," *Lasers Surg. Med.* 11: 419 (1991).

sitivity or ranging resolution.[67] We have also found that OCDR has sufficient sensitivity to detail optical scattering within transparent structures such as the lens and cornea. Thus, OCDR is a potential clinical tool for the quantitative assessment of lens opacity and cataract progression. No objective technique for evaluating cataracts currently exists with sufficient reliability for routine clinical use. In preliminary studies, we have induced reversible "cold" cataracts[66] in enucleated bovine eyes and have investigated the correlation between the temperature dependent lens opacity and OCDR backscatter intensity.

We have also developed a birefringence sensitive OCDR system which can characterize the phase retardation of light reflected from different depths in biological tissue independent of probe orientation. Birefringence may be characteristic of particular tissue infrastructure due the directionality of fibrous nerve, muscular and connective tissue,[68] and may enhance contrast between different tissue structures when coupled with OCDR.

1.14.3 Optical Coherence Tomography

We have recently developed a new medical imaging technique called optical coherence tomography (OCT) which extends the ranging capabilities of single-axis OCDR and provides two-dimensional cross sectional images of optical reflectivity in tissue.[69] OCT functions in analogy to ultrasound B-mode imaging and measures cross sectional tomographic images by performing multiple longitudinal OCDR measurements taken at a series of lateral sample locations. A computer controlled stage translates the point of measurement a small lateral distance after each single longitudinal scan. The digitized scan sequences characterizing the tissue cross-section are mapped using image processing software to a gray-scale or false color image. Unlike x-ray computed tomography or magnetic resonance imaging, OCT does not require large amounts of computation for image reconstruction. As in the single scan case, the longitudinal resolution is determined by the source coherence length (17 μm FWHM), while the probe beam spot diameter determines the lateral resolution (9 μm FWHM). The optical sectioning capability of OCT is similar to confocal microscopy. Ranging resolution, however, is not limited by the available numerical aperture. Thus, OCT is useful for transpupillary imaging of the posterior eye and in endoscopic imaging.

In collaboration with the New England Eye Center and Wellman Laboratories, we have demonstrated OCT in a wide range of clinically relevant biological systems.[69] In vitro anterior eye tomographs provide comprehensive measurements of anterior chamber depth and corneal contour. These measurements address clinical problems such as narrow angle glaucoma diagnosis and fitting contact lenses. Backscattering from within transparent tissues such as cornea and lens is also clearly evident in these tomographs, which may also be clinically useful in assessing corneal opacity or cataract progression. OCT images of an in vitro retina in a resected eye show enhanced scattering from the retinal nerve fiber layer (RNFL) and retinal pigment epithelium. RNFL and total retinal thickness may be directly extracted from the image, suggesting a potential quantitative diagnostic tool for direct measurement of RNFL degeneration and open-angle glaucoma progression.[70] Currently, no quantitative method exists for the in situ evaluation of retinal nerve fiber loss. We have also examined OCT images in optically turbid media such as the artery. Tomographs of in vitro human coronary artery samples suggest that OCT can distinguish between the different scattering properties of fatty calcified arterial plaque versus fibro-usatheromatous plaque. Thus, a fiber optic OCT probe coupled to an endoscope might be potentially useful in distinguishing normal from diseased arterial walls in laser angioplasty surgeries.

---

[67] E.A. Swanson, D. Huang, M.R. Hee, J.G. Fujimoto, C.P. Lin, and C.A. Puliafito, "High-speed Optical Coherence Domain Reflectometry," *Opt. Lett.* 17: 151 (1992).

[68] R.N. Weinred, A.W. Dreher, A.C. Coleman, H. Quigley, B. Shaw, and K. Reiter, "Histopathologic Validation of Fourier-ellipsometry Measurements of Retinal Nerve Fiber Layer Thickness," *Arch. Opthalmol.* 108: 557 (1990).

[69] D. Huang, E.A. Swanson, C.P. Lin, J.S. Schuman, W.G. Stinson, W. Chang, M.R. Hee, T. Flotte, K. Gregory, C.A. Puliafito, and J.G. Fujimoto, "Optical Coherence Tomography," *Sci.* 254: 1178 (1991).

[70] H.A. Quigley and E.M Addicks, "Quantitative Studies of Retinal Nerve Fiber Layer Defects," *Arch. Opthalmol.* 100: 807 (1982).

1.15 Overview of the EUV Laser Effort

Professor Peter L. Hagelstein and his research group are very close to the commencement of experiments in search of gain at near 200 Å in low-Z or mid-Z nickel-like ions. The oscillator and pre-amplifier have been upgraded; the power amplifier is functional and awaits the completion of short pulse experiments; the target chamber is operational; some degree of target alignment capability is available; finally, two principal EUV spectral diagnostics have been installed and have taken data. These projects are described in the following sections. Plans for the near future include experiments at full power in search of gain at 191 Å in Ni-like molybdenum and similar studies in neighboring elements.

1.16 Nd:glass Amplifier Development

Sponsor

U.S. Department of Energy
Grant DE-FG02-89 ER14012-A003

Project Staff

Martin H. Muendel, Michele M. Bierbaum, Professor Peter L. Hagelstein

The upper laser state in the Mo laser at 191 Å is excited by 150-250 eV electrons; a 5-J, 10-GW laser beam is required to create a high-temperature plasma over a long cylindrical gain region. Such lasers are not readily available, and we have constructed a laser-amplifier system at 1.05 μm for driving the Mo-laser. The system consists of a zig-zag slab Nd:glass power amplifier which we have designed and constructed and a commercially available master oscillator and pre-amplifier. The various parts of the laser system are described below.

The oscillator is a standard active-modelocked, Q-switched Nd:YLF system generating 100 psec pulses at about 50 μJ. These pulses are apodized to give a supergaussian beam profile and are amplified to the 50 mJ level by an Nd:phosphate glass rod preamplifier operating in double pass.

A square apodizer and a vacuum spatial filter have been added following the preamplifier in order to produce a clean square beam profile. The apodizer works using a highly serrated aperture, with the low frequency spatial Fourier components corresponding to the required apodization. Passing the beam through the spatial filter results in removal of the high frequency modulation, and the resulting square beam exhibits a "top-hat" intensity profile with steep yet smoothly curved edges (to give the beam good propagation characteristics). A small vacuum system encompassing the region of the spatial filter pinhole is necessary in order to prevent atmospheric breakdown in the high intensity region near the laser focus; this system has been built and installed.

The beam is relayed by the spatial filter to the glass slab, which it traverses three times at a gain of 5× per pass to bring the total output energy to about 5 J. Two anamorphic prism pairs have been implemented to expand the beam to a rectangular cross section that matches the slab's clear aperture closely.

We have demonstrated energies in the 15-20 J range in 100 nsec pulses (non-modelocked); the damage limit for our system for such pulses is around 50 J. For modelocked, 100 psec pulses, we have been gradually bringing up the energy to the desired 5 J while watching for the onset of nonlinear self-focusing.

We have designed and fabricated an f/6 cylindrical lens doublet for the final focusing optic which is corrected for spherical aberration and coma and should be essentially diffraction-limited. The rectangular beam from the slab is thus imaged in one dimension to the target and tightly ($\tilde{1}0$ μm) focused in the other, which should result in a highly uniform line focus.

The slab amplifier's zig-zag rectangular geometry allows it to run at repetition rates over 0.5 Hz in spite of its quite large (20 cm^2) clear aperture. The limiting agent to the system's rep rate is the 1cm-diameter glass preamp rod, which has a thermal recovery time of 20-30 sec due to thermal lensing in the straight-through cylindrical geometry. We have purchased a large (0.8 cm diameter) Nd:YLF rod with which we intend to replace the glass rod. The crystalline YLF host has a tenfold higher thermal conductivity as well as lower thermal lensing than phophate glass, which should raise the preamp rep rate to over 0.5 Hz. Also, the sixfold higher gain cross section and lower nonlinear index of Nd:YLF make it a superior material for amplification of short pulses of very high peak power.

The combination of high output energy, high peak power and high repetition rate make this laser system unique. With the system at full output and, soon, at full rep rate, we expect it to serve as a powerful and flexible tool in our short wavelength gain studies.

1.17 Spectral Measurements of a Ni-like Mo Plasma

Sponsor

U.S. Department of Energy
Grant DE-FG02-89 ER14012-A003

Project Staff

Dr. Santanu Basu, James G. Goodberlet, Professor Peter L. Hagelstein

We are investigating gain at 191 Å between 4d and 4p levels in Mo XV in a laser produced plasma.[71] The condition for gain requires a temperature of around 200 eV and an electron density of 1.2×10^{19} cm^{-3} for production of MoXV ions, and excitation of the ground-state $3d^{10}$ electrons to the upper laser state. The upper laser state decays to 4f state by electron collisional excitation and to the lower laser level by radiation.

We have constructed two spectrometers for laser diagnostics: one is based on a Harada flat-field grating[72] and the other one uses a concave grating[73] with very little astigmatism. The spectra of Mo taken with the Harada grating spectrometer is shown in figure 3. The Mo spectrum was obtained using a train of 80-ps pulses, the energy per pulse being 7 mJ. The laser beam was focused with a f-15 spherical lens to a measured spot size of 41 μm, which produced 3.3×10^{12} W/cm^2 intensity on the target. This intensity level is comparable to the design intensity for the gain experiment. The spectrometer was calibrated using a carbon target and noting the positions of the following lines; C VI 1s-2p at 33.736 Å, C V 1s-3p at 40.268 Å, and 1s-2p at 40.268 Å. In the Mo spectrum, we noted the 3d-4p lines of Mo XVI at 46.86 Å, Mo XV at 50.44 Å, and MO XIV at 52.75 Å The results indicate that at the design intensity level for the gain experiment, Ni-like ions will be present in the plasma.

The streaked concave grating spectrometer (SCGS) uses a 32 x 30 mm concave grating of 1-m radius of curvature with 3600 lines per mm. The grating is used at near normal incidence which

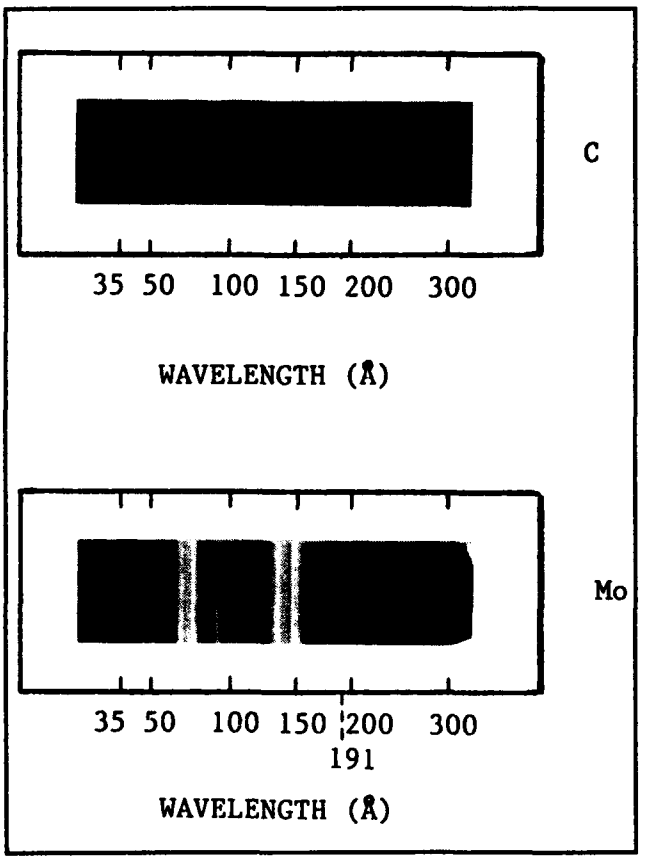


Figure 3. *The spectrum of Mo plasma taken with a flat-field Harada grating spectrometer and an Al spectral filter. The spectrum of C was used for calibration.*

produces a nearly stigmatic image, at the cost of negligible reflectivity at less than approximately 180 Å. The image magnification is 2.2, and the minimum astigmatic blur is estimated to be only 663 μm, which will make the SCGS a valuable diagnostic tool for time resolved and spectrally resolved imaging of the plasma. A streak camera with 12.5-mm wide photocathode is used to obtain temporal information on the x-ray spectrum over a 22 Å range.

Calibration for this spectrometer was carried out with Al as target material and at an incident intensity of $2 - 5 \times 10^{12}$ W/cm^2. Polaroid 107 which has a dynamic range of only 100 was used to record the spectrum in our first experiment. The

---

[71] P.L. Hagelstein, S. Basu, M.H. Muendel, J.P. Braud, D. Tauber, S. Kaushik, J. Goodberlet, T.-Y. Hung, and S. Maxon, "The MIT Short-Wavelength Laser Project: A Status Report," *Proceedings of the International Colloquium on X-Ray Lasers*, York, United Kingdom, 1990, p. 255; S. Basu, M. Muendel, J. Goodberlet, S. Kaushik, and P.L. Hagelstein, "A Search for Gain at 191 Å," *Proceedings SPIE International Symposium on Optical Applied Science and Engineering*, San Diego, California, July 1991.

[72] T. Kita, T. Harada, N. Nakano, and H. Kuroda, *Appl. Opt.* 22(4): 512 (1983).

[73] U. Feldman, G.A. Doschek, D.K. Prinz, and D.J. Nagel, *J. Appl. Phys.* 47(4): 1341 (1976).

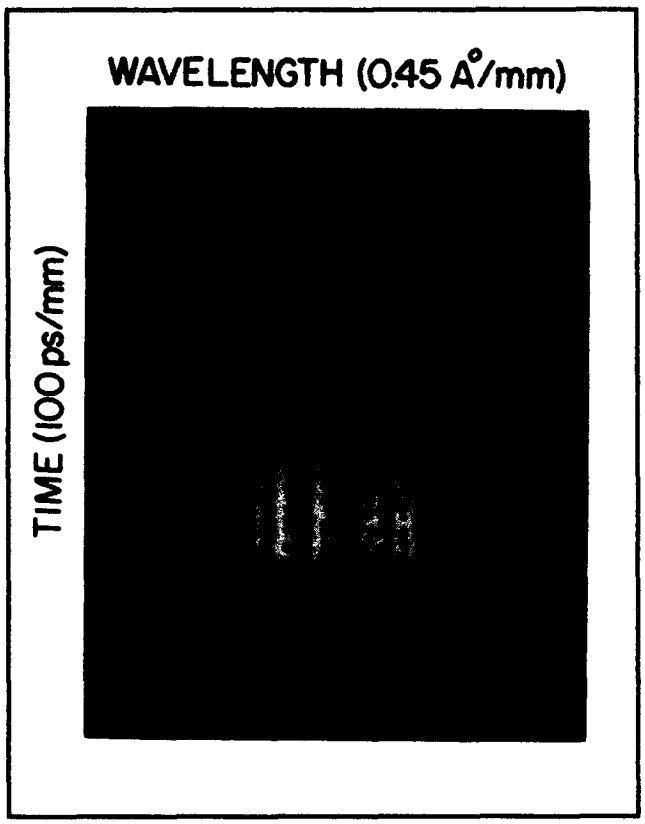


Figure 4. Calibration of the streaked concave grating spectrometer (SCGS). The spectral lines shown in this photograph are (from left to right): Al VII, 239.03 Å, Al VII, 240.77 Å, Al VI, 243.77 Å, Al VIII, 247.35 Å, O V, 248.46 Å, Al VIII, 250.14 Å, Al VIII, 251.35 Å,

data is shown in figure 4. The bright line at the center of the photograph is the Al VI line at 243.766 Å. The two lines on the extreme right at 250.139 Å (Al VII) and 251.347 Å (Al VIII) are separated by 1.21 Å and are clearly resolved. The spectral resolution at 240 Å was estimated to be $0.6Å(\lambda/\Delta\lambda = 400)$. The SCGS also allows us to look at the x-ray spectrum over a number of pump pulses which are separated by 7.5 ns.

In our design, both the spectrometers are installed inside of the chamber. The design has proved to be very efficient, since it is compact and it minimizes the impact of external vibrations on the diagnostic system. We envision the x-ray laser system to be operated routinely by one person in a university setting. Except for the externally applied pump beam, the completely enclosed x-ray laser head functions not much differently from commercially available optical laser heads. We have diagnosed laser produced plasma using a flat-field spectrometer, and a streaked concave grating spectrometer and these instruments are now ready to measure gain down to a gain-length product of 1.

1.18 Progress in EUV Laser Kinetics Modeling

Sponsor

U.S. Department of Energy
Grant DE-FG02-89 ER14012-A003

Project Staff

Professor Peter L. Hagelstein

The analysis of laser kinetics for x-ray lasers historically has relied extensively on large numerical simulation models which use several hundred levels to model the population dynamics. We have recently succeeded in developing an effective three-level model which accurately reproduces the temperature and density dependence of the population dynamics of the upper and lower laser states in mid-Z nickel-like ions obtained from the large models.

We have found[74] that the fractional inversion density is well approximated by

$$\frac{N^*}{N_o} = \frac{C_{uo}}{C_u}\left[\frac{x}{1+x} - \zeta\frac{x}{(1+x)^{1/3}}\right]$$

where N^* is the inversion density on the $3d^94d^1S - 3d^94p^1P$ laser transition, and N_0 is the ground state $3d^{10}$ population. The collisional rate up to the laser state is C_{uo}, and the collisional destruction rate of the upper laser state is C_u. The parameter x is the electron density normalized to the upper state equilibration density

$$x = \frac{C_u}{A_u}$$

where A_u is the radiative decay rate of the upper laser state. The parameter ζ describes the efficiency with which the ground state is populated, and evaluates to

$$\zeta = \frac{1}{3}\frac{A_u}{A_l}\frac{C_{lo}^*}{C_{uo}}$$

[74] P.L. Hagelstein, "Development of the MIT Short Wavelength Laser," *Proceedings SPIE International Symposium on Optical Applied Science and Engineering*, San Diego, California, July 1991.

In this formula, A_l is the radiative decay rate of the lower state, and C_{l_0} is the total collisional rate up to the lower laser state which would be obtained by taking the zero-density limit of the excitation cross section for all direct and indirect processes.

This result has allowed us to optimize analytically the optimum plasma temperature and electron density for maximum gain for mid-Z nickel-like ions. The optimum temperature occurs near $kT_e = \Delta E/2$, where ΔE is the excitation energy to the upper state. The optimum density occurs near

$$x \approx \left[\frac{3}{5\zeta}\right]^{3/2}$$

valid to within about 20% in regimes of interest.

We have verified independently that our proposed operating point for Ni-like Mo is in fact optimum, and have found scaling relations for neighboring elements. Interestingly enough, scaling to low Z appears to be problematic in Ni-like ions using a 1 μ driver, due to the very low density (and hence low gain) which occurs under optimum plasma conditions.

1.19 Laser Cavities in the Soft X-Ray Region

Sponsor

U.S. Department of Energy
Grant DE-FG02-89 ER14012-A003

Project Staff

John Paul Braud, Professor Peter L. Hagelstein, Dr. Santanu Basu, Tsen-Yu Hung

The primary motivation in developing laser cavities is to make a significant improvement in the beam quality and efficiency of extraction of stored energy in the gain medium. We have been working on whispering-gallery optics for short-wavelength laser cavities.[75]

We have made a major step forward in the analysis of beam propagation in whispering-gallery mirrors (WGMs). Our previous work in this area had led to the development of what we called the "whispering-gallery equation," which describes the evolution of a beam's transverse structure as it propagates along the surface of a WGM. During the past year, we have managed to solve this equation analytically; the solutions that we found are quasi-adiabatic local normal modes having curved wavefronts.

This progress in the area of analysis has in turn clarified the problem of design. Since the beginning of this project, an important goal has been the development of elongated mirror shapes leading to reduced beam divergence relative to the more obvious circular design. In the past year, we discovered a new class of mirror shapes, the so-called "quadratic family," whose performance in this regard is vastly superior to any designs considered previously. The primary virtue of a rotationally symmetric design is the relative ease of manufacture.

We have also made progress in establishing surface finish requirements for WGMs. We have developed a coupled-mode approach to describe the effect of surface imperfections and thereby established fabrication tolerances. The finish requirements for WGMs were found to be qualitatively different from those appropriate to more conventional optics.

We are also continuing to explore the use of unstable resonators. The high gain and short lifetime typical of short-wavelength laser amplifiers match up ideally with the large output coupling and rapid spatial-mode formation characteristic of unstable resonators. Moreover, unstable resonators can rely on diffractive output coupling and thereby avoid the use of beamsplitters, which are enormously inefficient at short wavelengths. The design of an unstable resonator with readily avail-

---

[75] T.-Yu Hung and P.L. Hagelstein, "Whisper Gallery Mirrors Reflectivities from 100 Å to 500 Å," *Proceedings of the International Conference on Lasers 90*, San Diego, California, 1990; T.-Yu Hung and P.L. Hagelstein, "Investigations of Whisper Gallery Mirrors for Extreme Ultraviolet (EUV) and Soft X-rays," *IEEE J. Quant. Electron.* (1992), forthcoming; J.P. Braud and P.L. Hagelstein, "Whispering-Gallery Laser Resonators—Part I: Diffraction of Whispering Gallery Modes," *IEEE J. Quant. Electron.* 27: 1069 (1991); J.P. Braud and P.L. Hagelstein, "Whispering-Gallery Laser Resonators—Part II: Analysis of Mirrors with Non-Uniform Curvature," *IEEE J. Quant. Electron.* 28: 254 (1992); J.P. Braud and P.L. Hagelstein, "Whispering-Gallery Laser Resonators—Part III: Mirror Design," submitted to *IEEE J. Quant. Electron.* (1992); J.P. Braud, "Polarizing Optics for the Soft X-ray Regime: Whispering-Gallery Mirrors and Multilayer Beamsplitters," *Proceedings of the SPIE International Symposium on Optical Applied Science and Engineering*, San Diego, California, July 1991; J.P. Braud, "Whispering-gallery Mirrors for Short-wavelength Laser Cavities: Shapes and Tolerances," *Proceedings of the SPIE International Symposium on Optical Applied Science and Engineering*, San Diego, California, July 1991.

able multilayer optics for our laser system is included in Basu and Hagelstein.[76]

1.20 Boltzmann Equation Studies

Sponsor

U.S. Department of Energy
Grant DE-FG02-89 ER14012-A003

Project Staff

Ann W. Morgenthaler, Professor Peter L. Hagelstein

A necessary step in the development of an x-ray laser is characterization of the collisionally-excited plasma produced by bombarding a high atomic number substrate with an intense electromagnetic field. If the density, velocity, and temperature profiles of the plasma are known, it is then possible to compute the expected laser gain directly. Much progress has been made in numerically simulating the hydrodynamics of x-ray laser plasmas, but usual assumptions of local thermal equilibrium are often insufficient to accurately calculate thermal conductivities, plasma viscosities, etc. As part of an attempt to produce a table-top x-ray/EUV laser, we are developing one- and two-dimensional hydrodynamics codes which will describe the behavior of non-Maxwellian coronal plasmas in the free-streaming limit where the linearized transport coefficients are typically inaccurate.

A general solution to the collisional Boltzmann equation is proposed, which consists of taking velocity moments of the scalar distribution function f(x, v; t). The velocity dependence thus disappears from the Boltzmann equation at the expense of solving an infinite number of coupled moment equations. It is our hope that only a few of these moment equations will be necessary to determine the behavior of the first three (namely, density, velocity, and temperature). If we define h, an infinite-dimensional column vector with components

$$h^{abc}(x, t) \equiv N < u_x^a u_y^b u_z^c > = \int d^3u\, u_x^a u_y^b u_z^c f(x, u; t) \quad (1)$$

where N is the plasma density, $u = v - < v >$ is the fluctuation velocity and a, b, and c take on the values of all non-negative integers, it is straightforward to show that the vectorized Boltzmann equation is:

$$Dh = h \bullet C \bullet h \quad (2a)$$

$$D = \frac{D}{Dt} + (\nabla \bullet < v >) + \quad (2b)$$

$$\left(\left(\frac{D < v >}{Dt} \right) - a \right) \bullet L^- + \nabla \bullet L^+ + L^+ \bullet (\nabla < v >) L^-$$

where $D/Dt = \partial/\partial t + < v > \bullet \nabla$ is the usual convective derivative and the raising and lowering operators L^+ and L^- are defined in component form as:

$$\begin{aligned} L_x^- \Phi^{abc} &= a\Phi^{a-1bc} & L_x^+ \Phi^{abc} &= \Phi^{a+1bc} \\ L_y^- \Phi^{abc} &= b\Phi^{ab-1c} & L_y^+ \Phi^{abc} &= \Phi^{ab+1c} \\ L_z^- \Phi^{abc} &= c\Phi^{abc-1} & L_z^+ \Phi^{abc} &= \Phi^{abc+1} \end{aligned} \quad (3)$$

where Φ^{abc} is any function indexed by the non-negative integers a, b, and c.

We have calculated exact formulas for the three-dyad *C* based on expanding the distribution function f in the eigenmodes of the spherical harmonic oscillator $\{|nlm>\}$ with the indices $n, l \in [0, n]$, $m \in [-l, l]$ analogous to the quantum numbers in the spherical harmonic oscillator problem. These functions (also called the Burnett basis) are products of spherical harmonics and associated Laguerre polynomials, with $|000>$ representing the local, shifted Maxwellian distribution. The full, non-linear Boltzmann equation may then be solved numerically for an arbitrarily anisotropic distribution, though clearly more moment equations will be needed if the distribution is severely non-Maxwellian.

The nonlinear problem is often linearized by assuming that one of the collision partners (represented by either h on the right side of equation 2a) is Maxwellian, and we can use our formulation to compute the linearized transport coefficients directly from the vectorized Boltzmann equation. The transport equations are found from a matrix equation having the form:

$$\sum_{n=0}^{\infty} J_{kn} A_n = b_k \qquad k = 0,1,2,... \quad (4)$$

where J is related to the linear collision matrix and b is also known; the transport coefficients are

[76] S. Basu and P.L. Hagelstein, "Design Analysis of a Short Wavelength Laser in an Unstable Resonator Cavity," *J. Appl. Phys.* 69(4): 15 (1991).

functions A_0 in this schematic description. Clearly, the first approximation to A_0 is just b_0/J_{00} and more sophisticated estimates can be made by truncating n at larger values. The Chapman-Enskog and Réisibois formulations only find the first approximation of the transport coefficients (and our formulation agrees exactly with their results). By vectorizing the Boltzmann equation and calculating the collision cross-sections exactly, it is easily possible to find the higher-order estimations of the transport coefficients. The thermal conductivity κ is typically approximated as

$$\kappa = \frac{75}{32\sqrt{\pi}} \frac{k(kT)^{5/2}}{e^4 m^{1/2} \ln \Lambda} \qquad (5)$$

which is also our first order result, and we can show that this linear conductivity is typically 20% too low. The transport coefficients converge rapidly as more terms in (4) are used, with 99% accuracy if n is truncated after n=4.

The next phase in this research will be to implement the non-linear equations in one- and two-dimensional form, since the laser plasma is not well described by the linear model. Adaptive Lagrangian codes with Newton-Raphson solvers will probably be the methods of choice.

1.21 Coherent Fusion Studies

Project Staff

Professor Peter L. Hagelstein, Isaac L. Chuang, Sumanth Kaushik, Irfan U. Chaudhary

The past year has seen advances in many areas of cold fusion research, and, in addition, a number of new effects have recently been reported. In this article, we will summarize briefly the current status of the field and review theoretical progress which we have made during the past year.

The primary effect associated with cold fusion research is the production of excess heat in electrochemistry experiments. During the past year, Pons and Fleischmann reported[77] obtaining completely reproducible heat excesses in the 20-50% regime, and described rather dramatic events where the excess power would be on the order of 10 times the input electrochemical power for periods of roughly half an hour. These high power events had been seen on eleven occasions as of the July meeting in Como, Italy; the new experiments benefited from the use of rods made of $Pd_{0.9}Ag_{0.1}$.

Reproducible heat was also reported by McKubre at SRI,[78] who described a recipe which had been discovered which produced excess heat on every occasion which the conditions of the recipe had been met. In total, the observation of about 100 bursts of excess heat was reported; these bursts occured during ten multimonth runs. Heat excesses of 10-20% were seen many times, measured with an accuracy of a few tenths of a per cent.

Heat in light water experiments has recently been reported by Mills and coworkers,[79] a result which is being viewed with skepticism by those who have observed heat in heavy water Pons-Fleischmann experiments. While still preliminary in that confirmations of the result have not yet been reported, the experimental claim is the generation of about a factor of 2 excess heat using nickel cathodes and a potassium carbonate electrolyte with very low current density ($\sim$ mA/cm^2), rather than using palladium cathodes and a LiOD electrolyte. This result is potentially important for numerous reasons: (1) Ni and light water are cheaper than Pd and heavy water, and (2) if correct, the result has the potential to demolish several classes of proposed mechanisms.

Very significant levels of ^{4}He have been reported from heat-producing Pons Fleischmann experiments.[80] The ^{4}He appears to be a byproduct of the heat process, but cannot quantitatively account for the heat produced.

Slow tritium production has been controversial since tritium contamination was claimed close to two years ago. Since that time, a number of groups have set up experiments in which tritium production is observed at the same time that pos-

---

[77] M. Fleischmann, presented at the Second Annual Cold Fusion Conference, Como, Italy, July 1991.

[78] M. McKubre, R. Rocha-Filho, S. Smedley, F. Tanzella, S. Crouch-Baker, T. Passell, and J. Santucci, "Isothermal Flow Calorimetric Investigations of the D/Pd System," *Proceedings of the Second Annual Cold Fusion Conference*, Como, Italy, July 1991.

[79] R. Mills and S. Kneizys, *Fusion Tech.* 20: 74-81 (1991).

[80] B.F. Bush, J.J. Lagowski, M.H. Miles, and G.S. Ostrom, "Helium Production During the Electrolysis of D_2O in Cold Fusion Experiments," *J. Electroanal. Chem.*, forthcoming.

sible metal contamination is assayed. Will et al. reported reproducible tritium production in palladium electrolysis using deuterated sulfuric acid;[81] Lanza described tritium production in a number of host alloys at similar levels;[82] Claytor reported tritium from his gas phase work.[83] Extremely high levels of tritium production have been claimed recently by Chien in electrolysis experiments.[84]

Observations of fast particle production are still being reported, with studies making some progress towards the determination of particle charge, mass and energy. Work on neutrons is continuing. Fleischmann recently described neutron observations from recent experiments of his group in a talk at MIT last December, in part to respond to the errors found in their initial neutron measurements.

We have been continuing our efforts to develop a theory which would apply to the Pons-Fleischmann effect and related anomalies which have been reported.[85] The premise of our current model is that energy transfer between nuclei and a lattice may occur through what amounts to a recoil effect, described by an interaction Hamiltonian of the form

$$\hat{H} = \int \hat{\Psi}_f[-\mu \bullet \hat{B}]\hat{\Psi}_i \wedge \hat{\psi}_n + \text{H.c.}$$

for magnetic dipole mediated neutron transfers, where the field operators describing nucleons in the lattice are of the form

$$\hat{\Psi}_i(\{r\}) = \sum_j \Phi_i(\{r - \hat{R}_j\})\hat{b}_i(j)$$

and where $\hat{R}_j$ is the lattice operator describing the center of mass of a nucleus at site j. This interaction Hamiltonian provides a natural description of recoil effects associated with neutron capture on a nucleus which is embedded in a lattice. This hamiltonian can be used to obtain lineshapes for direct conventional neutron capture in a lattice.

The transfer of a nuclear quantum of energy to lattice phonons in this theory requires a very high nonlinearity, which is provided naturally through the recoil effects contained in the interaction hamiltonian given above. The essential physics of the transfer is contained in the hamiltonian resulting from averaging over all coordinates except for phonon coordinates

$$\hat{H} = \sum_m \hbar\omega_m \hat{a}_m^\dagger \hat{a}_m + [V(t)e^{-i\hat{S}} + \text{H.c.}]$$

where V(t) is a high frequency (MeV) signal from the nuclear states, and where $e^{-i\hat{S}}$ is a Duschinsky operator which scales and translates according to

$$e^{-i\hat{S}}\Psi_L(q) = C\Psi_L(A \bullet q + b)$$

This operator takes into account the fact that the lattice differs before and after the capture process.

Energy transfer may occur if the high frequency nuclear signal can be demodulated. If a multimode phonon state is constructed from a product of single mode states,

$$\Psi_L = \prod_m \psi_m(q_m, t)$$

then self-consistent hamiltonians for each individual mode can be obtained of the form

$$\hat{H}_m = \hbar\omega_m \hat{a}^\dagger \hat{a} + V(t) < e^{-i\hat{S}} >_{\overline{m}}$$

If a very large number of modes can be locked, then the self-consistent single mode potential $V(t) < e^{-i\hat{S}} >_{\overline{m}}$ can be demodulated to have a low

---

[81] F. Will, K. Cedzynska, M-C Yang, J.R. Peterson, H.E. Bergeson, S.C. Barrowes, W.J. West, and D.C. Linton, "Studies of Electrolytic and Gas Phase Loading of Palladium with Deuterium," *Proceedings of the Second Annual Cold Fusion Conference*, Como, Italy, July 1991, p. 373.

[82] F. Lanza, presented at the Second Annual Cold Fusion Conference, Como, Italy, July 1991.

[83] T. Claytor and F. Lanza, presented at the Second Annual Cold Fusion Conference, Como, Italy, July 1991.

[84] C. Chien and T.C. Huang, "Tritium Production by Electrolysis of Heavy Water," unpublished, 1991.

[85] P.L. Hagelstein, "Coherent and Semi-Coherent Neutron Transfer Reactions I: The Interaction Hamiltonian," *J. Fusion Tech.* (1992), forthcoming; P.L. Hagelstein, "Coherent and Semi-Coherent Neutron Transfer Reactions II: Dipole Potential Operators," submitted to *J. Fusion Tech.*; P.L. Hagelstein, "Coherent and Semi-Coherent Neutron Transfer Reaction Mechanisms," submitted to *J. Fusion Tech.*

frequency component. To lowest order in the single mode potential, coherent states will be generated; to higher order, squeezed states are generated. Future efforts will focus on the relative contributions of each effect.

This model appears to have the potential to lead to the basic effect, and results in mean-field mode equations which may be be solved self-consistently.

The theory leads to a donor and acceptor nucleus description of coherent neutron transfer reactions (see figure 5). Heat in Pons-Fleischmann experiments is proposed to be due to the transfer of neutrons from deuterons to ^{6}Li nuclei; tritium comes about from neutron transfer to deuterons; ^{4}He and a high energy beta is evolved following neutron capture on ^{7}Li The light water experiments could be accounted for by neutron transfers on ^{39}K.

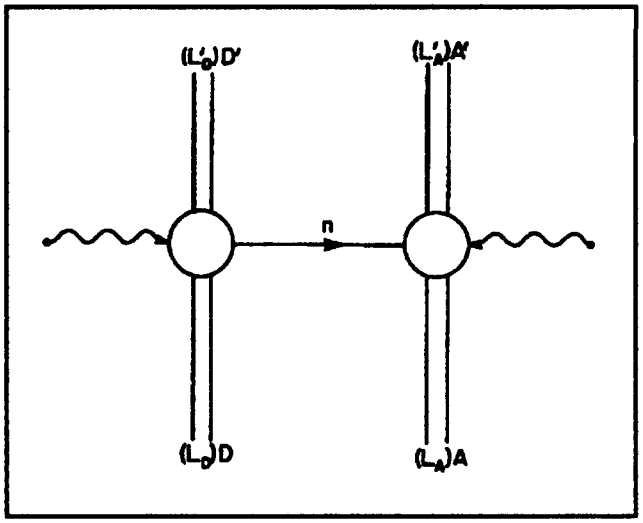
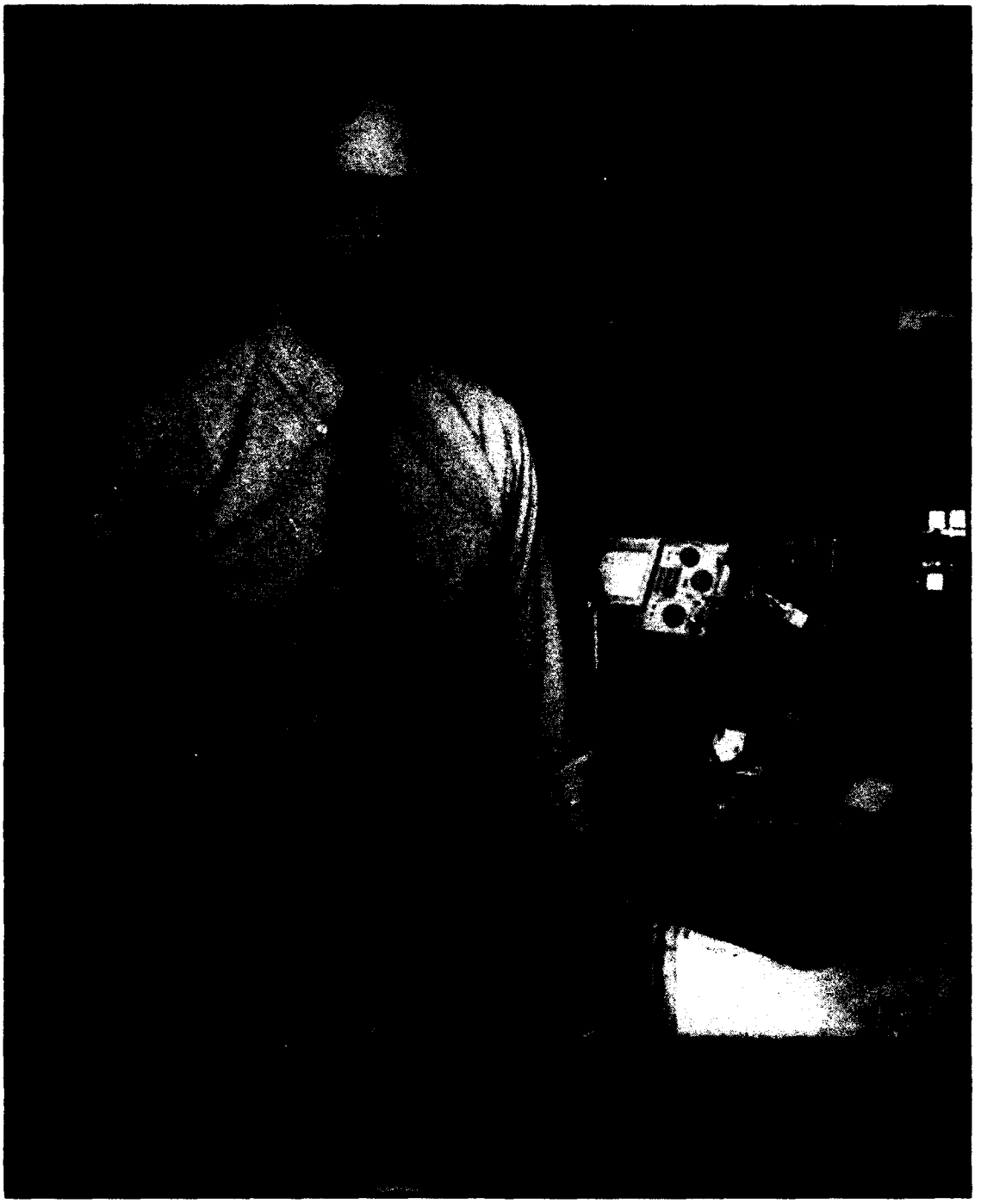


Figure 5. A general two-step coherent neutron transfer reaction for heat production. D and A refer to donor and acceptor nuclei before the transfer and primed variables refer to post-transfer variables. L_D and L_A refer to the host lattice.



Professor Jeffrey H. Shapiro

Chapter 2. Optical Propagation and Communication

Academic and Research Staff

Professor Jeffrey H. Shapiro, Dr. Robert H. Rediker, Dr. Ngai C. Wong

Visiting Scientists and Research Affiliates

Dr. Lance G. Joneckis[1]

Graduate Students

D. Shane Barwick, Bradley T. Binder, L. Reginald Brothers, Christopher J. Corcoran, Boris Golubovic, Thomas J. Green, Jr., Dicky Lee, Suzanne D. Lau, Robert E. Mentle, Phillip T. Nee, Brian K. Pheiffer, Scott R. Shepard, Ke-Xun Sun, Peter T. Yu

Technical and Support Staff

Barbara A. King

2.1 Introduction

The central theme of our programs has been to advance the understanding of optical and quasi-optical communication, radar, and sensing systems. Broadly speaking, this has entailed: (1) developing system-analytic models for important optical propagation, detection, and communication scenarios; (2) using these models to derive the fundamental limits on system performance; and (3) identifying, and establishing through experimentation the feasibility of techniques and devices which can be used to approach these performance limits.

2.2 Squeezed States of Light

Sponsors

Maryland Procurement Office
Contract MDA 904-90-C-5070
National Science Foundation
Grant ECS 87-18970

Project Staff

Professor Jeffrey H. Shapiro, Dr. Ngai C. Wong, Dr. Lance G. Joneckis, Scott R. Shepard, Ke-Xun Sun

The squeezed states of light are minimum uncertainty states for the quadrature components of the electromagnetic field which possess an asymmetric noise distribution between the two quadratures. The standard minimum uncertainty state that appears in quantum optics is the Glauber coherent state; it has an equal noise division between the two quadratures and is the quantum analog of the classical electromagnetic wave. Squeezed states are nonclassical and are of interest because their asymmetric noise division can lead to lower noise in photodetection measurements than that achievable with coherent states of the same energy. These noise reductions have been shown, theoretically, to afford significant benefits in interferometric precision measurements and novel guided-wave optical communication devices. We have pursued a vigorous program of experimental and theoretical research on squeezed-state and related nonclassical light.

2.2.1 Experiments

We have employed optical parametric downconversion in a type-I phase-matched $LiNbO_3$:MgO crystal in our efforts to generate nonclassical light. Above threshold, the optical parametric oscillator (OPO) has generated sub-shot-noise intensity correlation—over 50 percent observed noise reduction in the differenced photocurrents from the signal and idler detectors. Our focus has been on the demonstration of squeezed amplification by use of a below-threshold optical parametric amplifier (OPA) in the gain-saturated regime.[2] Under

---

[1] Laboratory for Physical Science, College Park, Maryland.

[2] N.C. Wong, "Squeezed Amplification in a Nondegenerate Parametric Amplifier," *Opt. Lett.* 16(21): 1698-1700 (1991).

gain saturation, the amplified output intensity of an injected coherent-state signal becomes amplitude squeezed, and the signal-to-noise ratio improves. Using a single-frequency diode-pumped YAG laser as the injection source, we have observed classical noise reduction in the signal output as a result of gain saturation. In particular, we have obtained a small-signal noise gain at 4 MHz that is ~ 1 dB lower than the large-signal gain at zero frequency.[3] Due to ~ 8 dB of excess noise of the YAG laser near 4 MHz, quantum noise saturation, and therefore signal-to-noise improvement has not been observed. To observe noise saturation in the quantum regime, we are presently working to reduce the excess intensity noise bandwidth of the YAG laser and to increase the photodetection bandwidth. Potential applications of an injection-seeded gain-saturated OPA include master oscillator output amplification and direct detection digital communication.

2.2.2 Theory

In a detailed study of the OPA or OPO with a strong mean field, we have identified the saturated gain regime in which an injection-seeded OPA generates amplitude squeezing in the signal output and the signal-to-noise ratio improves.[2] Above threshold, an injection-seeded OPO is found to generate more single-beam squeezing at a lower pump level than an unseeded one.

As an application of squeezing and OPOs in the area of precision measurements, a two-arm OPO has been analyzed and proposed as an active gravity-wave detector.[4] The signal and idler waves are internally separated such that the signal beam propagates along one arm of the OPO and the idler beam along the orthogonal arm. By monitoring the phase shift of the signal-idler beat frequency, a sensitive measure of the gravity-wave-induced differential path displacement in the OPO's two interferometer arms is obtained. Furthermore, we have shown that the external phase noise exhibits time-dependent squeezing.

In addition to the OPO/OPA theory, we have been continuing our fundamental attack on the ultimate limits of quantum phase measurement and have renewed our effort to elucidate time constant effects in quantized self-phase modulation. Recent work on quantum phase measurement has focused on two-mode, phase-conjugate detection. Here we have theoretically demonstrated a quantum communication system which affords zero error probability digital communication at finite root-mean-square photon number. This concept also has applications to precision measurements, i.e., it affords the possibility of analog phase-sensing with absolute precision to a prescribed number of decimal places. We have established the optimal state, in a root-mean-square photon number sense, for use with phase-conjugate measurement, and we have obtained the performance of this system in the presence of loss.[5] We found that in the low-loss regime phase-conjugate communication is less sensitive to loss than is number-state communication.

Our work on quantum self-phase modulation is a renewal of earlier research on the Kerr-effect nonlinearity.[6] Previously, we had identified the need to include a material time constant in the quantum theory of such interactions. Whereas the earlier work assumed a phase-insensitive (coherent state) input, our new results allow for an arbitrary phase-sensitive (squeezed state) input.[7] We are concentrating our attention on identifying experimentally accessible quantum artifacts of this time constant. It appears that the inclusion of a small amount of broadband classical input noise may well provide the key—it leads to homodyne noise spectra which diverge from the coupled-mode limit in a manner that depends on the value of the quantum time constant.

---

[3] N.C. Wong, K.X. Sun, and J.H. Shapiro, "Squeezed Amplification in a Gain-Saturated Parametric Amplifier," Paper presented at the Optical Society of America Annual Meeting, San Jose, California, November 3-8, 1991.

[4] N.C. Wong, "Gravity-Wave Detection via an Optical Parametric Oscillator," *Phys. Rev. A*, forthcoming.

[5] J.H. Shapiro, "Phase-Conjugate Quantum Communication at Zero Error Probability with Finite Average Photon Number," paper presented at the Optical Society of America Annual Meeting, San Jose, California, November 3-8, 1991.

[6] R.K. John, J.H. Shapiro, and P. Kumar, "Classical and Quantum Noise Transformations Generated by a Kerr Nonlinearity," *Digest of the International Quantum Electronics Conference*, Baltimore, Maryland, April 26-May 1, 1987.

[7] L.G. Joneckis and J.H. Shapiro. "Classical and Quantum Noise Transformations Generated by a Kerr Nonlinearity," paper presented at the Optical Society of America Annual Meeting, San Jose, California, November 3-8, 1991.

2.2.3 Publications

Ho, S.T., P. Kumar, and J.H. Shapiro. "Quantum Theory of Nondegenerate Multiwave Mixing. II. Adiabatic Elimination via Slowly Varying Amplitude Approximation." *Phys. Rev. A* 43(7): 3939-3948 (1991).

Ho, S.T., P. Kumar, and J.H. Shapiro. "Quantum Theory of Nondegenerate Multiwave Mixing. III. Application to Single-Beam Squeezed State Generation." *J. Opt. Soc. Am. B* 8(1): 37-57 (1991).

Ho, S.T., N.C. Wong, and J.H. Shapiro. "Single-Beam Squeezed-State Generation in Sodium Vapor and its Self-Focusing Limitations." *Opt. Lett.* 16(11): 840-842 (1991).

Joneckis, L.G., and J.H. Shapiro. "Classical and Quantum Noise Transformations generated by a Kerr Nonlinearity." Paper presented at the Optical Society of America Annual Meeting, San Jose, California, November 3-8, 1991.

Shapiro, J.H. "Going Through a Quantum Phase." Paper presented at the Workshop on Squeezed States and Uncertainty Relations, College Park, Maryland, March 28-30, 1991.

Shapiro, J.H. "Phase-Conjugate Quantum Communication at Zero Error Probability with Finite Average Photon Number." Paper presented at the Optical Society of America Annual Meeting, San Jose, California, November 3-8, 1991.

Shapiro, J.H., and S.R. Shepard. "Quantum Phase Measurements: A System-Theory Perspective." *Phys. Rev. A* 43(7): 3795-3818 (1991).

Shepard, S.R. "On the Measurement of Time for the Quantum Harmonic Oscillator." Paper presented at the Workshop on Squeezed States and Uncertainty Relations, College Park, Maryland, March 28-30, 1991.

Wong, N.C. "Squeezed Amplification in a Nondegenerate Parametric Amplifier." *Opt. Lett.* 16(21): 1698-1700 (1991).

Wong, N.C. "Gravity-Wave Detection via an Optical Parametric Oscillator." *Phys. Rev. A*, forthcoming.

Wong, N.C. "Squeezed Amplification in a Gain-Saturated Parametric Amplifier." Paper presented at the Conference on Quantum Electronics and Laser Science, Baltimore, Maryland, May 12-17, 1991.

Wong, N.C., K.X. Sun, and J.H. Shapiro. "Squeezed Amplification in a Gain-Saturated Parametric Amplifier." Paper presented at the Optical Society of America Annual Meeting, San Jose, California, November 3-8, 1991.

Wong, N.C. "Gravitational Wave Detection via an Optical Parametric Oscillator." Paper presented at the Optical Society of America Annual Meeting, San Jose, California, November 3-8, 1991.

2.3 Optical Frequency Division

Sponsors

National Institute of Standards and Technology
Grant 60-NANBOD-1052
U.S. Army Research Office
Grant DAAL03-90-G-0128

Project Staff

Dr. Ngai C. Wong, Dicky Lee, Phillip T. Nee, L. Reginald Brothers

An optical parametric oscillator (OPO) efficiently converts an input pump into two intense, coherent subharmonic outputs whose frequencies are tunable and whose sum frequency equals the pump frequency. By measuring the output frequency difference relative to a microwave source, the output frequencies are precisely determined, and the OPO functions as an optical frequency divider.[8] Optical parametric dividers (OPDs) can be operated in series or in parallel to measure, compare, and synthesize frequencies from optical to microwave, with high precision and resolution. This new technique of optical frequency division will be important in precision measurements, optical frequency standards, and coherent optical communications.

We have successfully phase locked the signal-idler output beat frequency of our two-element KTP OPO to a microwave synthesized signal at 9.36 GHz, thus demonstrating the OPO approach to

[8] N.C. Wong, "Optical Frequency Division Using an Optical Parametric Oscillator," *Opt. Lett.* 15(20): 1129-1131 (1990).

tunable optical frequency division.[9] The demodulated signal-idler beat spectrum of the phase-locked OPO shows a beatnote linewidth of no more than a few Hz, indicating that the output frequency linewidths are limited mostly by the pump laser frequency noise rather than the inherent OPO phase diffusion noise. The design of our two-element KTP OPD permits systematic and continuous frequency tuning. Together with its low threshold (40 mW) and high conversion efficiency (30%), the KTP OPD can be useful in potential applications such as optical communications.

We have proposed the use of OPDs to generate a 10 THz, precision optical frequency comb.[10] By pumping a set of 10 OPDs at 750 nm wavelength, the outputs at 1.5 μm wavelength serve as major frequency markers at 0.5 THz frequency intervals. Strong external phase modulation of the OPD outputs is used to maintain the phase-locked loops and to provide minor frequency markers at ~ 20 GHz intervals. In a dense fiber-based optical communication network, this scheme greatly simplifies the identification of channel frequencies over the entire bandwidth with kHz precision and accuracy, thus increasing its channel capacity.

As an application in the field of precision measurements, we have analyzed theoretically the use of a two-arm OPO as an active gravity-wave detector.[11] The signal and idler waves are internally separated such that the signal beam propagates along one arm of the OPO and the idler beam along the orthogonal arm. By monitoring the phase shift of the signal-idler beat frequency, a sensitive measure of the gravity-wave-induced differential path displacement in the OPO's two interferometer arms is obtained. The advantages of a low-loss all-solid-state OPO detector include its insensitivity to pump frequency noise and signal detection in a quiet radio frequency region.

2.3.1 Publications

Lee, D., and N.C. Wong. "Tunable Optical Frequency Division Using a Phase-Locked Optical Parametric Oscillator." *Opt. Lett.* 17(1): 13-15 (1992).

Wong, N.C. "Gravitational Wave Detection via an Optical Parametric Oscillator." Paper presented at the Optical Society of America Annual Meeting, San Jose, California, November 3-8, 1991.

Wong, N.C. "Gravity-Wave Detection via an Optical Parametric Oscillator." *Phys. Rev. A,* forthcoming.

Wong, N.C. "Precise Optical Frequency Comb Generation based on Optical Parametric Oscillators." Paper presented at the Optical Society of America Annual Meeting, San Jose, California, November 3-8, 1991.

Wong, N.C. "Proposal for a 10 THz, Precision Optical Frequency Comb Generator." Submitted to *IEEE Photonics Tech. Lett.*

Wong, N.C., and D. Lee. "Experimental Demonstration of a Tunable Optical Frequency Divider." Paper presented at the American Physical Society, Spring Meeting, Washington, D.C., April 22-25, 1991.

Wong, N.C., and D. Lee. "Optical Parametric Division." Invited paper. Accepted for presentation at the 46th Symposium on Frequency Control, Hershey, Pennsylvania, May 27-29, 1992.

Wong, N.C., and D. Lee. "A Tunable Optical Parametric Oscillator for Precision Measurements." Paper presented at the Optical Society of America Annual Meeting, San Jose, California, November 3-8, 1991.

2.4 Laser Radar System Theory

Sponsor

U.S. Army Research Office
Contract DAAL03-87-K-0117

Project Staff

Professor Jeffrey H. Shapiro, Bradley T. Binder, Thomas J. Green, Jr., Robert E. Mentle

Coherent laser radars represent a true translation to the optical frequency band of conventional microwave radar concepts. Owing to the enormous

[9] D. Lee and N.C. Wong, "Tunable Optical Frequency Division Using a Phase-Locked Optical Parametric Oscillator," *Opt. Lett.* 17(1): 13-15 (1992).

[10] N.C. Wong. "Proposal for a 10 THz, Precision Optical Frequency Comb Generator," submitted to *IEEE Photonics Tech. Lett.*

[11] N.C. Wong, "Gravity-Wave Detection via an Optical Parametric Oscillator," *Phys. Rev. A,* forthcoming.

wavelength disparity between microwaves and light, laser systems offer vastly superior space, angle, range, and velocity resolution as compared to their microwave counterparts. However, the resolution benefits associated with the shortness of laser wavelengths are accompanied by the penalties of this wavelength region: the ill-effects of atmospheric optical wave propagation in turbulent or turbid conditions, and the speckle patterns resulting from target roughness on wavelength scales. The ensuing trade-off between resolution advantages and propagation/speckle disadvantages makes it likely that laser radars will fill new application niches, rather than supplant existing microwave systems.

We have been working to quantify the preceding issues through development and experimental validation of a laser radar system theory. Our work includes a collaboration arrangement with the Opto-Radar Systems Group of the MIT Lincoln Laboratory, whereby the experimental portions of the research are carried out with measurements from their CO_2 laser radar test beds.

2.4.1 Target Detection and Recognition Theory

We have been developing the appropriate target-detection theory for multipixel multidimensional laser radar imagers, including those systems which augment their active-sensor channels with a forward-looking infrared (FLIR) passive channel. Our development of generalized likelihood-ratio tests (GLRTs) and associated receiver operating characteristics (ROCs) for this problem has addressed the realistic case of detecting a spatially-resolved, speckle target embedded in a spatially-resolved, speckle background. The target, if it is present, has unknown azimuth, elevation, range, and reflectivity. The background reflectivity is also unknown. Results of theory, computer simulation, and experiments have supported and quantified the intuitive notion that additional sensor dimensionality significantly improves detection performance. In recent work, we have removed the previous restriction of coarse-range (2-D) pulsed imager operation, by introducing the correct statistical model for fine-range (3-D) pulsed-imager operation.[12] We have also eliminated the assumption that the background's planar range profile is known, by using the expectation-maximization algorithm to obtain maximum-likelihood background range estimates.[13] This approach is both calculationally convenient and amenable to generalization to higher-order range fits. Finally, we have extended our framework to include the problem of maximum-likelihood target recognition, providing, for the first time, near-optimal processor structure and performance results for this M-ary decision task.[14]

2.4.2 Laser Radar Tomography

Through collaboration with the Laser Radar Measurements Group of the MIT Lincoln Laboratory, we have completed an investigation of the effects of target speckle on tomographic laser radar imaging.[15] Impulse-response descriptions for the mean image behavior of Doppler-time-intensity (DTI) and range-time-intensity (RTI) operation have been obtained. These impulse responses show space-variant effects commensurate with results obtained from experiment and simulation. Carrier-to-noise ratio and signal-to-noise ratio formulas were also derived for both DTI and RTI imagers. We found that speckle noise can be suppressed, without resolution loss, by increasing the number of projections employed.

2.4.3 Publications

Binder, B.T. *Laser Radar Tomography: The Effects of Speckle.* Ph.D. diss., Dept. of Electr. Eng. and Comput. Sci., MIT, 1991.

Green, T.J., Jr., and J.H. Shapiro. "Maximum-Likelihood Laser Radar Range Profiling with the Expectation-Maximization Algorithm." Submitted to *Opt. Eng.*

---

[12] T.J. Green, Jr., J.H. Shapiro, and M.M. Menon, "Target Detection Performance Using 3-D Laser Radar Images." *Proc. SPIE* 1471: 328-341 (1991).

[13] T.J. Green, Jr., and J.H. Shapiro, "Maximum-Likelihood Laser Radar Range Profiling with the Expectation-Maximization Algorithm," submitted to *Opt. Eng.*

[14] T.J. Green, Jr., *Three-Dimensional Object Recognition Using Laser Radar,* Ph.D. diss., Dept. of Electr. Eng. and Comput. Sci., MIT, 1992.

[15] B.T. Binder, *Laser Radar Tomography: The Effects of Speckle,* Ph.D. diss., Dept. of Electr. Eng. and Comput. Sci., MIT, 1991.

Green, T.J., Jr. *Three-Dimensional Object Recognition Using Laser Radar.* Ph.D. diss., Dept. of Electr. Eng. and Comput. Sci., MIT, 1992.

Green, T.J., Jr., J.H. Shapiro, and M.M. Menon. "Target Detection Performance Using 3-D Laser Radar Images." *Proc. SPIE* 1471: 328-341 (1991).

Mentle, R.E., and J.H. Shapiro. "Track-While-Image in the Presence of Background." *Proc. SPIE* 1471: 342-353 (1991).

2.5 Fiber-Coupled External-Cavity Semiconductor High Power Laser

Sponsor

U.S. Navy - Office of Naval Research
Grant N00014-89-J-1163

Project Staff

Dr. Robert H. Rediker, Christopher J. Corcoran, D. Shane Barwick

During 1991, quantitative experiments and associated theory were performed towards the understanding of the physics of the fiber-coupled external-cavity semiconductor high-power laser. The understanding that has been gained is also relevant in general to semiconductor laser arrays within external cavities and to monolithic semiconductor diode arrays. The issue of phasing the outputs from the coherent ensemble of elements in the array, which has been addressed in this work, is important for all arrays. Polarization, phasing the inputs to the external cavity, and coherence of the output from the external cavity have been studied.

The threshold current of the ensemble increases as the polarization of the radiation input to the cavity from one of the fibers is changed from the cavity's lowest threshold mode (TE). In addition, the output polarization of the ensemble rotates away from TE by up to 5 degrees. The experimental results are in agreement with theory.

The output spectrum of the ensemble tunes in wavelength and passes through a series of secondary modes of operation as the optical-path-length of one of the fiber inputs is increased. At these new wavelengths, the ensemble operates with lower output power in the dominant mode and greater output power in the side modes. At these new wavelengths the total power output was also reduced. A computer simulation found the intersections of the resonant frequencies of the fiber inputs to the cavity, computed the gain at these wavelengths (including the effects of non-perfect anti-reflection coating on the front facet of each laser diode), and predicted the output power in each of these modes. The program also tracked the maximum-gain wavelength of the ensemble as the optical-path-length of a single fiber is increased and predicted the wavelength tuning of the ensemble. The wavelength tuning results are in agreement with experimental data. At higher wavelength shifts, however, the predicted output power in the predominant operating modes is higher than the experimental results.

The coherence between different pairs of the five gain elements decreases with increasing spatial separation between the fiber inputs to the cavity. The coherence also decreases with larger slit widths in the spatial filter inside the cavity. The results are explained based on spontaneous emission inside the five separate gain elements and the action of the spatial filter. The coherence does not depend on phase changes of the optical inputs into the external cavity.

Publications

Corcoran, C.J., and R.H. Rediker. "Operation of Five Individual Lasers as a Coherent Ensemble by Fiber Coupling into an External Cavity." *Appl. Phys. Lett.* 59(7): 759-761 (1991).

Corcoran, C.J., R.H. Rediker, and K. Rauschenbach. "Effects on the Operation of an External-Cavity Laser of Phase Differences Between Multiple Inputs into the Cavity." Paper presented at the IEEE Lasers and Electro-Optical Society (LEOS) Annual Conference, San Jose, California, November 4-7, 1991.

Rediker, R.H, K.A. Rauschenbach, and R.P. Schloss. "Operation of a Coherent Ensemble of Five Diode Lasers in an External Cavity." *IEEE J. Quantum Electron.* 27(6): 1582-1593 (1991).

2.6 Analog Processing of Optical Wavefronts Using Integrated Guidod-Wave Optics

Sponsor

U.S. Air Force - Office of Scientific Research
Contract F49620-90-C-0036

Project Staff

Dr. Robert H. Rediker, Donald E. Bossi, Suzanne D. Lau, Brian K. Pheiffer, Boris Golubovic

In wavefront sensing and correction, it is envisioned that 10^3-10^4 basic modules would be used. In integrated optics, as in integrated circuits, it is important to relax the requirements on individual components and require that the operation of the integrated optics (circuits) be independent of significant component variations. The wavefront is sensed by interferometers between the multiplicity of through waveguides with the arms of the interferometers evanescently coupled to adjacent waveguides. The input powers to the interferometer arms will not be equal as a result of (1) the input power to the waveguide array being nonuniform and (2) unequal coupling by the evanescent couplers.

A Y-junction interferometer phase measurement technique has been developed which is independent of the power or power ratio in the input arms. The technique is intended for use in the basic module of the proposed integrated optical system for use at GaAs wavelengths that produces a flat-phase output wavefront. A proof-of-concept AlGaAs guided-wave Mach-Zehnder interferometer was employed to demonstrate measurement and correction of a phase difference between the arms using this technique. Results have been obtained for cases of successive steps in the phase difference between the interferometer arms, of random phase differences, and of intentional power imbalance between the arms. Power ratios greater than 10:1 between the arms have been created by applying a high voltage to a phase modulator in one arm so that power is absorbed via electro-absorption and/or by forward-biasing a modulator in one arm so that power is absorbed by carrier absorption. The experimental results on the phase measurement and phase correction have been independent of power imbalance up to these ratios of greater than 10:1.

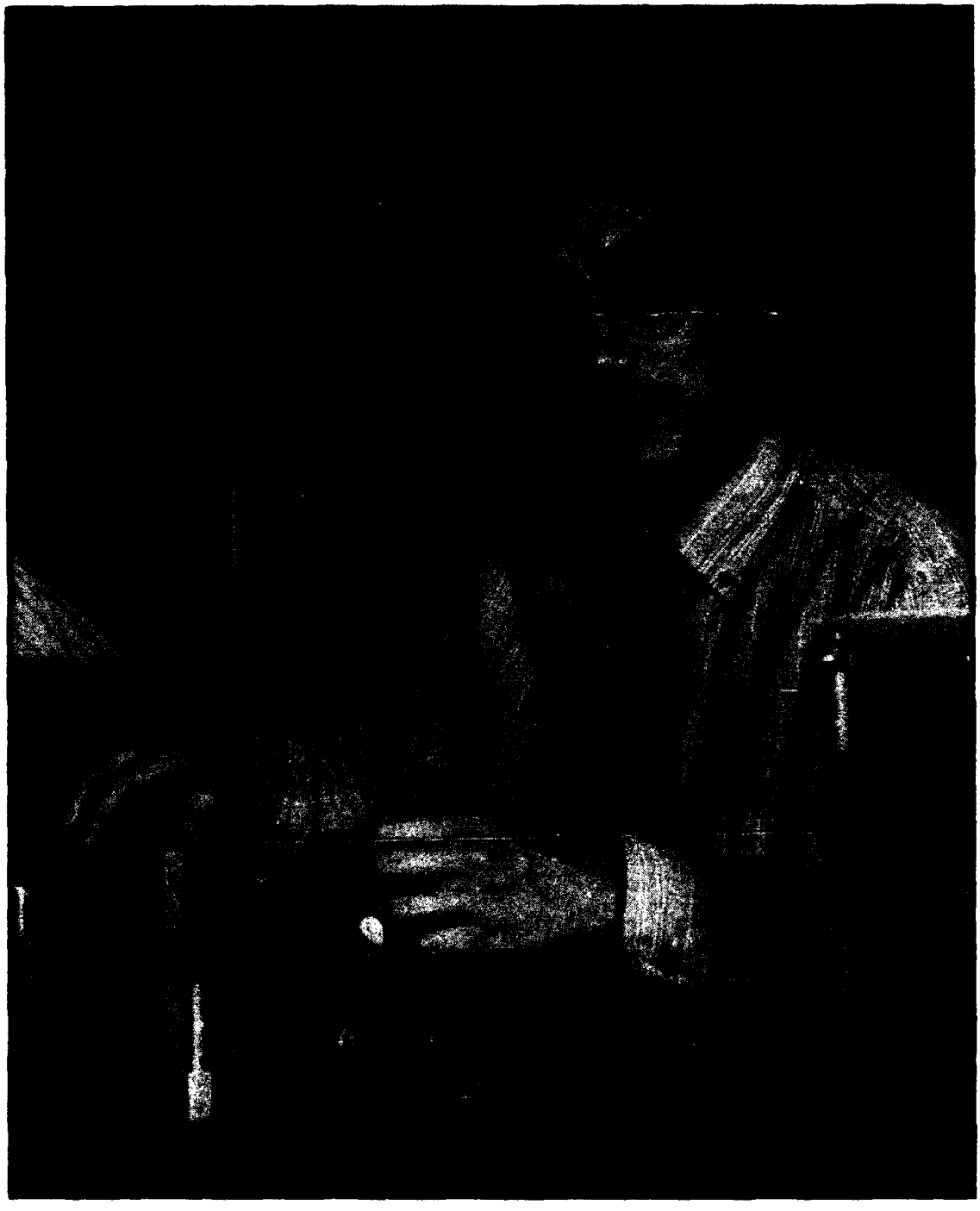
The Mach-Zehnder interferometer was fabricated using a dielectric-loaded strip waveguide structure. The modal characteristics of these waveguides were modelled theoretically and compared to experimental results. The waveguide propagation loss was less than 1 dB/cm measured at 862 nm by a Fabry-Perot technique. The abrupt bend and Y-junction insertion loss was measured as a function of angle. The abrupt bend insertion loss was $\approx$0.20 dB/bend for 0.5 degree angle and the Y-junction insertion loss was $\approx$0.37 dB for a 1.0 degree full angle. Phase modulators were fabricated by a selective Be ion implantation, followed by rapid thermal annealing, to form a p^+-n-n^+ structure. The phase in the waveguides was modulated via the electrooptic effect by reverse biasing the p-n structure. The compositions of the AlGaAs epilayers were chosen to minimize electroabsorption at the desired operating wavelengths and voltages. The phase modulators were modelled by a perturbation analysis and a more exact series solution analysis of the waveguide in the presence of an electric field. The more exact analysis is generally applicable to any arbitrary waveguide structure with index profile $n^2(x)$ that can be expressed as a polynomial function of position x.

Publications

Bossi, D.E., W.D. Goodhue, L.M. Johnson, and R.H. Rediker. "Reduced-Confinement GaAlAs Tapered Waveguide Antennas for Enhanced Far-Field Beam Directionality." *IEEE J. Quantum Electron.* 27(3): 687-695 (1991).

Lau, S.D., J.P. Donnelly, C.A. Wang, R.B. Goodman, and R.H. Rediker. "Optical Wavefront Phase Tilt Measurement and Correction Using AlGaAs Integrated Guided-Wave Components." Paper presented at the Integrated Photonics Research Topical Meeting, Monterey, California, April 9-11, 1991, pp. 124-125.

Lau, S.D., J.P. Donnelly, C.A. Wang, R.B. Goodman, and R.H. Rediker. "Optical Phase Difference Measurement and Correction Using AlGaAs Integrated Guided-Wave Components." *IEEE Photon. Tech. Lett.* 3(10): 902-904 (1991).



Professor Qing Hu

Chapter 3. High-Frequency (>100 GHz) Electronic Devices

Academic and Research Staff

Professor Qing Hu

Graduate Students

Edouard A. Garcia, Rajesh K. Gupta, Brian R. Jacobson, Jurgen H. Smet, Rolf A. Wyss

Undergraduate Students

Andrew E. Lan, Huy X. Le, Scott R. Velazquez, Noah D. Zamdmer

Technical and Support Staff

Barbara A. King

3.1 Millimeter Wave and Infrared Superconducting Focal-plane Receiver Arrays

Sponsor

Defense Advanced Research Projects Agency
Contract MDA972-90-C-0021
National Aeronautics and Space Administration
Grant NAG2-693

Project Staff

Professor Qing Hu, Brian R. Jacobson, Edouard A. Garcia, Rolf A. Wyss in collaboration with MIT Lincoln Laboratory, IBM Corporation, and AT&T Bell Laboratories

Millimeter wave and far-infrared frequencies remain one of the most underdeveloped frequency ranges, even though the potential applications in remote sensing and communication are significant. This is because the millimeter wave and far-infrared frequency range falls between two other frequency ranges in which conventional semiconductor devices are usually operated. One is the microwave frequency range, and the other is the near-infrared and optical frequency range. Semiconductor devices which utilize the classical diffusive transport of electrons, such as diodes and transistors, have a high frequency limit. This limit is set by the time it takes for electrons to travel a certain distance. Currently, electron mobility and the smallest feature size which can be fabricated by lithography limit the frequency range to below 100 GHz. It is not very likely that this limit can be pushed much higher. Semiconductor devices based on quantum mechanical interband transitions, however, are limited to frequencies higher than those corresponding to the semiconductor energy gap, which is higher than 10 THz for most bulk semiconductors. Therefore, a large gap exists from 100 GHz to 10 THz in which very few devices are available.

The gap energies of conventional superconductors, such as Nb, are in the range of 100 GHz to 2 THz. This coincidence makes superconducting devices natural candidates for millimeter and submillimeter wave applications. At millimeter wave frequencies, the superconducting video detectors have been demonstrated to have quantum efficiency $e/\hbar\omega$, that is, a transport of one electron for one incoming photon; while the superconducting coherent receivers have been demonstrated to have their sensitivities limited only by the zero-point fluctuation of vacuum. Such receivers have been used widely in astrophysical studies. More applications are feasible in space-based communication and far-infrared spectroscopy which requires ultimate sensitivity.

We are currently developing a novel quasioptical scheme to couple the millimeter-wave and infrared signals to the superconducting devices through a combination of an etched horn antenna and a planar antenna supported by a thin ($\sim 1\ \mu$m) membrane, as shown in figure 1. This scheme combines the advantages of easy fabrication of lithographic thin-film structures and high antenna efficiencies of horn antennas. Because of the absence of substrate losses in this scheme, it is expected that a THz receiver can be constructed using all-Nb superconductor-insulator-superconductor (SIS) junctions. More important, because of the cumbersome mechanical structures used in conventional waveguide technology, microwave receivers have been single-element devices, as opposed to CCD imaging arrays at optical frequencies. Spatial scan has been

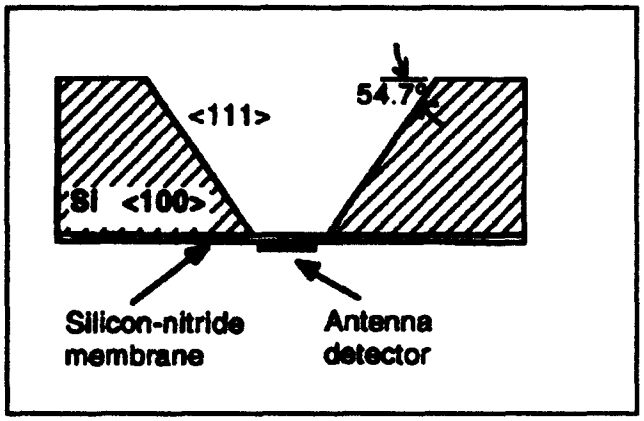


Figure 1. Example of anisotropic etching in a <100> silicon wafer. The opening of the wafer yields a pyramidal horn with a flare angle of 35.5°.

achieved mechanically. Using the novel quasi-optical scheme mentioned above, focal-plane detector arrays can be easily fabricated lithographically on a single Si wafer, as shown in figure 2, and far-infrared imaging becomes highly feasible.

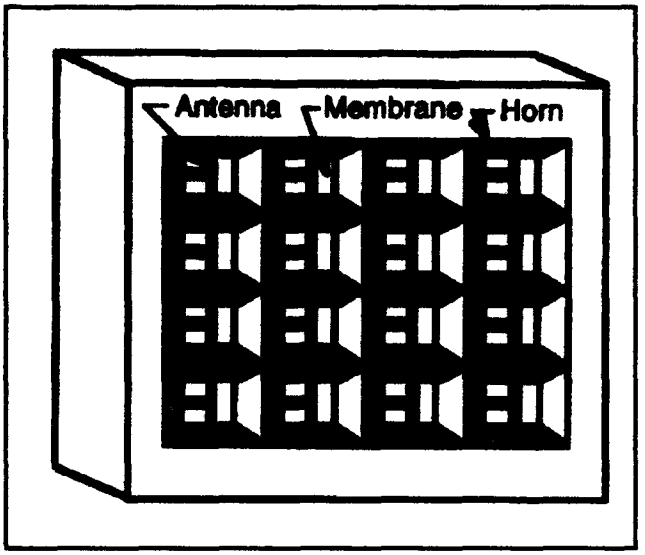


Figure 2. Perspective view of a two-dimensional horn imaging array.

3.2 Photon-assisted Quantum Transport in Quantum Point Contacts

Sponsor

National Science Foundation
Grant ECS 91-09330

Project Staff

Professor Qing Hu, Rolf A. Wyss in collaboration with Cristopher C. Eugster and Professor Jesús A. del Alamo

Quantum transport has been one of the most active fields in solid-state physics in recent years. Advances in material preparation have made quantum phenomena profound in electron transport for many semiconductor quantum devices such as quantum point contacts, quantum dots, quantum wires, quantum wells, superlattices, etc. In clean samples and at low temperatures, electrons can travel through the whole sample without suffering phase-destructive scattering. Extensive work has been done to study various features of such phase-coherent quantum transport. However, the experiments reported so far are limited to dc transport measurements or far-infrared spectroscopy measurements.

It is well known in the field of superconducting tunneling that photons can assist the tunneling process, provided the tunneling is elastic so that electrons do not suffer inelastic scattering. In a broad sense, elastic tunneling is a phase-coherent quantum transport in a classically forbidden region. Therefore, all the results of photon-assisted tunneling can be applied to the study of photon-assisted quantum transport in semiconductor devices. The study of the photon-assisted quantum transport can substantially improve our understanding of quantum transport phenomena. Novel long-wavelength optoelectronic devices may also emerge from this research.

In this NSF-sponsored project, we are studying the interaction between far-infrared photons and ballistic electrons in a quantum point contact (see schematic shown in figure 3(a)). The ballistic transport of electrons through the quantum point contact can be analyzed using an electron waveguide (see cross section shown in figure 3(b)). The width d of the waveguide can be varied by the gate voltage. Thus, the number of waveguide modes (subbands below the Fermi energy) which contribute to the source/drain conduction can be modulated by the gate voltage. Because electrons are fermions which obey Pauli's exclusion principle, each waveguide mode contributes exactly $2e^2/\hbar$ to the source/drain conductance. At certain negative gate voltages, such as shown in figure 3(b), the Fermi energy is suppressed below the first subband. Under this bias condition, the electron waveguide is pinched off, and the source/drain conductance is zero in the absence of radiation.

However, in the presence of radiation with appropriate polarity and photon energy, a source/drain current can be induced when the gate voltage is below the pinch off. The coupling of coherent radiation at ~300 GHz to the quantum point contact of submicron size is via a planar antenna

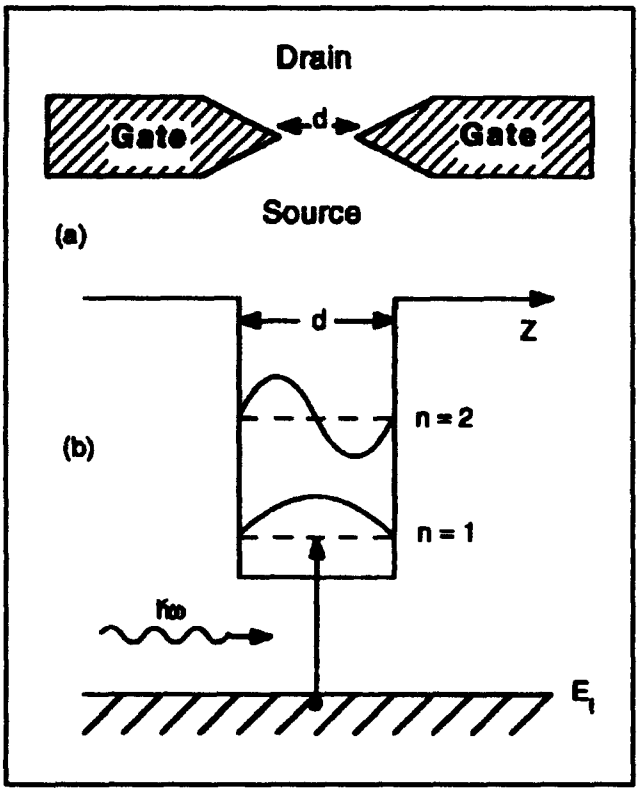


Figure 3. (a) Schematic of a quantum point contact. (b) Schematic of an electron waveguide which can be used to analyze the transport of electrons through the quantum point contact shown in (a).

with terminals that also serve as the split-gate of the quantum point contact, as shown in figure 4. In this scheme, the electrical field of the radiation is polarized perpendicular to the source/drain conduction path. Thus, intersubband transition can be excited by the far-infrared photons. At a gate voltage slightly below the pinch off (~ 1 mV), we have observed a photon-induced source/drain current with an amplitude comparable to that corresponding to the first quantized conductance step. We are currently optimizing the coupling efficiency of our system and carrying out a systematic study of photon-induced source/drain current as functions of the frequency and power of far-infrared radiation.

3.3 High-Tc Superconducting Josephson Devices

Sponsor

Defense Advanced Research Projects Agency
Contract MDA 972-90-C-0021

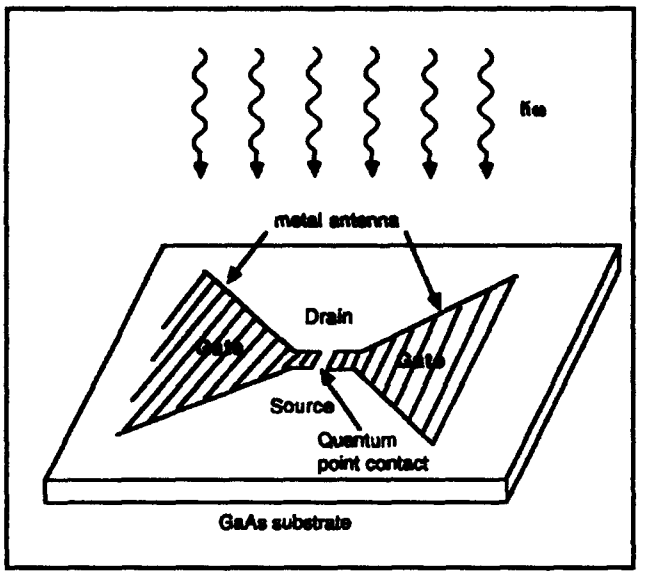


Figure 4. Schematic of an antenna-coupled quantum point contact (or electron waveguide). The incident radiation is usually focused by a lens onto the planar antenna, which in turn focuses the photon field into the small gap region between the two antenna terminals.

Project Staff

Professor Qing Hu, Rajesh K. Gupta, Scott R. Velazquez in collaboration with Twente University, The Netherlands

Many superconducting analog devices have been demonstrated to have higher sensitivities, higher speed and frequency limit, and lower power dissipation than competing semiconductor devices. Among them, the most successful ones are SQUIDs (Superconducting QUantum Interference Devices) and millimeter-wave detectors.

The discovery of superconductors with the superconducting transition temperature higher than liquid nitrogen temperature (high-Tc superconductors) has opened up new and exciting possibilities in electronic device technology. High temperature version of the superconducting devices mentioned above will find a much wider-range application wherever refrigeration is a problem. The key element of all superconducting analog and digital devices is the Josephson junction. This junction is formed by two superconductors weakly coupled together electrically. The supercurrent flowing through the Josephson junction oscillates at the Josephson frequency f = 2eV/h (500 GHz/mV), when a voltage is applied across the junction. Most of the useful applications of Josephson devices result from this high-frequency oscillation, such as high-frequency and high-speed signal processors and high-sensitivity SQUID magnetometers whose high precision results from averaging over many cycles of the Josephson oscillations.

In collaboration with the Dutch group headed by Professor Horst Rogalla, which is the leading group in fabricating high-Tc Josephson junctions with the most desirable properties, we are studying the response of high-Tc Josephson junctions to radiations at 100 GHz and above. We are also studying the effect of random noise, such as thermal and shot noise, on the performance of high-Tc Josephson devices. The immediate results of this research will be the development of liquid nitrogen cooled millimeter-wave and infrared detectors. Such devices will be very useful in extensive space-based sky and earth surveys, such as the one in the NASA's project "Mission to the Planet Earth," in which the detectors can be passively cooled by radiative cooling and in far-infrared spectroscopy. The study of the high-frequency response and noise effect will benefit all the future development of superconducting signal processors using high-Tc Josephson junctions.

3.4 Far-infrared (THz) Lasers Using Multiple Quantum Wells

Project Staff

Professor Qing Hu, Jurgen H. Smet, Edouard A. Garcia in collaboration with Professor Clifton G. Fonstad

Semiconductor quantum wells are man-made quantum mechanical systems in which energy levels can be chosen by changing the sizes of the quantum wells. Typically, the frequency corresponding to the intersubband transitions is in the far-infrared or THz range. Naturally, long-wavelength photoelectric devices, such as far-infrared lasers, which utilize the intersubband transitions, have been proposed and subsequently studied. Significant progress has been made recently toward this goal. Large oscillator strengths of intersubband transitions have been observed in far-infrared absorption spectroscopy experiments. An intersubband spontaneous emission with a power level of $\sim 10^{-7}$ W has been observed. Although these preliminary results are encouraging, two major challenges to building a quantum-well far-infrared laser remain. One is to achieve a high degree of population inversion between two subband levels, and the other is the confinement of photons within the active region. Optical pumping suffers from low efficiency and low modulation speed, thus it will be difficult to achieve a sufficient gain to maintain a lasing oscillation, so that optical pumping will be unsuitable for communication applications. As far as optical confinement is concerned, the usual dielectric waveguide confinement method, commonly used in optical and near-infrared laser systems, is not applicable at far-infrared frequencies because the confinement (on the order of a wavelength) is too large compared to the dimensions of the active region.

In this project, we will use a novel MQW (multiple quantum-well) device to circumvent these two problems. In this device, with an energy band diagram that is shown in figure 1 with and without a dc bias voltage, electrons are injected selectively into an upper subband level of a wide lasing quantum well through a narrow filter quantum well. After relaxing into a lower subband in the lasing well, the electrons are then removed selectively to a collector through another narrow filter quantum well. This filter well prevents the electrons in the upper subband level from tunneling out to the collector. Using this method of selective injection and removal, a high degree of population inversion can be achieved if the tunneling rate of the electrons from the ground state to the collector is greater than the relaxation rate of the electrons from the upper subband to the ground state. Our calculation indicates that this should easily be achieved.

In the proposed MQW laser device, a parallel-plate waveguide that confines the photons can be formed between a heavily doped semiconductor injector and collector. At a doping level of $2 \times 10^{18}/cm^3$, we can raise the plasma frequency in the injector and collector to about 17 THz. It has been reported that the electron mobility, m, for such a high doping level is 5×10^3 cm^2/Vs. This plasma is mostly reflective with a penetration depth as short as 0.8 μm for a lasing frequency in the range of 1-8 THz. This confinement is sufficiently tight so that the lasing threshold current density is on the order of several hundred A/cm^2, which should be achievable.

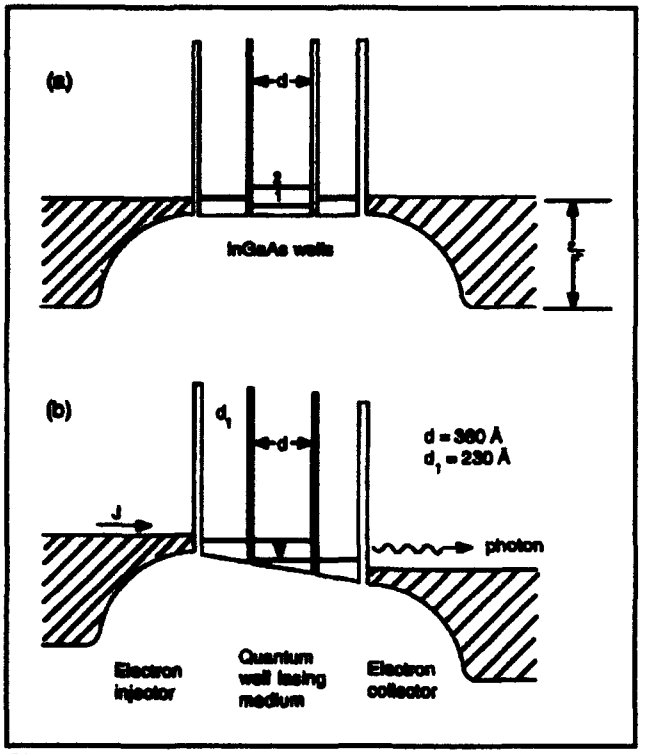


Figure 5. Band profiles (not drawn in proportion) of the proposed far-infrared laser device under (a) zero-bias, and (b) lasing condition in which Vbias ~ (E2 – E1)/e≈20 mV. The device consists of one narrow quantum-well energy filter on both sides of the lasing quantum well. The width of the narrow filter wells (made of $In_{0.53}Ga_{0.47}As$) is approximately 230Å so the energy of its first subband lies in between the first two subbands in the wide lasing well whose width is approximately 360Å, which will have a radiation frequency of 5 THz due to the intersubband transitions.

3.5 Research Facility

We have cryogenic systems which can cool devices down to 1.5 K. Each experimental set-up is equipped with low-noise electronic data acquisition systems which are capable of measuring current signals at subnonamp levels and voltage signals at submicrovolt levels. We also have microwave sweeper and spectrum analyzer up to 20 GHz. The most unique pieces of equipment in Professor Hu's group are various millimeter-wave and infrared sources which can generate coherent and incoherent radiation up to 30 THz. These include: Gunn oscillators at W-band frequencies (75-110 GHz); a frequency doubler, tripler, and quadrupler using Schottky diodes at 200, 300, and 400 GHz; an optically pumped far-infrared laser which generates coherent radiation up to 8 THz; and an infrared Fourier transform spectrometer which is capable in performing linear spectroscopy from 45 GHz to 30 THz and beyond.

3.6 Publications

Hu, Q., C.A. Mears, and P.L. Richards. "Millimeter Wave Superconducting Receivers." *IEEE MTT-S Digest* 409: (1991).

Hu, Q., and S. Feng. "Feasibility of Far-infrared Lasers Using Multiple Semiconductor Quantum Wells." *Appl. Phys. Lett.* 59: 2923 (1991).

Mears, C.A., Q. Hu, P.L. Richards, A. Worsham, and D.E. Prober. "Quantum Limited Quasiparticle Mixers at 100 GHz." *IEEE Trans. Magn.* MAG-27: 3363 (1991).

Mears, C.A., Q. Hu, and P.L. Richards. "The Effect of the Quantum Susceptance on the Gain of Superconducting Quasiparticle Mixers." *IEEE Trans. Magn.* MAG-27: 3384 (1991).

Nahum, M., Q. Hu, P.L. Richards, N. Newman, and S.A. Sachtjen. "Fabrication and Measurement of a High Tc Superconducting Microbolometer." *IEEE Trans. Magn.* MAG-27: 3081 (1991).

Zitkovsky, I.D., Q. Hu, T.P. Orlando, J. Melngailis, and M. Shepard. "Fabrication of High Tc Superconducting Weaklinks Using Focused Ion Beams." *Appl. Phys. Lett.* 59: 727 (1991).

Section 4 Surfaces and Interfaces

Chapter 1 Statistical Mechanics of Surface Systems and Quantum-Correlated Systems

Chapter 2 Synchrotron X-Ray Studies of Surface Disordering

Chapter 3 Chemical Reaction Dynamics at Surfaces

Chapter 4 Semiconductor Surface Studies

Chapter 5 Epitaxy and Step Structures on Semiconductor Surfaces

Chapter 1. Statistical Mechanics of Surface Systems and Quantum-Correlated Systems

Academic and Research Staff

Professor A. Nihat Berker

Graduate Students

Daniel P. Aalberts, Alexis Falicov, William C. Hoston, Jr., Roland R. Netz

1.1 Introduction

Sponsor

Joint Services Electronics Program
Contract DAAL03-89-C-0001
Contract DAAL03-92-C-0001

Our objectives are to develop, using renormalization-group theory and other methods of statistical mechanics, microscopic theories of quantum spin and electronic systems. Our approach is particularly suited to systems with fluctuations due to finite temperatures, impurities, surfaces or other geometric constraints.

1.2 Renormalization-Group Approach to Electronic Systems

Project Staff

Alexis Falicov, Professor A. Nihat Berker

High-T_c superconductivity, metallic magnetism, the metal-insulator transition, and heavy fermion behavior are all phenomena produced by the strong correlations of electrons in narrow energy bands. It is therefore important to study theoretical models that incorporate the strong correlation effects of electrons. The tJ model is such a system. It is defined on a lattice with one spherically symmetric orbital per site by the Hamiltonian

$$H_{tJ} = P\,[\,-t\,\Sigma_{<ij>,\sigma}\,(c^{+}_{i\sigma}\,c_{j\sigma} + \text{h.c.}) + J\,\Sigma_{<ij>}(\vec{s}_i\vec{s}_j - n_i n_j/4)]\,P,$$

where P is an operator that projects out all doubly occupied sites, $c^{\dagger}_{i\sigma}$ and $c_{i\sigma}$ are creation and annihilation operators for an electron in a Wannier state at site i with z-component of spin σ, n_i is the electron number operator that counts the total number of electrons at site i, and $\vec{s}_i$ is the spin operator. This Hamiltonian can be interpreted in two ways: (1) In the case of small J, the system can be thought of as the large U limit of the single-band Hubbard model of electronic systems. The antiferromagnetic exchange comes as a result of a virtual process where one electron hops onto a singly occupied nearest-neighbor site and then hops back. The energy gain for such a process is of the order of t^2/U since a doubly occupied site has energy U. (2) The system can also be thought of as an electronic system with a "super" exclusion principle where no two electrons (like or unlike spins) are allowed on the same site. The second interpretation does not put any restriction on the size of J.

There are few rigorous results available on this system: (1) At half filling, the system reduces to a Heisenberg antiferromagnet. (2) At $2t = \pm J$, the model has been solved by the Bethe-ansatz technique. (3) In one dimension and $J = 0$, the model has been solved also by the Bethe-ansatz technique. Other attempts to study this model have focused on the ground state and first few excited states. We have decided, instead, to focus on the thermodynamic properties of this system. Our method, the renormalization-group approach, involves solving a statistical mechanics problem by a recursive elimination of the degrees of freedom. Since the Hamiltonian involves a regular lattice, this problem is well suited for the position-space renormalization-group method. The solution is obtained in an expanded space with Hamiltonian

$$H = P\,[\,-t\,\Sigma_{<ij>,\sigma}\,(c^{+}_{i\sigma}c_{j\sigma} + \text{h.c.}) + \Sigma_{<ij>}\,(J\vec{s}_i\vec{s}_j + Vn_in_j) + \mu\Sigma_i n_i]\,P.$$

Because of the non-commutativity of quantum operators, new techniques of renormalization-group theory had to be developed.

We have obtained the renormalization-group flows for the effective coupling constants for one-, two-, and three-dimensional systems. The flows determine the phase diagrams and all thermodynamic

properties. In one dimension, we find, as expected, no finite-temperature phase transition. In two dimensions, we find a single finite-temperature critical point, as previous workers conjectured but were unable to derive. In three dimensions, our preliminary results indicate a rich finite-temperature phase diagram with novel phases, phases transition behaviors, and conductivity phenomena. Our results are also confirmed by our exact small-cluster calculations.

1.3 Phase Diagrams of Semiconductor Alloys

Project Staff

William C. Hoston, Jr., Roland R. Netz, Professor A. Nihat Berker

A study of ternary compounds on face-centered-cubic lattices has been started. The aim of the work is to elucidate the phase behavior of ternary and quaternary semiconductor alloys. These alloys have received recent attention for both fundamental and technological reasons. It has been found that these alloys can exist in the zincblende, chalcopyrite, or possibly stannite structures, involving two interpenetrating fcc lattices on which up to four atomic species exist. One atomic species occupies one of the fcc lattices while three other atomic species may (chalcopyrite, stannite) or may not (zincblende) order on the other fcc lattice. At present, not much is known about the chalcopyrite structure seen in the experimentally obtained III-V compounds. There is great interest in learning how stable this chalcopyrite phase is against other possible structures.

In recent work by K.E. Newman and collaborators, the Blume-Emery-Griffiths model has been adopted for the study of the zincblende to chalcopyrite or stannite transitions. This model is a spin-1 Ising model with Hamiltonian

$$H = J \Sigma_{<ij>} s_i s_j + K \Sigma_{<ij>} s_i^2 s_j^2 - \Delta \Sigma_i s_i^2, \quad s_i = 0, \pm 1.$$

The three spin values are each associated with a different species of atom, A, B, or C, which exist on one of the fcc lattices. The other fcc lattice is considered occupied by atomic species D. The systems under consideration have the composition $[(AB)_{1-x}C_{2x}]D_2$.

The model includes interactions between the A, B, and C atoms. The parameters J and K in the Hamiltonian above are fixed as combinations of these interaction energies. They are chosen so as to give the chalcopyrite structure at low temperature ($J < 0$) and to control the phase transition between the chalcopyrite and the zincblende. Δ controls the relative densities of the species (AB) and C.

As a preliminary study, we have completed the global phase diagram study of the Blume-Emery-Griffiths model. We found six new phase diagrams, including novel multicritical topology and two new ordered phases. Thus, we determined that the phase diagram of this simple spin system includes nine distinct topologies and three ordered phases. These results were obtained by a global mean-field theory with four independent order parameters.

It is important to note, however, that the choice of $J < 0$ makes the model on the fcc lattice frustrated, which requires analysis beyond mean-field theory. We have developed a new method, which we have called "hard-spin mean-field theory," that incorporates the hard-spin condition of local degrees of freedom and thereby conserves frustration. We have tested this method on frustrated triangular and stacked triangular lattices with the spin-1/2 Ising model, obtaining excellent results. We are now applying the method to the Blume-Emery-Griffiths model. Our future studies of semiconductor alloys will also include renormalization-group theory.

1.4 Quantum Spin Systems

Project Staff

Daniel P. Aalberts, Professor A. Nihat Berker

We are interested in calculating the thermodynamic properties of quantum mechanical systems at low temperatures, where the distinctive quantum phenomena are important. The first model we consider is the $s = 1/2$ XXZ model, with Hamiltonian

$$H = \Sigma_{<ij>} [J (s_i^x s_j^x + s_i^y s_j^y) + J_z s_i^z s_j^z].$$

This model in two dimensions is of interest in high-T_c superconductors; it is also of general interest to develop our ability to do the statistical mechanics of quantum systems and to extract, thereby, the quantitative properties of their elementary excitations.

We map this d-dimensional quantum system quantitatively onto a (d+1)-dimensional classical system with complicated interactions. For the ferromagnetic quantum system, we have been able to obtain magnon dispersion relations and magnon-magnon interactions. Eventually, we expect to apply our method to antiferromagnetic

quantum systems, where even the ground state presents a many-body problem.

1.5 Publications

Alerhand, O.L., A.N. Berker, J.D. Joannopoulos, D. Vanderbilt, R.J. Hamers, and J.E. Demuth. "Finite-Temperature Phase Diagram of Vicinal Si(100) Surfaces: Alerhand et al. Reply." *Phys. Rev. Lett.* 66(7): 962 (1991).

Berker, A.N. "Absence of Temperature-Driven First-Order Phase Transitions in Systems with Random Bonds." *J. Appl. Phys.* 70(10): 5941-5945 (1991).

Berker, A.N., and K. Hui. "Absence of Temperature-Driven First-Order Phase Transitions in Systems with Random Bonds." In *Science and Technology of Nanostructured Magnetic Materials.* Eds. G.C. Hadjipanayis and G.A. Prinz. New York: Plenum, 1991.

Berker, A.N., R.G. Caflisch, and M. Kardar. "Statistical Mechanics of Phase Transitions with a Hierarchy of Structures." In *Hierarchically Structured Materials.* Ed. I.A. Aksay. Pittsburgh: Materials Research Society, 1992.

Hoston, W., and A.N. Berker. "Multicritical Phase Diagrams of the Blume-Emery-Griffiths Model with Repulsive Biquadratic Coupling." *Phys. Rev. Lett.* 67(8): 1027-1030 (1991).

Hoston, W., and A.N. Berker. "Dimensionality Effects on the Multicritical Phase Diagrams of the Blume-Emery-Griffiths Model with Repulsive Biquadratic Coupling: Mean-Field and Renormalization-Group Studies." *J. Appl. Phys.* 70(10): 6101-6103 (1991).

Hoston, W. *Multicritical Phase Diagrams of the Blume-Emery-Griffiths Model with Repulsive Biquadratic Coupling: Mean-Field and Renormalization-Group Studies.* S.M. thesis, Dept. of Physics, MIT, 1991.

Netz, R.R. "New Phases and Multiple Reentrance of the Blume-Emery-Griffiths Model with Repulsive Biquadratic Coupling: Monte Carlo Renormalization-Group Theory." *Europhys. Lett.* 17(4): 373-377 (1992).

Netz, R.R., and A.N. Berker. "Monte Carlo Mean-Field Theory and Frustrated Systems in Two and Three Dimensions." *Phys. Rev. Lett.* 66(3): 377-380 (1991).

Netz, R.R., and A.N. Berker. "Hard-Spin Mean-Field Theory: Formulation for Ising, XY, and Other Models." *J. Appl. Phys.* 70(10): 6074-6076 (1991).

Netz, R.R., and A.N. Berker. "Monte Carlo Mean-Field Theory and Frustrated Systems in Two and Three Dimensions: Netz and Berker Reply." *Phys. Rev. Lett.* 67(13): 1808 (1991).

Netz, R.R., and A.N. Berker. "Smectic C Order, In-Plane Domains, and Nematic Reentrance in a Microscopic Model of Liquid Crystals." *Phys. Rev. Lett.* 68(3): 333-336 (1992).

Netz, R.R., and A.N. Berker. "Microscopic Liquid Crystal Theory of Nematic Reentrance, Smectic C Ordering, and In-Plane Domain Formation." In *Phase Transitions in Liquid Crystals.* Ed. S. Martellucci. New York: Plenum, 1992.

Netz, R.R. "Microscopic Theory of the Ripple Phase." In *Structure and Conformation of Amphiphilic Membranes.* Ed. R. Lipowsky. Berlin: Springer-Verlag, 1992.

Netz, R.R. *Frustration in Magnetic, Liquid Crystal, and Surface Systems: Monte Carlo Mean-Field Theory.* S.M. thesis, Dept. of Physics, MIT, 1991.

Meeting Papers

American Physical Society Meeting, Cincinnati, Ohio, March 18-22, 1991.

Berker, A.N. "Quenched Fluctuation Induced Second-Order Phase Transitions."

Hoston, W., and A.N. Berker. "New Multicritical Phase Diagrams from the Blume-Emery-Griffiths Model with Repulsive Biquadratic Interactions."

Netz, R.R., and A.N. Berker. "Monte Carlo Mean-Field Theory and Frustrated Systems in Two and Three Dimensions."

American Physical Society Meeting, Indianapolis, Indiana, March 16-20, 1992.

Aalberts, D.P., and A.N. Berker. "Hard-Spin Mean-Field Theory: Variational Free Energy and First-Order Phase Transitions."

Berker, A.N., and R.R. Netz. "Smectic C Order, In-Plane Domains, and Nematic Reentrance in a Frustrated Microscopic Model of Liquid Crystals."

Netz, R.R. "Symmetry-Breaking Fields in Frustrated Ising Systems on Square and Cubic Lattices."

Netz, R.R. "Multiple Reentrance and New Phases from the Blume-Emery-Griffiths Model in Three Dimensions: Monte Carlo Renormalization-Group Theory."

International Conference on Thermodynamics and Statistical Mechanics, Berlin, Germany, August 2-8, 1992.

Berker, A.N. "Critical Behavior Induced by Quenched Disorder."

Netz, R.R., and A.N. Berker. "Smectic C/A_2 Order, Domains, Reentrance in a Microscopic Model of Liquid Crystals."

International Liquid Crystal Conference, 14th, Pisa, Italy, June 21-26, 1992.

Netz, R.R. and A.N. Berker. "Smectic C Order, Nematic Reentrance, Domains, and Smectic A_1–Smectic A_2 Transitions in a Frustrated Microscopic Model of Liquid Crystals."

Magnetism and Magnetic Materials-Intermag Conference, Pittsburgh, Pennsylvania, June 18-21, 1991.

Berker, A.N. "Absence of Temperature-Driven First-Order Phase Transitions in Systems with Random Bonds."

Hoston, W., and A.N. Berker. "New Multicritical Phase Diagrams from the Blume-Emery-Griffiths Model with Repulsive Biquadratic Interactions."

Netz, R.R., and A.N. Berker. "Monte Carlo Mean-Field Theory and Frustrated Systems in Two and Three Dimensions."

NATO Advanced Study Institute on Liquid Crystals, Erice, Italy, May 2-12, 1991.

Berker, A.N. "Microscopic Theory of Polar Liquid Crystals and Multiply Reentrant Phase Diagrams."

Netz, R.R., and A.N. Berker. "The Mean-Field Theory for Frustration, Layered Magnets, and Reentrant Liquid Crystals."

Statistical Mechanics Meeting, 65th, New Brunswick, New Jersey, May 15-17, 1991.

Hoston, W., and A.N. Berker. "Bicritical and Tetracritical Phase Diagrams of the BEG Model: Dimensionality Effects."

Netz, R.R., and A.N. Berker. "Microscopic Theory of Smectic A and C Phases of Frustrated Liquid Crystals."

Chapter 2. Synchrotron X-Ray Studies of Surface Disordering

Academic and Research Staff

Professor Robert J. Birgeneau, Dr. Kenneth I. Blum, Dr. Do-Young Noh

Graduate Students

William J. Nuttall, Monte J. Ramstad

Technical and Support Staff

Elizabeth M. Salvucci

2.1 Introduction

Sponsor

Joint Services Electronics Program
Contract DAAL03-89-C-0001
Contract DAAL03-92-C-0001

In this research program we use modern x-ray scattering techniques to study structures and phase transitions in thin films and on surfaces. We have two principal experimental facilities, one at MIT and the other at the National Synchrotron Light Source at Brookhaven National Laboratory. At MIT, we have four high-resolution computer-controlled x-ray spectrometers using high-intensity, rotating anode x-ray generators. The angular resolution can be made as fine as 1.8 seconds of arc, which enables us to probe the development of order from distances of the order of the x-ray wavelength ~1Å up to 30,000Å. The sample temperature can be varied between 2 K and 500 K with a relative accuracy of 2×10^{-3} K. At the National Synchrotron Light Source, in collaboration with IBM, we have three fully instrumented beam lines. Two of these beam lines allow us to make studies with photons varying in energy between 3 and 12 keV; the third has a fixed energy of 17 keV. These facilities make possible high-resolution scattering experiments with a flux of more than three orders of magnitude larger than that of a rotating anode x-ray generator, opening up a new generation of experiments.

Several years ago, as part of this JSEP program, we built an x-ray-compatible, high vacuum single crystal apparatus. This enabled us to use synchrotron radiation to study the structures and transitions occurring at a single surface, and such experiments are now becoming routine. As a result of our recent research, we determined that a new chamber allowing access to a wider range of reciprocal space was required. In collaboration with Professor Simon G.J. Mochrie, we have designed, built and are now commissioning this second-generation x-ray surface facility.

Our basic scientific objective is to understand the morphologies and microscopic structures of simple semiconductor and metal surfaces at high temperatures. Possible phase changes include surface roughening, surface reconstruction, melting, amorphization and dilution. These phenomena are particularly interesting on stepped surfaces, where there may be an interplay between step structures, faceting, reconstruction, and roughening.

2.2 Metal Surface Studies

In 1987 we reported a detailed study of a possible roughening transition of the Ag(110) surface. Specifically, we discussed the detailed line shape of the Ag($1\bar{1}0$) surface peak for temperatures between 100°C and 525°C. At ~450°C we observed a crossover to a pure power law lineshape, indicative of a rough surface, for the near-surface diffraction. Above 450°C the profiles could be described by the power law singularity form $(Q - Q_{110})^{-2+\eta}$ with η changing rapidly with temperature. Accordingly, we identified 450°C as the roughening temperature.

Our more recent experiments and those by others on crystals with very small miscuts ($\sim 0.5°$) suggest that the story may be more complicated. Specifically, the experiments suggest that below ~450°C to 500°C, the Ag(110) surface may be facetted. In order to explore this further, we have begun a systematic set of experiments on vicinal Ag(110) crystals with miscuts in the ($1\bar{1}0$) direction of up to 4°. Our initial experiments on a crystal miscut by $\sim 2.3°$ indeed show facetted behavior below ~500°C. Further experiments should elucidate the full nature of the roughening-facetting transition on this prototypical noble metal surface.

2.3 Semiconductor Surface Studies

2.3.1 Stepped Si(111) Surfaces

The behavior of vicinal surfaces (surfaces cut a few degrees away from low index facets) involves essential aspects of surface structures including equilibrium crystal shapes, roughening, faceting, and surface reconstruction. The stability of vicinal surfaces is determined by the shape of the equilibrium crystal surface. By studying a series of vicinal surfaces with various surface normals, one can map out the equilibrium crystal shape. A vicinal surface, when it is stable, forms a structure consistent with low-index terraces separated by steps whose spacing is usually incommensurate with the bulk substrate lattice. As in the case of incommensurate domain wall problems, there can not be true long range order in the structure of the incommensurate steps. This is due to the overwhelming amplitude of the long wavelength thermal fluctuations in two-dimensional systems with continuous symmetry. As a result, an incommensurate stepped surface is rough in an exact sense. A vicinal surface becomes unstable when the free energy of a nearby low index facet is lowered drastically by some mechanisms such as reconstruction. One might expect that the lowering of free energy of a low-index facet would break a vicinal surface into a low-index facet and rough faces with a higher misorientation angle.

We have carried out a detailed synchrotron x-ray scattering study of a vicinal Si(11$\bar{1}$) surface misoriented by 3.5° toward the (11$\bar{2}$) direction. At temperatures higher than the "7 x 7-to-1 x 1" transition, we find that the surface is composed of steps with a mean separation of ~ 60Å which are correlated beyond 3000Å. Below the transition, the surface is split into the large (> 3000Å) perfectly flat (111) facets together with stepped regions whose misorientation angle increases as temperature is decreased. The transition is first order, indicating that it is induced by the 7 x 7 reconstruction of the (111) facets. In the facetted phase, the facet angle α follows the law $\tan \alpha \sim |T_c - T|^{(\lambda-1)/\lambda}$ with $\lambda = 2.3^{+0.8}_{-0.5}$. This disagrees somewhat with the theoretical predication $\lambda = 3/2$ for models in which the interaction between steps is entropic in character.

At temperatures above 1110 K, we observed two step superlattice peaks bracketing the (10) position of the (111) surface. Figure 1 shows high resolution longitudinal and transverse scans through the first-order step peak at 1120 K. The simplest model leads us to believe that this peak results from the ordering of steps by the entropic repulsion. To test this idea quantitatively, we fit the high temperature peak profile to a 2D power law singularity of the form

$$S(\vec{q}) = (q_H^2 + Bq_K^2)^{(-2+\eta_1)/2}$$

convolved with the instrumental resolution function. Figure 1 shows the optimal simultaneous fits to the longitudinal and transverse scans with $h = 0.6 \pm 0.1$ and $B = 15 \pm 7$. It is evident that the power law form fits the data very well. The large value of η_1 is fully consistent with scattering from a rough surface whose height variance diverges logarithmically with distance. We note that as in the stripe domain commensurate-incommensurate problem the Pokrovsky-Talapov model leads to the prediction $\eta_1 = 2/9$, independent of temperature. This is in clear disagreement with our results. More elaborate models of the interaction between the steps are needed to explain the large value of η_1.

More recently, we have been studying the behavior of vicinal Si(111) at very high temperatures. Remarkably, we find that at ~1300 K there is a second phase transition in the step structure which mimics a surface melting transition. We are currently exploring this new-found phenomenon.

2.4 Publications

Blum, K.I., D.Y. Noh, A. Mak, K.W. Evans-Lutterodt, J.D. Broch, G.A. Held, and R.J. Birgeneau. "Structure and Phase Transitions of Ge(111) and Si(111) Surfaces at High Temperatures." In *Surface X-Ray and Neutron Scattering*. Vol. 61, pp. 27-31. Springer Proceedings in Physics. Ed. H. Zabel and I.K. Robinson. Berlin/Heidelberg: Springer-Verlag, 1992.

Keane, D.T., P.A. Bancel, G.L. Jordan-Sweet, G.A. Held, A. Mak, and R.J. Birgeneau. "Evidence for Two-Step Disordering of the Au(110) 1 x 2 Reconstructed Surface." *Surf. Sci.* 250: 8 (1991).

Mak, A., K. Evans-Lutterodt, K.I. Blum, D.Y. Noh, J.D. Brock, G.A. Held, and R.J. Birgeneau. "Synchrotron X-ray Diffraction Study of the Disordering of the Ge(111) Surface at High Temperatures." *Phys. Rev. Lett.* 66: 2002 (1991).

Noh, D.Y., K. Blum, M.J. Ramstad, and R.J. Birgeneau. "Long Range Separation of Steps on Vicinal Si(111)." *Phys. Rev. B* 44: 10969 (1991).

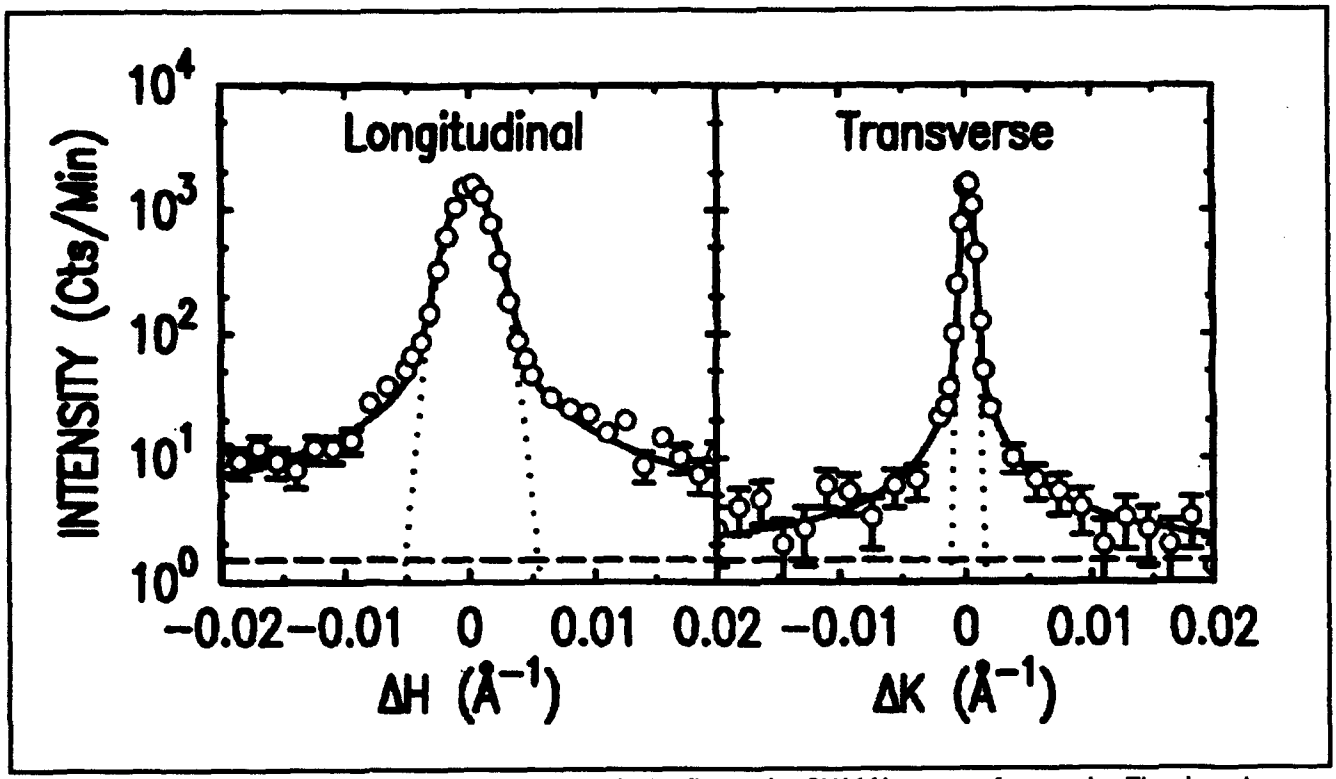
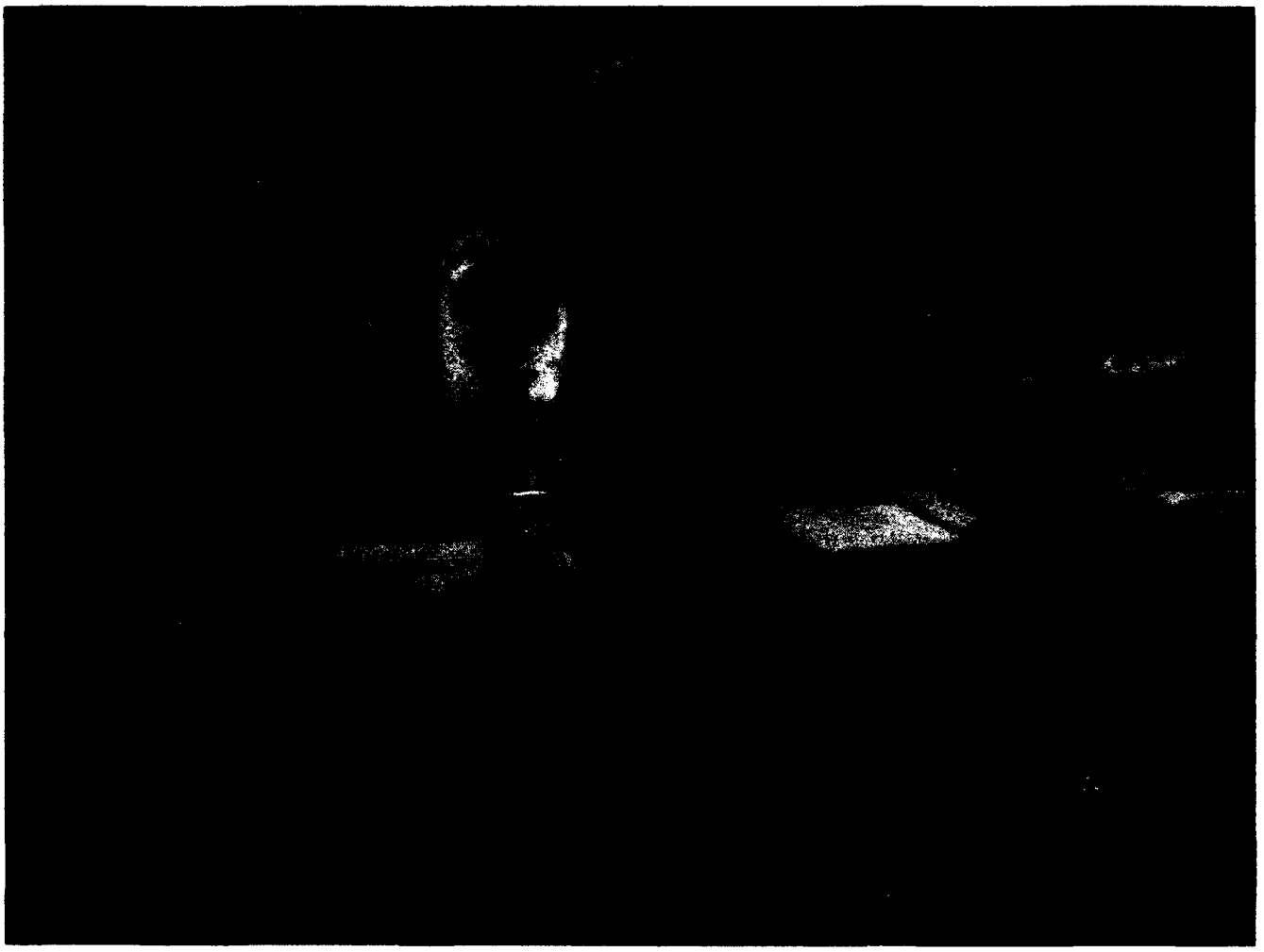


Figure 1. Longitudinal and transverse scans through the first order Si(111) step surface peak. The dotted curves are the resolution. The solid curves are the result of fits to the power-law lineshape with $\eta = 0.6$ and B = 15.



Professor Sylvia T. Ceyer

Chapter 3. Chemical Reaction Dynamics at Surfaces

Academic and Research Staff

Professor Sylvia T. Ceyer, Dr. Yulin Li, Dr. David P. Pullman, Dr. Arthur L. Utz

Graduate Students

Sean P. Daley, Theodore R. Trautman, Julius J. Yang

Undergraduate Students

Gerald R. Cain

Technical and Support Staff

Anne Stollerman

3.1 Dynamics of the Reaction of F_2 with Si(100)

Sponsor

Joint Services Electronics Program
Contract DAAL03-89-C-0001
Contract DAAL03-92-C-0001

Project Staff

Professor Sylvia T. Ceyer, Dr. Yulin Li, Dr. David P. Pullman, Julius J. Yang, Gerald R. Cain

As we have shown previously, F_2 reacts with Si(100) with very close to unity probability ($\sim$ 0.95) up to one monolayer of coverage, contrary to popular belief. We have now also shown that the sites for fluorine adsorption under these conditions are the dangling bonds and that the adsorbed fluorine does not lift the reconstruction. This was accomplished using a new technique of He atom diffraction that we have recently implemented in our molecular beam-ultrahigh vacuum surface scattering apparatus. The experiment is carried out by directing a well-characterized, monoenergetic beam of He atoms at the surface and monitoring the angular distribution of the diffracted atoms. This arrangement adds a powerful new structural probe to our experimental capabilities. While the binding of fluorine to the dangling bonds along with the maintenance of the surface dimer bond is not surprising, our results show the first experimental evidence for it. No experimental information about this system had been available previously because the common structural probes, electron diffraction techniques, are not sensitive to halogens.

Publications

Ceyer, S.T. , D.J. Gladstone, M. McGonigal, and M.T. Schulberg. "Molecular Beams: Probes of the Dynamics of Reactions on Surfaces." In *Physical Methods of Chemistry*. 2nd ed. Eds. B.W. Rossiter, J.F. Hamilton, and R.C. Baetzold. New York: Wiley, 1991. Forthcoming.

3.2 Dynamics of the Reaction of F_2 with Fluorinated Si(100)

Sponsor

Joint Services Electronics Program
Contract DAAL03-89-C-0001
Contract DAAL03-92-C-0001

Project Staff

Professor Sylvia T. Ceyer, Dr. Yulin Li, Dr. David P. Pullman, Julius J. Yang, Gerald R. Cain

We have previously shown that the reaction probability of F_2 with a clean Si(100) surface decays from near unity to zero as the fluorine coverage increases to one monolayer. This lack of reactivity with the fluorinated Si surface is the source of the misconception that F_2 does not react with Si. The lack of reactivity with the fluorinated surface precludes the build up of a sufficient layer of fluorine to produce the volatile etch product, SiF_4. However, we have also previously shown that if the kinetic energy of the incident F_2 molecule is increased above a threshold value of 6 kcal/mol ($\sim$ 0.25 eV), the dissociation probability of F_2 with a fluorinated Si surface increases linearly with the normal component of kinetic energy. This is a result of a barrier to dissociation that is overcome by translational energy of the incident molecule.

The enhancement in the dissociation probability allows enough fluorine to be deposited to form the etch product, SiF_4. This result establishes that Si can be etched with low energies using molecular beam techniques and without the use of plasmas. The low energies afforded by molecular beam techniques prevent the introduction of radiation damage or defects into the Si lattice, which are typical results of plasma etching.

We have begun a new project aimed at determining the origin of the barrier to dissociation of F_2 on the fluorinated surface. The hypothesis is that the barrier to F_2 dissociation is largely associated with breaking the Si surface dimer bond. To test this hypothesis, we are using He atom diffraction as a probe of the surface structure after exposure to the energetic F_2. Preliminary measurements indicate that the disappearance of the dimer bond, as measured by the half order diffraction feature, correlates well with the increase in the dissociation probability as a function of the F_2 incident translational energy in the normal direction. This result may be the first determination of the physical origin of a reaction barrier in any semiconductor system.

3.3 New Mechanisms for Surface Processes

Sponsor

National Science Foundation
Grant CHE 90-20623

Project Staff

Professor Sylvia T. Ceyer, Dr. Arthur L. Utz, Andrew D. Johnson, Sean P. Daley, Theodore R. Trautman

We report the first detection and identification of vibrational modes of buried species by high resolution electron energy loss spectroscopy (HREELS) and the observation of a new mechanism for absorption of adsorbates, collision-induced absorption, as applied to the interaction of hydrogen with Ni(111).

Subsurface or bulk sites of a Ni single crystal are populated with atomic hydrogen by exposure of the (111) face of the Ni crystal at 130 K to atomic hydrogen. Atomic hydrogen is generated by thermal dissociation of H_2 over a hot tungsten filament positioned 0.25 inches from the crystal surface. This results in a flux of both atomic and molecular hydrogen to the front surface of the crystal. The H^+ ions and electrons generated by the filament are shown to play no role in the following observations. Both atomic H and H_2 result in population of the threefold hollow surface sites up to a surface saturation coverage of 1 ML. The HREEL spectrum at 1 ML is characterized by the Ni-H asymmetric stretch at 955 cm^{-1} and the Ni-H symmetric stretch at 1170 cm^{-1}, and the thermal desorption spectrum exhibits two maxima at 340 and 380 K. Further exposure to atomic H results in the appearance of a new feature in the HREEL spectrum at 800 cm^{-1} and in the thermal desorption spectrum at 180-220 K. The loss feature at 800 cm^{-1}, for which an impact scattering mechanism is operable, is identified as a Ni-H vibration of bulk H by the similarity of the dependence of its intensity on electron impact energy to the dependence of the electron inelastic mean free path on electron energy. At 3 eV impact energy, the intensity of the 800 cm^{-1} loss feature is large but decreases monotonically to almost zero as the impact energy is increased beyond 15 eV. This kind of dependence of the intensity of a loss feature associated with a bulk vibrational mode is expected because the inelastic mean free path of an electron, which is 80 Å at 3 eV, rapidly drops to 1 Å as the energy is increased above the plasmon frequency of the metal (15 eV), where plasmon creation is the predominant energy loss mechanism which shortens the mean free path. In contrast, the intensity of the two loss features associated with surface chemisorbed H exhibits almost no dependence on electron energy with the exception of a resonance at 7 eV. As much as an equivalent of 8 monolayers of hydrogen have been absorbed into the bulk.

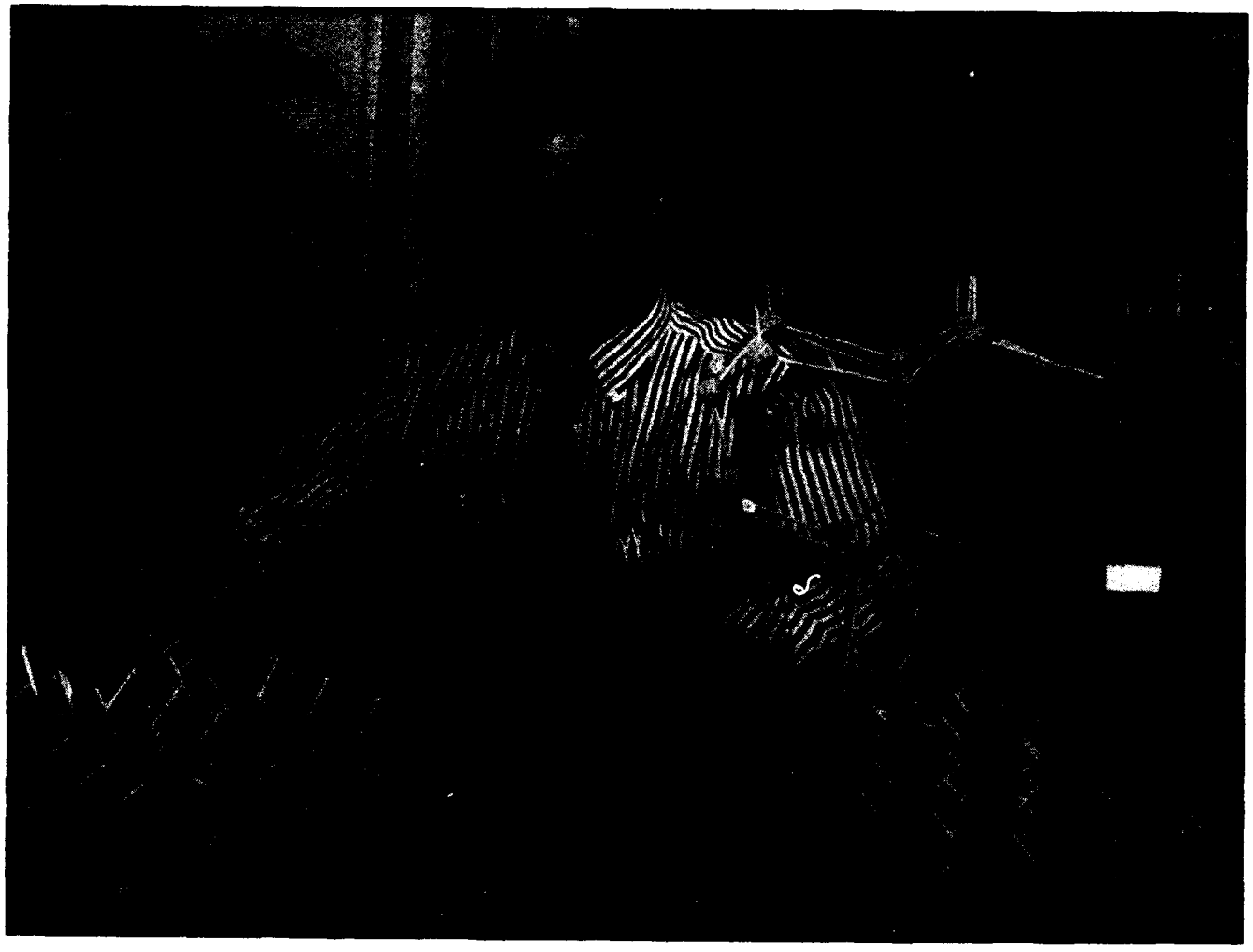
Subsurface or bulk sites of Ni can also be populated via a newly observed mechanism, collision-induced absorption. A beam of monoenergetic Kr or Xe atoms, produced by the supersonic expansion of Kr or Xe seeded in He, is directed at a monolayer of atomic hydrogen chemisorbed on Ni(111). The impacts of the incident inert gas atoms are observed to induce the absorption of the chemisorbed hydrogen. The hydrogen thus absorbed is identified by the appearance of (1) a loss feature at 800 cm^{-1} and (2) a feature at 180-220 K in the thermal desorption spectrum, consistent with the study of atomic hydrogen absorption. The absorption probability scales linearly with the energy of the incident Xe atom above a threshold energy of 2.5 eV. Collision-induced absorption may play a significant role in the mechanism for hydrogen absorption in the high pressure environments of a hydrogen storage cell where the hydrogen saturated surface is continually subject to bombardment by a large flux of energetic particles.

Publications

Johnson, A.D. ***Dynamics of Hydrogen Absorption into the Ni(111) Bulk: Spectroscopic Identification and Chemistry of Subsurface Hydrogen.*** Ph.D. diss., Dept. of Chem., MIT, 1991.

Johnson, A.D., K.J. Maynard, S.P. Daley, Q.Y. Yang and S.T. Ceyer. "Hydrogen Embedded in Ni: Production by Incident Atomic Hydrogen and Detection by High Resolution Electron Energy Loss." *Phys. Rev. Lett.* 67: 927 (1991).

Maynard, K.J., A.D. Johnson, S.P. Daley and S.T. Ceyer. "A New Mechanism for Absorption: Collision Induced Absorption." *J. Chem. Soc.,* Faraday Discussion (1991). Forthcoming.



Professor John D. Joannopoulos

Chapter 4. Semiconductor Surface Studies

Academic and Research Staff

Professor John D. Joannopoulos, Dr. Arnaldo Dal Pino, Dr. Robert D. Meade

Graduate Students

Tomas A. Arias, Kyeongjae Cho, Andrew M. Rappe, Jing Wang

4.1 Introduction

Sponsor

Joint Services Electronics Program
Contract DAAL03-89-C-0001
Contract DAAL03-92-C-0001

Understanding the properties of surfaces of solids and the interactions of atoms and molecules with surfaces has been of extreme importance both from technological and academic points of view. The recent advent of ultrahigh vacuum technology has made microscopic studies of well-characterized surface systems possible. The way atoms move to reduce the energy of the surface, the number of layers of atoms involved in this reduction, the electronic and vibrational states that result from this movement, and the final symmetry of the surface layer are all of utmost importance in arriving at a fundamental and microscopic understanding of the nature of clean surfaces, chemisorption processes, and the initial stages of interface formation.

The theoretical problems associated with these systems are quite complex. However, we are currently at the forefront of solving for the properties of real surface systems. In particular, we are continuing toward our goal of calculating the total ground-state energy of a surface system from "first principles," so that we can provide accurate theoretical predictions of surface geometries. Our efforts in this program have concentrated in the areas of surface growth, surface reconstruction geometries, structural phase transitions, and chemisorption.

4.2 Heteroepitaxial Growth

Epitaxial growth of dissimilar semiconductor materials holds significant potential for technological applications and has been the subject of major international efforts in recent years. Nevertheless, relatively little theoretical work has been performed to understand the fundamental interactions governing the initial stages of growth and the structure of the first few monolayers in these systems. Of particular interest is the prototypical system involving growth of GaAs on Si(100) substrates. Since growth typically begins with an As overlayer, one first needs to understand this seemingly simple system. Experimentally, it is observed that the adsorption of As on a stepped Si(100) surface can drastically rearrange the distribution of steps of the original surface. These changes in surface morphology are controlled by different factors, including temperature, coverage of As, and the type and density of steps on the original surface. The structure of the the As-covered Si(100) surface [henceforth Si(100):As] determines many of the properties of the final epitaxial film.

In particular, it has been observed that GaAs grown epitaxially on Si(100) can have two orientations, related by a 90 degree rotation, with respect to the Si(100). This puzzling observation, the so-called sublattice-orientation (or allocation) dilemma, has not been understood. Naively, this could be explained if the first epilayer above the Si substrate could be selected to be a Ga or As layer. However, bond strength and other theoretical arguments, as well as experimental evidence, show this selective wetting of the Si(100) surface by As or Ga does not occur.

In this work we have performed theoretical calculations which show that As adsorbed on a vicinal Si(100) surface with double-layer steps either *can grow directly on top of the Si surface, or can rearrange the surface so that it replaces the original top Si layer.* The former structure is metastable and results from growth at low temperatures. The latter has lower energy and occurs for growth at substrate temperatures where surface diffusion is activated. Replacing adsorption by substitution changes the sublattice of the diamond structure exposed at the surface and corresponds to a 90 degree rotation of the crystal orientation about the surface normal. The resulting two configurations of the stepped Si(100):As surface are related by a 90 degree rotation, but otherwise differ only in the type of steps present at the surface. Their difference in energy, which we calculate from first principles, is related to the relaxation of stress at surface steps. This result shows that the rear-

rangement of steps upon As adsorption controls the orientation of an epitaxial GaAs film.

Both Si(100) and Si(100):As surfaces have 2 x 1 reconstructions where surface atoms (Si in the first case and As in the second) form dimers arranged in parallel rows. A simple picture for the adsorption of As on Si(100) is that the Si dimers break and As dimers are formed on top, perpendicular to the original Si dimers. This rotates the orientation of the surface dimers by 90°. A single-domain Si(100) 2 x 1 surface would result in a single-domain Si(100):As 1 x 2 surface. STM images show that the orientation of the As dimers depends on the substrate temperature T_s during deposition. For low initial temperatures ($T_s \leq 400°C$) the surface reconstruction rotates from 2 x 1 to 1 x 2, as the simple picture describes.

We begin by considering a single-domain Si(100) 2 x 1 surface, as typically used in growth experiments. These are obtained by using double-layer-stepped vicinal surfaces misoriented towards the [011] direction. Here we will restrict ourselves to the case where both the starting Si(100) and the final Si(100):As surfaces are double-layer stepped and the As coverage is one complete monolayer. These are the conditions relevant to typical growth conditions. On the clean Si(100) surface the Si dimers are parallel to the step edges. Double-layer steps with dimers perpendicular to the edge have much higher energy and are not observed. In principle, there are two types of double-layer steps on the Si(100):As surface. Type A, where the As dimers are perpendicular to the step edge [Figure 1(a)], and type B, where the As dimers are parallel to the edges [Figure 1(b)]. The reconstruction of the surface is 1 x 2 with type-A steps, and 2 x 1 with type-B steps. Figure 1 shows steps with a simple edge termination, where Si atoms are fourfold coordinated and As atoms are threefold coordinated with a doubly occupied lone-pair orbital. This is the same bonding configuration that passivates the flat Si(100):As surface. Other step reconstruction we considered, which are discussed later in this chapter, were found to have higher energies.

To determine the relative stability of the 1 x 2 and 2 x 1 stepped Si(100):As surfaces, we compare the energies of surfaces with type-A and type-B steps, respectively. We calculate total energies from first principles within the framework of density-functional theory in the local-density approximation, using norm-conserving pseudopotentials.

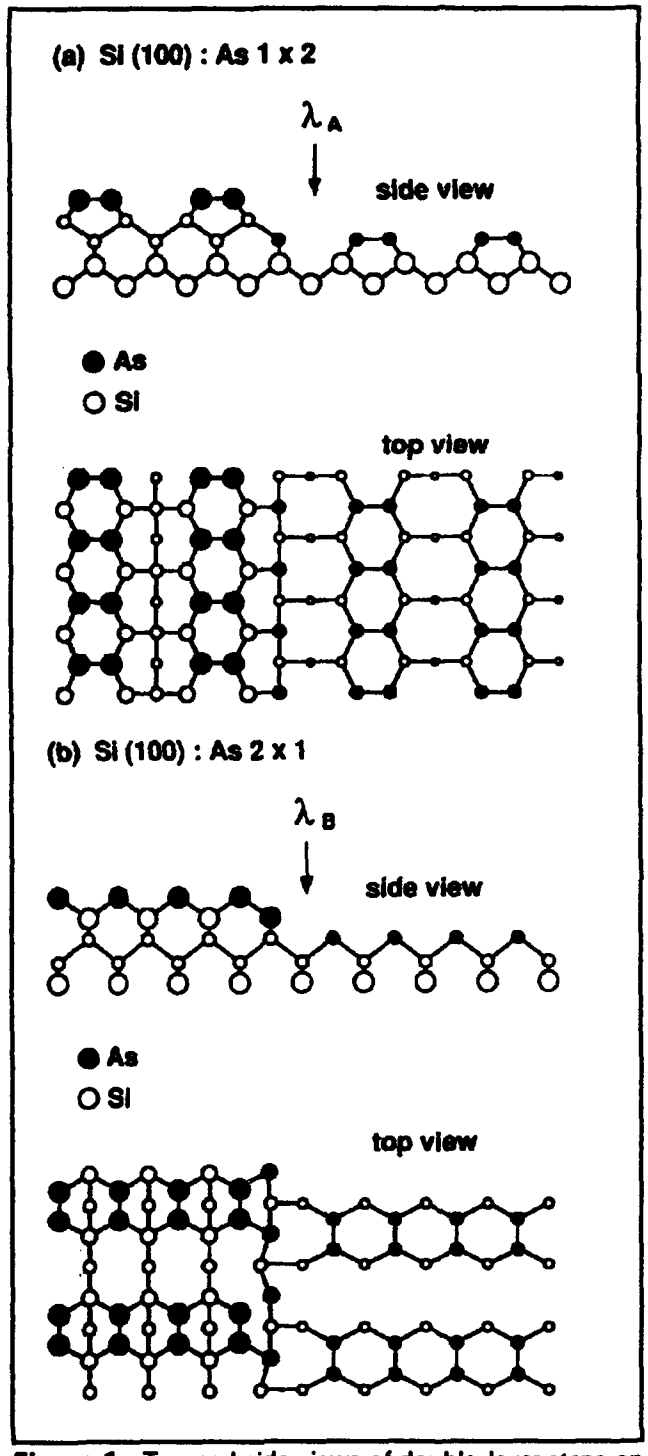


Figure 1. Top and side views of double-layer steps on Si(100):As surfaces. (a) Type-A steps: As dimers perpendicular to the step edge. (b) Type-B steps: As dimers parallel to the step edge (edge relaxation is illustrated in the top view, see text). Larger circles on top views represent atoms closer to the surface. The two circle sizes on side views represent front and back [01$\bar{1}$] planes.

The calculated energy difference between type-A and type-B steps of Si(100):As is

$$\lambda_A - \lambda_B = (200 \pm 20)\ \text{meV/a}, \qquad (1)$$

where λ_A and λ_B are the energies of type-A and type-B steps, respectively, and a = 3.80Å is the unit length along the step. This energy difference is large enough to change the surface from one step configuration to the other. Indeed, an energy difference of ~ 110 meV/a between single- and double-layer steps on vicinal Si(100) surfaces (for a surface misorientation larger than ~ 3-4°) drives the surface to have a majority of double-layer steps. It should be noted that the calculated step energies represent step-formation plus step-step-interaction energies, and the large size of these systems makes it prohibitive to increase the separation between steps and systematically separate these two contributions. However, it is assumed that the latter is approximately eliminated from the problem by taking energy differences between stepped surfaces and that this difference does not change significantly with larger step separations.

An inspection of figure 1 shows no obvious electronic origin for the large energy difference between type-A and type-B steps. In both cases the Si and As atoms have ideal bonding configurations, and there is no particular atom or bond whose relaxation or rehybridization might explain this result. We find that the energy difference is related to the relaxation of surface stress. The Si(100):As surface is under a large tensile stress, both parallel and perpendicular to the As dimers, that results from the tendency of the As atoms to from 90 degree bond angles and pull themselves up from the surface. This stress introduces a torque on surface steps, which allows a lateral contraction of the surface in the region near the steps, at the expense of introducing bulk strain.

Figure 2 shows the response of type-A and type-B steps to the tensile surface stress. Type-A steps lead to a large lateral contraction. This contraction is ~ 3.5% for the first layer of Si atoms, most of it within two lattice constants from the step edge (see inset in figure 2), and decays to zero deeper into the bulk. The surface As dimers, perpendicular to the step edge, are ~ 2% shorter than their calculated value on a flat Si(100):As surface. The relaxation type-B steps is different, even though the strength the tensile stress is calculated to be approximately equal both parallel and perpendicular to the surface dimers [the large energy difference in equation (1) is consistent with this]. Figure 2 shows that type-B steps undergo almost no contraction. Still, the relaxed coordinates suggest that the surface stress has been significantly reduced. Although we have not directly calculated the stress remaining on the stepped

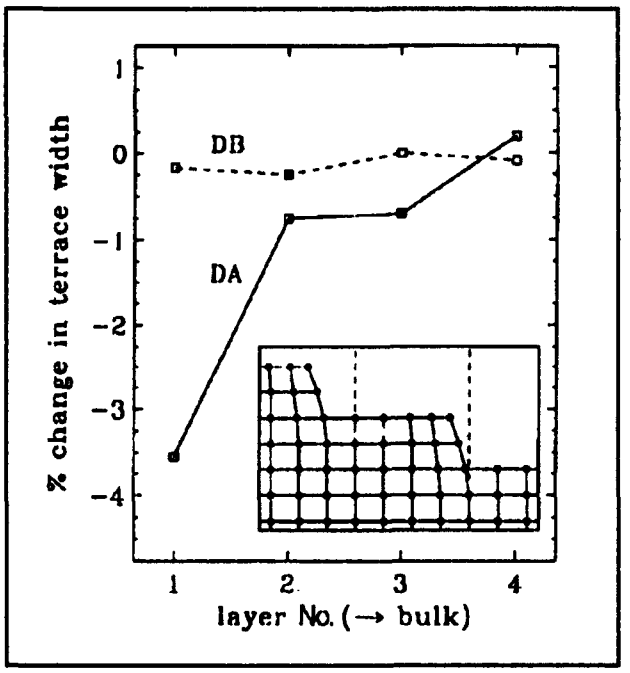


Figure 2. Layer-by-layer lateral contraction for a surface with type-A (solid line) and type-B (dashed line) steps as a function of penetrate into the bulk. Layer No. 1 denotes the first layer of Si atoms below the surface As dimers. Inset: Schematic representation of lateral contraction for a surface under tensile stress, defined with respect to the ideal terrace width shown by the vertical dashed lines.

surface (such calculations are beyond current capabilities), the lack of strain in the subsurface of type-B steps provides evidence of reduced surface stress. On flat Si(100):As subsurface strain forces a displacement of atoms from their ideal bulk positions. Atoms in third and fourth layers that are underneath surface dimers shift up, and subsurface atoms that are between dimer rows shift down. For type-A steps this distortion is further enhanced. On the other hand, for type-B steps the relaxed positions of the subsurface atoms are close to their ideal bulk value. This lack of strain in the subsurface for type-B steps is consistent with the reduction of surface stress.

We now address the implications of these results to growth experiments. Our calculations show that the Si(100):As 1 x 2 surface with type-A steps is a metastable structure. This surface results from the growth of As directly on top of the initial Si surface. Experimentally, it is obtained by depositing As at low substrate temperatures, where the As overlayer caps the surface and freezes any surface mobility. However, if the temperature is high enough during As deposition to activate surface diffusion, the surface can then reach the lower-energy configuration with type-B steps. This explains the surprising experimental observations. We note that this change in step type

requires a large rearrangement of the surface, but similar step redistributions requiring mass transport across the surface have been observed when the initial Si surface has single-layer steps. The transformation from type-A to type-B step may occur through other intermediate step configurations, including single-layer steps, and a complete conversion may not occur because of the large amount of mass transport required. This may further depend on the flux of As, and on whether As_2 or As_4 gas sources are used. Also, if surface diffusion is completely frozen or defects pin the edges of steps, type-A steps with a rebonded edge may occur on terraces that originally had an odd number of lattice sites, and both types of type-A steps may appear on the low-temperature surface. In principle, the surface with type-B steps ought to be reached from the surface with type-A steps upon annealing. However, As begins to leave the surface before this change occurs, and mixtures of steps with different heights are then observed.

It should be noted that since the driving force for the rotation of the As surface dimers is the difference in energy between type-A and type-B steps, as the surface misorientation becomes smaller and the density of steps decreases, the energy gain by step rearrangement diminishes. On nearly flat surfaces only the $2 \times 1 \rightarrow 1 \times 2$ change in orientation of Si to As surface dimers should be observed.

For the heteroepitaxial growth of GaAs on Si(100), our results predict the sequence of orientations of the Si and then As surface dimers in the growth process of Si(100)→Si(100):As→GaAs/Si(100). For low initial substrate temperatures, the predicted sequence is $2 \times 1 \rightarrow 1 \times 2 \rightarrow 4 \times 2$, and for high initial temperatures the sequence is $2 \times 1 \rightarrow 2 \times 1 \rightarrow 2 \times 4$. The final orientation of the GaAs epilayer depends on whether the equilibrium Si(100):As surface is attained, illustrating the interplay between kinetics and energetics in epitaxial crystal growth. This result explains the sublattice orientation dilemma and brings into a coherent picture experiments that seemed to be in contradiction. Also, type-A and type-B steps on Si(100):As may promote different nucleation channels for growth, leading to epitaxial films with different characteristics.

4.3 Molecules

In order to begin to address problems associated with molecules interacting with solid surfaces, it is important to test the applicability of the theoretical tools (developed for condensed matter systems) for isolated molecules. Moreover, if successful, these tools could be used to study large heterogeneous nonperiodic systems such as biological molecules that may consist of extended organic fragments, metal ions, and solvent water molecules. As a first step in this direction, *ab initio* theoretical calculations were performed on a large number of molecules with a variety of sizes and functional groups consisting of the first-row elements. These include the simple molecules H_2, H_2O, CH_4 and NH_3 that are constituents of the "biotic-soup" of the primordial atmosphere, neutral glycine which is the simplest amino acid, and formamide, which models the peptide-bond between amino acids in a protein.

Table I lists the results of our theoretical calculations (LDAP-PW) and compares them with both experimental values and quantum chemistry (MP2/6-31G*) Hartree Fock calculations.

Overall agreement of LDAP-PW with experiment and MP2 calculations is excellent. Average deviations from experiment and MP2 are 0.030Å and 0.034Å for bond lengths and 0.5 degrees and 1.0 degrees for bond angles. If the hydrogen-bonded system 3-hydroxy-acrylaldehyde is not included in the averages, the bond-length deviations become 0.017Å and 0.024Å respectively.

Upon closer examination, certain trends become apparent within the data contained in Table I. The most striking pattern is that a LDAP-PW calculation of a bond distance between two heavy (non-hydrogen) atoms is almost always closer to experiment than the corresponding MP2 result. Conversely, bonds involving at least one hydrogen are almost always calculated more accurately using MP2. In addition, bond angles which include zero or one hydrogen atom are almost always more accurate using LDAP-PW, while those including two hydrogens are usually better reproduced by MP2. We believe that these effects are due to the use of the LDA rather that a more accurate exchange-correlation functional. The small size of hydrogen makes its charge density change over a short length scale. It appears likely that gradient corrections to LDA will improve these results. Another trend which we have observed is that long bonds are reproduced more poorly than short bonds by the LDAP-PW. This effect is also probably due to the use of the LDA. As the atoms in a bond separate, they act more like free atoms, and the LDA does a poorer job on free atoms than on covalent materials. This effect is particularly striking in the O-O bond of H_2O_2 and the hydrogen bond in 3-hydroxyacrylaldehyde.

These results show that the LDAP-PW method can produce accurate structural parameters for molecules. The data suggest that the method which uses plane waves, pseudopotentials, and supercells may be a useful alternative to standard *ab initio* quantum mechanical methods for calcula-

Molecule	Parameter	Exp	MP2	Δ^1_e	LDAP-PW	Δ^2_e	Δ_G
H_2	r(HH)	0.742	0.738	0.004	0.776	0.034	0.038
O_2	r(OO)	1.208	1.242	0.034	1.183	0.025	0.059
N_2	r(NN)	1.098	1.131	0.033	1.099	0.001	0.032
P_2	r(PP)	1.893	1.936	0.043	1.875	0.018	0.061
CO	r(CO)	1.128	1.151	0.023	1.138	0.010	0.013
CO_2	r(CO)	1.162	-	-	1.170	0.008	-
H_2O	r(OH)	0.958	0.969	0.011	0.976	0.018	0.007
	<(HOH)	104.5	104.0	0.5	104.0	0.5	0.0
CH_4	r(CH)	1.092	1.090	0.002	1.102	0.010	0.012
NH_3	r(NH)	1.012	1.017	0.005	1.028	0.016	0.011
	<(HNH)	106.7	106.3	0.4	105.7	1.0	0.6
PH_3	r(PH)	1.420	1.415	0.005	1.440	0.020	0.025
	<(HPH)	93.3	94.6	1.3	91.6	1.7	3.0
H_2O_2	r(OO)	1.452	1.467	0.015	1.414	0.038	0.053
	r(OH)	0.965	0.976	0.011	0.982	0.017	0.006
	<(OOH)	100.0	98.7	1.3	100.2	0.2	1.5
	ω(HOOH)	119.1	121.3	2.2	118.7	0.4	2.6
N_2H_2	r(NN)	1.252	1.267	0.015	1.233	0.019	0.034
	r(NH)	1.028	1.036	0.008	1.052	0.024	0.016
	<(NNH)	106.9	105.4	1.5	107.2	0.3	1.8
H_2CO	r(CO)	1.208	1.221	0.013	1.205	0.003	0.016
	r(CH)	1.116	1.104	0.012	1.135	0.019	0.031
	<(HCH)	116.5	115.6	0.9	116.4	0.1	0.8
C_2H_2	r(CC)	1.203	1.218	0.015	1.196	0.007	0.022
	r(CH)	1.061	1.066	0.005	1.058	0.003	0.008
HNC	r(NC)	1.169	1.187	0.018	1.178	0.009	0.009
	r(HN)	0.994	1.002	0.008	1.018	0.024	0.016
HNO	r(NO)	1.212	1.237	0.025	1.188	0.024	0.049
	r(HN)	1.063	1.058	0.005	1.093	0.030	0.035
	<(HNO)	108.6	107.3	1.3	109.2	0.6	1.9
Formamide	r(CO)	1.193	1.224	0.031	1.217	0.024	0.007
($HCONH_2$)	r(CN)	1.376	1.361	0.015	1.365	0.011	0.004
	<(OCN)	124.7	124.8	0.1	124.9	0.2	0.1
Glycine	r(C=O^1)	-	1.218	-	1.204	-	0.014
($NH_2CH_2CO^1O^2H$)	r(CO^2)	-	1.358	-	1.345	-	0.013
	r(CC)	-	1.515	-	1.535	-	0.020
	r(NC)	-	1.451	-	1.460	-	0.009
	<(O^1CO^2)	-	123.2	-	123.7	-	0.5
	<(O^2CC)	-	111.4	-	111.9	-	0.5
	<(O^1CC)	-	125.4	-	124.4	-	1.0
	<(CCN)	-	114.9	-	114.8	-	0.1
$H_2PO_4^{-1}$	r(PO)	-	1.510	-	1.482	-	0.028
	r(P-OH)	-	1.680	-	1.640	-	0.040
	<(HO-P-OH)	-	101.1	-	101.2	-	0.1
	<(O-P-OH)	-	106.9	-	107.1	-	0.2
	<(O-P-O)	-	126.2	-	125.2	-	1.0
3-hydroxy-	r(O-H)	0.969	0.994	0.025	1.079	0.110	0.085
acrylaldehyde	r(O...H)	1.680	1.694	0.014	1.418	0.262	0.276
(HOCHCHCHO)							

Table I. A comparison of LDAP-PW geometry optimizations with experiment and with MP2. Δ^1_e and Δ^2_e are the deviations of the MP2 and LDAP-PW calculations from experiment, and Δ_G is the deviation of LDAP-PW from the MP2 values.

tions on chemical systems. Future work will include more realistic density functionals and tests of energetics of chemical transformations. In addition, research is continuing to develop more efficient energy minimization algorithms and superior pseudopotentials. These changes will improve the efficiency and accuracy of the method for the study of periodic and aperiodic chemical and biochemical systems.

4.4 Publications

Alerhand, O., J. Wang, J.D. Joannopoulos, E. Kaxiras, and R. Becker. "Adsorption of As on Stepped Si(100): Resolution of the Sublattice Dilemma." *Phys. Rev. Rapid Comm.* B44: 6534 (1991).

Alerhand, O., J. Wang, J.D. Joannopoulos, and E. Kaxiras. "Growth of As Overlayers on Vicinal Si(100)." *J. Vac. Sci. Tech.* B9: 2423 (1991).

Arias, T., M. Payne, and J.D. Joannopoulos. "Precise and Efficient Ab-Initio Molecular Dynamics." *Phys. Rev. B.* Forthcoming.

Joannopoulos, J.D., P. Bash and A. Rappe. "Modern Iterative Minimization Techniques in Quantum Chemistry." *Chem. Des. Automat. News* 6(8): pages (1991).

Rappe, A., and J.D. Joannopoulos. "The Design of Convergent and Transferable Ab-Initio Pseudopotentials." *Proceedings of the Nato Advanced Study Institute,* Aussois, France, 1991.

Rappe, A., J.D. Joannopoulos and P. Bash. "A Test of the Planewaves for the Study of Molecules from First Principles." *J. Amer. Chem. Soc.* Forthcoming.

Wang, J., M. Needels, and J.D. Joannopoulos. "Surface and Fracture Energies in GaAs." In *Surface Physics and Related Topics.* Teaneck, New Jersey: World Scientific Publ., 1991. pp. 314.

Chapter 5. Epitaxy and Step Structures on Semiconductor Surfaces

Academic and Research Staff

Professor Simon G.J. Mochrie, Dr. Kenneth I. Blum

Graduate Students

Douglas L. Abernathy

5.1 Structure and Phase Behavior of the Si(113) Surface

Sponsor

Joint Services Electronics Program
Contract DAAL03-89-C-0001
Contract DAAL03-92-C-0001

Recently, our efforts under JSEP have been directed towards implementation of a design for an ultra-high-vacuum (UHV) chamber for surface x-ray scattering. The design and assembly of the UHV chamber and its associated diffractometer are now complete, and a first set of experiments using the new chamber at the MIT-IBM Beamline (X20) at the National Synchrotron Light Source has been carried out.

Our initial program (in collaboration with R.J. Birgeneau) is to study the Si(113) surface.[1] Si(113) is interesting for a number of reasons, which involve both possible technological applications and interest in the basic physics of surfaces. Firstly, we note that Si(113) is a stable facet with a surface energy comparable to that of the (111) or (001) orientation.[2] Reports of superior epitaxial growth on Si(113)[3] make the structure of this surface and its temperature dependence especially worthy of study.

An unreconstructed (113) surface may be envisaged as a sequence of (001) terraces separated by (111) steps. (The terraces are a single atomic row wide.) The corresponding surface unit cell contains two different types of surface atom: two-fold coordinated atoms deriving from the (001) terrace with two dangling bonds and three-fold coordinated atoms from the (111) step with a single dangling bond (see figure 1, which is taken from the article by Myles and Jacobi[4]). As noted by others before,[5] this aspect of the (113) surface leads to the possibility of two different adsorption sites. This feature may alleviate the problem of twinning that occurs in the growth of III-V semiconductors on flat Si(001).[6] Furthermore, in a III-V material, the (113) surface is non-polar, in contrast to the (001) and (111) surfaces, which makes it especially interesting for heteroepitaxy.

The clean Si(113) surface reconstructs to form either a (1x3) or a (2x3) surface mesh. The (1x3) structure appears to be the equilibrium configuration,[7] but the precise atomic geometry of the Si(113) (1x3) reconstruction has yet to be established experimentally Moreover, convincing calculations of the structure of Si(113) do not currently exist. At elevated temperatures ($\gtrsim$840K), the surface reverts from its (1x3) structure to a structure with true (1x1) symmetry of bulk (113)

---

1 B.F. Olshanetsky and V.I. Mashanov, *Surf. Sci.* III: 414 (1981); D.J. Chadi, *Phys. Rev. B* 29: 785 (1984).

2 J.M. Gibson, M.L. McDonald, and F.C. Unterwald, *Phys. Rev. Lett.* 55: 1765 (1985).

3 G.H. Olsen, T.J. Zamerowski, and F.Z. Hawrylo, *J. Cryst. Growth* 59: 654 (1982); S.L. Wright, M. Inada, and H. Kroemer, *J. Vac. Sci. Technol.* 21: 534 (1982).

4 U. Myles and K. Jacobi, *Surf. Sci.* 220: 353 (1989).

5 D.J. Chadi, *Phys. Rev. B* 29: 785 (1984); U. Myles and K. Jacobi, *Surf. Sci.* 220: 353 (1989); J. Knall, J.B. Pethica, J.D. Todd, and J.H. Wilson, *Phys. Rev. Lett.* 66: 1733 (1991).

6 K. Fujikawa, *J. Cryst. Growth* 77: 509 (1986).

7 Y.N. Yang, E.D. Williams, R.L. Park, N.C. Barlett, and T.L. Einstein, *Phys. Rev. Lett.* 64: 2910 (1991).

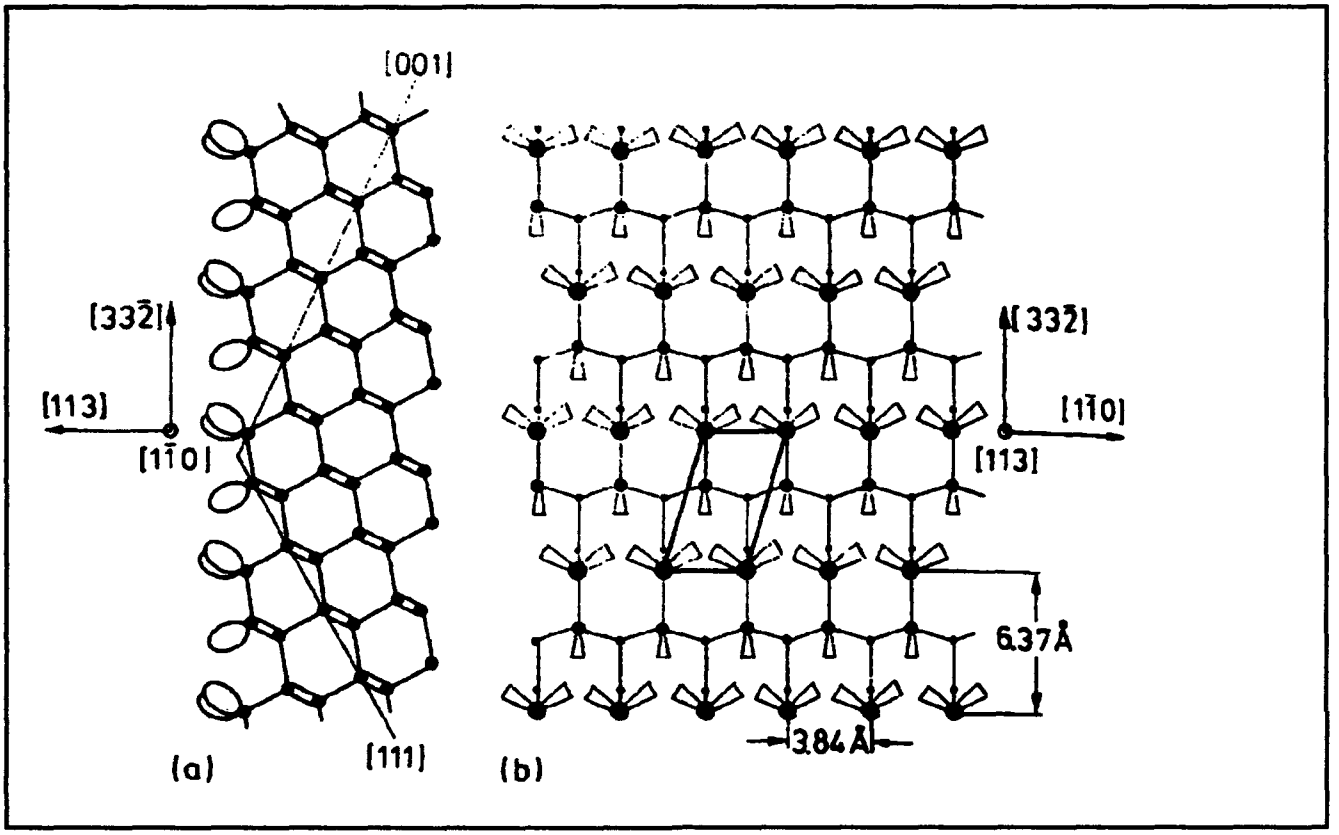


Figure 1.

planes.[7] It has been suggested that the phase transformation between these two surface configurations falls into a particular "universality class," that of the chiral, three state Potts model.[8] Our initial experiments, aimed at studying this aspect, were carried out on a (1x3) reconstructed surface, produced by annealing at 1500 K and subsequently cooling to below the (1x3)-to-(1x1) transformation temperature ($\gtrsim$840K). The presence of commensurate "1/3-order" rods, located between the rods of scattering associated with bulk periodicities, indicates a (1x3) reconstruction of the crystal surface. A scan across one such rod—the (4,2/3) rod (we employ the units of the unreconstructed surface unit cell)—is shown for several temperatures in figure 2 on a logarthmic intensity scale. The lowest profile shown corresponds to a temperature of 750 K. Evidently, the reconstruction is readily observable. In addition, the width of this profile determines that the reconstruction is translationally well-ordered on length scales of $\cong$ 4000Å. (Other measurements establish that the existence of peaks associated with a (2x3) structure is excluded at the 10^{-4} level.) The additional profiles in figure 2 illustrate the behavior observed on warming through the phase transformation. The commensurate 1/3-order rod becomes weaker, and at the same time a broad, incommensurate peak may be seen emerging towards smaller wave vector (smaller K). Least-mean-squares fits (solid lines) reveal that the width of the incommensurate peak is proportional to its displacement from the commensurate position, suggesting that the disordering indeed falls within the universality class proposed.

Experiments to investigate the detailed atomic structure in the commensurate phase are planned for the near future. Another interesting possibility is that of surface roughening, which may occur at very high temperatures. Experiments to investigate this aspect are also forthcoming.

[8] Y.N. Yang, E.D. Williams, R.L. Park, N.C. Barlett, and T.L. Einstein, *Phys. Rev. Lett.* 64: 2910 (1991); D.A. Huse and M.E. Fisher, *Phys. Rev. B* 29: 239 (1984).

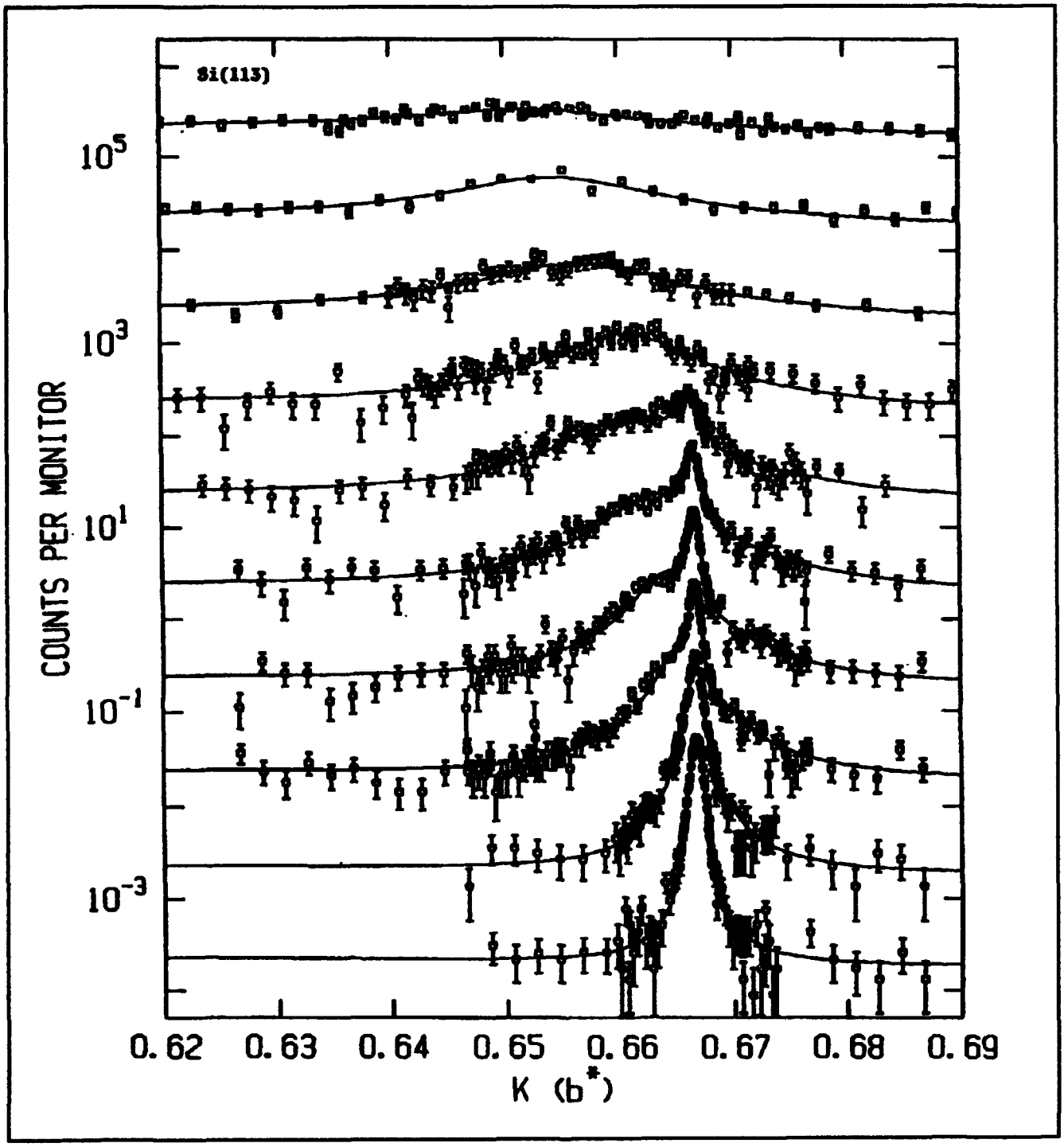


Figure 2.

Publications

Abernathy, D.L., S.G.J. Mochrie, D.M. Zehner, G. Grübel, and D. Gibbs. "Orientational Epitaxy and Lateral Structure of the Hexagonally Reconstructed Pt(001) and Au(001) Surfaces." *Phys. Rev. B* 45 (1992). Forthcoming.

Gibbs, D., G. Grübel, D.M. Zehner, D.L. Abernathy, and S.G.J. Mochrie. "Orientational Epitaxy of the Hexagonally Reconstructed Pt(001) Surface." *Phys. Rev. Lett.* 67: 3117 (1991).

Part II Applied Physics

Section 1 Atomic, Molecular and Optical Physics

Section 2 Plasma Physics

Section 3 Electromagnetics

Section 4 Radio Astronomy

Section 1 Atomic, Molecular and Optical Physics

Chapter 1 Quantum Optics and Photonics

Chapter 2 Basic Atomic Physics

Chapter 1. Quantum Optics and Photonics

Academic and Research Staff

Professor Shaoul Ezekiel

Visiting Scientists and Research Affiliates

Dr. Philip R. Hemmer,[1] Dr. Mara G. Prentiss,[2] Dr. Elias Snitzer,[3] John D. Kierstead[1]

Graduate Students

John J. Donoghue, M. Selim Shahriar, Stephen P. Smith, Farhad Zarinetchi

Technical and Support Staff

Margaret M. McCabe

1.1 Error Sources in a Fiber Optic Resonator Gyroscope

Sponsor

Charles S. Draper Laboratories
Contract DL-H-418468

Various forms of optical inertial rotation sensors based on the Sagnac effect have been under development since the advent of the laser in 1960. These include active techniques, such as the ring laser gyro[4] and passive techniques employing ring resonators[5] or interferometers.[6] In the past few years, low-loss single-mode optical fibers have been incorporated into both interferometers[7] and resonators.[8] Here, we describe some error sources of a fiber-optic resonator inertial rotation sensor that has been under study in our laboratory.

In the presence of an inertial rotation rate Ω normal to the plane of a ring cavity, the nonreciprocal phase shift induced by the Sagnac effect[9] causes the cavity resonances in the clockwise (CW) and counterclockwise (CCW) directions to be separated by a frequency Δf given by

$$\Delta f = \frac{4A}{\lambda P}\Omega \qquad (1)$$

where A is the area enclosed by the resonator, P is the optical perimeter, and λ is the wavelength of the light.

In order to measure Δf in a passive resonator, two counterpropagating beams are introduced into the cavity and the frequency of each beam is adjusted to coincide with the center of the corresponding cavity resonance. Thus, the frequency difference

---

1 Rome Air Development Center, Hanscom Air Force Base, Bedford, Massachusetts.

2 Professor, Harvard University, Cambridge, Massachusetts.

3 Professor, Rutgers University, New Brunswick, New Jersey.

4 A.H. Rosenthal, "Regenerative Circulatory Multiple Beam Interferometry for the Study of Light Propagation Effects," *J. Opt. Soc. Am.* 52: 1143 (1962).

5 S. Ezekiel and S.R. Balsamo, "Passive Ring Resonator Laser Gyroscope," *Appl. Phys. Lett.* 30: 478 (1977).

6 W.R. Carrington and R. Fredricks, *Development of an Optical Rate Sensor,* Final Report to the U.S. Navy Office of Naval Research N00014-73-C-0377, Lear Siegler, Inc., Grand Rapids, Michigan, November 1973.

7 V. Vali and L.W. Shorthill, "Fiber Ring Interferometer," *Appl. Opt.* 15: 1099 (1976).

8 R.E. Meyer and S. Ezekiel, "Fiberoptic Resonator Gyroscope," presented at the IEE First International Conference on Optical Fiber Sensors, London, April 26-28, 1983.

9 E.J. Post, "Sagnac Effect," *Rev. Mod. Phys.* 39: 475 (1967); H.J. Arditty and H.C. Lefevre, "Sagnac Effect in Fiber Gyroscopes," *Opt. Lett.* 6: 401 (1981).

between the two beams is simply Δf and is directly proportional to the rotation rate, as shown in equation 1. Figure 1 shows simplified gyro setups for a cavity in reflection (top) and for a cavity in transmission (bottom).

In order to hold each beam at the center of a cavity resonance, the frequency of each beam is modulated before it enters the cavity.[10] After emerging from the cavity, the beams fall on a detector whose signal is demodulated with a phase sensitive detector (PSD) to yield a discriminant which has a zero crossing at the center of the resonance, and this is used by the servo to hold the beam at the cavity resonance.

In practice, there are other sources of nonreciprocal phase shifts besides the Sagnac effect that constitute error sources in the gyroscope, and these must be drastically reduced, if not eliminated, to achieve ultimate performance. Here, we will discuss some of the major error sources and the research that is currently underway.

One major source of error is the coupling of the counterpropagating beams through backscattering from either inside or outside the cavity. This coupling between the two beams will cause a "dead zone" for a range of small rotation rates, similar to that observed in the bulk-optic ring laser gyro.[11]

One method of eliminating this effect is to "wash out" the interference between the beams by sinusoidally modulating the frequency of one of the beams so that its J_0 components are suppressed.[10] In this way, the interference between the beams occurs around the harmonics of the modulation frequency, where it can be easily removed by suitable filtering.

However, even with the interference between the two beams washed out, the residual intensity backscattering still can cause problems by affecting the servo loops if both directions use the same modulation frequency. To avoid the effects of intensity backscattering, different modulation frequencies need to be used in the two directions.[12]

Another error source is due to lineshape asymmetry, caused by loss in the coupler for a cavity in reflection. For example, when different

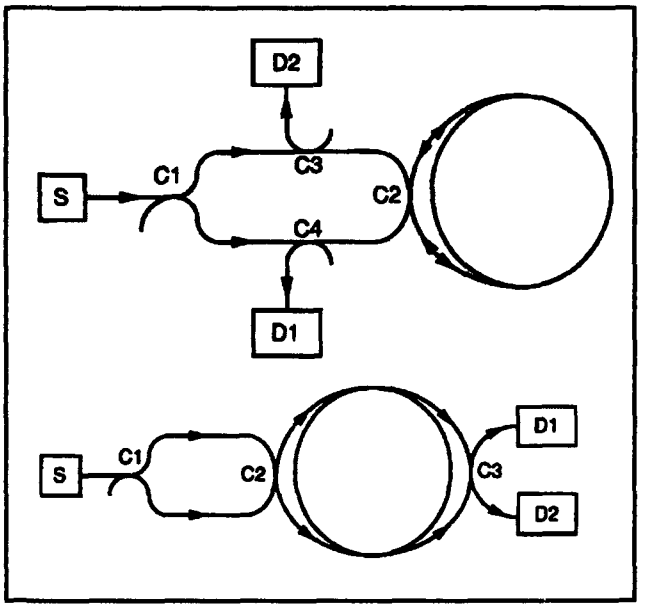


Figure 1. Simplified schematic of a ring resonator gyroscope using a resonator in reflection (top) and transmission (bottom).

modulation frequencies are used, the zero crossing of the discriminants in each direction are dependent on the exact parameters of the applied modulation. In this way, an offset is generated between the counterpropagating directions, which will vary with changes in modulation, or cavity, parameters.

Another problem caused by asymmetry is that the quadrature signal from the PSD is not zero at the center of the effective cavity resonance. It is important to note that for a symmetric resonance, the quadrature signal from the PSD is always zero at the center of the resonance, hence changes in the phase of the PSD do not cause any offset errors. In contrast, with a non-zero quadrature, changes in the PSD phase will cause gyro offsets.

Further, the magnitude of the quadrature offset is influenced by a number of factors including modulation rate and depth, as well as cavity backscattering. Thus, even if the phase of the PSD is constant, offset errors can be generated due to quadrature variations.

Several possible methods of minimizing the errors due to lineshape asymmetry are being explored including careful selection of modulation para-

---

[10] G.A. Sanders, M.G. Prentiss, and S. Ezekiel, "Passive Ring Resonator Method for Sensitive Inertial Rotation Measurements in Geophysics and Relativity," *Opt. Lett.* 7: 569 (1981).

[11] F. Aronowitz, "The Laser Gyro," in *Laser Applications*, ed. M. Ross (New York: Academic Press, 1971).

[12] K. Iwatsuki, K. Hotate, and M. Higashiguchi, "Effect of Rayleigh Backscattering in an Optical Passive Ring-resonator Gyro," *Appl. Opt.* 23: 3916 (1984).

meters and the use of multiple modulation frequencies. However, by using a cavity in transmission, there is no lineshape asymmetry and these errors can be avoided.

Another important source of error is polarization driven. A ring cavity can, in general, support two eigen polarizations which typically have different resonance frequencies, and for maximum resonance size, the input beam is usually matched into one of these eigen polarizations. However, if the second eigen polarization is partially excited, it will pull the resonance frequency of the main polarization. If the input polarizations are exactly the same in the two directions, these resonance pulls will be the same in each direction, but if the polarizations are not matched, the pulls will cause a gyro offset. Further, if the eigen polarizations are not exactly orthogonal, or if there are polarization sensitive elements after the cavity, the resonance pulls can be greatly enhanced.

Several solutions to these polarization-driven errors are possible. First, eliminating the second eigen polarization by the use of a single polarization fiber resonator will eliminate the polarization cross talk problems. Second, the input polarization can be actively locked to a cavity eigen polarization ensuring that the input polarizations are the same in both directions and that they are exactly matched into an eigen polarization. Third, cavities made from polarization maintaining fiber with a 90 degree rotated splice have eigen polarizations that are spaced by exactly half a cavity free spectral range.[13] This nulls the neighboring line resonance pull and greatly improves the temperature sensitivity of the eigen polarizations as compared to a standard polarization preserving fiber resonator.

Finally, the optical Kerr effect,[14] which causes a nonreciprocal phase shift due to a mismatch in the counterpropagating intensities, influences both the cavity in reflection and the cavity in transmission.

1.2 Stimulated Brillouin Fiber Laser Gyroscope

Sponsor

Charles S. Draper Laboratories
Contract DL-H-418468

Research is in progress on a new fiber optic ring laser gyroscope. This gyroscope is based on two counterpropagating stimulated Brillouin scattering (SBS) lasers[15] in the same single-mode fiber optic ring resonator. In the presence of inertial rotation normal to the plane of the resonator, a difference frequency is automatically generated between the counterpropagating SBS lasers which is directly proportional to the rotation,[16] as predicted by the Sagnac effect.[17] The operation of such a gyro is very similar to that of the bulkoptic ring laser gyro (RLG) that is based on two counterpropagating He-Ne lasers that share the same ring resonator.[18] Unlike the passive interferometeric fiber gyro,[19] the SBS fiber gyro does not require external means for

---

[13] G.A. Sanders, R.B. Smith and G.F. Rouse, "Novel Polarization Rotating Ring Resonator for Rotation Sensing," *Proc. SPIE,* 1169 (Bellingham, Washington: SPIE, 1989), pp. 1169-74; Fiber Optic and Laser Sensors VII Conference, Boston, Massachusetts, September 5-7, 1989.

[14] S. Ezekiel, J.L. Davis, and R. Hellwarth, "Intensity Dependent Nonreciprocal Phase Shift in a Fiberoptic Gyroscope," in *Fiber Optic Sensors*, eds. S. Ezekiel and H.J. Arditty (Berlin: Springer-Verlag, 1982), p. 332.

[15] S.P. Smith, F. Zarinetchi, and S. Ezekiel, "Fiberoptic Ring Laser Gyro," *Proceedings of OFS '89,* Paris, France, 1989.

[16] P.J. Thomas, H.M. van Driel, and G.I.A. Stegeman, "Possibility of Using an Optical Fiber Brillouin Ring Laser for Inertial Sensing," *Appl. Opt.* 19: 1906 (1980); K.O. Hill, B.S. Kawasaki, and D.C. Johnson, "cw Brillouin Laser," *Appl. Opt. Lett.* 28: 608 (1976); D.R. Ponikvar and S. Ezekiel, "Stabilized Single-frequency Stimulated Brillouin Fiber Ring Laser," *Opt. Lett.* 6: 398 (1981); L.F. Stokes, M. Chodorow, and H.J. Shaw, "All-fiber Stimulated Brillouin Ring Laser with Submilliwatt Pump Threshold," *Opt. Lett.* 7: 509 (1982); P. Bayvel and I.P. Giles, "Evaluation of Performance Parameters of Single-mode All-fiber Brillouin Ring Lasers," *Opt. Lett.* 14: 581 (1989); F. Zarinetchi, S.P. Smith, and S. Ezekiel, "Stimulated Brillouin Fiber-optic Laser Gyroscope," *Opt. Lett.* 16: 229 (1991).

[17] A.H. Rosenthal, "Regenerative Circulatory Multiple Beam Interferometry for the Study of Light Propagation Effects," *J. Opt. Soc. Am.* 52: 1143 (1962).

[18] W.M. Macek and D.T.M. Davis, Jr., "Rate Sensing with Travelling Wave Ring Laser," *Appl. Phys. Lett.* 2: 67 (1963).

[19] V. Vali and L.W. Shorthill, "Fiber Ring Interferometer," *Appl. Opt.* 15: 1099 (1976).

the measurement of nonreciprocal phase shifts induced by rotation.

Figure 2 shows a simplified schematic diagram of a SBS fiber laser gyroscope. Light from a 2 mW He-Ne laser at 1.15 μm is split into two beams, labelled P1 and P2, which are frequency shifted by acousto-optic (A/O) modulators. The beams are then coupled into counterpropagating directions of a single mode, fiber optic resonator which is 25 meters long, has a finesse of 250, and is wrapped around a 7.5 cm cylindrical drum. For maximum effective pump power in the resonator, beam P1 is held at the center of a cavity resonance using a servo loop, not shown in the figure.

With the pump input power about 60 μW, the SBS threshold for this cavity, SBS lasers B1 and B2, which are pumped by P1 and P2 respectively, are observed. These SBS lasers outputs are combined and fall on detector D.

Figure 3a shows the difference frequency between B1 and B2, when a sinusoidal rotation is applied to the cavity, and figure 3b shows the corresponding rotation angle. As seen in the figure, the difference frequency varies linearly with the rotation rate, as predicted by the Sagnac effect, and hence is 90 degrees out of phase with the rotation angle in figure 3b. However, it is important to notice that for a range of low rotation rates, i.e., when the rotation angle near its maximum or minimum values, the beat frequency goes to zero, demonstrating the so called "lock-in" zone that is caused by the coupling of the counterpropagating lasers through backscattering inside the resonator. Lock-in, which has been extensively studied in the bulkoptic He-Ne RLG, must be removed to achieve high precision measurements.

One method of removing lock-in in the SBS fiber gyro is to mechanically dither the gyro in the same manner as the bulkoptic RLG.[20] However, with a SBS gyro, it is possible to avoid lock-in completely by generating the counterpropagating lasers in different longitudinal modes of the cavity. In this way, backscattering within the cavity cannot couple the SBS lasers, since the lasers are at different frequencies. For example, to separate the SBS lasers by 12 longitudinal modes, i.e., $\Delta q = 12$, the frequency of pump P1 is shifted with respect to P2 by 12 free spectral ranges (FSR) using the A/O modulators shown in figure 2.

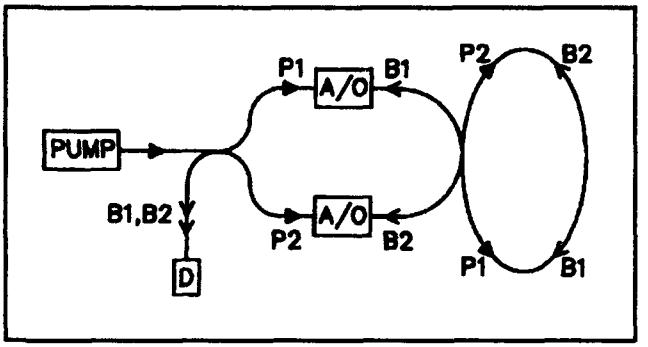


Figure 2. Simplified schematic of a SBS fiber ring laser gyroscope.

Figure 4a shows the frequency difference between the SBS lasers with $\Delta q = 12$ and a sinusoidal rotation applied to the cavity, and figure 4b shows the corresponding rotation angle. Similar to $\Delta q = 0$, the change in the difference frequency between the lasers is directly proportional to the applied rotation rate. However, in this case there is no lock-in zone for low rotation rates, and the difference frequency smoothly follows the applied rotation rate. In addition, the difference frequency is not zero for zero rotation, but is at a fixed frequency offset that, in this case, corresponds to 12 FSRs, or 92.4 MHz.

There are a number of factors that influence the stability of this offset that are being investigated. Some of these include temperature, fiber birefringence, backscattering, optical Kerr effect, and dispersion pulls.

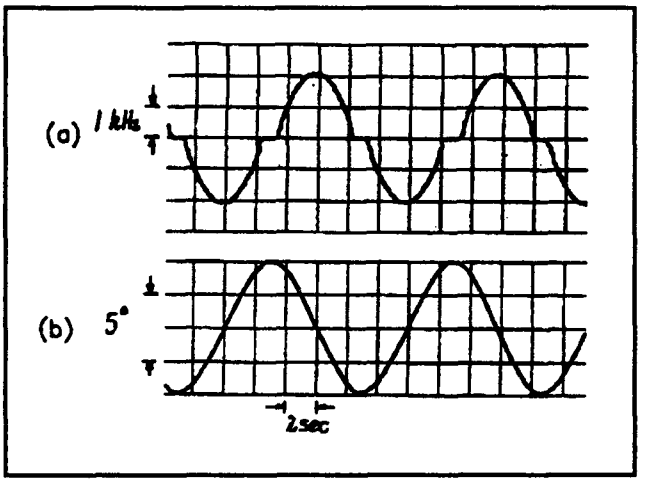


Figure 3. Simultaneous recording of (a) difference frequency between SBS lasers and (b) angle of the applied rotation.

[20] F. Aronowitz, "The Laser Gyro," in *Laser Applications*, ed. M. Ross (New York: Academic Press, 1971).

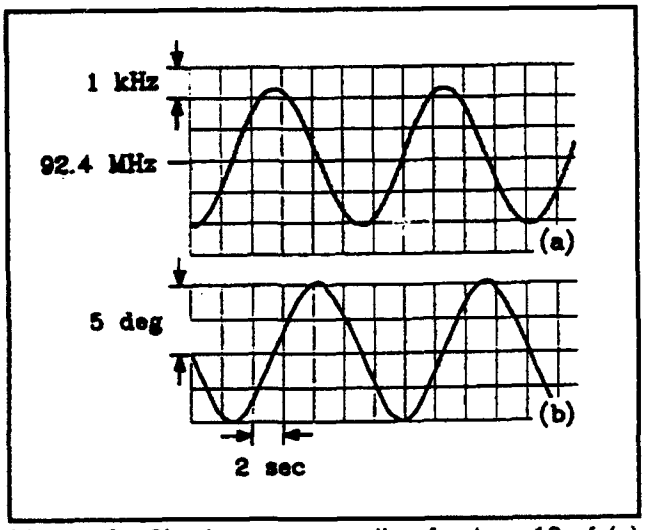


Figure 4. Simultaneous recording for $\Delta q = 12$ of (a) difference frequency between SBS lasers and (b) angle of the applied rotation.

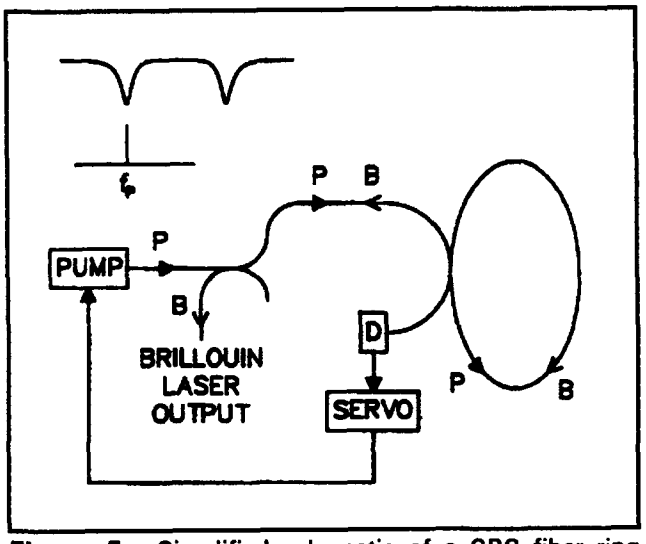


Figure 5. Simplified schematic of a SBS fiber ring laser.

1.3 Applications of Stimulated Brillouin Fiber Lasers

Sponsor

Charles S. Draper Laboratories
Contract DL-H-418468

The development of low threshold stimulated Brillouin scattering (SBS) fiber lasers has created a variety of fiberoptic devices and sensors for a wide range of applications.

Briefly stated, stimulated Brillouin scattering[21] is a nonlinear process in which an intense beam of light, the pump, propagating in a single mode fiber generates gain for a counterpropagating beam, the SBS beam, which is downshifted in frequency from the pump by $(2v_a/c)f_p$, where v_a is the speed of sound in the fiber, c is the speed of light in the fiber, and f_p is the frequency of the pump light. For example, for a pump wavelength of 1 μm in quartz, the center of the Brillouin gain is downshifted by about 15 GHz.

The pump power needed to achieve SBS can be greatly reduced by generating the SBS inside a fiber ring cavity, as illustrated in figure 5. By holding the pump, in the direction labelled P, at the center of a cavity resonance by the use of a servo, the pump power inside the resonator can be enhanced. If the resulting round trip SBS gain is greater than the cavity losses, SBS lasing will occur along the direction opposite to that of the pump,[22] labelled B in the figure. The absolute linewidth of the SBS laser was shown to be less than 1 kHz,[23] and with better acoustic and thermal isolation, this linewidth can be further reduced.

Since the SBS laser is downshifted in frequency from the pump, it can be used as a simple, wideband frequency shifter. A large frequency shift with respect to the pump, 15 GHz with a 1 μm pump, can be achieved without requiring sophisticated wideband electronics. Only a relatively simple servo is needed to hold the pump laser near the center of a cavity resonance. Moreover, even

---

21 R.Y. Chiao, C.H. Townes, and B.P. Stoicheff, "Stimulated Brillouin Scattering and Coherent Generation of Intense Hypersonic Waves," *Phys. Rev. Lett.* 12: 592 (1964).

22 K.O. Hill, B.S. Kawasaki, and D.C. Johnson, "cw Brillouin Laser," *Appl. Opt. Lett.* 28: 608 (1976); D.R. Ponikvar and S. Ezekiel, "Stabilized Single-frequency Stimulated Brillouin Fiber Ring Laser," *Opt. Lett.* 6: 398 (1981); L.F. Stokes, M. Chodorow, and H.J. Shaw, "All-fiber Stimulated Brillouin Ring Laser with Submilliwatt Pump Threshold," *Opt. Lett.* 7: 509 (1982).

23 S.P. Smith, F. Zarinetichi, and S. Ezekiel, "Narrow Linewidth Stimulated Brillouin Fiber Laser and Applications," *Opt. Lett.* 16: 393 (1991).

larger frequency shifts may be generated using higher order SBS lasers.[24]

There are also many applications for two SBS lasers generated in the same resonator, as shown in figure 6. In the figure, two independent pump lasers, in the directions labelled P1 and P2 respectively, are coupled into opposite directions of the same ring cavity and locked to different longitudinal modes of the cavity, using servos not shown in the figure. The corresponding SBS lasers, in the directions labelled B1 and B2, will have approximately the same frequency separation as the pump lasers. However, the beat between the SBS lasers will be very narrow, since they share the same cavity, and any fluctuations in the optical length of the cavity are common to both lasers.

Figure 7 shows an example of such a beat between two SBS lasers, centered at 507 MHz, which has been detected and is displayed on an electronic spectrum analyzer. The observed linewidth of 30 Hz was limited by the instrumental linewidth of the spectrum analyzer; this implies that the actual linewidth is much narrower than 30 Hz and should be close to the Schawlow-Townes limit. In contrast, the corresponding beat between the pump lasers, which were intentionally jittered, was almost 100 kHz. Thus, the beat between the two lasers can be detected and used as a microwave, or even millimeter wave source, limited only by the detector response and the tunability of the pump lasers.

SBS lasers also have a number of other applications in, for example, the generation of wideband amplitude modulated laser beams for use in absolute distance and ranging measurements. These lasers can also be used to generate two laser sources with correlated frequency jitter for fast flow laser Doppler velocimeters (LDV) and high resolution, two-photon interactions for the development of atomic clocks.

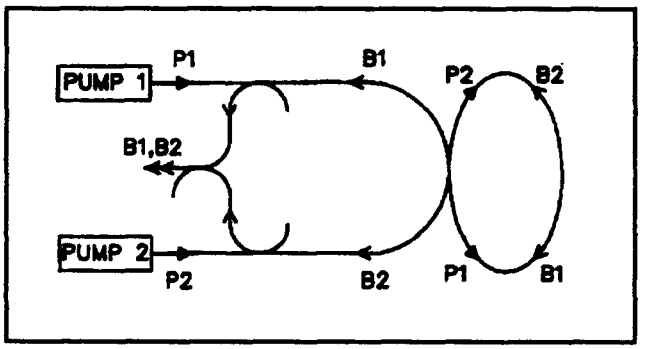


Figure 6. Simplified schematic of common cavity SBS lasers.

There are also a number of sensor applications for common cavity SBS lasers that take advantage of their narrow beat. An immediate application of SBS lasers is in the development of a fiber ring laser gyroscope,[25] which takes advantage of the directionality of the SBS gain tc generate two counterpropagating SBS lasers at the same frequency in a single cavity.

In addition to the fiber ring laser gyroscope, common cavity SBS lasers open the way for a new class of fiber optic sensors.[26] For example, by generating the SBS laser separated by an integer number of cavity free spectral ranges, it is possible to measure temperature in an inherently digital method that does not require a "reference arm." The change in the beat frequency between the SBS lasers is directly proportional to the change in temperature, with the scale factor determined by the frequency separation of the lasers and the temperature coefficient of the optical length of the fiber cavity. Thus, by changing the frequency spacing of the SBS lasers, the scale factor of the sensor can be adjusted. This concept may also be extended to measurement of other physical quantities such as magnetic and electric fields, acceleration, and acoustics.

---

[24] S.P. Smith, F. Zarinetichi, and S. Ezekiel, "Narrow Linewidth Stimulated Brillouin Fiber Laser and Applications," *Opt. Lett.* 16: 393 (1991).

[25] F. Zarinetchi, S.P. Smith, and S. Ezekiel, "Stimulated Brillouin Fiber-optic Laser Gyroscope," *Opt. Lett.* 16: 229 (1991).

[26] S.P. Smith, F. Zarinetchi, and S. Ezekiel, "Stimulated Brillouin Scattering Fiber Laser for Novel Fiber Sensor Applications," *Proceedings of the OFS '92*, Monterey, California, 1992.

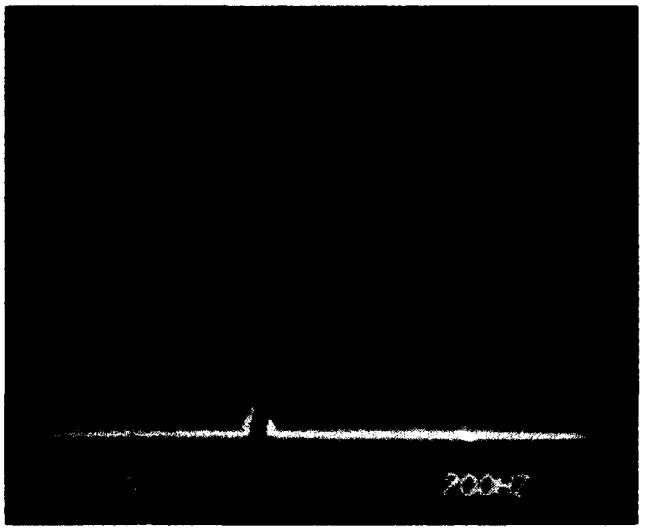


Figure 7. Spectrum of beat note between two common cavity SBS lasers centered at 507 MHz.

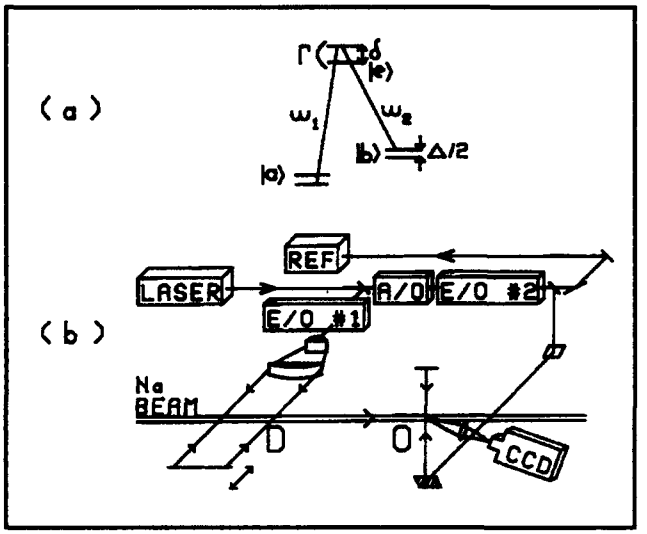


Figure 8. (a) Schematic of the three-level Λ system. (b) Perspective diagram of the experimental setup used to observe atomic beam deflection.

1.4 First Observation of Deflection and Cooling of Three-level Atoms in Raman Resonant Standing Wave Optical Fields

Sponsors

U.S. Air Force - Electronic Systems Division
Contract F19628-89-K-0300
U.S. Navy - Office of Naval Research
Grant N0014-91-J-1808

The interaction of two laser fields with a three-level atom in the Λ configuration has been of increasing interest in recent years. The force due to two counter-propagating traveling waves has already cooled such atoms below the single photon recoil limit.[27] Recently, theoretical solutions have shown that the force on a stationary three-level atom in standing wave fields is unbounded, with spatial variations on length scales both much longer and much shorter than an optical wavelength.[28] Here we show experimental verification of the existence of the long-range component of this force by deflecting an atomic beam of three-level sodium atoms using two Raman resonant standing wave laser fields. In addition, we show the existence of damping forces.

These observations open the possibility of developing an all-optical, deep neutral atom trap with a stimulated restoring force. Most atoms in a Raman trap would be in the ground states, so that the collisional lifetime of the atoms would be much longer than in magneto-optic traps. As a result, the Raman force could ultimately lead to high densities of cold and dark atoms in traps. Such a dense collection of atoms in transparent superposition states could find applications as novel, low intensity nonlinear optical materials.[29] Moreover, a Raman trap could be directly used as a Raman-atomic clock, since the dark state is not light shifted.[30]

A schematic diagram of the three-level Λ system is shown in figure 8a. The experimental setup used to observe deflection of a sodium atomic beam is shown schematically in figure 8b. Atomic beam deflection data obtained with the setup of figure 8 are shown in figure 9. For this data we chose to use the maximum laser power available (200 mW/cm^2) in the deflection zone. The detunings were then optimized ($\Delta = -16$ MHz,

[27] A. Aspect, E. Arimondo, R. Kaiser, N. Vansteenkiste, and C. Cohen-Tannoudji, *Phys. Rev. Lett.* 61: 826 (1988).

[28] S. Shahriar, P.R. Hemmer, N.P. Bigelow, and M.G. Prentiss, Quantum Electronics and Laser Science Conference, May 1991; M.G. Prentiss, N.P. Bigelow, S. Shahriar, and P.R. Hemmer, *Opt. Lett.* 16: 1695 (1991).

[29] S. Shahriar and P.R. Hemmer, *Phys. Rev. Lett.* 65: 1865 (1990).

[30] P.R. Hemmer, S. Shahriar, V.D. Natoli, and S. Ezekiel, *J. Opt. Soc. Amer. B* 6: 1519 (1989).

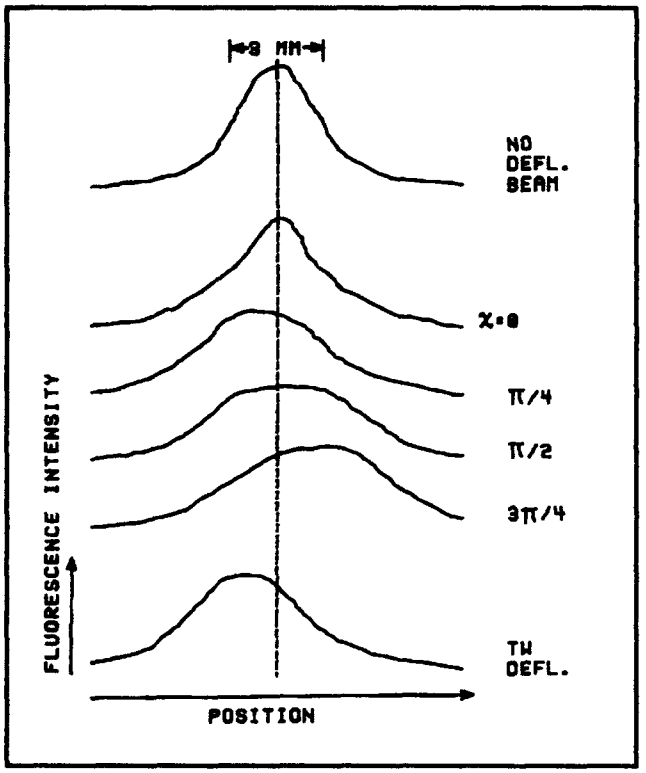


Figure 9. Data showing atomic beam deflection. Traces are obtained by digitizing single lines of stored video images.

$\delta = 4.4$ MHz) to observe the cleanest deflection. Here, the top trace shows the atomic beam profile with the deflecting laser blocked. The next four traces show the deflection obtained for standing wave fields having relative phase shifts of $\chi = 0, \pi/4, \pi/2$, and $3\pi/4$ as labeled. Finally, the bottom trace in the figure is obtained with the retroreflected deflecting laser beam blocked showing the spontaneous deflection. As can be seen, the deflection basically behaves as $\sin(2\chi)$ When the value of Δ is reversed, the stimulated deflection is reversed at every value of χ, while the spontaneous deflection remains unchanged. These observations are in qualitative agreement with theoretical prediction.

As we have pointed out, the deflection force changes sign when the sign of Δ is reversed. This property can be helpful in designing an all-optical trap. Briefly stated, one can conceivably design a B-field gradient such that the value of Δ is antisymmetric with respect to the zero field point, which would be the trap center. Of course, in order for such a trap to work, one would need a mechanism for cooling. We have performed numerical calculations for the friction force and have found evidence that, when averaged over an optical wavelength, it varies strongly as a function of χ. We have found experimental evidence (not shown) of such phase dependent cooling, being at its maximum at the phase where the deflection is at maximum.

In summary, we have observed the phase dependent deflection and cooling of a sodium atomic beam by two standing waves simultaneously near resonance with both components of a Λ three-level system. Qualitative agreement between theory and experiment is achieved. Potential applications to high-density, dark atom traps are currently being investigated. Such dark atom traps may be useful in nonlinear optics and as a Raman-atomic clock.

1.5 Origin of the Optical Force on the Raman Dark State in Two Standing Waves

Sponsors

U.S. Air Force - Electronic Systems Division
Contract F19628-89-K-0300
U.S. Navy - Office of Naval Research
Grant N0014-91-J-1808

Recently, the optical force on three-level atoms has been investigated for several promising applications. The force associated with coherent population trapping due to counterpropagating traveling wave fields has cooled atoms below the single photon limit.[31] On the other hand, three-level atoms in two standing waves have been cooled as well as deflected, with potential applications to a novel, high density trap.[32] There have been disparate calculations of the force on an atom in two standing wave excitation fields,[33] which have not discussed the underlying physical processes in any detail. Here we describe the origin of the force on stationary atoms in terms of the evolution of the

[31] A. Aspect, E. Arimondo, R. Kaiser, N. Vansteenkiste, and C.Cohen-Tannoudji, *Phys. Rev. Lett.* 61: 826 (1988).

[32] P. Hemmer, S. Shahriar, M. Prentiss, D. Katz, K. Berggren, and J. Mervis, accepted for presentation at the Quantum Electronics and Laser Science Conference, 1992.

[33] J. Javanainen, *Phys. Rev. Lett.* 64: 519 (1990); S. Chang, B.M. Garraway, and V.G. Minogin, *Opt. Comm.* 77: 19 (1990).

normal modes of the atom field system.[34] We show that most of the qualitative features of the force can be derived by inspection without actually solving the optical Bloch equations (OBEs).

We recall[35] first that, in steady state, the Raman system is in the dark state as long as Δ, the difference detuning (see figure 8a), vanishes. To take advantage of this, we choose to express the Raman interaction in a representation wherein the dark state is one of the basis states. For non-zero but small values of Δ, the Raman intercation can then be represented as a perturbative excitation into states that are orthogonal to the dark state. We find that if δ, the common detuning (see figure 8a) vanishes, the optical force is only on the dark state, thus futher simplifying the analysis.

To start with, we restrict the calculation to the regime wherein the Rabi frequencies are much weaker than the natural lifetime. This allows us to eliminate the excited state by invoking the adiabatic following approximation.[36] We are then left with a two-level system coupled by Δ. This problem is then solved perturbatively, since Δ is assumed to be small. The resulting expression for the optical force on a three-level system for the case of two standing waves with equal amplitudes and a phase difference of $\pi/4$ is illustrated in figure 10. Figure 10a shows the Rabi frequencies. The force expression is plotted and compared to the exact solution of the optical Bloch equations (OBEs) in figure 10b. The solid curve is a plot of the perturbative estimate, and the circles correspond to the OBE solution. The lowest order force estimate agrees well with the OBE result. However, unlike the OBE solution, the perturbative solution can be interpreted physically, enabling us to understand the origin of the sharp structures.

Not only does the force in the Λ system show sub-optical-wavelength behavior, but it can show strong rectification (i.e., non-zero value when averaged over an optical wavelength). One case in which the origin of this rectification can be clearly illustrated is when Δ is large, so that the reduced two level interaction is saturated. The force expression in this case can also be found by

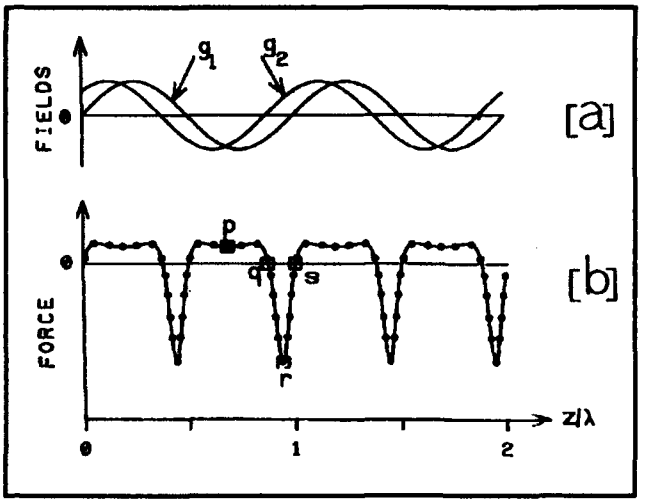


Figure 10. (a) The Rabi frequencies. (b) Sub wavelength structure in the optical force, computed by a perturbative estimate (solid line), and compared with the exact solution of the optical Bloch Equations (circles).

mere inspection, as is illustrated in figure 11. The rectified component of this force as a function of χ, the phase difference between the standing waves, is shown by the solid line. The dotted curve is the rectified force computed using the exact solution of the OBEs. Again, there is reasonably good agreement.

To summarize, we have used the normal modes of the atom field to physically model the origins of novel structures that appear in the force on a Λ system atom under standing wave excitation. In particular, we have identified a situation where the force is only on the dark state, thus leading to simple, closed form expressions for the force. Finally, our estimated results agree well with solutions of the OBEs in the regions where the approximations used are valid. Future work will involve using the normal modes of the atom-field system to model phase χ dependent cooling.

We are grateful to AT&T Bell Laboratories and the Laboratory for Laser Energetics (LLE) in Rochester, New York for their support of this project.

---

[34] H.R. Gray, R.M. Whitley, and C.R. Stroud, Jr., *Opt. Lett.* 3: 218 (1978).

[35] P.R .Hemmer, G.P. Ontai, and S. Ezekiel, *J. Opt. Soc. Amer. B* 3: 219 (1986).

[36] P.R. Hemmer and M.G. Prentiss, *J. Opt. Soc. Amer. B* 5: 1613 (1988); P.R. Hemmer, M.S. Shahriar, V.D. Natoli, and S. Ezekiel, *J. Opt. Soc. Amer. B* 6: 1519 (1989).

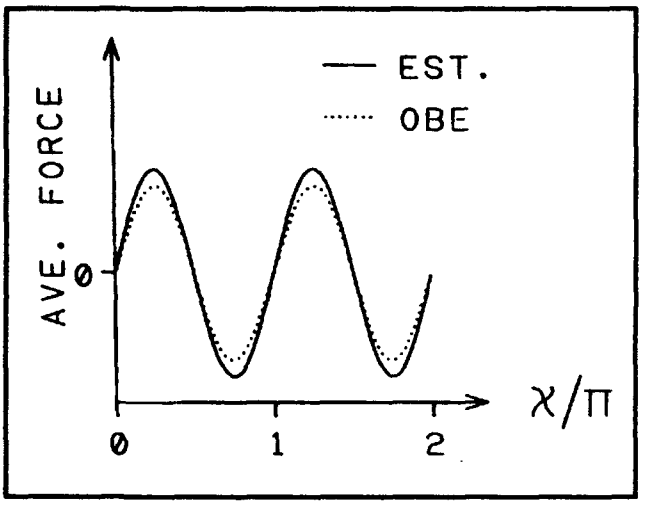


Figure 11. Wave-length averaged force as a function of the standing wave phase difference, computed by a perturbative estimate (solid line), and compared with the exact solution of the optical Bloch Equations (dotted line).

Publications

Hemmer, P., M. Prentiss, and S. Shahriar. "Optical Force on the Raman Dark State in Two Standing Waves." *Opt. Commun.* Forthcoming.

Prentiss, M., N. Bigelow, S. Shahriar, and N. Bigelow. "Forces on Three Level Atoms Including Coherent Population Trapping." *Opt. Lett.* 16: 1695 (1991).

Prentiss, M.G., N. Bigelow, M.S. Shahriar, P.R. Hemmer, K. Berggren, J. Mervis, S. Ezekiel. "Laser Manipulation of Atoms and Ions." Enrico Fermi International School of Physics, Course CXVIII. Milan, Italy, July 1991.

Shahriar, S., P. Hemmer, N. Bigelow, and M. Prentiss. "Forces on Three Level Atoms Including Trapped State Contribution." In *Quantum Electronics and Laser Science.* Technical Digest Series. Washington, D.C.: Optical Society of America, 1991. pp. 186.

1.6 Optical Data Storage with Raman Excited Microwave Spin Echoes

Sponsor

U.S. Air Force - Electronic Systems Division
Contract F19628-89-K-0030

Recently, there has been a great deal of interest in the use of optical photon echoes for information storage and processing.[37] However, so far experimental demonstrations have been restricted to spectral hole burning materials operating at liquid He temperatures. Information has been stored using microwave spin echoes in room temperature materials,[38] but the data rates and storage densities achievable are orders of magnitude below those of optical echo techniques. The proposed scheme, which makes use of an optically excited microwave spin echo, is capable of data rates and storage densities comparable to optical echo techniques, but potentially at much higher temperatures (provided a suitable material can be found). In contrast to multilevel optical echoes, the Raman excited microwave coherences could store information which is spread over times much longer than the homogeneous decay time of the optical coherence.

The basic architecture of the proposed scheme is illustrated in figure 12. A three-level system is used, which can be excited by two near resonant optical transitions (resonance Raman) or one near resonant microwave transition (see figure 8a). As shown, information is first input as an optical pulse train (two unequal amplitude pulses in the figure). The optical input beam contains both optical frequencies needed to excite the resonance Raman transition. The Raman interaction creates a coherence which depends on phase differences in the two optical frequencies. This phase sensitivity, combined with dephasing of the ground state coherence due to inhomogeneous broadening, allows both the temporal and phase information contained in the optical fields to be stored via a process analogous to spectral hole burning. To recall this information, a π-pulse must be applied. Since the Raman coherence directly translates into a microwave coherence[39] this can be accomplished with a microwave π-pulse. The ground state

---

[37] M.K. Kim and R. Kachru, "Storage and Phase Conjugation of Multiple Images Using Backward-stimulated Echoes in Pr^{3+}:LaF_3," *Opt. Lett.* 12: 593 (1987).

[38] S. Fernbach and W.G. Proctor, "Spin-echo Memory Device," *J. Appl. Phys.* 26: 170 (1955).

[39] M.S. Shahriar and P.R. Hemmer, "Direct Excitation of Microwave-spin Dressed States Using a Laser-excited Resonance Raman Interaction," *Phys. Rev. Lett.* 65: 1865 (1990).

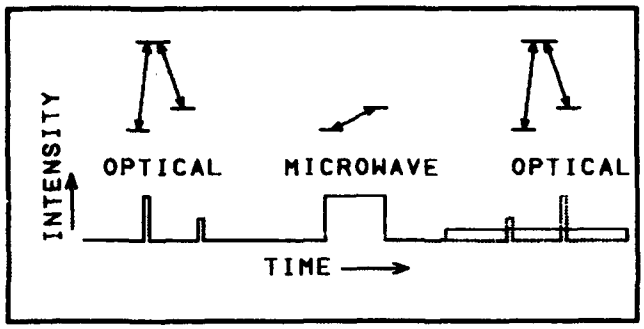


Figure 12. Schematic showing proposed architecture for optical data storage with Raman-microwave spin echoes. The dotted lines on the right side show the microwave spin echoes which are detected by an optical Raman probe (superimposed solid line).

coherences will then rephase at the appropriate time where they can be detected optically, as bright and dark areas, using an optical Raman probe, as shown in figure 12.

Figure 13a shows the theoretical input pulse train and figures 13b and 13c show the optically detected echo pulses for in and out of phase optical Raman probing fields, respectively. As shown, both positive and negative versions of the input information can be retrieved. These traces were produced using density matrix equations that had been developed to explain experimentally observed optical-microwave interactions.[39]

In summary, we have studied the process whereby resonant Raman excitation is used to store information in ground state spin-coherences that are long-lived and inhomogeneously broadened. A microwave π-pulse is used to rephase the coherences, so that the information can be restored via Raman detection of spin echoes. These techniques promise to combine the advantage of optical echo (high resolution) and spin echo (long lived) so that photon echo based optical data storage may possibly be achieved in room temperature materials.

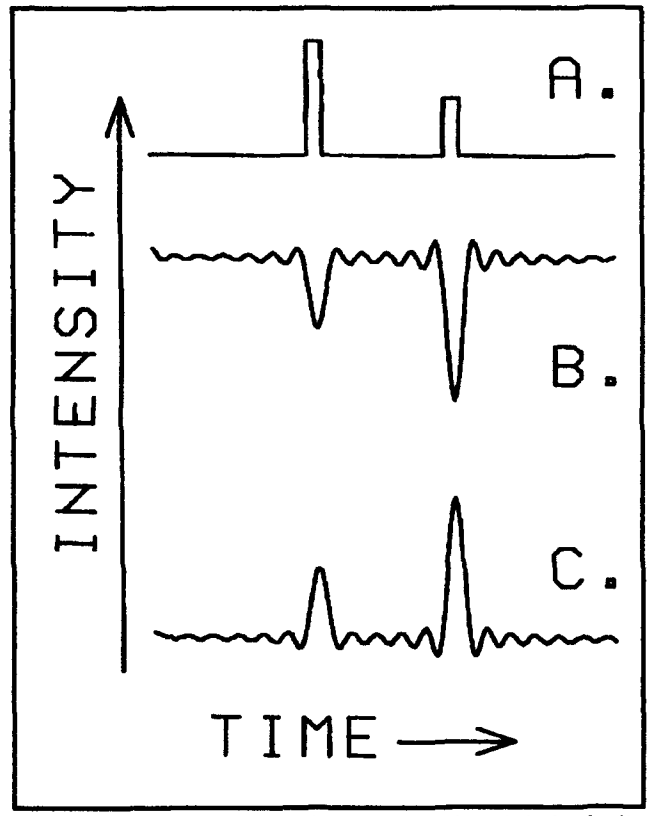


Figure 13. (a) Input optical pulse train. (b) Optically detected output microwave pulse train for in-phase Raman probe fields. (c) Output for out of phase Raman probe.



Professor Daniel Kleppner

Chapter 2. Basic Atomic Physics

Academic and Research Staff

Professor Daniel Kleppner, Professor David E. Pritchard, Dr. Kristian Helmerson, Dr. Wolfgang Ketterle

Visiting Scientists and Research Affiliates

Dr. Tomaz Catunda, Dr. Theodore W. Ducas,[1] Dr. Chun-ho Iu, Dr. Alexander Martin, Dr. H. Joerg Schiedmeyer

Graduate Students

Kevin R. Boyce, Pin P. Chang, Michael W. Courtney, Kendall Davis, Frank DiFilippo, Christopher R. Ekstrom, Troy D. Hammond, Jeffrey R. Holley, Hong Jiao, Michael A. Joffe, David W. Keith, Robert P. Lutwak, Marc-Oliver Mewes, Vasant Natarajan, Scott N. Paine

Undergraduate Students

John E. Berberian, Charles G. Freeman, James A. Grimm, Matthew J. Marjanovic, David Mitchell, Wan Morshidi, Lee-Peng Ng, Quentin A. Turchette, Peter S. Yesley

Technical and Support Staff

Carol A. Costa

2.1 The Diamagnetic Rydberg Atom

Sponsors

National Science Foundation
Grant PHY 89-19381
U.S. Navy - Office of Naval Research
Contract N00014-90-J-1322

Project Staff

Dr. Chun-ho Iu, Michael W. Courtney, Dr. Tomaz Catunda, Hong Jiao, Professor Daniel Kleppner, David Mitchell, Lee-Peng Ng

A highly excited hydrogen atom in a strong magnetic field, the so-called "diamagnetic hydrogen atom," is among the simplest nonseparable systems in quantum mechanics. Understanding it can be expected to provide a key to the more general aspects of nonseparable systems. The problem is also attracting attention in the context of nonlinear dynamics because its classical behavior displays a transition from orderly to disorderly motion as the energy is increased in a fixed magnetic field. One can study the quantum structure of the system in this regime both theoretically and experimentally. Thus, the diamagnetic hydrogen atom provides an ideal testing ground for studying the relation between quantum structure and disorderly classical motion, a subject sometimes called "quantum chaos."

We have developed techniques for carrying out high resolution laser spectroscopy on the lithium atom in a strong magnetic field. The difference between lithium and hydrogen is minor for Rydberg atoms.

The experiment uses a lithium atomic beam which is excited by two c.w. lasers. The first laser excites the atoms from the 2S state to the 3S state by a two-photon transition and the second laser excites the atoms to Rydberg states. The excited atoms are detected by electric field ionization. We typically operate in magnetic fields near 6T. We can determine the energy within $10^{-3}\,cm^{-1}$, and the magnetic field within 5 gauss.

The Hamiltonian for the diamagnetic hydrogen atom, in atomic units, is

$$H = \frac{p^2}{2} - \frac{1}{r} + \frac{1}{2} L_z B + \frac{1}{8} B^2 \rho^2. \qquad (1)$$

There are no general solutions to this problem, and perturbation theory is not applicable in the positive energy regime. In previous years, our experimental

[1] Department of Physics, Wellesley College, Wellesley, Massachusetts.

results[2] have helped to stimulate theoretical advances. However, the productivity of the research was limited by difficulties associated with our antique superconducting magnet. Our major effort during this past year has been to rebuild the apparatus with an up-to-date magnet that was provided by the National Science Foundation. Figure 1 presents a schematic diagram of the apparatus.

The new magnet employs a split coil configuration and provides 7T. The four inch bore allows a significantly larger interaction region and more convenient optical access than previously possible. Rydberg atoms are sensitive to stray electric fields, and stray fields were a limiting factor in our previous work. Figure 2 shows the new interaction region in which stray electric fields are greatly reduced because the surfaces are farther from the interaction volume. In addition, stray electric fields parallel to the magnet axis can be cancelled by an applied field. In addition, an electric field can be applied as an additional probe of the system. Another improvement in the interaction region is the collection of light from the fluorescent decay of the intermediate 2P state. One mirror focuses light onto a fiber bundle. Another doubles the area of collection by focusing light back to the point of interaction.

A scintillator and fiber bundle have replaced the surface barrier diode for detection of Rydberg atoms. After the atoms are ionized, they are accelerated to the scintillator by a 15 KV potential. The light is carried to a photomultiplier by the fiber bundle. This detection method permits reliable counting of single ions. As a result, our signal is highly linear to the number of Rydberg atoms produced.

We have observed that in a certain regime the system displays one-dimensional behavior. It is useful to write the Hamiltonian for the diamagnetic hydrogen atom as

$$H = H_\rho + H_z + H', \tag{2}$$

where

$$H_\rho = \frac{p_\rho^2}{2} + \frac{1}{2} L_z B + \frac{1}{8} B^2 \rho^2,$$

$$H_z = \frac{p_z^2}{2} - \frac{1}{|z|},$$

and

$$H' = \frac{1}{|z|} - \frac{1}{r}.$$

H_ρ is the Hamiltonian of an electron in a magnetic field, H_z is the Hamiltonian of one-dimensional Hydrogen, and H′ is a perturbation to the otherwise trivial Hamiltonian. Although the perturbing potential is not small (in fact it is singular for the entire z = 0 plane) it has been shown[3] that parts of the experimental spectrum can be understood simply in terms of the unperturbed Hamiltonian as a superposition of the spectra of one-dimensional Hydrogen and an electron in a magnetic field.

Using the stray electric field in the old apparatus, we have studied the Stark splitting of the one-dimensional hydrogen atom that is approximated by magnetic confinement of the electron transverse to the magnetic field. Figure 3 shows an example of the Stark splitting. The levels correspond to the Rydberg level of n = 70. The electric field was about 80 mV/cm. The predicted Stark splitting is 0.050 cm^{-1}, and the measured splitting from figure 3 is 0.047 cm^{-1}. This observation of the one-dimensional Stark splitting further confirms the regular behavior of the quantum system. We plan to measure the Stark splitting in a variety of electric fields to see how closely our system resembles one-dimensional hydrogen.

---

[2] D. Delande, A. Bommier, and J.C. Gay, *Phys. Rev. Lett.* 66: 141 (1991); C. Iu, G.R. Welch, M.M. Kash, D. Kleppner, D. Delande, and J.C. Gay, *Phys. Rev. Lett.* 66: 145 (1991).

[3] C. Iu, G.R. Welch, M.M. Kash, L. Hsu, and D. Kleppner, *Phys. Rev. Lett.* 63: 1133 (1989).

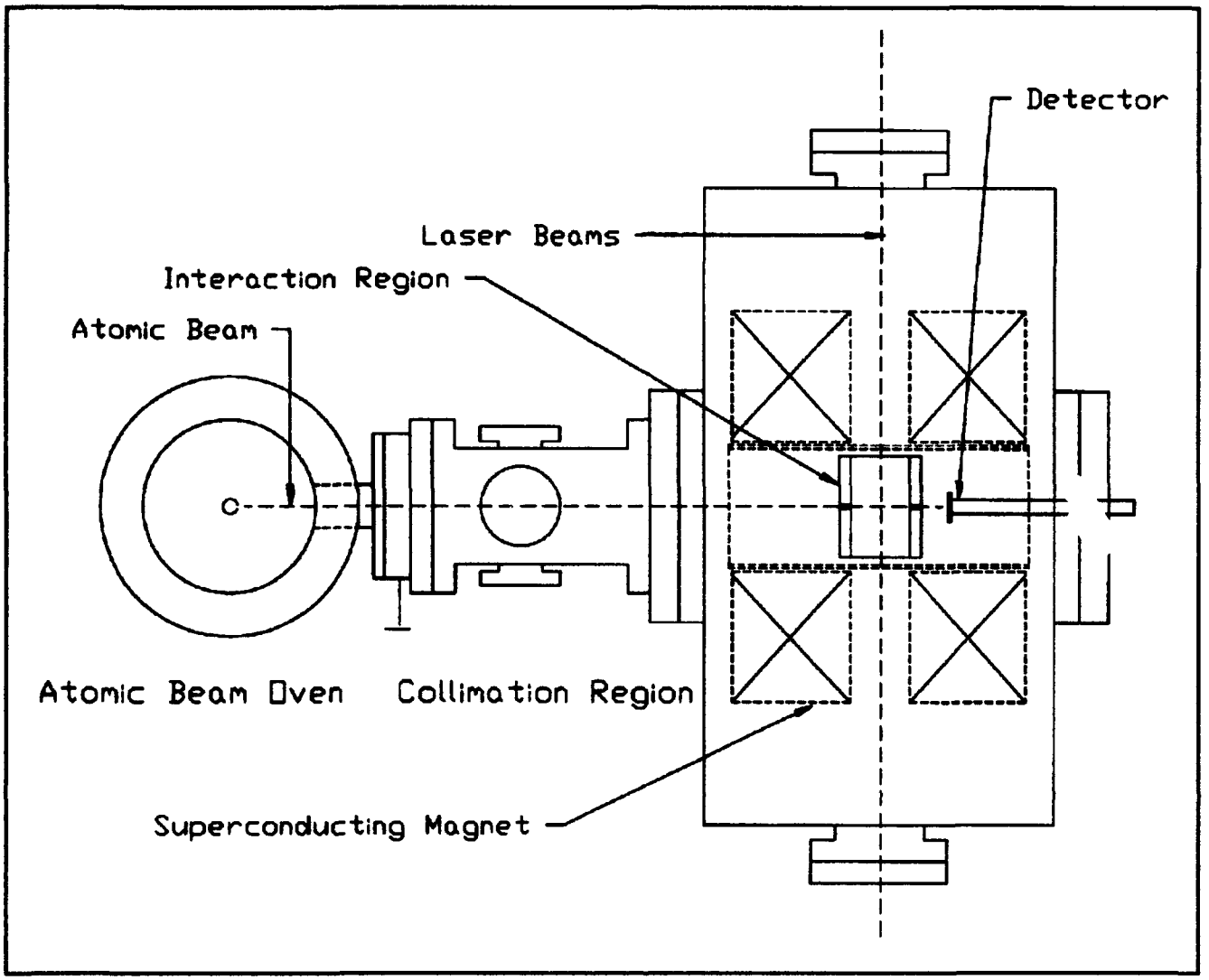


Figure 1. Superconducting magnet and atomic beam apparatus.

Publications

Iu, C., G.R. Welch, M.M. Kash, D. Kleppner, D. Delande, and J.C. Gay. "The Diamagnetic Rydberg Atom: Confrontation of Calculated and Observed Spectra." *Phys. Rev. Lett.* 66: 145 (1991).

Kleppner, D., C. Iu, and G.R. Welch. "Positive Energy Spectroscopy of the Diamagnetic Lithium System." *Comments At. Mol. Phys.* 25: 301 (1991).

Theses

Iu, C. *Energy Level Structure of Atoms in Magnetic Fields.* Ph.D. diss. Dept. of Physics, MIT, 1990.

Mitchell, D. *The Onset of Chaos for a Semi-Classical Alkali Atom in a Uniform Electric Field.* B.A. thesis, Dept. of Physics, MIT, 1991.

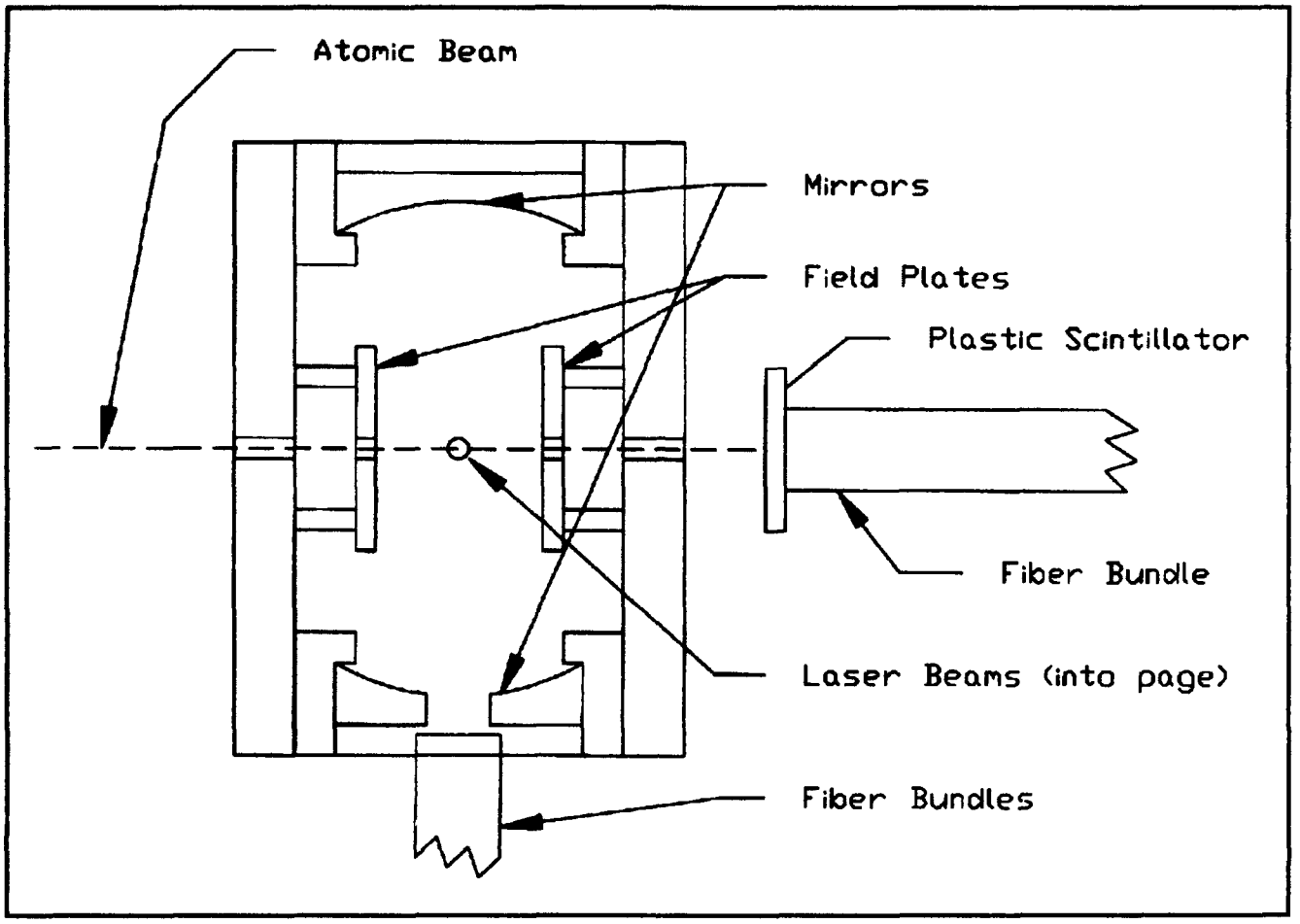


Figure 2. Interaction region.

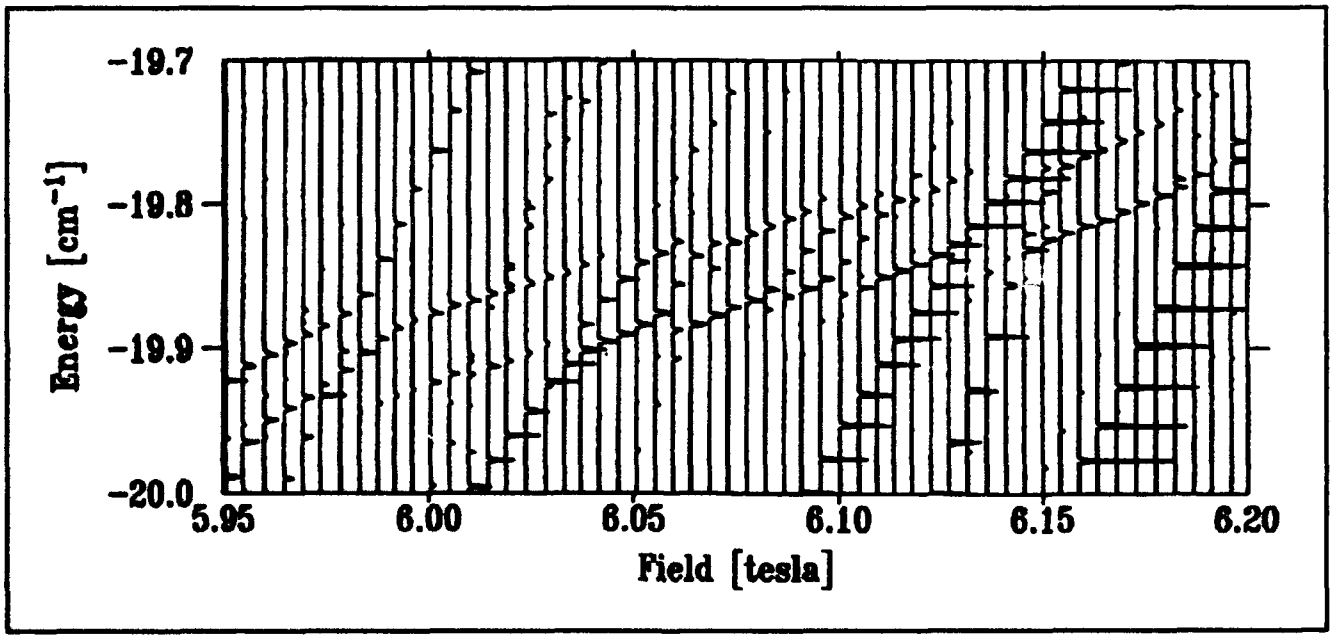


Figure 3. One-dimensional Stark splitting near 6 T, n = 70. The electric field is approximately 80 mV/cm.

2.2 Millimeter-Wave Frequency Measurement of the Rydberg Constant

Sponsors

Joint Services Electronics Program
Contract DAAL03-89-C-0001
Contract DAAL03-92-C-0001
National Science Foundation
Grant PHY 89-19381

Project Staff

Pin P. Chang, Jeffrey R. Holley, Robert P. Lutwak, Scott N. Paine, Dr. Theodore W. Ducas, Professor Daniel Kleppner

The Rydberg constant, R_∞, relates the wavelengths of the spectrum of atomic hydrogen to practical laboratory units. As such, R_∞ is the natural unit for measurements of numerous atomic properties. Experiments using laser spectroscopy have determined R_∞ to nearly 1 part in 10^{10}.[4] Although R_∞ is the most accurately measured fundamental constant, high-precision experiments which depend on R_∞ as an auxiliary constant demand a more accurate determination. For example, new experiments to determine the Lamb shift in the ground state of atomic hydrogen will be limited by uncertainties in R_∞. The accuracy of optical measurements has reached the limit of precision of wavelength metrology. Further progress in measuring R_∞ requires a frequency measurement, making use of the modern definition of length in terms of time intervals and the defined speed of light.

We are attempting to advance the accuracy of R_∞ by directly measuring cR_∞, the "Rydberg frequency." By initially preparing highly excited "Rydberg" states of atomic hydrogen, we are able to measure millimeter-wave transitions to nearby states with the full precision of frequency metrology.

The goal of our experiment is three-fold. First is the evaluation of cR_∞. Second is the measurement of the ground state Lamb shift. Because our measurements involve high angular momentum states for which the Lamb shift is extremely small, a comparison of our results with optical measurements of transitions between low-lying states will yield an improved measurement of the Lamb shift. Third is the precise frequency calibration of the spectrum of hydrogen to provide an independent check on forthcoming optical frequency measurements based on laser spectroscopy.

Our experiment is performed in an atomic beam configuration to provide a long interaction time and reduce Doppler and collisional perturbations. Atomic hydrogen is excited to the state (n=29, m=0) by two-photon stepwise absorption. The atoms are then transferred to the longer lived "circular" state (n=29,m=28) by the method of crossed electric and magnetic fields.[5] The atoms then enter a region of uniform fields in which the frequency of the transition (n=29,m=28) → (n=30,m=29) is measured. The atoms interact with the millimeter-wave radiation at two locations in a Ramsey separated oscillatory fields geometry. The final state distribution of the atoms is measured by a state-selective electric field ionization detector. The resonance signal is observed as a transfer of atoms from the n=29 state to the n=30 state as the millimeter wave frequency is tuned across the transition.

Figure 4 illustrates the main features of the apparatus. Atomic hydrogen or deuterium is produced by dissociation of H_2 or D_2 in a radio frequency discharge. The beam is cooled by collisions with the walls of a cryogenically cooled thermalizing channel in order to slow the beam and thereby increase the interaction time. The atoms are excited to the state (n=29,m=28) by two-photon stepwise excitation in the circular state production region. The development of the hydrogen beam and optical systems was described in the 1990 *RLE Progress Report Number 133.* The magnetic field necessary to transfer the atoms to the circular state is provided by permanent magnets. The electric field is produced by an arrangement of strip electrodes that causes the direction of the field to rotate. A detector in the circular state production region monitors the efficiency of the laser excitation and momentum transfer processes.

After the atoms are prepared in the circular state, the beam enters the interaction region. Because Rydberg atoms interact strongly with external fields, accurate measurement of the energy level structure requires careful control of the interaction environment. Thermal radiation is reduced by cooling the interaction region to ~ 10 K by a liquid helium flow system. The ambient magnetic field is shielded by a double-wall high permeability

[4] M.G. Boshier et al., *Phys. Rev. A* 40: 6169 (1989); P. Zhao et al., *Phys. Rev. A* 39: 2888 (1989); F. Biraben et al., *Phys. Rev. Lett.* 62: 621 (1989).

[5] D. Delande and J.C. Gay, *Europhys. Lett.* 5: 303 (1988).

shield. The small electric field, necessary to define the quantization axis of the atoms, is applied with high uniformity by field plates with corrective strip electrodes along the sides. The millimeter waves intersect the atomic beam at two locations separated by 50 cm. The millimeter-wave optics were described in the 1990 *RLE Progress Report Number 133.*

The state distribution of the atoms emerging from the interaction region is analyzed by an electric field ionization detector. The atoms enter a region of increasing electric field produced by a ramped plate held at constant potential. The atoms in the state (n=30), which ionize at lower field, are collected in the first detector, while atoms in the state (n=29), which ionize at higher field, are collected at the second detector. An important feature of the detector is that it provides time resolution. The atomic beam is pulsed, and the time-resolved signal from the detector allows different velocity classes to be observed independently.

During this past year we have observed millimeter wave transitions in each of the two millimeter wave beams. In this fashion, we have observed the (n=29 → n=30) transition in both hydrogen and deuterium, as well as the (n=27 → n=28) transition in hydrogen. A typical resonance signal is shown in figure 5. In addition, we have observed "Rabi oscillations" in each of the millimeter wave beams. Recently, we have begun experiments to study signals from interactions with both millimeter-wave beams in the Ramsey separated oscillatory fields geometry. Sample interference data is shown in figure 6.

Improvements to increase the signal-to-noise ratio are underway, and we anticipate starting on high accuracy measurements in the coming year.

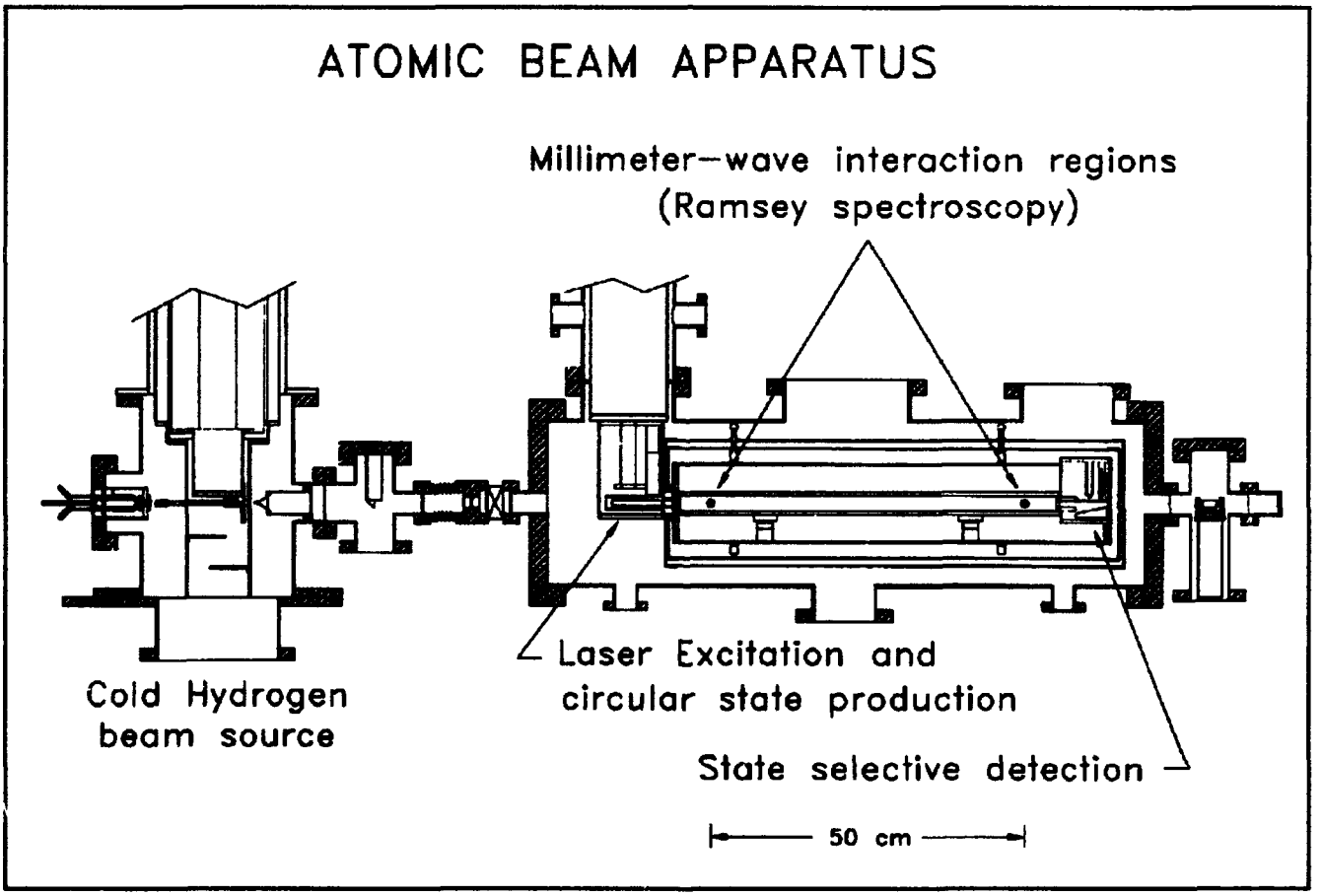


Figure 4. Schematic diagram of the atomic beam apparatus.

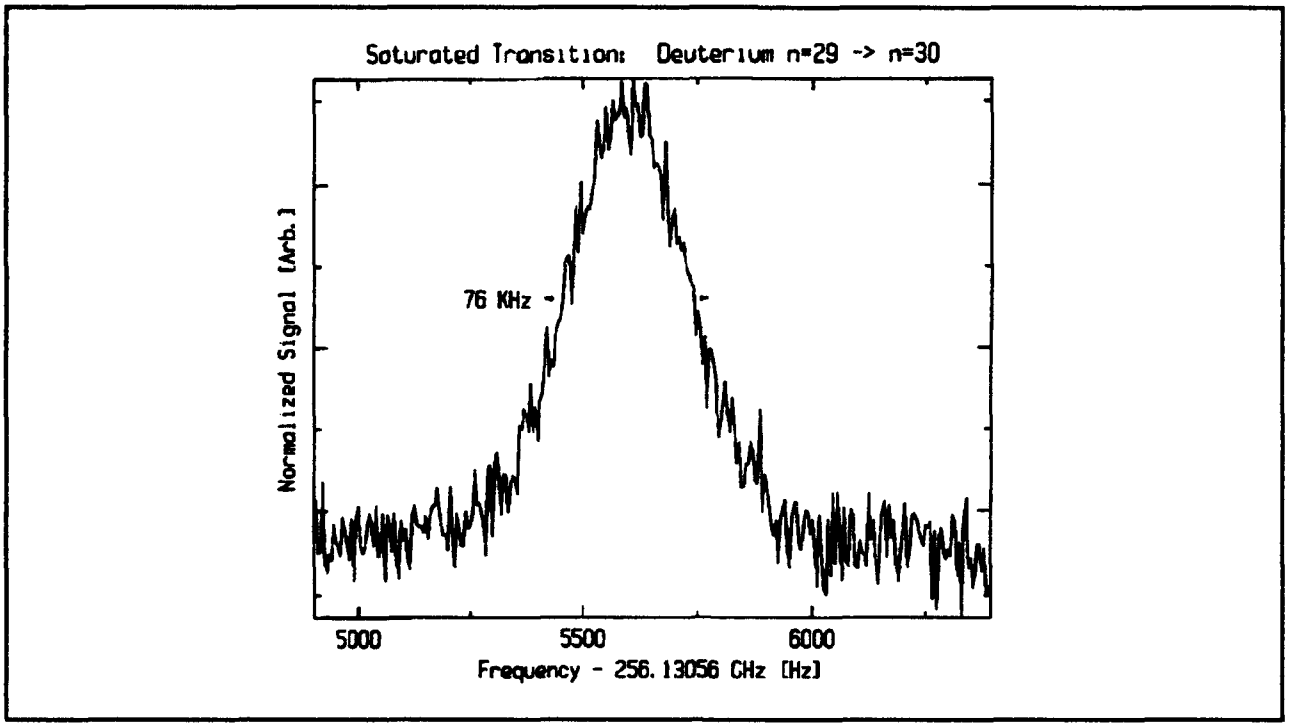


Figure 5. Typical signal for the (n=29,m=28) → (n=30,m=29) transition in atomic deuterium. The width of the resonance line is close to the time-of-flight limit as the atoms cross the millimeter wave beam.

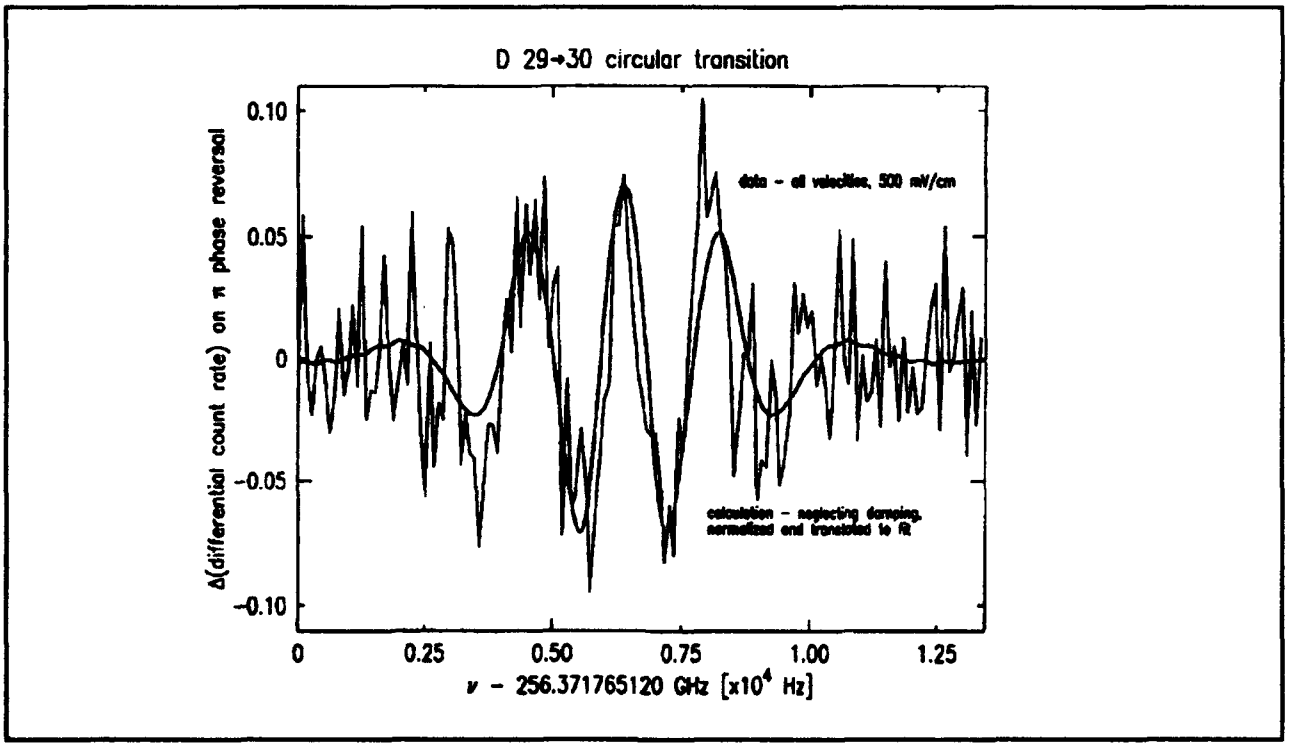


Figure 6. First results for the a narrow linewidth "Ramsey" fringe for the transition n=29,m=28 → n=30,m=29) in deuterium.

2.3 Atom Interferometry

Sponsors

Joint Services Electronics Program
Contract DAAL03-89-C-0001
Contract DAAL03-92-C-0001
U.S. Army Research Office
Contract DAAL03-89-K-0082
U.S. Navy - Office of Naval Research
Grant N00014-89-J-1207

Project Staff

John E. Berberian, Christopher R. Ekstrom, Troy D. Hammond, David W. Keith, Marc-Oliver Mewes, Dr. H. Joerg Schiedmeyer, Quentin A. Turchette, Professor David E. Pritchard

During 1991, we demonstrated the first atom interferometer.[6] Using transmission gratings, which we fabricated,[7] as optical elements for atom deBroglie waves, we constructed a three grating atom interferometer which physically separates atom waves before recombining them. Our demonstration was closely followed by two demonstrations of atom interferometers which used laser light as the beam splitters.[8]

Atom interferometers will make possible qualitatively new types of experiments involving inertial effects, studies of atomic and molecular properties, and tests of fundamental physics, and may ultimately open the way to making ultra-small structures using atom holograms.

- The relatively large mass and low velocity of atoms makes atom interferometers especially sensitive to inertial effects such as rotation, acceleration, and gravity. Sagnac rotation has been observed in agreement with theoretical predictions,[9] and sensitivity to gravitational acceleration at the 3×10^{-6} level has been demonstrated.[10] Atom interferometers may become the best absolute accelerometers and gravimeters in the next few years.
- Atom interferometers can be applied to a number of experiments in fundamental physics: tests of quantum mechanics such as the Aharonov-Casher effect,[11] measurement of the equality of proton and electron charges, and a precise measurement of the momentum of a photon. This latter measurement should produce a new high precision value for the fundamental constants $N_A\hbar$.
- Interferometers for atoms and molecules will offer more accurate ways to measure intrinsic properties of these particles, like their polarizability. They will also open up new areas of study, such as measurements of the "index of refraction" of a gas for a particle beam which passes through it.

Our interferometer consists of three 400 nm period transmission gratings, mounted 0.66 m apart on separate translation stages inside the vacuum envelope. During operation, the 0^{th} and 1^{st} order beams from the first grating strike the middle grating (which is 140 μm wide) where they are diffracted in the 1^{st} and -1^{st} orders so that they converge at the third grating. At the second (middle) grating the beams have widths of 30 μm (FWHM) and are separated by 27 μm. The first two gratings form an interference pattern in the plane of the third grating, which acts as a mask to sample this pattern. The detector, located 0.30 m beyond the third grating, records the flux transmitted by the third grating. Figure 7 shows the design of the interferometer.

The data necessary to determine the interferometer phase contrast are acquired by modulating the position of one grating relative to the other two and simultaneously recording the signal from the atom counting electronics as well as the signal from an optical interferometer used to measure the relative position of the gratings. After removing data obscured by noise spikes from the hot wire, the atom count rate data are averaged into bins according to relative grating position, resulting in the fringe pattern shown in figure 8.

---

[6] D.W. Keith, C.R. Ekstrom, Q.A. Turchette, and D.E. Pritchard, *Phys. Rev. Lett.* 66: 2693 (1991).

[7] D.W. Keith and M.J. Rooks, *J. Vac. Sci. Technol. B* 9: 2846 (1991).

[8] F. Riehle, T. Kisters, A. Witte, J. Helmcke, and J. Borde, *Phys. Rev. Lett.* 67: 177 (1991); M. Kasevich and S. Chu, *Phys. Rev. Lett.* 67: 181 (1991).

[9] F. Riehle, T. Kisters, A. Witte, J. Helmcke, and J. Borde, *Phys. Rev. Lett.* 67: 177 (1991).

[10] M. Kasevich, S. Chu, *Phys. Rev. Lett.* 67: 181 (1991).

[11] Y. Aharonov and A. Casher, *Phys. Rev. Lett.* 53: 319 (1984).

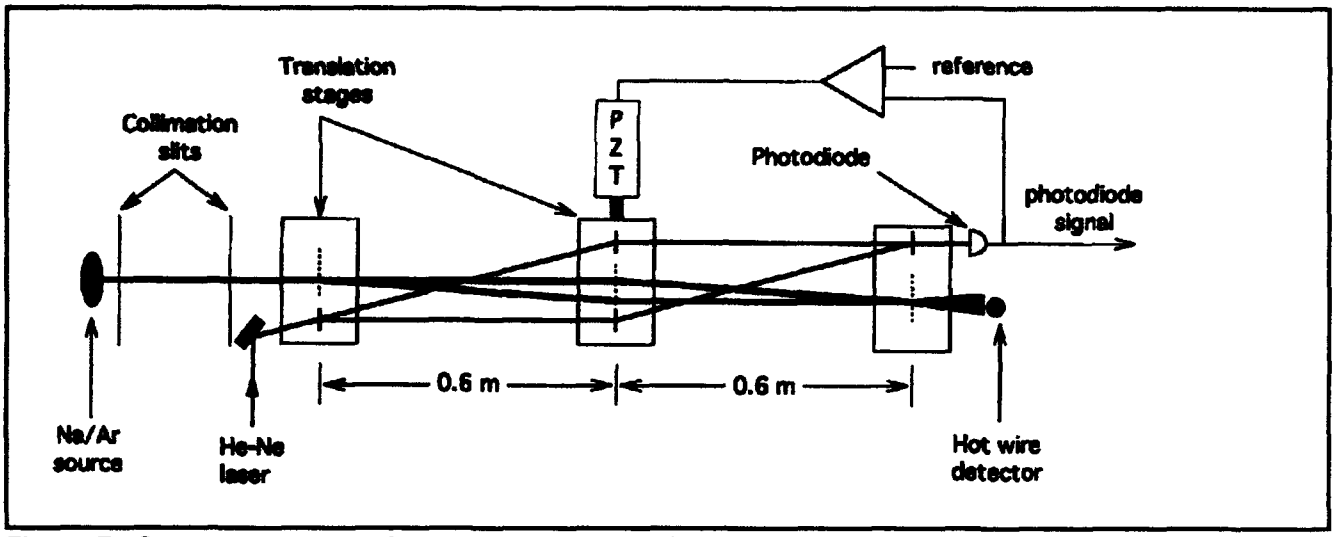


Figure 7. Our current atom interferometer with laser interferometer stabilization system (Not to scale).

The peak-to-peak amplitude of our interference signal is 70 Hz, which enables us to determine the interferometer phase to a precision of 0.1 rad in 1 min. The excellent long-term stability of our position stabilization system provides measured atom-interferometer phase drift of less than 0.1 rad over 10 minutes.

The key component of our interferometer is the set of three matched transmission diffraction gratings which we constructed during two visits at the National Nanofabrication Facility (NNF) at Cornell University. The first trip resulted in the development of a new process for fabricating atom optics. The process allows fabrication of precisely positioned openings in thin silicon nitride membranes mounted in silicon frames. The pattern created in the membrane is determined by an electron beam writer, making the process quite versatile. This process was used to create the diffraction gratings used in the interferometer. In addition, several zone plates (atom lenses) were also built and successfully demonstrated later. During our second trip, we devised ways to reduce the electron beam writing time. This decreased thermal drift during the writing period assured higher overall accuracy and also increased our overall productivity. We made a wide variety of diffraction gratings with various heights and periods between 100 and 300 nm as well as an assortment of single and double slits.

We have recently started construction of an interaction region that will allow us to perform several experiments including measurement of the Aharonov-Casher phase shift, the electric polarizability of the ground state of sodium, and the index of refraction for sodium passing through noble gas atoms.

The scientific future of atoms interferometers looks bright: (1) Atom beam sources are inexpensive and intense relative to other particle beams/sources (e.g., neutrons, electrons), (2) several techniques have now been demonstrated to make interferometers for them, and (3) the atoms which may be used in them come with a wide range of parameters such as polarizability, mass, and magnetic moment. This assures the applicability of these instruments to a wide range of measurements of both fundamental and practical interest.

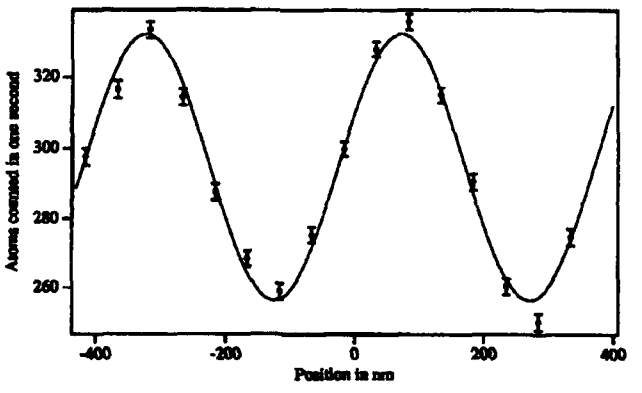


Figure 8. Interference signal from 400 seconds of data. Hot wire detector background of 40 Hz is subtracted. The solid line is a least squares fit to the data with a 400 nm period. The error bars are purely statistical and slightly underestimate the super-Poissonian character of the hot wire background.

Publications

Keith, D.W., C.R. Ekstrom, Q.A. Turchette, and D.E. Pritchard. "An Interferometer for Atoms." *Phys. Rev. Lett.* 66: 2693 (1991).

Keith, D.W., and M.J. Rooks. "Free-standing Gratings and Lenses for Atom Optics." *J. Vac. Sci. Technol. B* 9: 2846 (1991).

Pritchard, D.E. "Atom Interferometers." *Opt. Photonics News,* p. 19 (November 1991).

Pritchard, D.E. "Atom Optics." In *Atomic Physics 12.* Ed. J.C. Zorn, R.R. Lewis, and M. Weiss. New York: American Journal of Physics, 1991, pp. 165-170.

Turchette, Q.A., D.E. Pritchard, and D.W. Keith. "Numerical Model of a Multiple Grating Interferometer." Submitted to *J. Opt. Soc. Am. B* (1991).

Theses

Keith, D.W. *An Interferometer for Atoms.* Ph.D. diss. Dept. of Physics, MIT, 1991.

Turchette, Q.A. *Numerical Model of a Three Grating Interferometer for Atoms.* S.B. thesis. Dept. of Physics, MIT, 1991.

2.4 Cooling and Trapping Neutral Atoms

Sponsors

Joint Services Electronics Program
Contract DAAL03-89-C-0001
Contract DAAL03-92-C-0001
U.S. Navy - Office of Naval Research
Grant N00014-90-J-1642

Project Staff

Dr. Kristian Helmerson, Dr. Alexander Martin, Dr. Wolfgang Ketterle, Kendall Davis, Charles G. Freeman, Michael A. Joffe, Wan Morshidi, Peter S. Yesley, Professor David E. Pritchard

Our current objective is to develop an intense source of slow atoms which will be used in studies of cold collisions, atom optics and atom interferometry. Slow atoms sources typically have fluxes of a few times 10^9 atoms/sec. Improvements by two to three orders of magnitude seem feasible and are crucial for many experiments.

Experiments with dense samples of cold neutral atoms promise new exciting discoveries in basic and applied physics. Due to the considerably reduced thermal motion of atoms they are ideal for high resolution spectroscopy and for more accurate atomic frequency standards.

- Collisions of ultra-cold atoms in such samples are characterized by a long deBroglie wavelength and dominated by weak long-range interactions. Since the collision duration for slow atoms greatly exceeds the radiative decay time, stimulated and spontaneous radiative transitions can take place during the collision. Slow collisions are therefore radically different from fast collisions studied so far and will become an exciting new field of atomic physics.[12]

- High density samples of atoms open possibilities for observing quantum collective effects such as Bose-Einstein condensation and collectively enhanced or suppressed radiative decay.

In 1991, we designed and built two sources of cold atoms based on two different principles: a "Diffuse Light Slower" and an "Inverted Zeeman Slower." We also completed the data analysis and modeling of the laser spectroscopy and laser cooling experiments performed in a magnetic trap.[13] In addition, one of us (K. Helmerson) completed his doctoral dissertation.[14]

The following discusses in more detail the progress made in the three areas mentioned above.

---

[12] P.S. Julienne and J. Vigu, "Cold Collisions of Ground- and Excited-state Alkali-metal Atoms," *Phys. Rev. A* 44: 4464 (1991).

[13] K. Helmerson, A. Martin, and D.E. Pritchard, "Laser and rf Spectroscopy of Magnetically Trapped Neutral Atoms," submitted to *J. Opt. Soc. Am. B*; K. Helmerson, A. Martin and D.E. Pritchard, "Laser Cooling of Magnetically Trapped Neutral Atoms," submitted to *J. Opt. Soc. Am. B*.

[14] K. Helmerson, *Laser Cooling and Spectroscopy of Magnetically Trapped Atoms,* Ph.D. diss., Dept. of Physics, MIT, 1991.

2.4.1 Slowing Atoms with Diffuse Light

We have demonstrated a new technique for slowing and brightening atomic beams which uses isotropic monochromatic laser light detuned to the red of the atomic resonance. The atoms compensate for the changing Doppler shift as they decelerate by absorbing photons at a variable angle in accordance with the Doppler resonance condition. The use of isotropic light and the automatic angle selection method of compensating for the changing Doppler shift distinguish diffuse light slowing from other light slowing schemes realized so far, and is technically simpler to implement.

In our experiments isotropic light was generated by shining laser light into a tube of diffusely reflecting material around the atomic beam (figure 9). Sodium atoms were slowed from approximately 300 m/s to below 100 m/s resulting in a continuous slow beam with a flux of greater than 10^9 atoms/s.[15] This performance is comparable with other slowing schemes and is limited by the light losses in the diffuse reflector. We are currently working on ways to reduce the loss in the diffuse reflector well below its current 1 per cent.

Since isotropic light cools all components of the velocity, a diffuse light slower produces a slow beam with a smaller divergence. Other advantages of diffuse light slowing are the simple experimental realization, tolerance to laser jitter, and absence of an intense slowing laser beam collinear with the slowed atoms which can interfere with subsequent experiments.

2.4.2 Inverted Zeeman Slower

In a Zeeman slower the changing Doppler shift as an atom slows is compensated by the Zeeman shift in an inhomogeneous magnetic field. This method has the advantage of producing a continuous beam of slow atoms and featuring practically unlimited velocity capture range. The original implementation of Zeeman slowing, however, encountered difficulties in producing beams of atoms with velocities lower than 200 m/s. The major problems were off-resonant slowing of atoms after they left the slower and substantial

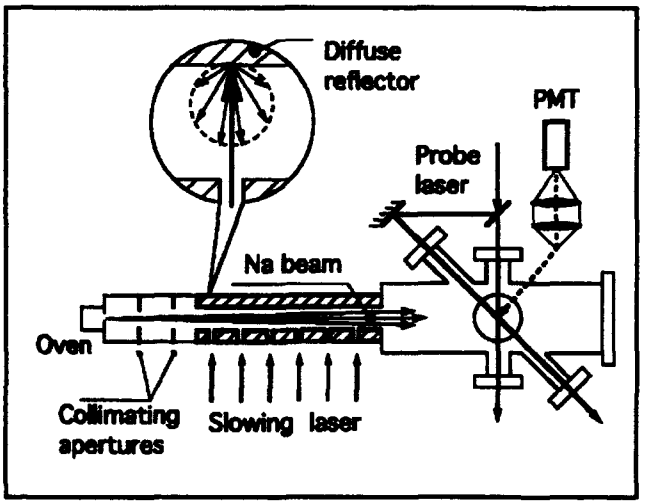


Figure 9. Schematic diagram of the experimental setup. A thermal sodium beam passes through the bore of a tube of diffusely reflecting material which is filled with laser light via six equally spaced small aperatures. Fluorescence-excitation spectra produced by laser beams perpendicular and at 45° to the atomic beam are used to observe the velocity distribution of the atoms as they emerge from the diffuse light cavity.

spreading of the slow atomic beam due to transverse heating.

To solve the first problem we chose the $|F=2,m=2> \rightarrow |F=3,m=3>$ cycling transition to slow sodium atoms. The transition requires a magnetic field increasing along the atoms trajectory (Inverted Zeeman slower). The magnetic field drops off rapidly after reaching its maximum thus quickly shifting atoms out of resonance and reducing off-resonant slowing. It seems therefore possible to perform subsequent atomic optics experiments without undue interference from the intense slowing laser beam.

We have built and tested an inverse Zeeman slower which allows for optical access to the slow atoms inside. Transverse laser cooling will increase the brightness of the resulting slow atom beam. Experiments are still in progress but preliminary results indicate that the performance is better than any other slower demonstrated so far. We have slowed about 50 per cent of the thermal beam down to velocities between 40 m/s and 100 m/s. After optimization we intend to use the slower for efficient loading of an atom trap.

---

[15] W. Ketterle, A.G. Martin, M. Joffe and D.E. Pritchard, "Slowing Atoms with Diffuse Laser Light," postdeadline paper, Seventh Interdisciplinary Laser Conference (ILS), Monterey, California, September 22-26, 1991.

2.4.3 Laser Cooling and Spectroscopy of Magnetically Trapped Neutral Atoms

During 1991, we concluded the data analysis and modeling of the experimental results obtained previously in a superconducting magnetic trap. This work can be divided into two parts:

1. Laser and rf spectroscopy of the trapped atoms:

   Laser absorption, fluorescence and rf spectra of the trapped atoms were modeled and interpreted to extract the energy distribution of the trapped atoms. The results of our model show that the atoms, when loaded into the trap, had an effective temperature of ~ 50 mK, comparable to the actual trap depth. We have shown how the rf spectra can give the energy distribution of the trapped atoms without prior knowledge of the shape of the trapping field potential. For our experiments, the energy distribution of the trapped atoms was well described by a Boltzman distribution, truncated at the energy corresponding to the highest energy trapped atom.[16]

2. Laser Doppler cooling of the trapped atoms:

   Our experiments have shown also how simple one-dimensional optical molasses can reduce the temperature of the trapped atoms to ~ 1 mK. The motion transverse to the cooling laser is cooled by the coupling between the different translational degrees of freedom provided by the trap. The cooling process was modeled, and the theoretical results show good qualitative agreement with the experimental data. The measurements indicated, and the model confirms, that for cooling rates that are low compared to the trap coupling time, ultimate temperatures a few times the Doppler limit can be achieved.[17]

Publications

Gould, P.L., P.J. Martin, G.A. Ruff, R.E. Stoner, J-L. Picque, and D.E. Pritchard. "Momentum Transfer to Atoms by a Standing Light Wave; Transition from Diffraction to Diffusion." *Phys. Rev. A* 43: 585 (1991).

Helmerson, K., A. Martin, and D.E. Pritchard. "Laser and rf Spectroscopy of Magnetically Trapped Neutral Atoms." Submitted to *J. Opt. Soc. Am. B.*

Ketterle, W., and D.E. Pritchard. "Trapping Ground State Atoms in Static Fields." Submitted to *App. Phys. B.*

Ketterle, W., A. Martin, M. Joffe, and D.E. Pritchard. "Slowing Atoms with Diffuse Laser Light." Submitted to *Phys. Rev. Lett.*

Theses

Freeman, C.G. *Diffuse Slowing of a Beam of Neutral Sodium Atoms.* S.B. thesis. Dept. of Physics, MIT, 1991.

Helmerson, K. *Laser Cooling and Spectroscopy of Magnetically Trapped Atoms.* Ph.D. diss. Dept. of Physics, MIT, 1991.

2.5 Precision Mass Spectroscopy of Ions

Sponsors

Joint Services Electronics Program
Contract DAAL03-89-C-0001
Contract DAAL03-92-C-0001
National Science Foundation
Grant PHY 86-05893
Grant PHY 89-21769

Project Staff

Kevin R. Boyce, Frank DiFilippo, James A. Grimm, Matthew J. Marjanovic, Vasant Natarajan, Professor David E. Pritchard

In 1991, we continued our program to substantially improve our precision mass measurement experiment. These improvements should allow us to reach a precision of about 10^{-11} in our mass measurements of individual atomic and molecular ions, the next step toward our ultimate goal of a few parts in 10^{12}. This capability will allow us to do a variety of experiments which address issues in both fundamental and applied physics, including:

---

[16] K. Helmerson, A. Martin, and D.E. Pritchard, "Laser and rf Spectroscopy of Magnetically Trapped Neutral Atoms," submitted to *J. Opt. Soc. Am. B.*

[17] K. Helmerson, A. Martin and D.E. Pritchard, "Laser Cooling of Magnetically Trapped Neutral Atoms," submitted to *J. Opt. Soc. Am. B.*

- The $^3H^+ - {}^3He^+$ mass difference, important in ongoing experiments to determine the electron neutrino rest mass;
- Determination of excitation and binding energies of atomic and molecular ions by weighing the small decrease in energy, $\Delta m = E_{bind}/c^2$;
- Determination of Avogadro's number N_A by weighing γ-rays—its accurate determination would permit the replacement of the "artifact" mass standard by an atomic mass standard; and
- Improvement of many traditional applications of mass spectroscopy by orders of magnitude improvement in both accuracy and sensitivity.

Our experimental approach is to measure ion cyclotron resonance on a single molecular or atomic ion in a Penning trap, a highly uniform magnetic field with axial confinement provided by weaker electric fields. We monitor the ion's oscillation along the magnetic field lines by detecting the currents induced in the trap electrodes. Working with only a single ion is essential because space charge from other ions leads to undesired frequency shifts. This work in trapping and precision resonance draws on techniques developed by Hans Dehmelt at the University of Washington and Norman Ramsey at Harvard, for which they shared the 1989 Nobel Prize.

We have developed techniques for driving, cooling, and measuring the frequencies of all three normal modes of Penning trap motion. Thus we can manipulate the ion position reproducibly to within 30 microns of the center of the trap, correcting for electrostatic shifts in the cyclotron frequency to great accuracy. We use a π-pulse method to coherently swap the phase and action of the cyclotron with the axial modes.[18] Therefore, although we detect only the axial motion directly, we can determine cyclotron frequency by measuring the phase accumulated in the cyclotron motion in a known time interval (figure 10).

In the past two years, we have built an entirely new Penning trap and detector, including a higher-Q resonant circuit and quieter RF SQUID, these have improved our signal-to-noise ratio by a factor of two. We have also constructed a new highly stable DC electric field supply, and added a pressure regulator to the liquid helium bath of our superconducting magnet to help stabilize the field. In addition, we have begun construction of ion optics and an external ion source that will allow us to make the ions in a discharge at room temperature and then load them into the trap. This will eliminate the problem of residual neutral gas in the trap when using volatile species such as hydrogen and helium, and should permit rapid cycling between two different ions which will dramatically increase measurement precision.

With all the improvements to the system, we foresee being able to resolve the existing 10 eV discrepancy between measurements of $m(^3H) - m(^3He)$ in the next year. In addition, we plan to demonstrate a classical squeezing technique which should reduce the thermal fluctuations of our measurement by a factor of three to five. After that, we plan to continue development of techniques to measure two ions of different mass simultaneously. The two-ion technique in combination with the various improvements made over the last two years should lead to precision in the range of 10^{-11}.[19]

Publications

Cornell, E.A., K.R. Boyce, D.L.K. Fygenson, and D.E. Pritchard. "Two Ions in a Penning Trap: Implications for Precision Mass Spectroscopy." *Phys. Rev. A.* Submitted for publication.

[18] E.A. Cornell, R.M. Weisskoff, et al., *Phys. Rev. A* 41: 312 (1990).

[19] E.A. Cornell, *Mass Spectroscopy Using Single Ion Cyclotron Resonance*, Ph.D diss., Dept. of Physics, MIT, 1990.

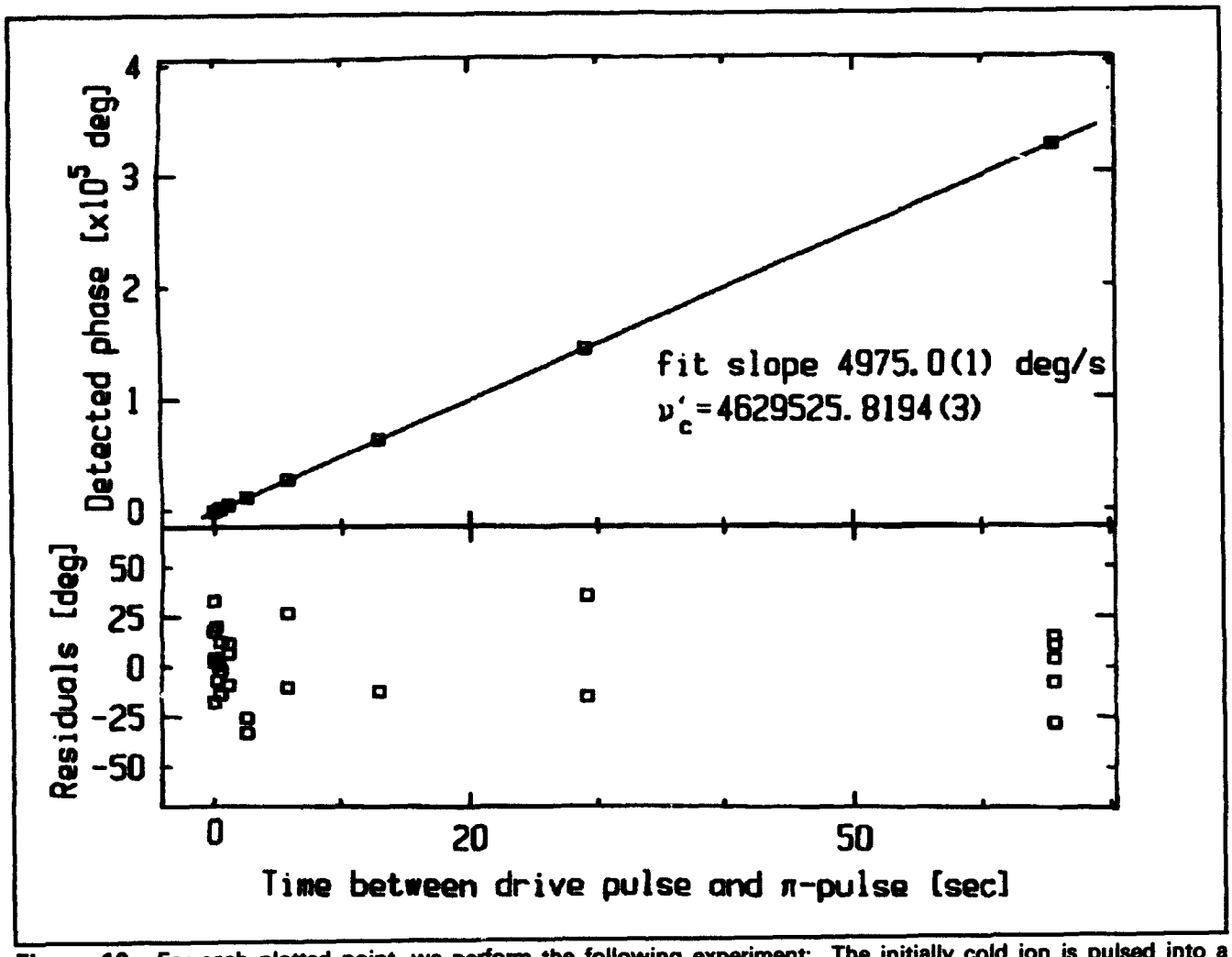


Figure 10. For each plotted point, we perform the following experiment: The initially cold ion is pulsed into a cyclotron orbit of known initial phase and then allowed to evolve "in the dark" for an indicated amount of time, t. Then a pulse is applied which exchanges cyclotron and axial motions, bringing the ion's cyclotron action and phase into the axial mode. As the ion's axial motion rings down, its phase is detected. The appropriate multiple of 360° is added, and a line is fitted to the points. The slope of the line is the frequency difference between the frequency generator and the trap cyclotron frequency.

Chapter 1. Plasma Dynamics

Academic and Research Staff

Professor George Bekefi, Professor Abraham Bers, Professor Bruno Coppi, Professor Miklos Porkolab, Professor Jonathan S. Wurtele, Dr. Chiping Chen, Dr. Shien-Chi Chen, Dr. Ronald C. Englade, Dr. Stefano Migliuolo, Dr. Abhay K. Ram, Dr. Barrett Rogers, Dr. Linda E. Sugiyama, Ivan Mastovsky

Visiting Scientists and Research Affiliates

Dr. Jean-Loup Delcroix,[1] Dr. Cesar Meirelles Filho,[2] Dr. Lazar Friedland,[3] Dr. Vladimir Fuchs,[4] Dr. Eli Jerby,[5] Dr. Pallavi Jha,[6] Dr. Christopher Lashmore-Davies,[7] Dr. Marco Nassi,[8] Dr. Leonid E. Zakharov,[9] Toru Hara,[10] Takahide Mizuno[11]

Graduate Students

Neer Asherie, Riccardo Betti, Palmyra E. Catravas, Carson C. Chow, Jeffrey A. Colborn, Manoel E. Conde, Darin Ernst, Wenian Hu, Mark K. Jablonski, Kenneth C. Kupfer, Michael C. Moldoveanu, Greg Penn, Steven D. Schultz, Gennady Shvets, Jared P. Squire, Richard E. Stoner, Luigi Vacca, Jesus Noel Villasenor, Pavel P. Volfbeyn

Undergraduate Students

Mustafa K. Ahmed, Daniel J.H. Chung, Jonathan C. Doan, Colin J. Taylor, Sasha K. Wood

Technical and Support Staff

Felicia G. Brady, Laura B. Doughty, Edward W. Fitzgerald, Kerry L. Gafney, Catherine Lorusso

1.1 Relativistic Electron Beams

Sponsors

National Science Foundation
Grant ECS 89-02990
U.S. Air Force - Office of Scientific Research
Grant AFOSR 89-0082-B
U.S. Army - Harry Diamond Laboratories
Contract DAAL02-89-K-0084
U.S. Department of Energy
Contract DE-AC02-90ER40591
U.S. Navy - Office of Naval Research
Grant N00014-90-J-4130

---

[1] Professor, University of Paris, Orsay, and Ecole Supérieure d'Electricité, France.

[2] Universidade de São Paulo, Brazil.

[3] Professor, Hebrew University of Jerusalem, Israel.

[4] Centre Canadien de Fusion Magnétique (CCFM), Quebec, Canada.

[5] Faculty of Engineering, Tel Aviv University, Tel Aviv, Israel.

[6] Physics Department, Lucknow University, Lucknow, India.

[7] Visiting Scientist, AEA Fusion, Culham Laboratory, United Kingdom.

[8] Politecnico di Milano, Milan, Italy.

[9] Kurchatov Institute of Atomic Energy, Moscow, U.S.S.R.

[10] Department of Nuclear Engineering, The University of Tokyo, Japan.

[11] The Institute of Space and Astronautical Science, Sagamihara, Kanagawa, Japan.

Project Staff

Professor George Bekefi, Professor Jonathan S. Wurtele, Ivan Mastovsky, Dr. Chiping Chen, Dr. Shien-Chi Chen, Toru Hara, Dr. Eli Jerby, Dr. Pallavi Jha, Takahide Mizuno, Palmyra E. Catravas, Manoel E. Conde, Wenian Hu, Gennady Shvets, Richard E. Stoner, Pavel P. Volfbeyn, Jonathan C. Doan, Daniel J.H. Chung, Colin J. Taylor, Sasha K. Wood, Felicia G. Brady

1.1.1 Experimental Study of a 33.3 GHz Free Electron Laser Amplifier with a Reversed Axial Guide Magnetic Field

The free electron laser (FEL) operating in a combined axial guide magnetic field and a helical wiggler field has been studied experimentally[12] and theoretically[13] over a period of many years, both in linear and nonlinear regimes. In all these studies, the axial magnetic field B_z is oriented so that the cyclotron rotation of the beam electrons is in the same direction as the rotation imposed by the helical wiggler field B_w. This leads to an increase[14] of the transverse electron velocity $v_\perp$ compared to what it would be in the absence of B_z, with potential benefits such as an enhanced radiation growth rate and efficiency. Indeed, when the cyclotron wavelength in the axial field $\lambda_c = 2\pi v_z/\Omega_z$, approaches the wiggler periodicity l_w the transverse electron excursions can become too large, the electrons strike the drift tube wall and are lost ($\Omega_z = eB_z/m_0\gamma$ is the cyclotron frequency in the guide field and $\gamma = [1 - (v_z/c)^2 - (v_\perp/c)^2]^{-1/2}$ is the relativistic energy factor). Thus, the "resonance" $\lambda_c = l_w$ becomes a dividing line for conventional FEL operation: at relatively weak axial fields, $\lambda_c > l_w$, we have the so called Group I regime, and for stronger fields such that $\lambda_c < l_w$, the Group II regime.

We report measurements using a new, hitherto unexplored configuration with a reversed axial magnetic field. The rotation of the electrons in the helical wiggler field B_w is now opposed by the presence of the guide field B_z and there is no longer the resonance at $\lambda_c = l_w$. The transverse electron velocity $v_\perp$ is diminished compared to what it would be in the absence of B_z (however, the latter reduction is partially compensated in our experiments by increasing B_w). We will show that a reversal of B_z yields higher radiation intensity and efficiency compared to what we were able to achieve with the conventional orientation of the axial magnetic field.

The three regimes of FEL operation (Group I, Group II, and Reversed Field) are displayed in figure 1 based on a particle trajectory calculation of v_z/c which neglects space charge and radiation and assumes that the electrons are undergoing ideal helical orbits in the combined B_z and B_w fields. The solid points illustrate the three parameter regimes of B_z where maximum radiation has been observed in our experiments.

A schematic of the FEL amplifier is shown in figure 2. A mildly relativistic electron beam (750 ± 50keV) is generated by a Marx capacitor bank (Physics International Pulserad 110 A). The electrons are emitted from a hemispherical graphite cathode by an explosive field emission process. The graphite anode acts as an emittance selector, allowing only a small fraction of the current to

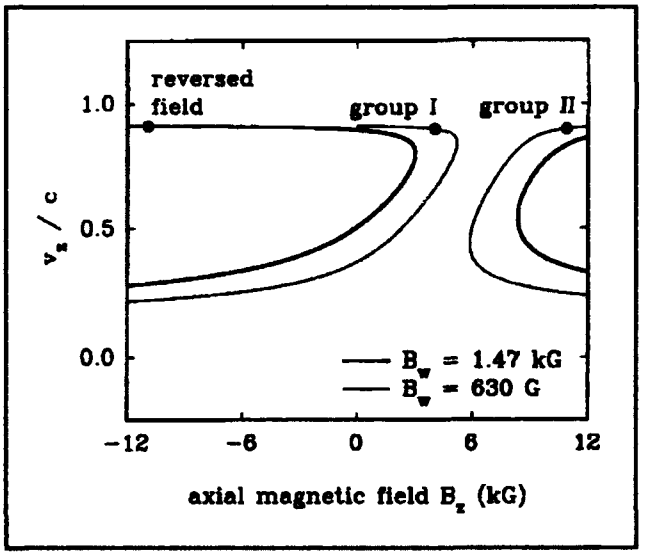


Figure 1. Ideal equilibrium electron orbits calculated for two different values of wiggler magnetic field. The solid points show the values of B_z where maximum power is observed for Group I, Group II and Reversed Field regimes.

[12] S.H. Gold, D.L. Hardesty, A.K. Kinkead, L.R. Barnett, and V.L. Granatstein, *Phys. Rev. Lett.* 52: 1218 (1984); J. Fajans, J.S. Wurtele, G. Bekefi, D.S. Knowles, and K. Xu, *Phys. Rev. Lett.* 57: 579 (1986); also, J. Fajans, G. Bekefi, Y.Z. Yin, and B. Lax, *Phys. Fluids* 28: 1995 (1985).

[13] A.K. Ganguly and H.P. Freund, *IEEE Trans. Plasma Sci.* 16: 167 (1988).

[14] L. Friedland, *Phys. Fluids* 23: 2376 (1980); P. Diament, *Phys. Rev. A* 23: 2537 (1981); H.P. Freund and A.K. Ganguly, *IEEE J. Quantum Electron.* QE-21: 1073 (1985).

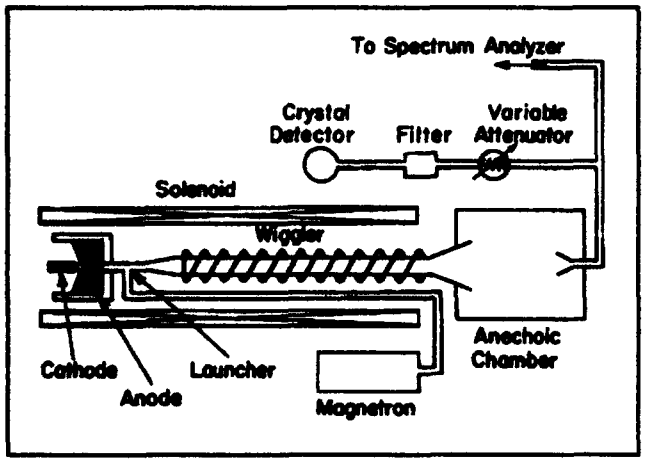


Figure 2. Free electron laser experimental setup.

propagate through its 2.54 mm radius and 62 mm long aperture. The electron beam current downstream from the emittance selector, and in the absence of the wiggler field, is illustrated in figure 3a, showing saturation at high B_z where all available electrons from the gun have made it through the anode hole. Using the technique of Prosnitz and Scharlemann,[15] we estimate the normalized RMS beam emittance to be $\varepsilon_n < 4.4 \times 10^{-2}$ cm-rad and the corresponding RMS axial energy spread to be $\Delta\gamma_z/\gamma_z < 1.5 \times 10^{-2}$. We observe from figure 3b that when the wiggler is turned on, an expected, very pronounced current loss occurs near resonance $\lambda_c = l_w$ with the conventional orientation of B_z. This happens because the transverse velocity of the electrons become too large and eventually they are lost to the waveguide walls. No significant current loss (also as expected) is seen with the magnetic field reversed (figure 3c).

The 50 period bifilar helical wiggler produced by current carrying helical wires has a period of 3.18 cm and provides a magnetic field whose magnitude on axis is adjustable up to 1.8 kG. The wiggler field intensity is slowly increased over the initial six periods, providing an adiabatic input for the electron beam. The system, including the gun, is immersed in a uniform axial magnetic field generated by a solenoid. The intensity of this field can be varied up to a maximum of 11.6 kG.

The two-meter long stainless steel drift tube has an internal radius of 0.51 cm and acts as a cylindrical waveguide whose fundamental TE_{11} mode has a cutoff frequency of 17.2 GHz. The system is designed to operate in this lowest waveguide mode.

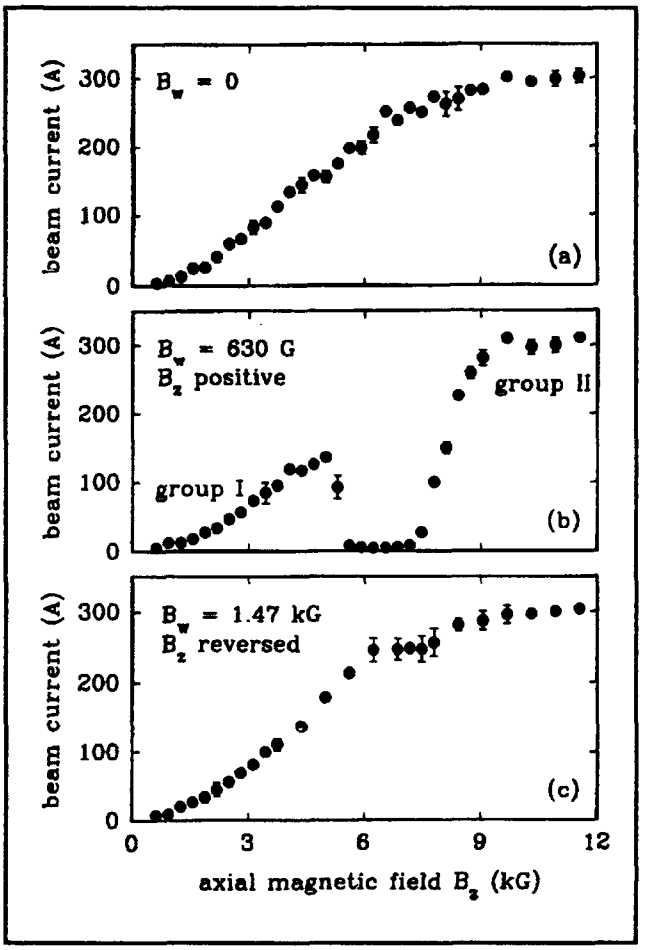


Figure 3. Electron beam current in the FEL as a function of the axial guide magnetic field B_z; (a) no wiggler magnetic field; (b) wiggler field B_w = 630 G and B_z in the conventional direction; (c) wiggler field B_w = 1.47 kG and B_z in the reversed direction.

A high power magnetron operating at 33.39 GHz is the input power source for the FEL amplifier. The wave launcher consists of a short section of circular waveguide of radius 0.31 cm into which 17 kW are coupled from a standard Ka-band rectangular waveguide. This section of circular waveguide supports only the fundamental TE_{11} mode for the operating frequency. Its radius is then adiabatically increased to the radius of the drift tube. A linearly polarized wave is thereby injected into the interaction region. Half of the incident power, with the correct rotation of the electric field vector, participates in the FEL interaction.

A parameter scan of the output power has been carried out in order to discover the optimum operating conditions for our three regimes, Group I, Group II and Reversed Field. Figure 4a illustrates

[15] D. Prosnitz and E.T. Scharlemann, *LLNL ATA Note* No. 229, February 1984.

the output power as a function of B_w at constant B_z, and figures 4b and 4c show how the power varies with B_z at constant B_w. It is seen that the maximum output power obtained in Group I and Group II regimes is approximately the same, 5 MW; however, the efficiency is much higher for the Group I regime since here the beam current is smaller. The output power for the reversed field case is higher by an order of magnitude and reaches a level of 61 MW.

The spatial growth of the electromagnetic wave intensity is determined from the measurement of the output power as a function of the length of the interaction region. This length is varied by changing the distance that the electron beam is allowed to propagate in the drift tube. Application of a strong magnetic field is sufficient to deflect the electrons into the waveguide wall and thereby terminate the interaction at that point. Figure 5 shows the result of this measurement for the three different regimes. In the Group I regime the power level reaches saturation at 5.8 MW corresponding to an efficiency of 9 percent. Operation in Group II shows the lowest efficiency (2 percent). The Reversed Field operation has by far the highest efficiency (27 percent), and exhibits no power saturation (Table 1).

Table 1. Summary of Experimental Results.

Parameter	Group I	Group II	Reversed Field
Frequency (GHz)	33.39	33.39	33.39
Beam energy (keV)	750	750	750
Beam current (A)	90	300	300
Guide field (kG)	4.06	10.9	-10.9
Wiggler field (kG)	0.63	0.63	1.47
Output power (MW)	5.8	4.2	61
Efficiency (%)	9	2	27

In conclusion, we have found that our free electron laser shows highest efficiency and highest power output when operated with reversed axial guide magnetic field. Table I summarizes our findings. We believe that the 27 percent efficiency of our system exceeds the efficiency of previous FELs with untapered wigglers. If the ~ 1 dB/m attenuation due to the stainless steel waveguide were subtracted from the measurements, the power and efficiency could be substantially higher. Moreover, figure 5c shows that our wiggler is too short to reach saturation, and much higher efficiency may well be possible with longer and/or tapered magnetic fields.

We note that our FEL falls into the so called Raman parameter regime where RF space charge effects must be allowed for, both in order to account for the radiation frequency and the power

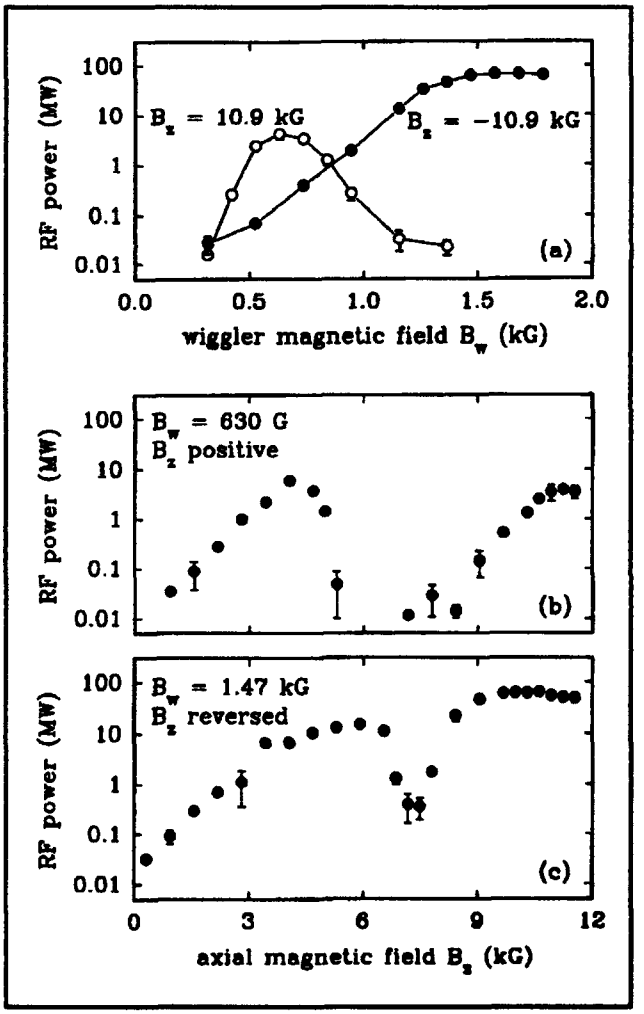


Figure 4. FEL output power as a function of B_z and B_w; (a) B_w scan for fixed B_z = 10.9 kG in each direction; (b) B_z scan in the conventional direction for fixed B_w = 630 G; (c) B_z scan in the reversed direction for fixed B_w = 1.47 kG.

output. A detailed theoretical understanding of the Reversed Field FEL is as yet unavailable due in part to some lack of understanding of the electron trajectories themselves. This is clearly shown in figure 4c, where a large, unexpected dip in output power occurs near $l_w \simeq -\lambda_c$ ($B_z \simeq -7.6$kG), but no such dip occurs either in the electron current (figure 3c) or in calculations based on ideal orbit theory. Thus, the ideal orbit model on which figure 1 is based needs substantial modification when B_z is reversed from its usual orientation. Such studies are now in progress.[16]

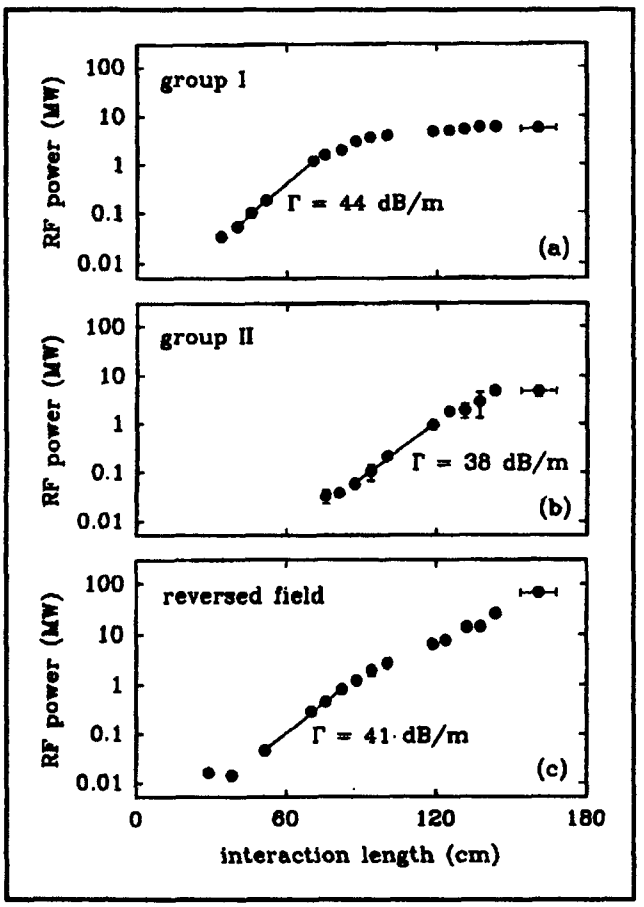


Figure 5. FEL output power as a function of interaction length; (a) Group I regime; (b) Group II regime; (c) Reversed Field regime. The Γs represent growth rate estimates over interaction regions indicated by the straight lines.

1.2 Plasma Wave Interactions—RF Heating and Current Generation

Project Staff

Professor Abraham Bers, Dr. Abhay K. Ram, Dr. Jean-Loup Delcroix, Dr. Vladimir Fuchs, Dr. Lazar Friedland, Dr. Christopher Lashmore-Davies, Mustafa K. Ahmed, Carson C. Chow, Mark K. Jablonski, Kenneth C. Kupfer, Michael C. Moldoveanu, Steven D. Schultz, Luigi Vacca

1.2.1 Introduction

The research work of this group is concerned with studies on the electrodynamics of plasmas and their applications. Attention is directed toward understanding the nonlinear dynamics of plasmas driven by high-frequency electromagnetic fields (as in RF heating and current drive of magnetically confined plasmas or in laser-plasma interactions) and the generation and propagation of unstable radiations from laser-plasma interactions and anisotropic electron distributions in space and astrophysical plasmas.

1.2.2 Spatio-Temporal Chaos in the Saturation of an Unstable Wave

Sponsors

Lawrence Livermore National Laboratory
Subcontract B-160456
National Science Foundation
Grant ECS 88-22475
U.S. Department of Energy
Contract DE-FG02-91-ER-54109

We have completed a major part of our study on spatio-temporal chaos (STC) in the nonconservative, nonlinear three-wave interaction (3WI).[17] In particular, we have found that STC arises in the saturation of an unstable wave coupled to two damped waves at lower frequencies. The ensuing saturated state exhibits the chaotic behavior of coherent structures and is characterized by a correlation length ξ which is small compared to the system size L; in turn, the system size is larger than the excitation length ℓ_E (at which energy is

[16] K.R. Chu and A.T. Lin, *UCLA Report* PPG-1373, September 1991, forthcoming; G. Shvets and J.S. Wurtele (private communication).

[17] C.C. Chow, *Spatiotemporal Chaos in the Nonlinear Three Wave Interaction,* Ph.D. diss., Dept. of Physics, MIT, 1991.

injected into the system by the unstable wave) and also larger than the dissipation length ℓ_D (at which energy leaves the system through the damped waves). Thus STC characterized by the conditions $\xi \ll L$ and $L > \ell_E \sim \ell_D$ is a new nonlinear state for a saturated instability in an extended medium, which is very different from either low-dimensional chaos or fully developed turbulence.[18] In the former case, $\xi > L$ so that the system is completely spatially correlated, and, in the latter case, $L > \ell_E \gg \ell_D$ so that energy is injected at some large scale and dissipated at a much smaller length scale (the inertial range lies in between these length scales) with coherent structures existing at a large number of scale lengths.

The main features of the STC that ensues in the saturation of an unstable wavepacket by mode coupling was described in *RLE Progress Report 133.* During the past year, we have attempted to develop an analytical basis for understanding and predicting this STC state. The usual perturbation analyses that start from linear instability (e.g., weak turbulence theory) cannot be used to access a description of STC. In STC, the nonlinearity is not weak; it is essential in establishing the coherent structures.

The approach we found useful was to start from the nonlinear state of the conservative 3WI and consider the nonconservative aspects as a perturbation. The conservative nonlinear 3WI is exactly integrable by inverse scattering (IST).[19] In particular, when the high-frequency (hf) wave has the middle group velocity of the three nonlinearly interacting waves, the solutions involve the exchange of envelope solitons between the three waves. In the non-conservative case, assuming the high-frequency wave is unstable for long wavelengths and stable (by diffusion-type damping) at short wavelengths, the dynamics proceed as follows. When the unstable wave envelope reaches an area threshold, it transfers solitons to the low-frequency (lf) waves when these are of non-zero amplitude, and, by this transfer, its envelope wavelengths become shorter; these shorter wavelengths, if not damped, begin to grow until they reach their soliton transfer threshold, and the process of depletion and growth repeats. Thus, from any random initial conditions, small scales are smoothed out by the diffusion-type damping and long scales grow until a soliton depletion threshold is reached which in turn generates smaller scales that may be damped. The steady state is arrived at when one attains a balance between the nonlinear conversion of long length scales to small length scales and the linear damping of the small scales. Thus, if the unstable wave has a growth rate γ_1 and its diffusive-type damping is characterized by a diffusion constant D, its steady-state correlation length will be of the order

$$\xi_1 \approx 2\pi\sqrt{\frac{D}{\gamma_1}} \qquad (1)$$

The low-frequency damped envelopes are in a state in which they are continuously fed with solitons (by the unstable high-frequency wave) which propagate with their group velocities and are damped; we identify these as quasi-solitons. From IST we can show that the size of these solitons are related to the IST bound state eigenvalue η of the high-frequency unstable envelope:

$$\xi_2 \approx 2/\eta \qquad (2)$$

In the simplest case of an envelope with one extremum, the bound state eigenvalue η is given by

$$\int (Q_1^2 - \eta^2)dx = \pi\left(n + \frac{1}{2}\right) \qquad (3)$$

where Q_1 is the Zakharov-Shabat (ZS) potential (proportional to the unstable wave envelope) and the integral is over the classical turning points of this potential.[19] In the STC state, the depleted, unstable high-frequency envelope will have some remaining area (IST "radiation") from which it grows before depleting again, and the low-frequency quasi-soliton envelope colliding with the high-frequency envelopes causes their depletion. Thus, two questions arise: Given that the hf, unstable envelope depletes from some initial envelope area (i.e., ZS eigenvalue), what is the remaining envelope area after depletion? (i.e., the leftover radiation); and what threshold area (i.e., threshold eigenvalue) is required for depletion? To address the first question, a multiple-time scale analysis around the IST solution for soliton decay was carried out assuming that growth and dissipation occur on a slower time scale than soliton depletion. The answer to the second question required a perturbation expansion in the Zakharov-Manakov (ZM) scattering space of the 3WI.[19] The mathematical details and results

[18] P.C. Hohenberg and B.I. Shraiman, *Physica D* 37: 109 (1989).

[19] D.J. Kaup, A. Reiman, and A. Bers, *Rev. Mod. Phys.* 51: 915 (1979).

from these IST perturbation analyses[20] gave the perturbed state eigenvalue of the unstable envelope as

$$\eta \approx 4\xi_1\gamma_1 + 2\gamma_2 \qquad (4)$$

where γ_2 is the damping rate of the lf wave, and the time required for the hf unstable envelope to grow after soliton depletion to the threshold for depletion as

$$t_g \approx \frac{1}{\gamma_1} \ln \frac{2\eta}{(2+\gamma_1)\ln 3} \qquad (5)$$

With these results one can obtain the quasi-soliton width given by (2) and the characteristic cycling time which is given by (5) plus the (generally very short) soliton depletion time.

The long-time behavior in the STC of this nonlinear 3WI was found to be characterized approximately by the diffusive-type damping associated with the unstable wave. Thus, the long-time scale for the hf unstable wave, τ_1, can be estimated as a diffusion time across the correlation length (1),

$$\tau_1 \approx \frac{D}{\xi_1^2} = \frac{(2\pi)^2}{\gamma_1} \qquad (6)$$

and for the lf damped wave, characterized by the quasi-soliton width, (2) with (4),

$$\tau_2 \approx \frac{4}{\eta^2 D} \qquad (7)$$

The results (1)-(7) describe all the characteristic scales in the STC ensuing from the saturation of an hf unstable wave by nonlinear coupling to lf damped waves in a soliton transfer interaction (i.e., the hf unstable wave having the middle group velocity). The validity of these results were corroborated by extensive numerical simulations.[20]

Finally, there remains only to estimate the average energy densities in the saturated state of the STC. These are obtained from the conservation equations for the nonlinearly interacting waves and the threshold eigenvalue η. With $\langle U_n \rangle \equiv \int_0^L \langle |a_n|^2 \rangle dx$, where a_n is the complex envelope amplitude of wave n = 1, 2, 3, the conservation equations show that

$$\langle U_2 \rangle \approx \frac{2}{3}\frac{\gamma_1}{\gamma_2}\langle U_1 \rangle \qquad (8)$$

$$\langle U_3 \rangle = \frac{\gamma_2}{\gamma_3}\langle U_2 \rangle \qquad (9)$$

with γ_1 the growth rate of the hf wave, and γ_2 and γ_3 the damping rates of the lf waves. In the saturated state, the hf unstable envelope has an amplitude related to its threshold eigenvalue η, which together with the eigenvalue quantization rule for a soliton, (3) with n = 0, allows us to estimate the average energy density of the saturated unstable wave as

$$\frac{\langle U_1 \rangle}{L} \approx \frac{1}{2}\left[\eta^2 + \left(\frac{\pi}{2\xi_1}\right)^2\right]$$

These estimates of the average energy densities in STC have been found to correspond closely to the amplitudes of the spectral energy densities determined from the correlation functions in the numerical simulations.[20]

The results of these studies have been presented at several conferences[21] and are being prepared for publication.

1.2.3 Current Drive by Lower Hybrid and Fast Alfvén Waves

Sponsor

U.S. Department of Energy
Contract DE-FG02-91-ER-54109

The most effective way of driving current using radio-frequency waves in present day tokamaks has been with lower hybrid waves (LHW). However, as is well known, in a high density and high temperature tokamak (ITER-type) these slow

---

[20] C.C. Chow, *Spatiotemporal Chaos in the Nonlinear Three Wave Interaction,* Ph.D. diss., Dept. of Physics, MIT, 1991.

[21] C.C. Chow, A. Bers, and A.K. Ram, "Spatio-Temporal Chaos in the Saturation of an Unstable Wavepacket," Proceedings of the International Sherwood Fusion Conference, April 22-24, 1991, Seattle, Washington, Paper 2D08; C.C. Chow, A. Bers, and A.K. Ram, "Spatiotemporal Chaos in the Three Wave Interaction," *Bull. Am. Phys. Soc.* 36: 2407 (1991); C.C. Chow, A. Bers, and A.K. Ram, Spatiotemporal Chaos in the Nonlinear Three Wave Interaction, *Proceedings of the III Potsdam–V Kiev International Workshop on Nonlinear Processes in Physics,* Clarkson University, Potsdam, New York, August 1-11, 1991, forthcoming.

LHWs will not be able to penetrate into the center of the plasma. They would damp away their energy and momentum onto electrons which are towards the edge of the plasma. Consequently, it is important to determine the effectiveness of other rf means of current drive by waves which can penetrate into the center of the plasma. Fast Alfvén waves (FAW) with frequencies below the lower hybrid frequency are able to penetrate into the core of a high temperature plasma and have been proposed as one of the means for driving currents.

Recent experiments on rf current drive in JET have brought forth some very interesting results. The current drive efficiency was found to be significantly enhanced at higher plasma temperatures when LHWs were used in conjunction with the FAWs. The FAW spectrum was such that these rf waves could not drive any current without LHWs. However, the current drive efficiency was enhanced only when the phase velocities of the FAW spectrum overlapped with the phase velocities of the LH spectrum.

We have begun a detailed analysis of current drive by LHWs in combination with FAWs in order to better understand the current drive efficiency in the presence of both types of waves. Some of the results were presented at the 1991 APS-DPP meeting[22] and in an invited presentation at the IAEA meeting in Arles, France.[23]

The LHW generated electron tail has an effective perpendicular energy (or perpendicular temperature) which can be an order of magnitude (or more) bigger than the bulk electron temperature.[24] This is due to the pitch angle scattering of the energetic electrons to higher perpendicular momenta. It has been shown that, when these effective increases in perpedicular temperature are taken into account, the theoretically calculated current drive efficiency is more than that evaluated in models where the tail electrons are assumed to have the same perpendicular temperature as the bulk electrons. In our initial calculations, we assumed that the effect of the FAW on these tail electrons was to increase their perpendicular energy. This was then shown to lead to an increase in the current drive efficiency. Two-dimensional Fokker-Planck simulations with a model FAW diffusion coefficient and the LHW diffusion coefficient showed that the FAW did enhance the perpendicular tail temperature.[25] This enhancement depended on the strength of the FAW diffusion coefficient, increasing as the diffusion coefficient strength was increased. There was a corresponding increase in the current drive efficiency. Below, we present some of these results.

The two-dimensional, relativistic Fokker-Planck code[26] was used to determine the effect of FAW on an electron distribution function which has an asymmetric tail in $p_\parallel$ due to LH waves.[22] The FAW diffusion coefficient was taken to be of the form given by Giruzzi and Fidone,[27] with the FAW spectrum assumed to be a symmetric Gaussian centered at $n_\parallel = 0$ with a half width of $\Delta n_\parallel = 2.3$. For the LH waves, we assumed $D_\delta^H/D_c = 50$, where D_c is the collisional diffusion coefficient with the LH spectrum extending from $v_\parallel/v_{Te} = v_1$ to v_2 where $v_1 = 4$ and $v_2 = c/(v_{Te}n_a)$ (n_a is the lowest accessible $n_\parallel$). For $n_a = 1.6$ and $T_e = 2$ keV, $v_2 = 10$ while for $T_e = 6$ keV, $v_2 = 5.77$. When considering the effect of the FAW, the FAW diffusion coefficient was assumed to be such that $D_\delta^W/D_c = 0.1$ when $|v_\parallel|/v_{Te} \geq 4.0$ and zero, otherwise. [This allows us to consider only the interaction of the FAW with the LH spectrum. The low phase velocity FAW are strongly affected by the existence of magnetically trapped electrons; they can also directly heat bulk electrons which would happen if we allow the FAW diffusion coefficient to extend into the bulk of the electron distribution function. However, our current code does not account for trapped electrons nor does it evolve

---

[22] A.K. Ram, A. Bers, V. Fuchs, and M.M. Shoucri, *Bull. Am. Phys. Soc.* 36: 2339 (1991).

[23] A. Bers and A.K. Ram, in *Proceedings of the IAEA Technical Meeting on Fast Wave Current Drive in Reactor Scale Tokamaks (Synergy and Complementarity with LHCD and ECRH)*, Arles, France, September 23-25, 1991.

[24] V. Fuchs, R.A. Cairns, M.M. Shoucri, K. Hizanidis, and A. Bers, *Phys. Fluids* 28: 3619 (1985).

[25] A.K. Ram, A. Bers, V. Fuchs, and M.M. Shoucri, *Bull. Am. Phys. Soc.* 36 (1991) 2339; A. Bers and A.K. Ram, in *Proceedings of the IAEA Technical Meeting on Fast Wave Current Drive in Reactor Scale Tokamaks (Synergy and Complementarity with LHCD and ECRH)*, Arles, France, September 23-25, 1991.

[26] M.M. Shoucri, V. Fuchs, and A. Bers, *Comput. Phys. Comm.* 46: 337 (1987).

[27] G. Giruzzi and I. Fidone, in "Controlled Fusion and Plasma Heating," *Proceedings of the 17th European Conference*, Amsterdam, 1990, ed. G. Briffod, A. Nijsen-Vis, and F.C. Schuller (European Physical Society, 1990), Vol. 14B, Part III, pp. 1279-1282.

the bulk temperature, and the conditions for its validity would breakdown if the diffusion coefficient were allowed to extend into the bulk of the distribution function.]

From the numerical code, we evaluated the current drive efficiency, η, and the effective perpendicular temperature in the LH induced tail of the distribution function:

$$T_p = \frac{T_\perp}{T_e} \quad \text{where} \quad T_\perp = \frac{\int dp_\perp \frac{p_\perp^3}{2} f_o}{\int dp_\perp p_\perp f_o} \qquad (1)$$

The other parameters used in the numerical program were: $Z_i = 1.6$, electron density = 2.4×10^{19} m^{-3}, $B_0 = 3.3$ Tesla, LH frequency = 3.7 GHz, and FAW frequency = 48 MHz (parameters similar to those in the JET experiment).

When the Fokker-Planck equation was solved with just the LH diffusion coefficient, we obtained the following results:

$$\text{for } T_e = 2 \text{ keV}: \quad T_p \approx 34, \quad \eta \approx 0.434 \qquad (2)$$

$$\text{for } T_e = 6 \text{ keV}: \quad T_p \approx 10, \quad \eta \approx 0.544 \qquad (3)$$

When the FAW diffusion coefficient was included along with the LH diffusion coefficient, we obtained:

$$\text{for } T_e = 2 \text{ keV}: \quad T_p \approx 55, \quad \eta \approx 0.608 \qquad (4)$$

$$\text{for } T_e = 6 \text{ keV}: \quad T_p \approx 16, \quad \eta \approx 0.683 \qquad (5)$$

Comparing (2) with (4), and (3) with (5), we clearly see that the effect of the FAW is to enhance the $T_\perp$ in the LH induced tail of the distribution function. This also gives an enhancement in the current drive efficiency. These increases in $T_\perp$ and η can be understood in terms of a simple analytical model developed primarily for the LH current drive.[28] It must, however, be remarked that this explanation of the observations on current drive by LHWs and FAWs is to be taken as only preliminary. For one thing, in the JET experiments the FAW not only interacts with the LHCD generated electron tail, but it also raises the electron temperature of the plasma. Our numerical simulations do not allow for the bulk electron temperature to evolve, and thus cannot account for the change in the current drive efficiency due electron bulk heating.

1.2.4 Space-Time Propagation of Electromagnetic Instabilites Across the Magnetic Field in Auroral Regions

Sponsor

National Aeronautics and Space Administration
Grant NAGW-2048

We have shown that the space-time analysis of instabilities leads to distinctly observable features that can identify whether an instability is absolute or convective.[29] An absolute instability has a narrow frequency bandwidth while a convective instability typically has a broad band emission. We have considered instabilities that propagate across an ambient, steady-state magnetic field, and are generated by relativistic, highly anisotropic, electron distribution functions. Such distribution functions arise in the auroral regions and are considered to be sources of the observed auroral kilometric radiation.[30] We have studied the propagation of the ordinary and the extraordinary (x) modes. The instabilities are generated at the electron cyclotron frequency (ω_{ce}) and its harmonics. For low electron densities, the x-mode is an absolute instability at ω_{ce} and a convective instability at the harmonics. As the density is increased the instability at ω_{ce} becomes convective while that at $2\omega_{ce}$ becomes absolute, thereby, leading to harmonic generation of radiation by a linear mechanism. Detailed results for these instabilities and the effect of a cold background plasma on the propagation of these instabilities are currently being studied.

---

[28] V. Fuchs, R.A. Cairns, M.M. Shoucri, K. Hizanidis, and A. Bers, *Phys. Fluids* 28: 3619 (1985).

[29] A.K. Ram and A. Bers, in *Physics of Space Plasmas, Proceedings of the 1990 Cambridge Workshop in Geoplasma Physics*, eds. T. Chang, G.B. Crew, and J.R. Jasperse (Cambridge, Massachusetts: Scientific Publishers, 1990).

[30] C.S. Wu and L.C. Lee, *Astrophys. J.* 230: 621 (1979).

1.2.5 Linear Instability Analysis of the Double Stream Cyclotron Maser

Sponsors

National Aeronautics and Space Administration
Grant NAGW-2048
National Science Foundation
Grant ECS 88-22475

The double stream cyclotron maser in which two copropagating beams, with different beam velocities, gyrate in a uniform axial magnetic field has been proposed as a source of millimeter wavelength radiation.[31] The interaction which leads to the radiation is between the slow cyclotron space charge of one beam and the fast cyclotron space charge of the other beam. This interaction leads to high frequency bunching. We have carried out a linear stability analysis of an electrostatic dispersion function derived for two "cold" beams from the fully relativistic Vlasov equation.[32] This linear analysis of the interaction shows that instabilities are generated near harmonics of the Doppler shifted electron cyclotron frequency (ω_{ce}) and also near the Doppler shifted half harmonics ($(n + 1/2)\omega_{ce}$ for n any integer). The region of instability depends on the values of $k_{\parallel}$ (the axial component of the wave vector). Including axial temperatures in the two beams eliminates the large $k_{\parallel}$ instabilities. Regions of interest to either space plasma physics or coherent em amplifying devices are currently being explored by further numerical studies.

1.2.6 Coupling of Positive and Negative Energy Waves in a Nonuniform Plasma

Sponsors

National Science Foundation
Grant ECS 88-22475
U.S.-Israel Binational Science Foundation
Grant 87-0057

Recently developed techniques for finding embedded pairwise mode couplings in high order systems and calculating the transmission coefficient in linear mode conversion for passive, stable plasmas have been extended to the treatment of coupling of positive and negative energy waves in nonuniform plasmas. In particular, the coupling of positive and negative energy waves in co-streaming, nonuniform electron beams has been treated in detail and the ensuing spatial amplification determined. A journal article on this work has been recently accepted for publication.[33]

1.2.7 Publications

Bers, A., V. Fuchs, and C.C. Chow. *Maximizing Absorption in Ion-Cyclotron Heating of Tokamak Plasmas.* Plasma Fusion Center Report PFC/JA-91-10, MIT, 1991.

Bers, A., and A.K. Ram. *Lower Hybrid and Fast Wave Current Drive—Status of Theory.* Plasma Fusion Center Report PFC/JA-92-3, MIT, 1992.

Bers, A., and A.K. Ram. "Signature of Absolute and Convective Instabilities with Application to Space Plasmas." *Bull. Am. Phys. Soc.* 36: 2462 (1991).

Bers, A., V. Fuchs, and C.C. Chow. "Maximizing Absorption in Ion-Cyclotron Heating of Tokamak Plasmas." *Proceedings of the EPS 18th Conference on Controlled Fusion and Plasma Physics,* Berlin, Germany, June 3-7, 1991. Forthcoming.

Bers, A., and A.K. Ram. "Lower Hybrid and Fast Wave Current Drive—Status of Theory." *Proceedings of the IAEA Technical Meeting on Fast Wave Current in Reactor Scale Tokamaks (Synergy and Complementarity with LHCD and ECRH),* Arles, France, September 23-25, 1991. Forthcoming.

Chow, C., A. Bers, and A.K. Ram. "Spatiotemporal Chaos in the Nonlinear Three Wave Interaction." *Proceedings of the III Potsdam—V Kiev International Workshop on Nonlinear Processes in Physics,* August 1-11, 1991.

---

[31] G. Bekefi, *J. Appl. Phys.*, forthcoming 1992.

[32] A. Bers and C.E. Speck, *Quarterly Progress Report* 78: 110-114, Research Laboratory of Electronics, MIT, July 1965; C.E. Speck and A. Bers, *Quarterly Progress Report* 80: 159-161, Research Laboratory of Electronics, MIT, January 1966; G. Bekefi, A.K. Ram, A. Bers, and C. Chen, *SPIE Proc.* 1992 OE LASE Conference, Los Angeles, California, January 1992.

[33] L. Friedland and A. Bers, "Hermitian Description of Interacting Inhomogeneous Electron Beams," *Phys. Fluids B,* forthcoming 1992.

Potsdam, New York: Clarkson University. Forthcoming.

Chow, C.C., A. Bers, and A.K. Ram. "The Three Wave Interaction and Spatiotemporal Chaos." Paper presented at the 1991 Cambridge Workshop on Theoretical Geoplasma Physics. *Physics of Space Plasmas (1991), SPI Conference Proceedings and Reprint Series.* Forthcoming.

Chow, C.C., A. Bers, and A.K. Ram. *Spatiotemporal Chaos in the Nonlinear Three Wave Interaction.* Plasma Fusion Center Report PFC/JA-92-2, MIT, 1992.

Chow, C.C., A. Bers, and A.K. Ram. "Spatio-Temporal Chaos in the Saturation of an Unstable Wavepacket." *Proceedings of the International Sherwood Fusion Conference,* Seattle, Washington, April 22-24, 1991, Paper 2D08.

Chow, C.C., A.K. Ram, and A. Bers. "Spatiotemporal Chaos in the Nonlinear Three Wave Interaction." *Research Trends in Physics: Chaotic Dynamics and Transport in Fluids and Plasmas.* Eds. I. Prigogine et al. New York: American Institute of Physics, 1992.

Chow, C.C., A. Bers, and A.K. Ram. "Spatiotemporal Chaos in the Three Wave Interaction." *Bull. Am. Phys. Soc.* 36: 2407 (1991).

Chow, C.C., A. Bers, and A.K. Ram. *The Three Wave Interaction and Spatiotemporal Chaos.* Plasma Fusion Center Report PFC/JA-92-1, MIT, January 1992.

Friedland, L., and A. Bers. "Hermitian Description of Interacting Inhomogeneous Electron Beams." *Phys. Fluids B.* Forthcoming.

Kupfer, K., and A. Bers. "Fast Electron Transport During Lower-Hybrid Current Drive." *Proceedings of the EPS 18th Conference on Controlled Fusion and Plasma Physics,* Berlin, Germany, June 3-7, 1991. Forthcoming.

Kupfer, K., and A. Bers. *Fast Electron Transport in Lower-Hybrid Current Drive.* Plasma Fusion Center Report PFC/JA-91-13, MIT, 1991.

Kupfer, K., A. Bers, and A.K. Ram. "Fast Electron Transport in Current Drive." *Proceedings of the International Sherwood Fusion Conference,* Seattle, Washington, April 22-24, 1991, Paper 2B05.

Kupfer, K., A. Bers, and A.K. Ram. "Fast Electron Transport During Lower-Hybrid Current Drive." *Phys. Fluids B* 3: 2783 (1991).

Kupfer, K., A. Bers, and A.K. Ram. *Fast Electron Transport During Lower-Hybrid Current Drive.* Plasma Fusion Center Report PFC/JA-91-9, MIT, 1991.

Ram, A.K., A. Bers, V. Fuchs, R.W. Harvey, and M.G. McCoy. "Current Drive by Lower Hybrid Waves in Combination with Fast Alfvén Waves," *Proceedings of the International Sherwood Fusion Conference,* April 6-8, 1992. Forthcoming.

Ram, A.K., and A. Bers. "Comments on Absolute and Convective Instabilities." *Geophys. Res. Lett.* 19: 143 (1992).

Ram, A.K., and A. Bers. "Space-Time Propagation of Electromagnetic Instabilities Across the Magnetic Field in Auroral Regions," *EOS Trans. Amer. Geophys. Union* 72: (1991).

Ram, A.K., A. Bers, V. Fuchs, L. Vacca, and M. Shoucri. "Current Drive by Fast Alfvén Waves and in Combination with Lower Hybrid Waves." *Bull. Am. Phys. Soc.* 36: 2339 (1991).

Ram, A.K., and A. Bers. "Propagation and Damping of Mode Converted Ion-Bernstein Waves in Toroidal Plasmas." *Phys. Fluids B* 3: 1059 (1991).

Ram, A.K., and A. Bers. "Absolute Versus Convective Analysis of Instabilities in Space Plasmas." Invited paper presented at the 1990 Cambridge Workshop on Theoretical Geoplasma Physics. In *Physics of Space Plasmas (1990),* SPI Conference Proceedings and Reprint Series, Number 10. Eds. T. Chang, G.B. Crew, and J.R. Jasperse. Cambridge, Massachusetts: Scientific Publishers, 1991.

Ram, A.K., and A. Bers. *Comments on Absolute and Convective Instabilities.* Plasma Fusion Center Report PFC/JA-91-8, MIT, 1991.

Ram, A.K., and A. Bers. *Absolute Versus Convective Analysis of Instabilities in Space Plasmas.* Plasma Fusion Center Report PFC/JA-91-4, MIT, 1991.

1.3 Physics of Thermonuclear Plasmas

Sponsor

U.S. Department of Energy
Contract DE-FG02-91ER-54109

Project Staff

Professor Bruno Coppi, Dr. Ronald C. Englade, Dr. Stefano Migliuolo, Dr. Marco Nassi, Dr. Barrett Rogers, Dr. Linda E. Sugiyama, Dr. Leonid E. Zakharov, Riccardo Betti, Darin Ernst

The main theme of this program is the theoretical study of magnetically confined plasmas in regimes of thermonuclear interest. A variety of physical regimes that fall in this category characterize both present-day experiments on toroidal plasmas (e.g., Alcator, TFTR, JET) as well as future experiments that will contain ignited plasmas. These will either involve first generation fuels, namely a deuterium-tritium mixture (Ignitor), or more advanced fuels such as deuterium-deuterium or deuterium-helium mixtures (Candor).

We are participating in a coordinated effort of collaboration between the design group of a U.S. compact ignition experiment and that of the European experiment (Ignitor). At MIT, the Alcator C-MOD experiment that combines the favorable features of an elongated plasma cross section with a high magnetic field is under construction. These features, which are also being planned for Ignitor, were originally proposed for a machine called Megator, which we designed in the early 1970s.

Presently, our research program follows two major avenues. First, the basic physical processes of thermonuclear plasmas (equilibrium, stability, transport, etc.) are being studied as they apply to existing or near-term future systems. In this effort, we closely collaborate with our experimental colleagues, as well as theorists from other research groups (e.g., Joint European Undertaking (JET), Princeton, Columbia). This work also involves time-dependent simulations of plasma discharges in the planned D-T burning Ignitor experiment, with particular attention being focused on the evolution of spatial profiles of plasma current and temperature. Collaboration with our colleagues at the Italian laboratories of Energia Nucleare e Energie Alternative (E.N.E.A.), as well as in-house code development by visiting scientists from Italy, plays a major role in this endeavor. Second, we explore advanced regimes of thermonuclear burning, including those employing low neutron yield fuels (^{3}D-He, and "catalyzed" D-D). We consider both the design of machines that will contain these very high temperature plasmas as well as the physics that govern their behavior.

We present below some of the salient results on work completed or presently being worked on by members of our research group.

1.3.1 Physics of Compact, High Field Ignition Experiments

Magnetically confined, toroidal experiments to investigate deuterium-tritium ignition conditions in a plasma can be designed on the basis of the presently known experimental results and theoretical understanding of plasma behavior. The most advantageous and least expensive designs incorporate an interlocking set of characteristics:[34] tight aspect ratio, relatively small size with significant vertical elongation, high toroidal and poloidal magnetic fields, large plasma currents, high plasma densities, good plasma purity, strong ohmic heating, good plasma and α-particle confinement, and robustness against ideal MHD and resistive plasma instabilities. We have proposed and developed the physics[35] and engineering ideas[36] behind

---

[34] B. Coppi, M. Nassi, and L. Sugiyama, "Physics Basis for Compact Ignition Experiments," *Proceedings of the 1991 International Atomic Energy Agency Conference on α-particle Physics*, Göteborg, Sweden, *Physica Scripta*, forthcoming (1992).

[35] B. Coppi, M. Nassi, and L. Sugiyama, "Physics Basis for Compact Ignition Experiments," *Proceedings of the 1991 International Atomic Energy Agency Conference on α-particle Physics*, Göteborg, Sweden, *Physica Scripta*, forthcoming (1992); L. Sugiyama and M. Nassi, *Free Boundary Current Ramp and Current Profile in a D-T Ignition Experiment*, RLE Report PTP 90/8, Res. Lab. of Electron., MIT, 1991, *Nucl. Fusion*, forthcoming (1992); B. Coppi, R. Englade, M. Nassi, F. Pegoraro, and L. Sugiyama, "Current Density Transport, Confinement and Fusion Burn Conditions," *Proceedings of the 13th International Conference on Plasma Physics and Controlled Nuclear Fusion Research*, Washington D.C., 1990 (Vienna, Austria: I.A.E.A., 1991), paper CN-53/D4-14.

[36] B. Coppi, M. Nassi, and L. Sugiyama, "Physics Basis for Compact Ignition Experiments," *Proceedings of the 1991 International Atomic Energy Agency Conference on α-particle Physics*, Göteborg, Sweden, *Physica Scripta*, forthcoming (1992); B. Coppi, R. Englade, M. Nassi, F. Pegoraro, and L. Sugiyama, "Current Density Transport, Confinement and Fusion Burn Conditions," *Proceedings of the 13th International Conference on Plasma Physics and*

such a design (the Ignitor Ult,[37] shown in figure 6), as part of an ongoing program of research into ignition experiments. In addition, we have studied the feasibility of using similar characteristics to design an experiment to study the next level of fusion burning, the D-^{3}He reaction.

Basic Physics Considerations for D-T Ignition

The ignition of a 50:50 deuterium-tritium plasma requires a minimum value of the parameter $n_o\tau_E \simeq 4 \times 10^{20}$ sec/m^3 in order to achieve ignition with $T_o \lesssim 15$ keV, where n_o is the peak plasma (electron) density, T_o the peak temperature, and τ_E the energy replacement time. Here ignition is defined to be the point when the plasma heating due to fusion α-particles, P_α, equals the plasma thermal losses P_L. Relatively high values of the plasma density, $n_o \simeq 10^{21}$ m^{-3}, then allows ignition to be considered at moderate values of τ_E, whose

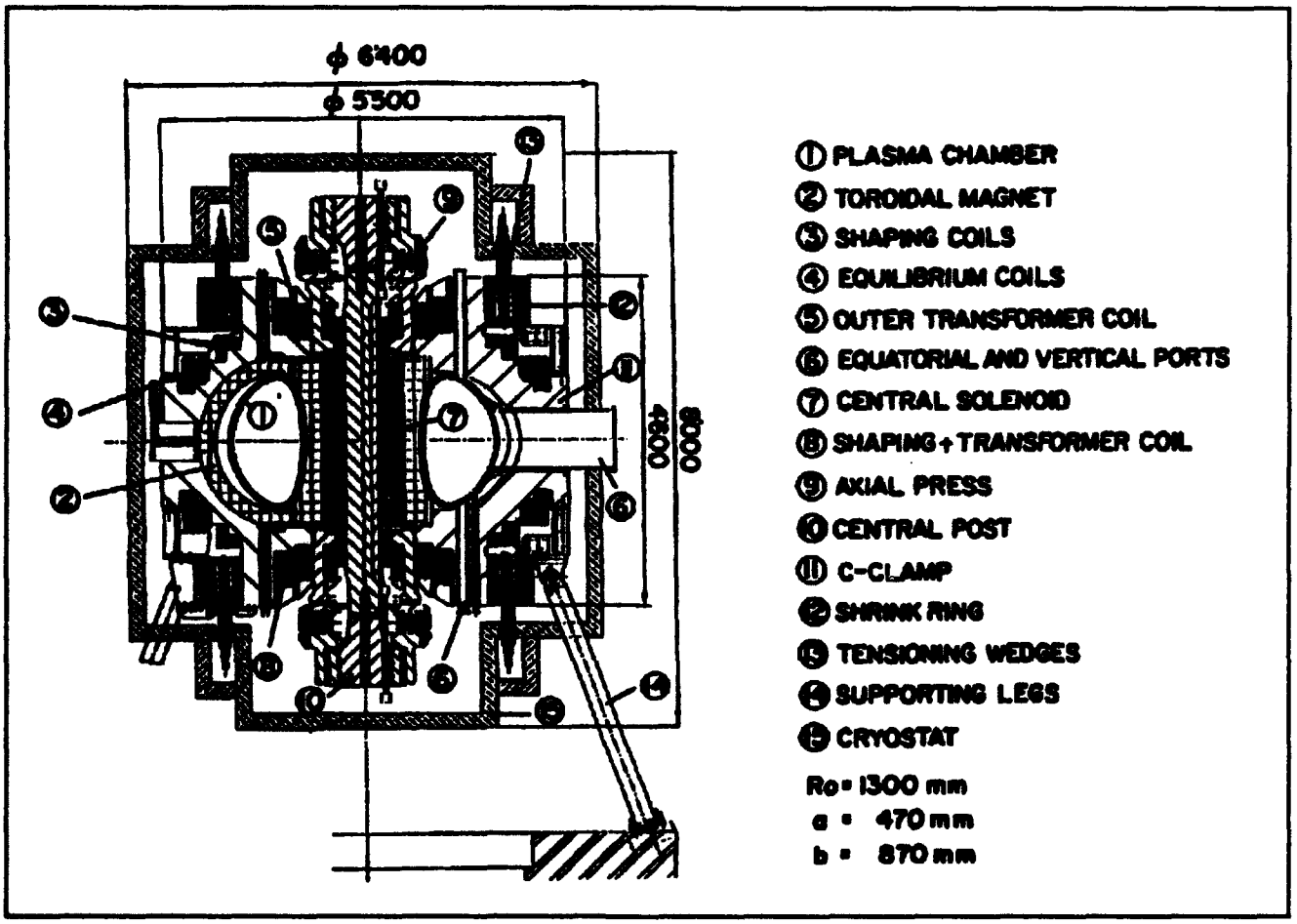


Figure 6. Cross section of the Ignitor Ult experiment, showing the major components of the machine.

Controlled Nuclear Fusion Research, Washington D.C., 1990 (Vienna, Austria: I.A.E.A., 1991), paper CN-53/D4-14; B. Coppi, "High Current Density Tritium Burner," RLE Report PTP 75/18, Res. Lab. of Electron., MIT, 1975; B. Coppi, *Comm. Plasma Phys. Cont. Fusion*, 3: 2 (1977); B. Coppi and The Ignitor Group, "Characteristics and Expected Performance of the Ignitor-U Experiment," *Proceedings of the Twelfth International Conference on Plasma Physics and Controlled Nuclear Fusion Research*, Nice, France, 1988 (Vienna, Austria: I.A.E.A., 1989), Vol. 3, p. 357.

[37] B. Coppi, R. Englade, M. Nassi, F. Pegoraro, and L. Sugiyama, "Current Density Transport, Confinement and Fusion Burn Conditions," *Proceedings of the 13th International Conference on Plasma Physics and Controlled Nuclear Fusion Research*, Washington D.C., 1990 (Vienna, Austria: I.A.E.A., 1991), paper CN-53/D4-14.

magnitude is less easy to predict with certainty. Both of these values should be achievable, based on the favorable confinement properties of high density plasmas that have been demonstrated by a series of high field experiments, the Alcator A and Alcator C at MIT and the FT/FTU devices at Frascati, Italy. The maximum plasma density n_o that can be supported correlates experimentally with the ratio B_T/R_o, where B_T is the toroidal magnetic field at the center of the plasma column, at major radius $R = R_o$. On the basis of the Alcator C machine, where $n_o \simeq 2 \times 10^{21}\ m^{-3}$ was achieved with $B_T \simeq 12.5$ T and $R_o = 0.64$ m, and the TFTR machine at Princeton, where even larger ratios of $n_o R_o/B_T$ were achieved, a configuration with $R_o \simeq 1.3$ m and $B_T \simeq 13$ T should be able to sustain reliably densities of $10^{21} m^{-3}$. Given B_T, the smallest R_o consistent with the structural and electromechanical requirements is advantageous.

A strong toroidal field also supports a high poloidal magnetic field and correspondingly large plasma current. A vertical elongation, e.g., $\kappa \simeq 1.8$, can be used to substantially increase the plasma current that can be carried for a given B_T and R. If the density actually correlates with the (volume) averaged toroidal current density, $< J_\phi >$, then a value somewhat less than $1 kA/cm^2$ should offer a considerable margin to obtain the desired peak density $n_o \sim 10^{21} m^{-3}$. High values of the poloidal field B_p produce a strong rate of ohmic heating, while large toroidal plasma currents I_p tightly confine the fast α-particles produced by the fusion reactions, so that they deposit their energy inside the central region of the plasma. The degradation of the plasma energy confinement that is commonly observed when externally injected (nonohmic) heating is applied is reduced at higher plasma current. In addition, the poloidal plasma beta β_p can be kept small at ignition, to improve the plasma stability and in particular to stabilize ideal MHD modes with mode numbers $m = 1$, $n = 1$ associated with sawtooth oscillations.

Large plasma density combined with good ohmic heating allows ignition at low plasma temperatures. This increases the overall margin of plasma stability due to low beta. It reduces the fusion power required for ignition, and, therefore, the thermal wall loads.

Plasma purity has been shown to improve with increasing plasma density, the effective charge $Z_{eff} = \sum n_i Z_i / n_e$ decreasing monotonically with n_e, in an extensive series of experiments starting with the Alcator A.[38] The major effect of impurities is to dilute the concentration of fusing nuclei, while a secondary effect is the increase the radiative power lost due to bremsstrahlung. If auxiliary heating is not used, Z_{eff} cannot exceed about 1.6 for D-T ignition, as shown in the next section.

Relatively high plasma edge densities also help to confine impurities to the scrape off layer, where the induced radiation helps to distribute the thermal wall loading more uniformly over the plasma chamber surface. The low ignition temperatures further help to keep the plasma clean, by reducing the thermal wall loading.

Peaked plasma density profiles should be maintained by external means such as a pellet injector if necessary. Peaked profiles maintain stability to η_i modes that enhance the ion thermal transport.[39] Since the neoclassical (Ware) particle pinch is relatively strong in a tight aspect ratio, high field configuration and considering that an anomalous inflow process is also present, pellets that penetrate partway into the plasma can be successfully used to produce peaked profiles near ignition.[40]

Plasma configurations, such as x-points, that concentrate the thermal (particle) heat flux on localized areas of the vessel wall, limit the amount of fusion power that can be handled. In addition, they limit the maximum possible plasma current that can be sustained. However, it may be desirable to operate with a detached plasma or an x-point, in order to limit the degradation of the plasma confinement caused by nonohmic heating by creating the conditions known to produce "H-mode" operation. These configurations can be obtained by sacrificing relatively little in the plasma and magnet parameters.

Divertors represent a more severe compromise, since they alter the design of the plasma chamber and the toroidal magnet. The major radius must be

---

[38] G.J. Boxman, B. Coppi, L.C.J.M. de Koch, et al., "Low and High Density Operation of Alcator," *Proceedings of the Seventh European Conference on Plasma Physics*, Lausanne, Switzerland, 1975 (Ecole Polytechnique Fédérale de Lausanne: Lausanne, Switzerland, 1976), Vol. 2, p. 14.

[39] B. Coppi, S. Cowley, P. Detragiache, R. Kulsrud, F. Pegoraro, and W.M. Tang, *Proceedings of the Tenth International Conference on Plasma Physics and Controlled Nuclear Fusion Research*, London, 1984 (Vienna, Austria: I.A.E.A., 1985), Vol. 2, p. 93; B. Coppi and W.M. Tang, *Phys. Fluids* 31: 2683 (1988).

[40] W. Houlberg, private communication (1991).

increased to accommodate a reliable divertor, reducing the ratio B_T/R and therefore the maximum plasma density. The magnetic fields are also reduced, lowering the plasma current and the ohmic heating, and increasing the plasma beta. A large injected heating system becomes necessary to replace the ohmic heating, and the resulting degradation of the plasma confinement makes low temperature ignition difficult. The divertor plates then would have to handle large thermal heat fluxes. There is no demonstrated advantage to using divertors in high density plasmas and the cumulative disadvantages make ignition difficult to attain and remove much of the rationale for using a compact, high field machine.

Shown in Table 2 is a detailed reference design for the Ignitor that incorporates the above features.[41]

Time Dependent D-T Ignition

Transient Processes and the Current Density Evolution

Our research[42] has underlined the importance of the transient nature of the ignition process. We have considered the time evolution of a free boundary plasma from the initial current ramp phase, when the plasma current, density, size, and toroidal magnetic field are raised to their maximum values, through ignition, using numerical simulation with the TSC code,[43] for the specific example of the Ignitor Ult device of Table 2.

Table 2. Design Parameters of the Ignitor Ult.	
$R_o \simeq 1.30$ m	Major radius
$a \times b \simeq 0.47 \times 0.87 m^2$	Minor radii
$\delta_G \simeq 0.4$	Triangularity
$I_p \lesssim 12$ MA	Toroidal plasma current
$B_T \lesssim 13$ T	Vacuum toroidal field at R_o
$< J_\phi > \lesssim 0.93$ kA/cm^2	Volume-average toroidal current density
$\bar{B}_p \lesssim 3.75$ T	Mean poloidal field
$q_\psi \simeq 3.6$	Edge magnetic safety factor
$t_R \simeq 3 \div 4$ sec	Ramp up time for I_p
$t_{FT} \simeq 4$ sec	Flat top time at maximum I_p and B_T
$P_{INJ} \lesssim 16$ MW	Injected heating power (ICRH at $f \simeq 130$ MHz)

The results show that the initial current ramp, when the toroidal current, plasma density, toroidal field, and plasma cross section are increased simultaneously, has important effects on the plasma energy balance and stability at ignition.[42] These effects arise from the relatively slow inward diffusion of the plasma current compared to the growth of the central temperature. The current ramp generates a inhomogeneous electric field in the plasma that is peaked off axis and allows large values of ohmic heating at high central temperature. The magnetic safety factor q (the inverse of the winding number of the magnetic field lines divided by 2π) can be easily maintained above unity or held to a very small $q < 1$ region during the current ramp. This is important to minimize the effects of plasma instabilities with poloidal and toroidal mode numbers $m/n = q = 1/1$ that can

---

[41] B. Coppi, M. Nassi, and L. Sugiyama, "Physics Basis for Compact Ignition Experiments," *Proceedings of the 1991 International Atomic Energy Agency Conference on α-particle Physics*, Göteborg, Sweden, *Physica Scripta*, forthcoming (1992); L. Sugiyama and M. Nassi, "Free Boundary Current Ramp and Current Profile in a D-T Ignition Experiment," Report PTP 90/8, Res. Lab. of Electron., MIT, 1991, *Nucl. Fusion*, forthcoming (1992); B. Coppi, R. Englade, M. Nassi, F. Pegoraro, and L. Sugiyama, "Current Density Transport, Confinement and Fusion Burn Conditions," *Proceedings of the 13th International Conference on Plasma Physics and Controlled Nuclear Fusion Research*, Washington D.C., 1990 (Vienna, Austria: I.A.E.A., 1991), paper CN-53/D4-14.

[42] B. Coppi, M. Nassi, and L. Sugiyama, "Physics Basis for Compact Ignition Experiments," *Proceedings of the 1991 International Atomic Energy Agency Conference on α-particle Physics*, Göteborg, Sweden, *Physica Scripta*, forthcoming (1992); L. Sugiyama and M. Nassi, "Free Boundary Current Ramp and Current Profile in a D-T Ignition Experiment," Report PTP 90/8, Res. Lab. of Electron., MIT, 1991, *Nucl. Fusion*, forthcoming (1992).

[43] S.C. Jardin, N. Pomphrey, and J. DeLucia, "Dynamic Modelling of Transport and Positional Control of Tokamaks," *J. Comp. Phys.* 66: 481 (1986).

destroy the good confinement in the center of the plasma. A more careful study[42] shows that the $q \leq 1$ region can also be kept small after the ramp, at least until the central temperature reaches high values and fusion alpha particles begin to appear, both of which have stabilizing effects for $m = 1$ modes. Furthermore, small amounts of externally injected heating (e.g., 5 MW) during the current ramp can maintain the very small size of the $q < 1$ region until well past ignition if central temperatures can be raised to $\lesssim 10$ keV by the end of the current ramp through the "freezing-in" of the central current density as the rate of inward, resistive diffusion decreases with temperature. Injected heating also reduces the magnetic flux consumption required to reach ignition, particularly if ignition occurs during the current ramp.

We have also been able to show that it is possible to simultaneously maintain q profiles that increase monotonically from the plasma center, without large regions of low magnetic shear (flat or even hollow q profiles) and with values of q at the edge of the plasma maintained within $3 < q_{\psi a} < 4$ during the current ramp, to beyond ignition. This avoids instabilities associated with internal plasma modes (e.g., "locked" or quasistationary modes) that are triggered during the current ramp and can lead to disruptions. Since hollow q profiles are usually associated with the excitation of internal macroscopic modes and enhanced or "anomalous" current penetration (cf. Sugiyama and Nassi[44]), while ignition is aided by a slow current penetration that keeps $q_o > 1$ for as long as possible, these precautions are not superfluous.

Energy Confinement at Ignition

A major question that faces ignition experiments is the degree of degradation expected in the plasma energy confinement near ignition. D-T ignition is easily achieved if the confinement remains at the optimal, ohmic heating levels. The strategy for a high field experiment is to maintain a high level of ohmic heating up to ignition, $P_\alpha \leq 2P_{OH}$, to reduce the degree of degradation. Since fusion alpha-particle heating possesses two important characteristics of ohmic heating that are not shared by any presently available form of injected heating—axisymmetric deposition and generation in the center of the plasma column—we expect that the degradation should not be as severe.

The requirement of relatively low edge q (high plasma current) means that special care must be devoted to maintaining $q > 1$ up to ignition. If only ohmic heating is contemplated, the steadily increasing size of the $q < 1$ region after the end of the current ramp imposes a more severe limit on the time in which the plasma can ignite and on the required energy confinement level, than the energy balance alone, assuming that the sawtooth oscillations that destroy the central peaking of the temperature cannot be avoided. Thus, ignition in the reference case, where $T_o \simeq 11$ keV, requires $\tau_E \simeq 0.66$ sec and ignition within approximately 1.5 sec of the end of the current ramp. Our theoretical analysis, on the other hand, indicates that Ignitor remains, *in all regimes, within the stability* limits of the ideal MHD and resistive $m = 1$, $n = 1$ modes that are presently known. On the other hand, moderate amounts of auxiliary heating, $P_{ICRH} \lesssim 15$ MW, allow ignition down to the expected limits required for $n_o\tau_E$, i.e., $\tau_E \lesssim 0.4$ sec, while maintaining very small $q = 1$ regions well beyond ignition. Similarly, if the requirement of small $q < 1$ region is dropped in the ohmic case, either on the basis of existing theoretical analyses or by envisioning an external means of stabilizing sawtooth oscillations, ignition can also occur at these values of τ_E and times of $t_i \simeq 5$-5.5 sec.

The importance of ohmic heating during the ignition sequence at high field and density means that a model for the electron thermal transport, like the one that has been adopted here, should include a diffusion coefficient that simulates ohmic regimes. It should reproduce at least typical toroidal loop voltages in steady state ohmic experiments, that are observed to be approximately a "universal" constant. In addition, the total diffusion coefficient should increase with injected heating and reproduce the degraded confinement observed in present experiments that are dominated by injected heating.

Plasma Density

Another major question for ignition is the effect of variation in the plasma density and its profile, since pellets injected to raise the density are unlikely to fully penetrate a high density plasma.

For a given level of thermal transport, there is an optimum density for fastest ignition. Higher density is more favorable under degraded conditions. Higher density, however, also increases the toroidal current penetration at a given time by lowering the electron temperature, producing larger $q < 1$ regions earlier than at lower density. A

[44] L. Sugiyama and M. Nassi, "Free Boundary Current Ramp and Current Profile in a D-T Ignition Experiment," Report PTP 90/8, Res. Lab. of Electron., MIT, 1991.

similar effect operates in the outer part of the plasma radius, when density profiles are broadened. Thus, for $n_{eo} = 1.1 \times 10^{21}$ m^{-3}, profile peaking factors $\alpha_n \equiv n_{eo}/ < n_e > = 1.9\text{-}2.9$, where $< n_e >$ is the volume average, with a fixed ratio of edge to central density $n_{es}/n_{eo} = 0.1$, give similar results for ignition, requiring $\tau_E \geq 0.67$ sec, at $t_I \leq 4.5$ sec, with $q = 1$ radius $r_1/a \leq 1/3$ on the horizontal midplane. Lower peaking factors rapidly lead to degraded ignition, for example $\alpha_n = 1.5$ yields $\tau_E = 0.70$ sec, $t_I = 4.7$ sec, and $r_1/a \simeq 0.45$. A lower central density, 6.5×10^{20}m^{-3} at the end of the current ramp, increasing to $8\text{-}9 \times 10^{20}$ by ignition, allows much broader profiles ($\alpha_n \lesssim 1$).

For related reasons, increasing the plasma density after the current ramp, is more advantageous than increasing the density during the ramp.

At high density, broad regions of low magnetic shear (flat q at $q < 1$) develop in the mid-region of the minor radius. This region may be unstable when its value of q approaches unity, since ideal MHD instabilities with $m = 1$ can occur. This is the major limit on the broad density profile cases, since at the reference thermal transport level even a very broad profile, $\alpha_n \simeq 0.1$, will ignite at the lower density.

Burning Conditions

Fusion ignition is thermally unstable in the low temperature interval we consider, due to the temperature dependence of the fusion reaction cross section. At ignition, by definition, $P_\alpha = P_L$, so that the plasma thermal energy is increasing as $dW/dt = P_{OH} + P_{INJ}$. Provision should be made to limit possible temperature excursions. However, there are intrinsic processes such as the rise of the central pressure that can overcome the stability threshold for $m = 1$, $n = 1$ modes and limit the temperature excursion naturally. Marginal ignition and sustained subignited states, partly supported by ohmic heating, are also of interest for studying fusion burning. An example has been given.[45]

Plasma Stability

A major concern for ignition is the stability of the plasma to central, sawtooth oscillations. The stability of modes with dominant poloidal mode number $m = 1$ has been discussed previously.[46] Additional considerations for instabilities driven by the current density profile have been discussed above. Other instabilities, such as shear Alfvén modes destabilized by fusion α particles, have been discussed,[45] based on the analysis reported in Betti and Friedberg.[47]

Engineering Design of a D-T Ignition Experiment

The main engineering problems encountered in designing a high field D-T ignition experiment arise from the need to:

- create and control different plasma configurations;
- induce the toroidal plasma current and maintain the plasma discharge for a time $\gtrsim 10\tau_E$ at ignition, where τ_E is the energy replacement time;
- operate with an acceptable thermal loading on the first wall;
- withstand the static, dynamic, electromagnetic, thermal, and disruptive loads with sufficient margin to provide an adequate reliability;
- provide access for the plasma diagnostics, pellet injector, radio frequency antennae, vacuum system, remote maintainance, etc.

Poloidal Magnetic Field System

The Ignitor Ult uses a highly optimized set of 14 up-down symmetric poloidal field coils, placed in proximity to the plasma column (figure 6), to induce the plasma current, create the desired plasma configurations, and maintain them against radial and vertical motions of the plasma.

Copper OHFC has been selected as the material for the central solenoid in order to maximize the

---

[45] B. Coppi, M. Nassi, and L. Sugiyama, "Physics Basis for Compact Ignition Experiments," *Proceedings of the 1991 International Atomic Energy Agency Conference on* α-particle *Physics*, Göteborg, Sweden, *Physica Scripta*, forthcoming (1992).

[46] B. Coppi, "High Current Density Tritium Burner," RLE Report PTP 75/18, Res. Lab. of Electron., MIT, 1975.

[47] R. Betti and J.P. Friedberg, "Stability of Alfvén Gap Modes in Burning Plasmas," Report PFC/JA-91-25 (Cambridge: MIT Plasma Fusion Center, 1991), submitted to *Phys. Fluids.*

current that it can carry, while a material with enhanced mechanical properties (GLIDCOP) is used for the other poloidal field coils in order to produce self-supporting structures. These other coils are located in a region of the machine where more space is available and carry high current for only a limited time during each discharge, so that electrical conductivity is not the major constraint.

The central solenoid consists of a double array of copper coils, each wrapped 32 times around the central steel pole of the machine. Each coil is provided with a cooling channel at its center, cooled by He gas. The initial temperature before a plasma discharge is about 30 K. The final temperature can reach a maximum of about 230 K, after a long pulse at the maximum plasma current I_p.

An assessment[48] of the magnetic flux variation linked with the plasma column has been carried out, and the results have been checked against the time dependent numerical analysis performed using the TSC code. The volt-second requirement at ignition is found to be less than 32 V s, under a range of assumptions on the values of the ion and electron thermal conductivity, effective charge, etc., for plasmas that reach ignition during the constant current ("flat top") phase of the discharge, at the maximum plasma current. The volt-second consumption during the flat top is about 1.5 V s per second, due to resistive losses and an increase in the plasma internal inductance. We note that use of injected heating, when the plasma reaches ignition during the current ramp, can reduce the volt-second requirement to as low as $\simeq 25$ V s, due to the lower plasma current at ignition and the higher plasma temperature that reduces the resistive losses. The poloidal field system has been designed to produce a flux variation of about 32 V s.

Several plasma configurations have been analyzed:[49]

- limiter configurations that fill the entire plasma chamber are useful to distribute the thermal loading on the chamber walls uniformly;
- transient double x-point configurations, used to reproduce the characteristics of the so-called H-regime of plasma confinement, where τ_E is only slightly degraded in the presence of injected heating, relative to ohmic heating regimes. They require I_p to be kept well below its design value. In addition, when the local thermal wall loading at the x-points exceeds desirable limits, the equilibrium can be changed to a limiter configuration.
- detached limiter configurations, which separate the plasma boundary from the first wall by a distance larger than a/10, to obtain the H-regime, a procedure suggested and confirmed by a significant set of experiments.[50]

The radial feedback system for the plasma size and position is mainly used to:

- control the plasma current density distribution and the magnetic safety factor during the plasma current ramp by changing the size and shape of the plasma cross section;
- maintain the plasma position with respect to the first wall and, possibly, control the transition between x-point and limiter configurations;
- control the radial position during vertical disruptions or other rapid change of the plasma internal inductance (l_i) or the poloidal beta (β_p).

A vertically elongated plasma configuration is potentially unstable to vertical motion. We have carried out extensive numerical simulations[51] with the TSC code of the plasma dynamics and the stability of the plasma/vacuum vessel/poloidal field coils system, taking into account, in the axisymmetric geometry of the system, the position of the diagnostic magnetic pick up coils, and the voltage limitations and time delay in the response of the power supplies. The vertical displacement time (τ_v), the inverse of the exponential growth rate of the plasma vertical position, has been estimated to be about 13.5 ms, taking into account the presence of the thick vacuum vessel and the poloidal

---

[48] M. Nassi, *Volt-sec Requirement and Relevant Margin in the Ignitor Device,* RLE Report PTP-90/1, Res. Lab. of Electron., MIT, 1990.

[49] G. Cenacchi, B. Coppi, L. Lanzavecchia, and M. Rulli, *Ideal MHD Equilibria and Poloidal Field Magnet System for Compact Ignition Experiments,* RLE Report PTP-88/14, Res. Lab. of Electron., MIT, 1988.

[50] N. Suzuki, A. Aikawa, K. Hoshino, et al., *Proceedings of the Twelfth International Conference on Plasma Physics and Controlled Nuclear Fusion Research,* Nice, France, 1988 (Vienna, Austria: I.A.E.A., 1989), Vol. 1, p. 207.

[51] M. Nassi, S.C. Jardin, C.E. Kessel, and N. Pomphrey, *Vertical Stability Analysis for Ignitor,* RLE Report PTP-91/10, Res. Lab. of Electron., MIT, 1991.

field coils connected in antiseries (so that currents induced in coils by the plasma can flow antisymmetrically).

Our results show that β_p and κ have only a weak effect on the plasma vertical motion. The weak influence of κ (for variations $\Delta\kappa = \pm 10\%$) is due to the presence of a close-fitting vacuum vessel.[52]

Toroidal Magnetic Field System

The Ignitor design has always used toroidal magnets made of copper plates, connected in series externally and supported by an appropriate steel structure against the vertical (axial) and horizontal (radial) electrodynamic forces. The loads on the inner leg of the toroidal magnet are supported by bucking between the toroidal and poloidal field coils (a sliding surface is provided at the interface between the toroidal magnet and the air core transformer), by wedging in the inner part of the toroidal field coils, and by an external structure which consists of:

- A set of steel plates or "C-clamps" surrounding each of the 24 modules of the toroidal magnet. The C-clamps are wedged on the outside to allow the unwedged part to rotate around an effective hinge under the effect of the bracing rings. Thus, only a small fraction of the vertical separating force is unloaded onto the central leg of the toroidal magnet.
- Two bracing rings maintaining the plate assembly and transferring the vertical separating force produced by the toroidal magnet to the effective outer shell formed by the steel plates.
- A central post filling the bore of the air core transformer that absorbs the centripetal force acting on the inner leg of the toroidal magnet and acts as a component of a central press. Vertical cuts are made in the post to reduce the effect of the induced currents.
- A vertical electromagnetic press connected to the central post that applies a compression preload on the inner leg of the toroidal magnet to reduce the electromagnetic load. The press is deactivated as soon as thermal expansion in the toroidal magnet becomes significant, or whenever the machine is operated with magnetic fields below the maximum value.

A hybrid cryogenic system[53] is adopted for cooling the toroidal magnet, using liquid N_2 and liquid He. After a current pulse corresponding to the maximum plasma current scenario, the temperature reaches about 230 K in the region facing the transformer (one-third of its volume) and about 95 K in the remaining part. The cooling of toroidal magnets with liquid N_2 is a well established procedure. The step from 80 K to 30 K then requires the use of He. Heat transfer takes place through forced convection in conduits within the coils. The same helium stream is passed through the magnet several times and recooled between passages. The estimated cooling time for the toroidal magnet is shorter than that required by the central solenoid.

Plasma Chamber

The plasma chamber has been designed to withstand both static and dynamic loads with good reliability, while minimizing weight, construction and assembly difficulties, and the overall cost. The result is a relatively thick chamber (17 mm in the inboard side and 26 mm in the outboard side), made of Inconel 625, divided in 24 sectors that can be assembled and joined by welding.

The chamber is mechanically supported and restrained by C-clamps, with long horizontal port ducts that allow for freedom of deformation under electromagnetic and thermal loads. It has been designed to withstand both vertical and axisymmetric disruptions with plasma current decay rates from 1 to 5 MA/ms. A two-dimensional numerical analysis[54] shows that the stresses are below the limit imposed by ASME rules. The plasma chamber also acts as a support for the first wall system. Vertical and equatorial access ports for the plasma diagnostics, the vacuum system, the pellet injector, and the auxiliary heating are provided. Six of the twelve equatorial ports (0.8×0.165 m^2) connect to recessed "pockets" (0.8×0.5 m^2) facing the plasma, which house the antennae of the ion cyclotron radio frequency (RF) heating system.

---

[52] C.E. Kessel and S.C. Jardin, "Vertical and Radial Plasma Position Control for BPX," *Proceedings of the Fourteenth Symposium on Fusion Engineering*, San Diego, California, 1991.

[53] A. Angelini and H. Quack, U.S. Patent No. 4,884,409, December 5, 1989.

[54] Consorzio CITIF, Report CTFFIGNN5251, Turin, Italy (1991).

First Wall System

The first wall is made of 20 mm thick tiles, that cover the entire inner surface of the plasma chamber, which can be replaced using the remote handling system. In principle, the entire first wall can function as a limiter to increase the area over which the heat load may be spread. Graphite reinforced by carbon fibers has been selected as the first wall material, primarily on the basis of its ability to withstand the expected effects of disruptions.

Numerical simulation[55] has shown that Ignitor can achieve ignition at low peak temperature ($T_o \gtrsim 11$ keV) and moderate α-particle heating power ($P_\alpha \simeq 18$ MW). About 26% of this power is lost by radiative processes ($P_R \simeq 4.6$ MW) from the main plasma, and the remaining 13.4 MW (74%) is transfered to the scrape off layer (SOL), where it is released to the first wall by radiative and convective-conductive energy transfer. Simple physical models[56] and experimental data from high density, high magnetic field experiments predict a high density, low temperature plasma in the SOL. This cold, dense SOL plasma shields the core plasma from impurity nuclei and experiences a strong radiative cooling. In particular, on the basis of an extensive series of observations made on high field machines, we estimate that at least 50 percent of the power transfered into the SOL will be released by radiation. Thus, $\simeq$ 63% (11.3 MW) of the total power is uniformly distributed to the first wall by radiation in the main plasma and in the SOL. The remaining $\sim$ 37% (6.7 MW) is non-uniformly distributed (with an estimated maximum peaking factor of 3) due to convection and conduction in the SOL.

We estimate the maximum local thermal wall loading to be about 0.9 MW/m^2 at ignition for a limiter plasma filling the entire plasma chamber and more if the plasma interacts only with the inner part of the first wall. If we assume that the ignited plasma eventually reaches $T_o \lesssim 15$ keV, where about 40 MW are supplied by the input power and the radiative losses from the main plasma are about $P_R \simeq 6$ MW, the corresponding wall loading is 2 MW/m^2.

Auxiliary Systems

Since ignition can be attained by ohmic heating alone, injected heating systems in compact high field experiments have a backup role to suppress, if necessary, the possible onset of sawtooth oscillations, control the temperature evolution and the current density profiles, and accelerate ignition.

An ICRH system with a frequency $\simeq$ 130 MHz and maximum power delivered to the plasma $P_J \simeq 16$ MW, has been adopted for Ignitor because of its demonstrated effectiveness in relatively high density plasmas. The antennae are placed in six housings inset into the vacuum chamber walls, each delivering 2.5 to 4.0 MW.

An injector of deuterium or deuterium-tritium pellets ($\sim$ 4 mm diameter) is considered, in addition to gas injection ("puffing"),[57] to create and maintain the desired plasma density profile. Pellet velocities of 2 km/s or higher that are required to reach the center of the plasma have already been achieved with existing technologies. Another use for a pellet injector that has been demonstrated recently is to condition the first wall by launching lithium pellets into the plasma column prior to regular hydrogenic discharges.[58]

1.3.2 Momentum Transport and Plasma Collective Modes

It is widely known that the transport properties of plasmas are not, with the exception of relatively few cases, adequately described by collisional processes alone. Rather, the presence of fine-scale collective modes typically gives rise to transport coefficients exceeding the collisional ones by two

---

[55] B. Coppi, M. Nassi, and L. Sugiyama, "Physics Basis for Compact Ignition Experiments," *Proceedings of the 1991 International Atomic Energy Agency Conference on α-particle Physics*, Göteborg, Sweden, *Physica Scripta*, forthcoming (1992); L. Sugiyama and M. Nassi, *Free Boundary Current Ramp and Current Profile in a D-T Ignition Experiment*, Report PTP 90/8, Res. Lab. of Electron., MIT, 1991, *Nucl. Fusion*, forthcoming (1992).

[56] A. Angelini and H. Quack, U.S. Patent No. 4,884,409, December 5, 1989; Consorzio CITIF, Report CTFFIGNN5251, Turin, Italy (1991).

[57] L. Sugiyama and M. Nassi, *Free Boundary Current Ramp and Current Profile in a D-T Ignition Experiment*, RLE Report PTP 90/8, Res. Lab. of Electron., MIT, 1991, *Nucl. Fusion*, forthcoming (1992).

[58] C. Ferro and R. Zanino, "Edge Parameters and Scrape-off Layer (SOL) Characteristics in Ignitor," ENEA Report RT/NUCL/90/31, ENEA CRE Frascati, Italy, 1990, *Proceedings of the Ninth International Conference on Plasma Surface Interaction*, Bournemouth, United Kingdom, 1990.

or more orders of magnitude. Although the so-called "anomalous" transport of particles and thermal energy has been studied extensively by many authors, relatively little attention has been paid to the anomalous transport of fluid momentum in plasmas. Over the last fifteen years, an abundance of cases have arisen in which the known collisional theories could not account for the observed momentum transport in laboratory and space as well as in astrophysical plasmas. Our work has focused on this problem in each of the three regimes.

In the auroral F-region of the earth's ionospere, regions in which the plasma flow velocity is strongly sheared tend to develop near auroral arcs.[59] Dynamics Explorer 2 satellite data has been used to study the spectral characteristics of density and electric field fluctuations in these regions,[60] and it was found that the canonical Kelvin-Helmholz instability can only be excited with wavelengths much larger than those in the 1 km range observed. We have proposed an explanation of the fluctuations in a new theory of collisional, electrostatic modes that are driven unstable by the sheared, *field-aligned* ion flow velocity[61] in partially ionized plasmas. The modes can be driven unstable by a moderate amount of velocity shear ($\simeq 3$ sec^{-1}) with wavelengths in the sub-km to several meter range. The resulting (anomalous) viscosity is derived from quasilinear theory, and a model for the nonlinear evolution of the mode is proposed. For the first time, an equation for the nonlinearly evolving normal mode amplitude is derived and solved. We then argued that these spatially localized modes give rise to a flattening of the profile of $V_{i\parallel}$, the ion flow velocity parallel to the magnetic field. This flattening effect begins in localized regions where the growth rate is largest and spreads by creating additional maxima and minima in $dV_{i\parallel}/dx$ at the edges of these regions. New normal modes then grow at the extrema, propagating the effect outward from the initial point of growth.

This work has been extended to include not only the presence of a flow $V_{i\perp} \neq 0$ across the magnetic field, but also its shear $dV_{i\perp}/dx \neq 0$.[62] The profile of $V_{i\perp}(x)$ has strong effects on the spatial topology of the aforementioned modes. In fact, it had been previously suggested that no normal modes localized in the x-direction (transverse to the magnetic field) can be found when $dV_{i\perp}/dx \neq 0$. However, this leaves no reasonable explanation for the observed fluctuations near auroral arcs in which shears are present in both $V_{i\parallel}$ and $V_{i\perp}$. After further investigation, we have found that indeed there are realistic profiles of $V_{i\perp} = V_{E\times B}(x)$ for which significant x-*localized, normal mode solutions exist.* We have described these modes in detail and have proposed a saturation model for the Kelvin-Helmholz instability, which is driven by $dV_{E\times B}/dx$, to explain the observed profiles of $V_{E\times B}$. We suggest two relevant mechanisms: quasilinear flattening and coupling to the short-wavelength collisional modes that are driven by $dV_{i\parallel}/dx$. Thus the K-H modes may provide the "seed" for the observed short wavelength fluctuations. We suggest, in addition, that "composite" modes viewed as spatial sequences of these modes are relevant to extended regions over which the shear of $V_{E\times B}$ is depressed. We have indeed shown the existence of localized, unstable modes driven by $dV_{i\parallel}/dx$ in both collisional and collisionless regimes. All of the modes are expected to have a pronounced effect on the spatial profile of $V_{i\parallel}$ through anomalous momentum transport.

In tokamak experiments heated by neutral beam co-injection,[63] the plasma rotates at nearly sonic $\simeq 5 \times 10^5$ m/s speeds in the toroidal direction. The beams are injected near the magnetic axis and result in a toroidal velocity profile that is peaked near the center of the plasma and decreases toward the edge. The heating has a similar effect on the ion temperature profile. The poloidal flow is complicated by the possibility of shock formation when the poloidal Alfvén Mach number exceeds unity, as the relevant Grad-Shafranov equation undergoes an elliptical-to-hyperbolic transition at this point. In the absence of such shocks, however, the classical, strongly collisional theory[64] predicts damping of the poloidal flow by parallel viscosity at a rate $\sim (\rho_i^2/a^2)(V_{Ti}/a^2\nu_{i\parallel})$, rapid

---

[59] M.C. Kelley and C.W. Carlson, *J. Geophys. Res.* 82: 2343 (1977).

[60] B. Basu and B. Coppi, *Geophys. Res. Lett.* 15: 417 (1988).

[61] B. Basu and B. Coppi, *J. Geophys. Res.* 94: 5316 (1989).

[62] B. Basu and B. Coppi, *J. Geophys. Res.* 95: 21213 (1990).

[63] S.D. Scott, et al., *Phys. Rev. Lett.* 64: 531 (1990); S.D. Scott et al., "Plasma Physics and Controlled Nuclear Fusion Research 1988," Paper I.A.E.A.-CN-50/E-3-5 (Vienna, Austria: I.A.E.A., 1989).

[64] J.W. Connor, S.C. Cowley, R.J. Hastie, and L.R. Pan, *Plasma Phys. and Cont. Fusion* 29: 919 (1987).

on the timescales of interest. Therefore, the remaining flow is predominantly toroidal and can easily be shown to be constant, to lowest order, on magnetic flux surfaces[64] with the magnetic field frozen into the flow. Shock formation is no longer possible as the relevant Grad-Shafranov equation is always elliptic. The collisional damping of the toroidal flow is determined primarily by perpendicular viscosity with a small gyroviscous contribution at a rate $\sim \nu_{ii}\rho_i^2/a^2$, as it is obvious that parallel viscosity cannot transport toroidal momentum across the magnetic field. The corresponding experimental rates and diffusivities are 30-100 times this[65] and are therefore "anomalous." In addition, it is well-documented that the experimental cross-field diffusivities of toroidal momentum, χ_ϕ, and ion thermal energy, χ_i, scale almost identically with the minor radius of the plasma column,[66] increasing toward the edge. This has led to suggestions by others that ion temperature gradient modes produce the anomalous transport of both.

Fluctuations traveling in both the electron and the ion diamagnetic directions have been observed, however, and the shape of the associated spectrum is independent of the toroidal flow velocity while acquiring a Doppler shift. This suggests anomalous transport by modes of the electron-drift type as well, and quite plausibly, those driven by the ion velocity gradient. We have written a report[67] describing two collective modes of the electron-drift type[68] driven unstable by the large ion flow velocity shear induced by NBI. The theory described is consistent with the aforementioned conditions. One mode requires large flow velocities in addition to shear, while the other, weaker instability does not require such high flow velocities but relies on the existence of a parallel ion viscosity. Recent experimental conditions in TFTR[66] are sufficient for the excitation of this weaker instability. Both instabilities are shown to produce momentum diffusivities χ_ϕ greatly exceeding the neoclassical result.

Following this work, we have obtained scaling laws for χ_ϕ employing the neoclassical parallel viscosity. In addition, we have compiled scalings for χ_ϕ for other "anomalous viscosity" theories in a form convenient for comparison with experimental data obtained from interpretation codes. To this end, transport equations describing the radial diffusion of toroidal momentum have been derived for axisymmetric systems, and a method for extracting χ_ϕ from experimental radial profile data has been developed.[69] This work is relevant to the interpretation of data taken on the JET machine as well as future machines in which the flux surfaces are very noncircular, and the data will be compared to cylindrical models.

Most recently, we have formulated arguments[69] showing the ways in which spatial and other symmetries of a given system affect the momentum transport. It is found that, in general, spatial symmetries simplify the form of the anomalous stress tensor as a function of the thermodynamic forces (i.e., gradients of temperature, velocity, etc.). Specifically, we have shown that for an axisymmetric torus with up-down symmetry, the only forces that contribute to the viscous stress are rank two, traceless, and symmetric tensors. This form is exactly that exemplified by the classical viscous stress due to velocity gradients. This result lends plausibility to the argument that the anomalous momentum transport in tokamak plasmas is due to velocity gradient driven modes.

Hospitality extended to one of our group, D. Ernst, by our colleagues at the Joint European Undertaking (JET) during the summer of 1990 and by the Institute of Fusion Studies at the University of Texas during the summer of 1991, has been particularly beneficial in this work.

---

[64] S.D. Scott, et al., *Phys. Rev. Lett.* 64: 531 (1990); S.D. Scott et al., "Plasma Physics and Controlled Nuclear Fusion Research 1988," Paper I.A.E.A.-CN-50/E-3-5 (Vienna, Austria: I.A.E.A., 1989).

[65] S.D. Scott et al., "Plasma Physics and Controlled Nuclear Fusion Research 1988," Paper I.A.E.A.-CN-50/E-3-5 (Vienna, Austria: I.A.E.A., 1989).

[67] B. Coppi, RLE Report PTP 89/2, Res. Lab. of Electron., MIT, 1989.

[68] B. Coppi, M.N. Rosenbluth, and R.Z. Sagdeev, *Phys. Fluids* 10: 582 (1967).

[69] D. Ernst, RLE Report PTP 91/3, Res. Lab. of Electron., MIT, 1991.

1.3.3 Collisional Electrostatic Impurity Drift Modes and the Isotopic Effect

Experiments performed on toroidal, magnetically confined plasmas indicate[70] that the energy confinement time scales roughly with $\sqrt{A_i}$ where $A_i = m_i/m_p$ is the atomic mass of the primary ion species. Most theoretical models predict the so-called gyro-Bohm transport scaling where the relevant diffusion coefficient is:

$$D \propto \frac{cT}{eB}\frac{\rho_i}{r_p} \qquad (1)$$

where ρ_i = ion Larmor radius $\propto \sqrt{m_i}$ and r_p = scale length representative of the source of free energy (e.g., density or temperature scale length). Now since $\tau \propto a^2/D$ where a = plasma cross-section, we see that these theories fail to predict the favorable scaling with atomic mass (hereafter called the "isotopic effect").

There exists one class of fluctuations encountered in collisionless and weakly collisional plasmas that apparently gives the required transport scaling: electrostatic impurity drift waves. To be more precise, these are modes that occur in the presence of impurities (i.e., additional ion species, heavier than Hydrogen or Deuterium), propagate in the electron diamagnetic direction (hence "drift wave") and require a gradient in the temperature of the primary ion species (though not necessarily in the impurity temperature).

These modes were first discovered[71] to occur in plasmas with uniform temperatures when the density profiles are reversed: $(dn_i/dx)(dn_I/dx) < 0$, where the subscripts i and I refer to the primary ion and the impurity respectively, and later[72] found to occur in plasmas with regular profiles, $(dn_I/dx)(dn_I/dx) > 0$, when an ion temperature gradient is present. Recently, it has been argued[73] that these modes occur at the edge of the plasma, and are responsible for the main part of the energy transport in that region. In that case, they ultimately determine the energy confinement time (energy cannot be lost faster than the speed predicted by the characteristics of these modes) and provide an explanation for the isotopic effect.

In the following, we sketch a derivation of the linear stability properties of these modes. We begin by considering a slab geometry, with sheared magnetic field $B = B_0(\hat{e}_z + \hat{e}_y x/L_s)$, and a set of fluid equations for the ions:[74]

$$\omega\frac{\tilde{n}_i}{n_i} + Z_i\omega_{*i}\frac{\tilde{e\phi}}{T_i} \qquad (2)$$

$$-[\omega - \omega_{*i}(1+\eta_i)]\frac{\rho_i^2}{2}\nabla_\perp^2\frac{\tilde{e\phi}}{T_i} - k_\parallel\tilde{u}_\parallel = 0$$

$$\omega\tilde{u}_\parallel = k_\parallel c_i^2\left(\frac{\tilde{n}_i}{n_i} + \frac{\tilde{T}_i}{T_i} + \frac{\tilde{e\phi}}{T_i}\right) \qquad (3)$$

$$(\omega + i\omega_\kappa)\frac{\tilde{T}_i}{T_i} + Z_i\eta_i\omega_{*i}\frac{\tilde{e\phi}}{T_i} \qquad (4)$$

$$-[\omega - \omega_{*i}(1+\frac{7}{2}\eta_i)]\frac{\rho_i^2}{3}\nabla_\perp^2\frac{\tilde{e\phi}}{T_i} - \frac{2}{3}k_\parallel\tilde{u}_\parallel = 0$$

where we have neglected perpendicular transport coefficents (of order ν^2/Ω^2 compared to parallel coefficients) and dropped parallel collisional viscosity, for simplicity (it contributes a small stabilizing term). Here $\omega_{*i} = k_y cT_i/Z_i eBL_n$ is the ion diamagnetic frequency (L_n is the density gradient scale length), $c_i^2 = T_i/m_i$, $\rho_i = c_i/\Omega_i$ (Ω_i= Larmor frequency) and $\omega_\kappa = 2\chi^0 k_\parallel^2 c_i^2/3\nu_i$ where χ^0 is a constant coefficient of order unity. The parallel wavenumber is $k_\parallel = k_y x/L_s$, and the temperature gradient parameter is $\eta_i = (d \ln T_i/dx)/(d \ln n_i/dx)$.

---

[70] G. Boxman, B. Coppi, L. DeKock, B. Meddens, A. Oomens, L. Ornstein, D. Pappas, R. Parker, L. Pieroni, S. Segre, F. Schuller, and R. Taylor, *7th European Conference on Plasma Physics and Controlled Fusion*, Lausanne, Vol. 4B, Part II, p. 14, (1975); A.G. Barsukov et al, in *Plasma Physics and Controlled Nuclear Fusion Research* (Vienna, Austria: I.A.E.A., 1983), Vol. 1, p. 83; J.G. Cordey et al, in *Plasma Physics and Controlled Nuclear Fusion Research* (Vienna, Austria: I.A.E.A., 1985), Vol. 1, p. 167; F. Wagner et al., in *16th European Conference on Plasma Physics and Controlled Fusion*, Venice, 1989, Vol. 13B, Part I, p. 195.

[71] B. Coppi, H.P. Furth, M.N. Rosenbluth, and R.Z. Sagdeev, *Phys. Rev. Lett.* 17: 377 (1966).

[72] B. Coppi, G. Rewoldt, and T. Schep, *Phys. Fluids* 19: 1144 (1976) and references therein.

[73] B. Coppi, in *Plasma Physics and Controlled Nuclear Fusion Research* (Vienna, Austria: I.A.E.A., 1991), Vol. 2, p. 413.

[74] A.B. Hassam, T.M. Antonsen, Jr., J.F. Drake, and P.N. Guzdar, *Phys. Fluids* B2: 1822 (1990).

Equations (2)-(4) are valid for any ion species. In the following, we shall consider the orderings:

$$k_\parallel c_i << \omega << k_\parallel c_i \qquad (5-a)$$

$$\omega \nu_i < k_\parallel^2 c_i^2 \qquad (5-b)$$

Then the impurities respond to the perturbation by simple E x B drift, while the primary ion response is weakly collisional ($\omega < \omega_{*i}$) and shorts out the parallel electric fields ($\tilde{p}_i = -e\tilde{\phi}$, to lowest order). The electron reponse is adiabatic, $\tilde{n}_e/n_e = e\tilde{\phi}/T_e$. Using quasi-neutrality, $Z_i\tilde{n}_i + Z_I\tilde{n}_I = \tilde{n}_e$, a simple analysis leads to the following dispersion equation:

$$\frac{d^2}{dX^2}\frac{e\tilde{\phi}}{T_i} - \left(X^2 + \frac{\alpha}{\beta}\right)\frac{e\tilde{\phi}}{T_i} = 0 \qquad (6)$$

where $X \equiv \sqrt{\beta}\, x/\rho_i$ and

$$\beta^2 \equiv \frac{4i\chi^0}{5\eta_i}\frac{k_y^2\rho_i^2 c_i^2}{L_s^2 \nu_i \omega_{*i}}$$

$$\times\left[\frac{T_i}{T_e} + Z_i\left(1 - \frac{Z_I n_I}{n_e} + \frac{Z_I n_I}{n_e}\sigma_I\frac{\omega_{*i}}{\omega}\right)\right] \qquad (7-a)$$

$$\alpha \equiv \frac{6}{5\eta_i}\left(\frac{2}{3} - \eta_i\right) + k_y^2\rho_i^2 \qquad (7-b)$$

and $\sigma_I \equiv d\ln n_I/d\ln n_i$.

This equation admits unstable, spatially localized modes for

$$\eta_i \geq \frac{2}{3}\left(1 + \frac{5}{6}k_y^2\rho_i^2\right) \qquad (8)$$

with

$$\omega = -Z_I k_y D_B \frac{1}{n_e}\frac{dn_I}{dx} \times \qquad (9)$$

$$\left[1 + Z_i\frac{T_e}{T_i}\left(1 - \frac{Z_I n_I}{n_e}\right) + \frac{9iZ_i}{5\chi^0}\frac{T_e}{T_i}\frac{\nu_i\omega_{*i}}{k_y^2 c_i^2}\left(\frac{L_s}{\rho_i}\right)^2 (2N+1)^{-2}\eta_i\left(\frac{\eta_i - 2/3}{\eta_i} - \frac{5}{6}k_y^2\rho_i^2\right)^2\right]^{-1}$$

where N is the radial quantum number and $D_B = cT_e/eB$ is the Bohm diffusion coefficient.

From (9) we notice that $\mathrm{Re}(\omega)/\omega_{*I} < 0$ for $\sigma_I > 0$ and that, for $\gamma \equiv \mathrm{Im}(\omega) < \mathrm{Re}(\omega)$, we have

$$\gamma \propto Z_I\eta_i\frac{\nu_i\omega_{*i}}{k_y^2\rho_i^2}\left(\frac{L_s}{\rho_i}\right)^2 \propto Z_I Z_i m_i^{-1/2} \qquad (10)$$

Referring to the well-known mixing length formula, $D \approx \gamma/k_\perp^2$ we see that $\tau_E \propto a^2/D \propto \sqrt{m_i}$, as observed experimentally. It also predicts that transport will not be better in Helium ($Z_i = 2$, $A_i = 3$) than in Hydrogen, also an observed property.

In addition, one can argue that as the mass ratio m_i/m_I is increased, the two thermal speeds v_{TI} and v_{Ti} get closer together and the "window of opportunity"

$$v_{TI} < \omega/k_\parallel < v_{Ti} \qquad (11)$$

decreases, leading to a dramatic narrowing in the spectrum of unstable modes. This has in fact been confirmed by a local analysis of the relevant kinetic theory[75] and further contributes to this "isotopic effect."

[75] S. Migliuolo, RLE Report PTP-90/11, Res. Lab. of Electron., MIT, 1990, and JET preprint P(90)34, submitted to *Nucl. Fusion*, 1991.

1.3.4 Two-Fluid MHD Description of the Internal Kink Mode

Oscillations in the central electron temperature and x-ray emission (so-called "sawtooth oscillations") are an important and well-known instability in tokamak experiments. It is widely believed that they are initiated by a mode with poloidal and toroidal mode numbers m/n = 1/1 known as the internal kink mode. This mode has been extensively studied theoretically using both fluid[76] and kinetic descriptions;[77] the results found in these two types of investigations, however, differ in the high-temperature and finite $\beta > 2\omega_{pi}^2/\omega_{pe}^2$ regimes (β is the ratio of plasma pressure to magnetic pressure and ω_{pi}, ω_{pe} are the ion and electron plasma frequencies, respectively) currently attained in toroidal machines such as Alcator, TFTR, and JET. In these regimes, the ion gyroradius exceeds the scale-length of plasma motions predicted by the fluid analysis of Ara et al.,[76] which is determined by either electron inertia (i.e., the collisionless plasma skin depth $d_e = c/\omega_{pe}$) or resistivity. As a fluid description is not expected to be valid in this circumstance, it has therefore been argued[78] that only kinetic theory can properly describe the behavior of kink modes in such experiments.

In recent work, we re-examined the two-fluid MHD theory of the internal kink mode. Unlike Ara et al.,[76] however, we did not assume that the electron velocity appearing in the two-fluid form of Ohm's law is divergenceless. We found that this assumption, which effectively eliminates the contribution of the Hall term in Ohm's law, is not valid in the regime mentioned above. Avoiding this assumption, furthermore, we showed that the results obtained from the two-fluid theory are in good agreement with those found from kinetic treatments (at least in the absence of hot particles). Thus, with a careful treatment of the Hall term, the two-fluid model appears to provide an adequate description of the internal kink mode in the parameter region of current tokamak experiments. This result may be useful in the numerical study of such experiments due to the relative simplicity of the two-fluid model compared to a kinetic description.

Returning to the apparent breakdown of the fluid theory, we note that the Hall term in our treatment introduces into the theory a new length $\rho_s \simeq c\sqrt{\beta/2}\,/\omega_{pi}$ of the order of the ion gyroradius (as calculated on the basis of the sum of the electron and ion temperatures), which becomes the characteristic scale of the plasma motion in the high temperature regimes referred to above. This scale, due to the decoupling of the ions from the magnetic field afforded by Hall's term, may greatly exceed the scale-length of the current sheets excited in the resonant region during the mode's development (e.g., the skin depth). Thus, the two-fluid theory does not predict that the characteristic scale of plasma motions falls below the ion gyroradius (as previously thought), which may account for the agreement between the MHD and kinetic results.

We also developed two variational approaches to calculating the linear growth rate. One of these formulations is in terms of a single function (the poloidal velocity profile) and provides an upper bound estimate for the growth rate. The other is in terms of two trial functions (the radial displacement and the helical magnetic flux perturbation) and leads to a lower bound estimate for this rate. The numerical implementation of the latter approach is also very efficient in the regimes discussed above, despite the presence of two very different scale lengths. The nonlinear generalization of the second approach, which is based only on the largest scale length, may be especially useful in numerical simulations involving these regimes.

---

[76] G. Ara, B. Basu, B. Coppi, G. Laval, M.N. Rosenbluth, and B.V. Waddel, *Annals of Physics* 112: 443 (1978).

[77] J.F. Drake, *Phys. Fluids* 21: 1777 (1978); G.B. Crew and J.J. Ramos; *Nucl. Fusion* 26: 1475 (1986); F. Pegoraro, F. Porcelli, and T.J. Schep, *Phys. Fluids* B1: 364 (1989); F. Porcelli, *Phys. Rev. Lett.* 66: 425 (1991); H.L. Berk, S.M. Mahajan, and Y.Z. Zhang, *Phys. Fluids* B3: 351 (1991); B. Coppi and P. Detragiache, RLE Report PTP-90/1, Res. Lab. of Electron., MIT, 1990, submitted to *Phys. Rev. Lett.*

[78] F. Pegoraro, F. Porcelli, and T.J. Schep, *Phys. Fluids* B1: 364 (1989).

1.4 Versator II Tokamak Research Program

Sponsor

U.S Department of Energy
Contract DE-AC02-78-ET-51013

Project Staff

Professor Miklos Porkolab, Jeffrey A. Colborn, Jared P. Squire, Jesus Noel Villasenor, Edward W. Fitzgerald

Versator II is a small tokamak facility (major radius R = 40 cm, minor radius a = 13 cm) with modest plasma parameters (magnetic field $B_0 \sim 1.3$ Tesla, density $n_e \sim 3 \times 10^{13}$ cm^{-3}, and plasma current $I_p \sim$ 10-80kA) which is used for fundamental studies of the interaction of electromagnetic waves with a fully ionized, nearly collisionless plasma. For this purpose, we use several high power (~ 100 kW) microwave sources to launch waves at frequencies near the electron-gyro frequency (f ~ 28-35 GHz) and the lower hybrid (ion-plasma) frequency (f = 800 MHz or 2.45 GHz). In the section below, we describe three different experimental projects which were carried out during the past year.

1.4.1 High Beta-Poloidal Experiments with Advanced X-ray Diagnostics

The purpose of this project is (1) to measure the spatial and energy distributions of fast electrons during rf current drive experiments, and (2) to study the equilibrium and stability of high beta poloidal plasmas in the Versator II tokamak. (Beta poloidal is the ratio of plasma pressure to poloidal magnetic pressure and is an important parameter for plasma equilibrium and stability.) In these discharges the plasma current and most of the plasma pressure are supplied by highly energetic electrons created by launched high power lower-hybrid plasma waves.[79] We have been mapping the spatial and velocity distributions of the current carrying fast electrons. With this information we can calculate realistic plasma current and pressure distributions. Along with other basic plasma parameters, we can then test theoretical predictions regarding the equilibrium and stability of these plasmas. Specifically, we would like to determine if these equilibria are in or near what is called the second stability regime.[80] In addition, at high beta poloidal significant bootstrap current[81] generation is expected, and we would like to verify its existence in the Versator experiment.

To accomplish this goal, we have developed two arrays of NaI detectors which measure the hard x-ray (20-500 kev) spectrum by utilizing pulse-height analyzers. With the x-ray detectors we look at plasma bremsstrahlung emission from the collision of the energetic electrons with plasma ions. To obtain spatial distributions we first constructed an array to view the plasma vertically from the bottom of the tokamak at different major radii (see figure 7). Next, we exploited the fact that bremsstrahlung emission becomes asymmetric with respect to the direction of the electron motion at high energies. We do this by measuring the x-ray emissions at various angles to the toroidal magnetic field. For this purpose we reconfigured the detectors into a tangential array which view through the plasma mid-plane at a full range of angles. Due to the excellent port access, historically this is the first NaI array capable of viewing all angles simultaneously (see figure 8). During the tangential x-ray measurements a single scannable detector was used to monitor the radial emission profile. The detector electronics can collect time integrated x-ray energy spectra and energy integrated time dependent data simultaneously on all detectors. With this data we can model the distribution of energetic electrons by calculating the expected x-ray emissions and iteratively fitting the model to the measured data.

In the past year, we have obtained x-ray energy spectra and profiles from mostly high beta poloidal rf driven plasmas, but some data has also been taken at lower beta poloidal for comparison. The radial profile data show an outward shift in major radius of the peak emission. This corresponds to the Shafranov shift of the inner magnetic flux surface. The shift helps confirm that the plasma is indeed in a high poloidal beta equilibrium. Also, we have found that the x-rays coming from the outer region of the plasma are more energetic. This can be explained by noting that higher phase velocity waves are accessible only to the low density (outside) region. At lower beta poloidal the emission profile does not have an outward shift; rather, we observe a secondary emission

---

[79] S.C. Luckhardt et al., *Phys. Rev. Lett.* 62: 1508 (1989).

[80] B. Coppi, A. Ferreira, J.W-K. Mark, and J.J. Ramos, *Nucl. Fusion* 19: 715 (1979).

[81] A.A. Galeev and R.Z. Sagdeev, *Sov. Phys.* JETP 26: 233 (1968).

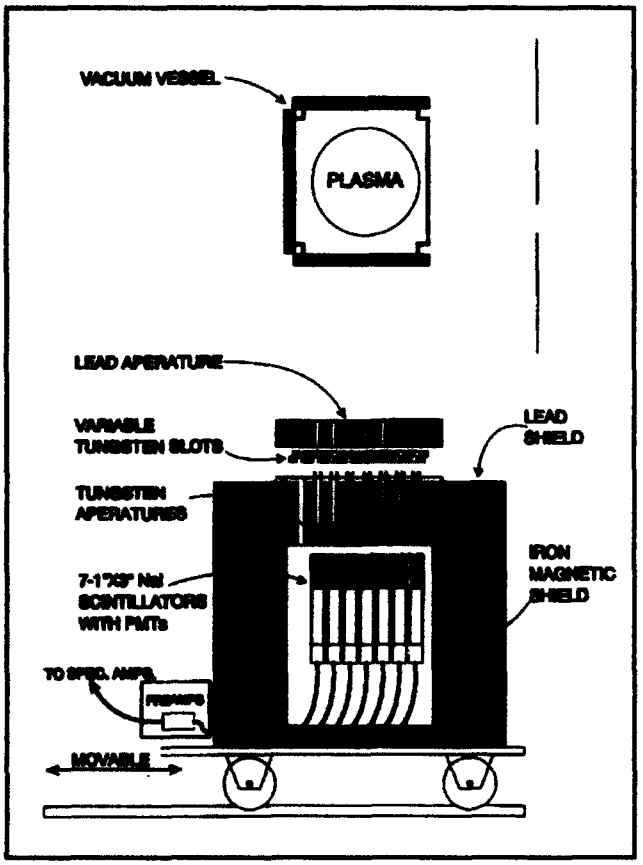


Figure 7. Perpendicular array.

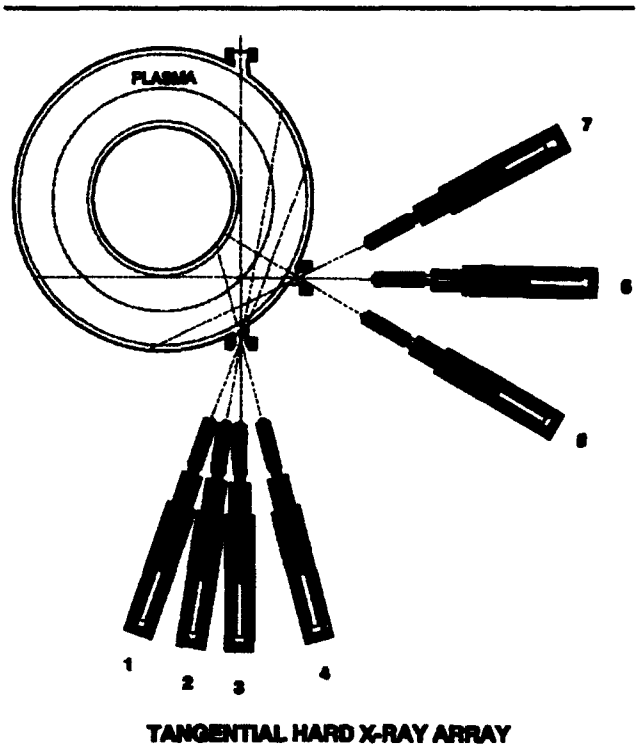


Figure 8. A view of the tangential array from above the tokamak.

peak toward the inside plasma major radius. This may be evidence of the tips of trapped particle banana orbits. The peak may correspond to a reflection point where the gradient in the toroidal magnetic field has converted all the trapped electron energy into perpendicular energy.

Using the tangential array, we observed a distinct asymmetry in the plasma x-ray emissions during rf current drive with unidirectional launched rf waves. There was as much as a factor of ten times greater high energy x-ray flux emitted in the co-current drive direction as compared to the counter-current drive direction. In the course of this study, symmetric injection of lower-hybrid waves was also examined. Current drive is not expected with this configuration, but at high poloidal beta nearly the same current was driven with symmetric injection as with the asymmetric current drive configuration (see figure 9a). The x-ray flux for the symmetric case was less by as much as a factor of 5, implying a strong reduction in the current carrying electron tail (see figure 9b). At the lower beta poloidal it was not possible to maintain the plasma current with the symmetric injection alone. We believe this is evidence that in high beta poloidal plasmas a major fraction of the plasma current may be supplied by bootstrap current. We have yet to model the electron distribution based on this data.

In 1992, we will continue analyzing the data collected during the past year. We will carry out theoretical numerical analysis using the ACCOME[82] code, partially developed at the Plasma Fusion Center (PFC). Given just a few external parameters this code calculates the self-consistent plasma equilibrium. It is the most sophisticated code of its kind available in the world. We will perform bremsstrahlung emission calculations with a code such as the one developed for the Alcator C lower-hybrid experiments at the PFC.[83] Information from this work should allow us to determine whether the equilibria obtained in Versator II is in second stability and whether bootstrap current is generated.

[82] P.T. Bonoli et al., *Nucl. Fusion* 30: 533 (1990).

[83] S. Texter et al., *Nucl. Fusion* 26: 1279 (1986).

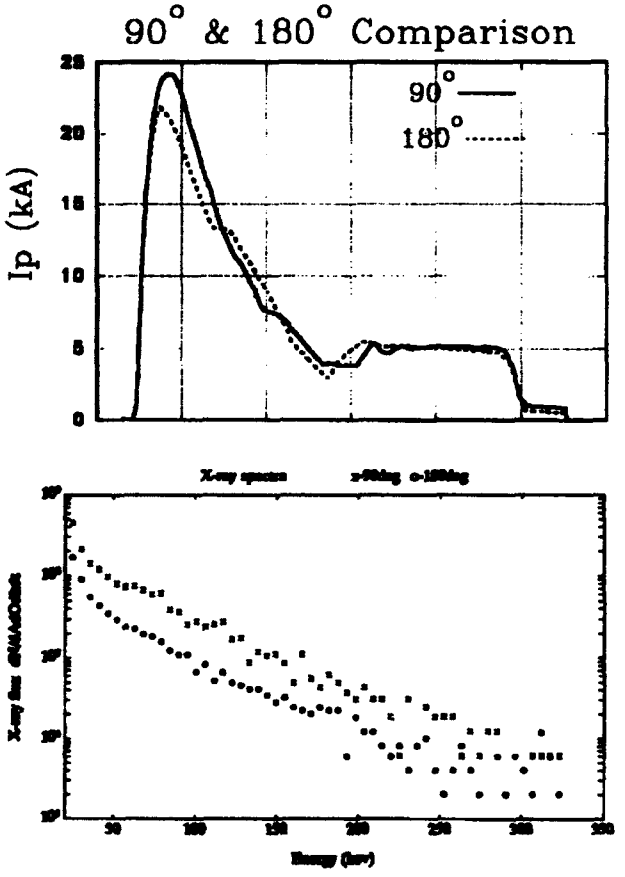


Figure 9. (a)(top) A comparison of current driven by asymmetric (90°) and symmetric (180°) rf injection. (b)(bottom) A comparison of the emitted x-ray spectra.

1.4.2 Fast Wave Current Drive Experiments

In previous progress reports, we have discussed a combined fast wave slow lower hybrid wave current drive experiment where two traveling waves are launched. Slow lower hybrid waves launched at 2.45 GHz by a conventional grill forms a suprathermal electron tail, which is then expected to absorb an 800 MHz fast wave spectrum launched by a specially built dielectric-loaded waveguide array. The available power at each of these frequencies is up to 100 kW at the sources. The fast wave antenna was successfully tested during last year's experimental runs and low power coupling results were consistent with theoretical predictions.

Recent high power experiments showed no clear sign of fast wave penetration into, and/or interaction with the plasma interior. In particular, no evidence of rf driven current or acceleration of suprathermal electrons was observed from hard x-ray detectors. Our code calculations indicate that according to linear wave theory a significant fraction of the power should have penetrated the plasma interior and also been absorbed by fast electrons. We conclude that the fast waves must be absorbed on the plasma surface, possibly by non-linear effects such as parametric decay or scattering by low frequency edge density fluctuations.

To further study the physics at the edge, we have installed a poloidal rf probe array on the plasma surface to look for evidence of such non-linear phenomena. In addition, a retarding potential analyzer was also installed to measure the fast electron distribution function near the plasma surface that may be formed by parametric decay. Early results show a low energy electron tail radially concentrated within a centimeter and located at the plasma periphery. The rf probes have also detected asymmetric broadening at the pump frequency, indicating some level of parametric decay activity. These results are under further study.

1.4.3 Current-Drive Experiments Using Electron Cyclotron Waves and Lower Hybrid Waves

During the past year, current-drive experiments were completed on the Versator II tokamak using electron-cyclotron (EC) and lower-hybrid (LH) waves. The experiments performed fall into three groups: (1) studies of the electron distribution function during LH current drive, (2) studies of the current drive efficiency of combined LH and EC waves, and (3) preionization and current drive experiments with EC waves. The results are presently under analysis, and attention is being focused primarily on the following issues.

During LH current-driven discharges, a two-temperature tail in the parallel electron distribution function has been observed using an improved electron-cyclotron transmission diagnostic. Analysis of this result has focused on modeling the discharges using a computer code, CQL3D, which computes the electron distribution function under the influence of LH waves, electric field, EC waves, and other power sources, if desired. The results of the code are being compared to the measured data to improve our understanding of the cause of the two-temperature feature.

Combined LH and EC current-driven discharges are presently being analyzed to determine the efficiency of this type of current drive and to learn as much as possible about the physical mechanisms that affect that efficiency. Our results indicate that, in many cases, the efficiency is considerably lower than predicted theoretically on Versator II. This may be due to enhanced electron losses or

trapping caused by EC and LH wave combination. This analysis is ongoing.

Effective preionization and current drive at low plasma densities has been achieved on Versator II using EC waves alone. The current drive efficiency is higher than expected for the low electron temperature ($J_e \approx 250$ eV) of the target plasmas. Preliminary analysis suggests that this may be due to the presence of a hot parallel electron tail preformed by the tokamak's toroidal electric field. The current-drive efficiency was found to be independent of the launch angle of the EC waves, but strongly dependent on plasma density, decreasing rapidly as the density was increased above 3×10^{12} cm^{-3}. A doctoral dissertation based on these results is being prepared by Jeffrey A. Colborn.

Section 3 Electromagnetics

Chapter 1 Electromagnetic Wave Theory and Applications

Chapter 1. Electromagnetic Wave Theory and Applications

Academic and Research Staff

Professor Jin Au Kong, Dr. Sami M. Ali, Dr. Son V. Nghiem, Dr. Robert T. Shin, Dr. Ying-Ching E. Yang, Dr. Yi Yuan, Dr. Herng A. Yueh, John W. Barrett, Barbara A. Roman

Visiting Scientists and Research Affiliates

Qizheng Gu,[1] Dr. Tarek M. Habashy,[2] Dr. Arthur K. Jordan,[3] Dr. Che Y. Kim,[4] Dr. Kevin O'Neill,[5] Dr. Soon Y. Poh,[6] Masanori Yamaguchi[7]

Graduate Students

David V. Arnold, Robert G. Atkins, William W. Au, Pierre Coutu, Hsiu C. Han, Yoshihisa Hara, Chih-Chien Hsu, Gregory T. Huang, Joel T. Johnson, Cheung-Wei Lam, Hongsing Lee, Kevin Li, Harold H. Lim, Ilya Lyubomirsky, Michael C. Moldoveanu, John H. Oates, David M. Sheen, M. Ali Tassoudji, Murat E. Veysoglu, Li-Fang Wang, Jiqing Xia

Undergraduate Students

Sean T. Hogarty, Jerome S. Khohayting, Yong Liu, Jean O. Nam

Technical and Support Staff

Margery E. Brothers, Anh Lieu, Wei Ming-Yu Lin, Kit-Wah F. Lai, Sarah L. Larson

1.1 ILS/MLS Frequency Management Assessment

Sponsor

U.S. Department of Transportation
Contract DTRS-57-88-C-00078TTD13

Project Staff

Professor Jin Au Kong, Dr. Robert T. Shin, Dr. Ying-Ching E. Yang, Qizheng Gu, John W. Barrett, M. Ali Tassoudji, Murat E. Veysoglu, Li-Fang Wang, Chih-Chien Hsu, Gregory T. Huang, Barbara A. Roman, Jean O. Nam, Yong Liu, Jerome S. Khohayting

Developed during World War II, the Instrument Landing System (ILS) is currently being used at airports worldwide as the standard precision approach guidance system to assist pilots landing during poor visibility weather conditions. It consists of three basic components: (1) a localizer to line up the airplane with the runway, (2) a glideslope for vertical glide path control, and (3) marker beacons for homing and position determination. To improve the range accuracy, Distance Measurement Equipment (DME) is often used as a replacement for the marker beacons in newer ILS.

The Microwave Landing System (MLS) was developed to overcome some of the problems and limitations associated with ILS. In order to install

---

[1] Shanghai Research Institute of Mechanical and Electrical Engineering, Shanghai, China.

[2] Schlumberger-Doll Research, Ridgefield, Connecticut.

[3] U.S. Navy, Office of Naval Research, Arlington, Virginia.

[4] Department of Electronics, Kyungpook National University, Taegu, Korea.

[5] Civil and Geotechnical Engineering, Department of the Army, Hanover, New Hampshire.

[6] Digital Equipment Corporation, Andover, Massachusetts.

[7] Tsukuba Research Laboratory, Hitachi Chemical Company, Tsukuba, Ibaraki, Japan.

ILS, flat terrain over an extended area is required since traditional glideslope antennas use ground reflection to generate desired radiation patterns. Furthermore, the clearance requirement around an ILS site is stringent to avoid guidance error caused by multipath interference. MLS overcomes these limitations by using much higher frequencies (5030 MHz - 5090 MHz) so that very narrow beams can be formed from antennas of reasonable sizes. The narrow beams can avoid most structures near the airport, and flat terrain is not required in front of the vertical guidance part of MLS. A benefit of the higher frequency band is that the number of channels available for MLS is five times that for ILS. There are 200 channels allocated for MLS in the band between 5030 MHz and 5090 MHz, in contrast to 40 channels for ILS in the 108-112 MHz (localizer) and 329-335 MHz (glideslope) bands. In order to accommodate future growth beyond the year 2015, the International Civil Aviation Organization (ICAO) has passed a resolution to expand MLS by 120 more channels up to 5126 MHz and allowed nations to use up to 5150 MHz.

MLS has more channel capacity than ILS available to satisfy the future requirements in the National Airspace System Plan. However, the user community, particularly aircarriers in the United States, because of fear of the high cost of conversing from ILS to MLS, constantly challenges the FAA's gloomy picture of the ILS spectrum. As a result, Congress has mandated that a detailed study explore the capacity of ILS to expand in major metropolitan areas where the FAA has identified potential frequency congestion and radio interference problems.

To address the concerns of the aviation community, this project is centered around building simulation software that can:

1. predict channel capacities of ILS and MLS in congested metropolitan areas (e.g., New York, Chicago, Los Angeles and Dallas/Fort Worth), as well as many other geographical areas;
2. perform quantitative analyses of in-band (aviation band) and out-of-band electromagnetic interferences; and
3. make quantitative assessments of electromagnetic interferences within the ILS/MLS service volume.

Based upon the above requirements, we established a methodology for implementing simulation software from theoretical studies of electromagnetic interference phenomena. In brief, first we locate potential interference sources, and then we use an electromagnetic propagation model to compute desired and interfering signal strengths. Then an interference analysis based upon safety standards, which are consistent with the receiver model, is performed. Finally, the interference analysis results for various locations are combined to make a channel capacity assessment. Accordingly, the following tasks have been identified:

1. identification of radiation sources, including in-band and out-of-band sources,
2. development of propagation models to be used to calculate interference levels,
3. development of receiver models to determine the quantitative effect of interference signals,
4. verification and validation of models through testing and checking against existing data, and
5. development of graphical user interface which allows for interactive retrieval of quantitative information on the assessment.

In this project, we have developed a computer simulation tool, EMSALS, which uses the databases of navigational and commercial radiowave transmitters to calculate the strengths of desired and undesired signals and generate an EM interference assessment based on user-selected assumptions. The first part of the software EMSALS/I (for ILS) has been used to analyze the frequency congestion and electromagnetic interference problems in the continental United States given the assumptions of the current level of FAA standard interference protection. Emphasis was first placed on ten complex metropolitan areas having a density of runways. Then the less densely populated regions were analyzed to determine ILS capacity across the entire continental United States (CONUS).

Based upon the current flight standards and interference protection criteria specified by the ICAO and FAA, computer simulations across the ten metropolitan areas predict shortfalls in ILS channel capacity. For example, ILS substantially fails to meet the precision landing runway requirements in the New York-Philadelphia-Washington DC area, even with several different priority schemes to optimize the number of available channels. The limitations of the ILS spectrum are best illustrated by the fact that as assignment priorities are changed, the number of available channels for specific regions over a large geographical area also changes. Assigning additional frequencies in one region can seriously reduce the channel availability in nearby regions. Analysis of other areas such as Denver and Chicago demonstrated that the limited ILS channel capacity could significantly impede expansion plans. Analysis of the regions outside the ten metropolitan areas also showed potentially significant shortfalls because of FM interference

problems. Using computer simulation, we have obtained the number of possible ILS installations at the candidate runways throughout the CONUS under the current FAA interference protection requirements. While the actual number may deviate from these because of different local conditions and equipment set-up, the over-all picture is that ILS will reach its capacity limit given the high demand for precision landing runways. The EMSALS/I software can also be used for detailed analysis of the local set-up.

The second part of the software, EMSALS/M (for MLS), was used to evaluate channel availability and to generate a frequency assignment plan given the assumptions of the current ICAO MLS channel assignment rules and interference protection standards. The channel assignments had to be carried out for ILS-to-MLS conversion sites as well as new candidates, including heliports which cannot be sited with ILS. The total number of candidate sites is over 1800.

Unlike the ILS analysis, the main concern was in-band interference because the MLS-band is currently well protected, and no proven out-of-band interference sources have been identified yet. The MLS analysis shows marked improvement in the congestion problems as compared to ILS availability. In addition to satisfying all existing and new qualified site requirements, there still remains channel capacity for future expansion.

1.2 Future Aircraft Landing System: Global Positioning System (GPS) and Synthetic Vision Sensors (SVS)

Sponsor

U.S. Department of Transportation
Contract DTRS-57-88-C-00078TTD30

Project Staff

Professor Jin Au Kong, Dr. Robert T. Shin, Dr. Ying-Ching E. Yang, Dr. Yi Yuan, Chih-Chien Hsu, M. Ali Tassoudji, Sean T. Hogarty, Yong Liu, Barbara A. Roman

Precision landing systems play an important role in continuing air travel service during adverse weather conditions. The Instrument Landing System (ILS) has been in service for the past five decades, and the Microwave Landing System (MLS) will be gradually replacing ILS within the next decade. These two systems require that ground equipment works properly; therefore, their usage is limited to locations where these setups are available. Two alternative technologies that do not require ground setups have been proposed as the future replacement for ILS and MLS: Synthetic Vision (SV) sensors and the Global Positioning System (GPS).

Specifically, it has been suggested that technologies such as Active Millimeter Wave (MMW) radar or passive Forward-looking Infrared (FLIR) could be used as approach and landing aids by aircraft for locating airport runways during approximately the last 1 nmi of flight. GPS is the newest satellite-based navigation system which distributes precision timing information on a continuous basis. With a constellation of 18 to 24 satellites in high altitude orbits, receivers at any position in the sky or on the ground can obtain signals from several satellites to derive three-dimensional positions to a very high degree of accuracy. It has also been suggested that the GPS can play a significant role during approach and landing either: (1) in conjunction with an SV sensor in which case GPS would provide sole-means guidance information until the SV sensor could be used to "see" the landing environment and then might provide supplementary guidance information; or (2) as an alternative to ILS and MLS, in which case the currently planned GPS would be augmented, for example, by ground-based differential stations at the airport.

The goals of our study are to:

1. assess the capability of present and projected future state-of-the-art active millimeter wave and passive infrared systems to serve as low-visibility approach and landing aids for civil aviation, and
2. evaluate GPS requirements and capabilities in specific areas which directly affect the feasibility of using GPS for precision approach, e.g., availability and integrity.

The approach employed for SV sensor evaluation is based on the generation of simulated images to portray the capabilities of active MMW and passive FLIR SV systems. MMW and FLIR images of the same scene for the same altitudes and visibility conditions are generated using validated computer models and software. Comparison of the visible MMW and IR images provides the assessment of the capabilities of SV sensors. Simulated FLIR images have been generated using InfraRed Modeling and Analysis (IRMA) program developed by the Air Force Armament Laboratory. This simulation has been under development for several years and is thoroughly validated. IRMA models both emission and propagation of long IR (8-12 μm), which has the best weather penetration capability.

Active MMW images are also generated using models and software from related projects. Preliminary simulation of 35 GHz sensor scene reveals the lack of depth information and resolution, but shows good weather penetration. Future work is required in the area of postprocessing in order to achieve better images.

1.3 Multilayer Media and Superconducting Electronics

Sponsors

Defense Advanced Research Projects Agency
Contract MDA972-90-C-0021
Digital Equipment Corporation
IBM Corporation
Joint Services Electronics Program
Contract DAAL03-89-C-0001
Contract DAAL03-92-C-0001
Schlumberger-Doll Research
U.S. Navy - Office of Naval Research
Grant N00014-90-J-1002
Grant N00014-89-J-1019

Project Staff

Professor Jin Au Kong, Dr. Robert T. Shin, Dr. Tarek M. Habashy, Dr. Sami M. Ali, Dr. Ying-Ching E. Yang, Dr. Soon Y. Poh, Dr. Herng A. Yueh, Dr. Son V. Nghiem, David M. Sheen, Robert G. Atkins, Hsiu C. Han, Jiqing Xia, Cheung-Wei Lam, Michael C. Moldoveanu, Hongsing Lee, Ilya Lyubomirsky

A method for the calculation of current distribution, resistance, and inductance matrices for a system of coupled superconducting transmission lines having finite rectangular cross-section is presented. These calculations allow accurate characterization of both high-T_c and low-T_c superconducting strip transmission lines. For a single stripline geometry with finite ground planes, the current distribution, resistance, inductance, and kinetic inductance are calculated as a function of the penetration depth for various film thicknesses. These calculations are then used to determine the penetration depth for Nb, NbN, and $YBa_2Cu_3O_{7-x}$ superconducting thin films from the measured temperature dependence of the resonant frequency of a stripline resonator. The calculations are also used to convert measured temperature dependence of the quality factor to the intrinsic surface resistance as a function of temperature for an Nb stripline resonator.

The frequency-dependent resistance and inductance of uniform transmission lines are calculated with a hybrid technique that combines a cross-section coupled circuit method with a surface integral equation approach. The coupled circuit approach is most applicable for low-frequency calculations, while the integral equation approach is best for high frequencies. The low-frequency method consists in subdividing the cross section of each conductor into triangular filaments, each with an assumed uniform current distribution. The resistance and mutual inductance between the filaments are calculated, and a matrix is inverted to give the overall resistance and inductance of the conductors. The high-frequency method expresses the resistance and inductance of each conductor in terms of the current at the surface of that conductor and the derivative of that current normal to the surface. A coupled integral equation is then derived to relate these quantities through the diffusion equation inside the conductors and Laplace's equation outside. The method of moments with pulse basis functions is used to solve the integral equations. An interpolation between the results of these two methods gives very good results over the entire frequency range, even when few basis functions are used. Results for a variety of configurations are obtained and are compared with experimental data and other numerical techniques.

A spectral domain dyadic Green's function formulation defining the fields inside a multilayer chiral medium due to arbitrary distribution of sources is developed. The constitutive parameters and the chirality of each layer are assumed to be different. The fields are obtained in terms of electric and magnetic type dyadic Green's functions. The singular behavior of these dyadic Green's functions in the source region is taken into account by extracting the delta function singularities. The fields in any layer are obtained in terms of appropriately defined global reflection and transmission matrices.

In order to understand the physical meaning of rational reflection coefficients in one-dimensional inverse scattering theory for optical waveguide design, we have studied the relation between the poles of the transverse reflection coefficient and the modes in inhomogeneous dielectrics. By using a stratified medium model, it is shown that these poles of the reflection coefficient have a one-to-one correspondence to the discrete modes, which are the guided and leaky modes. The radiation modes have continuous real values of transverse wave numbers and are not represented by the poles of the reflection coefficient. Based on these results, applications of the Gel'fand-Levitan-Marchenko theory to optical waveguide synthesis with the rational function representation of the transverse reflection coefficient are discussed.

We developed an inversion algorithm referred to as the Renormalized Source-Type Integral Equation

approach. The objective of this method is to overcome some of the limitations and difficulties of the iterative Born technique. It recasts the inversion, which is nonlinear in nature, in terms of the solution of a set of linear equations; however, the final inversion equation is still nonlinear. The derived inversion equation is an exact equation which sums up the iterative Neuman (or Born) series in a closed form and; thus, is a valid representation even in the case when the Born series diverges; hence, the name *Renormalized* Source-Type Integral Equation (STIE) Approach. This renormalized STIE approach has been applied to underground soil moisture inversion and formation inversion in the borehole geometry.

Several recent papers discuss techniques for reducing the parasitic circuit capacitance of millimeter-wave planar air bridge type GaAs Schottky barrier diodes by completely etching away the semi-insulating material under the active region and transferring the device to a second carrier that is better suited, both electrically and mechanically, to the intended high frequency application. This technique and a similar procedure are being explored as a means of producing a semi-integrated subharmonically pumped two-diode mixer for use in 640 GHz. For this application, a planar antiparallel diode pair is incorporated into the center of a pair of low pass microstrip filters formed on an insulating GaAs substrate. An appealing substitute for millimeter and submillimeter wavelength applications is fused quartz which has an order of magnitude lower loss tangent, one-third the dielectric constant, and is much more mechanically rigid than GaAs. Using known techniques, it is possible to thin an entire GaAs wafer to a thickness on the order of 1-3 microns and then transfer the remaining active layer onto quartz. An interesting question that arises as a result of this procedure is the effect of the ultrathin GaAs layer on the filter characteristics. A three-dimensional finite difference time domain (FD-TD) method is used to calculate the response of the filter both with and without the GaAs layer.[8] It is shown that even a very thin layer of high dielectric constant material can have a noticeable effect on the filter response. The FD-TD analysis agreed fairly well with measured response and could be used for subsequent design.

In the last few years there has been an increasing interest in the interaction of electromagnetic fields with chiral media. A chiral medium is a subset of the wider class referred to as bianisotropic. Such media are characterized by linear constitutive relations that couple the electric and magnetic field vectors by three independent scalars. A rigorous formulation deals with the problem of radiation of electric and magnetic sources embedded in a layered lossless chiral medium. The fields are obtained in terms of dyadic Green's functions of electric or magnetic type represented in two-dimensional spectral-domain form. First, the spectral domain dyadic Green's functions of electric and magnetic types for an unbounded chiral medium are derived. The singular behavior of the various dyadic Green's functions in the source region is investigated and taken into account by extracting the delta function singularities. Finally, introducing global upward and downward reflection and transmission matrices, the dyadic Green's functions in any layer of the stratified chiral medium are derived.

The growth of epitaxial Fe film on GaAs was first demonstrated using molecular beam epitaxy. Deposition of such films by ion-beam sputtering was reported and their application to microwave filters has previously been discussed. A theoretical analysis is performed to the analysis of a tunable band-stop filter using epitaxial Fe films on [011] GaAs, in which the Fe layer is part of a microstrip line that runs along either a [100] or a [110] direction, the easy and hard directions of magnetization of the Fe film, respectively.[9] The analysis indicates that peak attenuation should occur at the ferromagnetic resonance (FMR) frequency and be proportional to the length of the microstrip line, and inversely proportional to the substrate thickness.

A rigorous approach to the problem of radiation of electric or magnetic sources in a stratified arbitrarily magnetized linear plasma.[10] The fields are obtained in terms of dyadic Green's functions of electric or magnetic type represented in the spec-

---

[8] P.H. Siegel, J.E. Oswald, R.G. Dengler, D.M. Sheen, and S.M. Ali, "Measured and Computed Performance of a Microstrip Filter Composed of Semi-Insulating GaAs on a Fused Quartz Substrate," *IEEE Microwave Guided Wave Lett.* 1(4): April (1991).

[9] V.S. Liau, T.W. Stacey, S. Ali, and E. Schloemann, "Tunable Band-Stop Filter Based on Epitaxial Fe Film on GaAs," *Proceedings of the 1991 IEEE MTT-S International Microwave Symposium,* Boston, Massachusetts, June 11-14, 1991, pp. 957-960.

[10] T.M. Habashy, S.M. Ali, J.A. Kong, and M.D. Grossi, "Dyadic Green's Functions in a Planar Stratified, Arbitrarily Magnetized Linear Plasma," *Radio Sci.* 26(3): 701-716 (1991).

tral domain. First, the dyadic Green's functions for an unbounded arbitrarily magnetized plasma is derived. The formulation is considerably simplified by using the KDB system of coordinates in conjunction with the Fourier transform. This leads to compact and explicit expressions for the dyadic Green's functions. The distributional singular behavior of the various dyadic Green's functions in the source region is investigated and taken into account by extracting the delta function singularities. Finally, the dyadic Green's function in any arbitrary layer is obtained in terms of appropriately defined global upward and downward reflection and transmission matrices. The field expressions for any arbitrary distribution of sources or linear antennas can be obtained by performing a convolution integral over the volume of the antenna weighted by the current density on the antenna.

The input impedance of a microstrip antenna consisting of two circular microstrip disks in a stacked configuration driven by a coaxial probe is investigated.[11] A rigorous analysis is performed using a dyadic Green's function formulation where the mixed boundary value problem is reduced to a set of coupled vector integral equations using the vector Hankel transform. Galerkin's method is employed in the spectral domain where two sets of disk current expansions are used. One set is based on the complete set of orthogonal modes of the magnetic cavity, and the other employs Chebyshev polynomials with the proper edge condition for disk currents. An additional term is added to the disk current expansion to properly model the current in the vicinity of the probe/disk junction. The input impedance of the stacked microstrip antenna including the probe self-impedance is calculated as a function of the layered parameters and the ratio of the two disk radii. Disk current distribution and radiation patterns are also presented. The calculated results are compared with experimental data and shown to be in good agreement.

A method for the analysis of complex frequency-dependent signal interconnections and planar circuits terminated with nonlinear load is investigated. The frequency-dependent portion of the system is first analyzed to get the scattering parameters and hence the impulse responses. Two different methods, depending on the complexity of the system, are used to get the scattering parameters: the three-dimensional finite-difference time-domain method and an analytical procedure. The nonlinear convolution equations governing the overall system are then derived and solved numerically. The transient responses of a pair of coupled dispersive microstrip lines, a corner discontinuity, and a microstrip switching circuit are presented.

We analysed three-dimensional (3-D) multichip module (MCM) interconnects. In this technology, the vertical interconnects consist of small conductor plated via holes etched by a photo lithography system. The via dimensions are in the same order as the microstrip and stripline widths to reduce the transmission line discontinuities. Two 3-D transitions are investigated: microstrip-via-stripline and microstrip-via-90 degree stripline. The finite-difference time-domain with nonuniform grid is applied to the analysis of these transitions. Electric field distribution and pulse propagation under the strip and the strip line are presented. The scattering parameters for various cases are calculated and compared. Geometrical effects such as different conductor extensions on top of the vias and different hole sizes in the reference plane are also investigated.

A method for calculation of the current distribution, resistance, inductance matrices for a system of coupled superconducting transmission lines having finite rectangular cross section is developed.[12] These calculations allow accurate characterization of both high-T_c and low-T_c superconducting transmission lines. For a single stripline geometry with finite ground planes, the current distribution, resistance, and kinetic inductance are calculated as a function of the penetration depth for various film thicknesses. These calculations are then used to determine the penetration depth for Nb, NbN, and $YBa_2Cu_3O_{7-x}$ superconducting thin films from the measured temperature dependance of the resonant frequency of a stripline resonator. The calculations are also used to convert measured temperature dependance of the quality factor to the intrinsic surface resistance as a function of temperature for an Nb stripline resonator.

The calculations of resistance and inductance are used for the determination of surface impedance of

---

[11] A.N. Tulintseff, S.M. Ali, and J.A. Kong, "Input Impedance of a Probe-Fed Stacked Circular Microstrip Antenna," *IEEE Trans. Antennas Propag.* 39(3): 381-390 (1991).

[12] D.M. Sheen, S.M. Ali, D.E. Oates, R.S. Withers, and J.A. Kong, "Current Distribution, Resistance, and Inductance for Superconducting Strip Transmission Lines," *IEEE Trans. Appl. Superconduct.* 1(2): 108-115 (1991); D.M. Sheen, S.M. Ali, D.E. Oates, R.S. Withers, and J.A. Kong, "Current Distribution in Superconducting Strip Transmission Lines," Proceedings of the 1991 IEEE MTT-S International Microwave Symposium, pp. 161-164, Boston, Massachusetts, June 11-14, 1991.

$YBa_2Cu_3O_{7-x}$ thin films using a stripline resonator.[13] The surface impedance as a function of frequency from 1.5 to 20 GHz, as function of temperature from 4K to the transition temperature (90 K), and as a function of the RF magnetic field from zero to 300 Oe, is obtained. At low temperatures the surface resistance of the films shows a very week dependance on the magnetic field up to 225 to 250 Oe. At 77 K, the surface resistance is proportional to the square of the field. The penetration depth shows a much weaker dependence on the field than does the surface resistance.

The Ginzburg-Landau (GL) theory is used to predict the nonlinear behavior in a superconducting stripline resonator as a function of input. A method for calculating the nonlinear inductance and the fractional change in the resonant frequency of a stripline resonator is presented. By solving the GL equations inside the superconducting strip, the spatial variation of the number density of superconducting electrons, and hence the spatial variation of the magnetic penetration depth are obtained for different values of input current. First, an infinite parallel plate transmission line is considered where the one-dimensional GL equations are solved. The two-dimensional case of stripline is then considered. Nonlinear inductances are calculated as functions of input current for different superconducting strip lines. Comparisons of the calculated resonance frequency shift with measurements for $YBa_2Cu_3O_{7-x}$ stripline resonators show excellent agreement.

A full-wave numerical analysis is applied to accurately characterize superconducting transmission lines embedded in a layered media. An integral equation formulation is developed by using a spectral domain Green's function for stratified media. Galerkin's method with roof top basis functions for the electric field distribution inside the superconductor is then employed to solve for the complex propagation constant. The thickness of the superconducting film is arbitrary in this analysis, and the formulation rigorously accounts for the anisotropy of the superconducting film. The propagation characteristics of a superconducting microstrip transmission line with a thin dielectric buffer layer are investigated. A superconducting stripline configuration with an air gap is also studied.

A full-wave analysis is applied to accurately characterize normal and superconducting coplanar strip lines (CPS) and coplanar waveguides (CPW). A volume integral equation formulation which rigorously considers the finite thickness, conductivity, and anisotropy of the strips, is developed. The phase and attenuation constants for copper CPS and CPW at 77 K and room temperatures are calculated and compared to experimental results obtained by short-pulse propagation measurements.

1.4 Remote Sensing of Earth Terrain

Sponsor

National Aeronautics and Space Administration
Grant NAGW-1617
Grant 958461

Project Staff

Professor Jin A. Kong, Dr. Robert T. Shin, Dr. Herng A. Yueh, Dr. Son V. Nghiem, Harold H. Lim, Robert G. Atkins, Hsiu C. Han, David V. Arnold, Murat E. Veysoglu, Chih-Chien Hsu, William W. Au, Joel T. Johnson, Pierre Coutu

A branching model is proposed for the remote sensing of vegetation. The frequency and angular response of a two-scale cylinder cluster are calculated to demonstrate the significance of vegetation architecture. The results indicate that it is necessary for theoretical remote sensing models to take into account the architecture of vegetation which plays an important role in determining the observed coherent effects. A two-scale branching model is implemented for soybeans with its internal structure and the resulting clustering effects considered. Furthermore, at the scale of soybean fields, the relative locations of soybean plants is described by a pair distribution function. The polarimetric backscattering coefficients are obtained in terms of the scattering properties of soybean plants and their pair distribution. Theoretical backscattering coefficients are evaluated using a hole-corrected pair distribution function. Backscattering coefficients calculated are in good agreement with extensive data collected from soybean fields. It is found that the hole-correction approximation, which prevents two soybean plants from overlaying each other, greatly improves the agreement between the model and these three data sets near normal incidence, by introducing destructive interference at small angles of incidence.

---

[13] D.E. Oates, C. Anderson, D.M. Sheen, and S.M. Ali, "Stripline Resonator Measurements of Z_sVSH_{rf} in $YBa_2Cu_3O_{7-x}$ Thin Films," *IEEE Trans. Microwave Theory Tech.* 39: 1522-1529 (1991).

In the past, when radiative transfer theory was applied to the modeling of vegetation, the average phase matrix of vegetation layer was approximated by an incoherent sum of the phase matrices of individual vegetation elements. In this research,[14] radiative transfer theory is applied to vegetation with clustered structures. To take into account vegetation structure in the radiative transfer theory, the phase matrix of a vegetation cluster is calculated by incorporating the phase interference of scattered fields from every component. Subsequently, the resulting phase matrix is used in the radiative transfer equations to evaluate the polarimetric backscattering coefficients from a layer of medium embedded with vegetation clusters. Theoretical results are illustrated for various kinds of vegetation clusters. It is found that the simulated polarization, frequency, and angular responses carry significant information regarding the structure of vegetation clusters and also agree with the signatures observed in measured multifrequency polarimetric synthetic aperture radar images.

We have also formulated the vector radiative transfer equation for passive microwave remote sensing of a vegetation canopy overlying a soil half-space and study the calculated brightness temperatures resulting from microwave thermal emission based on the first order iterative solution. A randomly distributed stem-leave model is employed to construct the phase matrix such that we can properly account for the effects of coherence and multiscale vegetation cluster.

For polarimetric remote sensing, geophysical media are modeled as layers containing randomly embedded scatterers. In media such as snow, ice, and vegetation canopy, scatterers can have various shapes, sizes, and permittivities that are significantly distinct from the background medium. The model studied in our research considers each type of the scatterers as a species which can takes on a shape, size, and complex permittivity different from other species. The effective permittivity of the random medium is derived under the strong permittivity fluctuation theory and polarimetric scattering coefficients are calculated for the layer configuration with the distorted Born approximation in the analytical wave theory which preserves the phase information. The multiple species in the random medium are considered as randomly oriented ellipsoids and described by multiple three-dimensional ellipsoidal correlation functions. The variances and correlation lengths of the correlation functions characterize the fluctuation strengths and the physical geometry of the scatterers, respectively. The result for the cross-polarized return σ_{hv} is non-zero even in the first order approximation. Due to the non-spherical shape and the random orientation of the scatterers, the correlation coefficient between the HH and VV returns has a magnitude different from unity and a small phase. The scattering coefficients are also used to calculate the Mueller matrix for synthesis of polarization signatures. The copolarized signature of the random medium has a rather straight distortion track and a recognizable pedestal.

The concept of polarimetry in active remote sensing has been extended to passive remote sensing.[15] The potential use of the third and fourth Stokes parameters U and V, which play an important role in polarimetric active remote sensing, is demonstrated for passive remote sensing. It is shown that by the use of the reciprocity principle the polarimetric parameters of passive remote sensing can be obtained through the solution of the associated direct scattering problem. These ideas are applied to study polarimetric passive remote sensing of periodic surfaces. The solution of the direct scattering problem is obtained by an integral equation formulation which involves evaluation of periodic Green's functions and normal derivative of those on the surface. Rapid evaluation of the slowly convergent series associated with these functions is observed to be critical for the feasibility of the method. New formulas, which are rapidly convergent, are derived for the calculation of these series. The study has shown that the brightness temperature of the Stokes parameter U can be significant in passive remote sensing. Values as high as 50 K are observed for certain configurations.

To verify our theory, a triangular corrugation pattern with height h = 2.5 cm and period p = 5 cm is made on the sandy soil surface covering 23 periods by length l = 160 cm and thickness d = 12.7 cm. A radiometer of 15° beam width oper-

---

[14] C.C. Hsu, S.H. Yueh, H.C. Han, R.T. Shin, and J.A. Kong, "Radiative Transfer Modeling of Vegetation Clusters," *Proceedings of the Progress in Electromagnetics Research Symposium*, p. 609, Boston, Massachusetts, July 1-5, 1991.

[15] S.V. Nghiem, M.E. Veysoglu, J.A. Kong, R.T. Shin, K. O'Neill, and A.W. Lohanick, "Polarimetric Passive Remote Sensing of a Periodic Soil Surface: Microwave Measurements and Analysis," *J. Electromag. Waves Appl.* 5(9): 997-1005 (1991); M.E. Veysoglu, H.A. Yueh, R.T. Shin, and J.A. Kong, "Polarimetric Passive Remote Sensing of Periodic Surfaces," *J. Electromag. Waves Appl.* 5(3): 267-280 (1991).

ating at 10 GHz is used in the experiment. The radiometer is mounted on a tripod at an elevation of 1.8 m height and directed toward the soil surface along the look direction determined by azimuthal angle ϕ and polar angle θ. Polarimetric brightness temperatures T_{Bh}, T_{Bv}, and T_{Bp} are measured respectively with horizontal, vertical, and 45° polarization orientations for $\theta = 20°, 30°$ and ϕ from 0° to 90°. From the measured temperatures, the third Stokes brightness temperatures U_B are obtained. Absolute values as high as 30-40 K of the third Stokes brightness temperatures are observed. A theoretical analysis of the data indicates that the high values of U_B are caused by the azimuthal asymmetry on the remotely sensed soil surface. It is also observed from the experiment that as T_{Bh} decreases, T_{Bv} increases, T_{Bp} decreases to a minimum at $\phi = 45°$ and then increases as ϕ takes on the increased values. For U_B, the trend is similar to that of T_{Bp}. These general trends are supported by our theoretical predictions of the polarimetric brightness temperatures.

In most of the scattering models, volume scattering and surface scattering effects have been investigated separately. We have studied the first order iterative solution to the vector radiative transfer equations for a two-layer medium with a diffuse top boundary and an irregular bottom boundary of Gaussian roughness.[16] The geometrical optics approach with shadowing correction are used in formulating the boundary conditions. We applied our formula with a phase matrix for randomly oriented spheroidal discrete scatterers to calculate the backscattering coefficients from soybean field in different growing stages and compare the results with the experimental measurements. Good agreement has been achieved for both the co-polarized and the cross-polarized data. It is observed that the presence of the rough surface can significantly enhance the backscattering at small incident angles and the levels of the cross-polarized return.

As an electromagnetic wave propagates through a random scattering medium, such as a forest, its energy is attenuated, and random phase fluctuations are induced. The magnitude of the random phase fluctuations induced is important in estimating how well a Synthetic Aperture Radar (SAR) can image objects within the scattering medium. The two-layer random medium model, consisting of a scattering layer between free space and ground, is used to calculate the variance of the phase fluctuations induced between a transmitter located above the random medium and a receiver located below the random medium.[17] The scattering properties of the random medium are characterized by a correlation function of the random permittivity fluctuations. The effective permittivity of the random medium is first calculated using the strong fluctuation theory, which accounts for large permittivity fluctuations of the scatterers. The distorted Born approximation is used to calculate the first-order scattered field. A perturbation series for the phase of the received field is then introduced, and the variance of the phase fluctuations is solved to first order in the permittivity fluctuations. The variance of the phase fluctuations is also calculated assuming that the transmitter and receiver are in the paraxial limit of the random medium, which allows an analytic solution to be obtained. The effects studied are the dependence of the variance of the phase fluctuations on receiver location in lossy and lossless regions, medium thickness, correlation length and fractional volume of scatterers, depolarization of the incident wave, ground layer permittivity, angle of incidence, and polarization.

1.5 SAR Image Interpretation and Simulation

Sponsors

National Aeronautics and Space Administration
Grant NAGW-1272
Grant NAGW-1617
Grant 958461
U.S. Army Corp of Engineers
Contract DACA39-87-K-0022
U.S. Navy - Office of Naval Research
Grant N00014-89-J-1107

Project Staff

Professor Jin Au Kong, Dr. Robert T. Shin, Dr. Ying-Ching E. Yang, Dr. Herng A. Yueh, Dr. Son V. Nghiem, Harold H. Lim, Robert G. Atkins, David V. Arnold, Hsiu C. Han, M. Ali Tassoudji, Murat E. Veysoglu, Yoshihisa Hara, Chih-Chien Hsu, William W. Au, Joel T. Johnson, Pierre Coutu

---

[16] H.C. Han, J.A. Kong, S.V. Nghiem, and T. Le Toan, "Analytical Solution of the Vector Radiative Transfer Equation with Rough Surface Boundary Condition," *Proceedings of Progress in Electromagnetics Research Symposium*, p. 536, Boston, Massachusetts, July 1-5 (1991).

[17] J. Fleischman, S. Ayasli, R.T. Shin, N.C. Chu, H.A. Yueh, and S.V. Nghiem, "Covariance of Phase and Amplitude Fluctuations of Electromagnetic Waves Propagating Through a Random Medium," *Proceedings of the Progress in Electromagnetics Research Symposium*, p. 617, Boston, Massachusetts, July 1-5 (1991).

Classification of terrain cover using polarimetric radar is an area of considerable current interest and research. A number of methods have been developed to classify ground terrain types from fully polarimetric synthetic aperture radar (SAR) images, and these techniques are often grouped into supervised and unsupervised approaches. Supervised methods, including both conventional Maximum Likelihood (ML) and more recent Multilayer Perceptron classifiers, have yielded higher accuracy than unsupervised techniques, but suffer from the need for human interaction to predetermine classes and training regions. In contrast, unsupervised methods determine classes automatically, but generally show limited ability to accurately divide terrain into natural classes. In this research, a new terrain classification technique is introduced, utilizing unsupervised neural networks to provide automatic classification, but employing an iterative algorithm which overcomes the poor accuracy of other unsupervised techniques.

Several types of unsupervised neural networks are first applied to the classification of SAR images,[18] and the results are compared with those of more conventional unsupervised methods. Neural network approaches include Adaptive Resonance Theory (ART), Learning Vector Quantization (LVQ), and Kohonen's self-organizing feature map. Conventional classifiers utilized are the migrating means clustering algorithm and the K-means clustering method. With both neural network and conventional classifiers, preprocessing is performed to reduce speckle noise and to stabilize the training process. Results show that LVQ is the best of the neural network techniques and that this method outperforms all of the conventional unsupervised classifiers. The accuracy of even the LVQ technique, however, is seen to remain below that of supervised methods.

To overcome this poor accuracy, an iterative algorithm is proposed in which the SAR image is reclassified using a Maximum Likelihood (ML) classifier. Training of the ML classifier is performed using a training data set first classified by the above unsupervised method, thus requiring no human intervention and preserving the unsupervised nature of the overall classification scheme. The process is then repeated iteratively, training a second ML classifier using data classified by the first. It is shown that this algorithm converges rapidly and significantly improves classification accuracy. Performance after convergence is seen to be comparable to that obtained with a supervised ML classifier, while maintaining the advantages of an unsupervised technique.

The new unsupervised and iterative algorithm developed in this research is applied to polarimetric SAR images of San Francisco and Beaufort sea ice acquired by the Jet Propulsion Laboratory. The results obtained for this imagery using the new algorithm are compared with the results obtained with other techniques and also with those obtained with single-feature classification. It is found in each case that the new fully polarimetric unsupervised algorithm yields classified images which compare closely with those obtained from optimally chosen, supervised algorithms.

A multivariate K-distribution is proposed to model the statistics of fully polarimetric radar returns from earth terrain.[19] Numerous experimental data have shown that the terrain radar clutter statistics is non-Gaussian, and an accurate statistical model for the polarimetric radar clutter is needed for various applications. In the terrain cover classification using the synthetic aperture radar (SAR) images, the application of the K-distribution model will provide better performance than the conventional Gaussian classifier. In the multivariate K-distribution model, the correlated polarizations of backscattered radar returns are characterized by a covariance matrix, and the clustering behavior of terrain scatterers is described by a parameter α. In the limit the parameter α approaches infinity, the multivariate K-distribution reduces to the multivariate Gaussian distribution. With the polarimetric covariance matrix and the α parameter extracted from the measurements, it is shown that the multivariate K-distribution model is well supported by the simultaneously measured C-, L- and P-band polarimetric SAR images provided by the Jet Propulsion Laboratory. It is also found that the α parameter appears to decrease from C- to P-band for forests, clear-cut areas in forests, and desert areas. The polarimetric covariance matrices of the various earth terrain media can be interpreted with the theoretical models for model validation and development of other classification algorithms. Also, the frequency-dependence of

[18] R. Kwok, Y. Hara, R.G. Atkins, S.H. Yueh, R.T. Shin, and J.A. Kong, "Application of Neural Networks to Sea Ice Classification Using Polarimetric SAR Images," International Geoscience and Remote Sensing Symposium (IGARSS '91), Helsinki University of Technology, Espoo, Finland, June 3-6, 1991.

[19] H.A. Yueh, J.A. Kong, J.K. Jao, R.T. Shin, H.A. Zebker, and T. Le Toan, "K-Distribution and Multi-Frequency Polarimetric Terrain Radar Clutter," *J. Electromag. Waves Appl.* 5(1): 1-15 (1991).

the α parameter is being investigated for various other radar clutter.

Polarimetric calibration algorithms using combinations of point targets and reciprocal distributed targets are developed.[20] From the reciprocity relations of distributed targets, an equivalent point target response is derived. Then the problem of polarimetric calibration using two-point targets and one distributed target reduces to that using three-point targets, which has been solved before. For calibration using one-point target and one reciprocal distributed target, two cases are analyzed with the point target being a trihedral reflector or a polarimetric active radar calibrator (PARC). For both cases, the general solutions of the system distortion matrices are written as a product of a particular solution and a matrix with one free parameter. For the trihedral-reflector case, this free parameter is determined by assuming azimuthal symmetry for the distributed target. For the PARC case, knowledge of one ratio of two covariance matrix elements of the distributed target is required to solve for the free parameter. Numerical results are simulated to demonstrate the usefulness of the algorithms developed.

1.5.1 Publications and Meeting Papers

Chan, C.H., S.H. Lou, L. Tsang, and J.A. Kong. "Electromagnetic Scattering of Waves by Random Rough Surface: a Finite-Difference Time-Domain Approach." *Microwave Opt. Tech. Lett.* 4(9): 355-359 (1991).

Fleischman, J., S. Ayasli, R.T. Shin, N.C. Chu, H.A. Yueh, and S.V. Nghiem. "Covariance of Phase and Amplitude Fluctuations of Electromagnetic Waves Propagating Through a Random Medium." *Proceedings of the Progress in Electromagnetics Research Symposium,* p. 617, Boston, Massachusetts, July 1-5, 1991.

Habashy, T.M., S.M. Ali, J.A. Kong, and M.D. Grossi. "Dyadic Green's Functions in a Planar Stratified, Arbitrarily Magnetized Linear Plasma." *Radio Sci.* 26(3): 701-716 (1991).

Han, H.C., J.A. Kong, S.V. Nghiem, and T. Le Toan. "Analytical Solution of the Vector Radiative Transfer Equation with Rough Surface Boundary Condition." *Proceedings of the Progress in Electromagnetics Research Symposium,* p. 536, Boston, Massachusetts, July 1-5 (1991).

Hsu, C.C., S.H. Yueh, H.C. Han, R.T. Shin, and J.A. Kong. "Radiative Transfer Modeling of Vegetation Clusters," *Proceedings of the Progress in Electromagnetics Research Symposium,* p. 609, Boston, Massachusetts, July 1-5, 1991.

Kwok, R., Y. Hara, R.G. Atkins, S.H. Yueh, R.T. Shin, and J.A. Kong. "Application of Neural Networks to Sea Ice Classification Using Polarimetric SAR Images." International Geoscience and Remote Sensing Symposium (IGARSS '91), Helsinki University of Technology, Espoo, Finland, June 3-6, 1991.

Le Toan, T., S.V. Nghiem, J.A. Kong, and H.C. Han. "Application of Random Medium Model to Remote Sensing of Vegetation." International Geoscience and Remote Sensing Symposium (IGARSS '91), Helsinki University of Technology, Espoo, Finland, June 3-6, 1991.

Lee, C.F., K. Li, S.Y. Poh, R.T. Shin, and J.A. Kong. "Electromagnetic Radiation from a VLSI Package and Heatskin Configuration." IEEE 1991 International Symposium on Electromagnetic Compatibility, Hyatt Cherry Hill, Cherry Hill, New Jersey, pp. 393-398, August 12-16, 1991.

Li, K., M.A. Tassoudji, R.T. Shin, and J.A. Kong. "Simulation of Electromagnetic Phenomema Using a Finite Difference-Time Domain Technique." *Proceedings of the 7th Annual Review of Progress in Applied Computational Electromagnetics,* Naval Postgraduate School, Monterey, California, pp. 38-55, March 18-22, 1991.

Liau, V.S., T.W. Stacey, S. Ali, and E. Schloemann. "Tunable Band-Stop Filter Based on Epitaxial Fe Film on GaAs." *Proceedings of the 1991 IEEE MTT-S International Microwave Symposium,* Boston, Massachusetts, June 11-14, 1991, pp. 957-960.

Melville, W.K., D.V. Arnold, E. Lamarre, J.A. Kong, R.H. Stewart, and W.C. Keller. "Direct Measurements of EM Bias at Ku and C Bands."

[20] H.A. Yueh, J.A. Kong, and R.T. Shin, "External Calibration of Polarimetric Radars Using Point and Distributed Targets," *Proceedings of the Third Airborne Synthetic Aperture Radar (AIRSAR) Workshop,* Jet Propulsion Laboratory, Pasadena, California, May 23-24, 1991.

Proceedings of the Progress in Electromagnetics Research Symposium, p. 168, Boston, Massachusetts, July 1-5, 1991.

Moldoveanu, M.C., and A.K. Jordan. "Theory of Non-Dispersive Electromagnetic Pulses: the Nonlinear Dirac Equation." *Proceedings of the Progress in Electromagnetics Research Symposium,* p. 676, Boston, Massachusetts, July 1-5 (1991).

Nghiem, S.V., M.E. Veysoglu, J.A. Kong, R.T. Shin, K. O'Neill, and A.W. Lohanick. "Polarimetric Passive Remote Sensing of a Periodic Soil Surface: Microwave Measurements and Analysis." *J. Electromag. Waves Applicat.* 5(9): 997-1005 (1991).

Oates, D.E., C. Anderson, D.M. Sheen, and S.M. Ali. "Stripline Resonator Measurements of Z_sVSH_{rf} in $YBa_2Cu_3O_{7-x}$ Thin Films." *IEEE Trans. Microwave Theory Tech.* 39: 1522-1529 (1991).

Schattenburg, M.L., K. Li, R.T. Shin, J.A. Kong, D.B. Olster, and H.I. Smith. "Electromagnetic Calculation of Soft X-Ray Diffraction from 01.μm-Scale Gold Structures." *J. Vacuum Sci. Tech.,* as part of the *Proceedings of the 35th International Symposium on Electron, Ion, and Photon Beams,* paper E84, Seattle, Washington, May 28-31, 1991.

Schattenburg, M.L., K. Li, R.T. Shin, J.A. Kong, and H.I. Smith. "Electromagnetic Calculation of Soft X-Ray Diffraction from Nanometer-Scale Gold Structures." *35th International Symposium on Electron, Ion, and Photon Beams,* Seattle, Washington, May 28-31, 1991.

Sheen, D.M., S.M. Ali, D.E. Oates, R.S. Withers, and J.A. Kong. "Current Distribution, Resistance, and Inductance for Superconducting Strip Transmission Lines." *IEEE Trans. Appl. Superconduct.* 1(2): 108-115 (1991).

Sheen, D.M., S.M. Ali, D.E. Oates, R.S. Withers, and J.A. Kong. "Current Distribution in Superconducting Strip Transmission Lines." *Proceedings of the 1991 IEEE MTT-S International Microwave Symposium,* pp. 161-164, Boston, Massachusetts, June 11-14, 1991.

Siegel, P.H., J.E. Oswald, R.G. Dengler, D.M. Sheen, and S.M. Ali. "Measured and Computed Performance of a Microstrip Filter Composed of Semi-Insulating GaAs on a Fused Quartz Substrate." *IEEE Microwave Guided Wave Lett.* 1(4): 78-80 (1991).

Taherian, M.R., D.J. Yuen, T.M. Habashy, and J.A. Kong. "A Coaxial-Circular Waveguide for Dielectric Measurement." *IEEE Trans. Geosci. Remote Sensing* 29(2): 321-330 (1991).

Tassoudji, M.A. C.C. Hsu, Y.E. Yang, R.T. Shin, J.A. Kong, and G. Markey. "Computer-Aided Spectrum Engineering Procedure for Instrument Landing System (ILS) and Microwave Landing System (MLS)." *Proceedings of the Progress in Electromagnetics Research Symposium,* p. 13, Boston, Massachusetts, July 1-5, 1991.

Tsuk, M.J., and J.A. Kong. "A Hybrid Method for the Calculation of the Resistance and Inductance of Transmission Lines with Arbitrary Cross-Sections." *IEEE Trans. Microwave Theory Tech.* 39(8): 1338-1347 (1991).

Tulintseff, A.N., S.M. Ali, and J.A. Kong. "Input Impedance of a Probe-Fed Stacked Circular Microstrip Antenna." *IEEE Trans. Antennas Propag.* 39(3): 381-390 (1991).

Veysoglu, M.E., H.A. Yueh, R.T. Shin, and J.A. Kong. "Polarimetric Passive Remote Sensing of Periodic Surfaces." *J. Electromag. Waves Appl.* 5(3): 267-280 (1991).

Yang, Y.E., J.A. Kong, R.T. Shin, B.F. Burke, E.M. Geyer, R.P. Arnold, and E.A. Spitzer. "Spectrum Management for Precision Landing Systems: Instrument Landing Systems (ILS) and Microwave Landing System (MLS)." *Proceedings of the Progress in Electromagnetics Research Symposium,* p. 8, Boston, Massachusetts, July 1-5, 1991.

Yueh, H.A., J.A. Kong, J.K. Jao, R.T. Shin, H.A. Zebker, and T. Le Toan. "K-Distribution and Multi-Frequency Polarimetric Terrain Radar Clutter." *J. Electromag. Waves Appl.* 5(1): 1-15 (1991).

Yueh, H.A., J.A. Kong, and R.T. Shin. "External Calibration of Polarimetric Radars Using Point and Distributed Targets." *Proceedings of the Third Airborne Synthetic Aperture Radar (AIRSAR) Workshop,* Jet Propulsion Laboratory, Pasadena, California, May 23-24, 1991.

Section 4 Radio Astronomy

Chapter 1 Radio Astronomy

Chapter 1. Radio Astronomy

Academic and Research Staff

Professor Bernard F. Burke, Professor David H. Staelin, Professor Jacqueline N. Hewitt, Dr. Philip W. Rosenkranz, John W. Barrett

Visiting Scientists and Research Affiliates

Dr. Michael Shao,[1] Dr. Alan Wright[2]

Graduate Students

Ashraf S. Alkhairy, Edmund Chalom, Grace H. Chen, Kevin G. Christian, Samuel R. Conner, John T. Delisle, John D. Ellithorpe, Paul W. Fieguth, André B. Fletcher, Eric J. Gaidos, Mark R. Griffith, Michael B. Heflin, Lori K. Herold, Michael S. Ho, Charles A. Katz, Joseph Lehár, Darren L. Leigh, Michael J. Schwartz

Undergraduate Students

Michael C. Petro, Jo-Ana Quirch

Technical and Support Staff

Wendy E. Hunter, Clare F. Smith

1.1 Extragalactic Radio Source Studies

Sponsor

National Science Foundation
Grant AST 88-19848
Grant AST 90-22501

Project Staff

Professor Bernard F. Burke, Professor Jacqueline N. Hewitt, John W. Barrett, Dr. Michael Shao, Dr. Alan Wright, Eric J. Gaidos, Samuel R. Conner, André B. Fletcher, Mark R. Griffith, Michael B. Heflin, Lori K. Herold, Joseph Lehár, Michael C. Petro, Jo-Ana Quirch

1.1.1 Measurement of the Hubble Constant

A definitive measurement of the time delay difference between quasar images in the gravitational lens system 0957+561 has been carried out. The time delay, reported provisionally in *RLE Progress Report Number 133,* is 513±40 days and leads to an evaluation of the Hubble Constant.[3] The apparent discrepancy with optical determination by other authors has been resolved in favor of the radio data. A complete account of the data has also been published.[4] The derived value of the Hubble Constant depends upon lens model and mean matter density in the universe. Our derived values fall between 42 and 69 km/sec/Mpc. The method is completely independent of traditional techniques, but the range of values is consistent with the optical determinations. Agreement of the various methods gives us some confidence that the scale of the universe is known to within a factor of two. Similar measurements of other gravitationally lensed quasars will lead to a better determination

---

[1] Jet Propulsion Laboratory, California Institute of Technology, Pasadena, California.

[2] Australian Telescope National Facility, Parkes Radio Observatory (CSIRO), Australia.

[3] Roberts, J. Lehár, J.N. Hewitt, and B.F. Burke, *Nature* 352: 43 (1991).

[4] J. Lehár et al., *Astrophys. J.* 384: 453-466 (1992); see also Rybicki, Press, and J.N. Hewitt, *Astrophys. J.* 385: 404, 416 (1992).

of the scale of the universe, as inferred from the Hubble constant.

1.1.2 Gravitational Lens Studies

A new example of an "Einstein ring," the source MG1549+3047, was discovered by Lehár in the course of his Ph.D. dissertation work at MIT.[5] The radio map is illustrated in figure 1. An Einstein ring is produced when a background source is well-aligned with a foreground symmetrical mass distribution that deflects the rays to form a ring-like image about the lens. Three of the five known examples of Einstein rings have been discovered in the course of National Science Foundation research under this grant and those preceding it. The ring phenomenon is not rare and leads to interesting astrophysical conclusions about distribution of matter in the universe. The size of the ring determines mean surface density of matter in the foreground lensing galaxy. All matter within the ring contributes to the observed image whether it is in the form of stars or "dark matter." For two of the three rings, system parameters are completely measurable, and mass-to-light ratio can be determined completely. MG1654+1346 and MG1549+3047 have values of M/L^B equal to 15.9 $\pm$2.3 and 16$\pm$3. These are probably the best values ever determined for elliptical galaxies.

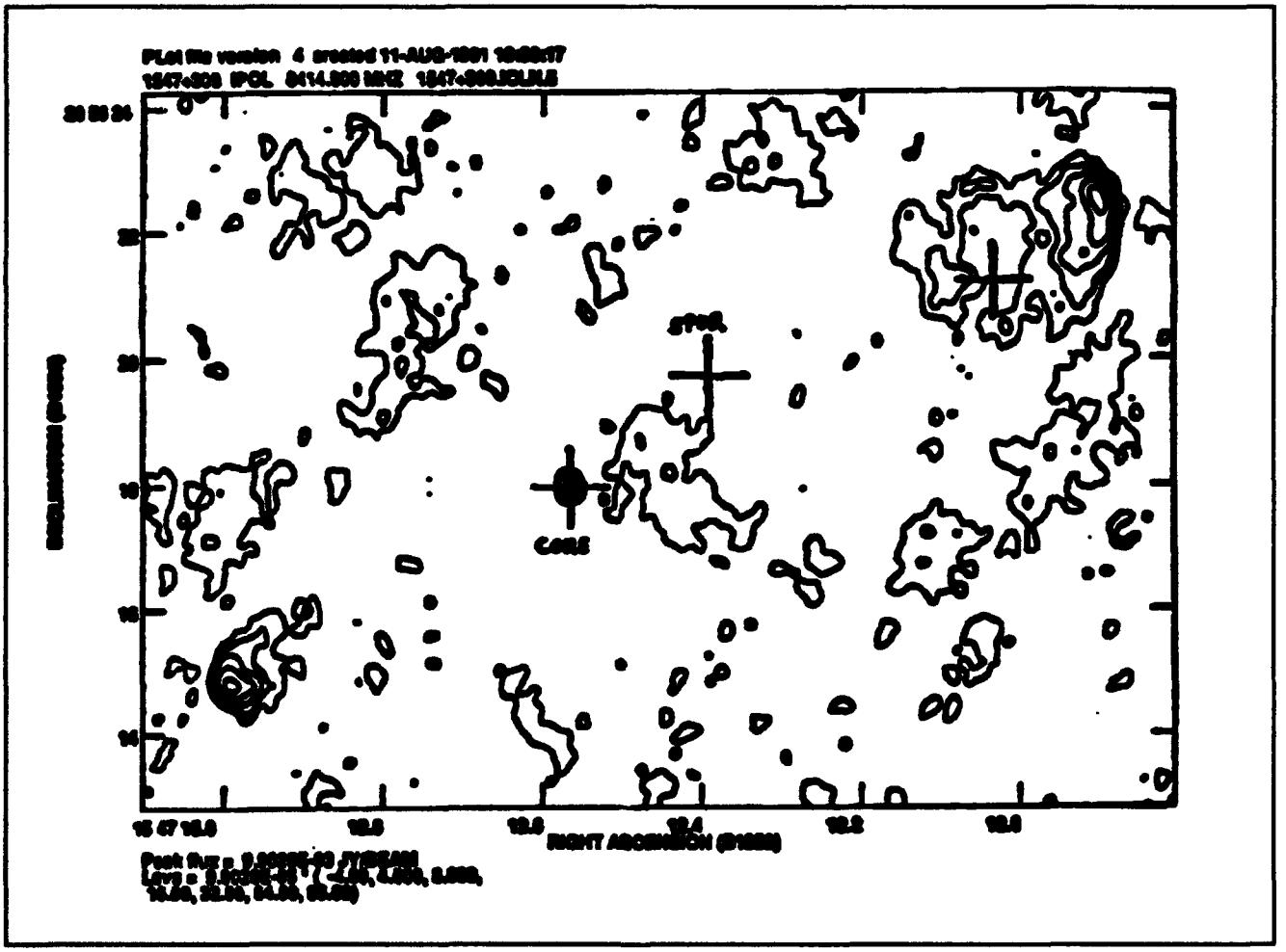


Figure 1. VLA Map of MG1549+3047. There is a bright galaxy at the position of the upper right hand cross, and the ring is roughly centered on the galaxy. The radio source is of the core-double type, and one lobe lies behind the lensing galaxy.

[5] J. Lehár, Ph.D. diss., Dept. of Phys., MIT, 1991.

1.1.3 Search for New Lenses

The systematic lens search project, carried out jointly with Professor Jacqueline Hewitt of MIT and Professor Edward Turner of Princeton University, is continuing. The Very Large Array (VLA) mapping of MG sources is the raw material, and the 4000 maps obtained in previous years have been used for the search. A new complex of Sun work stations, operated jointly with Professor Hewitt, is producing a final map catalog, with each map being cleaned and self-calibrated. S. Conner is coordinating the work. An additional 2000 sources were mapped by the VLA, and data reduction is progressing. J. Lehár's 1991 thesis[6] described the first 500 of these sources, from which his new Einstein ring was later discovered. A closely-related class of gravitational lens has been recognized for some time: quadruple sources. These have essentially the same morphology as the rings, and similarly, the characteristics of the foreground galaxy can be studied. Professor Hewitt has used the material from the MG survey to demonstrate that the source MG0414+0354 belongs to the same class. Our estimate that approximately one in 400 MG sources is measurably lensed continues to be valid.

1.1.4 The Parkes-MIT-NRAO (PMN) Southern Hemisphere Survey

During 1990, a completely new radio survey of the Southern Hemisphere was completed, using the Parkes Telescope, the National Radio Astronomy Observatory (NRAO) multifeed 6-cm receiver, and carried out under the principal leadership of Mark Griffith, an MIT graduate student, with the vital collaboration of Dr. Alan Wright of CSIRO. The first preliminary results were illustrated in the previous *RLE Progress Report Number 133.* A far more complete survey is now in the final stages of preparation, and an example of the radio source distribution for the Southern Hemisphere is illustrated in figure 2. The survey will increase the number of known Southern Hemisphere radio sources by an order of magnitude. The observations have been processed by the MIT Cray computer, and the completed survey should be finished by early summer 1992.

At the same time, we are planning to search this body of data for new examples of lensing. The southernmost sources would have to be studied by the Australian telescope, but there is a large part of the southern sky which is accessible to the VLA. We have carried out an initial investigation of over 1000 sources from the PMN survey using the VLA in the A configuration at X-band. The observations were carried out in the summer of 1991 and are now being reduced.

1.1.5 Search for Highly Redshifted, Pregalactic Hydrogen Clouds

Hydrogen complexes, located at great distances and from an earlier age when galaxies and clusters of galaxies had not been formed, may be observable. This was a project of speculative nature, but the Arecibo Observatory was interested in pursuing the work which could be carried out simultaneously along with its other observations. Initial calculations are encouraging. Fortunately, we have found that the multichannel receiver that is needed for this task can be copied from an existing design by Professor Paul Horowitz at Harvard University. We have proposed that a prototype should be built and tested at Arecibo and that construction of a full-scale receiver should follow. The 1.5 meter band, corresponding to a redshift of 6, would be an optimum area to search. The proposal has gained credibility from Uson's recent announcement that a large hydrogen complex has been discovered by the VLA at a redshift of 3.3.

[6] J. Lehár, Ph.D. diss., Dept. of Phys., MIT, 1991.

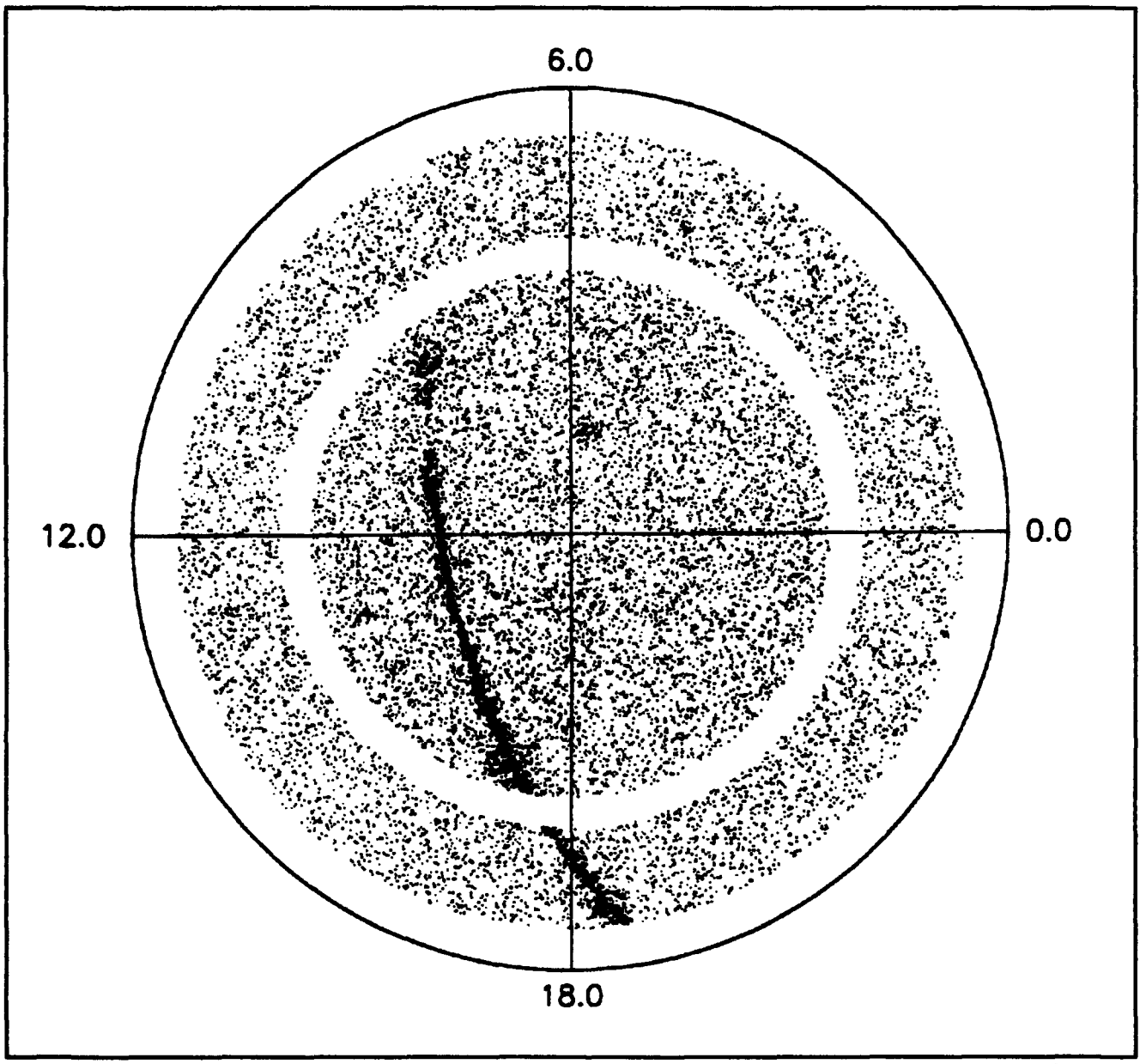


Figure 2. A map of 18,524 sources in the Southern Sky. The plane of the Milky Way is clearly visible. The large Magellanic cloud is the small cluster of sources in the upper right-hand quadrant. The empty circle marks the zenith strip as seen at the Parkes Telescope, and these observations have not yet been analyzed.

1.2 Studies of Gravitational Lenses

Sponsors

Alfred P. Sloan Fellowship
National Science Foundation
Presidential Young Investigator Award

Project Staff

Professor Jacqueline N. Hewitt, Grace H. Chen, Charles A. Katz

Gravitational lenses provide radio astronomers with the opportunity to examine many long-standing problems in astrophysics. For example, through modeling the light-bending effects of a gravitational field, one can infer the quantity and distribution of matter responsible for gravitational lensing. Because dark matter in the universe is not well understood, these independent measurements are proving to be helpful. However, the robustness of this technique is strongly dependent on the degree to which one can reconstruct the mass distribution reliably. Reliable reconstruction is possible if sufficient structure in the lensed image can be measured, and it is facilitated if the mass distribution is highly symmetric. These conditions are met by several gravitational lens systems including MG1131+0456 and MG0414+0534, both radio sources whose lensed properties were discovered in the VLA gravitational lens search described in Section 1.1.3.

An Einstein ring is a particularly symmetric case of gravitational lensing in which the background source is imaged into a ring. MG1131+0456 was the first "Einstein ring" discovered.[7] In MG1131+0456, an intrinsically normal radio source consisting of two radio lobes and a compact object, possibly the active galactic nucleus, is lensed in such a way that one of its lobes is imaged into a ring, and the compact object is doubly imaged. We are continuing our analysis of this object by measuring its polarization and spectral properties. Figure 3 shows a radio image (8 GHz frequency) in which complex polarization structure is evident. We will use these data to reconstruct the gravitational potential that is responsible for imaging.

MG0414+0534 consists of multiple images of a background object, with a configuration that is typical of an elliptically symmetric gravitational lens. Data collected at optical and radio wavelengths provide compelling evidence that the source is lensed and, furthermore, that the background source appears to have unusual properties.[8] Figure 4 shows an 8 GHz radio image that demonstrates that there are four components. Previously collected data with lower resolution could only prove unambiguously the presence of three components. Models of gravitational lenses predict that four components should be present, and this prediction is supported by the image shown in figure 4.

The radio images presented here were computed from data acquired with the National Radio Astronomy Observatory's Very Large Array telescope.

1.3 Radio Interferometry of Nearby dMe Stars

Sponsors

National Aeronautics and Space Administration
Grant NAGW-2310
David and Lucile Packard Fellowship

Project Staff

Professor Jacqueline N. Hewitt, John D. Ellithorpe

dMe stars are dwarf M stars that show evidence of surface activity. For some time, they have been known to flare strongly at optical and radio wavelengths, and, more recently, it has been demonstrated that many dMe stars exhibit low-level quiescent emission that is detectable in Very Long Baseline Interferometry (VLBI). The detection of dMe stars on VLBI baselines makes possible measurement of the position of these stars with high precision, and astrometric detection of planetary companions may be feasible. The astrometric monitoring program was continued with second-epoch measurements of the dMe stars AD Leo, EV Lac, and YZ CMi.

---

[7] J.N. Hewitt, E.L. Turner, D.P. Schneider, B.F. Burke, G.I. Langston, and C.R. Lawrence, *Nature* 333: 537 (1988).

[8] J.N. Hewitt, E.L. Turner, C.R. Lawrence, D.P. Schneider, and J.P. Brody, *Astronom. J.*, forthcoming.

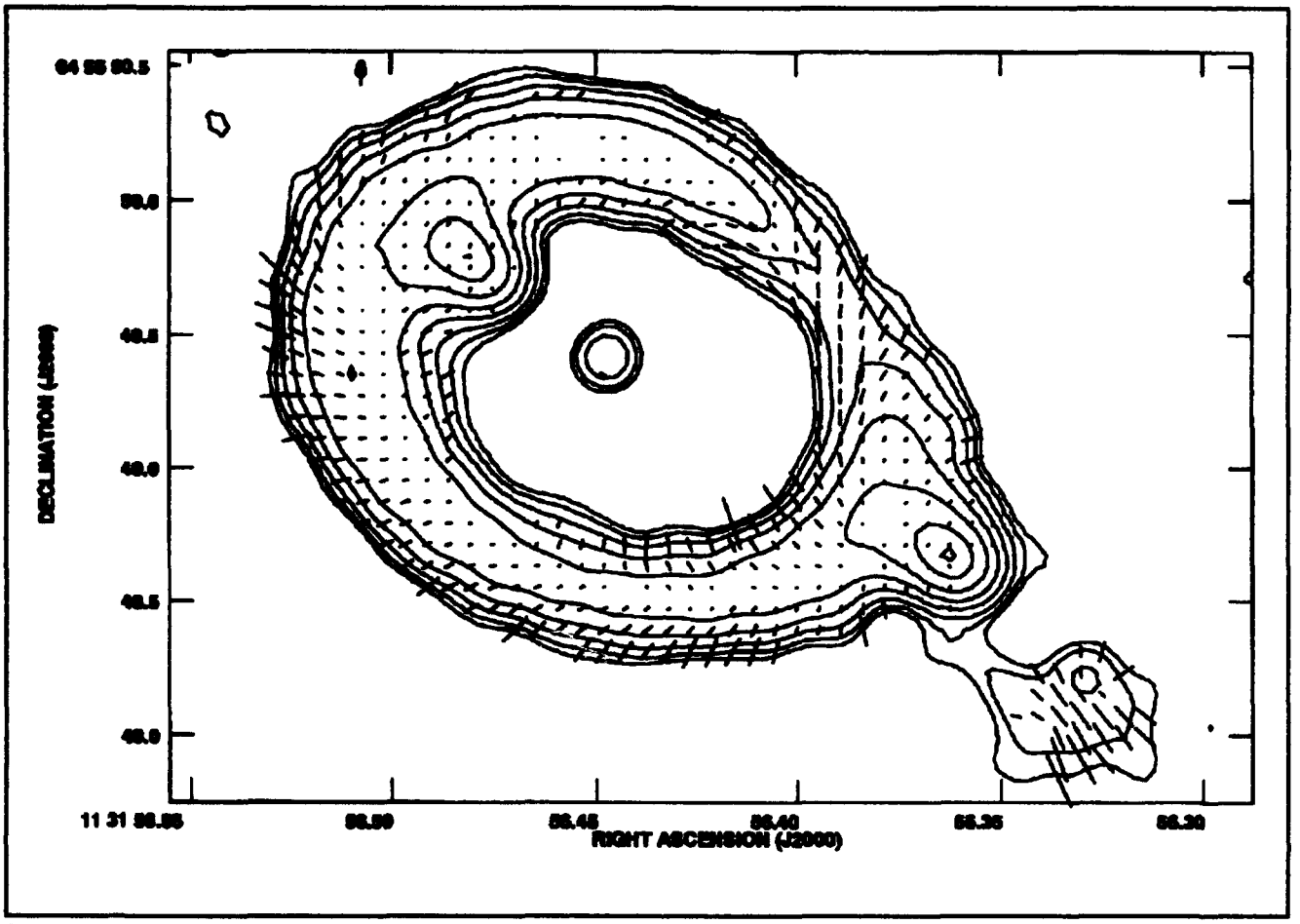


Figure 3. 8 GHz radio image of the Einstein ring gravitational lens MG1131+0456. The contours trace the surface brightness of the source, and the line segments represent its linear polarization. The length of each line segment is proportional to the percentage polarization, and the position angle of each line segment gives the orientation of the electric field vector.

1.4 Tiros-N Satellite Microwave Sounder

Sponsor

SM Systems and Research Corporation

Project Staff

Professor David H. Staelin, Dr. Philip W. Rosenkranz, Michael S. Ho

This project provides scientific support to the National Oceanic and Atmospheric Administration (NOAA) for its Advanced Microwave Sounding Unit (AMSU). The AMSU is scheduled to be launched on NOAA's polar-orbiting weather satellites in the mid-1990s and also on follow-on satellites. In our research effort, we emphasize development of atmospheric transmittance algorithms, estimates of surface emissivity and precipitation, and issues related to instrument design and specification.

A study of measurements made by an existing satellite radiometer, the Special Sensor Microwave Imager (SSM/I), has yielded information on the sensitivity of ocean surface emissivity to wind stress at 19 and 85 GHz.[9] This information will be used to design algorithms for the AMSU, which has an 89-GHz channel.

Measurements made by H.J. Liebe at the Institute for Telecommunication Sciences in Boulder, Colorado, of microwave attenuation in dry air have been analyzed to extract coefficients describing the

[9] P.W. Rosenkranz, "Rough-Sea Microwave Emissivities Measured with the SSM/I," 1992, forthcoming.

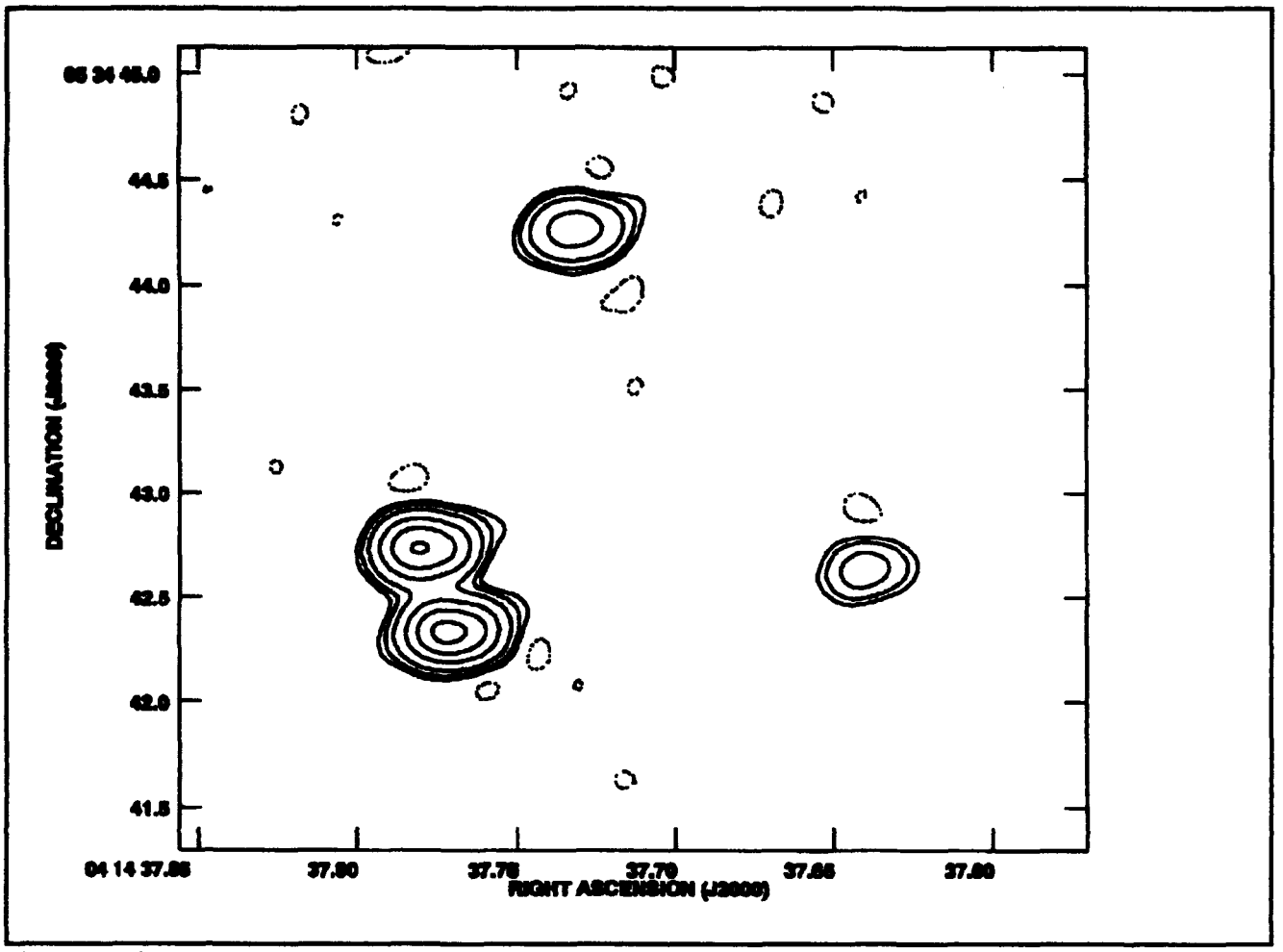


Figure 4. 8 GHz radio image of the four-image gravitational lens MG0414+0456. The contours trace the surface brightness of the source.

mixing of overlapping oxygen lines.[10] These coefficients will improve the accuracy of atmospheric transmittance models, particularly with respect to temperature dependence.

1.5 Earth Observing System: Advanced Microwave Sounding Unit

Sponsor

National Aeronautics and Space Administration/
Goddard Space Flight Center
Contract NAS 5-30791

Project Staff

Professor David H. Staelin, Dr. Philip W. Rosenkranz, Michael J. Schwartz

The AMSU will provide microwave-band measurements to the Atmospheric Infrared Sounder (AIRS), which will be a facility instrument on NASA's planned Earth Observing System (EOS). In this effort, we are developing algorithms for retrieval of temperature and humidity profiles, precipitation, sea ice, land snow cover, and other parameters. Presently, we are planning that temperature and humidity profiles obtained from AMSU will provide initial conditions for the AIRS infrared retrieval algorithm. Currently, our work is focused on simulation efforts and on developing a rapid (as distinguished from line-by-line) microwave transmittance algorithm.

[10] H.J. Liebe, P.W. Rosenkranz, and G.A. Hufford, "Atmospheric 60-GHz Oxygen Spectrum: New Laboratory Measurements and Line Parameters," submitted for publication.

1.6 High-Resolution Passive Microwave Imaging of Atmospheric Structure

Sponsor

National Aeronautics and Space Administration/
Goddard Space Flight Center
Grant NAG5-10

Project Staff

Professor David H. Staelin, Dr. Philip W. Rosenkranz, John W. Barrett, Michael J. Schwartz

The MIT Microwave Temperature Sounder (MTS) is a dual-band radiometer, incorporating an imaging spectrometer at 118 GHz and a tunable fixed-beam radiometer at 52-54 GHz. This instrument is flown on the NASA ER-2 high-altitude aircraft. During July and August 1991, we participated in the Convection and Precipitation/Electrification (CaPE) experiment which observed subtropical convective systems.

The data taken during this series of flights, which included two overpasses of Hurricane Bob, provided the highest resolution observations in these frequency bands of a hurricane. On other flights, upward-observed profiles of atmospheric brightness temperature were obtained. These data will help us to resolve apparent discrepancies with theoretical calculations of brightness temperatures that had been observed in previous experiments.

1.7 Characterization of Dolphin Whistles

Project Staff

Professor David H. Staelin, Kevin G. Christian

Dolphins emit whistles resembling bird song. In this project, we are exploring methods for compressing these signals so that repetitious song elements can be rapidly identified. Identifying song elements rapidly with minimal training presents the most challenging aspect of the project.

This year the dolphin song database was expanded, and a broad class of robust measures of whistle parameters was designed. Our current research involves developing methods for selecting combinations of measures which most efficiently capture unique elements in these whistles and permit compact representation and efficient recall from a computer database. These algorithms should also be useful for diagnosing acoustic and other signals produced by machinery, manufacturing processes, and other environments.

1.8 Rapid Precision Net-Form Manufacturing

Sponsor

Leaders for Manufacturing Program

Project Staff

Professor David H. Staelin, John T. Delisle, Darren L. Leigh, Paul W. Fieguth

Algorithms were improved for estimating the shape of manufactured objects with a precision of microns at very high data rates.[11] The experiment involves use of a previously developed four-axis stage with a scannable volume of $\sim$ 20 cubic inches. A 512^2 pixel CCD camera was used with a field of view adjustable down to 1 mm^2. The system is fully computer controlled and can receive up to 30 frames per second.

1.9 Conformal Experiment Design

Sponsor

Leaders for Manufacturing Program

Project Staff

Professor David H. Staelin, Ashraf S. Alkhairy

Optimization of operating parameters for products and manufacturing processes are often determined by experiment in cases where theoretical analysis is inadequate. The performance of these products and processes is often limited because of the high cost of these experiments; experimentation simply ceases when the allocated budget is depleted or the allotted time period ends. With most conventional techniques for experiment design, such as those of Taguchi and Box, on the order of N^2 experiments are required, where N is the approximate number of important parameters. Using

[11] J.T. Delisle, *Three-dimensional Profiling Using Depth of Focus,* S.M. thesis, Dept. of Physics, MIT, 1991.

newly developed techniques, Dr. Ashraf Alkhairy[12] has shown that in many cases of practical interest, only the order of N experiments is sufficient to get excellent results.

These new techniques, called "conformal experiment design," are used to probe the complexity of the product or process space and guide definition of efficient sets of experiments. This new approach conforms to the process or product of interest by taking advantage of any intrinsic simplicity and by better matching the chosen quality cost functions and statistical models to the problem at hand. This involves performing a series of experiments which ends when those experiments suggest that all unaccounted second-order interactions are negligible; the implication is then that all higher-order interactions are probably negligible too. Previously existing methods often overlooked some of these interactions, even with N^2 experiments, and thus yielded inferior results.

The impact of these new, more efficient methods for experiment design can be enormous when processes and products are characterized by too many significant parameters for N^2 experiments to be practical. Experimental optimization can therefore now be employed for larger and more complex systems or subsystems with larger values of N, leading to significantly superior performance over cases where sequential optimizations of subsets of the same N parameters are performed.

---

[12] Alkhairy, A.S., *Optimal Product and Manufacturing Process Selection—Issues of Formulation and Methods for Parameter Design*, Ph.D. diss., Dept. of Electr. Eng. and Comput. Sci., MIT, 1991.

Part III Systems and Signals

Section 1 Computer-Aided Design

Section 2 Digital Signal Processing

Section 1 Computer-Aided Design

Chapter 1 Custom Integrated Circuits

Chapter 2 Computer-Aided Fabrication System Structure

Chapter 1. Custom Integrated Circuits

Academic and Research Staff

Professor Jonathan Allen, Professor John L. Wyatt, Jr., Professor Srinivas Devadas, Professor Jacob K. White, Professor Dimitri A. Antoniadis, Professor Berthold K.P. Horn, Professor Hae-Seung Lee, Professor Tomaso Poggio, Professor Stephen D. Senturia, Professor Charles G. Sodini, Dr. Sami M. Ali, Dr. John G. Harris

Visiting Scientists and Research Affiliates

James H. Kukula[1]

Graduate Students

Robert C. Armstrong, Kelly S. Bai, Donald G. Baltus, Steven J. Decker, Lisa G. Dron, Ibrahim M. Elfadel, Kamyar Eshghi, Mikko Hakkarainen, Frederick P. Herrmann, Mattan Kamon, Craig L. Keast, Songmin Kim, Stan Y. Liao, Jennifer A. Lloyd, Steve Leeb, Andrew Lumsdaine, David R. Martin, Ignacio S. McQuirk, Keith S. Nabors, Lisa A. Pickelsimer, Khalid Rahmat, Mark W. Reichelt, Mark N. Seidel, Amelia H. Shen, Luis M. Silveira, David L. Standley, Ricardo Telichevsky, Clay M. Thompson, Christopher B. Umminger, Filip J. Van Aelten, Paul C. Yu

Technical and Support Staff

Dorothy A. Fleischer, Susan E. Nelson

1.1 Custom Integrated Circuits

Sponsors

Analog Devices
IBM Corporation

Project Staff

Professor Jonathan Allen, Robert C. Armstrong, Donald G. Baltus, Lisa A. Pickelsimer, Mark W. Reichelt, Filip J. Van Aelten

The overall goal of VLSI computer-aided design (CAD) research is to provide the means to produce custom integrated circuits quickly, correctly, and economically. Traditionally, correctness has been checked at several representational levels of abstraction, such as layout (via design rule checking), and circuit and logic representations (both via simulation). These techniques for checking correctness are usually local to the particular representational level involved and, while these techniques are important components of the overall design testing, they do not attempt to provide for alignment and consistency checks between the different representational levels and an input behavioral specification. In addition, they do not characterize the set of possible designs at each representational level corresponding to the initial functional specification in a way that ranges over a variety of performance levels. For this reason, there is an increasing need to provide CAD tools that serve as a framework for design exploration, thus providing the desired performance together with consistently aligned representations at all levels.

This research group studies a variety of research topics with an emphasis on performance-directed synthesis of custom VLSI designs. An overview of the viewpoint that motivates these projects has recently been provided in a major survey paper[2] in which the need for coordinating a design optimization process over the several levels is emphasized. Since design exploration is so central to the production of high-performance designs, emphasis is placed on how performance can be characterized at the several levels of representation and how overall optimal performance can be achieved in an integrated way. In addition to the basic issues of circuit optimization, architectures for digital signal processing have been studied because of the highly parallel nature of the algorithms involved and the need for a very high level of real-time performance in these systems. Emphasis on devel-

[1] IBM Corporation.

[2] J. Allen, "Performance-Directed Synthesis of VLSI Systems," *Proc. IEEE* 78(2): 336-355 (1990).

oping formally specified systems has been increased so that the design space can be comprehensively searched and verification of the resultant design can be confirmed in terms of the initial behavioral specification. Current projects focus on design methodologies for very high-speed clocked circuits, design of highly optimized array architectures for digital signal processing, and provision of a VLSI design database that provides for incremental consistency maintenance.

There has been a continuing evolution of circuit styles that seek to provide high performance in a minimal space. Thus, in CMOS technology, static designs are utilized, but precharge-evaluate methodologies have also been employed to provide speed, minimize the number of transistors, and increase the utilization of n-channel devices (rather than slower p-channel devices). Recently, examples of a new circuit style called *True Single-Phase Clocking* (TSPC) have been published.[3] This style provides for clock speeds of several hundred megahertz in modest CMOS technologies. While these results have been confirmed, an analysis to explain the speed has not been provided, and no overall design methodology for these circuits has been demonstrated. In her Master's thesis research project, Pickelsimer is providing both the required insight into the cause of the high-speed performance as well as a comprehensive design methodology for these circuits which will cover both combinational and sequential circuits. In addition, comparisons are provided with several CMOS circuit styles which include simulations based on layouts of commonly used circuit modules. These contributions are expected to promote the utilization of TSP clocked circuits for a wide variety of applications and provide an important capability to the circuit aspect of performance-directed synthesis.

In the survey of performance-directed synthesis by Allen, the need for integrated performance optimization across multiple levels of representation was pointed out. In order to gain concrete experience for these techniques,[4] Baltus has extended his work on the generation of custom layout from netlist specifications to the systematic exploration of array-like digital signal processing architectures from a high-level functional specification. In this way, designs can be optimized at a high level in a meaningful way with realistic delay models. The input specification for this algorithm is expressed in a language called FLASH, which affords several improvements over the commonly used SILAGE language.[5] FLASH designs are then converted to data dependence graphs, and some elements of these graphs are reused and indexed to provide a compact representation that does not grow with the size of the repetitive array aspect of the problem. Techniques to optimize scheduling without commitment to allocation have been provided for array designs in several dimensions, and novel architectures have been obtained for a variety of common signal processing tasks (such as finite impulse response filters). This process of deriving schedules, coupled with the following allocation process, constitutes a comprehensive search of the architectural design space under the given cost function and has already produced many useful but nonintuitive designs. Another novel aspect of this project is the introduction of an affine delay model, which corresponds to the utilization of elements in arbitrary positions within the array by a particular element of the array. By controling this delay model, it is possible to study several different designs which vary in the amount of communication delay from source modules to the destination module which requires these inputs. This project makes many new contributions to architectural design for digital signal processing systems including scheduling optimization with affine delay models, multidimensional mapping from the original design space to two-dimensional implementation spaces, and strong coupling between layout performance considerations and communication constraints at the architecture level.

Armstrong has been studying the design of an incremental consistency maintenance schema in a multirepresentation VLSI database. Here, the goal is to develop a design that automatically, incrementally, and continuously provides for consistent alignment of all levels of design abstraction. That is, from the start of the design process, all levels are kept in alignment through the introduction of explicit correspondence zones between adjacent representational levels. This project has required the elaboration of complex database schemas, constraint evaluation, and maintenance of broad utility among the overall structural representations,

---

[3] J. Yuan and E. Svensson, "High-Speed Circuit Technique," *IEEE J. Solid-State Circ.* 24(1): 62-70 (1989).

[4] D. Baltus and J. Allen, "SOLO: A Generator of Efficient Layouts from Optimized MOS Circuit Schematics," *Proceedings of the 25th Design Automation Conference,* Anaheim, California, June 1988, pp. 445-452.

[5] P.N. Hilfinger, "A High-Level Language and Silicon Compiler for Digital Signal Processing," *Proceedings of the IEEE 1985 Custom Integrated Circuits Conference,* Portland, Oregon, May 1985, pp. 213-216.

and a substantial implementation that employs over 50,000 lines of code on a contemporary workstation.[6] This project is now being extended in several different ways to include coupling to other design modules, introduction of new schema compilers, and extension of the basic methodology to functional (nonstructural) representations.

There is increasing interest in overall CAD systems where the database is central and surrounded by specific applications for design and verification at a variety of different levels of representation, such as in the database just described. Plans are underway to build a client server architecture that will consist of coordinated workstation, mainframe, and large disk system environments interconnected with high-speed fiberoptic switching. This system will serve as a test bed for the combined utilization of high-performance workstations and mainframe-based storage for high-speed, reliable database access. This environment also provides a structure in which distributed parallel algorithms can run in a coherent way within an overall environment that supports other specialized, nonparallel CAD algorithms.

1.2 Analog VLSI Systems for Integrated Image Acquisition and Early Vision Processing

Sponsors

National Science Foundation/Defense Advanced Research Projects Agency
Grant MIP 88-14612

Project Staff

Professor John L. Wyatt, Jr., Professor Berthold K.P. Horn, Professor Hae-Seung Lee, Professor Charles G. Sodini, Professor Tomaso Poggio, Steven J. Decker, Lisa G. Dron, Ibrahim M. Elfadel, Kamyar Eshghi, Mikko Hakkarainen, Dr. John G. Harris, Frederick P. Herrmann, Craig L. Keast, David R. Martin, Ignacio S. McQuirk, Mark N. Seidel, David L. Standley, Clay M. Thompson, Christopher B. Umminger, Paul C. Yu

1.2.1 Project Overview

In real-time machine vision the sheer volume of image data to be acquired, managed and processed leads to communications bottlenecks between imagers, memory and processors, and to very high computational demands. We are designing and testing experimental *analog* VLSI systems to overcome these problems. The goal is to determine how the advantages of analog VLSI—high speed, low power and small area—can be exploited and its disadvantages—limited accuracy, inflexibility and lack of storage capacity—can be minimized. The work is concentrated on *early* vision tasks, i.e., tasks that occur early in the signal flow path of animal or machine.

Completed designs include seven different chips for image filtering and edge detection, moment extraction to determine object position and orientation, image smoothing and segmentation, depth determination from stereo image pairs, scene depth determination jointly from stereo depth and surface shading, and camera motion determination. The typical subsystem is physically very small and performs one or more computationally intensive image-processing tasks at hundreds to thousands of frames per second using only tens to hundreds of milliwatts.

There is no single design strategy, but each of the designs has many of the following features:

- sensors (typically on-chip) and processing circuitry tightly coupled,
- parallel computation,
- analog circuits for high throughput, low latency, low power and small area,
- selection of tasks and algorithms requiring low to moderate precision,
- special emphasis on computations that map naturally to physical processes in silicon, e.g., to relaxation processes or to resistive grids,
- emphasis on charge-domain processing, e.g., CCD and switched-capacitors, for maximal layout density and compatibility with CCD sensors,
- sufficiently fast processing that requires no long-term storage circuitry,

[6] R.C. Armstrong, *A Formal Approach to Incremental Consistency Maintenance in Multirepresentation VLSI Databases*, Ph.D. diss., Dept. of Electr. Eng. and Comput. Sci., MIT, 1992.

- careful matching of algorithms, architecture, circuitry and (often custom) fabrication for maximum performance, and
- modular design, with a standardized input and output, for compatibility between subsystems.

1.2.2 Recent Progress

This project has shown experimentally that continuous-time CMOS and clocked CMOS/CCD systems, appropriately designed, can perform extremely fast early vision processing at a minimum cost in power and area.

Perhaps the most exciting results are the seven analog vision chip designs described below. All have been fabicated either as complete systems or in the form of test chips containing each of the cells needed in the final array. The image filtering and edge detection chip and the moment chip have been fabricated in system form with on-chip imagers, and testing has been completed. Advanced versions of these two systems are now being developed by their inventors, who have graduated from MIT. The CMOS/CCD and the unclocked CMOS image smoothing and segmentation chips have been fabricated in both test-cell form and as complete systems with on-chip imagers. The former versions have been tested, and testing is now underway for the system versions of these two chips. The depth-from-stereo chip and the depth-from-stereo-and-surface-shading chip are intended as components of larger systems and do not have on-chip imagers. The former has been fabricated with a redesign currently under fabrication, and the latter has been fabricated in a one-dimensional form. Both will be tested soon. The camera motion chip has been fabricated and tested in test-cell form, and a complete system with on-chip imager will be fabricated soon. The tested systems all operate at very high speeds (1,000 to 5,000 frames per second), and all systems were designed for speeds in that same range.

We have also developed a 1.75 micron CCD/CMOS process on campus for vision chip fabrication. The CCD enhancements were developed by this project, and the process is now successfully run by staff so that other designers can use it. The CCD/CMOS image smoothing and segmentation chip was fabricated in this process.

These and other developments are described in more detail below.

1.2.3 Vision Chip Designs

NMOS/CCD Imager and Parallel, Pipelined Filter for Edge Detection

Woodward Yang, working with Dr. Alice Chiang at Lincoln Laboratory and Professor Tomaso Poggio, has designed and tested a 64×64 NMOS/CCD imager and analog filter chip. It consists of a high fill-factor CCD imager and a parallel, pipelined processor that convolves the image with a 7×7 Laplacian of a Gaussian mask to enhance edges. All 64 rows of the image are fed in parallel to a fully pipelined analog processor that is pitch-matched to the imager. The entire system operates at 1,000 frames/second on a 10 MHz clock and consumes only 40 mW on-chip. The processor design minimizes area by carrying out delay, division and summing operations entirely in the charge domain and therefore occupies only 15 percent of the total chip area. The chip was conservatively designed using 4 micron design rules, prior to the creation of the MOSIS and campus CMOS/CCD processes. Dr. Yang, now an assistant professor at Harvard, is making a 2 micron redesign for MOSIS fabrication. The entire system would scale to 256×256 pixels in a 1 micron process.[7]

Continuous-Time CMOS Moment Chip for Object Position and Orientation

David L. Standley has completed and tested a novel, very specialized chip that rapidly determines the location and orientation of an object in its field of view. The design principle, discovered by Professor Berthold Horn, is entirely new. The location and orientation are most accurately determined to sub-pixel resolution by a least-squares technique using five linear and quadratic grey-scale moments, specifically the intensity-weighted averages of 1, x, y, xy and $x^2 - y^2$. These functions are all *harmonic*, i.e., their Laplacian vanishes identically, and therefore they can be processed very efficiently by a uniform resistive grid. The circuit exploits this new principle to reduce the order of the calculation for an N×N image from N^2 (one addition and multiplication per *pixel*) to 4N (one

[7] W. Yang, "Analog CCD Processors for Image Filtering," *SPIE International Symposium on Optical Engineering and Photonics in Aerospace Sensing*, Orlando, Florida, April 1991, pp. 114-127.

operation pair only on each current leaving the *boundary* of the resistive grid) and then to 4 (one operation on the current leaving each *corner* of a surrounding square made of 4 resistive lines). The chip has a phototransistor array driving a 30×30 resistive grid and was fabricated in a 2 micron MOSIS process. It operates in continuous time at 5,000 frames/second (governed by relaxation time to 1 percent error) on 25 mW. Orientation measurement is less accurate than position, with worst case error of 10 degrees for uncalibrated measurements and 2 degrees for calibrated measurements of a diamond-shaped object. Dr. Standley, presently employed at Rockwell International, is developing a larger 2-chip version of this system.[8]

We have filed U.S. patent applications for Drs. Yang and Standley's chips. Both are described in more detail in the conference papers included in the bibliography at the end of this section.

CMOS/CCD Imager and Fully Parallel Smoothing and Segmentation Chip

Image segmentation and smoothing systems perform linear smoothing on approximately uniform regions of an image while preserving or enhancing edges by nonlinear operations. When the smoothing operation is quite strong the output image is approximately piecewise constant in intensity with sharp edges, a reduced-bandwidth form that is suitable for rapid subsequent processing by analog or digital systems. Craig Keast, working with Professor Charles Sodini, has designed, simulated and fabricated a CMOS/CCD imager and processor chip to perform rapid image acquisition, smoothing and segmentation. The fabrication was done on campus in the CMOS/CCD process Mr. Keast developed as an enhancement to MIT's baseline 1.75 micron CMOS process (see CMOS/CCD Fabrication Process section).

The architecture uses standard CCD imaging techniques to transfer image brightness into signal charge. The Gaussian smoothing operation is approximated by a discrete binomial convolution of the image with a controllable support region. The design incorporates segmentation circuits with variable threshold control at each pixel location to enhance edge localization in the image. Once processed, the image can be read out using a standard CCD clocking scheme.

Currently, wafers from the first run are being evaluated using Polaroid's CCD test system. First order testing of a 4×4 processor array showed functionality of the three system operations: Imaging, Smoothing (spatial low pass filtering), and Smoothing with Segmentation. Detailed sensitivity analysis along with a comparison between measured and simulated data is currently underway. After the characterization of the 4×4 array is complete, the testing focus will shift to the much larger 40×40 imager and processor array that has also been fabricated.[9]

Continuous-Time CMOS Imager and Smoothing and Segmentation System with Resistive Fuses

As an alternative to the clocked system described above, a network consisting of a grid of vertical and horizontal resistors can perform the normally mutually exclusive functions of image smoothing and segmentation simultaneously, when *resistive fuses* are employed as horizontal resistors. Resistive fuses are nonlinear resistors that act like

---

[8] D. Standley, "An Object Position and Orientation IC with Embedded Imager," *IEEE J. Solid-State Circuits*, 26(12): 1853-1860 (1991); J.L. Wyatt, Jr., C. Keast, M. Seidel, D. Standley, B. Horn, T. Knight, C. Sodini, H.-S. Lee, and T. Poggio, "Analog VLSI Systems for Image Acquisition and Fast Early Vision Processing," submitted to *Int. J. of Comput. Vision*; B.K.P. Horn, "Parallel Networks for Machine Vision," in *Research Directions in Computer Science: An MIT Perspective*, eds. A. Meyer, G.V. Guttag, R.L. Rivest, and P. Szolovits (MIT Press: 1991), pp. 531-572; D. Standley and B. Horn, "An Object Position and Orientation IC with Embedded Imager," *Proceedings IEEE International Solid State Circuits Conference*, San Francisco, California, February 13-15, 1991, pp. 38-39; J.L. Wyatt, Jr., D.L. Standley, and W. Yang, "The MIT Vision Chip Project: Analog VLSI Systems for Fast Image Acquisition and Early Vision Processing," *Proceedings IEEE International Conference on Robotics and Automation*, Sacramento, California, April 1991, pp. 1330-1335; D. Standley and B.K.P. Horn, "Analog CMOS IC for Object Position and Orientation," *SPIE International Symposium on Optical Engineering and Photonics in Aerospace Sensing*, Orlando, Florida, April 1991, pp. 194-201; D. Standley, *Analog VLSI Implementation of Smart Vision Sensors: Stability Theory and an Experimental Design*, Ph.D. diss., Dept. of Electr. Eng. and Comput. Sci., MIT, 1991.

[9] J.L. Wyatt, Jr., C. Keast, M. Seidel, D. Standley, B. Horn, T. Knight, C. Sodini, H.-S. Lee, and T. Poggio, "Analog VLSI Systems for Image Acquisition and Fast Early Vision Processing," submitted to *Int. J. of Comput. Vision*; C.L. Keast, and C.G. Sodini, "An Integrated Image Acquisition, Smoothing and Segmentation Focal Plane Processor," submitted to 1992 VLSI Circuit Symposium.

positive linear resistors for small applied voltages, but their current begins to decrease and eventually becomes quite small for large applied voltages. Thus the fuse "breaks" when the voltage difference between two adjacent pixels is large, inhibiting smoothing at the edges. Since a large number of resistive fuses are needed in a grid, the simplicity and size of the resistive fuse circuit becomes critical.

This project has developed a variety of very compact resistive fuse circuits as described in the section on Special Circuits for Vision Chips. Paul Yu, working with Professor Hae-Seung Lee, has designed a 32×32 array, using one of these fuse types with a 32×32 imager and a read-out system. It has been fabricated through MOSIS, and initial tests seem to indicate that it works correctly. More extensive testing is now underway.[10]

CMOS/CCD Stereo Chip

Mikko Hakkarainen and Professor Hae-Seung Lee have completed the design of a high-speed stereo vision system in analog VLSI technology. Three stereo algorithms have been considered, and a simulation study examined details of the interaction between algorithm and analog VLSI implementation: the Marr-Poggio-Drumheller algorithm was shown to be best suited for this technology. Particular attention was paid to the fact that analog signal processing accuracy is limited to about 8 bits (1 part in 256). Hakkarainen and Lee have shown that several stages of the algorithm only require about 4 bits of accuracy, and about 6 bits is sufficient throughout.

They have proposed an analog CMOS/CCD system implementation of the Marr-Poggio-Drumheller algorithm. The system consists of six modules: two imagers, two image filters (that perform a spatial band-pass operation), a shift-and-correlate module, and a vote taker. The shift-and-correlate module compares the band-pass filtered left and right images pixel-by-pixel in parallel, and generates match data (degree of matching) for all possible shift (disparity) values for each pixel. This module does most of the processing in the overall stereo system, and thus presents both a speed and functionality bottleneck. For this reason, the shift-and-correlate module was selected for VLSI implementation, the other blocks being initially emulated by a digital computer.

CMOS/CCD signal processing technology is well suited for the shift-and-correlate module due to the ability of a CCD device to function as an analog memory, subtractor, and shift register. A 40×40 absolute-value-of-difference array, the core processor of the shift-and-correlate module, has been fabricated through MOSIS in a 2 micron CMOS/CCD process. This array performs a pixel-wise comparison between two input arrays (band-pass filtered left and right images). The chip size limitation imposed by MOSIS has kept the number of pixels in this prototype design at 40×40, although a 64×64 array would fit on a full size 1.2 cm × 1.2 cm 2-micron chip.

At a 10 Mhz clock rate for the prototype CCD processor, a remarkable 2,000 image frame pairs can be processed per second for a disparity range of 10 pixels. This experimental array has a serial input structure for interfacing purposes. However, in a full stereo system the input would be column parallel for both left and right images. In such a case, a 64×64 system would reach 9,000 image frame pairs per second for a 10 MHz clock and a 16 pixel disparity range.

A complete test system has been designed, and one 40×40 chip has been fabricated. Errors in the first chip were corrected in a second design, which is now being fabricated while the test system is under construction.[11]

Switched-Capacitor System for Merging Depth and Slope Estimates

Mark Seidel is working with Professor Wyatt and Thomas F. Knight[12] on a switched-capacitor chip to robustly compute the depth of a scene by merging depth estimates (possibly from a stereo algorithm) with surface slope estimates from a shape-from-shading algorithm. This multisensor image fusion design uses the least-squares properties of certain switched-capacitor systems to compute a dense depth map given noisy or sparse

---

[10] P.C. Yu, S.J. Decker, H.-S. Lee, C.G. Sodini, and J.L. Wyatt, Jr., "CMOS Resistive Fuses for Image Smoothing and Segmentation," *IEEE J. Solid-State Circuits*, forthcoming; H.-S. Lee and P. Yu, "CMOS Resistive Fuse Circuits," *Symposium on VLSI Circuits*, Oiso, Japan, May 1991, pp. 109-110.

[11] M. Hakkarainen, J. Little, H.-S. Lee and J.L. Wyatt, Jr., "Interaction of Algorithm and Implementation for Analog VLSI Stereo Vision," *SPIE International Symposium on Optical Engineering and Photonics in Aerospace Sensing*, Orlando, Florida, April 1991, pp. 173-184.

[12] MIT Dept. of Electr. Eng. and Comput. Sci.

depth and slope input. A 1-D version has been fabricated through the MOSIS system, and testing will begin soon.[13]

CMOS/CCD Imager and Focus-of-Expansion Chip for Camera Motion

Ignacio McQuirk and Professors Berthold Horn and Hae-Seung Lee are developing a chip that determines the direction of camera translation directly from a time-varying image sequence with a real-time analog VLSI system. Professor Horn's algorithm assumes a fixed world; there is no restriction on the shapes of the surfaces in the environment, only an assumption that the imaged surfaces have some texture, that is, spatial variations in reflectance. It is also assumed that the camera is stabilized so that there is no rotational motion. The focus of expansion (FOE) is the projection of the camera translation vector onto the image plane and gives the direction of camera motion. The FOE is the image of the point towards which the camera is moving and the point from which other image points appear to be receding. Knowledge of the location of the FOE in the case of pure translation also allows coarse calculation of the depth map of the imaged world up to a scale factor ambiguity, as well as the associated time to impact.

Through extensive simulation on synthetic images, various possible algorithms for estimating the FOE were compared in terms of accuracy, robustness, and feasibility for single-chip analog VLSI implementation with on-chip imaging circuitry. Based on these studies, an algorithm was chosen for implementation.

The method chosen for estimating the FOE is based on least squares analysis. It minimizes the sum of squares of the differences at every picture cell between the observed time variation of brightness and the predicted variation given the assumed position of the FOE. The minimization is not straightforward because the relationship between the brightness derivatives depends on distance to the surface being imaged and that distance is not only unknown, but also varies from picture cell to picture cell. Stationary points, where brightness is constant (instantaneously), play a critical role. Ideally, the FOE would occur at the intersection of the tangents to the iso-brightness contours at these stationary points. In practice, image brightness derivatives are hard to estimate accurately given that the image itself is quite noisy. Hence the intersections of tangents from different stationary points may be quite scattered. Reliable results can nevertheless be obtained if the image contains many stationary points, and the point is found that has the least weighted sum of squares of perpendicular distances from the tangents at the stationary points.

A variety of system architectures and circuit designs were explored, and one was chosen for realization in analog VLSI. McQuirk has designed a preliminary CMOS/CCD version of the FOE chip which estimates the FOE, using on-chip CCD imaging circuitry and a row-parallel processing scheme. The chip will accommodate both electrical and optical input. Electrical input makes it possible to distinguish algorithmic performance from chip performance. The full FOE chip will be tested and characterized with electrical and optical input. A control processor, timing generator, and the required CCD clock drivers will be designed to complete the FOE system.

Several components of the FOE chip have been fabricated through MOSIS in a test chip. Agreement between expected and actual circuit behavior has been excellent. The next steps of the project include testing the CCD FOE chip components, revising the design if necessary, and fabricating the preliminary version of the chip. Required support circuitry for the chip will also be designed and constructed. Then full testing of the system with electrical and optical input will begin.[14]

1.2.4 CMOS/CCD Fabrication Process for Vision Chips

Craig Keast and Professor Charles Sodini have developed a four-phase, buried-channel CCD capability to enhance MIT's 1.75 micron baseline CMOS process. This enhancement allows CCD operations such as image-to-charge conversion, spatial shifting, analog storage, and many other linear signal processing functions necessary for early vision processing. It uses an additional implant step, a second gate oxidation, a second level of polysilicon, and an additional etching step, adding two more lithographic levels to the 13

---

[13] J.L. Wyatt, Jr., C. Keast, M. Seidel, D. Standley, B. Horn, T. Knight, C. Sodini, H.-S. Lee, and T. Poggio, "Analog VLSI Systems for Image Acquisition and Fast Early Vision Processing," submitted to *Int. J. Comput. Vision.*

[14] Horn, B.K.P., "Parallel Networks for Machine Vision," in *Research Directions in Computer Science: An MIT Perspective*, eds. A. Meyer, G.V. Guttag, R.L. Rivest and P. Szolovits (MIT Press, 1991), pp. 531-572.

mask double-metal CMOS process. In addition, this process allows the fabrication of high quality poly-to-poly capacitors with low voltage and temperature coefficients that are useful in many analog MOS applications. The process utilizes a 23 nm gate dielectric for high transconductance and a 42 nm poly-to-poly capacitor insulator. The first run processed yielded functional CCD shift registers and CMOS transistors. The CCDs fabricated in this process now perform well, with a transfer efficiency of about 0.99999 and a dark current of 1 nA/cm^2. This technology is currently being used to fabricate some of the designs in this project.[15]

1.2.5 Special Circuits for Vision Chips

Switched-Capacitor Resistive Grids

Resistor networks can perform several useful computations for machine vision problems. Most IC processes, however, are not designed for implementing large resistor networks on the image plane. The resistivity values are usually too low to make large-valued resistors in a reasonable area. Chris Umminger and Professor Sodini investigated the use of switched capacitor networks as an alternative to resistor networks for performing these computations. They showed that a mapping can be made from any resistor network to an equivalent switched capacitor network that will have the same node voltage solution in steady state. However, it takes several switching cycles for the charge to be distributed in the SC network before steady state is reached. Their results indicate that SC networks can be used in moderate resolution systems (250×250 pixels) operating at video rate without the settling time of the networks becoming a problem. A chip was fabricated and successfully tested which implemented some switched capacitor networks for image smoothing in one dimension. By varying the clocking scheme applied to the network, they were able to adjust the amount of smoothing performed. It was found that under certain conditions these networks are susceptible to charge-pumping; proper design can circumvent this problem.[16]

Compact Resistive Fuse Circuits

Resistive fuse circuits were described in the Vision Chip Designs section. The original concept and circuit implementation were created by John Harris at the California Institute of Technology, who has now become a postdoctoral student with this project.

Previous implementations require a large number of transistors, at least 33 per fuse. We have developed several much smaller designs that enable the fabrication of much denser grids.

Steven Decker and Professor Wyatt have designed a 4-FET depletion mode fuse that Steve and Professor Sodini have fabricated in an enhancement to MIT's CMOS process. The device has been tested and works essentially as expected.

Although the four-transistor fuse is quite compact, its behavior is not adjustable and the depletion mode FETs require custom processing. Professor Lee has designed two slightly larger fuses that avoid both these problems. One fuse uses seven small FETs, and the other uses 11; both can be fabricated in a standard CMOS process. Furthermore, both the linear resistance and off-voltage parameters can be varied, offering the flexibility of controlling the space constant and the threshold of smoothing independently. Professor Lee and Paul Yu have designed and fabricated a prototype 11-transistor circuit through MOSIS, which was found to be fully functional. The silicon area for each fuse is 75 μm by 105 μm. We have filed a U.S. patent application for these compact fuse designs.[17]

Simulation of Analog Vision Chips

Andrew Lumsdaine and L. Miguel Silveira, under the supervision of Professor Jacob K. White, developed the CMVSIM program for simulating grid-based analog circuit arrays on the Connection Machine. The program was designed specifically for robotic vision chips and has built-in functionality for handling images as input and output. CMVSIM has two intended uses. The first

---

[15] C.L. Keast and C.G. Sodini, "An Integrated Image Acquisition, Smoothing and Segmentation Focal Plane Processor," submitted to 1992 VLSI Circuit Symposium.

[16] C.B. Umminger and C.G. Sodini, "Switched Capacitor Networks for Monolithic Image Processing Systems," submitted to *IEEE Trans. Circuits Syst.*

[17] P.C. Yu, S.J. Decker, H.-S. Lee, C.G. Sodini, and J.L. Wyatt, Jr., "CMOS Resistive Fuses for Image Smoothing and Segmentation," *IEEE J. Solid-State Circuits*, forthcoming; S.J. Decker, *A Resistive Fuse for Image Segmentation and Smoothing*, S.M. thesis, Dept. of Electr. Eng. and Comput. Sci., MIT, 1991.

is in simulating algorithms, whereby CMVSIM is used to simulate grids of idealized circuit elements so that a designer can tune the idealized network realization of a particular algorithm. The second, and more important, use is in simulating actual VLSI circuits, where CMVSIM is used to simulate a VLSI circuit at an analog level. It is in this arena that CMVSIM's capabilities are so important, because VLSI realizations of vision circuits can easily have hundreds of thousands of devices, and yet the circuit must be simulated in its entirety at an analog level. Such a capability is well beyond that of a conventional circuit simulation program running on a serial computer. Since CMVSIM can simulate very large circuits in a reasonable amount of time, it allows the incorporation of a simulation phase into the design cycle of grid-based analog signal processors.

1.2.6 Theory and Algorithms

Settling Time of Large Switched-Capacitor Networks

At least some image processing algorithms formulated as minimization problems can be implemented using networks of switches, capacitors, and independent voltage sources (SC networks). In seeking bounds on the settling time of these networks, Mark Seidel and Professor Wyatt have discovered a method for deriving closed-form zero-state step response bounds for discrete-time systems characterized by M-matrices. This new result provides rigorous bounds that can replace the empirical approximations currently used to estimate settling times in switched-capacitor grids.[18]

Texture Synthesis and Halftoning Using Markov Random Fields

Using a novel formulation of the Gibbs energy of a Markov random field in terms of generalized graylevel co-occurrences that he calls *aura measures*, Ibrahim Elfadel, working with Professors Yuille, Horn and Wyatt, has been able to gain a deeper understanding of the textural patterns synthesized by using Gibbs random fields (GRF). In particular, with the use of aura measures, he has generalized the "boundary length" optimization principle of first-order binary MRF models to any order and to any number of graylevels. His work has also led to a new insight into the meaning of co-ocurrences: they relate the behavior of the texture pattern during the synthesis procedure to physically meaningful phenomena such as mixing, separation, crystallization and precipitation in multiphase fluids.

Underlying the notion of an aura measure is a new set-theoretic concept called the *aura* set. This concept was introduced to give precise meaning to the intuitive notion of one subset of a lattice being in the neighborhood of another subset.

Even more important is Elfadel's discovery that the descriptive "power" of GRF models could be quite limited if the model parameters are not chosen appropriately. When organized in a matrix indexed by the graylevels, the aura measures form an aura matrix that is also a generalization of the co-occurrence matrix. For instance, detailed analysis supported by numerical simulation for the autobinomial GRF model has shown that the ground state of the isotropic attractive case has a tridiagonal aura matrix, while the isotropic repulsive case has an antitridiagonal matrix. In the general anisotropic case, his results mean that there are grayscale patterns that are impossible to model using the ground states of the autobinomial GRF model.

These results indicate, apparently for the first time, a relationship between a texture synthesis model and its co-occurrence matrix. Moreover, the restrictions imposed on the possible ground state patterns should be taken into account before modeling images with Markov/Gibbs random fields.

Within the framework of GRF image models but along another research direction, Elfadel has shown how methods developed in the context of statistical physics can be used to analyze gray scale texture synthesis procedures based on the Monte Carlo probabilistic paradigm. In particular, using the mean-field equations of the texture GRF, the existence of a bifurcation point indicating the presence of a phase transition in the textural pattern has been demonstrated. Using simulations, he has shown that a number of interesting phenomena occur at the bifurcation temperature, e.g., a sudden decrease in energy, sharp peaks in similarity measures between textural patterns, and sudden saturation of the mean-field variables. The mean-field results allows him to argue that for texture synthesis, it is sufficient to simulate the

[18] M.N. Seidel and J.L. Wyatt, Jr., "Settling-Time Bounds for Switched-Capacitor Networks," *Proceedings of the IMACS World Congress on Computation and Applied Mathematics*, Dublin, Ireland, July 1991, pp. 1669-1670.

mean-field equations near the bifurcation temperature.[19]

Algorithm for Effortless Least-Squares Camera Calibration

Accurate camera calibration is important for many of the subsystems we propose to build and for other applications. A major part of this task is accurate determination of *internal* camera parameters, specifically the exact *focal length* and the *center of projection* coordinates that describe the lens position precisely in relation to the focal plane. Existing methods are accurate but slow and laborious because they involve constructing calibration arrays with very accurately-known positions and angles relative to the camera.

Professor Wyatt has discovered that one can, in principle, determine the internal camera parameters by processing images of 3-D spheres without requiring precise knowledge of their sizes or of their positions in relation to the camera. Jesus Dominguez has carried out an initial set of simulations under the supervision of Professors Wyatt and Horn that indicate accuracies of better than 1 pixel on a 454×576 pixel image can be obtained using images of only three spheres. Further work is planned with Gideon Sten to explore the possibilities of this method.[20]

Multiscale Method for Image Segmentation and Bandwidth Compression

Lisa Dron, working with Professor Horn, has invented a robust method of image segmentation that appears to work well in computer simulations. The basic idea is to segment an image between two nodes of a grid wherever the difference in intensities at the two nodes exceeds a threshold at *all of several different scales* of spatial low-pass filtering. (The threshold can vary with the scale.) The method is *robust* in that local noise spikes in the image are averaged out with filtering and do not contribute false edges, and it is *accurate* because the unfiltered image plays a role, since threshold must be exceeded there as well. Bandwidth compression is achieved by retaining intensity values only at nodes adjacent to edges. Intensities elsewhere are obtained by spatial averaging using a resistive grid. The method looks promising for analog VLSI implementation, and Ms. Dron is planning a chip based on these two novel ideas.[21]

Extremum Principles for Resistive Fuse Networks

The operation of resistive fuse networks has previously been explained in the literature on an ad-hoc basis. Professor Wyatt has shown that the operation of these networks can now be understood in terms of a network extremum principle involving a scalar function known as the *co-content*. This insight enables one to understand the operation of these networks in terms of the *graduated nonconvexity* algorithm in the computer vision literature. Andrew Lumsdaine, working with Professor Wyatt, has developed continuation methods

---

[19] I.M. Elfadel and R.W. Picard, "On a Unifying Neighborhood-Based Framework for Morphological Analysis and Co-Occurrence Methods," submitted to *IEEE Trans. Pattern Anal. Mach. Intell.*; R.W. Picard and I.M. Elfadel, "Texture Modeling: Markov/Gibbs Random Fields, Co-Occurrence, and Boundary Length Optimization," submitted to *IEEE Trans. Pattern Anal. Mach. Intell.*; R.W. Picard and I.M. Elfadel, "On the Structure of Aura Matrices for the Markov/Gibbs Texture Model," submitted to *J. Math. Imag. Vision*; R.W. Picard, I.M. Elfadel and A.P. Pentland, "Markov/Gibbs Texture Modeling: Aura Matrices and Temperature Effects," *1991 IEEE Computer Society Conference on Computer Vision and Pattern Recognition*, Lahaina, Maui, Hawaii, June 3-6, 1991, pp. 371-377; I.M. Elfadel and A.L. Yuille, "Mean-Field Theory for Grayscale Texture Synthesis using Markov Random Fields," *SPIE Conference on Stochastic Methods in Signal Processing, Image Processing, and Computer Vision*, San Diego, California, July 1991, 1569: 248-259.

[20] J. Dominguez, *Effortless Internal Camera Calibration Using the Images of Spheres*, S.B. thesis, Dept. of Electr. Eng. and Comput. Sci., MIT, 1991.

[21] L. Dron, "The Multi-Scale Veto Model: A Two-Stage Analog Network for Edge Detection and Image Reconstruction," submitted to *Int. J. Comput. Vision*; L. Dron, "An Analog Model of Early Visual Processing: Contour and Boundary Detection in the Retina," *Proceedings of the SPIE Intelligent Robots and Computer Vision X*, November 14-15, 1991, Boston, Massachusetts, forthcoming.

(i.e., "deterministic annealing") that drive these networks toward good solutions.[22]

1.2.7 Publications of the MIT Analog Vision Chip Project

Journal Articles

Dron, L. "The Multi-Scale Veto Model: A Two-Stage Analog Network for Edge Detection and Image Reconstruction." Submitted to *Int. J. Comput. Vision*.

Elfadel, I.M., and R.W. Picard. "On a Unifying Neighborhood-Based Framework for Morphological Analysis and Co-Occurrence Methods." Submitted to *IEEE Trans. Pattern Anal. Mach. Intell.*

Lumsdaine, A., J.L. Wyatt, Jr., and I.M. Elfadel. "Nonlinear Analog Networks for Image Smoothing and Segmentation." *J. VLSI Signal Proc.* 3: 53-68 (1991).

Picard, R.W., and I.M. Elfadel. "Texture Modeling: Markov/Gibbs Random Fields, Co-Occurrence, and Boundary Length Optimization." Submitted to *IEEE Trans. Pattern Anal. Mach. Intell.*.

Picard, R.W., and I.M. Elfadel. "On the Structure of Aura Matrices for the Markov/Gibbs Texture Model." Submitted to *J. Math. Imag. Vision*.

Standley, D. "An Object Position and Orientation IC with Embedded Imager." *IEEE J. Solid-State Circuits* 26 (12): 1853-1860 (1991).

Umminger, C.B., and C.G. Sodini. "Switched Capacitor Networks for Monolithic Image Processing Systems." Submitted to *IEEE Trans. Circuits Syst.*

Wyatt, J.L., Jr., C. Keast. M. Seidel, D. Standley, B. Horn, T. Knight, C. Sodini, H.-S. Lee, and T. Poggio. "Analog VLSI Systems for Image Acquisition and Fast Early Vision Processing." Submitted to *Int. J. Comput. Vision*.

Yu, P.C., S.J. Decker, H.-S. Lee, C.G. Sodini, and J.L. Wyatt, Jr. "CMOS Resistive Fuses for Image Smoothing and Segmentation" *IEEE J. Solid-State Circuits.* Forthcoming.

Book Chapters

Horn, B.K.P. "Parallel Networks for Machine Vision." in *Research Directions in Computer Science: An MIT Perspective.* Eds. A. Meyer, G.V. Guttag, R.L. Rivest and P. Szolovits. MIT Press, 1991, pp. 531-572.

Lumsdaine, A., J.L. Wyatt, Jr., and I.M. Elfadel. "Nonlinear Analog Networks for Image Smoothing and Segmentation." In *Parallel Processing on VLSI Arrays.* Ed. J.A. Nossek. Norwell, Massachusetts: Kluwer Academic Publishers, 1991. pp. 53-68.

Conference Papers

Dron, L. "An Analog Model of Early Visual Processing: Contour and Boundary Detection in the Retina." *Proceedings of the SPIE Intelligent Robots and Computer Vision X*, November 14-15, 1991, Boston, Massachusetts. Forthcoming.

Elfadel, I.M., and A.L. Yuille. "Mean-Field Theory for Grayscale Texture Synthesis using Markov Random Fields." *SPIE Conference on Stochastic Methods in Signal Processing, Image Processing, and Computer Vision*, San Diego, California, July 1991, 1569: 248-259.

Hakkarainen, M., J. Little, H.-S. Lee, and J.L. Wyatt, Jr. "Interaction of Algorithm and Implementation for Analog VLSI Stereo Vision." *SPIE International Symposium on Optical Engineering and Photonics in Aerospace Sensing*, Orlando, Florida, April 1991, pp. 173-184.

Keast, C.L., and C.G. Sodini. "An Integrated Image Acquisition, Smoothing and Segmentation Focal Plane Processor." Submitted to 1992 VLSI Circuit Symposium.

Lee, H.-S., and P. Yu. "CMOS Resistive Fuse Circuits." *Symposium on VLSI Circuits*, Oiso, Japan, May 1991, pp. 109-110.

Picard, R.W., I.M. Elfadel and A.P. Pentland. "Markov/Gibbs Texture Modeling: Aura Matrices and Temperature Effects." *IEEE Computer Society Conference on Computer Vision and Pattern Recognition*, Lahaina, Maui, Hawaii, June 3-6, 1991, pp. 371-377.

---

[22] A. Lumsdaine, J.L. Wyatt, Jr., and I.M. Elfadel, "Nonlinear Analog Networks for Image Smoothing and Segmentation," *J. VLSI Signal Proc.* 3: 53-68 (1991).

Seidel, M.N., and J.L. Wyatt, Jr. "Settling-Time Bounds for Switched-Capacitor Networks." *Proceedings of the IMACS World Congress on Computation and Applied Mathematics*, Dublin, Ireland, July 1991, pp. 1669-1670.

Standley, D., and B. Horn. "An Object Position and Orientation IC with Embedded Imager." *Proceedings of the IEEE International Solid State Circuits Conference*, San Francisco, California, Feb. 13-15, 1991, pp. 38-39.

Standley, D., and B.K.P. Horn. "Analog CMOS IC for Object Position and Orientation." *SPIE International Symposium on Optical Engineering and Photonics in Aerospace Sensing*, Orlando, Florida, April 1991, pp. 194-201.

Wyatt, J.L., Jr., D.L. Standley, and W. Yang. "The MIT Vision Chip Project: Analog VLSI Systems for Fast Image Acquisition and Early Vision Processing." *Proceedings of the IEEE International Conference on Robotics and Automation*, Sacramento, California, April 1991, pp. 1330-1335.

Yang, W. "Analog CCD Processors for Image Filtering." *SPIE International Symposium on Optical Engineering and Photonics in Aerospace Sensing*, Orlando, Florida, April 1991, pp. 114-127.

Theses

Decker, S.J. *A Resistive Fuse for Image Segmentation and Smoothing.* S.M. thesis, Dept. of Electr. Eng. and Comput. Sci., MIT, 1991.

Dominguez, J. *Effortless Internal Camera Calibration Using the Images of Spheres.* S.B. thesis, Dept. of Electr. Eng. and Comput. Sci., MIT, 1991.

McQuirk, I.S. *Direct Methods for Estimating the Focus of Expansion in Analog VLSI.* S.M. thesis, Dept. of Electr. Eng. and Comput. Sci., MIT, 1991.

Standley, D.L. *Analog VLSI Implementation of Smart Vision Sensors: Stability Theory and an Experimental Design.* Ph.D. diss., Dept. of Electr. Eng. and Comput. Sci., MIT, 1991.

1.3 Mixed Circuit/Device Simulation

Sponsors

IBM Corporation
U.S. Navy - Office of Naval Research
Grant N00014-91-J-1698

Project Staff

Andrew Lunsdaine, Mark W. Reichelt, Professor Jacob White, Professor Jonathan Allen

The enormous computational expense and growing importance of mixed circuit/device simulation, as well as the increasing availability of parallel computers, suggest that specialized, easily parallelized algorithms can be developed for transient simulation of MOS devices. In earlier work on the WORDS program (Waveform Overrelaxation Device Simulator), the easily parallelized waveform relaxation (WR) algorithm was shown to be a computationally efficient approach to device transient simulation even on a serial machine, though the WR algorithm typically requires hundreds of iterations to achieve an accurate solution.

In order to use WORDS in a mixed circuit/device simulator, we have been investigating ways of making WORDS more robust and efficient. We determined how to compute the terminal currents accurately using different timepoints at different mesh nodes and improved the timestep selection procedure by determining how to refine the timesteps as WR iterations proceed (reducing the total computation by as much as a factor of 2 by using only a few coarse timesteps in early iterations). The more accurate, electric field dependent mobility model was also implemented.

We found experimental evidence that WR using standard overrelaxation acceleration can produce oscillatory results and are investigating methods for eliminating this phenomenon. A frequency-dependent overrelaxation algorithm using lowpass filtering was developed,[23] as well as a waveform conjugate-direction approach.[24] Experimental

[23] A. Lumsdaine, M. Reichelt, and J. White, "Conjugate Direction Waveform Methods for Two-Dimensional Transient Simulation of MOS Devices," *Proceedings of the International Conference on Computer-Aided Design*, Santa Clara, California, November 1991.

[24] M. Reichelt, J. White, and J. Allen, "Frequency-Dependent Waveform Overrelaxation for Transient Two-Dimensional Simulation of MOS Devices," *Proceedings of NUPAD IV*, Seattle, Washington, 1992, forthcoming.

results indicate that both approaches reduce the number of waveform iterations required by more than a factor of seven.

1.4 Simulation Algorithms for Clocked Analog Circuits

Sponsors

IBM Corporation
National Science Foundation
PYI MIP 88-58764
U.S. Navy - Office of Naval Research
Contract N00014-87-K-0825

Project Staff

Luis M. Silveira, Steve Leeb, Professor Jacob White

A challenging problem in the area of analog circuits is the simulation of clocked analog circuits like switching filters, switching power supplies, and phase-locked loops. These kinds of circuits are computationally expensive to simulate using conventional techniques because they are all clocked at a frequency whose period is orders of magnitude smaller than the time interval of interest to the designer. To construct such a long time solution, a program like SPICE or ASTAP must calculate the behavior of the circuit for many high frequency clock cycles. The basic approach to making simulation of these circuits more efficient is to exploit only the property that the behavior of such a circuit in a given high frequency clock cycle is similar, but not identical, to the behavior in the preceding and following cycles. Therefore, by accurately computing the solution over a few selected cycles, an accurate long time solution can be constructed. Such approaches are known as *"envelope-following" algorithms.*[25]

In our recent work, we have been trying to make the envelope-following algorithm more robust and efficient by exploiting the fact that the envelope of "quasi-algebraic" components in the solution vector need not be computed. An automatic method for determining the quasi-algebraic solution components has been derived, and experimental results demonstrate that this modified method reduces the number of computed clock cycles when applied to simulating closed-loop switching power converters.[26]

1.5 Numerical Simulation of Short Channel MOS Devices

Sponsors

IBM Corporation
National Science Foundation
PYI MIP 88-58764

Project Staff

Jennifer A. Lloyd, Khalid Rahmat, Professor Dimitri A. Antoniadas, Professor Jacob White

The model used in conventional device simulation programs is based on the drift-diffusion model of electron transport, and this model does not accurately predict the field distribution near the drain in small geometry devices. This is of particular importance for predicting oxide breakdown due to penetration by "hot" electrons. There are two approaches for more accurately computing the electric fields in MOS devices: one is based on adding an energy equation to the drift-diffusion model, and the second is based on particle or Monte-Carlo simulations.

In the first approach, an energy balance equation is solved along with the drift-diffusion equations so that the electron temperatures are computed accurately. This combined system is numerically less tame than the standard approach, and must be solved carefully. We have developed a two-dimensional device simulator in which an energy balance equation is solved for electron temperature along with the usual drift-diffusion equations. The program avoids temperature instabilities produced by previous discretization approaches through the use of a careful application of exponential-fitting to the energy equation. Drain currents for silicon MOSFETs predicted by the simulator, using one set of model parameters, match well with experimental data for devices over a range of channel lengths from 0.90 μm to 0.16 μm. Also, a method to compute substrate current has been derived which uses the electron temperature provided by the simulator. The computed substrate currents match well with measured data, for the regime

---

[25] J. White and S. Leeb, "An Envelope-Following Approach to Switching Power Converter Simulation," *IEEE Trans. Power Electron.* 6(2): 303-308 (1991).

[26] M. Silveira and J. White, "A Modified Envelope-Following Approach to Clocked Analog Circuit Simulation," *Proceedings of the International Conference on Computer-Aided Design,* Santa Clara, California, November 1991.

above subthreshold, for MOSFETs with channel lengths as short as 0.16 μm.[27]

In the area of Monte Carlo device simulation, we are focusing on transient calculations with self-consistent electric fields. Specifically, we are trying to apply the recently developed implicit particle methods on very simple three-dimensional structures.

1.6 Efficient Three-Dimensional Interconnect Analysis

Sponsors

Digital Equipment Corporation
IBM Corporation
National Science Foundation
PYI MIP 88-58764
U.S. Navy - Office of Naval Research
Grant N00014-91-J-1698

Project Staff

Keith S. Nabors, Songmin Kim, Dr. Sami M. Ali, Professor Jacob White

We have developed a multipole-accelerated algorithm for computing the capacitance of complicated 3-D geometries and have implemented the algorithm in the program FASTCAP. The method is an acceleration of the boundary-element technique for solving the integral equation associated with the multiconductor capacitance extraction problem. Boundary-element methods become slow when a large number of elements are used because they lead to dense matrix problems which are typically solved with some form of Gaussian elimination. This implies that the computation grows as n^3, where n is the number of panels or tiles needed to accurately discretize the conductor surface charges. Our new algorithm, which is a generalized conjugate residual iterative algorithm with a multipole approximation to compute the iterates, reduces the complexity so that accurate multiconductor capacitance calculations grow nearly as nm where m is the number of conductors. For practical problems which require as many as 10,000 panels, FASTCAP is more than two orders of magnitude faster than standard boundary-element based programs.[28]

Recent work on FASTCAP includes: (1) improvements to the basic multipole-accelerated algorithm[29], (2) linking the FASTCAP program to the solid modeler used in the MIT Micro-Electrical-Mechanical CAD (MEMCAD) system, and (3) adding the capability to analyze problems with conductors embedded in arbitrary piecewise-constant dielectric regions.[30] With these improvements, the capacitance calculation method gives more accurate results for more intricate problems and retains the linear time complexity of the basic algorithm. The FASTCAP program and manuals are available from MIT.

Recently, it has been suggested that sufficiently accurate integrated circuit cross-talk simulations can be performed by computing the time evolution of electric fields both inside and outside three-dimensional integrated circuit conductors via a finite-difference discretization of Laplace's equation. We have derived a boundary-element approach to the same calculation, as boundary-element methods require that only conductor surfaces be discretized, and the difficulty constructing volume meshes associated with finite-difference methods is avoided. Two boundary-element approaches have been investigated, and experiments show that the straight-forward approach leads to unacceptable discretization errors, and a less intuitive second approach yields good results even with coarse surface meshes. This boundary-

---

[27] K. Rahmat, J. White, and D. Antoniadas, "Simulation of Very Short Channel MOSFETs Including Energy Balance," *Proceedings of the International Electron Devices Meeting,* Washington, D.C., December 1991.

[28] K. Nabors and J. White, "FastCap: A Multipole-Accelerated 3-D Capacitance Extraction Program," *IEEE Trans. Comput.-Aided Des.* 10 (11): 1447-1459 (November 1991); K. Nabors, T. Korsmeyer, and J. White, "Multipole-Accelerated Preconditioned Iterative Methods For Solving Three-Dimensional Mixed First and Second Kind Integral Equations," *Proceedings of the Copper Mountain Conference on Iterative Methods,* Copper Mountain, Colorado, April 1992, forthcoming.

[29] K. Nabors, S. Kim, J. White, and S. Senturia, "Fast Capacitance Extraction of General Three-Dimensional Structures," *Proceedings of the International Conference on Computer Design,* Cambridge, Massachusetts, October 1991; K. Nabors and J. White, "Fast Capacitance Extraction of General Three-Dimensional Structures," *IEEE Trans. Microwave Theory Tech.*, forthcoming.

[30] K. Nabors and J. White, "Multipole-Accelerated 3-D Capacitance Extraction Algorithms for Structures with Conformal Dielectrics," *Proceedings of the 29th Design Automation Conference,* Anaheim, California, June 1992, forthcoming.

element approach makes it possible to perform true three-dimensional transient interconnect analyses in less than a minute on a scientific workstation.[31]

Currently, we are working on development of a multipole-accelerated 3-D inductance analysis program.

1.7 Parallel Numerical Algorithms

Sponsor

U.S. Navy - Office of Naval Research
Grant N00014-91-J-1698

Project Staff

Andrew Lumsdaine, Mark W. Reichelt, Luis M. Silveira, Ricardo Telichevsky, Professor William Dally, Professor Jacob White

We are taking an application-oriented approach to developing parallel numerical algorithms and are focusing on circuit and device simulation. Application programs and techniques are being developed for both massively parallel SIMD machines like the Connection Machine, or on MIMD machines like the Intel hypercube. In addition, we are also trying to understand fundamental aspects of the interaction between architecture and certain numerical algorithms.

For example, the direct solution of circuit simulation matrices is particularly difficult to parallelize, in part because methods like parallel nested dissection are ineffective due to the difficulty of finding good separators. For that reason, general sparse matrix factorization techniques are being studied, and in particular, the interaction between sparse matrix data structures, computer memory structure, and multiprocessor communication is being investigated. To focus this work, a special-purpose processor for circuit simulation, the Numerical Engine (NE), is under development. Preliminary design is complete, and register-transfer level simulation results indicate that the specialized processor can achieve up to 80% of its peak floating-point performance for sparse matrix factorization and nearly 90% of its peak performance on model evaluation.

Explicit integration methods avoid matrix solution and are therefore also interesting algorithms to use on parallel processors. For this reason, we investigated some of the properties of the recently developed explicit exponentially-fit integration algorithms. The results were not very encouraging, though the theoretical investigation undertaken yielded several new insights about these methods.[32]

Over the last year, CMVSIM, a program for circuit-level simulation of grid-based analog signal processing arrays on a massively parallel processor has been used to evaluate several signal processor architectures. CMVSIM uses the trapezoidal rule to discretize the differential equations that describe the analog array behavior, Newton's method to solve the nonlinear equations generated at each time-step, and a block conjugate-gradient squared algorithm to solve the linear equations generated by Newton's method. Excellent parallel performance is achieved through the use of a novel, but very natural, mapping of the circuit data onto the massively parallel architecture. The mapping takes advantage of the underlying computer architecture and the structure of the analog array problem. Experimental results demonstrate that a full-size Connection machine can provide a 1400 times speedup over a SUN-4/280 workstation.[33]

An easily parallelized approach to solving large systems of time-dependent differential equations is the waveform relaxation algorithm. In such an approach, the differential equation system is broken into subsystems which are solved independently, each subsystem using guesses about the behavior of the state variables in other subsystems. Waveforms are then exchanged between the subsystems, and the systems are resolved with, hopefully, improved information about the other subsystems. This process is continued until convergence is achieved. Recent work on theoretical aspects of these methods has answered several long-standing questions about multirate stability.[34]

---

[31] D. Ling, S. Kim, and J. White, "A Boundary-Element Approach to Transient Simulation of Three-dimensional Integrated Circuit Interconnect," *Proceedings of the 29th Design Automation Conference,* Anaheim, California, June 1992, forthcoming.

[32] H. Neto. L. Miguel Silveira, J. White, and L.M. Vidigal, "On Exponential Fitting For Circuit Simulation," *IEEE Trans. Comput.-Aided Des.*, forthcoming.

[33] A. Lumsdaine, *Theoretical and Practical Aspects of Parallel Numerical Algorithms for Initial Value Problems, with Applications,* Ph.D. diss., Dept. of Electr. Eng. and Comput. Sci., 1991.

Also, a new conjugate-direction based acceleration to the waveform relaxation algorithm has been derived and applied to solving the differential-algebraic system generated by spatial discretization of the time-dependent semiconductor device equations. Numerical experiments demonstrate that when used to perform two-dimensional transient simulations of MOS devices, the waveform conjugate-direction method is more than an order of magnitude faster than standard waveform relaxation.[35]

1.8 Microelectromechanical Computer-Aided Design

Sponsors

Federal Bureau of Investigation
National Science Foundation
Felloship MIP 88-58764

Project Staff

Mattan Kamon, Professor Martin A. Schmidt, Professor Stephen D. Senturia, Professor Jacob White

High fabrication costs and increasing microsensor complexity is making computer simulation of the realistic geometries necessary, both to investigate design alternatives and to perform verification before fabrication. At MIT, we are developing a MicroElectroMechanical Computer-Aided Design (MEMCAD) system to make it possible for microsensor designers to easily perform realistic simulations. Carefully selected commercial software packages have been linked with specialized database and numerical programs to allow a designer to enter easily a three-dimensional microsensor geometry and perform quickly both mechanical and electrical analysis. The system currently performs electromechanical analyses, such as calculating the capacitance versus pressure (or force) curve for both a square diaphragm deformed by a differential pressure and a rectangular beam deflected by a centrally applied force.[36]

1.9 Techniques for Logic Synthesis, Formal Verification and Testing

Sponsors

IBM Corporation
Grant/Fellowship
U.S. Navy - Office of Naval Research
Contract N0014-87-K-0825

Project Staff

Professor Srinivas Devadas, James H. Kukula, Kelly S. Bai, Stan Y. Liao, Amelia H. Shen, Filip J. Van Aelten

1.9.1 Introduction

Integrated circuits, whether they are manually designed or automatically synthesized, must meet many different specifications. For example, limits on circuit delay, layout area, and power consumption are typically placed. Reliability restrictions are also placed, for example in the form of noise margins or non-susceptibility to electron-migration-induced failure. The designed circuit also has to be checked for correct functionality and whether it meets its performance goals. The fabricated circuit has to be tested in order to ensure that the fabrication steps are error-free.

At MIT, we are working on various aspects of automated synthesis, as well on design verification and test problems. We are developing logic optimization methods that target not only the area, performance and power consumption of the synthesized design, but also the testability of the designed circuit. We are developing verification mechanisms at the behavioral, logic and circuit

---

[34] J. White and F. Odeh, "A Connection between the Convergence Properties of Waveform Relaxation and the A-stability of Multirate Integration Methods," *Proceedings NASECODE VII*, Copper Mountain, Colorado, April 1991; J. White and F. Odeh, "Connecting the Convergence Properties of Waveform Relaxation and the A-stability of Multirate Integration Methods," *COMPEL*, December 1991.

[35] A. Lumsdaine, and J. White, "Accelerating Dynamic Iteration Methods with Application to Semiconductor Device Simulation," *Proceedings of the Copper Mountain Conference on Iterative Methods*, Copper Mountain, Colorado, April 1992, forthcoming.

[36] B. Johnson, S. Kim, J. White, and S. Senturia, "MEMCAD Capacitance Calculations for Mechanically Deformed Square Diaphragm and Beam Microstructures," *Proceedings Transducers 91*, San Francisco, California, June 1991; S.D. Senturia, R.M. Harris, B.P. Johnson, S. Kim, K. Nabors, M.A. Shulman, and J.K. White, "Computer-Aided Design System for Microelectromechanical Systems (MEMCAD)," *IEEE J. Microelectromech. Syst.* 1 (1): 3-13 (1992).

schematic levels that can check whether the circuit implementation has the correct logical functionality and meets the desired performance requirements prior to embarking on the fabrication process. Finally, we are developing methods for efficient test generation at the logic level, so fabricated integrated circuits can be easily tested for correctness.

In the following, we describe our work in the areas of timing, circuit, and behavioral verification, sequential logic synthesis for area and performance, combinational logic synthesis for low power, and test generation.

1.9.2 Timing Analysis and Verification

Over the past year, several projects have been undertaken in the areas of timing analysis and verification. Timing analysis tools are essential to the performance verification problem. The tools we have developed operate on logic-level descriptions of an integrated circuit. The work described in this section has been done in collaboration with Professor Sharad Malik of Princeton University, Dr. Kurt Keutzer and Dr. Albert Wang of Synopsys, Inc.

Timing Simulation

Timing simulation is a very common method for conclusively verifying the timing behavior of a design.

We have shown that in simulating a vector pair in a combinational circuit, the number of events at a gate is bounded above by the number of paths from the primary inputs to that gate. We have discovered a family of circuits, parameterizable by the depth of the circuit, in which the number of events at a gate is precisely the number of paths from the primary inputs to that gate. Thus, the number of events at the output of a circuit can be exponential in either the size or depth of a circuit. This shows that event-driven timing simulation can have exponential complexity, and this fact has been observed in practice on widely-used timing simulators.

We made the observation that to answer the question: "Does an event occur in this circuit at any time at or after τ?," we do not need a full history of the circuit activity before time τ. In other words, an event-driven timing simulation approach is likely to compute much more information, in the form of events, than is necessary to resolve the question at hand. To fully explore the ramifications of this observation we have developed a *calculus of event simulation* and applied this calculus to different models of timing behavior. Using these results we can reduce the number of events that need to be evaluated in a circuit simulation. The upper bound on the number of events at a gate g that need to be evaluated to determine if an event occurs after time τ is equal to the number of paths from primary inputs to g of length greater than or equal to τ. For example, on the circuit family mentioned above, the number of events evaluated at a gate is reduced exponentially by our procedure. Over a large class of circuits the number of events required to simulate random vector pairs was reduced by a factor of 2 to 10.

False Path Identification

We have addressed the problem of accurately computing the delay of a combinational logic circuit in the floating mode of operation. (In this mode the state of the circuit is considered to be unknown when a vector is applied at the inputs.) It is well known that using the length of the topologically longest path as an estimate of circuit delay is a poor estimate of circuit delay since this path may be false, i.e., *it cannot propagate an event.* Thus, the true delay corresponds to the length of the longest true path. This forced us to examine the conditions under which a path is true. We introduced the notion of static co-sensitization of paths which leads to the necessary and sufficient conditions for a path to be true. We have applied these results to develop a delay computation algorithm with the unique feature of being able to determine simultaneously the truth or falsity of entire sets of paths. This algorithm uses conventional stuck-at-fault testing techniques to arrive at a delay computation method that is both correct and computationally practical even for particularly difficult circuits.

Statistical Analysis

An important problem in high performance circuit design is to predict the percentage of fabricated circuits that will achieve a certain performance level (or clock speed). Accurate and efficient means of answering this question have not been developed thus far.

We have developed efficient methods to compute an exact *probability distribution* of the delay of a combinational circuit, given probability distributions for the gate and wire delays. The derived distribution gives the probability that a combinational circuit will achieve a certain performance, across the possible range. Then this information can be used to predict the expected performance of the entire circuit. We have defined the notion of a *correct* approximation, based on convex inequality, which never overestimates the percentage

of circuits that will achieve any given performance. We have shown that, given the assumption that all the topologically longest paths are responsible for the delay, our computation technique provides a correct probabilistic measure in the sense given above.

Nevertheless, false paths in a circuit may result in needlessly pessimistic probability distributions. Having defined a notion of falsity of paths when dealing with probability distributions on gate and wire delays, we give methods to identify and to ignore false paths in our probabilistic analysis to obtain correct and accurate answers to the performance prediction question.

Certified Timing Verification

The floating delay of a circuit is the delay under a single-vector static analysis condition that makes conservative assumptions about the state of the circuit before the single vector is applied (see the section above on False Path Identification). The transition delay of a circuit is the delay under a multivector dynamic-analysis condition that makes no assumptions about the state of the circuit before the vector sequence is applied but does allow for the possibility for monotonic speed-up at gates. Recently it has been shown that the transition delay of a circuit is bounded above by the floating delay, and it has been conjectured that this bound is tight in the presence of monotonic speed-ups. We have refuted this conjecture and demonstrated for the first time that the transition delay of a circuit *can differ* from the floating delay even in the presence of arbitrary monotonic speed-ups in the circuit.

We have used this result to motivate our derivation of a procedure which directly computes the transition delay of a circuit. The result of this procedure is a vector sequence which excites an event along the longest sensitizable path of the circuit under consideration. The most practical application of this result is in *certified timing verification*. In this scenario, the vector sequence generated by the transition delay calculator is applied by a timing simulator with more accurate timing models to certify the results of static timing verification. Such a procedure promises to give the high accuracy of timing simulation with the computational efficiency and comprehensive path coverage of static timing verification.

1.9.3 Asynchronous Circuit Verification

We have addressed the problem of verifying that the gate-level implementation of an asynchronous circuit with given or extracted bounds on wire and gate delays is equivalent to a specification of the asynchronous circuit behavior described as a classical flow table.

We have developed a procedure that extracts the complete set of possible flow tables from a gate-level description of an asynchronous circuit under the fixed or bounded wire delay models. Given an extracted flow table and the initial flow table specification, we have implemented procedures to construct a product flow table to check for machine equivalence under various modes of operation.

The modes of operation we have considered are fundamental mode and non-fundamental mode. We have considered single output change and multiple output change flow tables, as well as single input change and multiple input change flow tables. Flow table extraction and equivalence checking procedures have been tailored for each mode of operation and each type of asynchronous flow table.

1.9.4 Behavioral Verification

The problem of implementation verification at the behavioral level has proven to be difficult because of the lack of a strong underlying theory similar to automata or switching theory. Pipelined, parallel and serial implementations of a given behavioral description can have dramatically different automata-theoretic terminal behavior.

String Theory

We have used string function theory to develop an efficient and formal methodology for the verification of logic implementations against behavioral specifications.

We have defined six primitive relations between string functions, other than strict automata equivalence, including delay, don't care times, parallelism, encoding, input don't care and output don't care relations. These relations have attributes; for instance, the delay relation has an attribute corresponding to the number of clock cycles of delay. Using string function theory, we have derived associated circuit transformations for each of these primitive relations and formally proven that the correspondence is correct.

During synthesis, these transformations can be applied in sequence to a circuit specification to

produce a logic-level implementation. Given an arbitrarily long sequence of behavioral transformations that correspond to primitive relations occurring in arbitrary order, we have shown that we can always produce a composite relation, wherein each primitive relation occurs at most once in a predetermined order, which also relates the specification and the implementation. We can derive a set of attributes for the composite relation, given the attributes in the transformation sequence. This is possible because we can prove that the primitive relations satisfy precedence and transitivity properties.

We have shown how we can apply the composite transformations with the appropriate attributes to the behavioral specification and logic implementation and verify the resultant behavioral specification against the resultant logic implementation with *one* automata equivalence check, using any currently available method. If the resultant specification and implementation are strictly automata equivalent, then the implementation is deemed to implement correctly the specification. Preliminary experimental results have been obtained that indicate that the procedure is viable for medium-sized circuits.

Compositional Verification

The strategy described in the previous section is only viable for medium-sized circuits because an equivalence check between two automata is required. The number of states in the automata can be astronomically large since both data and control memory elements are treated uniformly and the number of states grows exponentially with the number of memory elements.

We have developed a compositional verification technique which allows for the efficient verification of the specific class of systems with synchronous globally timed control. In such systems, a single controller directs the data through the data path and decides (globally) when to move the data. These systems are verified against a specification in an applicative language such as SILAGE, which can be viewed as describing a maximally parallel synchronous machine. Both implementation and specification have string functions (input/output mappings) associated with them, and correctness is taken to mean that a certain relation holds between these string functions. These relations extend beyond strict input/output equivalence, and provide room for various behavioral transformations.

Sufficient conditions for the validity of these relations have been developed, which can be verified efficiently. They consist of the combinational correctness of the data path modules and the validity of a number of past-tense Computation Tree Logic (CTL) formulae with respect to the controller. The latter can be verified using forward finite state machine (FSM) traversal algorithms. In this way, the verification of the composite machine is reduced to the separate verification of data path modules and controller.

1.9.5 Sequential Logic Synthesis

Problems in the area of synthesis of sequential machines from State Transition Graph descriptions and the optimization of logic-level sequential circuits have been addressed. The goal is to obtain logic-level implementations that are minimal in terms of area and/or delay.

Theoretical Results on State Encoding

A prime-factorization-based approach to encoding N-state counters, where N can be arbitrary, has been developed. First, an analytical expression for the number of cubes in an optimal two-level implementation of a 2^k-state counter under a radix-2 encoding was derived. A lower bound for the number of cubes in a radix-2 encoding of an arbitrary N-state counter was also derived.

We have shown that there is a deep and interesting relationship between the prime factorization of a whole number N, and encoding a N-state counter. Factoring the number N into prime factors and encoding the smaller submachines separately can result in an encoding that requires substantially fewer cubes than a radix-2 encoding. Analytical expressions for the number of cubes in a prime-factorization-based encoding of a N-state counter, as well as upper bounds for the ratios of the number of cubes in a prime-factorization-based encoding to a radix-2 encoding for classes of counters have been derived.

Prime-factorization-based encoding algorithms provably perform better than radix-2 encoding for counters, and also lend insight into the algebraic structure of sequential machines.

Finite State Machine Decomposition

Current state assignment strategies almost exclusively employ a two-step strategy, where in the first step relationships are derived between states, and in the second step states are encoded taking into account these relationships. We have developed methods for state assignment based on the premise that optimal state assignment corresponds to finding an optimal general decomposition of a finite state machine.

We have arrived at two methods, the first of which performs multiway decomposition on the initial State Transition Graph (STG) based on the notion of transition pairs. The resulting submachines are encoded using constraint satisfaction methods. In the second method, we incrementally construct a state encoding for the given machine, one bit at a time. A 2^n-state machine is encoded in n steps, by repeated general decomposition of a 2^i-state machine into a 2^{i-1}-state submachine and a 2-state submachine. The 2-state submachine is encoded — an extra bit is added to the incremental encoding, and the process continues with the decomposition of the 2^{i-1}-state submachine.

Experimental results validate the use of decomposition-based techniques to solve the encoding problem.

Sequential Optimization at the Logic Level

Many sequential logic circuits are directly designed at the logic level without recourse to State Transition Graph descriptions. For this reason, it is important to be able to operate upon logic-level descriptions of finite state machines and optimize their area or performance characteristics.

We are in the process of investigating use of re-encoding techniques for sequential circuit optimization. In this method, we identify a good encoding for the sequential circuit by using symbolic encoding algorithms that operate on a symbolic description of the circuit which has been extracted from its logic-level implementation. Once this encoding has been identified, we re-encode the circuit, by adding encoding and decoding circuitry. We then re-optimize the circuit using combinational logic optimization algorithms.

The above process may be time-consuming for large circuits. We are developing latch selection algorithms that allow us to focus on the control logic of a design, and extract symbolic information for portions of the design, rather than the entire design.

1.9.6 Combinational Logic Synthesis for Low Power

Very little work has been done in the automated synthesis of circuits for low power consumption. While circuit style selection and power supply voltage reduction affect power dissipation considerably, given a specification of desired logical function, different logic-level implementations of the specification can have significantly different power consumptions for a particular circuit style and power supply voltage. In order to arrive at synthesis strategies that minimize power dissipation, we first have to develop efficient power estimation methods.

Probabilistic Power Dissipation Analysis

The work described here has been done in collaboration with Professor Jacob White, Dr. Kurt Keutzer of Synopsys, Inc., and Dr. Abhijit Ghosh of Mitsubishi Laboratories.

We have addressed the problem of estimating the average switching activity of VLSI sequential circuits, under random input sequences. This measure can be used to (1) gauge the power dissipation of the sequential circuit and (2) make architectural or design-style decisions during the VLSI synthesis process.

Switching activity is strongly affected by gate delays and, for this reason, we have used a general delay model in estimating switching activity. This model takes into account glitching at gate outputs in the circuit and models the inertial delay of a gate. Our method takes into account correlation caused at internal gates in the circuit due to reconvergence of input signals. In combinational circuits, uncorrelated input patterns with uniform switching rates are typically assumed, simplifying the problem of switching activity estimation. However, in sequential circuits the input sequence applied to the combinational portion of the circuit is highly correlated because some of the inputs to the combinational logic are flip-flop outputs representing the state of the circuit. We have developed exact and approximate methods to probabilistically estimate switching activity in sequential circuits that automatically compute the switching rates and correlations between flip-flop outputs.

Synthesis for Low Power

In our experiments with probabilistic power analysis, we noted that power consumption depended quite significantly on the gate-level structure of a combinational or sequential circuit. We then became interested in gauging exactly what logic structures corresponded to low power realizations. With this information we can tailor a logic optimization strategy to produce circuit topologies that consume the least amount of power.

In particular, we have established for dynamic CMOS circuits that are precharged low (high) that implementing AND (OR) gates near the inputs of the circuit and OR (AND) gates near the circuit outputs results in lower power consumption. We are currently precisely characterizing our all obser-

vations and developing a common subexpression extraction technique (for use in multilevel logic minimization) that minimizes the power consumption of a combinational circuit, while attempting to reduce the area as well.

1.9.7 Testing and Synthesis for Testability

Work in the test generation of sequential circuits is being pursued, as well as the synthesis of combinational circuits for easy testability.

Sequential Test Generation

A new approach has been developed for the state justification and differentiation processes in test generation for sequential circuits. In previously proposed algorithms, the justification and differentiation processes employ the enumeration of Boolean product terms or cubes. Cube enumeration, however, is not efficient. This is because when a Boolean function is represented by cubes, the number of cubes may grow unreasonably large. With this representation, only one cube can be enumerated at a time. This results in a depth-first search for justification sequences. Thus, the operations are very time-consuming.

Ordered binary decision diagrams (OBDDs) provide an alternative representation for Boolean functions. It has been shown that many Boolean functions and operations benefit from this representation. The algorithms we have developed use OBDDs for the justification and differentiation processes in sequential test generation. With OBDDs, the search for justification sequences can be done in a breadth-first manner or depth-first manner. In the case of breadth-first search, all cubes of a given Boolean expression can be searched at once. Experimental results demonstrate the superior efficiency of this approach over previous techniques. Speed improvements of over an order of magnitude have been achieved on industrial benchmarks.

Synthesis for Random Pattern Testability

Built-In Self Test (BIST) techniques are becoming increasingly popular. In order to use BIST efficiently, it is important that the design be amenable to random testing. Typically, designs are not very testable by random patterns. Our solution is to guide the logic optimization process to produce circuit topologies that are inherently random pattern testable.

The random pattern testability of a design is influenced by the probabilities that a random vector produces a *1* or a *0* at each wire in the circuit. In order for the design to be randomly testable, it is intuitive that each wire in the circuit be easily controlled to a *0* and easily controlled to a *1*. For instance, if the probability that a wire is at a *1* on a randomly applied input vector is strictly zero, it means the wire is redundant for a stuck-at-0 fault. An easily randomly testable design will have close to *0.5* probabilities for each wire in the circuit being a *1/0* on a randomly applied input vector. We are compiling a set of logic transformations that satisfy this condition, and are developing a logic optimization strategy that uses these transformations to improve the random testability of a given design.

1.9.8 Publications

Journal Publications

Ashar, P., A. Ghosh, and S. Devadas. "Boolean Satisfiability and Equivalence Checking Using General Binary Decision Diagrams." *Integration, the VLSI Journal.* Forthcoming.

Bryan, M.J., S. Devadas, and K. Keutzer. "Necessary and Sufficient Conditions for Robust Stuck-Open Fault Testability in Multilevel Networks." *IEEE Trans. Comput.-Aided Des.* Forthcoming.

Devadas, S. "Optimizing Interacting Finite State Machines Using Sequential Don't Cares." *IEEE Trans. Comput.-Aided Des.* 10(12): 1473-1484 (1991).

Devadas, S., and K. Keutzer. "Synthesis of Robust Delay-Fault Testable Circuits: Theory." *IEEE Trans. Comput.-Aided Des.* 1: 87-101 (1992).

Devadas, S., and K. Keutzer. "Synthesis of Robust Delay-Fault Testable Circuits: Practice." *IEEE Trans. Comput.-Aided Des.* 11(3): 277-300 (1992).

Devadas, S., and K. Keutzer. "Validatable Nonrobust Delay-Fault Testable Circuits Via Logic Synthesis." *IEEE Trans. Comput.-Aided Des.* Forthcoming.

Devadas, S., K. Keutzer, and J.K. White, "Estimation of Power Dissipation in CMOS Combinational Circuits Using Boolean Function Manipulation." *IEEE Trans. Comput.-Aided Des.* 11(3): 373-383 (1992).

Ghosh, A., S. Devadas and A.R. Newton. "Test Generation and Verification for Highly Sequen-

tial Circuits." *IEEE Trans. Comput.-Aided Des.* 10(5): 652-667 (1991).

Ghosh, A., S. Devadas, and A.R. Newton. "Heuristic Minimization of Boolean Relations Using Testing Techniques." *IEEE Trans. Comput.-Aided Des.* Forthcoming.

Ghosh, A., S. Devadas, and A.R. Newton. "Sequential Test Generation and Synthesis for Testability at the Register-Transfer and Logic Levels." *IEEE Trans. Comput.-Aided Des.* Forthcoming.

Conference Proceedings

Ashar, P., A. Ghosh, and S. Devadas. "Boolean Satisfiability and Equivalence Checking Using General Binary Decision Diagrams." *Proceedings of the International Conference on Computer Design: VLSI in Computers and Processors,* Boston, October 1991.

Ashar, P., S. Devadas, and K. Keutzer. "Resynthesis of Combinational Logic Circuits for Robust Gate-Delay-Fault Testability." *Proceedings of the International Test Conference,* Nashville, Tennessee, October 1991.

Cheng, K-T., S. Devadas, and K. Keutzer. "A Partial-Scan Approach to Robust Delay-Fault Test Generation for Sequential Circuits." *Proceedings of the International Test Conference,* Nashville, Tennessee, October 1991.

Devadas, S., K. Keutzer, and S. Malik. "Delay Computation in Combinational Logic Circuits: Theory and Algorithms." *Proceedings of the International Conference on Computer-Aided Design,* Santa Clara, California, November 1991.

Devadas, S., K. Keutzer, and A.S. Krishnakumar. "Design Verification and Reachability Analysis Using Algebraic Manipulation." *Proceedings of the International Conference on Computer Design: VLSI in Computers and Processors,* Boston, October 1991.

Devadas, S., H-F. Jyu, K. Keutzer, and S. Malik. "Statistical Timing Analysis of Combinational Logic Circuits." *Proceedings of the International Workshop on Timing Issues in the Specification and Synthesis of Digital Systems (TAU92),* Princeton, New Jersey, March 1992.

Devadas, S., K. Keutzer, S. Malik, and A. Wang. "Certified Timing Verification and the Transition Delay of a Circuit." *Proceedings of the International Workshop on Timing Issues in the Specification and Synthesis of Digital Systems (TAU92),* Princeton, New Jersey, March 1992.

Devadas, S., K. Keutzer, S. Malik, and A. Wang. "Computation of Floating Mode Delay in Combinational Logic Circuits: Practice and Implementation." *Proceedings of the International Workshop on Timing Issues in the Specification and Synthesis of Digital Systems (TAU92),* Princeton, New Jersey, March 1992.

Devadas, S., K. Keutzer, S. Malik, and A. Wang. "Efficient Timing Simulation for Delay Computation." *Proceedings of the MIT/Brown Conference on Advanced Research in VLSI and Parallel Systems,* Providence, Rhode Isand, March 1992.

Kukula, J., and S. Devadas. "Finite State Machine Decomposition By Transition Pairing." *Proceedings of the International Conference on Computer-Aided Design,* Santa Clara, California, November 1991.

Van Aelten, F., J. Allen, and S. Devadas. "Verification of Relations Between Synchronous Machines." *Proceedings of the International Conference on Computer-Aided Design,* Santa Clara, California, November 1991.

Van Aelten, F., J. Allen, and S. Devadas. "Compositional Verification of Systems with Synchronous Globally Timed Control." *Proceedings of the MIT/Brown Conference on Advanced Research in VLSI and Parallel Systems,* Providence, Rhode Island, March 1992.

Van Aelten, F., S. Devadas, and A. Ghosh. "Test Generation and Verification at the Behavorial Level." *Proceedings of the Third Synthesis and Simulation Meeting and International Exchange (SASIMI) Workshop,* Kobe, Japan, April 1992.

Chapter 2. Computer-Aided Fabrication System Structure

Academic and Research Staff

Professor Donald E. Troxel, Michael B. McIlrath, Wilberto Martinez, Thomas J. Lohman

Graduate Students

Michael L. Heytens, Kyle K. Iwai, Abbas Kashani, Weng-Yew Ko

Technical and Support Staff

Francis M. Doughty

2.1 CAFE—The MIT Computer-Aided Fabrication Environment

Sponsor

Defense Advanced Research Projects Agency
MDA 972 88-K-0008

2.1.1 Research Goals and Objectives

CAFE (Computer-Aided Fabrication Environment) is a software system being developed at MIT for use in the fabrication of integrated circuits and microstructures. The distinguishing feature of CAFE is that it can be used in all phases of process design, development, planning, and manufacturing of integrated circuit wafers. This manufacturing software system is unique because a process flow representation is developed and integrated into actual fabrication operations.

Presently CAFE provides day-to-day support to research and production facilities at MIT with both flexible and standard product capabilities. This software system provides a platform for work in several active research areas including "technology" (process and device) computer-aided design (TCAD), process modeling, manufacturing quality control, and scheduling.

2.1.2 Architecture

The CAFE architecture is a computer integrated manufacturing (CIM) framework for the deployment and integration of integrated circuits and process design and manufacturing software. CAFE uses an object-oriented database model which is implemented in a layered manner on top of a relational database. Our database schema is based on GESTALT, an object-oriented extensible data model. GESTALT is a layer of abstraction which maps user defined objects onto existing data... systems (e.g., a relational DBMS) and shields application programs from the details of the underlying database. The integration architecture includes the conceptual schema and models used to represent the integrated circuit manufacturing domain in CAFE, and the user and programmatic interfaces with its various applications. Two important CAFE applications relate process simulation and actual wafer fabrication to the same process flow representation.

2.1.3 Process Flow Representation

During the past year, progress in process flow representation (PFR) was made in three major areas: fundamental modeling, application to fabrication at MIT, and cooperative efforts with industry to define and test a process representation standard.

A high level conceptual model for describing and understanding semiconductor manufacturing process knowledge is a crucial component both of the research program and CAFE implementation. Driven by the needs of process control and optimization research, including sophisticated modeling, design, and experimental model verification, our fundamental conceptual process model has evolved from a two-stage generic process model into one which is part of a more general process modeling framework. The two-stage model is treated as a special case.

To take advantage of an opportunity to apply our research, extensive effort was directed toward industrial efforts in Technology (process and device) CAD Framework (TCAD) to define a broadly applicable semiconductor process representation (SPR) standard. Based largely on the conceptual process model described above, a high

level information model of semiconductor processes is being developed in conjunction with Motorola, IBM, and Texas Instruments, as well as other representatives from industry and universities. A prototype SPR implementation and programming interface was developed and employed in the TCAD Framework demonstration in August 1991.

2.1.4 CAFE Applications

The fabrication of wafers with a process represented as a PFR involves several steps. A suitable PFR for the specific process must be created and installed. Wafer lots must be created and associated with this specific PFR. These lots must then be "started" to create a task data structure which is isomorphic to the hierarchical structure of the PFR.

At this point, actual machine operations can be scheduled and reservations made for both machines and operators. Finally, the machine operations can be performed, instructions given to the operator and machines, and data collected from the operator or machine and entered into the database.

An experimental fabrication run of the MIT baseline CMOS process was made in which all operations were driven by the CAFE system using a PFR representation of the process. We have been evaluating the results of this experiment, performed in conjunction with the Integrated Circuits Laboratory staff, and preparing a plan for expanding use of PFR in the lab to other processes including research processing.

Current work involves the implementation of hierarchical scheduling, real time process control using PFR, and integration of a microelectromechanical TCAD system using PFR.

2.1.5 Publications

Boning, D.S., M.B. McIlrath, P. Penfield, and E. Sachs, "A General Semiconductor Process Modeling Framework." *IEEE Trans. Semicond. Manufact.* Forthcoming.

Ko, W.-Y. *Graphical Framework for Computer-Aided Fabrication Environment's Process Flow Representation.* S.M. thesis, Dept. of Electr. Eng. and Comput. Sci., MIT, 1991.

McIlrath, M. "A General Semiconductor Process Modeling Framework." Presentation at the Semiconductor Research Corporation (SRC) Computer Integrated Manufacturing of Integrated Circuits (CIM-IC) Workshop, Raleigh, North Carolina, August 21-23, 1991.

McIlrath, M. *Current Concepts in Semiconductor Process Representation.* CFI Document No. 91-T-2. Austin, Texas: CAD Framework Initiative, 1991.

McIlrath, M. "Semiconductor Process Representation (SPR) Server Prototyping." Presentation at the Technology Computer-Aided Design (TCAD) Working Group, San Francisco, California, June 21, 1991 (see CFI Document No. 91-M-8).

McIlrath, M. "Report on SPR Prototyping." Presentation at the TCAD SPR Working Group, Palo Alto, California, August 10, 1991 (see CFI Document No. 91-M-10).

McIlrath, M. "TCAD Framework Architectural Issues." Presentation at the TCAD Framework Plenary Session, Palo Alto, California, August 10, 1991 (see CFI Document No. 91-M-10).

McIlrath, M. "Mini-SPR Prototype Programming Interface." Unpublished technical report delivered to the TCAD SPR Working Group, June 21, 1991.

McIlrath, M. "TCAD Framework Architectural Issues." Unpublished technical report delivered to the TCAD Framework Group, Palo Alto, California, August 10, 1991.

Section 2 Digital Signal Processing

Chapter 1 Digital Signal Processing Research Program

Chapter 2 Advanced Television and Signal Processing Program

Chapter 3 Combined Source and Channel Coding for High-Definition Television

Chapter 1. Digital Signal Processing Research Program

Academic and Research Staff

Professor Alan V. Oppenheim, Professor Arthur B. Baggeroer, Professor Gregory W. Wornell, Giovanni Aliberti

Visiting Scientists and Research Affiliates

Dr. Bruce R. Musicus,[1] Dr. Ehud Weinstein[2]

Graduate Students

Paul E. Beckmann, Saurav Dev Bhatta, John R. Buck, Kevin M. Cuomo, Steven H. Isabelle, Jacek Jachner, Warren M. Lam, James M. Njeru, James C. Preisig, Michael D. Richard, Stephen F. Scherock, Andrew C. Singer, Kathleen E. Wage, Taylen J. Wong, Kambiz C. Zangi

Technical and Support Staff

Deborah A. Gage

1.1 Introduction

The Signal Processing Research Program is directed at the development of new algorithms and their applications in a variety of areas. In addition to specific projects being carried out on campus, there is close interaction with MIT Lincoln Laboratory and the Woods Hole Oceanographic Institution. The application areas that we are primarily involved with are speech, image, and underwater acoustic signal processing. In addition to algorithm development and applications, there are a number of projects directed at issues of algorithm implementation. Also affecting our research directions is the recognition that while, historically, signal processing has principally emphasized numerical techniques, it will increasingly exploit a combination of numerical and symbolic processing, a direction that we refer to as knowledge-based signal processing.

1.2 Oceanographic Signal Processing

Sponsor

U.S. Navy - Office of Naval Research
Grant N00014-91-J-1628

Project Staff

Professor Arthur B. Baggeroer

Our research programs involve the application of signal and array processing to problems in ocean and structural acoustics and geophysics. They require an understanding of both signal processing and wave propagation; moreover, most employ data from laboratory or field experiments, so an appreciation of real world issues such as noise, sensor calibrations and modeling errors is needed. Several of the topics provide the opportunity to participate in oceanographic cruises. (So far, over a dozen students have been able to participate.)

---

[1] Bolt, Beranek, and Newman, Cambridge, Massachusetts.

[2] Department of Electrical Engineering, Systems Division, Faculty of Engineering, Tel-Aviv University, Israel; adjunct scientist, Department of Applied Ocean Physics and Engineering, Woods Hole Oceanographic Institution, Woods Hole, Massachusetts.

1.2.1 Arctic Acoustics

MIT and the Woods Hole Oceanographic Institution have participated in seven experiments on the polar ice cap in the high Arctic since 1977. These programs have used large arrays to conduct studies of acoustic propagation under the ice, elastic wave propagation in the ice, ambient noise, seismic reflection and refraction, and long-range reverberation. The signal processing involves short-time spectral analysis, directional, or frequency wavenumber, spectrum estimation, source localization, matched field processing, and geophysical inverse theory.

1.2.2 Heard Island Experiment for Acoustic Monitoring of Global Warming

Sponsor

Vertical Arrays for the Heard Island Experiment
Award No. SC 48548

The Heard Island Experiment is a feasibility study for using acoustics to monitor global warming. The speed of sound in the ocean changes 4.6 m/s/degree C, so very small differences in temperature lead to significant changes in travel time when signals propagate over long ranges. A loud sound source transmitted signals from Heard Island in the southern Indian Ocean for nine days in early 1991. Receivers from nine countries aboard 14 ships were keyed to listen to the signals. We deployed two 1.4 km, 32-element vertical arrays off Bermuda and Monterey—17,000 km from the source—to listen to these signals. The objectives of this experiment are (1) to determine if the signals can be detected, and (2) to estimate the accuracy of the travel time of the modes.

1.2.3 Structural Acoustics

When sound impinges on a complicated object, it scatters into many different paths in the structure. These processes may involve reflection, mode conversion into elastic waves, and scattering. Analytic calculation of the structure response is usually intractable, so determining the energy partitioning among all the scattered signals requires both experiments and simulation using finite element and/or finite difference methods in combination with high-resolution array processing. This array processing must resolve the scattered signal components which are both transient and overlapped temporally and spatially; moreover, the signals are often measured in the nearfield so wavefront curvature and inhomogeneities become important. The research topic involves working with both experimental data and synthetics generated using finite differences to estimate both energy partitioning and scattered signals.

1.2.4 Signal Processing for Large Aperture Arrays

Adaptive processing for arrays with a small number of sensors has an extensive literature; however, when the number of sensors becomes large, there are a number of outstanding problems. The basic problem is that the statistical characterization of the ambient field requires an amount of data which exceeds the short-term stationarity of the field. Introducing adaption can lead to a situation where more sensors lead to poorer performance because the additional degrees of freedom are not well characterized. The research concerns developing adaptive array processing algorithms where the statistical characterization of the ambient field with a large number of sensors is incorporated.

1.2.5 Matched Field Processing

Matched field processing is used in underwater acoustics for processing data from large arrays when the inhomogeneity of the signal field is important. It is especially applicable to vertical arrays used for low frequency, long-range propagation. There are two major applications of matched field methods: (1) determine the location (range, depth and bearing) of an acoustic source; (2) determine the sound speed of the acoustic channel knowing the location of the source and receiver (tomography). Matched field processing can improve the resolution performance of an array by a factor of 100 by exploiting the coherence among the multipath, or modes, in the acoustic propagation. Some of the important research topics include developing robust methods which are tolerant of environmental uncertainties and determining "optimum array geometries" and adaptive processing which incorporates the mesoscale dynamics of the ocean.

1.3 Fault-Tolerant Algorithms and Architectures for Digital Signal Processing

Sponsors

Charles S. Draper Laboratories, Inc.
Contract DL-H-418472
Defense Advanced Research Projects Agency/
U.S. Navy - Office of Naval Research
Grant N00014-89-J-1489
Rockwell Corporation
Doctoral Fellowship

Project Staff

Dr. Bruce R. Musicus, Professor Alan V. Oppenheim, Paul E. Beckmann

In many digital signal processing applications, there is a high cost of failure, and continuous, error-free operation is needed. Traditionally, the problem of fault-tolerance has been solved through the use of modular redundancy. Several copies of the system operate in parallel, and their outputs are compared with voter circuitry. Modular redundancy is a very general technique and can be applied to any system. However, it does not take advantage of the details of a specific problem and thus requires substantial amounts of overhead (100% for single error detection, 200% for single error correction).

Recently, an alternative method of protecting signal processing operations called Algorithm-Based Fault-Tolerance (ABFT) has emerged.[3] It promises redundancy requirements and performance advantages similar to existing error-correcting codes. Operands are encoded using a high-level error-correcting code, and algorithms are modified to operate on the encoded data. The specific coding scheme chosen must commute with the operation being performed. ABFT thus combines the design of algorithms, architectures, and fault-tolerant systems, and results in more reliable, less costly systems.

Applications of ABFT have thus far all been linear systems, and the data encoding and fault detection/correction techniques can be described using standard linear error-correcting codes. Extension of ABFT to other operations has been limited by the absence of suitable coding schemes.

In this research, we have two major goals. First, to develop a unifying framework capable of explaining coding schemes used in existing ABFT systems. Second, to apply this framework to extend ABFT to a wider range of systems, both linear and nonlinear. Substantial progress has already been made in both areas. By using a group theoretical approach, we have shown that the encoding scheme must define an algebraic homomorphism between the original operands and their encoded form. For the important class of systematic-separate codes, this homomorphism reveals the form which the redundant information must take, enabling all applicable coding schemes to be determined. Future work will focus on describing signal processing algorithms as operations in algebraic groups.

1.4 Imaging Ice-cracks Using Diffraction Tomography

Sponsors

Defense Advanced Research Projects Agency/
U.S. Navy - Office of Naval Research
Grant N00014-89-J-1489
MIT - Woods Hole Oceanographic Institution
Joint Program

Project Staff

Professor Alan V. Oppenheim, Dr. S.D. Rajan, Saurav Dev Bhatta

This research deals with the development of an effective method for locating and observing the propagation of cracks in sea-water ice using diffraction tomography.

Ordinary tomography refers to the cross-sectional reconstruction of an object using transmission data. For geophysical applications, the data generally consist of travel time measurements of acoustic or electromagnetic waves. The objects are considered to be embedded in a homogeneous medium which contains the wave source and the receivers. As we deal with objects whose scale lengths approach the wavelength of the transmitted wave, the reconstruction from ordinary tomography becomes increasingly poor. Similar problems result when the coverage of the viewing angles is limited. Diffraction tomography, which uses the scattered (or diffracted) field to reconstruct the objects, performs much better in such cases. It can also yield a higher resolution.

---

[3] J.A. Abraham, "Fault-tolerance Techniques for Highly Parallel Signal Processing Architectures," *SPIE Highly Parallel Signal Proc. Arch.* 614: 49-65 (1986).

The main problems with applying such tomographic techniques in sea-water ice arise from the fact that the medium (ice) is inhomogeneous and elastic. The first step in the research consists of evaluating how good a reconstruction we can get using the fluid approximation. The second step involves modifying existing reconstruction algorithms, which assume a homogeneous inelastic embedding medium, to take into account the inhomogeneity and elasticity of the ice. We will focus primarily on ART (algebraic reconstruction techniques) type algorithms.

1.5 Implementation and Evaluation of a Dual-Sensor Time-Adaptive EM Algorithm for Signal Enhancement

Sponsors

Defense Advanced Research Projects Agency/
U.S. Navy - Office of Naval Research
Grant N00014-89-J-1489
Grant N00014-90-J-1109

Project Staff

Professor Alan V. Oppenheim, Dr. Ehud Weinstein, John R. Buck

This research describes the implementation and evaluation of an adaptive time-domain algorithm for signal enhancement from multiple-sensor observations. The algorithm is first derived as a noncausal time-domain algorithm, then converted into a causal, recursive form. A more computationally efficient gradient-based parameter estimation step is also presented. The results of several experiments using synthetic data are shown. These experiments first illustrate that the algorithm works on data meeting all the assumptions made by the algorithm, then provide a basis for comparing the performance of the algorithm against the performance of a noncausal frequency-domain algorithm solving the same problem. Finally, an evaluation is made of the performance of the simpler gradient-based parameter estimation step.

This work was completed in August 1991.

1.6 Quantitative Comparisons of Dolphin Signature Whistles

Sponsors

Defense Advanced Research Projects Agency/
U.S. Navy - Office of Naval Research
Grant N00014-89-J-1489

Project Staff

Professor Alan V. Oppenheim, John R. Buck

Marine mammal biologists have been interested in the identification and comparison of whistles from various dolphins for some time. The Bottle-nose Dolphin, *Tursiops truncatus*, is of particular interest because there is strong evidence that the whistles of this species are individually specific, i.e., the shape of the plot of the fundamental frequency against time of the whistle is unique to a given individual. This is generally referred to as the signature whistle hypothesis. There are varying explanations for why this occurs, but almost all researchers agree that the majority of the whistles made by a particular dolphin will exhibit the time-frequency contour characteristic of that individual and that most of the whistles not matching the individual's own signature whistle are imitations of the signature whistles of other members of the dolphin's social group.

Unfortunately, biologists have almost exclusively had to rely on qualitative judgments of similarity based on looking at printouts of spectrograms. This requires considerable investment of time until a particular researcher accumulates a sufficient mental library of contours to recognize and compare whistles within a large population. Because of the subjective nature of the judgments, the degree of similarity between two whistles can also be disputed by different researchers.

This work uses techniques from speech processing to develop a quantitative measure of similarity between dolphin signature whistles. The algorithm first extracts the contour of the primary frequency from the whistle, then compares the contour against a library of known contours to find a best fit for the unknown whistle. Like human speech, dolphin whistles are subject to fluctuations in the registration and duration of the various segments. The algorithm for comparison uses the technique of dynamic time warping to obtain the best possible registration of contours, subject to continuity restrictions.

Preliminary results indicate that the algorithm performs as well or better than any other quantitative method of signature whistle comparison.

1.7 Applications of Synchronization in Chaotic Systems

Sponsors

Defense Advanced Research Projects Agency/
U.S. Navy - Office of Naval Research
Grant N00014-89-J-1489
Lockheed Sanders, Inc./
U.S. Navy - Office of Naval Research
Contract N00014-91-C-0125
U.S. Air Force - Office of Scientific Research
Grant AFOSR-91-0034

Project Staff

Professor Alan V. Oppenheim, Kevin M. Cuomo

This research is concerned with the analysis, synthesis, and application of synchronizing chaotic dynamical systems. A chaotic system is a nonlinear deterministic system whose behavior is erratic, irregular, and similiar in many respects to stochastic processes. Two well-known examples of systems which can behave chaotically are the Lorenz and the Rossler systems. The signals that evolve in these systems form a highly structured set in the system's state space; however, scalar observations often appear unstructured and exhibit a broad Fourier spectrum. These characteristics of a nonlinear system would seem to defy synchronization; however, a chaotic system which can be decomposed into a drive system and a stable response subsystem will synchronize by coupling the drive and response systems with a common drive signal.[4]

The ability to synchronize remote systems through the use of a common drive signal suggests several novel signal processing and communication applications. We are currently exploring the use of chaotic signals and systems for spread spectrum communication and signal masking purposes.[5] We plan to develop a theoretical and computational framework to analyze and synthesize synchronizing chaotic systems that have specific signal properties and to obtain performance bounds of these new systems.

1.8 Signal Processing Applications of Chaotic Dynamical Systems

Sponsors

AT&T Laboratories Doctoral Program
Defense Advanced Research Projects Agency/
U.S. Navy - Office of Naval Research
Grant N00014-89-J-1489
Lockheed Sanders, Inc./
U.S. Navy - Office of Naval Research
Contract N00014-91-C-0125
U.S. Air Force - Office of Scientific Research
Grant AFOSR-91-0034

Project Staff

Professor Alan V. Oppenheim, Steven H. Isabelle

Researchers in areas ranging from animal behavior and medicine to economics and geophysics have found evidence of chaotic behavior in an enormous number of empirically gathered time series. Indeed, the sheer volume of apparently random phenomena which appear to have a deterministic explanation underscores the need for signal processing techniques specifically tailored to the unique charateristics of chaotic signals. In particular, because chaotic signals can generally be observed only indirectly, e.g., through some propagation channel or nonideal laboratory instrumentation, a signal's chaotic structure may be partially obscured by additive noise and convolutional distortion. Consequently, algorithms for reducing these distortions are an important component of signal processing systems for chaotic signals. This research explores the effects of convolutional distortion on chaotic signals along with techniques for reducing such distortions.

In general, the limiting trajectory of a chaotic system will be a highly structured set in the state space, while the scalar output will appear erratic and unstructured. It is this "hidden" structure that makes the signal interesting and allows for a simple description. One measure of structure which has been used to characterize a chaotic signal is the fractal dimension of its strange attractor. We are examining the effect of convolution on fractal dimension and using these results to develop deconvolution algorithms. The major challenge here is developing optimal computa-

---

[4] L.M. Pecora and T.L. Carroll, "Synchronization in Chaotic Systems," *Phys. Rev. Lett.* 64: 821-824 (1990); T.L. Carroll and L.M. Pecora, "Synchronizing Chaotic Circuits," *IEEE Trans. Circuits Syst.* 38: 453-456 (1991).

[5] K.M. Cuomo, A.V. Oppenheim, and S.H. Isabelle, *Spread Spectrum Modulation and Signal Masking Using Synchronized Chaotic Systems*, RLE TR-570 (Cambridge: MIT Research Laboratory of Electronics, 1992).

tionally efficient techniques which are uniformly applicable to a broad class of chaotic signals.

1.9 High-Resolution Direction Finding for Multidimensional Scenarios

Sponsor

U.S. Navy - Office of Naval Research
Grant N00014-91-J-1628

Project Staff

Professor Alan V. Oppenheim, Jacek Jachner

Recently, there has been considerable interest in High-Resolution Techniques for direction finding and time series analysis. Recent results[6] have improved our understanding of High-Resolution direction finding techniques in the following areas:

- Beamformer design for Beamspace approaches,
- Analytical expressions for the threshold SNR at which algorithms can resolve closely-spaced sources,
- Cramer-Rao lower bounds on the variances of unbiased estimators of direction, and
- Covariance matrix eigenstructure for closely-spaced sources.

The results are applicable to far-field planar scenarios in which the location of each source is specified by a single angular parameter.

Many practical applications of DF techniques are multidimensional in nature, requiring estimation of a vector of parameters. For example, two angular parameters are necessary in 3-D far-field problems (e.g., azimuth, elevation). Three parameters may be required in some 3-D emitter localization problems (e.g., range, azimuth, elevation). Extension of 1-D approaches to multi-D is not always direct, as several high-resolution techniques, including MinNorm and minimum dimension Beamspace algorithms fail to uniquely locate sources for multi-dimensional scenarios. This research explores the multidimensional Direction Finding problem, and extends recent 1-D results to multi-D scenarios.

1.10 Wavelet-Based Representation and Algorithms for Generalized Fractal Signals

Sponsors

Defense Advanced Research Projects Agency/
U.S. Navy - Office of Naval Research
Grant N00014-89-J-1489
U.S. Air Force - Office of Scientific Research
Grant AFOSR-91-0034

Project Staff

Professor Gregory W. Wornell, Warren M. Lam

Numerous signals and phenomena in nature can be modeled as generalized fractals. Indeed, it can be readily shown that generalized fractals constitute a much richer class of signal models that includes the familiar ARMA signals.

Despite the wide extent to which generalized fractals can be used in modeling, no satisfactory algorithms have been developed for the analysis of such signals. In the classical ARMA framework, the power spectral density (psd) of a signal is typically modeled as a sum of one-pole terms. Consequently, the psd is approximated as having sections that decay as integral powers of frequency. The psd of a generalized fractal process, on the other hand, consists of sections that decay as fractional powers of frequency. Standard methods for analyzing ARMA processes, therefore, are inadequate for the solving of problems involving generalized fractal processes.

Recently, the use of the discrete wavelet transform has made practical the analysis of 1/f or fractal processes.[7] We have been successful in applying similar methods to the analysis of a broader class of fractal processes whose psd is white at low frequencies and fractional at high frequencies. Parameter estimation problems involving such first order fractal processes have been formulated and solved. By decomposing a generalized fractal

---

[6] H.B. Lee and M.S. Wengrovitz, "Resolution Threshold of Beamspace MUSIC for Two Closely Spaced Emitters," *IEEE Trans. ASSP*, 38: 1545-1559 (1990); H.B. Lee and M.S. Wengrovitz, "Beamformer Preprocessing for Enhanced Resolution by the MUSIC Algorithm," *IEEE Trans. ASSP*, forthcoming; H.B. Lee, "The Cramer-Rao Bound on Frequency Estimates of Signals Closely Spaced in Frequency," *IEEE Trans. ASSP*, forthcoming; H.B. Lee, "Eigenvalues and Eigenvectors of Covariance Matrices for Signals Closely Spaced in Frequency," submitted to *IEEE Trans. ASSP*.

[7] G.W. Wornell, "A Karhunen-Loeve-like Expansion for 1/f Processes via Wavelets," *IEEE Trans. Info. Theory* IT-36: 859-861 (1990).

signal into a sum of one-pole fractal terms and applying the discrete wavelet transform, we investigate the possibility of an efficient algorithm for analyzing generalized fractals.

1.11 Signal Processing for Ocean Acoustic Tomography

Sponsors

Defense Advanced Research Projects Agency/
U.S. Navy - Office of Naval Research
Grant N00014-89-J-1489
MIT - Woods Hole Oceanographic Institution
Joint Program

Project Staff

Professor Alan V. Oppenheim, Dr. John L. Spiesberger, James M. Njeru

An average sound speed profile over a 1000 km section of the northeast Pacific Ocean is obtained using Ocean Acoustic Tomography from data acquired during the 1987 SVLA experiment on a long 900 m 120-hydrophone vertical acoustic array.

In particular, we pulse compress the received signal with a phase-only matched filter. The signal, centered at 80 Hz, is phase-modulated by a maximal length sequence. A fast m-sequence cross-correlation algorithm based on the Hadamard transform is used. In addition, wideband Doppler correction and coherent averaging of repetitions of the signal are performed.

The tomographic inversion is initialized from a range averaged climatological profile. Multipaths are identified from ray theory. The identified arrivals are inverted for a range-independent sound speed profile change estimate. Estimates of source and array position error are also obtained. For the limited data set used, the sound speed change estimate is found to be insignificant and a significant instrument position estimate is obtained.

This work, which is being done under the MIT-Woods Hole Oceanographic Institution Joint Program, is co-supervised by Dr. John L. Spiesberger of the Woods Hole Oceanographic Institution, Woods Hole, Massachusetts.

1.12 Chaotic Signaling in Binary Data Transmission and Detection

Sponsors

Defense Advanced Research Projects Agency/
U.S. Navy - Office of Naval Research
Grant N00014-89-J-1489
U.S. Air Force - Office of Scientific Research
Grant AFOSR-91-0034

Project Staff

Professor Gregory W. Wornell, Haralabos C. Papadopoulos

Chaotic waveforms provide a rich family of signals whose behavior and properties are currently explored in various signal processing contexts. Classical signal processing corresponds to processing signals that are either deterministic and predictable or stochastic. Chaotic signals provide a qualitatively different workspace. Signals generated from chaotic systems are not predictable even though they are completely deterministic. They are very sensitive to infinitesimal changes in initial conditions so that longterm predictability is impossible. Chaotic waveforms provide excellent candidates for use in a variety of contexts in signal processing due to their resemblance to random signals and their ease of implementation.

In this project, we are considering a very common problem in classical signal processing: the transmission of a binary data stream via waveform representation. Chaotic signals are introduced in coding the binary stream. Chaotic waveforms may prove very powerful in this context due to their ease of implementation, noise-like appearance, and broadband spectra. The signals used in such communication schemes have their own distinct dynamical behavior and characteristics. Given a sequence of noisy observations, we may readily set up a binary hypothesis test in order to detect the original binary stream.

A preliminary heuristic detection algorithm that has already been implemented shows that signal detection with sufficiently high SNR may be accomplished if sufficiently long sequence representations are used. More sophisticated algorithms are explored which take into account properties of the distinct dynamical behavior of the chaotic signals that are used to code the binary stream.

1.13 Adaptive Matched Field Processing in an Uncertain Propagation Environment

Sponsors

Defense Advanced Research Projects Agency/
U.S. Navy - Office of Naval Research
Grant N00014-89-J-1489
General Electric Foundation
Graduate Fellowship in Electrical Engineering
MIT - Woods Hole Oceanographic Institution
Joint Program
National Science Foundation
Grant MIP 87-14969
Graduate Fellowship
U.S. Navy - Office of Naval Research
Grant N00014-91-J-1628

Project Staff

Professor Alan V. Oppenheim, James C. Preisig

Adaptive array processing algorithms have achieved widespread use because they are very effective at rejecting unwanted signals (i.e., controlling sidelobe levels) and in general have very good resolution (i.e., have narrow mainlobes). However, many adaptive high-resolution array processing algorithms suffer a significant degradation in performance in the presence of environmental mismatch. This sensitivity to environmental mismatch is of particular concern in problems such as long-range acoustic array processing in the ocean where the array processor's knowledge of the propagation characteristics of the ocean is imperfect. An Adaptive Minmax Matched Field Processor has been developed which combines adaptive matched field processing and minmax approximation techniques to achieve the effective interference rejection characteristic of adaptive processors while limiting the sensitivity of the processor to environmental mismatch.

The derivation of the algorithm is carried out within the framework of minmax signal processing. The optimal array weights are those which minimize the maximum conditional mean squared estimation error at the output of a linear weight-and-sum beamformer. The error is conditioned on the propagation characteristics of the environment and the maximum is evaluated over the range of environmental conditions in which the processor is expected to operate. The theorems developed using this framework characterize the solutions to the minmax array weight problem and relate the optimal minmax array weights to the solution to a particular type of Wiener filtering problem. This relationship makes possible the development of an efficient algorithm for calculating the optimal minmax array weights and the associated estimate of the signal power emitted by a source at the array focal point. An important feature of this algorithm is that it is guaranteed to converge to an exact solution for the array weights and estimated signal power in a finite number of iterations.

The Adaptive Minmax Matched Field Processor can also be interpreted as a two-stage Minimum Variance Distortionless Response (MVDR) Matched Field Processor. The first stage of this processor generates an estimate of the replica vector of the signal emitted by a source at the array focal point, and the second stage is a traditional MVDR Matched Field Processor implemented using the estimate of the signal replica vector.

Computer simulations using several environmental models and types of environmental uncertainty have shown that the resolution and interference rejection capability of the Adaptive Minmax Matched Field Processor is close to that of a traditional MVDR Matched Field Processor which has perfect knowledge of the characteristics of the propagation environment and far exceeds that of the Bartlett Matched Field Processor. In addition, the simulations show that the Adaptive Minmax Matched Field Processor is able to maintain its accuracy, resolution, and interference rejection capability when its knowledge of the environment is only approximate and, therefore, it is much less sensitive to environmental mismatch than is the traditional MVDR Matched Field Processor.

1.14 State and Parameter Estimation with Chaotic Systems

Sponsors

Defense Advanced Research Projects Agency/
U.S. Navy - Office of Naval Research
Grant N00014-89-J-1489
Lockheed Sanders, Inc./
U.S. Navy - Office of Naval Research
Contract N00014-91-C-0125

Project Staff

Professor Alan V. Oppenheim, Michael D. Richard

Chaotic systems are nonlinear dynamical systems characterized by extreme sensitivity to initial conditions. A signal generated by a chaotic system may appear random, despite its having been generated by a low-order, deterministic dynamical system. Both random and chaotic signals lack longterm predictability; but, in contrast to truly random signals, chaotic signals exhibit short-term

predictability. Evidence of chaotic behavior has been reported in many diverse disciplines, including physics, biology, engineering, and economics.

We are exploring techniques for state and parameter estimation with chaotic systems. We have implemented the extended Kalman filter,[8] a recursive state estimator for nonlinear systems, and several related algorithms,[9] and have evaluated their effectiveness as state estimators for chaotic systems. Preliminary results have shown these algorithms to perform reasonably well. But, these results have also shown these algorithms to suffer potentially unacceptable deficiencies when applied to chaotic systems.

More recently, we have developed and begun testing several related novel, state-estimation techniques which are loosely motivated by maximum likelihood state estimation.[10] The techniques exploit a distinguishing property of all chaotic systems—the simultaneous existence of stable and unstable manifolds.[11] The combination of these techniques with an Estimate-Maximize (EM) algorithm is also being considered. Finally, we plan to ascertain the value of various state-estimation techniques in improving the short-term predictability of chaotic signals.

1.15 Causal Filters with Negative Group Delay

Sponsors

Defense Advanced Research Projects Agency/
U.S. Navy - Office of Naval Research
Grant N00014-89-J-1489
National Science Foundation
Graduate Fellowship

Project Staff

Professor Alan V. Oppenheim, Stephen F. Scherock (Independent Research)

Traditional prediction schemes often assume an input signal with a fixed (ARMA) model. The performance of such schemes degrades as the input signal deviates from the model. In particular, a fixed linear predictor performs poorly when the characteristics of the signal vary with time (as would the output of a frequency-hopping transmitter). This research investigates the design of filters which have a negative group delay characteristic over a desired frequency range. Since negative group delay corresponds to positive time advance, one might initially think that all filters of this type were noncausal, therefore unrealizable in real time. In fact, causal filters with negative group delay can be realized. Such filters could provide a new framework for predicting a signal that is only known to lie within a certain band.

Two filter design algorithms have been implemented, one for FIR filters and one for IIR filters. The FIR filter design algorithm is based on minimizing prediction error over a band and reduces to a Weiner predictor in extreme cases. The IIR design algorithm uses the complex cepstrum to specify group delay, then attempts to find a rational Z transform matching the desired cepstrum. The quality of the filters has been characterized with two new error measures.

Further work may include the development of new design algorithms and theoretical bounds on performance.

---

[8] A. Jazwinski, *Stochastic Processes and Filtering Theory* (New York: Academic Press, 1970); M.D. Richard, "State Estimation with Discrete-Time Chaotic Systems Using the Extended Kalman Filter," unpublished technical report, September 1991.

[9] A. Willsky, Course Notes for 6.433 "Recursive Estimation," unpublished, 1989.

[10] M.D. Richard, "State Estimation with Discrete-Time Chaotic Systems Using the Extended Kalman Filter," unpublished technical report, September 1991.

[11] J. Eckmann and D. Ruelle, "Ergodic Theory of Chaos and Strange Attractors," *Rev. of Mod. Phys.* 57(3), Part 1: 617-656 (1985).

1.16 Codebook Prediction: A Nonlinear Signal Modeling Paradigm

Sponsors

Defense Advanced Research Projects Agency/
U.S. Navy - Office of Naval Research
Grant N00014-89-J-1489
Lockheed Sanders, Inc./
U.S. Navy - Office of Naval Research
Contract N00014-91-C-0125
U.S. Air Force - Office of Scientific Research
Grant AFOSR-91-0034

Project Staff

Professor Gregrory W. Wornell, Professor Alan V. Oppenheim, Andrew C. Singer

A standard assumption made in signal processing is that an observed signal is the product of a linear, time-invariant system. Signals of this class have a rich history for which the mathematics is tractable, and many techniques have been explored. Based on this assumption, many linear methods of signal prediction and smoothing are used in applications such as speech and image coding and forecasting. However, many signals of interest arise from physical processes that are inherently nonlinear. Consequently, nonlinear dynamical system models may be much better suited to these phenomena.

Recently, the subject of nonlinear dynamics in general, and chaotic dynamics in particular, has attracted increased attention in the research literature. A number of new paradigms for signal modeling have emerged. While initial attention had focused on the study of the richness of behavior and properties of such systems, now there is considerable interest in the problems of modeling data based on this class of systems and addressing problems of signal processing for them. We are presently considering a number of these problems, based on the preliminary work of Farmer, Casdagli, Abarbanel, and others which address problems of prediction and smoothing based on a state space framework.

1.17 Synthesis, Analysis, and Processing of Fractal Signals

Sponsors

Canada Natural Sciences and Engineering
Research Council
Defense Advanced Research Projects Agency/
U.S. Navy - Office of Naval Research
Grant N00014-89-J-1489
Lockheed Sanders, Inc.
National Science Foundation
Grant MIP 87-14969
U.S. Air Force - Office of Scientific Research
Grant AFOSR-91-0034

Project Staff

Professor Gregory W. Wornell

Fractal geometry arises in a truly extraordinary range of natural and man-made phenomena. The 1/f family of fractal random processes, in particular, are appealing candidates for data modeling in a wide variety of signal processing scenarios involving such phenomena. In contrast to the well-studied family of ARMA processes, 1/f processes are typically characterized by persistent long-term correlation structure. However, the mathematical intractability of such processes has largely precluded their use in signal processing. We introduce and develop a powerful Karhunen-Loeve-like representation for 1/f processes in terms of orthonormal wavelet bases that considerably simplifies their analysis. Wavelet-based representations yield highly convenient synthesis and whitening filters for 1/f processes and allow a number of fundamental detection and estimation problems involving 1/f processes to be readily solved. In particular, we obtain robust and computationally efficient algorithms for parameter and signal estimation with 1/f signals in noisy backgrounds, coherent detection in 1/f backgrounds, and optimal discrimination between 1/f signals. Results from a variety of simulations are presented to demonstrate the viability of the algorithms.

In contrast to the statistically self-similar 1/f processes, homogeneous signals are governed by deterministic self-similarity. Orthonormal wavelet bases play an equally important role in the representation of these signals, and, in fact, are used to construct orthonormal "self-similar" bases. The spectral and fractal characteristics of homogeneous signals make them appealing candidates for use in a number of applications. As one potential example, we consider the use of homogeneous signal sets in a communications-based context. In particular, we develop a strategy for embedding information into a homogeneous waveform on all time-scales. The result is a unique multirate modulation strategy that is well-suited for use with noisy channels of simultaneously unknown duration and bandwidth. Computationally efficient modulators and demodulators are developed for the scheme, and the results of a preliminary performance evaluation are presented. Although not yet a fully developed protocol, "fractal modulation" represents a novel and compelling paradigm for communication.

1.18 Active Noise Cancellation

Sponsors

Defense Advanced Research Projects Agency/
U.S. Navy - Office of Naval Research
Grant N00014-89-J-1489
U.S. Air Force - Office of Scientific Research
Grant AFOSR-91-0034

Project Staff

Professor Alan V. Oppenheim, Kambiz C. Zangi

Unwanted acoustic noise is a by-product of many industrial processes and systems. With active noise cancellation (ANC), one introduces secondary noise sources to generate an acoustic field that interferes destructively with the unwanted noise, thereby eliminating it. Examples of such unwanted noise include machinery noise, aircraft cabin noise, and fan noise.

Traditional active noise cancellation systems assume that the statistical characteristic of the primary noise is known a priori. Furthermore, almost all of the existing systems use two microphones and, as a result, suffer from an acoustic feedback between the cancelling speaker and the input microphone.[12]

We have developed an adaptive active noise cancellation system which uses one microphone, and therefore has no feedback problem. This system uses the estimate maximize (EM) algorithm to simultaneously estimate the noise statistics and the transfer function between the cancelling speaker and the microphone. An optimal cancelling signal is then generated based on these estimates.[13]

We have also developed a two microphone version of the above system which does not suffer from the feedback problem and is more intelligent in using the outputs of the microphones.

We are currently studying the problem of noise cancellation in a volume. A topic of fundamental interest is finding analytically simple ways to describe the sound field over a volume from measurements made at a finite set of points in that volume. Similarly, we would like to find ways to alter the sound field in a desired manner using only a finite number of sources.

---

[12] L.J. Eriksson, M.C. Allie, and C.D. Bremigan, "Active Noise Control Using Adaptive Digital Signal Processing," *Proc. ICASSP*, New York, 1988, pp. 2594-2597.

[13] E. Weinstein, A. Oppenheim, and M. Feder, *Signal Enhancement Using Single and Multi-Sensor Measurements*, RLE TR-560 (Cambridge: MIT Research Laboratory of Electronics, 1990); A. Oppenheim, E. Weinstein, K. Zangi, M. Feder, D. Gauger, "Single Sensor Active Noise Cancellation Based on the EM Algorithm," submitted to *IEEE Trans. on Signal Proc.*, 1991; M. Feder, A. Oppenheim, and E. Weinstein, "Methods for Noise Cancellation Based on the EM Algorithm," *Proc. ICASSP*, April 1987, pp. 201-204.



Professor Jae S. Lim with Research Assistants (from left) Lon E. Sunshine and Peter A. Monta

Chapter 2. Advanced Television and Signal Processing Program

Academic and Research Staff

Professor Jae S. Lim, Giampiero Sciutto

Graduate Students

John G. Apostolopoulos, Babak Ayazifar, Matthew M. Bace, David M. Baylon, Michael S. Brandstein, Shiufun Cheung, Ibrahim A. Hajjahmad, John C. Hardwick, Eddie F. Lee, Peter A. Monta, Aradhana Narula, Julien J. Nicolas, Lon E. Sunshine, Chang Dong Yoo

Technical and Support Staff

Debra L. Harring, Cindy LeBlanc

2.1 Introduction

The present television system was designed nearly 35 years ago. Since then, there have been significant developments in technology which are highly relevant to the television industry. For example, advances in the very large scale integration (VLSI) technology and signal processing theories make it feasible to incorporate frame-store memory and sophisticated signal processing capabilities in a television receiver at a reasonable cost. To exploit this new technology in developing future television systems, Japan and Europe established large laboratories which are funded by government or industry-wide consortia. The lack of this type of organization in the United States was considered detrimental to the broadcasting and equipment manufacturing industries, and in 1983 the Advanced Television Research Program (ATRP) was established at MIT by a consortium of American companies.

Currently, the consortium members include ABC, Ampex, General Instrument, Kodak, Motorola, NBC, NBC Affiliates, PBS, Tektronix, and Zenith. The major objectives of the ATRP are:

1. To develop the theoretical and empirical basis for the improvement of existing television systems, as well as the design of future television systems.
2. To educate students through television-related research and development and to motivate them to undertake careers in television-related industries.
3. To facilitate continuing education of scientists and engineers already working in the industry.
4. To establish a resource center to which problems and proposals can be brought for discussion and detailed study.
5. To transfer the technology developed from this program to the industries.

The research areas of the program include the design of a channel-compatible advanced television (ATV) system, a receiver-compatible ATV system and digital ATV system, and development of transcoding methods. Significant advances have already been made in some of these research areas. A digital ATV system has been designed and is scheduled to be tested in 1992 by the Federal Communications Commission (FCC) for its possible adoption as the U.S. HDTV standard for terrestrial broadcasting.

In addition to research on advanced television systems, the research program also includes research on speech processing. Current research topics include development of a new speech model and algorithms to enhance speech degraded by background noise. We are also investigating methods to display spectrograms more efficiently.

2.2 ATRP Facilities

The ATRP facilities are currently based on a network of eight Sun-4 workstations. There is approximately 14.0 GB of disk space distributed among the various machines. Attached to one of the Sun-4s is a VTE display system with 256 MB of RAM. This display system is capable of driving the Sun-4 monitors or a 29-inch Conrac monitor in the lab at rates up to 60 frames/sec. In addition to displaying high-resolution, real-time sequences, ATRP facilities include a Metheus frame buffer which drives a Sony 2k×2k monitor. For hard copy output, the lab uses a Kodak XL7700 thermal imaging printer which can produce 2k×2k color or black and white images on 11-inch × 11-inch photographic paper.

Other peripherals include an Exabyte 8 mm tape drive, a 16-bit digital audio interface with two channels and sampling rates up to 48 kHz per channel, and an "audio workstation" with power amplifier, speakers, CD player, tape deck, etc. Additionally, the lab has a 650 MB optical disk drive, a CD-ROM drive, and two laser printers. For preparing presentations, ATRP facilities also include a MacIntosh SE30 microcomputer, a Mac IIx, and an Apple LaserWriter.

To support the growing computation needs of the group, several additional Sun-4 workstations will be installed in the near future. They will have 24-bit color displays, local disk storage, and digital signal processing boards to assist with computation-intensive image processing. Some of the existing machines may also be supplemented with these DSP boards. In addition, the group will be purchasing image scanning equipment.

We are considering installing a fast network (FDDI) to augment the current 10 Mbps Ethernet. The new network would enable much faster data transfer to display devices, and it would support large NFS transfers more easily.

2.3 Coding of the Motion-Compensated Residual for an All-Digital HDTV System

Sponsor

Advanced Television Research Program

Project Staff

John G. Apostolopoulos

An All-Digital High-Definition Television System is being developed at MIT to transmit higher quality video and audio information in the same channel bandwidth as today's conventional television. To achieve this goal, the system must reduce redundant information which exists because of the high correlation inherent to video and audio.

For normal television broadcasts, the image from one frame to the next is very similar. In order to reduce this temporal redundancy, motion-estimation/motion-compensation is applied to the HDTV video to predict the current frame from the previous frame. The error in this prediction, also referred to as the motion-compensated residual (MC-residual), is then coded and transmitted over the channel. The focus of this research is to determine the optimal method to represent and encode the MC-residual so that the highest quality video can be produced within the limited available bit rate (approximately 0.2 to 0.35 bits/pixel).

To reduce the spatial redundancy of the MC-residual, a transform/subband filtering scheme must be applied. Toward this goal, the Block DCT, the Lapped Orthogonal Transform, and the Multi-scale schemes are examined. A number of important observations/considerations have arisen from this work:

1. Both the Block DCT and the Lapped Orthogonal Transform suffer from structured blocking artifacts that are visually degrading. The Multi-scale scheme, on the other hand, does not suffer from these artifacts.
2. The Multi-scale scheme can be implemented using a number of filterbanks, but the precise filterbank chosen is critical to its performance. For example, the original filterbank utilized for the Multi-scale scheme resulted in detracting ripple artifacts. A new filterbank eliminated these artifacts, but at the expense of reduced coding efficiency.
3. The MC-residual is more highpass in nature than a typical image, and, to take advantage of this, new frequency decompositions should be investigated.
4. Also, as the temporal prediction may be in error, a spatially adaptive inter/intra-coding scheme is found to be essential in order to achieve the highest quality reconstructed video.

This research was completed in August 1991.

2.4 Motion-Compensated Vertico-Temporal and Spatial Interpolation

Sponsor

Advanced Television Research Program

Project Staff

Babak Ayazifar

In this project, we examine the application of a motion-estimation algorithm to the field and line-rate conversion issues which exist in the process of converting video signals from European to American standards and vice-versa.

Topics explored are simultaneous temporal and vertical interpolation of image sequences and also strictly spatial interpolation of individual frames (e.g., line and column doubling) using a novel generalized form of the well known "spatio-temporal" constraint equation-based motion estimation algorithms.

This work was completed in January 1992.

2.5 Design of a Channel-Compatible HDTV System

Sponsors

Adams-Russell Electronics, Inc.
Advanced Television Research Program
National Science Foundation Fellowship
Grant MIP 87-14969

Project Staff

Matthew M. Bace, Lon E. Sunshine

The MIT-Hybrid High-Definition Television System is a video coding scheme designed to deliver high-quality video through a standard 6 MHz terrestrial broadcast channel. It is intended to be applied to a progressively scanned source which has a spatial resolution of 720×1280 pixels and a temporal resolution of 30 frames per second. The MIT-Hybrid System makes use of a hybrid modulation scheme which allows it to deliver 10 million bits and 10 million samples per second through a standard 6 MHz terrestrial broadcast channel. Some of the digital bandwidth is set aside for four channels of CD-quality audio.

The primary basis for the MIT-Hybrid System is spatial subband decomposition and block adaptive selection of important subband coefficients. Several additional measures are incorporated to combat channel noise, most notably adaptive amplitude modulation (pre-emphasis) of the selected high spatial frequency components and a hybrid analog/digital representation of important low-frequency components.

Energy compaction is achieved by spatially transforming 8 × 8 blocks into their subband representation. An 8-band, 16-tap LOT-type filter bank is applied in both the vertical and horizontal directions. In order to minimize the complexity and the storage requirements of the system, no temporal filtering is performed.

Subband coefficient selection is done on a block adaptive basis. The Y, I, and Q components are each handled separately. For each component, every 8 × 8 block (in its transform domain representation) is divided into several zones. The selection procedure starts with the computation of the average energy in each zone in every block of the frame. Then the most energetic zones in the entire frame are selected. Thus, the number of zones (and coefficients as well) selected may vary from one block to another. Some of the zones are always selected, such as the luminance (Y) DC component, and some are never selected, such as the high frequency I and Q coefficients.

Channel noise is combatted primarily through two techniques. A hybrid representation, which uses digital information to make each analog coefficient more robust in the presence of noise, is applied to the low frequency coefficients in the Y, I, and Q components. The number of bits used for a particular coefficient depends on the number of bits used for coding the zonal selection information, as well as the actual coefficient itself. The DC luminance coefficient, for example, is allocated the most bits. The high-frequency coefficients are protected from channel degradation by adaptive amplitude modulation. In this procedure, several of the selection zones are grouped together, and one digital value is used to scale all the coefficients in those zones by the same amount. Since one digital value is used for several coefficients, the overall digital requirement for adaptive modulation is less than that for the hybrid representation. Adaptive modulation, while being effective for combating noise in the high-frequency coefficients, is not suitable for the low-frequency components. Therefore, another scheme (such as the hybrid representation) must be employed.

2.6 Multirate Systems and Structures for Image and Video

Sponsor

Advanced Television Research Program

Project Staff

David M. Baylon

Recently, there has been a growing interest in scalable and extensible systems for image and video. Such systems are desirable in many applications because they can interface with a wide variety of source material and output devices without requiring significant modification to the system. For example, a high resolution input source can be displayed on either a high-resolution or lower resolution monitor with only slight modifications to the receiver.

This research focuses on determining how to optimally process image and video for such applications. One aspect under study involves signal representation. Because data rate is constrained in many applications, we are focusing on efficient representations that allow for data rate reduction without sacrificing quality of the resynthesized image and video. However, the algorithms for data rate reduction will allow for variable data rate reduction, so that resolution and quality can be

traded-off for bandwidth in a particular application. Both intraframe and interframe algorithms are being studied.

Another aspect of this research involves multirate/multistage structures. Multirate schemes allow resynthesis at different scales, so that image and video can be displayed on devices that may differ in size. We are investigating structures for implementing such schemes in a multistage fashion. Conditions under which single-stage structures can be implemented in a multistage fashion are also being studied. Particular attention is given to reconstructed image and video quality and computational complexity.

2.7 Development of a 1.5 Kbps Speech Vocoder

Sponsors

National Science Foundation Fellowship
U.S. Navy - Office of Naval Research
Grant N00014-89-J-1489

Project Staff

Michael S. Brandstein

The recently developed Multi-Band Excitation Speech Model has been shown to accurately reproduce a wide range of speech signals without many of the limitations inherent in existing speech model based systems.[1] The robustness of this model makes it particularly applicable to low bit rate, high quality speech vocoders. In Griffith and Lim,[2] a 9.6 Kbps speech coder based on this model was first described. Later work resulted in a 4.8 Kbps speech coding system.[3] Both of these systems have been shown to be capable of high quality speech reproduction in both low and high SNR conditions.

The purpose of this research is to explore methods of using the new speech model at the 1.5 Kbps rate. Results indicate that a substantial amount of redundancy exists between the model parameters. Current research is focused on exploiting these redundancies to quantize these parameters more efficiently. Attempts are also underway to simplify the existing model without significant reduction in speech quality.

This research was completed in June 1990.

2.8 A New Method for Representing Speech Spectrograms

Sponsors

National Science Foundation
Grant MIP 87-14969
U.S. Navy - Office of Naval Research
Grant N00014-89-J-1489

Project Staff

Shiufun Cheung

The spectrogram, a two-dimensional time-frequency display of a one-dimensional signal, is used extensively in speech research. Existing spectrograms are generally divided into two types, wideband spectrograms and narrowband spectrograms, according to the bandwidth of the analysis filters used to generate them. Due to the different characteristics of the two types of spectrograms, they are employed for different purposes. The wideband spectrogram is valued for its quick temporal response and is used for word boundary location and formant tracking. On the other hand, the narrowband spectrogram, with its high frequency resolution, is primarily used for measuring the pitch frequency.

Various attempts have been made to improve the spectrographic display. Past efforts include development of (1) neural spectrograms which use critical bandwidth analysis filters in imitation of the human auditory system and (2) better time-frequency distributions such as the Wigner distribution.

In this research, we propose a different approach. The spectrogram is viewed as a two-dimensional digital image instead of a transformed one-dimensional speech signal. Image processing techniques are used to create an improved spectrogram which preserves the desirable visual

---

[1] D.W. Griffin and J.S. Lim, "A New Model-Based Speech Analysis/Synthesis System," *IEEE International Conference on Acoustic, Speech and Signal Processing,* Tampa, Florida, March 26-29, 1985, pp. 513-516.

[2] D.W. Griffin and J.S. Lim, "A High Quality 9.6 kbps Speech Coding System," *IEEE International Conference on Acoustic, Speech and Signal Processing,* Tokyo, Japan, April 8-11, 1986.

[3] J.C. Hardwick, *A 4.8 Kbps Multi-Band Excitation Speech Coder,* S.M. thesis, Dept. of Electr. Eng. and Comput. Sci., MIT, 1988.

features of the wideband and narrowband spectrograms. This transforms a speech processing problem into an image processing problem.

Among the techniques investigated are geometric-mean merge, smaller-value merge, and use of pseudocolor. In geometric-mean merge, spectrograms are combined by evaluating the geometric mean of corresponding short-time Fourier transform magnitudes. In smaller-value merge, the combined spectrogram displays only the smaller value of the corresponding pixels in wideband and narrowband spectrograms. With pseudocolor, the spectrograms are combined by mapping the wideband spectrogram to one color and the narrowband spectrogram to another color.

These techniques are found to be simple and effective. However, since a standard for objective measure in the form of an "ideal spectrogram" does not exist, evaluation of the above schemes is difficult.

This research was completed in June 1991.

2.9 Transform Coding for High-Definition Television

Sponsor

Advanced Television Research Program

Project Staff

Ibrahim A. Hajjahmad

The field of image coding is useful for many areas. Foremost of these areas is the reduction of channel bandwidth needed for image transmission systems, such as HDTV, video conferencing, and facsimile. Another area is reduction of storage requirements. One class of image coders is known as transform image coder.[4] In transform image coding, an image is transformed to another domain more suitable for coding than the spatial domain. The transform coefficients obtained are quantized and then coded. At the receiver, the coded coefficients are decoded and then inverse transformed to obtain the reconstructed image.

One transform which has shown promising results is the Discrete Cosine Transform (DCT).[5] The DCT is a real transform with two important properties that make it very useful in image coding. One is the energy compaction property, in which a large amount of energy is concentrated in a small fraction of the transform coefficients (typically low frequency components). This property allows us to code a small fraction of the transform coefficients with a small sacrifice in quality and intelligibility of the coded images. Second is the correlation reduction property. In the spatial domain there is a high correlation among image pixel intensities. The DCT reduces this correlation, and redundant information does not have to be coded.

Currently, we are investigating the use of the DCT for bandwidth compression. New adaptive techniques are also being studied for quantization and bit allocation that can further reduce the bit rate without reducing image quality and intelligibility.

2.10 A Dual Excitation Speech Model

Sponsors

U.S. Air Force - Electronic Systems Division
Contract F19628-89-K-0041
U.S. Navy - Office of Naval Research
Grant N00014-89-J-1489

Project Staff

John C. Hardwick

One class of speech analysis/synthesis systems (vocoders) which have been extensively studied and used in practice are based on an underlying model of speech. Even though traditional vocoders have been quite successful in synthesizing intelligible speech, they have not been successful in synthesizing high quality speech. The Multi-Band Excitation (MBE) speech model, introduced by Griffin, improves the quality of vocoder speech through the use of a series of frequency dependent voiced/unvoiced decisions. The MBE speech model, however, still results in a loss of quality as compared to the original speech. This degradation is caused in part by the voiced/unvoiced decision process. A large number of frequency regions contain a substantial amount of both voiced and unvoiced energy. If a region of this type is declared voiced, then a tonal or hollow quality is added to the synthesized speech. Similarly, if the region is declared unvoiced, then addi-

---

[4] J.S. Lim, *Two-Dimensional Signal and Image Processing*, (Englewood Cliffs, New Jersey: Prentice Hall, 1990); R.J. Clarke, *Transform Coding of Images*, (London: Academic Press, 1985).

[5] N. Ahmed, T. Natarajan, and K.R. Rao, "Discrete Cosine Transform," *IEEE Trans. Comput.* C-23: 90-93 (1974).

tional noise occurs in the synthesized speech. As the signal-to-noise ratio decreases, classification of speech as either voiced or unvoiced becomes more difficult, and, consequently, degradation is increased.

A new speech model has been proposed in response to the aforementioned problems. This model is referred to as the Dual Excitation (DE) speech model due to its dual excitation and filter structure. The DE speech model is a generalization of most previously developed speech models, and, with the proper selection of the model parameters, it reduces to either the MBE speech model or to a variety of more traditional speech models.

We are currently examining use of this speech model for speech enhancement, time scale modification, and bandwidth compression. Additional areas of study include further refinements of the model and improvements of the estimation algorithms.

2.11 Design of an HDTV Display System

Sponsor

Advanced Television Research Program

Project Staff

Eddie F. Lee

Several years ago, a video filter and display unit were built by graduate students to aid in the development of an HDTV system. This unit could read large amounts of digital video data from memory, filter the data, and display the data at a high rate on a large, high-resolution monitor. Unfortunately, this display system is very complex and highly unreliable; and there is very little documentation to help diagnose any problems with the system.

This project involves the design of a new, simpler, and more reliable display system. Since little documentation is available, the older system is being analyzed to determine input specifications.

2.12 Signal Processing for Advanced Television Systems

Sponsor

Advanced Television Research Program

Project Staff

Peter A. Monta

Digital signal processing will play a large role in future advanced television systems. Major applications are: (1) source coding to reduce the channel capacity necessary to transmit a television signal and (2) display processing such as spatial and temporal interpolation. Present-day television standards will also benefit significantly from signal processing designed to remove transmission and display artifacts. This thesis will focus on algorithms and signal models designed to enhance current standards (both compatibly and with some degree of cooperative processing at both transmitter and receiver) and improve proposed HDTV systems.

The American television standard, NTSC, could be improved in a number of ways with a receiver with a high-quality display and significant computation and memory. Interlace artifacts, such as line visibility and flicker, can be removed by converting the signal to a progressive format prior to display. Color cross-effects can be greatly reduced with accurate color demodulators implemented with digital signal processing. If the original source material is film, an advanced receiver can recover a much improved image by exploiting structure in the film-NTSC transcoding process; such an algorithm has been implemented and tested.

Similar ideas apply to HDTV systems. For example, film will be a major source material well into the next century, and HDTV source coders should recognize film as a special case, trading off inherent reduced temporal bandwidth for better spatial resolution.

2.13 Relative Importance of Encoded Data Types in an All-Digital HDTV System

Sponsor

Advanced Television Research Program

Project Staff

Aradhana Narula

The Federal Communications Commission (FCC) has regulated that transmission of HDTV signals must be restricted to occupy only the same 6 MHz channel bandwidth that has been allocated for the current television system, NTSC signals. In order to fulfill this requirement and still provide the high quality images that HDTV is designed for, digital image processing techniques must be applied. An efficient coding technique is needed to compress the enormous amount of information into as few bits as possible while maintaining a high degree of

picture resolution and quality. The amount of information which must be transmitted is compressed by taking advantage of the inherent redundancy both within a single image and between subsequent picture frames, taking into account the capabilities and limitations of the human visual system.

Video compression techniques essentially form a new representation of image sequences. In the original representation, each data value corresponds to only one pixel. The data in the new representation, however, affects blocks of pixels, the size of the block varying with different types of data. For example, control information includes frame synchronization data, type of video signal, and level of quantization; in general, information that affects the entire frame. Other values of data may only affect blocks of 32×32 pixels or 8×8 size blocks. As a result of using an efficient coding scheme, the effect of transmission errors becomes more serious. A bit error in the original representation can only affect one pixel, but, in the compressed representation, the error could destroy blocks of pixels or even the entire frame. To reduce the effect of the channel errors, it is necessary to add redundancy back into the data through the use of channel coding. Some bits are more vital to the image than others, and thus it may be useful to protect the more important bits to a greater extent. In this research, the relative importance of the different types of data in video compressed representation will be determined.

2.14 Transmission of HDTV Signals in a Terrestrial Broadcast Environment

Sponsor

Advanced Television Research Program

Project Staff

Julien J. Nicolas

High-Definition Television Systems currently being developed for broadcast applications require 15-20 Mbps to yield good quality images for approximately twice the horizontal and vertical resolutions of the current NTSC standard. Efficient transmission techniques must be found in order to deliver this signal to a maximum number of receivers while respecting the limitations stipulated by the FCC for over-the-air transmission. This research focuses on the principles that should guide the design of these transmission systems.

The major constraints related to transmission of broadcast HDTV include (1) a bandwidth limitation (6 MHz, identical to NTSC); (2) a requirement for simultaneous transmission of both NTSC and HDTV signals on two different channels (Simulcast approach); and (3) a tight control of the interference effects between NTSC and HDTV, particularly when the signals are sharing the same frequency bands. Other considerations include complexity and cost issues of the receivers, degradation of the signal as a function of range, etc.

A number of ideas are currently under study. Most systems proposed to date use some form of forward error-correction in order to combat channel noise and interference from other signals. The overhead data reserved for the error-correction schemes represent up to 30 percent of the total data, and it is therefore worthwhile trying to optimize these schemes. Current work is focusing on the use of combined modulation/coding schemes capable of exploiting specific features of the broadcast channel and the interference signals. Other areas of interest include the use of combined source/channel coding schemes for HDTV applications and multiresolution coded modulation schemes.

2.15 Hybrid Analog/Digital Representation of Analog Signals

Sponsor

Advanced Television Research Program

Project Staff

Lon E. Sunshine

Transform coding has been shown to be an effective way to represent images, allowing for significant amount of data compression while still enabling high-quality reproduction of the original picture. One result of transform coding of images is that, at a given signal-to-noise ratio (spatially), low-frequency components are much more sensitive to additive noise that high-frequency components.

In the MIT-CC television system, we must employ a noise reduction technique that is able to eliminate the effect of additive noise at low frequencies. We represent these analog (continuous-amplitude) coefficients by a hybrid analog/digital signal. This representation consists of a new analog value plus a discrete-valued piece of side information. The advantage of using this hybrid format is that we can reduce the noise added to a particular coefficient by at least 6 dB for each bit used in the side information.

In our research we consider the task of determining the "best" hybrid representation for an image. Here, "best" is characterized by a tradeoff between sufficient noise reduction, simplicity in implementation, and minimization of necessary side information.

This work was completed in February 1992.

2.16 An Iterative Method for Designing Separable Wiener Filter

Sponsor

Advanced Television Research Program

Project Staff

Chang Dong Yoo

One of the most common problems in signal processing is noise cancellation or reduction. If the statistics of the undegraded signal and the noise are given, the optimal solution that minimizes the mean square error between recovered signal and undegraded original signal is the Wiener filter. In this work, we impose an additional constraint of separability on the two-dimensional filter design problem. The motivation for developing these algorithms is clearly computational efficiency. This design problem is not the same as trying to fit a separable filter to an ideal two-dimensional filter. It has been shown that the solution to this problem can be obtained by computing the SVD of the ideal two-dimensional filter. In this work, a method is being studied to go directly from the statistics of the signals to the coefficient of the separable filter without the intermediate step of computing the ideal unconstrained two-dimensional filter.

A set of nonlinear equations in the design parameters is derived and an iterative algorithm to solve them is presented. Application of this filter towards images is being explored.

Chapter 3. Combined Source and Channel Coding for High-Definition Television

Academic and Research Staff

Professor William F. Schreiber

Graduate Students

Michael O. Polley, Susie J. Wee

3.1 Project Description

Terrestrial broadcasting of High-Definition Television (HDTV) in the channels currently being used for today's televison system presents the system designer with many difficult problems. One difficulty is spectrum efficiency, i.e., to get the most service—the largest number of programs to each viewer and the highest quality image and sound—within a given overall spectrum assignment. This is complicated by the fact that channel capacity to the various receivers within the viewing area of each station varies widely. The second most important problem relates to analog channel impairments—ghosts, noise, interference, and frequency distortion. These problems actually set the limit for received image quality in most homes.

In addition, there are many characteristics which are desirable in any new television system. These include: (1) an undiminished service area for each station, (2) a practical transition scenario, (3) affordable costs to broadcasters and viewers, and (4) interoperability among systems with various applications and resolutions. The FCC has also expressed a strong desire for nondisruptive improvement over time, a property that could be readily achieved with the appropriate kind of interoperability.

The purpose of this project is to devise solutions to these problems and to achieve the characteristics listed above. To this end, we are now simulating a two-stage spread-spectrum system. In this scheme, the signal is divided into a number, N, of frequency components that become the separate signals in a code-division multiplex system. Each sample of each ac-component is multiplied by one of a number, N, of orthogonal pseudo-random (PN) sequences, thus being spread to the full channel bandwidth. The product signals are added together and transmitted. At the receiver, the sum-of-products signal is multiplied, in turn, by each of the PN sequences and integrated over the sequence length. The components can be separated perfectly since there are just N orthogonal sequences of length N. The main advantage of this technique is that the relative SNR of the various frequency components can be assigned arbitrarily while maintaining a signal format that appears to be white random noise.

This scheme can be used equally well with a wide variety of source-coding methods, analog and digital, and intraframe or interframe. In the method being used, which relies on intraframe processing only, both digital and analog data are transmitted. The analog data comprises the adaptively selected high-frequency subband samples. (They could be DCT coefficients.) The digital data comprises dc and low-frequency subband information, audio, data required to interpret the analog information, *and ancillary data.* The 6-MHz channel has capacity for 10 Mbits/second plus 10 M analog samples/second using a hybrid QAM format in which the analog information, processed as discussed for code-division (spread-spectrum) multiplexing, rides on top of the digital data.

The hybrid signal samples are subjected to a second spread-spectrum operation. They are divided into a large number of parallel data streams. A number of streams is used such that the symbol length is substantially longer than the differential time delay of the multipath signals. Each symbol is multiplied by a PN sequence as for the analog information, added together, and decoded at the receiver as described above. This has the effect of suppressing multipath, since all delayed replicas of the signal arrive within one symbol period and the autocorrelation functions of the sequences are nearly zero for all delays other than zero.

An additional advantage of the second spread-spectrum operation is that the several streams of hybrid data can be assigned different power levels. This extends the range at which some kind of picture can be received, since the highest-power component can be detected at lower CNR than the lower-power component(s). For example, if the 10-Mb/s digital data stream is divided into two 5-Mb/s streams, then at the lowest CNR, a low-resolution image can be reconstructed. At a 6 dB

higher CNR, all 10 Mb/s plus 5 Msamples/second are recoverable, making a better picture, while another 6 dB gives all 10 Msamples/second. A soft threshold of this type is essential for high spectrum efficiency when transmission of each signal is from a single centrally located transmitter, since this arrangement results in widely varying SNR at the various receivers.

Code-division multiplex permits the transmission of components whose total bandwidth is larger than the channel bandwidth, at the cost of lower SNR in the recovered image. Thus, more than 10 Msamples/second can be transmitted, giving a soft threshold and a graceful degradation of quality with distance. By extension, it is also possible to have coders of different resolutions "talk to" decoders of different resolutions, giving good interoperability.

Software simulation of the system is proceeding. The first monochrome still images have been produced and confirm our expectations for the viability of this method.

Part IV Language, Speech and Hearing

Section 1 Speech Communication

Section 2 Sensory Communication

Section 3 Auditory Physiology

Section 4 Linguistics

Section 1 Speech Communication

Chapter 1 Speech Communication

Chapter 1. Speech Communication

Academic and Research Staff

Professor Kenneth N. Stevens, Professor Jonathan Allen, Professor Morris Halle, Professor Samuel J. Keyser, Dr. Marie K. Huffman, Dr. Michel T. Jackson, Dr. Melanie Matthies, Dr. Joseph S. Perkell, Dr. Stefanie Shattuck-Hufnagel, Dr. Mario A. Svirsky, Seth M. Hall

Visiting Scientists and Research Affiliates

Dr. Shyam S. Agrawal,[1] Dr. Tirupattur V. Ananthapadmanabha,[2] Dr. Vladimir M. Barsukov, Dr. Corine A. Bickley, Dr. Suzanne E. Boyce, Dr. Carol Y. Espy-Wilson,[3] Dr. Richard S. Goldhor,[4] Dr. Robert E. Hillman,[3] Eva B. Holmberg,[5] Dr. Caroline Huang,[6] Dr. Harlan Lane,[7] Dr. John Locke,[8] Dr. John I. Makhoul,[9] Dr. Sharon Y. Manuel, Dr. Carol Ringo,[10] Dr. Anthony Traill,[11] Dr. David Williams,[12] Giulia Arman Nassi, Torstein Pedersen,[13] Jane Webster[14]

Graduate Students

Abeer A. Alwan, Hwa-Ping Chang, Marilyn Y. Chen, Helen M. Hanson, Mark A. Johnson, Ronnie Silber, Lorin F. Wilde

Undergraduate Students

Kerry L. Beach, Venkatesh R. Chari, Anna Ison, Sue O. Kim, Laura Mayfield, Bernadette Upshaw, Monnica J. Williams

Technical and Support Staff

D. Keith North, Arlene E. Wint

---

1 CEERI Centre, CSIR Complex, New Delhi, India.

2 Voice and Speech Systems, Bangalore, India.

3 Boston University, Boston, Massachusetts.

4 Audiofile, Inc., Lexington, Massachusetts.

5 MIT and Department of Speech Disorders, Boston University, Boston, Massachusetts.

6 Dragon Systems, Inc., Newton, Massachusetts.

7 Department of Psychology, Northeastern University, Boston, Massachusetts.

8 Massachusetts General Hospital, Boston, Massachusetts.

9 Bolt, Beranek and Newman, Cambridge, Massachusetts.

10 University of New Hampshire, Durham, New Hampshire.

11 University of Witwatersrand, South Africa.

12 Sensimetrics, Inc., Cambridge, Massachusetts.

13 University of Karlsruhe, Germany.

14 Massachusetts Eye and Ear Infirmary, Boston, Massachusetts.

1.1 Introduction

The overall objective of our research in speech communication is to gain an understanding of the processes whereby (1) a speaker transforms a discrete linguistic representation of an utterance into an acoustic signal, and (2) a listener decodes the acoustic signal to retrieve the linguistic representation. The research includes development of models for speech production, speech perception, and lexical access, as well as studies of impaired speech communication.

Sponsors

C.J. Lebel Fellowship
Dennis Klatt Memorial Fund
National Institutes of Health
- Grant T32-DC00005
- Grant R01-DC00075
- Grant F32-DC00015
- Grant R01-DC00266[15]
- Grant P01-DC00361[16]
- Grant R01-DC00776[17]

National Science Foundation
- Grant IRI 89-10561
- Grant IRI 88-05680[15]
- Grant INT 90-24713[18]

1.2 Studies of the Acoustics, Perception, and Modeling of Speech Sounds

1.2.1 Liquid Consonants

An attribute that distinguishes liquid consonants (such as /l/ and /r/ in English) from other consonants is that the tongue blade and tongue dorsum are shaped in such a way that there is more than one acoustic path from the glottis to the lips. One of these paths passes over the midline of the vocal tract over much of its length whereas the other, shorter, path traverses around the side of the tongue dorsum and blade in the oral portion of the tract. Measurements of the acoustic spectra of sounds produced when the vocal tract is in such a position show some irregularities in the frequency range 1.5 to 3.5 kHz. Extra spectral peaks and valleys not normally seen in nonnasal vowels or in glides are often evident in the spectrum, and some of the peaks have amplitudes that deviate from the amplitudes expected for vowels.

In an effort to understand the acoustic basis for these spectral properties, we have initiated a theoretical study of the behavior of a vocal-tract model in which there is a bifurcation of the acoustic path. Equations for the vocal-tract transfer function (from glottal source to lip output) have been developed and the transfer function has been calculated and displayed for dimensions that are estimated to be within the expected range for liquids. One outcome of this preliminary analysis is that an additional pole and zero is introduced into the transfer function in the expected frequency range (2.0 to 3.0 kHz) when the length of the tract over which there is more than one path is in the range 6-8 cm. This additional pole-zero pair is associated with the acoustic propagation time around the two portions of the split section of the tube. Further theoretical work must be supplemented by additional data on the configurations of the airways for liquids and by improved estimates of the acoustic losses for these types of configurations.

1.2.2 Fricative Consonants

The need to further describe the acoustic properties of fricatives is evident in rule-based speech synthesis, where these sounds continue to present intelligibility problems. In order to provide a baseline measure of intelligibility, identification tests have been performed with natural fricative-vowel tokens and corresponding synthetic tokens, generated using a research version of Klatt's text-to-speech rule-based system. All the strident alveolar (s, z) and palatal ($\int$, ζ) fricatives were identified correctly. The weaker labiodental (f, v) and dental (θ, δ) fricatives were frequently confused with each other. As expected, intelligibility of text-to-speech fricatives was poorer than natural speech.

Acoustic analysis was performed to determine differences between natural and synthetic stimuli that could account for observed differences in intelligibility. Our results confirmed the need for

---

[15] Under subcontract to Boston University.

[16] Under subcontract to Massachusetts Eye and Ear Infirmary.

[17] Under subcontract to Massachusetts General Hospital.

[18] U.S.-Sweden Cooperative Science Program.

improved modelling of the source changes at the fricative-vowel boundary. Intelligibility of synthetic labiodental and dental fricatives is poorer than natural, even when formant transitions appear to be reproduced accurately. Natural tokens showed subtle noise amplitude variations that were not found in synthetic stimuli. Aspiration noise was found more frequently for [f] than [θ] for natural stimuli, while no text-to-speech tokens included aspiration. Offset of noise and onset of voicing at the fricative-vowel boundary was too abrupt for voiced synthetic stimuli. Preliminary results suggested speaker dependencies in the observed noise variations and time-dependent emergence of high-frequency peaks. We plan to apply our results to modify rules for manipulating speech sources and evaluate the effect of these changes on the intelligibility and naturalness of synthetic fricatives.

1.2.3 Acoustic Properties Contributing to the Classification of Place of Articulation for Stops

The production of stop consonants generates several kinds of acoustic properties: (1) the spectrum of the initial transient and burst indicating the size of the cavity anterior to the constriction; (2) place-dependent articulatory dynamics leading to different time courses of the noise burst, onset of glottal vibrations and formant transitions; (3) formant transitions indicating the changing vocal tract shape from the closed position of the stop to a more open configuration of the following vowel. A study has been initiated to measure the relative contributions of these acoustic properties to the classification of the consonantal place of articulation using a semi-automatic procedure. The acoustic data consisted of a number of repetitions of voiceless unaspirated stops in meaningful words spoken by several female and male speakers. The spectra averaged over the stop release and at the vowel onset were used as the acoustic features. Speaker independent and vowel independent classification was about 80% using either the burst or vowel onset spectrum, and a combined strategy led to higher accuracy. These results, together with further acoustic analysis of the utterances, suggest that additional acoustic properties related to articulatory dynamics, such as the detailed acoustic structure of the burst, the time course of the formant transitions, and the voice onset time, should be included in a model for stop-consonant recognition.

1.2.4 Modeling Speech Perception in Noise: the Stop Consonants as a Case Study

A doctoral thesis on this topic by Abeer A. Alwan was completed during the past year. The abstract for that thesis follows:

This study develops procedures for predicting perceptual confusions of speech sounds in noise by integrating knowledge of the acoustic properties which signal phonetic contrasts of speech sounds with principles of auditory masking theory. The methodology that was followed had three components: (1) quantifying acoustic correlates of some phonological features in naturally-spoken utterances and using the results to generate synthetic utterances, (2) developing a perceptual metric to predict the level and spectrum of the noise which will mask these acoustic correlates, and (3) performing a series of perceptual experiments to evaluate the theoretical predictions.

The focus of the study was the perceptual role of the formant trajectories in signalling the place of articulation for the stop consonants /b, d/ in consonant-vowel syllables, where the vowel was either /ɑ/ or /ɛ/. Nonsense syllables were chosen for the perceptual study so that lexical effects such as word frequency did not bias subjects' responses. Computer-generated, rather than naturally-spoken, syllables were used to provide better control of the stimuli.

In the analysis/synthesis stage, the acoustic properties of the stop consonants /b, d/ imbedded in naturally-spoken CV syllables were quantified and the results were then used to synthesize these utterances with the formant synthesizer KLSYN88. In the context of the vowel /ɑ/, the two synthetic syllables differed in the *F*2 trajectory: the *F*2 trajectory was falling for /dɑ/ and was relatively flat for /bɑ/. In the C/ɛ/. context, both *F*2 and *F*3 trajectories were different for the consonants: *F*2 and *F*3 were flat for /dɛ/, whereas they were rising for /bɛ/.

A metric was then developed to predict the level of noise needed to mask a spectral peak corresponding to a formant peak. The metric was based on a combination of theoretical and empirical results. Two types of masking were studied: within-band masking (where the formant was within the bandwidth of the noise masker) and above-band masking (where the formant was above the upper cutoff frequency of the masker). Results of auditory masking theory, which was established primarily for pure tones, were used successfully to predict within-band masking of formant peaks. The predictive measure in this case was the signal-to-noise ratio in a critical band

around the formant frequency. The applicability of the results of masking theory to formant peaks was tested by conducting a series of discrimination and detection experiments with synthetic, steady-state vowels.

In the above-band masking case, it was found that predictions based on the two methods known for predicting aspects of this kind of masking (ANSI standards and Ludvigsen) did not agree with experimental results. An empirical algorithm was developed to account for the experimental data.

In the final stage of the study, a series of identification tests with synthetic CV utterances in noise was conducted. Two noise maskers were used in the experiments: white noise, and band-pass noise centered around the *F2* region. The spectral prominences associated with *F2* and *F3* have a lower amplitude during the transitions from the consonant than in the steady-state vowel, so that it is possible, using a steady-state noise, to mask portions of a formant transition without masking the formant peak in the vowel. Subjects' responses were analyzed with the perceptual metric developed earlier. Results showed that when the *F2* transition for C/*a*/ or the *F2* and *F3* transitions for C/ɛ/ were masked by noise, listeners interpreted the stimuli as though the formant transitions were flat. That is, /d*a*/ was heard as /b*a*/ and /bɛ/ was heard as /dɛ/.

It was also found that when only the *F2* trajectory is masked, achieved by selectively masking *F2* with a band-pass noise masker, then amplitude differences in the *F3* and *F4* regions could be used as cues for place information in the C/*a*/ case even though the trajectories of these higher formants did not differ for the two consonants.

1.2.5 Unstressed Syllables

We are continuing acoustic and perceptual studies of the vowels and consonants in unstressed syllables in utterances produced with different speech styles. Our aim is to determine what attributes of these syllables are retained and what attributes are modified or deleted when reduction occurs. We hope that the results of these studies can contribute to the development of models for lexical access that are valid for various speech styles.

In one study we have examined the acoustic manifestation of /ð/ in the definite article **the** when this article occurs in different phonetic environments. In particular we have looked at the sequence **in the** in a large number of sentences produced by several speakers. In almost all of these utterances, acoustic analysis indicates that the underlying consonant /ð/ is produced as a nasal consonant. That is, the consonant is produced with a dental closure, and the velopharyngeal opening from the preceding nasal consonant spreads through the dental closure. Production of this underlying voiced fricative as a [-continuant] consonant is a common occurrence (e.g., in absolute initial position, or following an obstruent, as in **at the** or **of the**), and consequently use of a stop-like closure following **in** is not unexpected. Comparison of the duration of the nasal murmur for the sequences **in a** and **in the** show that the duration for the latter sequence is consistently longer, with the dividing point being at about 50 ms.

In a second group of studies, we are examining the acoustic evidence for the presence of unstressed vowels in bisyllabic utterances like **below** and **support**, so that they are distinguished from the monosyllabic words **blow** and **sport**. Acoustic measurements for several speakers producing these utterances show that the speakers' attempts to implement the unstressed vowels can take several forms. These forms are consistent with a view that there are two basic requirements for an unstressed vowel. One is that the airway above the glottis should be less constricted during the vowel than in the adjacent consonants, and the other is that the glottis assumes a configuration that is narrower than that in the adjacent consonants if those consonants are obstruents. Both of these adjustments contribute to the generation of a maximum amplitude in some part of the frequency range to signal the presence of the vowel. One manifestation of these intended movements in our data is an increase in the time from the release of the first consonant to the release of the second consonant for the two-syllable utterance relative to the one-syllable one. Other acoustic measurements (such as aspiration in /p/ of **support**, and changes in spectrum amplitudes and formant frequencies between the two consonant releases in **below**) also provide evidence for the unstressed vowel. Preliminary listening tests with synthetic versions of one of these word pairs (**support-sport**) have demonstrated the perceptual importance of these various acoustic attributes.

A third set of experiments has compared the temporal and amplitude characteristics of stop consonants in post- and prestressed positions in an utterance. The data show consistent reduction in closure duration and in voice onset time for consonants in post-stressed positions. Burst amplitudes (in relation to the following vowel) for post-stressed stops are less than those for prestressed stops when the consonants are voiceless but not when they are voiced. Poststressed velar stop consonants show considerable variability in

duration and in the degree to which they exhibit imprecise releases with multiple bursts.

These studies of unstressed syllables are consistent with the notion that the intention to produce the components of these syllables can take many different acoustic forms. Models of lexical access must be sensitive to these different acoustic attributes.

1.2.6 Reductions in Casual Speech in German

For each language, there are modifications or reductions that occur in the production and acoustic patterns of utterances when they are spoken casually compared to when they are spoken carefully. Many of these reductions are language-specific, but it is expected that some of the principles governing the reductions might be universal across languages. In a preliminary effort to uncover some of these principles, a study of reductions in casual speech in German has been undertaken.

Several sentences were spoken by three speakers of German, at four speech rates ranging from careful to rapid. Acoustic characteristics of a number of components of these sentences were measured. These included measurements of the durations of several types of units, and measurements of formant frequencies and glottal vibration characteristics for selected vowels and consonants. For the more casual or rapid speech modes, the sentence durations were shorter, with function words and unstressed vowels contributing more to the duration reduction than content words and stressed vowels. The durations of the nasal consonant regions of the sentences were reduced less than other portions of the sentences. The presence of a nasal consonant (or a sequence with nasal consonants) was always preserved in the rapid utterances, whereas the distinction between voiced and voiceless obstruent consonants was often neutralized. Vowel formant frequencies for stressed vowels in content words showed greater stability with changes in rate than did the formants for unstressed vowels or vowels in function words. Some of the reductions that occur in function words in German appear to be more extreme than reductions in function words in English.

1.3 Speech Synthesis

1.3.1 Synthesis of Syllables for Testing with Different Populations of Listeners

Ongoing improvements in procedures for synthesizing consonant-vowel and vowel-consonant syllables have led to the creation of a wide inventory of synthesized syllables. One use of these syllables has been testing the phonetic discrimination and identification capabilities of an aphasic population that is being studied by colleagues at Massachusetts General Hospital. Pairs of syllables have been synthesized which differ in one phonetic feature, such as [bα-vα] (stop-continuant), [wα-vα] (sonorant-obstruent), [nα-lα] (nasal-nonnasal). Contrasts of these sorts have been studied infrequently in the past. More commonly used contrasts such as place ([bα-dα-gα],[αm-αn]) have also been synthesized. We attempted to create highly natural-sounding stimuli by manipulating every acoustic characteristic which has been observed to contribute to the phonetic contrast in question. The other acoustic characteristics of the pair of stimuli were identical. This synthesis approach facilitated the creation of continua between pairs of stimuli. Several continua have been generated by varying each acoustic parameter which differs between the endpoints in nine steps. These continua are being presented informally to normal-hearing listeners in order to assess their naturalness and will be used in studies at Massachusetts General Hospital. An initial goal of the research with aphasic listeners is to determine whether individuals or groups of individuals show a pattern in phonetic discrimination indicating that ability to discriminate some features is a prerequisite for discriminating others.

1.3.2 Synthesis of Non-English Consonants

The flexibility of the glottal source in the KLSYN88 synthesizer should make it capable of generating obstruent consonants with a variety of laryngeal characteristics. Hindi (as well as a number of other languages) contrasts stop consonants on the dimensions of both voicing and aspiration. These stop consonants can be produced with four different places of articulation. All of these consonants have been generated (in consonant-vowel syllables) with the synthesizer. Of particular interest are the voiced aspirated stops. Synthesis of these consonants requires that vocal-fold vibration continue through much of the closure interval, with glottal spreading initiated just prior to the consonantal release. The glottal parameters

are adjusted to give breathy voicing in the few tens of milliseconds after release, followed by a return to modal voicing. All syllables were judged to be adequate by native listeners.

The synthesizer has also been used to generate click sounds for perception tests by speakers of a Khoisan language that uses an inventory of clicks. Generation of the abrupt clicks /ǀ/ and /ǂ/ required that a transient source be used to excite the parallel resonant circuits of the synthesizer, with appropriate adjustment of the gains of the circuits to simulate the resonances of the oral cavity that are excited by the release of the tongue tip or tongue blade.

1.4 Studies of Speech Production

1.4.1 Degradation of Speech and Hearing with Bilateral Acoustic Neuromas

We have begun a project in which we are studying the relation between speech and hearing in people who become deaf from bilateral acoustic neuromas (NF2). The primary goal of this study is to add to the understanding of the role of hearing in the control of adult speech production. The rationale and approach to this work is similar to our ongoing work on the speech production of cochlear implant patients. Speech acoustic and physiological parameters will be recorded and speech perception will be tested in a group of (still hearing) NF2 patients who are at risk of losing their hearing. The same production parameters will be recorded at intervals for the subset of patients from the initially-recorded group who suffer further hearing loss. Thus far, we have begun the recruitment of patients from across the country, we have ordered several special-purpose transducers, and we have nearly completed the design of a comprehensive test protocol.

1.4.2 Trading Relations Between Tongue-body Raising and Lip Rounding in Production of the Vowel /u/

Articulatory and acoustic data are being used to explore the following hypothesis: the goals of articulatory movements are relatively invariant acoustic targets, which may be achieved with varying and reciprocal contributions of different articulators. Previous articulatory studies of similar hypotheses, expressed entirely in articulatory terms, have been confounded by interdependencies of the variables being studied (lip and mandible or tongue body and mandible displacements). One case in which this complication may be minimized is that of lip rounding and tongue-body raising (formation of a velo-palatal constriction) for the vowel /u/. Lip rounding and tongue-body raising should have similar acoustic effects for /u/, mainly on the second formant frequency, and could show reciprocal contributions to its production; thus, we are looking for negative correlations in measures of these two parameters. We are using an Electro-Magnetic Midsagittal Articulometer (EMMA) to track movements of midsagittal points on the tongue body, upper and lower lips and mandible for large numbers of repetitions of utterances containing /u/ in controlled phonetic environments. Initial analyses from four subjects of articulatory displacements at times of minima in absolute velocity for the tongue body during the /u/ (i.e., "articulatory targets") show evidence against the hypothesis for one subject and weakly in favor of the hypothesis for the other three.

We are currently examining: (1) trading relations between the two parameters as a function of time over the voiced interval of each vowel, and (2) relations among the transduced measures of tongue raising and lip protrusion, the resulting vocal-tract area-function changes (using measurements from dental casts and video recordings of facial movements), and changes in the vowel formants (using an articulatory synthesizer).

1.4.3 Refinements to Articulatory Movement Transduction

We have concluded that our EMMA system almost always produces sufficiently accurate measurements of the positions of articulatory structures, but we have observed in experiments with subjects (see 1.4.2 above) that there can be circumstances under which measurement error may approach or exceed acceptable limits. We are currently running bench tests to explore this issue, with the goal of developing procedures and criteria for the objective assessment of measurement error.

In order to make the original EMMA electronics function with a revised transmitter configuration, it was necessary to design and implement a phase correction circuit. This circuit has now been hard wired and installed in a box which plugs into the main unit.

1.4.4 Modeling of the Lateral Dimension in Vocal-Fold Vibration

The forces which drive vocal-fold vibration can be simulated using the Ishizaka-Flanagan two-mass model, but the model misses some of the subtleties of actual fold vibration. In particular, acoustic studies by Klatt and Klatt indicate that during breathy voicing, the vocal folds close gradually along their length, rather than all at once as in the two-mass model. We have developed a model, based on the two-mass model, which treats the fold surface as a pair of beam elements which are acted upon by the glottal pressure, a compressive stress which is proportional to the fold displacement, and a shear stress which is proportional to the deformation of the fold's inner surface. Rather than assuming a single displacement for the entire length of the fold, the displacement is smoothly interpolated from the arytenoid cartilage, through the middle of the fold, to the anterior commissure. With two degrees of freedom, the model is capable of imitating the two-mass model for tightly adducted arytenoid cartilages, and of simulating gradual fold closure during breathy voicing.

1.5 Speech Production Planning

Our studies of the speech production planning process have focussed on developing and testing models of two aspects of phonological processing: segmental (primarily the serial ordering of sublexical elements) and prosodic (particularly the phenomenon of apparent stress shift).

1.5.1 Segmental Planning

Earlier analyses of segmental speech errors like "parade fad" → "farade pad" showed that word-position similarity is an important factor in determining which segments of an utterance will interact with each other in errors, even when word stress is controlled. This result supports the view that word structure constrains the serial ordering process (i.e., the process which ensures that the sub-parts of words occur in their appropriate locations in an utterance). In fact, for some kinds of speech errors, up to 80 percent occur in word-onset position. The predeliction for word-onset errors, at least in English, may arise from a difference in processing for these segments. We are testing this hypothesis with a series of error elicitation experiments to determine whether the asymmetry is found only for the planning of syntactically-structured utterances.

1.5.2 Prosodic Planning

Recent theories of phonology have addressed the question of the location of prominences and boundaries in spoken language. These two aspects of utterances are not fully determined by syntactic and lexical structure, but instead suggest the necessity of a separate hierarchy of prosodic constituents, with intonational phrases at the top and individual syllables at the bottom. One aspect of this theoretical development has been the positing of a rhythmic grid for individual lexical items in which the columns correspond to the syllables in the utterance and the rows to degrees of rhythmic prominence. It has been argued that this grid representation should be extended to entire utterances, partly on the basis of the occurrence of apparent "stress shift." Stress shift occurs when the major perceptual prominence of a target word is heard not on its main-stess syllable (as in "massaCHUsetts") but on an earlier syllable (as in "MAssachusetts MIRacle") in certain rhythmic configurations.

Our acoustic and perceptual analyses of this phenomenon have shown that in many cases the perception of apparent stress shift is the result of the disappearance of a pitch marker from the main-stress syllable ("CHU" in the above example) when the target word appears in the longer phrase. This disappearance of the pitch accent leaves an impression of relative prominence on the earlier syllable "MA-," even though its duration does not systematically increase. Although the rise in fundamental frequency on the early syllable may be greater when the target word occurs in the longer phrase, just as a stress shift account would predict, this increased rise is also found for phrases like "MONetary POLicy," where no shift can occur because the first syllable of the target word is the main stress syllable. This result suggests that the increased *F0* movement is associated with the length of the phrase, rather than with the migration of rhythmic prominence to the left in the target word.

In summary, it appears that apparent stress shift is at least in part a matter of where the pitch accents in an utterance are located, raising the possibility that speakers tend to place pitch accents near the beginnings of prosodic constituents. We are currently testing this hypothesis with paragraphs in which the target word occurs early vs. late in its intonational phrase. We are testing this possibility in both elicited laboratory speech read aloud, and in a corpus of FM radio news speech. If we can demonstrate that pitch accent placement is at least partially determined by the beginning of a new prosodic constituent, and that pitch accents can be reliably detected in the signal, we will have a basis for proposing that listeners make use of the occur-

rence of pitch accents to help them determine which portion of an utterance to process as a constituent.

1.5.3 Integration of Segmental and Prosodic Planning

We have begun a series of experiments to explore the possibility that the segmental and prosodic aspects of production planning interact. Initial results suggest that metrically regular utterances (with repeated use of the same stress pattern) provoke fewer segmental errors than metrically irregular utterances. This preliminary finding is compatible with Shattuck-Hufnagel's hypothesis that the serial ordering process for sublexical elements occurs during the integration of syntactic/morphological information with the prosodic framework of the planned utterance. It may be that, when the prosody of an utterance is partially predictable, with stresses occurring at regular intervals, the planning process is less demanding and serial ordering operates more reliably.

1.6 Speech Research Relating to Special Populations

1.6.1 A Psychophysically-based Vowel Perception Model for Users of Pulsatile Cochlear Implants

Pulsatile multichannel cochlear implants that encode second formant frequency as electrode position (*F*0-*F*2 strategy) represent different vowels by stimulating different electrodes across the electrode array. Thus, the ability of a subject to identify different vowels is limited by his ability to discriminate stimulation delivered to different electrodes. A vowel perception model was developed for users of such devices. This model is an extension of the Durlach-Braida model of intensity resolution. It has two parts: an "internal noise" model that accounts for vowel confusions made as a consequence of poor perceptual sensitivity, and a "decision" model that accounts for vowel identification errors due to response bias. The decision model postulates that each stimulus is associated with a "response center" which represents the sensation expected by the subject in response to that stimulus. To test the vowel perception model we used d' scores in an electrode identification experiment with a male subject and predicted this subject's vowel confusion matrix employing three sets of response centers. The "natural" set was determined by places that would be maximally stimulated by each vowel in a normal cochlea; the "optimal" response center was determined by places actually stimulated by each vowel during the vowel identification experiment; and the "good fit" set used response centers that were manually adjusted to improve the model's prediction of the real matrix. Model predictions were tested against a vowel confusion matrix obtained from the same subject in a separate study.

Results using the optimal set of response centers are encouraging: the model predicted successfully some characteristics of the confusion matrix, in spite of a five-year lapse between the experiment that provided sensitivity data and the experiment where the confusion matrix was obtained. Nevertheless, there were discrepancies between predicted and real confusion matrices. These discrepancies are interestingly biased—the subject frequently mistook some vowels for other vowels with higher *F*2. These errors are consistent with a set of response centers that are close to the optimal set, but somewhat shifted in the direction of the natural set. One implication of these preliminary results is that cochlear implant users make use of the central nervous system's plasticity but at the same time this plasticity may not be unlimited.

1.6.2 The Effect of Fixed Electrode Stimulation on Perception of Spectral Information

This study was carried out in collaboration with Margaret W. Skinner and Timothy A. Holden of the Department of Otolaryngology-Head and Neck Surgery, Washington University School of Medicine, Saint Louis. The study attempts to find the underlying reasons for improvements in speech perception by users of the Nucleus cochlear implant when they employ the new Multipeak stimulation strategy instead of the older *F*0-*F*1-*F*2 strategy. For voiced sounds, the *F*0-*F*1-*F*2 strategy stimulates two channels every pitch period: these electrodes are chosen based on instantaneous estimates of *F*1 and *F*2. The Multipeak strategy stimulates two additional channels in the basal region of the cochlea. Channels 4 and 7 are typically used for voiced sounds, with delivery of pulses whose energy is proportional to the acoustic energy found in the 2.0-2.8 kHz and 2.8-4.0 kHz ranges.

We designed an experiment that employed a Multipeak-like condition, a *F*0-*F*1-*F*2 condition and a control condition, where fixed-amplitude pulses were sent to channels 4 and 7. Two subjects were tested using vowel and consonant identification tasks. The control condition provided vowel identification performance at least as good as the Multipeak condition, and significantly better than the *F*0-*F*1-*F*2 condition. Consonant identifi-

cation results for the control condition were better than for the *F*0-*F*1-*F*2 condition, but not as good as for the Multipeak condition. These results suggest that part of the improvement observed with the Multipeak strategy is due to stimulation of the fixed basal channels, which act as perceptual "anchors" or references, allowing subjects to identify the position of electrode pairs that vary in position along the electrode array.

1.6.3 Acoustic Parameters of Nasal Utterance in Hearing-Impaired and Normal-Hearing Speakers

One of the more prevalent abnormalities in the speech of the hearing impaired that contributes to reduced intelligibility is inadvertent nasality. Theoretically, a wider first formant should reflect a greater loss of sound energy within the nasal cavity, which has a relatively large surface area compared to the oral cavity of vowels. A more prominent spectral peak in the vicinity of 1 kHz should reflect a larger velopharyngeal opening, according to a theoretical analysis of a nasal configuration based on admittance curves. From acoustic analysis of the speech of hearing-impaired children, reduced first formant prominence and the presence of an extra pole-zero pair between the first and second formants characterize spectra of nasalized vowels. The difference between the amplitude of the first formant and the amplitude of the extra peak, *A*1-*P*1, was a measure that correlated with listener judgments of the degree of vowel nasalization. To obtain further validation of these parameters as measures of nasalization, *A*1 and the pole-zero spacing were systematically manipulated in synthetic utterances. Perceptual experiments with synthesized, isolated static vowels [i],[I],[o],[u] showed that both parameters contributed to the perception of nasality. Another perceptual experiment with a number of synthesized words (of the form bVt) gave results indicating somewhat different relative importance of the two parameters. Correlation of *A*1-*P*1 with the average nasality perception judgments of ten listeners was found for both groups of stimuli. Another acoustic characteristic of speech of the hearing-impaired children is the change of the extra peak amplitude over time within the vowel due to their lack of coordination of movement of the velum with movement of other articulators. From a pilot test, time variation of the first formant bandwidth and frequency of the nasal zero had a greater effect on nasality judgments when the average *A*1-*P*1 was small. This finding suggests that a somewhat nasalized vowel is perceived to be even more nasal when there is large velum movement during production of the vowel.

1.7 Models for Lexical Representation and Lexical Access

As we continue to develop models for lexical access from acoustic patterns of speech, we have been attempting to organize and refine the representation of words, segments, and features in the lexicon. The present version of the model of the lexicon organizes phonological segments into four classes according to the way the features are represented in the sound.

Two of these classes are (1) the vowels and (2) the glides and syllabic consonants. A distinguishing attribute of both these classes is that the spectrum of the sound that is produced when the segments are implemented is either relatively fixed or changes only slowly. There are no acoustic discontinuities, and all of the features of the segments are derived from the spectra sampled over a relatively long time interval and how these spectra change with time. Both classes are produced with a source at the glottis. Within this group of segments, the vowels are considered to form a class, in that the vocal tract does not have a narrow constriction that gives a distinctive acoustic attribute. They are characterized entirely by their formant pattern, and no articulator can be regarded as primary. The glides and syllabic consonants, on the other hand, have spectral characteristics that are imposed by forming a constriction with a particular articulator.

A third class of segments (traditionally classified as [+consonantal]) is produced by making a narrow constriction with a specific articulator. Formation or release of this constriction creates a discontinuity in the sound. The landmark generated by this discontinuity forms a nucleus around which acoustic information about the various features of the consonant is located, possibly over a time interval of $\pm$ 50 milliseconds or more. The fourth class consists of the clicks. The sound is of high intensity and relatively brief. The features identifying a click are contained in the spectral characteristics within a few milliseconds of the click release. These clicks are not directly relevant to English, except that they highlight the contrast between sounds that are of high intensity and concentrated in time (the clicks) and sounds of lower intensity where evidence for the features is spread over a longer time interval around an acoustic discontinuity.

In the proposed lexical representation, the classes of segments and features within these classes are organized in a hierarchical fashion. In the case of

consonants, a distinction is made between features designating the primary articulator that forms the constriction and features designating the activity of other articulators.

As a part of a project in which automatic procedures for lexical access are being developed, we are building a computer-based lexicon of words in which the representation of features for the segments in the words reflects the classification noted above. There are currently about 150 words in the lexicon. The marking of feature values within the lexicon includes the possibility of labeling a feature as being subject to modification by the context. For example, in the word **bat**, the features designating place of articulation for the final consonant are subject to modification (as in **bat man**) but the feature [-continuant] is not. A second component of the implementation of the lexical access model is to develop automatic procedures for identifying landmarks and determining the features whose acoustic correlates appear in the vicinity of the landmarks. Initial efforts in this direction are in progress.

1.8 Speech Analysis and Synthesis Facilities

Several modifications have been made to the Klattools that are used for analysis and synthesis of speech. The KLSYN88 synthesizer has been augmented to include the possibility of selecting a new glottal source (designed by Dr. Tirupattur Ananthapadmanabha) that has potential advantages and flexibility relative to the current inventory of glottal sources in the synthesizer. An inverse filtering capability has also been incorporated in the synthesizer program to allow for the possibility of generating a glottal source derived from a natural utterance.

The KLSPEC analysis program has been modified to include the possibility of obtaining a spectrum that is an average of a number of DFT spectra sampled at one-ms intervals over a specified time span. This type of averaging is especially useful when examining the spectra of noise bursts and fricative consonants. It also has application when using a short time window for measuring the spectrum of a voiced sound to avoid the necessity of careful placement of the window within each glottal period.

1.9 Publications

1.9.1 Published Papers

Alwan, A. "Modelling Speech Perception in Noise: A Case Study of the Place of Articulation Feature." *Proceedings of the 12th International Congress of Phonetic Sciences* 2: 78-81 (1991).

Bickley, C.A. "Vocal-fold Vibration in a Computer Model of a Larynx." In *Vocal Fold Physiology*. Eds. J. Gauffin and B. Hammarberg. San Diego: Singular, 1991, pp. 37-46.

Boyce, S.E., R.A. Krakow, and F. Bell-Berti. "Phonological Underspecification and Speech Motor Organisation." *Phonology* 8: 219-236 (1991).

Burton, M.W., S.E. Blumstein, and K.N. Stevens. "A Phonetic Analysis of Prenasalized Stops in Moru." *J. Phonetics* 20: 127-142 (1992).

Halle, M., and K.N. Stevens. "Knowledge of Language and the Sounds of Speech." In *Music, Language, Speech and Brain.* Eds. J. Sundberg, L. Nord, and R. Carlson. Basingstoke, Hampshire: Macmillan Press, 1991, pp. 1-19.

Kuhl, P.K., K. Williams, F. Lacerda, K.N. Stevens, and B. Lindblom. "Linguistic Experience Alters Phonetic Perception in Infants by Six Months of Age." *Sci.* 255: 606-608 (1992).

Lane, H., J.S. Perkell, M. Svirsky, and J. Webster. "Changes in Speech Breathing Following Cochlear Implant in Postlingually Deafened Adults." *J. Speech Hear. Res.* 34: 526-533 (1991).

Perkell, J.S. "Models, Theory and Data in Speech Production." *Proceedings of the 12th International Congress of Phonetic Sciences* 1: 182-191 (1991).

Perkell, J.S., E.B. Holmberg, and R.E. Hillman. "A System for Signal Processing and Data Extraction from Aerodynamic, Acoustic and Electroglottographic Signals in the Study of Voice Production." *J. Acoust. Soc. Am.* 89: 1777-1781 (1991).

Price, P.J., M. Ostendorf, S. Shattuck-Hufnagel, and C. Fong. "The Use of Prosody in Syntactic Disambiguation." *J. Acoust. Soc. Am.* 90: 1956-2970 (1991).

Price, P.J., M. Ostendorf and S. Shattuck-Hufnagel. "Disambiguating Sentences Using Prosody." *Proceedings of the 12th International Congress of Phonetic Sciences* 2: 418-421 (1991).

Shattuck-Hufnagel, S. "Acoustic Correlates of Stress Shift." *Proceedings of the 12th International Congress of Phonetic Sciences* 4: 266-269 (1991).

Stevens, K.N. "Some Factors Influencing the Precision Required for Articulatory Targets: Comments on Keating's Paper." In *Papers in Laboratory Phonology I.* Eds. J.C. Kingston and M.E. Beckman. Cambridge: Cambridge University Press, 1991, pp. 471-475.

Stevens, K.N. "Vocal-fold Vibration for Obstruent Consonants." In *Vocal Fold Physiology.* Eds. J. Gauffin and B. Hammarberg. San Diego: Singular, 1991, pp. 29-36.

Stevens, K.N. "The Contribution of Speech Synthesis to Phonetics: Dennis Klatt's Legacy." *Proceedings of the 12th International Congress of Phonetic Sciences* 1: 28-37 (1991).

Stevens, K.N., and C.A. Bickley. "Constraints Among Parameters Simplify Control of Klatt Formant Synthesizer." *J. Phonetics* 19: 161-174 (1991).

Svirsky, M.A., and E.A. Tobey. "Effect of Different Types of Auditory Stimulation on Vowel Formant Frequencies in Multichannel Cochlear Implant Users." *J. Acoust. Soc. Am.* 89: 2895-2904 (1991).

Wilde, L.F., and C.B. Huang. "Acoustic Properties at Fricative-vowel Boundaries in American English." *Proceedings of the 12th International Congress of Phonetic Sciences* 5: 398-401 (1991).

1.9.2 Papers Submitted for Publication

Holmberg, E., R. Hillman, J. Perkell, and C. Gress. "Relationships Between SPL and Aerodynamic and Acoustic Measures of Voice Production: Inter- and Intra-speaker Variation." *J. Speech Hear. Res.*

Perkell, J., M. Svirsky, M. Matthies, and M. Jordan. "Trading Relations Between Tongue-body Raising and Lip Rounding in Production of the Vowel /u/." *PERILUS,* the working papers of the Department of Phonetics, Institute of Linguistics, Stockholm. Forthcoming.

Perkell, J., and M. Matthies. "Temporal Measures of Anticipatory Labial Coarticulation for the Vowel /u/: Within- and Cross-Subject Variability." *J. Acoust. Soc. Am.*

Perkell, J., H. Lane, M. Svirsky, and J. Webster. "Speech of Cochlear Implant Patients: A Longitudinal Study of Vowel Production." *J. Acoust. Soc. Am.*

Shattuck-Hufnagel, S. "The Role of Word and Syllable Structure in Phonological Encoding in English." *Cognition.* Forthcoming.

Stevens, K.N. "Lexical Access from Features." Workshop on Speech Technology for Man-Machine Interaction, Tata Institute of Fundamental Research, Bombay, India, 1990.

Stevens, K.N. "Speech Synthesis Methods: Homage to Dennis Klatt." In *Talking Machines: Theories, Models, and Applications.* Eds. G. Bailly and C. Benoit. New York: Elsevier. Forthcoming.

Stevens, K.N. "Models of Speech Production." In *Handbook of Acoustics.* Ed. M. Crocker. New York: Wiley. Forthcoming.

Stevens, K.N., S.E. Blumstein, L. Glicksman, M. Burton, and K. Kurowski. "Acoustic and Perceptual Characteristics of Voicing in Fricatives and Fricative Clusters." *J. Acoust. Soc. Am.* Forthcoming.

Stevens, K.N. "Phonetic Evidence for Hierarchies of Features." In *LabPhon3.* Ed. P. Keating. Los Angeles: University of California. Forthcoming.

Svirsky, M., H. Lane, J. Perkell, and J. Webster. "Effects of Short-Term Auditory Deprivation on Speech Production in Adult Cochlear Implant Users." *J. Acoust. Soc. Am.* Forthcoming.

Wightman, C., S. Shattuck-Hufnagel, M. Ostendorf, and P.J. Price. "Segmental Durations in the Vicinity of Prosodic Phrase Boundaries." *J. Acoust. Soc. Am.* Forthcoming.

Section 2 Sensory Communication

Chapter 1 Sensory Communication

Chapter 1. Sensory Communication

Academic and Research Staff

Professor Louis D. Braida, Professor Richard M. Held, Dr. Joan M. Besing, Lorraine A. Delhorne, Nathaniel I. Durlach, Dr. Donald K. Eddington, Dr. Susan L. Goldman, Seth M. Hall, Dr. Xiao Dong Pang, Dr. William M. Rabinowitz, Dr. Christine M. Rankovic, Dr. Charlotte M. Reed, Dr. Mandayam A. Srinivasan, Dr. Rosalie M. Uchanski, Dr. Victor W. Zue, Dr. Patrick M. Zurek

Visiting Scientists and Research Affiliates

Dr. Richard L. Freyman, Dr. Kenneth W. Grant, Dr. Janet D. Koehnke, Dr. Jack Kotik, Dr. Neil A. Macmillan, Wei Min, Dr. Karen L. Payton, Dr. Patrick M. Peterson

Graduate Students

Santosh Ananthraman, Jyh-Shing Chen, Kiran B. Dandekar, Paul Duchnowski, Joseph A. Frisbie, Eric M. Fuchs, Julie E. Greenberg, Wolfgang G. Knecht, Gregory R. Martin, Matthew H. Power, Michael T. Richey, Barbara G. Shinn-Cunningham, Robert W. Stadler, Hong Z. Tan

Undergraduate Students

Susan E. Bach, Belinda Chen, Swaroop Gantela, Rajashi Ghosh, Andrew H. Grant, Rogeve Gulati, Darby A. Hailes, John M. Hedgcock, Albert G. Hong, Mary A. Hou, Michael H. Lim, Sandra Y. Ma, Alexa Ogno, Prashun R. Patel, Charles A. Reisman, Alexander P. Rigopulos, Diane E. Ronan, Brian A. Rubin, Sumeet Sandhu, Leon L. Ting

Technical and Support Staff

Ann K. Dix, Eleanora M. Luongo, Timothy J. Stellmach, Michael T. Tuyo

1.1 Introduction

The Sensory Communication Group is conducting research on (1) the auditory and tactual senses, (2) auditory, visual, and tactual aids for individuals who are hearing-impaired or deaf, and (3) human-machine interfaces for teleoperator and virtual-environment systems (involving the visual as well as the auditory and tactual senses). Within the domain of hearing aids, research is being conducted on systems that bypass the outer and middle ear and directly stimulate the auditory nerve electrically (cochlear prostheses), as well as on systems that stimulate the ears acoustically. The research on taction is focused not only on speech reception for the totally deaf, but also on the ability of the human hand to sense and manipulate the environment. Within the domain of human-machine interfaces, topics of special interest concern the development of principles for mapping the human sensorimotor system into non-anthropomorphic slave mechanisms (or the equivalent in virtual space) and the ability of the human sensorimotor system to adapt to alterations of normal sensorimotor loops caused by the presence of the interface.

1.2 Hearing Aid Research

Sponsor

National Institutes of Health
Grant 5 R01 DC00117

Project Staff

Dr. Joan M. Besing, Professor Louis D. Braida, Lorraine A. Delhorne, Paul Duchnowski, Nathaniel I. Durlach, Joseph A. Frisbie, Dr. Susan L. Goldman, Gregory R. Martin, Matthew H. Power, Dr. Christine M. Rankovic, Dr. Charlotte M. Reed, Dr. Rosalie M. Uchanski, Dr. Victor W. Zue, Dr. Patrick M. Zurek

This research is directed toward the development of improved hearing aids for people suffering from hearing impairments that cannot be treated medically. Since the major problem for most people with impaired hearing is a degraded ability to understand speech, and since medical treatments are available for abnormalities of the outer and middle ear, our work is directed towards aids that better match speech signals to residual auditory function in people with impairments central to the middle ear. More specifically, the research is

directed at improving speech reception for people with sensorineural impairments. The work performed during the past year can be divided into four project areas: linear amplification, speech token variability, prediction of speech intelligibility, and aids to speechreading.

1.2.1 Linear Amplification

This research has focused on (1) methods for prescribing and automatically controlling the frequency response of hearing aids, and (2) analysis of perceptual integration of acoustic speech cues across frequency. Work in the first area has included a theoretical analysis of suggested prescriptive methods for fitting frequency-gain characteristics to individual listeners[1] and a study of the use of adaptive frequency-gain characteristics to combat the effects of background interference on target speech intelligibility.[2] Work is also underway on the development of real-time signal-processing implementations of systems with adaptive frequency-gain characteristics. In the second area, we have studied the combination of cues arising from various spectral bands of speech and applied models of perceptual integration[3] to the analysis of the resulting consonant confusions.

1.2.2 Speech Token Variability

Performance in intelligibility tests for speech segments depends on the set of segments to be identified, characteristics of the talker, and the number and variability of the speech tokens chosen to represent a given segment. Speech perception experiments, which systematically controlled the number of tokens for each speech segment, have been completed for American English vowels and for normal hearing listeners. For both vowel identification and discrimination tasks, performance generally is (1) highest when only one token represents each segment and (2) roughly equal when four and sixteen tokens represent each segment.[4] The first result indicates that the use of a single token for each speech segment can lead to the use of artifacts as perceptual cues and to artificially high performance. Two additional experiments are in progress. The first is measuring the effect of number of tokens on vowel identification with cochlear implant users as listeners. The second, a vowel discrimination experiment, was designed so that its results allow development of a relationship between discriminability and previously measured physical attributes of the same vowel segments.

1.2.3 Prediction of Speech Intelligibility

This project involves development of computational methods for predicting the intelligibility of speech subjected to a waveform degradation. The approach employs a model of the human auditory system which reduces a speech waveform to a sequence of discrete symbols, each representing a prototypical vector of parameter values measured in a single frame of speech. The perceptual effect of the transformation is estimated by assessing the transmitted information between the symbol sequence derived from an untransformed (input) speech signal and that derived from a transformed (output) speech signal. Current efforts[5] are underway to assess the model's ability to predict the effects of linear filtering and additive noise on speech intelligibility.

---

[1] C.M. Rankovic and P.M. Zurek, "Evaluation of Prescriptive Fitting Procedures Using the AI Model," *ASHA* 33: 164 (1991).

[2] C.M. Rankovic, R.L. Freyman, and P.M. Zurek, "Potential Benefits of Varying the Frequency-Gain Characteristic for Speech Reception in Noise," *J. Acoust. Soc. Am.* 91: 354-362 (1992); C.M. Rankovic, P.M. Zurek, and R.L. Freyman, "Potential Benefits of Varying the Frequency-Gain Characteristic for Speech Reception in Noise for Hearing-Impaired Individuals," *J. Acoust. Soc. Am.* 90: 2319 (1991); P.M. Zurek, "Interference Reduction for the Hearing Impaired." *J. Acoust. Soc. Am.* 89: 1957 (1991).

[3] L.D. Braida, "Crossmodal Integration in the Identification of Consonant Segments," *Quart. J. Exper. Psych.* 43A(3): 647-677 (1991).

[4] R.M. Uchanski, K.M. Millier, D.E. Ronan, C.M. Reed, and L.D. Braida, "Effects of Token Variability on Resolution for Vowel Sounds," *J. Acoust. Soc. Amer.* 90(4): 2254 (1991); R.M. Uchanski, K.M. Millier, C.M. Reed, and L.D. Braida, "Effects of Token Variability on Vowel Identification," in *The Processing of Speech: From the Auditory Periphery to Word Recognition* (Berlin: Mouton de Gruyter, 1992).

[5] M.H. Power and L.D. Braida, " A Physical Measure of Consistency Among Speech Parameter Vectors: Application to Speech Intelligibility Determination," *J. Acoust. Soc. Am.* 90: 2327 (1991).

1.2.4 Aids to Speechreading

Our study of aids to speechreading has focused on (1) developing a system for the preparation of audiovisual test stimuli, and (2) evaluating the effectiveness of Cornett's manual Cued Speech system. Our research in this area requires a large corpus of speech materials that can be randomly accessed for presentation in experiments. We have begun to develop an automated facility for recording selected audiovisual recordings onto laser disks, preparing taped audiovisual tests from the laser disks, and randomly accessing recorded segments as required in identification experiments. This facility incorporates a laser-disk recorder/player system that can be operated under computer control. Results obtained with subjects who are highly experienced (8 to 25 years) in the reception of Cued Speech indicate that manually cued speech is much more intelligible than lipread speech, and under typical conversational conditions is received nearly perfectly. Work is currently underway to develop an automatic cueing system capable of generating cues that supplement speechreading as effectively as manually produced cues. Experienced receivers of Cued Speech will be tested on their ability to receive sentence materials in which cues are generated synthetically. Specified error structures will be introduced into the cues to determine the performance that must be achieved by effective automatic cueing systems.

1.3 Multimicrophone Hearing Aids

Sponsor

National Institutes of Health
Grant 5 R01 DC00270

Project Staff

Nathaniel I. Durlach, Julie E. Greenberg, Wolfgang G. Knecht, Dr. Xiao Dong Pang, Dr. William M. Rabinowitz, Robert W. Stadler, Dr. Patrick M. Zurek

The long-term goal of this research is the development of sensory aids that improve the ability of hearing-impaired listeners to function in complex acoustic environments through the use of microphone arrays. Since the reception of speech is the most important problem for the hearing impaired, the target signal of primary interest is speech.

To enhance monaural speech reception, we envision a microphone array that resolves the incoming signals into simultaneous directional channels, followed by a coding operation that transforms these resolved signals in such a way that resolution is preserved at the perceptual level after the signals are summed for presentation to a single ear.[6] Such a system would permit the monaural listener (like the normal binaural listener) to monitor all directions simultaneously, to detect and localize in the same operation, and to focus on a single direction. Our current work on the microphone array is directed toward the creation of a single directional channel containing the target signal (assumed to arise from a target source straight ahead of the listener) and the reduction of interference from sources directionally distinct from the target source. Parallel processing of array outputs to achieve simultaneous multiple directional channels will be considered only after further progress on the coding problem has been achieved.

Work during the past year has focused on assessments of modifications to the basic beamforming algorithm and performance in reverberant environments.

1.3.1 Adaptive Beamforming: Controlling Adaptation

The adaptive beamforming algorithm that has been the focus of much of our work, the Griffiths-Jim beamformer,[7] can be viewed as a simple preprocessor operating in conjunction with an adaptive noise canceller (ANC).[8] Two of the problems encountered with this beamforming system are associated with, and can be described more simply in terms of, the ANC. The first problem is known as misadjustment and is due to fluctuations in the adaptive filter's weights. The second problem, known as misalignment, comes from leakage of the target signal into the reference channel, which

---

[6] N.I. Durlach, R.C. Corbett, M.V. McConnell, W.M. Rabinowitz, P.M. Peterson, and P.M. Zurek, "Multimicrophone Monaural Hearing Aids," RESNA 10th Annual Conference, San Jose, California, 1987.

[7] L.J. Griffiths and C.W. Jim, "An Alternative Approach to Linearly Constrained Adaptive Beamforming," *IEEE Trans. Antennas Propag.* AP-30: 27-34 (1982).

[8] B. Widrow, J.R. Glover, Jr., J.M. McCool, J. Kaunitz, C.S. Williams, R.H. Hearn, J.R. Zeidler, E. Dong, Jr., and R.C. Goodlin, "Adaptive Noise Cancelling: Principles and Applications," *Proc. IEEE* 63: 1692-1716 (1975).

is ideally free of the desired target for best estimation of the interfering jammer. Both problems increase in severity with input target-to-jammer power ratio (TJR). We have developed two methods (based on output power and intermicrophone correlation) to control adaptation and reduce the high-TJR problems of misalignment and misadjustment in a two-microphone Griffiths-Jim beamformer.[9] Both methods exploit the fact that speech exhibits a high degree of fluctuation and has pause periods; these methods are attempts to sense the TJR and to adapt only in intervals when the TJR is small. Figure 1 shows the results of computer simulations in an anechoic environment with a speech target and a single jammer for both aligned and misaligned arrays. The plot shows performance as measured by intelligibility-weighted gain from the input to the output of the system, as a function of TJR at the system input. These results demonstrate the effectiveness of both methods for controlling adaptation; together, the two modifications significantly improved performance at high TJRs.

1.3.2 Adaptive Beamforming: Performance in Reverberation

We have also considered the effect of reverberation on system performance.[10] Initial studies have shown that reverberation degrades performance due to effects associated with both target and jammer. Reverberant target degrades performance by violating the assumption that the target signal arrives from a known direction. Reverberant jammer is cancelled only when it falls within the time span of the adaptive filter, so jammer is cancelled less effectively when the room impulse response exceeds that span. Future work will consider methods to overcome the problems associated with reverberation.

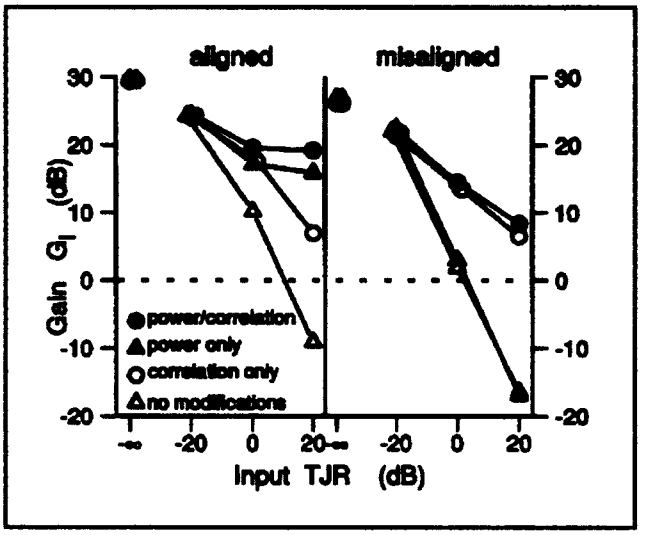


Figure 1. Results of computer simulations showing the effects of adaptation-control methods with a two-microphone array perfectly aligned and misaligned by 10 degrees. Plots show the gain, G_I, in the effective target-to-jammer ratio from input to output of the system, as a function of input target-to-jammer ratio. The environment was anechoic, and the target and jammer were separated by 45 degrees in azimuth. The array was a free-space, 26-cm broadside array.

1.4 Cochlear Prostheses

Sponsor

National Institutes of Health
Grant 5 P01 DC00361[11]

Project Staff

Professor Louis D. Braida, Lorraine A. Delhorne, Dr. Donald K. Eddington, Dr. William M. Rabinowitz

The overall goal of this research project is to determine and understand the potential and limitations of cochlear prostheses and to develop improved prostheses. Residual sensorineural hearing is measured prior to implantation in connection with subject selection and to provide baseline data for later comparison. Following implantation, auditory performance is evaluated by studying psychophysical performance, discrimination of speech ele-

[9] J.E. Greenberg and P.M. Zurek, "Evaluation of an Adaptive Beamforming Method for Hearing Aids," *J. Acoust. Soc. Am.*, forthcoming.

[10] J.E. Greenberg and P.M. Zurek, "Adaptive Beamformer Performance in Reverberation," paper presented at the 1991 IEEE Workshop on Applications of Signal Processing to Audio and Acoustics, Mohonk, New York, October 20-23, 1991.

[11] Subcontract from Massachusetts Eye and Ear Infirmary. Dr. Joseph B. Nadol, M.D., Principal Investigator.

ments, and comprehension of speech and the acoustic environment. Attempts are made to identify and measure central processing abilities that are relevant to speech-reception performance with an implant and that may help explain the large intersubject variations observed. Also, for comparison purposes, speech-reception tests are performed using a promising multichannel tactile vocoder. To minimize differential learning effects in the comparison, these tests are restricted to discrimination of speech segments. Further research focuses on alternative speech-processing schemes to achieve improved implant performance. This research capitalizes on analytic results from other parts of our research and the direct accessibility of the implanted electrode array (via a percutaneous plug).

During the past year, work has focused on evaluation of overall performance using the present Ineraid prosthesis and alternative speech processing for improved implant performance. The latter work is performed with Dr. Donald K. Eddington of RLE and Drs. Joseph Tierney and Marc Zissmann of MIT Lincoln Laboratory, and stems from an ongoing collaboration with colleagues at Duke University and the Research Triangle Institute. Progress in alternative processing[12] is described in Part IV, Section 3, Chapter 1, *Auditory Physiology*.

1.4.1 Cochlear Protheses: Overall Performance

A study was completed documenting implantees' speech-reception abilities at a variety of different levels and establishing relationships among different tests.[13] Twenty postlingually-deafened adult users of the Ineraid multichannel cochlear implant were tested on audio, visual, and audiovisual recognition of words embedded in two sentence corpora (with differing degrees of difficulty) and audio-only recognition of isolated monosyllabic words, consonant identification, and vowel identification. Quantitative relations among audio-only scores were assessed using power-law transformations[14] that can account for the benefit of sentence context and the relation between word and phoneme recognition. Across the broad range of performance that existed among the subjects, substantial order was observed among measures of speech reception along the continuum from recognition of words in sentences, words in isolation, speech segments, and the retrieval of underlying phonetic features. Correlations exceeded 0.85 among direct and sentence-derived measures of isolated word recognition as well as among direct and word-derived measures of segmental recognition. Results from a variety of other studies involving presentation of limited auditory signals, single-channel and multichannel implants, and tactual systems revealed similar patterns. Finally, for all of these prostheses, improving the reception of consonantal place cues was identified as key to producing the greatest potential gains in speech reception.

1.5 Binaural Hearing

Sponsor

National Institutes of Health
Grant 2 R01 DC00100[15]

Project Staff

Nathaniel I. Durlach, Dr. Patrick M. Zurek

The long-term goal of this program is (1) to develop an integrated, quantitative theory of binaural interaction that is consistent with psychophysical and physiological data on normal and impaired auditory systems, and (2) to apply our results to the diagnosis and treatment of hearing impairments.

Experimental research in this area has focused on identifying the stimulus variables responsible for in-head lateralization of auditory images. It is well established that the interaural relations that exist early after the onset of a sound have a strong influence on where the subsequent sound image is

---

[12] B.S. Wilson, C.C. Finley, D.T. Lawson, R.D. Wolford, D.K. Eddington, and W.M. Rabinowitz, "New Levels of Speech Recognition with Cochlear Implants," *Nature* 132: 236-238.

[13] W.M. Rabinowitz, D.K. Eddington, L.A. Delhorne, and P.A. Cuneo, "Relations Among Different Measures of Speech Reception in Subjects Using a Cochlear Implant," *J. Acoust. Soc. Am.*, forthcoming.

[14] A. Boothroyd and S. Nittrouer, "Mathematical Treatment of Context Effects in Phoneme and Word Recognition," *J. Acoust. Soc. Am.* 84: 101-114 (1988).

[15] Subcontract from Boston University. Professor H. Steven Colburn, Principal Investigator.

heard.[16] It is believed that this effect allows very good sound source localization in highly reverberant environments. Our recent work has confirmed that such effects measured using an acoustic pointer correspond well with measurements of interaural parameter resolution.[17] Further work has shown that the influence of the onset cue can extend over a relatively long (hundreds of milliseconds) subsequent stimulus, depending on both the ambiguity of the interaural cues in the subsequent stimulus and on whether it appears to constitute a separate "auditory object."[18]

1.6 Clinical Applications of Binaural Hearing

Sponsor

National Institutes of Health
Grant 7 R29 DC00428[19]

Project Staff

Dr. Patrick M. Zurek

Hearing with two ears provides advantages for (1) detecting and localizing sounds and (2) understanding speech in noisy environments. Part of the reason for binaural advantages stems from the fact that the ears are on opposite sides of the head, leading to differential diffraction, or "head-shadow," effects on spatially-separated target and interference sources and hence better signal-to-noise ratio at one ear or the other. The other source of binaural advantages is the auditory system's processing of the simultaneous right- and left-ear signals for enhanced detectability. The various factors leading to binaural advantages directional effects under anechoic conditions with a single interference source have recently been summarized.[20] Figure 2 shows the effect of interference direction on speech reception when listening with either the right ear only, the left only, or binaurally.

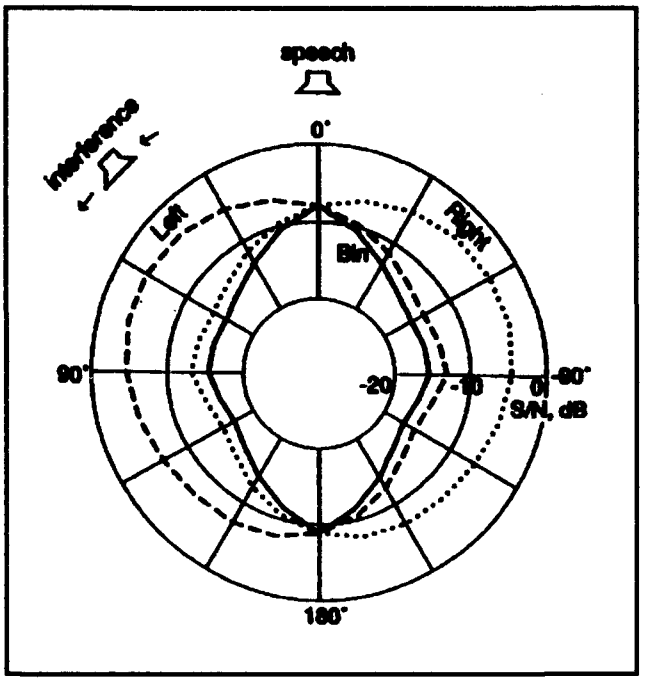


Figure 2. This polar plot shows the signal-to-noise ratio, S/N, needed at the input to the loudspeakers for constant intelligibility of the straight-ahead target as a function of the azimuthal direction of the interference. Lower S/N indicates easier listening or greater immunity from noise. Lines indicate performance when listening with the right ear alone, the left ear alone, or both ears (binaural).

Experimental work in this project is motivated by the desire to apply our understanding of binaural advantages in speech reception to the prescription of hearing aids, both monaural and binaural, as well as to test that understanding further. In particular, this work is focusing on comparisons between the performance of listeners with sensorineural impairments and listeners with normal hearing on tests of binaural detection, localization, and contralateral masking with various amplification patterns applied at the two ears.

---

[16] P.M. Zurek, "The Precedence Effect," in *Directional Hearing*, eds. W.A. Yost and G. Gourevitch (New York: Springer-Verlag, 1987); P.M. Zurek, "A Note on Onset Effects in Binaural Hearing," submitted to *J. Acoust. Soc. Am.*

[17] B.G. Shinn-Cunningham, P.M. Zurek, and N.I. Durlach, "Adjustment and Discrimination Measurements of the Precedence Effect," submitted to *J. Acoust. Soc. Am.*

[18] R.L. Freyman and P.M. Zurek, "Influence of Onset Cues in Lateralization," *J. Acoust. Soc. Am.* 89: 1995 (1991).

[19] Subcontract from University of Connecticut; Dr. Janet D. Koehnke, Principal Investigator.

[20] P.M. Zurek, "Binaural Advantages and Directional Effects in Speech Intelligibility," in *Acoustical Factors Affecting Hearing-Aid Performance*, eds. G.A. Studebaker and I. Hochberg, forthcoming.

1.7 Tactile Communication of Speech

Sponsor

National Institutes of Health
Grant 2 R01 DC00126

Project Staff

Lorraine A. Delhorne, Nathaniel I. Durlach, Michael T. Richey, Hong Z. Tan, Dr. William M. Rabinowitz, Dr. Charlotte M. Reed, Dr. Mandayam A. Srinivasan

Previous research on (1) tactual communication of speech among the deaf-blind in which the tactual stimulation is achieved by direct physical contact with the speaker and (2) tactual aids that transform acoustic signals into patterns of tactual stimulation and thus function at a distance has led us to the following conclusions: (1) The tactual sense is capable of receiving continuous speech at nearly normal speaking rates with nearly zero error rates; (2) Subjects are capable of integrating a relatively impoverished tactual signal with visual speechreading to achieve essentially normal speech-reception performance; (3) Limitations on the speech-reception performance obtained with current tactual aids are due primarily to inadequacies in the design of the aids and/or in the *training* received with these aids; and (4) There are no fundamental scientific obstacles to eliminating these inadequacies and achieving much improved speech reception for a wide range of patients. Conclusions (1) and (2) are based on (a) extrapolations of results obtained with relatively crude experimental devices on subjects with relatively limited training;[21] (b) tactual communication performance exhibited by the deaf-blind using direct-contact methods;[22] and (c) preliminary results on the ability of individuals who are experienced in the visual reception of Cued Speech to integrate visual speechreading with direct-contact tactual cueing. Conclusions (3) and (4) *are* essentially corollaries of conclusions (1) and (2).

With the above research as background, our ultimate general goal can be stated simply as follows: To develop schemes for processing acoustic signals and displaying these processed signals to the tactual sense so that, when accompanied by equivalent training, they provide speech-reception performance comparable to that demonstrated for the direct-contact methods. Discussion of our progress during the past year is divided into the following subsections: (a) Basic study of encoding and display schemes, (b) Tactual supplements to speechreading, (c) Evaluation of practical aids, and (d) Completion of work on natural methods of tactual communication. Recent reports of our work are available in Reed et al.[23] and Pang et al.[24]

1.7.1 Basic Study of Encoding and Display Schemes

Previous research on transmitting information through the tactual (i.e., cutaneous, proprioceptive, kinesthetic) sense has been confined almost exclusively to *stimulation of the skin; manipulation* of joint angles (i.e., hand postures) has been essentially ignored. Research is now underway to determine information transfer rates achieved by manipulation of joint angles, as well as by both joint angle manipulation and cutaneous stimulation combined. New devices to drive the hand are being developed and preliminary discrimination and identification experiments are being performed. The results of a preliminary study of joint-

---

[21] N.I. Durlach, C.E. Sherrick, and J.D. Miller, "Sensory Substitution: Visual and Tactual Methods," in *Speech Communication Aids for the Hearing Impaired: Current Status and Needed Research,* Report of CHABA Working Group 95 by C.S. Watson, R.A. Dobie, N.I. Durlach, H. Levitt, J.D. Miller, C.E. Sherrick, F.B. Simmons, G.A. Studebaker, R.S. Tyler, and G.P. Widin, *J. Acoust. Soc. Am.* 90: 637-685 (1991); C.M. Reed, N.I. Durlach, and L.D. Braida, "Research on Tactile Communication of Speech: A Review," *ASHA Monog.* 20 (1982); C.E. Sherrick, "Basic and Applied Research on Tactile Aids for Deaf People: Progress and Prospects," *J. Acoust. Soc. Am.* 75: 1325-1342 (1984).

[22] C.M. Reed, W.M. Rabinowitz, N.I. Durlach, L.D. Braida, S. Conway-Fithian, and M.C. Schultz, "Research on the Tadoma Method of Speech Communication," *J. Acoust. Soc. Am.* 77: 247-257 (1985).

[23] C.M. Reed, W.M. Rabinowitz, N.I. Durlach, L.A. Delhorne, L.D. Braida, J.C. Pemberton, B.D. Mulcahey, and D.L. Washington, "Analytic Study of the Tadoma Method: Improving Performance through the Use of Supplementary Tactual Displays," *J. Speech Hear. Res.*, 1992, forthcoming; C.M. Reed, N.I. Durlach, and L.A. Delhorne, "Natural Methods of Tactual Communication," in *Tactile Aids for the Hearing Impaired,* ed. I.R. Summers (London: Whurr, 1992).

[24] X.D. Pang, H.Z. Tan, and N.I. Durlach, "Manual Discrimination of Force Using Active Finger Motion," *Percept. Psychophys.* 49: 531-540 (1991).

angle resolution using the proximal interphalangeal joint of the human right index finger indicate that the JND for joint position is roughly 2.5 degrees (regardless of metacarpal phlangeal joint position) and that information transfer of position sense for this joint is roughly 1.8 bits. Work on joint-angle resolution will be extended to include additional relevant parameters; in addition, studies of thickness resolution are being designed to address the inherent difficulty of isolating thickness as an independent variable.

1.7.2 Tactual Supplements to Speechreading

A study comparing the effectiveness of a simple, low-bandwidth supplement to speechreading presented auditorally versus tactually has been completed.[25] The signal consisted of a 200-Hz tone modulated by the envelope of an octave band of speech centered at 500 Hz. The resulting signal was used to drive a high-performance single-channel vibrator for tactile stimulation or Koss earphones for auditory stimulation. Performance through speechreading alone (which averaged 30 percent correct on the CUNY sentences employed for these tests) was improved by nine percentage points with the tactile supplement compared to 23 points with the auditory supplement. Thus, although the tactile supplement improved speechreading ability, the size of the improvement was smaller than that obtained through auditory presentation of the same information. One possible explanation for the poorer tactile performance is that the ability of the skin to follow changes in modulation is inferior to that of the ear. Preliminary results of measurements of AM modulation resolution for auditory and tactile signals indicate that tactile resolution is roughly 6 dB poorer than auditory resolution for 200 Hz carriers and roughly 45 dB poorer for 400 Hz carriers.

1.7.3 Evaluation of Practical Aids

Our research in this area has focused on evaluations of performance through the Tactaid VII device[26] both with normal-hearing laboratory subjects and with profoundly deaf subjects wearing this device in the field. Segmental discrimination scores through the tactile device alone were similar for both groups of subjects (roughly 73 percent correct for discrimination of 14 consonant and 8 vowel contrasts). On connected speech materials, however, the laboratory-trained normal-hearing subjects did not show the same benefits to speechreading through the Tactaid VII as did the group of four profoundly deaf subjects. Despite a wide range of speechreading ability among these four deaf subjects, each demonstrated improvements to speechreading on CUNY sentences of roughly 10 percentage points. Evaluations of performance with the Tactaid VII are continuing with both laboratory and field subjects.

1.7.4 Completion of Work on Natural Methods of Tactual Communication

During the past year, we have completed a manuscript summarizing research conducted with experienced deaf-blind users of three natural methods of tactual communication: (1) Tadoma (in which speech is understood by using the hand to sense the mechanical actions of the face associated with speech production), (2) tactual reception of sign language, and (3) tactual reception of fingerspelling.[27] In addition, detailed analyses of data obtained on the reception of sign language through the tactual and visual senses have been completed.

1.8 Super Auditory Localization for Improved Human-Machine Interfaces

Sponsor

U.S. Air Force - Office of Scientific Research
Grant AFOSR 90-0200

---

[25] J.M. Besing, C.M. Reed, and K.W. Grant, "Tactual Presentation of Low-Bandwidth Envelope Signals: Benefits to Speechreading," *ASHA* 33: 212 (1991).

[26] A. Ogno, *The History of Tactile Aids for the Deaf: A Case Study of Audiological Engineering Corporation*, S.B. thesis, Dept. of Mech. Eng., MIT, 1991.

[27] C.M. Reed, N.I. Durlach, and L.A. Delhorne, "Natural Methods of Tactual Communication," in *Tactile Aids for the Hearing Impaired*, ed. I.R. Summers (London: Whurr Publishers Limited, 1992).

Project Staff

Nathaniel I. Durlach, Eric M. Fuchs, Professor Richard M. Held, Wei Min, Dr. Xiao Dong Pang, Dr. William M. Rabinowitz, Barbara G. Shinn-Cunningham

The normal human auditory system suffers from a number of deficiencies in its ability to localize sound sources. The auditory system determines the distance or elevation of a source poorly, is substantially worse at detecting changes in azimuth when the source is off to the side than when it is in front or back, and occasionally makes front-back confusions when the head is motionless. However, when localization is considered in the context of human-machine interfaces such as those employed in teleoperator or virtual-environment systems, there is an opportunity to recode source location in a manner that improves localization. In other words, one can transform the acoustical cues available to the listener for determining source location (i.e., alter the manner in which source location is represented in the binaural acoustic stimulus) in such a way that the listener achieves super localization.

The principal research questions in attempting to achieve super localization concern the ability of the human operator to adapt to such transformations and to switch back and forth between the normal cue system and the altered cue system rapidly and reliably. Although certain consequences of these transformations can be predicted theoretically from our models of normal human audition, those involving perceptual learning and adaptation cannot be predicted. A major goal of the research is to determine, understand, and model the perceptual effects of these transformations.

The planned research involves the study of adaptation to a wide range of transformations using a specially designed virtual-environment system for presenting the transformed localization cues, a variety of training procedures to achieve adaptation, and localization tests to measure adaptation that include detection and localization in multiple-source environments and dynamic tests of localization constancy, as well as discrimination and identification of single sources. To the extent that reliable and reversible adaptation can be demonstrated, the results of this research will provide important new options for improved interface design. Further background in this area can be found in Durlach.[28]

Work has continued on the development of appropriate virtual environment displays, head-motion trackers, and software. In addition, a series of identification experiments have been conducted using a transformation of the relation between azimuth and head-related transfer function such that azimuthal space is magnified in front and minified off to the side. Initial changes in resolution and response bias (from those encountered before the transformation was introduced) were as expected; however, the expected decay of response bias over exposure time that was expected to result from sensorimotor adaptation did not occur. Further experiments using revised procedures are now being initiated to determine the conditions necessary for response-bias decay.

1.9 Research on Reduced-Capability Human Hands

Sponsor

U.S. Navy - Office of Naval Research
Grant N00014-90-J-1935

Project Staff

Lorraine A. Delhorne, Nathaniel I. Durlach, Dr. Xiao Dong Pang, Dr. Mandayam A. Srinivasan

The general objectives of our research on hand function are (1) to increase basic knowledge of manual sensing and manipulation, (2) aid in the design and evaluation of artificial hands for robotic and teleoperator systems, and (3) improve clinical diagnosis and treatment of hand impairments. Reports of some of our previous work in this general area are available in Durlach et al.[29] and Pang et al.[30]

The particular research being conducted in this grant focuses on the ability of the human hand to

---

[28] N.I. Durlach, "Auditory Localization in Teleoperator and Virtual-Environment Systems: Ideas, Issues, and Problems," *Perception*, forthcoming.

[29] N.I. Durlach, L.A. Delhorne, A. Wong, W.Y. Ko, W.M. Rabinowitz, and J.M. Hollerbach, "Manual Discrimination and Identification of Length by the Finger-Span Method," *Percept. Psychophys.* 46(1): 29-38 (1989).

[30] X.D. Pang, H.Z. Tan, and N.I. Durlach, "Manual Discrimination of Force Using Active Finger Motion," *Percept. Psychophys.*, forthcoming.

sense and manipulate the environment under various types of constraints. Such constrained hand performance is being studied in connection with hand-design questions in the area of teleoperator systems. Determination of how performance degrades as various capabilities of the normal human hand are eliminated provides important background for hand-design decisions. The constraints to be studied are imposed by experimental gloves and local anesthetics, as well as by various types of hand impairments (resulting from injuries, birth defects, or diseases).

The main effort in this project during the past year involved testing the capabilities of various constrained hands on a set of tasks previously employed by the U.S. Navy to compare two different teleoperator systems, one employing a telerobot with a complex anthropomorphic hand and one employing a telerobot that used a simple gripper. The results of our tests indicated that the given set of tasks could be accomplished nearly as well with a simple one degree of freedom gripper as with a normal human hand. These results were consistent with those obtained by the Navy using the teleoperator systems and indicated either that (1) the additional degrees of freedom available in the complex anthropomorphic hand were not worthwhile or (2) the selected tasks were not representative of the whole set of tasks with which the system would realistically be faced. Overall, these results emphasized the need to develop a set of "generator" tasks with the following properties: (1) knowledge of performance on this set of tasks enables one to predict performance on any task in the given universe of tasks, and (2) no smaller set of tasks provides comparable predictive accuracy.

1.10 Mechanistic Modeling of Primate Fingerpad

Sponsor

National Institutes of Health
Grant 5 R29 DC00625

Project Staff

Kiran B. Dandekar, Dr. Mandayam A. Srinivasan

Whenever we touch an object, the source of all tactile information is the spatio-temporal distribution of mechanical loads on the skin at the contact interface. The relationship between these loads and the resulting stresses and strains at the nerve terminals within the skin plays a fundamental role in the neural coding of tactile information. Although empirical determination of the stress or strain state of a mechanoreceptor is not possible at present, mechanistic models of the skin and subcutaneous tissues enable prediction and verification of peripheral neural response. The research under this grant is directed towards applying analytical and computational mechanics to analyze the biomechanical aspects of touch—the mechanics of contact, the transmission of the mechanical signals through the skin, and their transduction into neural impulses by the mechanoreceptors.

1.10.1 Determination of Geometric and Material Properties of the Primate Finger Tip

The first step in performing mechanistic analyses of the primate finger tip is to determine its geometric and material properties. We have indented the fingerpads of humans and monkeys in vivo using a line load delivered by a sharp wedge and photographed the resulting skin surface deflections. We have shown that the homogeneous elastic model of the finger tip only roughly approximates the experimental data, while a simple alternative model, which views the finger tip as an elastic membrane filled with an incompressible fluid (like a "waterbed") predicted the observed profiles very well.[31] In order to empirically determine the in vivo compressibility of the finger tip, we designed an apparatus containing a chamber in which human subjects can submerge their finger tips in water. Indentation of the finger tip by a plunger caused a change in the water level in an attached tube, which enabled the measurement of the resulting change in volume of the finger tip. Preliminary results indicate that the finger tip is almost incompressible, with the highest change in volume (about 3 percent) occuring at the greatest depth of indentation (4 mm). We plan to investigate the effect of the shape of the plunger on the compressibility of the finger tip, and use this information in our finite element models described below.

1.10.2 Finite Element Analyses of Two-Dimensional Models

We have performed linear and nonlinear finite element analyses of a series of mechanistic models of the fingerpad under a variety of mechanical

[31] M.A. Srinivasan, "Surface Deflection of Primate Fingertip Under Line Load," *J. Biomech.* 22(4): 343-349 (1989).

stimuli.[32] The models range from a semi-infinite medium to cylindrical distal phalanx, composed of either a homogeneous elastic material or a thick elastic shell containing a fluid. Simulations of the mechanistic aspects of neurophysiological experiments involving mapping of receptive fields with single point loads, determination of spatial resolution of two-point stimuli, and indentations by single bars as well as periodic and aperiodic gratings have been carried out. We have also solved the nonlinear contact problem of indentations by cylindrical objects.

The large number of numerical calculations needed even for the linear models necessitated the use of the MIT supercomputer. The results show, for example, that the strain energy density at the receptor site is a leading contender for the relevant stimulus that causes the responses recorded from slowly adapting afferent fibers. More generally, we have demonstrated the power of computational mechanics in investigating the relationship between tactile stimuli imposed on the skin and the resulting peripheral neural response. The analyses are being extended both in terms of the mechanical stimuli applied on the fingerpad as well as the geometrical and material properties of the finger tip.

1.10.3 Tactile Sensing of Microtexture, Shape, and Softness

We have been collaborating with Dr. LaMotte of Yale University School of Medicine in conducting psychophysical and neurophysiological studies on how we sense by touch alone the microtextures, shapes and softnesses of objects.[33] By using methods of photolithography, we etched submicron-high bar gratings on glass plates. We have shown that humans can detect extremly fine textures composed of parallel bars only 50 nanometers high.[34] Our earlier neurophysiological recordings with bigger texture elements indicate that when such fine textures are stroked, skin vibrates and causes Pacinian Corpuscles to respond, thus enabling detection of the microtexure.[35] Based on a theoretical analysis of the mechanics of contact, we have demonstrated that the receptors respond to the low-pass filtered versions of surface pressures.[36] Thus curvature of the skin surface under an object, which we know from differential geometry is approximated by the second spatial derivative of surface deflection, is coded without differentiating (which is a noise enhancing process), but by exploiting its relation to surface pressure. We have now designed and fabricated a high performance tactile stimulator controlled by a PC through transputers. Our ongoing experiments on shape sensing involve the use of precisely manufactured cylindrical, ellipsoidal, and spherical surfaces as stimuli. Human discriminability of compliance of objects depends on whether the object has a deformable or rigid surface. When the surface is deformable, the spatial pressure distribution within the contact region is dependent on object compliance, and hence information from cutaneous mechanoreceptors is sufficient for discrimination of subtle differences in compliance. When the surface is rigid, kinesthetic information is necessary for discrimination, and the discriminability is much poorer than that for objects with deformable surfaces.

---

[32] M.A. Srinivasan and K. Dandekar, "Role of Mechanics in Cutaneous Mechanoreceptor Response," Society for Neuroscience Abstracts, 1991.

[33] M.A. Srinivasan, "Tactual Interfaces: The Human Perceiver," in *Human-Machine Interfaces for Teleoperators and Virtual Environments,* eds. N.I. Durlach, T.B. Sheridan, and S.R. Ellis, NASA Conference Publication 10071, 1991; M.A. Srinivasan, and R.H. LaMotte, "Tactile Discrimination and Representation of Texture, Shape, and Softness," in *Human-Machine Interfaces for Teleoperators and Virtual Environments,* eds. N.I. Durlach, T.B. Sheridan, and S.R. Ellis, NASA Conference Publication 10071, 1991.

[34] R.H. LaMotte and M.A. Srinivasan, "Surface Microgeometry: Neural Encoding and Perception," in *Information Processing in the Somatosensory System,* eds. O. Franzen and J. Westman, Wenner-Gren International Symposium Series (New York: Macmillan Press, 1991).

[35] M.A. Srinivasan, J.M. Whitehouse, and R.H. LaMotte, "Tactile Detection of Slip: Surface Microgeometry and Peripheral Neural Codes," *J. Neurophysiol.* 63(6): 1323-1332 (1990).

[36] M.A. Srinivasan and R.H. LaMotte. "Encoding of Shape in the Responses of Cutaneous Mechanoreceptors," In *Information Processing in the Somatosensory System,* Eds. O. Franzen and J. Westman, Wenner-Gren International Symposium Series (New York: Macmillan Press, 1991).

1.10.4 Development of a Computational Theory of Touch

Although the "hardware" of the tactile apparatus in humans and robots are different, they have the common feature of mechanosensors embedded in a deformable medium. Thus, the computational problem of coding (predicting sensor response for a given mechanical stimulus at the surface) and decoding (inferring the mechanical stimulus at the surface by suitably processing the sensor response) need similar mechanistic analyses for their solution. We have developed such a "computational theory" for an idealized medium subjected to arbitrary pressure or displacement loading conditions, and give explicit formulae for the coding and decoding problems.[37]

In collaboration with Dr. Annaswamy of the Department of Mechanical Engineering at MIT, we have investigated some of the identification and control problems that occur in the context of manipulation, when compliance is present in the end-effectors as well as in the object.[38] In order to understand the fundamental aspects of these tasks, we have analyzed the problem of identification of compliant objects with a single finger contact, as well as under a two-finger grasp. Assuming that the finger and the compliant object are constrained to deform along a single spatial dimension, we have carried out parameter identification using either force or displacement inputs to the rigid backing of the end-effector. Based on this analysis, control strategies are developed to achieve a desired manipulation of the object in the workspace. Animated graphical renderings are being developed to visually illustrate the presence or absence of slipping and crushing during an active manipulation task. The theoretical results can be used to generate testable hypotheses for human or robot experiments on tactual sensing.

1.11 Biomechanics of Skin-Object Contact

Sponsor

U.S. Navy - Office of Naval Research
Grant N00014-91-J-1454

Project Staff

Jyh-Shing Chen, Dr. Mandayam A. Srinivasan

As mentioned earlier, in any task involving physical contact with objects, the source of all tactile information is the spatio-temporal distribution of mechanical loads on the skin at the contact interface. These loads, specified as pressure, displacements, etc., depend on the geometrical and material properties of both the contacting entities, as well as the overall forces of interaction. In this new project, we wish to determine the growth and motions of contact regions over time between the human fingerpad and carefully chosen transparent test objects whose microtexture, shape or softness is varied in a controlled manner. Towards this end, we will obtain and analyze high resolution video-images of the contact regions in synchrony with the contact force measurements. The results will lead to a deeper understanding of the data we have already obtained for these test objects, namely, electrophysiologically recorded responses of cutaneous mechanoreceptive afferent fibers, and psychophysically determined human discriminabilities.

Our initial goal is to record video images and forces of contact under active touch, where subjects press or stroke various transparent specimens mounted on a force transducer. Accordingly, we have conducted an extensive literature and product survey, as well as designed a videomicroscopy system and a force sensing system, both interfaced to a computer. The videomicroscopy system consists of a set of video zoom lenses attached to a high-resolution CCD camera, whose output can either be digitized directly at about 5 frames/s, or stored on a laserdisk at real-time frame rates (30 frames/s) for off-line digitization. The zoom lenses enable continuous variation of the magnification, with the field of view covering the entire fingerpad, or just a few fingerprint ridges. High contrast images are achieved with coaxial lighting. Transparent specimens can be attached to custom-made, six-axis force sensors that can measure contact forces up to 500 gwt. at about 10-bit resolution. We are beginning a set of experiments with human subjects on the relationship between the contact force, contact area and compliance of the object.

---

[37] M.A. Srinivasan, "Tactile Sensing in Humans and Robots: Computational Theory and Algorithms," Newman Laboratory Technical Report, Dept. of Mech. Eng., MIT, 1988.

[38] A.M. Annaswamy and M.A. Srinivasan, "Adaptive Control for Grasping and Manipulation of Compliant Objects with Compliant Fingerpads," *Proceedings of the American Control Conference*, Boston, Massachusetts, 1991; A.M. Annaswamy, M.A. Srinivasan, and S. Weibel, "Identification for Grasping and Manipulation of Compliant Objects with Compliant Fingerpads," Submitted to *IEEE Trans. Autom. Control*, 1992.

1.12 Publications

Annaswamy, A.M., and M.A. Srinivasan. "Adaptive Control for Grasping and Manipulation of Compliant Objects with Compliant Fingerpads." *Proceedings of the American Control Conference*, Boston, Massachusetts, 1991.

Besing, J.M., C.M. Reed, and K.W. Grant. "Tactual Presentation of Low-Bandwidth Envelope Signals: Benefits to Speechreading." *ASHA* 33: 212 (1991).

Braida, L.D. "Crossmodal Integration in the Identification of Consonant Segments." *Quart. J. Exper. Psych.* 43A(3): 647-677 (1991).

Durlach, N.I. "Auditory Localization in Teleoperator and Virtual Environment Systems." *Perception* 20: 543-554 (1991).

Freyman, R.L., and P.M. Zurek. "Influence of Onset Cues in Lateralization." *J. Acoust. Soc. Am.* 89: 1995 (1991).

Grant, K.W., L.D. Braida, and R.J. Renn. "Single-band Envelope Cues as an Aid to Speechreading." *Quart. J. Exper. Psych.* 43A(3): 621-645 (1991).

Grant, K.W., and L.D. Braida. "Evaluating the Articulation Index for Audiovisual Input." *J. Acoust. Soc. Am.* 89: 2952-2960 (1991).

Greenberg, J.E., and P.M. Zurek. "Evaluation of an Adaptive Beamforming Method for Hearing Aids." *J. Acoust. Soc. Am.* Forthcoming.

LaMotte, R.H., and M.A. Srinivasan. "Surface Microgeometry: Neural Encoding and Perception." In *Information Processing in the Somatosensory System.* Eds. O. Franzen and J. Westman. Wenner-Gren International Symposium Series. New York: Macmillan Press, 1991.

Ogno, A. *The History of Tactile Aids for the Deaf: A Case Study of Audiological Engineering Corporation.* S.B. thesis. Dept. of Mech. Eng., MIT, 1991.

Pang, X.D., H.Z. Tan, and N.I. Durlach. "Manual Discrimination of Force Using Active Finger Motion." *Percept. Psychophys.* 49: 531-540 (1991).

Power, M.H., and L.D. Braida. "A Physical Measure of Consistency Among Speech Parameter Vectors: Application to Speech Intelligibility Determination." *J. Acoust. Soc. Am.* 90: 2327 (1991).

Rabinowitz, W.M., D.K. Eddington, L.A. Delhorne, and P.A. Cuneo. "Relations Among Different Measures of Speech Reception in Subjects Using a Cochlear Implant." *J. Acoust. Soc. Am.* Forthcoming.

Rankovic, C.M., R.L. Freyman, and P.M. Zurek. "Potential Benefits of Adaptive Frequency-Gain Characteristics for Speech Reception in Noise." *J. Acoust. Soc. Am.* 91: 354-362 (1992).

Rankovic, C.M., and P.M. Zurek. "Evaluation of Prescriptve Fitting Procedures Using the AI Model." *ASHA* 33: 164 (1991).

Rankovic, C.M., P.M. Zurek, and R.L. Freyman. "Potential Benefits of Adaptive Frequency-Gain Characteristica for Speech Reception in Noise for Hearing-Impaired Individuals." *J. Acoust. Soc. Am.* 90: 2319 (1991).

Reed, C.M., M.H. Power, N.I. Durlach, L.D. Braida, K.K. Foss, J.A. Reid, and S.R. Dubois. "Development and Testing of Artificial Low-Frequency Speech Codes." *J. Rehabil. Res. Dev.* 28: 67-82 (1991).

Reed, C.M., N.I. Durlach, and L.A. Delhorne. "Natural Methods of Tactual Communication." In *Tactile Aids for the Hearing Impaired.* Ed. I.R. Summers. New York: Taylor and Francis. Forthcoming.

Reed, C.M., W.M. Rabinowitz, N.I. Durlach, L.A. Delhorne, L.D. Braida, J.C. Pemberton, B.D. Mulcahey, and D.L. Washington. "Analytic Study of the Tadoma Method: Improving Performance through the Use of Supplementary Tactual Displays." *J. Speech Hear. Res.* Forthcoming.

Srinivasan, M.A. "Tactual Interfaces: The Human Perceiver," in *Human-Machine Interfaces for Teleoperators and Virtual Environments,* Eds. N.I. Durlach, T.B. Sheridan, and S.R. Ellis. NASA Conference Publication 10071, 1991.

Srinivasan, M.A., and K. Dandekar. "Role of Mechanics in Cutaneous Mechanoreceptor Response." Society for Neuroscience Abstracts, 1991.

Srinivasan, M.A., and R.H. LaMotte. "Encoding of Shape in the Responses of Cutaneous Mechanoreceptors." In *Information Processing in the Somatosensory System.* Eds. O. Franzen and J. Westman. Wenner-Gren International Symposium Series. New York: Macmillan Press, 1991.

Srinivasan, M.A., and R.H. LaMotte. "Tactile Discrimination and Representation of Texture, Shape, and Softness." In *Human-Machine Interfaces for Teleoperators and Virtual Environments* Eds. N. Durlach, T.B. Sheridan, and S.R. Ellis. NASA Conference Publication 10071, 1991.

Uchanski, R.M., K.M. Millier, D.E. Ronan, C.M. Reed, and L.D. Braida. "Effects of Token Variability on Resolution for Vowel Sounds." *J. Acoust. Soc. Amer.* 90: 2254 (1991).

Uchanski, R.M., K.M. Millier, C.M. Reed, and L.D. Braida. "Effects of Token Variability on Vowel Identification." In *The Processing of Speech: From the Auditory Periphery to Word Recognition.* Berlin: Mouton de Gruyter, 1992.

Wilson, B.S., C.C. Finley, D.T. Lawson, R.D. Wolford, D.K. Eddington, and W.M. Rabinowitz. "New Levels of Speech Recognition with Cochlear Implants." *Nature* 132: 236-238 (1991).

Woods, W.S., A. Kulkarni, H.S. Colburn, A. Rigopulos, X.D. Pang, N.I. Durlach, and E.M. Wenzel. "On the Externalization of Auditory Images." *Presence.* Forthcoming.

Zurek, P.M. "Probability Distributions of Interaural Phase and Level Differences in Binaural Detection Stimuli." *J. Acoust. Soc. Am.* 90: 1927-1932 (1991).

Zurek, P.M. "Detectability of Transient and Sinusoidal Otoacoustic Emissions." *Ear Hear.* Forthcoming.

Zurek, P.M. "Interference Reduction for the Hearing Impaired." *J. Acoust. Soc. Am.* 89: 1957 (1991).

Theses

Hedgcock, J.M. *Development and Testing of a System to Evaluate Manual Tracking Ability.* S.B. thesis. Dept. of Elect. Eng. and Comput. Sci., MIT, 1991.

Knecht, W. *A Nonlinear Extension of a Beamformer for Multi-Microphone Speech Processing.* S.M. thesis. Dept. of Physics, MIT, 1991.

Reisman, C.A. *Envelope Modulation Spectra of Bandpass Filtered Speech.* S.B. thesis. Dept. of Electr. Eng. and Comput. Sci. MIT, 1991.

Section 3 Auditory Physiology

Chapter 1 Signal Transmission in the Auditory System

Chapter 1. Signal Transmission in the Auditory System

Academic and Research Staff

Professor Lawrence S. Frishkopf, Professor Nelson Y.S. Kiang, Professor William T. Peake, Professor William M. Siebert, Professor Thomas F. Weiss, Dr. Alice M. Berglund, Dr. Peter A. Cariani, Dr. Bertrand Delgutte, Dr. Donald K. Eddington, Dr. Dennis M. Freeman, Dr. John J. Guinan, Jr., Dr. William M. Rabinowitz, Dr. John J. Rosowski

Visiting Scientists and Research Affiliates

Ellen Carlisle, Patricia A. Cuneo, Dr. Sunil Puria, Dr. Jay T. Rubinstein, Frank J. Stefanov-Wagner, Meng Y. Zhu

Graduate Students

Kristin J. Dana, Charles Q. Davis, Scott B.C. Dynes, Farzad Ehsani, Michael P. McCue, Jennifer R. Melcher

Technical and Support Staff

Janice L. Balzer, David A. Steffens

1.1 Introduction

Sponsors

National Institutes of Health
Grants 5 R01 DC00194, P01 DC00119, F32 DC00073, 5 R01 DC00473, 2 R01 DC00238, 2 R01 DC00235, 5 P01 DC00361, T32 DC00006
Whitaker Health Sciences Fund

Research on the auditory system is carried out in cooperation with two laboratories at the Massachusetts Eye and Ear Infirmary (MEEI). With the Eaton-Peabody Laboratory for Auditory Physiology, we pursue basic investigations with the objectives of (1) understanding the anatomical structures and physiological mechanisms that underlie vertebrate hearing, and (2) applying that knowledge to clinical problems. Studies of cochlear implants in humans are carried out at the MEEI Cochlear Implant Research Laboratory. The goal of cochlear implant research is to provide speech communication for the deaf by electrically stimulating intracochlear electrodes to elicit patterns of auditory nerve fiber activity that the brain can learn to interpret.

1.2 Signal Transmission in the External and Middle Ear

1.2.1 Structure-Function Relations in Middle Ears

Project Staff

Dr. John J. Rosowski, Professor William T. Peake, David A. Steffens

The goal of our work is to understand the relationship between the structure of the external and middle ear and their functions. In this approach, we determine how inter-specific variations in ear structure lead to functional differences. In the past year, we have investigated these issues using three basic techniques: (1) correlation of basic structural features of the middle ears of different mammals with differences in hearing ability, (2) description of signal processing by the external and middle ear based on measurements of function combined with a simple model, and (3) new functional measurements in the gerbil, a species with several peculiar auditory adaptations.

Specifically, in a paper[1] on the middle-ear function of one of the earliest known mammals, the relationship between the size of middle-ear structures and limits of hearing in modern mammals

[1] J.J. Rosowski and A. Graybeal, "What Did Morganucodon Hear?" *Zoolog. J. Linnean Soc.* 101:131-168 (1991).

was used to predict the auditory capabilities of the early mammal. This work points out that the middle ears of early mammals are similar to those of shrews and other small mammals with good high-frequency and poor low-frequency hearing. A subsequent book chapter[2] tested and expanded these predictions. The two papers argue that early mammals were capable of hearing high-frequency sounds and shed light on how the mammalian ear differs from that of other vertebrates.

A framework for understanding the role of the external and middle-ear in determining the shape of the audiogram and variations in susceptibility to damage by different noises was developed.[3] This work explains why low-frequency noise is less damaging to human hearing than high-frequency noise.

Methods for assessing the efficacy of middle-ear acoustic-power transmission were reviewed[4] with the conclusion that consideration of the external and middle ear together leads to the best assessment of optimum middle-ear function.

The significance of non-ossicular sound transmission through the normal and abnormal middle ear of both men and cats was predicted based on a new model.[5] This analysis suggests that direct acoustic stimulation of the cochlear window plays a major role in determining residual hearing in certain middle-ear disorders. The paper makes recommendations for middle-ear reconstructive surgery including the size of the residual middle-ear air spaces and stiffness of any round-window shield.

The acoustic input impedance of the gerbil middle ear and middle-ear air spaces was measured.[6] The middle-ear air spaces of the gerbil were found to play a significant role in determining the exceptional sensitivity of the gerbil ear to low frequency sounds. However, a flaccid tympanic membrane and ossicular chain were found to be necessary codevelopments of a low-frequency ear.

1.3 Basic and Clinical Studies of the Auditory System

1.3.1 Subproject 1: Middle Ear and Measurement of Middle-Ear Transfer Function

Project Staff

Dr. John J. Rosowski, Professor William T. Peake, Dr. Sunil Puria

The animal work described above is complemented by direct measurements of middle-ear function in a human temporal-bone preparation.

Measurements of the motion of the human malleus in response to sound[7] demonstrate that mallear motion can be described as simple rotation only for frequencies below 500 Hz. At higher frequencies the motion can be better described as a combination of rotational and translational components. This result conflicts with the popular description of middle-ear mechanical action and has implications for the design of middle-ear prostheses.

Together with Dr. S.N. Merchant at the Massachusetts Eye and Ear Infirmary, we have made some preliminary measurements of the input impedance of the stapes and cochlea in human temporal bones. These measurements specify the load on the middle ear and are essential for understanding

---

[2] J.J. Rosowski, "Hearing in Transitional Mammals: Predictions from the Middle-ear Anatomy and Hearing Capabilities of Extant Mammals," in *The Evolutionary Biology of Hearing*, eds. D.B.Webster, A.N. Popper, and R.R. Ray (New York: Springer-Verlag, 1991), pp. 625-631.

[3] J.J. Rosowski, "The Effects of External- and Middle-ear Filtering on Auditory Threshold and Noise-induced Hearing Loss," *J. Acoust. Soc. Am.* 90: 124-135 (1991).

[4] W.T. Peake and J.J. Rosowski, "Impedance Matching, Optimum Velocity and Ideal Middle Ears," *Hear. Res.* 53: 1-6 (1991).

[5] W.T. Peake, J.J. Rosowski, and T.J. Lynch III, "Middle-ear Transmission: Acoustic Versus Ossicular Coupling in Cat and Human," *Hear. Res.* 57: 245-268 (1992).

[6] M.E. Ravicz, J.J. Rosowski, and H.F. Voigt, "Sound-power Collection by the Auditory Periphery of the Mongolian Gerbil Meriones Unguiculatus: I. Middle-ear Input Impedance," submitted to *J. Acoust. Soc. Am.*

[7] K.M. Donahue, J.J. Rosowski, and W.T. Peake, "Can the Motion of the Human Malleus be Described as Pure Rotation?" Abstracts of the 14th Midwinter Research Meeting of the Association for Research in Otolaryngology 53 (1991).

middle-ear function. The preparation we are developing will also enable us to test fundamental assumptions of cochlear function including whether the volume velocity of the oval and round window are equal.[8]

Publications

Donahue, K.M., J.J. Rosowski, and W.T. Peake. "Can the Motion of the Human Malleus be Described as Pure Rotation?" Abstracts of the 14th Midwinter Research Meeting of the Association for Research in Otolaryngology 53 (1991).

Merchant, S.N., M.E. Ravicz, and J.J. Rosowski. "The Acoustic Input Impedance of the Stapes and Cochlea in Human Temporal Bones." Abstracts of the 15th Midwinter Research Meeting of the Association for Research in Otolaryngology. Forthcoming.

Peake, W.T., and J.J. Rosowski. "Impedance Matching, Optimum Velocity and Ideal Middle Ears." *Hear. Res.* 53: 1-6 (1991).

Peake, W.T., J.J. Rosowski, and T.J. Lynch III. "Acoustic Coupling to Cochlear Windows." Abstracts of the Fourteenth Midwinter Meeting of the Association for Research in Otolaryngology, p. 121 (1991).

Peake, W.T, J.J. Rosowski, and T.J. Lynch III. "Middle-ear Transmission: Acoustic vs. Ossicular Coupling in Cat and Human." *Hear. Res.* 57: 245-268 (1992).

Ravicz, M.E., J.J. Rosowski, and H.F. Voigt. "Sound-power Collection by the Auditory Periphery of the Mongolian Gerbil Meriones Unguiculatus: I. Middle-ear Input Impedance." Submitted to *J. Acoust. Soc. Am.*

Rosowski, J.J. "The Effects of External- and Middle-ear Filtering on Auditory Threshold and Noise-induced Hearing Loss." *J. Acoust. Soc. Am.* 90: 124-135 (1991).

Rosowski, J.J. "Hearing in Transitional Mammals: Predictions from the Middle-ear Anatomy and Hearing Capabilities of Extant Mammals." In *The Evolutionary Biology of Hearing.* Eds. D.B. Webster, A.N. Popper, and R.R. Ray. New York: Springer-Verlag, 1991, pp. 625-631.

Rosowski, J.J., and A. Graybeal. "What Did Morganucodon Hear?" *Zoolog. J. Linnean Soc.* 101:131-168 (1991).

1.4 Cochlear Mechanisms

Project Staff

Professor Thomas F. Weiss, Professor Lawrence S. Frishkopf, Dr. Dennis M. Freeman, Kristin J. Dana, Farzad Ehsani, Charles Q. Davis

Our goal is to study the mechanisms by which the motion of macroscopic structures in the inner ear produce motions of the mechanically sensitive hair bundles of sensory receptor (hair) cells. Except for certain populations of hair cells found in lizards, auditory hair cells are surmounted by a gelatinous tectorial membrane. Because of its strategic location, the tectorial membrane plays an important role in the mechanical stimulation of hair bundles. However, there have been few direct observations of the tectorial membrane, and many of its critical properties remain obscure.

Based on its biochemical composition and ultrastructure, the tectorial membrane is a polyelectrolyte gel similar to those found in many connective tissues. The mechanical properties of such gels are intimately connected to their electrochemical properties. As a step toward understanding its physiochemical properties, we have investigated the effect of the ionic environment on the size and structure of the tectorial membrane of the chick cochlea. In our experiments, the cochlear duct was dissected, placed in an ionic solution, and opened to expose the sensory receptor organ. The tectorial membrane was lifted off the organ and attached to the glass floor of an experimental chamber. Latex beads (2-5 μm in diameter) were allowed to settle on the tectorial membrane. Video images of the tectorial membrane were obtained, and the positions of beads were measured as a function of time while the ionic composition of the solution perfusing the tectorial membrane was systematically altered. These measurements indicate how changes in the dimensions and geometry of the tectorial membrane were caused by changes in composition of the solution.

Measurements of the tectorial membrane were obtained in both high potassium (endolymph-like)

[8] S.N. Merchant, M.E. Ravicz, and J.J. Rosowski, "The Acoustic Input Impedance of the Stapes and Cochlea in Human Temporal Bones," Abstracts of the 15th Midwinter Research Meeting of the Association for Research in Otolaryngology, forthcoming.

and high sodium (perilymph-like) solutions at a number of calcium concentrations. At a fixed calcium concentration, the dimensions of the tectorial membrane change if the sodium and potassium concentrations are changed. For example, when the calcium concentration was maintained at a low value (20 μmol/L), substitution of sodium ions for potassium caused swelling of the tectorial membrane. The swelling had a large magnitude, often increasing the thickness of the tectorial membrane by more than a factor of two, and a slow time course, often continuing for hours. Subsequent perfusion with a high potassium solution caused the tectorial membrane to shrink. The time course of shrinking was almost an order of magnitude faster than that of swelling. Generally the shrinking did not completely reverse the previous swelling. Permanent changes in the structure of the tectorial membrane tended to persist after a long exposure to a high sodium solution.

For both high potassium and high sodium solutions, the tectorial membrane shrunk as calcium was increased from μmol/L to mmol/L concentrations. When calcium concentration was held constant at 2 mmol/L, substitution of sodium for potassium had little effect. For both high potassium and high sodium solutions, addition of the calcium chelator EGTA, which reduced the calcium concentration to levels appreciably below 1 μm/L, induced swelling. If the perfusate contained 1 mmol/L EGTA, substitution of sodium for potassium had little effect.

Many of the exposures to perfusion solutions that were long enough for the changes in dimensions of the tectorial membrane to come to steady-state led to irreversible changes in the tectorial membrane. Therefore, we began to study the effects of brief (15 minute) exposures to test solutions. The responses for brief exposures are consistent with those for long exposures. However, the effects of brief exposures are more nearly reversible, and we have been able to measure responses to brief exposures of as many as 20 different ionic solutions in a single preparation. Thus, we should be able to characterize more fully the dependence of dimensions of the tectorial membrane on ionic composition of the perfusion solution. Such a characterization is necessary if we are to understand the gel properties of the tectorial membrane.

The initial experiments with the isolated tectorial membrane preparation revealed that its microstructure changes systematically and reversibly in different ionic solutions. To capture these differences in microstructure and quantify changes in the volume of the tectorial membrane, we are developing a system for analyzing effects of lymph composition on the three-dimensional structure of the tectorial membrane using video-enhanced microscopy and computer-aided image reconstruction. The image of the tectorial membrane is magnified using a compound microscope equipped with differential interference contrast (Nomarski) optics. The magnified image is projected onto a video camera connected to a video digitizer. A sequence of images is recorded at different focal planes of the microscope. This sequence of two-dimensional images contains information about the three-dimensional structure of the tectorial membrane.

Although Nomarski images are sensitive to variations in the refractive index of the specimen (i.e., the tectorial membrane), Nomarski images are not simple maps of refractive index. Implicit in the optical system are a number of systematic transformations of the underlying variations in refractive index. We have implemented numerical algorithms to undo these transformations and recover the underlying variations in refractive index. The optical transformations are characterized by measuring a sequence of video images at different focal depths of a microscopic (0.25 μm diameter) plastic sphere. This sequence, which approximates the point-spread function of the optical system, is used to implement a "deconvolution" system that reduces optical blurring in the plane of the images and also removes out-of-focus information (from nearby planes) that contaminates each image. The enhanced two-dimensional images will be used to construct a three-dimensional representation of the tectorial membrane. This representation will allow measurements of the dimensions of the tectorial membrane (including its volume, thickness, length, and width) as well as its microstructure.

1.4.1 Stimulus Coding in the Auditory Nerve and Cochlear Nucleus

Project Staff

Dr. Bertrand Delgutte, Dr. Peter A. Cariani

The goal of our research is to understand neural mechanisms for the processing of complex acoustic stimuli at the level of the auditory nerve and cochlear nucleus. During the past year, we have focused on the coding of the pitch of complex periodic tones such as voiced speech and musical sounds. We have recorded the responses of auditory-nerve fibers to both harmonic and inharmonic stimuli similar to those used in psychophysical experiments on pitch perception. Neural responses were analyzed in the form of autocorrelograms, which display the probability distribution of all interspike intervals (1st, 2nd, 3rd, etc). Aggregate autocorrelograms were formed by

adding the interval distributions for large numbers of auditory-nerve fibers innervating all regions of the cochlea. For harmonic stimuli which produce a strong pitch at the fundamental frequency, the most frequent interspike interval in the aggregate autocorrelogram always corresponded to the fundamental period of the stimulus. For inharmonic stimuli that have multiple, ambiguous pitches (such as amplitude-modulated tones), aggregate autocorrelograms showed multiple prominent intervals whose relative strengths corresponded roughly to the relative salience of the different pitches. For amplitude-modulated noise, which has a much weaker pitch than amplitude-modulated tones, interspike intervals were much less concentrated near specific values than for modulated tones. These results show that information for pitch determination is available in a relatively simple form in the interspike intervals of auditory-nerve fibers, and are consistent with pitch theories stating that pitch corresponds to the most frequent interspike interval in the entire auditory nerve.

If an interspike interval code is used for pitch, what neural mechanisms could be employed to discriminate between different pitches? One possibility is that cells in the cochlear nucleus with regular "chopper" firing patterns might preferentially synchronize to specific interspike-intervals in their auditory nerve inputs. An array of such elements tuned to different intervals could implement an autocorrelation-like periodicity detector. In order to test this idea, a simple model of a neuron exhibiting "chopping" behavior, preferred interspike intervals, and band-pass modulation transfer functions was developed. The integrate-to-threshold model has a nonmonotonic threshold recovery function with a "superexcitable" phase following a refractory one. The presence of a superexcitable phase implies that the neuron will have relatively higher discharge rates and modulation gain in response to amplitude-modulated tones whose modulation frequency is within a certain range. The model predicts that the peak of superexcitability should coincide with the interspike interval predominant at the onset of chopping. We are currently recording from cochlear nucleus units with chopper discharge patterns in order to test the model predictions.

Publications

Cariani, P., and B. Delgutte. "Interspike Interval Distributions of Auditory-nerve Fibers in Response to Variable-pitch Complex Stimuli." *Abstr. Assoc. Res. Otolaryngol.* 15 (1992).

Delgutte, B., and P. Cariani. "Coding of the Pitch of Harmonic and Inharmonic Complex Tones in the Interspike Intervals of Auditory-nerve Fibers." In *Audition, Speech, and Language.* Ed. M.E.H. Schouten. Berlin: Mouton-De Gruyter. Forthcoming.

Delgutte, B. "Fundamental Issues in Auditory Modeling." Proceedings of the IEEE ASSP Workshop on Applications of Signal Processing to Speech and Audio Coding, 1991.

1.5 Electrical Stimulation of the Auditory Nerve

Project Staff

Dr. Bertrand Delgutte, Scott B.C Dynes

This research studies physiological mechanisms of electrical stimulation of the auditory nerve with the expectation that such information will help design improved cochlear implants. For this purpose, we are recording the responses of auditory-nerve fibers to electric currents applied through electrodes inserted into the cochlea. Recent results[9] have shown that a speech processor in which brief current pulses are applied in rapid succession through different electrodes provides better speech reception in cochlear-implant patients than a processor delivering continuous analog signals. In the hope of better understanding the physiological basis for these improvements, we are studying the responses of auditory nerve fibers to pairs of brief rectangular electrical pulses separated by a delay. For delays smaller than 0.5 msec, the presence of a subthreshold first pulse either decreased (sensitization) or increased (masking) the threshold for the second pulse. The amount of sensitization was always greater than that of masking. The time course of these effects, as well as the asymmetry between sensitization and masking were predicted by a nonlinear, biophysical model of myelinated nerve fibers developed by J.T. Rubinstein. These physiological results resemble inter-pulse interactions found in behavioral thresholds of cochlear-implant patients. They suggest

[9] B.S. Wilson, C.C. Finley, D.T. Lawson, R.D. Wolford, D.K. Eddington, and W.M. Rabinowitz, "Better Speech Recognition with Cochlear Implants." *Nature* 352: 236-238 (1991).

that increasing pulse rate in interleaved-pulses speech processors may not lead to further improvements in speech reception because this would increase interactions between pulses applied through different electrodes.

Publications

Dynes, S.B.C., and B. Delgutte. "Phase Locking of Auditory-nerve Discharges to Sinusoidal Electric Stimulation of the Cochlea." *Hear. Res.* Forthcoming.

1.6 Middle-Ear Muscle Reflex

Project Staff

Dr. John J. Guinan, Jr., James B. Kobler

Our aim is to determine the structural and functional basis of the acoustically elicited middle-ear muscle reflexes. During the past year, data analysis and writing have been done to prepare for publication our results on the sound-frequency selectivities of single stapedius motoneurons in ketamine-anesthetized and decerebrate cats. Stapedius-motoneuron tuning curves were very broad, similar to the tuning of the overall acoustic reflexes as determined by electromyographic recordings. The lowest thresholds were usually for sound frequencies between 1 and 2 kHz although many tuning curves also had a second sensitive region in the 6-12 kHz range. The broad tuning of stapedius motoneurons implies that inputs derived from different cochlear frequency regions (which are narrowly tuned) must converge at a point central to the stapedius-motoneuron outputs, possibly at the motoneuron somata. There were only small differences in tuning among the four previously described groups of stapedius motoneurons categorized by sensitivity to ipsilateral and contralateral sound. The thresholds and shapes of stapedius-motoneuron tuning curves support the hypothesis that the stapedius acoustic reflex is triggered by summed activity of low-spontaneous-rate auditory-nerve fibers with both low and high characteristic frequencies (CFs). Excitation of high-CF auditory-nerve fibers by sound in their tuning curve "tails" is probably an important factor in eliciting the reflex. In general, the most sensitive frequency for stapedius motoneurons is higher than the frequency at which stapedius contractions produce the greatest attenuation of middle-ear transmission. This is consistent with the hypothesis that the main function of the stapedius acoustic reflex is to reduce the masking of responses to high frequency sounds produced by low-frequency sounds. A manuscript describing these data has been submitted.[10]

Also during the past year, data analysis and writing have been done to prepare for publication our results on (1) the growth of simultaneous masking of cat auditory-nerve fiber responses to high-frequency tones by low frequency noise, and (2) the effects of stapedius-muscle contractions on the masking of responses in the auditory nerve.

Publications

Kobler, J.B., J.J. Guinan, Jr., S.R. Vacher, and B.E. Norris, "Acoustic-Reflex Frequency Selectivity in Single Stapedius Motoneurons of the Cat." Submitted to *J. Neurophys.*

1.7 Cochlear Efferent System

Project Staff

Dr. John J. Guinan, Jr., Michael P. McCue

Our aim is to understand the physiological effects produced by medial olivocochlear efferents which terminate on outer hair cells in the mammalian cochlea.

During the past year, work has been done on several ongoing projects: (1) a project which measures efferent effects on stimulus frequency otoacoustic emissions (SFEs) to test hypotheses about the role of outer hair cells in controlling the "cochlear amplifier," (2) a project in which efferent effects on SFEs are contrasted with two-tone suppression effects on SFEs (both of these agents appear to influence the "cochlear amplifier" but at different sites), and (3) a project to determine the correspondence between the number of medial efferents that fire and the magnitude of the effects produced.

During the past year, we have also begun work aimed at comparing the time courses of the many reported efferent effects. Preliminary work suggests that all of these effects may not follow the same basic time course which would imply that more than one mechanism is involved.

[10] J.B. Kobler, J.J. Guinan, Jr., S.R. Vacher, and B.E. Norris, "Acoustic-Reflex Frequency Selectivity in Single Stapedius Motoneurons of the Cat," submitted to *J. Neurophys.*

1.8 Cochlear Implants

Project A: Models of Current Spread and Nerve Excitation during Intracochlear Stimulation

Project Staff

Dr. Donald K. Eddington, Dr. Jay T. Rubinstein

The basic function of a cochlear prosthesis is to elicit patterns of activity on the array of surviving auditory nerve fibers by stimulating electrodes that are placed in and/or around the cochlea. By modulating these patterns of neural activity, these devices attempt to present information that the implanted subject can learn to interpret. The spike activity patterns elicited by electrical stimulation depend on several factors: the complex, electrically heterogeneous structure of the cochlea, the geometry and placement of the stimulating electrodes, the stimulus waveform, and the distribution of exitable auditory nerve fibers. An understanding of how these factors interact to determine the activity patterns is fundamental to designing better devices and to interpreting the results of experiments involving intracochlear stimulation of animal and human subjects. As a first step towards this understanding, *the goal of this project is to construct* a software model of the cochlea that predicts the distribution of potential produced by the stimulation of arbitrarily placed, intracochlear electrodes and to use these potential distributions as inputs that drive models of auditory nerve fibers.

This year we directed effort at testing the three-dimensional, finite difference model of the human cochlea that predicts the potential distribution produced in this structure by electrical stimulation using model electrodes of arbitrary position and geometry. Both the measurements of scala tympani potentials and psychophysical measures of the interaction between two simultaneously stimulated electrodes made in subjects implanted with intracochlear electrodes and reported last year were continued and confirmed the asymmetric potential distributions predicted by the model.

We have continued the development of linear and nonlinear models of extracellular excitation of myelinated and unmyelinated nerve fibers by considering the case of terminated fibers. Cable models developed to simulate stimulation near the terminal of a passive fiber show that the predicted cathodal threshold can be an order of magnitude lower than predicted by the infinite length models used to date. In addition to the obvious relevance of such models to stimulation of the cochlea (where dendrites of auditory nerve fibers terminate), these models are also of general interest since they predict that in regions where some fibers terminate and others do not, cathodal electrical stimulation will tend to excite the fibers that terminate.

Publications

Eddington, D.K., G. Girzon, and P.A. Cuneo. "An Electroanatomical Model of Intracochlear Electrical Stimulation II: Tests of Model Predictions for Monopolar Electrodes." Submitted to *Hear. Res.*

Girzon, G., and D.K. Eddington. "An Electroanatomical Model of Intracochlear Electrical Stimulation I: Formulation, Solution and Predictions for Monopolar Electrodes." Submitted to *Hear. Res.*

Project B: New Sound Processors for Auditory Prostheses

Project Staff

Dr. Donald K. Eddington, Dr. William M. Rabinowitz

Our collaboration with colleagues at Duke University and the Research Triangle Institute in the development of new processing algorithms to improve the speech reception of cochlear implant users has resulted in laboratory-based systems that increase the average single-syllable word recognition scores by 20 percentage points for the seven subjects tested (Wilson et al., 1991). In order to make the continued development of new algorithms and their testing in our larger subject population more efficient, we decided to design and build a local, laboratory-based, real-time signal-processing system in collaboration with Joseph Tierney amd Marc Zissman of Lincoln Laboratory.

The resulting system includes a digital signal processing (DSP) board (Sonitech Corporation, based on a Texas Instruments TMS320C30 DSP chip) that connects to a SUN IPC workstation. The serial output port of the DSP board is connected to a custom I/O system that includes two channels of A/D conversion (50 kHz/channel) and eight channels of D/A conversion (>100,000 kHz/channel). Two channels of input provide the ability to investigate binaural processing and the eight channels of output allow for stimulation of up to eight intracochlear electrodes. The eight output channels are isolated from the 120V AC power and converted to current source signals by custom electronics before being connected to a subject's implanted electrode array. Custom software provides the flexible interface that enables the experimenter to specify the parameters and

configuration of the processing algorithm to be implemented.

Initial tests of the system concentrated on simulating the subject's commercial, four-channel analog processor in which the analog output of each of four bandpass filters is directed to an implanted electrode. Tests of this system were made in our best performing subject and demonstrated equivalence in both subjective impressions and objective measures of word recognition. A new system designed to reduce the interference caused by simultaneously activating electrodes was also implemented. It uses the envelopes of bandpass filter outputs to modulate biphasic pulse trains that are interleaved and, therefore, delivered nonsimultaneously to as many as six electrodes. Initial tests of this system made use of a 24 consonant test (aCa context) in the same best performing subject. Scores measured using the commercial processor ranged between 73% and 85% and between 95% and 99% using the interleaved system.

Publications

Wilson, B.S., C.C. Finley, D.T. Lawson, R.D. Wolford, D.K. Eddington, and W.M. Rabinowitz. "Better Speech Recognition with Cochlear Implants." *Nature* 352: 236-238 (1991).

Section 4 Linguistics

Chapter 1 Linguistics

Chapter 1. Linguistics

Academic and Research Staff

Professor Morris Halle, Professor Noam A. Chomsky

1.1 Introduction

The work of the Linguistics group is directed towards a better understanding of the mental capacities of human beings through the study of the nature, acquisition and use of language. Language is a uniquely human faculty: only humans appear to be capable of learning and using a language, and every normal human acquires knowledge of one or more languages.

We are trying to understand how this linguistic knowledge is represented in the speaker's mind. The central issues of linguistics research are:

1. What is the nature of linguistic knowledge? What do speakers of a particular language such as Latvian, Spanish or Walpiri know, and how does knowledge of one language resemble or differ from that of another language?
2. How do speakers acquire this knowledge?
3. How do speakers put this knowledge to use in producing and understanding utterances?
4. What are the physiological mechanisms that provide the material basis for storage, acquisition and utilization of linguistic knowledge?

Our ability to answer these questions differs considerably, and our research reflects these differences. At present, we have progressed further with regard to answering the questions posed by item one and have made less progress with item four. Currently, our research is heavily concentrated on issues concerned with the nature of the knowledge that characterizes fluent speakers of various languages. However, we are making a significant effort to solve the other questions also.

We are studying these topics along a number of parallel lines. Linguists have investigated the principles by which words are concatenated to form meaningful sentences. These principles have been the primary domain of inquiry into the disciplines of syntax and semantics. Phonology studies the sound structure of words while morphology examines the manner in which different languages combine different meaning-bearing units (specifically, stems, prefixes, suffixes and infixes) to form words. The latter topic has attracted increasing interest in recent years and will probably become more prominent in our research efforts in the future.

1.2 Abstracts of Doctoral Dissertations

The following are abstracts of dissertations submitted in 1991 to the Department of Linguistics and Philosophy in partial fulfillment of the requirements for the degree of Doctor of Philosophy in Linguistics.

1.2.1 Morphology After Syntax: Pronominal Clitics in Romance

M. Eulalia Bonet i Alsina

Abstract

This dissertation is primarily concerned with non-transparent output forms in Romance pronominal clitic combinations. The position is taken that pronominal clitics constitute hierarchical structures of *morphological features*. Each clitic is a subset of the structure shown below:

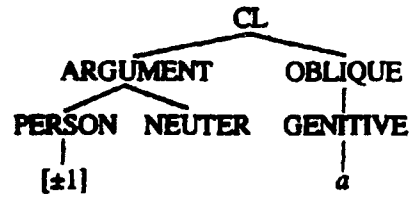


Figure 1.

In addition, clitics might contain an Agreement node, dependent on the most specific node dominated by [ARGUMENT], with the private features [feminine] and [plural].

It is assumed, with Kayne (1975) and later work, that pronominal clitics are generated in argument position at D-structure and are ajoined to an Infl node by S-structure. S-structure contains fully

specified syntactic feature matrices, as argued for in Lumsden (1987). The morphological structures schematized in figure 1 are created in the mapping from S-structure to the Morphology Component (cf. Halle (1989) and related work). Within the Morphology Component, morphological rules might alter in certain contexts the original structure assigned to a specific clitic. In this fashion, most non-trasparent forms are derived, predicting that an important subset of the non-transparent output forms will have the same surface form as other clitics of the language instead of becoming an arbitrary phonological sequence.

The surface order of clitics is established in the Morphology Component through mapping to a template. Some other non-transparent forms are obtained at this point, when two clitics (or morphological features) compete for the same slot. Since only one of them can be mapped, the other one simply does not surface.

Phonological information not present in the syntax is introduced within the Morphology Component by spell-out rules, providing the input to PF, which deals only with phonological processes.

The type of account presented in this dissertation voids the need for filters that rule out sequences of phonologically identical sequences, criticized often in the literature.

1.2.2 On the Typology of Wh-Questions

Lisa Lai Shen Cheng

Abstract

This thesis proposed that the typological distinctions among languages with respect to the formation of wh-questions can be attributed to the availability of question particles and the properties of wh-words. It is argued that the availability of question particles correlated with the lack of syntactic wh-movement. A theory of Clausal Typing is proposed to account for this correlation. In particular, languages employ either question particles or syntactic wh-movement to type a clause as a wh-question. It is shown that the Principle of Economy of Derivation predicts that (a) no language has the options of alternating between the two methods of Clausal Typing and thus there are no languages with "optional movement" of wh-words and (b) movement of one wh-word is sufficient to type a clause as a wh-question. Apparent counterexamples to the proposal are discussed. It is argued that in languages with apparent optional fronting of wh-words (e.g., Egyptian Arabic), sentences with a clause-initial wh-word are clefts. In addition, it is shown that in languages which front multiple wh-words in multiple questions, the wh-words are morphologically complex and need to satisfy a licensing requirement independent of Clausal Typing.

The internal structure of wh-words in an in situ language, namely Mandarin Chinese, is also examined. It is shown that wh-words in Mandarin are indefinite NPs, which lack quantificational force, and they are polarity sensitive. In addition, two LF operations are discussed: Quantifier Raising and LF wh-movement. It is shown that the lack of scope ambiguities in Mandarin can be attributed to lexical properties of indefinite NPs. Arguments for and against LF wh-movement as well as the landing site of wh-words at LF are examined. It is shown that evidence against LF wh-movement does not hold, and arguments against adjuction of wh-words to IP and LF will be provided.

1.2.3 Resumptive Chains in Restrictive Relatives, Appositives and Dislocation Structures

Hamida K. Demirdache

Abstract

This thesis proposes that *wh*-operators in (headed) restrictive and non-restrictive relatives are resumptive chains. A resumptive chain can have *+wh*-features or *−wh*-features. If it has *−wh*-features, it can be either a null pronoun or an overt pronoun. It can have either of the two interpretations that pronouns have. Thus, in restrictive relatives, it has a bound variable interpretation. In appositive relatives, it is a referring pronoun (or what Evans (1982) calls an E-type pronoun). This resumptive chain can be created at S-structure or at LF. In particular, it is argued that what has been called (misleadingly) in the literature a "resumptive pronoun" in languages like Hebrew or Irish (i.e., a pronoun that freely alternates with gaps in certain positions) is an instance of in situ relativization: an overt *−wh*-pronoun in situ at S-structure creates an operator-variable chain at LF. It does not have the same range of interpretations as a trace created at S-structure because it is not a variable at S-structure. In contrast, the *wh*-operator in appositive relatives never has a bound variable interpretation. An analysis of appositives is proposed based on Emonds' (1979) *Main Clause Hypothesis*. It is argued that appositive clauses are lifted at LF out of the matrix clause containing their antecedent. The relation between the appositive pronoun and its antecedent is treated on a par with anaphora

across discourse, except in one respect: anaphora is obligatory precisely because of the *wh*-features of the pronoun. Finally, it is argued that, under the above proposal, the (Clitic)Left-Dislocation construction discussed by Cinque (1991) must be a wh-movement construction. The clitic-pronoun is a *–wh*-operator in-situ at S-structure, on a par with the pronoun that appears in Hebrew relatives. However, it has the syntactic properties and the interpretation of the *+wh*-operator in appositive relatives.

1.2.4 The Syntax of Argument-Structure-Changing Morphology

Mika C. Hoffman

Abstract

The study of the causative and applicative constructions in Bantu languages gives us an insight into some complex applications of theories of argument structure and Case theory. This thesis develops a theory of lexical complementation which gives a unified account of causative and applicative constructions and double object constructions of all types: all these multiple object constructions are examples of predicate-predicate complementation. Causatives are examples of VP-VP complementation, while applicatives, locative alternation verbs, and dative double object verbs are examples of VP-PP complementation. Complementation involving PP is examined in some detail, as a theory of Preposition Inversion is developed and shown to be responsible for applicative asymmetries. In addition, a theory of licensing involving movement to functional head accounts for a number of object properties in Bantu.

1.2.5 Topics in Conditionals

Sabine Iatridou

Abstract

This thesis is concerned with a number of issues that pertain to the syntax and semantics of conditional constructions.

In chapter 1, there is a treatment of basic syntactic properties that characterize the relationship between the IF-clause and the matrix clause, as well as relationships internal to the IF-clause. Some similiarities between if and other elements that introduce clauses are discussed.

In chapter 2, there is a typology of conditional constructions with respect to their meaning and syntactic properties. It is argued that there are three different types of conditionals, if the semantic and syntactic relationship between the IF-clause and the matrix clause is taken into account. The contrasts between two conditional types is assimilated to the contrasts between appositive and restrictive relative clauses, and between BECAUSE- AND SINCE-clauses.

In chapter 3, it is argued that conditional then has a meaning, and a specific proposal is advanced to account for its distribution on semantic grounds.

In chapter 4, there is a discussion of the syntactic properties of conditional then, and a general proposal is put forth for the syntactic environments in which its presence is restricted.

1.2.6 The Semantics of the English Progressive

Katherine Susan Kearns

Abstract

This thesis proposes that the English progressive semantically modifies the relation between events and times, and that this semantics uniformly underlies a variety of apparently disparate readings of the progressive. Chapter 2 begins with Jespersen's observation that the progressive presents an event as a temporal frame around a given time. This intuition may be expressed as follows: where t is a given time, and t' is the time of an event e, a progressive sentence reporting e asserts that t', the event time, properly contains the framed time t. In this view, a progressive sentence entails the existence of an event of greater duration than the framed time t. The author demonstrates that the temporal frame reading is not an entailment of the progressive but arises by implicature; the existence of an event of greater duration than the framed time t is implicated but not entailed. The author also shows that restrictions on the framed time t proposed elsewhere, claiming that t must be an instant, or that t must be non-initial and non-final in t', are incorrect.

Drawing on the constrasting readings of present progressive sentences and simple present tense sentences with event predicates, it has also been claimed that the progressive has a metaphysical character, reporting actual phenomena, while the simple present tense, interpreted as a habitual predication, reports characteristics of the "structure of the world." The author argues that the progressive/non-progressive contrast in the

present tense is basically temporal: the progressive, unlike the (habitual) simple present tense, explicitly dates or temporally locates reported events. The different readings at issue follow by implicature arising from this contrast.

In chapter 3, the author addresses certain problems with the progressive of state predicated, including habituals. Having argued that the progressive is not ill-formed or false with state predicates per se, the author offers an account of the temporary or limited duration reading of progressive state predicates in terms of the implicature outlined in chapter 2 for the progressive/non-progressive contrast in the present tense. Drawing also on a modified version of Carlson's (1977) distinction between individual-level and stage-level predications, the author argues that where a simple tense state predicate has the individual level reading, the progressive form implicates temporariness because it explicitly dates or temporally locates the state described. The author also reviews a class of psychological state predicates and argues that certain of these resist the progressive because the explicit dating of a state or event expressed by the progressive is anomalous.

A very old traditional observation, holding that the progressive is a "definite tense," contrasting with the "indefinite" perfect, is addressed in chapter 4; definite tense forms make reference to specific times and indefinite forms to non-specific times. This classification is seen as resting on the pre-Russellian view of the articles a and the, developed more recently as the Familiarity Theory of Definiteness. The author argues for a quantificational analysis of the novelty and familiarity effects and claims that the original definite/indefinite classification of verb forms should be captured by differences in the quantification over times. In present perfect sentences event times are existentially quantified, and in progressive sentences, the framed time is bound by quantificational the.

Finally, in chapter 5 the author discusses the Imperfective Paradox and the two main types of response to it. Dowty (1979) is the chief example of the first approach, which is to analyze the progressive as a kind of counterfactual. The author explores the essential components of this view and argues that certain inadequacies indicated the correctness of the second view. The second view holds that the paradox is only apparent, because the predicate found in a progressive sentence is not the same as the predicate in the corresponding non-progressive sentence; the troublesome entailments are not valid on this view. The author presents additional evidence for the second view and also argues that the two distinct readings are found in the uninflected predicate, which is ambiguous.

1.2.7 The Aspectual Nature of the Thematic Relations: Locative and Temporal Phases in English and Chinese

Elizabeth Mary Klipple

Abstract

This thesis investigates the properties of elements on the "border" of thematic structure. It deals primarily with various sorts of locative and temporal phrases, with the aim of elucidating which of these phrases should be considered to be thematically related to the verb, and what the factors are which determines this division. It is proposed that the Internal/External distinction is the major dividing line between thematic and non-thematic elements; an element is "internal" if it adds to the information about the internal aspectural structure of the event denoted in a sentence; it is external if it does not contribute information about this structure. Thus, thematic structure is closely tied to aspect and event structure.

This approach predicts that certain elements which are normally not considered to be relevant to thematic relations should be included as part of thematic structure. These elements are locative phrases indicating goal, direction, path, source, and posture, and temporal phrases indicating iteration and duration, measure phrases, and resultatives.

It is further maintained that there is a tight syntax/semantics correlation and that the semantic property of contributing to the internal aspectural structure of an event corresponds to the syntactic property of being within the lowest projection of the VP.

Chapter 2 provides syntactic evidence in English for the internal/external distinction, and shows that for the most part the types of phrases predicted to be event-internal are also VP-internal. Chapter 3 presents evidence from Mandarin Chinese; in this language, the surface order of the various types of locatives and temporals provides a strong argument for the distinction as drawn by the author.

In chapter 4, the author looks at binding relations between various types of VP-internal and VP-external phrases, in order to probe the structure of the VP. The author considers the proposal of Larson (1988) that all post-verbal PPs are within

the VP, but shows that in fact it is better to treat these elements as VP or IP adjuncts, as is traditionally done.

In chapter 5, the author explores in more detail the semantic properties of internal locatives and temporals. Goal and Posture phrases are argued to be secondary predicates which combine with the main verb, on a par with the resultative complements. Direction, path, and durative phrases are modifiers of a parameter associated in the lexicon with the main predicate. Iterative phrases are taken to be something like numerals which quantify subparts of the event. Finally, the author compares her approach with the theories of Gruber and Jackendoff and that of Davidson (1967) as modified by Parson (1990).

1.2.8 On Embedded Interrogatives and Predicates That Embed Them

Utpal Lahiri

Abstract

This thesis deals with certain issues in the interpretation of embedded interrogatives, in particular, the role of the notion *answer* to a question in the interpretation of embedded interrogatives. Chapter 1 discusses a certain view about the interpretation of embedded interrogatives derived from Hintikka (1976) and Berman (1991) and raises problems for the view that embedded interrogative complements of predicates like *know* are open sentences. The author discusses the phenomenon of Quantificational Variability, viz., the fact that certain adverbs of quantification restrict the interpretation of structures containing interrogatives embedded under predicates like *know* in a way they do not for predicates like *knows*. The author argues that the distinction between two classes of predicates is not between factive and non-factives, but between those predicates that are true of questions and an agent only if their proposition-taking counterpart is true of the agent and some answer to the question. The author also argues that certain predicates require their embedded interrogatives to be interpreted as whole answers rather than the way expected of the open sentence view.

In chapter 2, the author examines possible syntactic evidence for the claim the the interrogative complements of predicates like *know* and predicates like *wonder* are syntactically distinct and shows that no such evidence is available in English. The author examines the case of Spanish which has been proposed to maintain such a distinction, and again show that the relevant distinction is between speech-act and non-speech-act verbs, and so is not directly relevant to the issue of which predicates allow Quantificational Variablility.

In chapter 3, the author develops an account of Quantificational Variability that highlights the ways in which answers to questions are relevant in interpreting embedded interrogatives. In order to do this, the author first distinguishes between two classes of adverbials of quantification, viz., adverbials of frequency and adverbials of quantity and precision and shows that only the latter are relevant to Quantificational Variablity. The author argues that *natural* answers to questions can be viewed as things with a Boolean part-structure and develops a theory of quantification for atomic Boolean algebras modeled on Higginbotham's treatment of mass-quantification. Since *natural* answers have an atomic Boolean part-structure, this analysis, which is needed independently, can be extended to interrogatives.

1.2.9 Effects of Head-Movement on Subjacency and Proper Government

Paul S. Law

Abstract

This dissertation offers a perspective from which to view the relationship between extraction and head-movement. In particular, it claims that bounding theory must take syntactic head-movement into account in defining bounding domains. The possibility of subject extraction is related to abstract verb movement to C, which is argued to be a consequence of the interaction between the Principle of Full Interpretation and various principles in the grammar is also claimed.

It is suggested that bounding domains be defined with respect to head-movement. Specifically, a potentially bounding category can be subsumed under another if their heads are morphologically merged. As a result, the dominating maximal projection comes to delimit the bounding domain. Evidence is presented to show that VP can be bounding in general and that cases where the bounding effect is seemingly absent are due to head-movement. It is also shown how this conception of bounding domains fits into a theory of bounding with two parameters which can annul bounding effects of maximal projections by complementation. A principled explanation obtains for why certain combinations of categories as bounding domains are possible, and why some others are not. The predicted four types of languages with respect to bounding variations are all attested. It is argued that in order to account for

the extraction asymmetry between adverbials and others, successive-cyclic movement should be strictly constrained by structure-preservation.

The apparent lack of the *that*-trace effect in some instances is suggested to have a principled explanation in terms of abstract verb movement to C, which is either a result of the Principle of Full Interpretation interacting with a theory of expletive replacement, or is due to some language-particular property like the verb-second constraint in most Germanic languages requiring movement of the finite verb to the empty C position at LF, if it is not already there at S-structure. One desirable consequence that immediately follows is that the class of proper head-governors can now be restricted to all and only lexical categories. It is suggested that abstract verb movement to C in relative clauses is independently justified by theory of predication, which requires a lexical category to fill the head of a constituent which is semantically a predicate. Consequently, the subject trace is properly head-governed by the verb in C. The possibility of abstract verb movement to C thus explains in a uniform way the anti-*that*-trace effect in relative clauses and the *that*-trace effect in complement clauses, without the assumption that the complementizers in these two types of constructions are different entities.

1.2.10 Tense and Temporal Order

Harry Leder

Abstract

This thesis investigates the nature of temporal reference in natural language. Reference to time enters into linguistic structures in two distinct ways, namely *tense* and *temporal modification* by adverbials.

The author starts by considering temporal modification, since it is noncontroversial here that an analysis in terms of predicates of events can be implemented straightforwardly. Events, then, are conceived along the lines of Davidson (1967a) and are assumed to be encoded in linguistic representations as proposed by Higginbotham (1985), etc. Being predicated of properties, viz. which are temporal *duration* and temporal location; the first of these answers to the question *How long?* the latter, to the question *when?* Both can be specified by means of temporal adverbials.

Taking the analysis of temporal adverbs as a guide, the author analyzes tenses as predicates of events as well, thereby placing in the context of the Davidsonian theory of adverbial modification the idea due to Kiparsky (1968), that tense is adverbial in nature. It is immediately obvious that tense is concerned only with temporal location, not with duration.

The author proposes to analyze the tenses as functional instances of the abstract ordering relation of events found at work in adverbial modification, and specifically in the temporal connectives or conjunctions. In the case of simple matrix clauses, tense establishes an ordering relation between the event purportedly described in the sentence and an utterance-event.

Analyzing the tenses as ordering relations predicts two possibilities for construing embedded tenses. One option, called Serial embedded tense, is for an embedded event to be placed in an ordering relation with the event of the next-higher clause. Alternatively, with what we call Parallel embedded tense, the embedded event is ordered relative to the utterance-event by its tense, independently of, and parallel to, the ordering of the matrix event *vis-à-vis the same utterance* event.

Both patterns are found to exist side by side in Latin, where Parallel and Serial tense are expressed by indicative and subjunctive tense-marking, respectively. But as we see in the latter part of this thesis, the author also finds evidence that both patterns are available in English. Parallel tense, subject to certain restrictions to be made precise, give rise to the "double access" reading discussed by Enç (1987), Ogihara (1989), and others, while Serial tense is responsible for the so-called "sequence of tense phenomena." Both of these are discussed in several frameworks; they provide crucial cases which permit sorting the different predictions made by competing analyses.

The view proposed here, which treats the tenses as two-place predicates of events is found to be superior to alternatives, both in its coverage of tense-phenomena and in its simplicity. The semantics of tense can be assimilated to known schemes for interpreting context-dependent expressions.

1.2.11 Investigations Into Grammatical Knowledge

James Douglas Saddy

Abstract

This work presents a case study into the nature of one brain-damaged individual's ability to comprehend sentences. The focus of the research is on the ability to construe quantificational scope ambiguities. Two broad results will emerge. First, the author demonstrates that the notion of comprehension as it is currently used in aphasic research is too narrow. In addition, the author argues against the position that linguistic impairments are the result of damage to an individual's grammatical knowledge. Secondly, the author demonstrates that evidence from aphasia can bear on a formal linguistic issue in an interesting way.

The aphasiological investigation (1) demonstrates that grammatical knowledge (competence) may be retained in a grammatism and (2) presents evidence of a hitherto unknown comprehension impairment that is tied to the event structure of a sentence.

The linguistic analysis of the aphasialogical data argues for the existence of a syntactically active abstract argument position associated with predicates, thus providing support for an extended Davidsonian view of argument structure. This approach also provides for an alternative account of the general nature of agrammatic receptive deficits in terms of an impaired ability to distinguish the properties of such arguments and links the pattern of deficit comprehension observed to the normal range of scopal interpretations attested in languages that do not distinguish nouns and verbs at the lexical level.

The particular pattern of the comprehension deficit exposed by the research leads one to conclude that universally quantified terms are understood as binding the event position in the syntactic representations generated. Definite and indefinite phrases, however, do not. The aphasic evidence suggests that indefinites are not quantificational. Nevertheless, both wide and narrow scope readings are attested. This leads us to question whether this pattern is due to the special nature of the deficit or whether it reflects a true distinction between the quantificational properties of indefinite existential and universal expressions in natural language.

Arguments from Heim and Berman are presented that support the notion that indefinites and WH expressions have no inherent quantificational force. The special syntactic and interpretational properties of WH expressions in Bahasa Indonesia are then presented as demonstration that scoped interpretation of indefinites may be available without movement.

This result allows the author to claim that in the agrammatic case, the normal application of core properties of grammar to a well formed syntactic representation obtain. The pattern of comprehension in the agrammatic case follows from a merging of the distinguishing characteristics of predicate types.

Appendices

Appendix A RLE Publications and Papers Presented

Appendix B Current RLE Personnel

Appendix C Milestones

Appendix D RLE Research Support Index

Appendix A. RLE Publications and Papers Presented

The first section of this bibliography includes papers and talks presented by RLE faculty, staff and students during 1991 and is in alphabetical order by conference name. Reprints of these papers may be obtained by contacting the authors directly.

Section 2 includes an alphabetical listing by author of journal articles that were published and accepted or submitted for publication. Book chapters by RLE authors are listed in Section 3. Section 4 of this bibliography lists RLE general publications and technical reports, and Section 5 is a list of RLE theses submitted during 1991. Section 6 contains miscellaneous publications.

A.1 Meeting Papers

A.1.1 Papers Presented

Acoustical Society of America Meeting, 121st, Baltimore, Maryland, April 29 - May 3, 1991.

Boyce, S., and C.Y. Espy-Wilson. "The F3 Trajectories of American English /r/'s."

Stevens, K.N. "Models for Voicing and Aspiration in Stop Consonants."

Zurek, P.M. "Interference Reduction for the Hearing Impaired."

Acoustical Society of America Meeting, 122nd, Houston, Texas, November 4-8, 1991.

Power, M.H., and L.D. Braida. "A Physical Measure of Consistency Among Speech Parameter Vectors: Application to Speech Intelligibility Determination."

Uchanski, R.M., K.M. Millier, D.E. Ronan, C.M. Reed, and L.D. Braida. "Effects of Token Variability on Resolution for Vowel Sounds."

American Association for the Advancement of Science, Annual Meeting, Washington, D.C., February 14-19, 1991.

Pritchard, D.E., K. Boyce, and E. Cornell. "Single Ion Mass Spectroscopy."

American Astronomical Society, 177th Meeting, Philadelphia, Pennsylvania, January 14-17, 1991.

Lehár, J., J.N. Hewitt, D.H. Roberts, and B.F. Burke. "VLA Determination of the Time Delay in 0957+561."

Markert, T., M.L. Schattenburg, T. Isobe, J. Bauer, C. Canizares, J. O'Connor, J. Porter, and H.I. Smith. "Investigations of Materials for Ultra-Thin Window X-ray Detectors."

American Physical Society, Division of Plasma Physics, 33rd Annual Meeting, Tampa, Florida, November 4-8, 1991.

Bers, A., and A.K. Ram. "Signature of Absolute and Convective Instabilities with Application to Space Plasmas."

Chan, H.W., C. Chen, and R.C. Davidson. "Numerical Study of Relativistic Multiresonator Magnetron."

Chow, C.C., A. Bers, and A.K. Ram. "Spatio-temporal Chaos in the Three Wave Interaction."

Conde, M.E., and G. Bekefi. "Experimental Study of a 33.3 GHz Free Electron Laser Amplifier with a Reversed Axial Guide Magnetic Field."

Nassi, M., B. Coppi, and L. Sugiyama. "Ignitor Fiducial Discharge."

Ram, A.K., A. Bers, V. Fuchs, and M. Shoucri. "Current Drive by Fast Alfvén Waves and in Combination with Lower Hybrid Waves."

Shvets, G., J. Wurtele, W. Moli, and A. Sessler. "Theoretical Analysis of Frequency Shifts by Ionization Fronts."

Sugiyama, L., and B. Coppi. "Near Term Experiments on Advanced Fusion."

Wurtele, J., and G. Shvets. "Theory of a Free Electron Laser Operating with a Reversed Axial Magnetic Field."

American Physical Society, March Meeting, Cincinnati, Ohio, March 18-22, 1991.

Alerhand, O.L. "Finite-Temperature Equilibrium Properties of Steps on Si(100) Surfaces."

Berker, A.N. "Quenched Fluctuation-Induced Second-Order Phase Transitions."

Hoston, W., and A.N. Berker. "New Multicritical Phase Diagrams from the Blume-Emery-Griffiths Model with Repulsive Biquadratic Interactions."

Meade, R.D., O.L. Alerhand, and M.L. Roukes. "Classical Buttiker Model of Ballistic Transport in Mesoscopic Junctions."

Melngailis, J. "Focused Ion Beam Patterning."

Netz, R.R., and A.N. Berker. "Monte Carlo Mean-Field Theory and Frustrated Systems in Two and Three Dimensions."

Rappe, A.M., and J.D. Joannopoulos. "Convergent and Transferable Pseudopotential for Ab-Initio LDA Calculations."

Rittenhouse, G., K. Early, and J.M. Graybeal. "A Novel Structure for a Three-Terminal Superconducting Resonant Tunneling Device."

Zhao, Y., D.C. Tsui, S.J. Allen, K. Ismail, H.I. Smith, and D.A. Antoniadis. "Spectroscopy of 2-Deg in a Grid Gate Patterned Heterostructure."

American Physical Society, Spring Meeting, Washington, D.C., April 22-25, 1991.

Chang, P., S. Paine, R. Lutwak, T. Ducas, and D. Kleppner. "Millimeter Wave Measurement of the Rydberg Constant."

Iu, C., M. Courtney, T. Catunda, H. Jiao, and D. Kleppner. "Observation of the Stark Effect in a One-dimensional Hydrogen-like Atom."

Kleppner, D. "'Quantum Chaos': An Experimental View."

Pritchard, D.E. "The Physics of Atom-Molecule Collisions: Regularities, Scaling and Dynamics."

Wong, N.C., and D. Lee. "Experimental Demonstration of a Tunable Optical Frequency Divider."

American Physical Society, Interdisciplinary Laser Science/LSTG Meeting, Monterey, California, September 23-27, 1991.

Ketterle, W., A. Martin, M.A. Joffe, and D.E. Pritchard. "Slowing Atoms with Diffuse Laser Light."

American Vacuum Society Meeting, Seattle, Washington, November 1991.

Kolodziejski, L.A. "Chemical Beam Epitaxy of II-VI Semiconductors" (invited paper).

Applied Computational Electromagnetics Society Conference, Monterey, California, March 19-22, 1991.

Li, K., M.A. Tassoudji, R.T. Shin, and J.A. Kong. "Simulation of Electromagnetic Phenomena Using a Finite Difference-Time Domain Technique."

Armed Forces Communication and Electronics Association, Eatontown, New Jersey, May 16, 1991.

Lim, J.S. "Advanced Television Systems."

Association for Research in Otolaryngology, 15th Midwinter Meeting, St. Petersburg Beach, Florida, February 2-6, 1991.

Donahue, K.M., J.J. Rosowski, and W.T. Peake. "Can the Motion of the Human Malleus be Described as Pure Rotation?"

Guinan, J.J. "Inhibition of Stimulus Frequency Emissions by Medial Olivocochlear Efferent Neurons in Cats."

Merchant, S.N., M.E. Ravicz, and J.J. Rosowski. "The Acoustic Input Impedance of the Stapes and Cochlea in Human Temporal Bones."

Peake, W.T., J.J. Rosowski, and T.J. Lynch III. "Acoustic Coupling to Cochlear Windows."

Association for Research in Vision and Ophthalmology, Annual Meeting, Sarasota, Florida, April 28 - May 3, 1991.

Huang, D., W.G. Stinson, J.S. Schuman, C.P. Lin, C.A. Puliatito, and J.G. Fujimoto. "High Resolution Measurement of Retinal Thickness Using Optical Coherence Reflectometry."

AT&T Bell Laboratories, Holmdel, New Jersey, April 7-8, 1991.

Melngailis, J. "Focused Ion Beam Microfabrication."

Conference on Atmospheric Transmission Models, Annual Review, Phillips Laboratory, Hanscom Air Force Base, Massachusetts, June 12, 1991.

Rosenkranz, P.W. "Overview of Line Coupling in the 5 mm Band of Oxygen."

Conference on Lasers and Electro-Optics/Quantum Electronics Laser Science, Baltimore, Maryland, May 12-17, 1991.

Cheng, T.K., H.J. Zeiger, A.S. Kazeroonian, E.P. Ippen, G. Dresselhaus, and M.S. Dresselhaus.

"Time-Resolved Coherent Phonon Study of the Insulator-Metal Phase Transition in Ti_2O_3."

Gabetta, G., D. Huang, J. Jacobson, M. Ramaswamy, H.A. Haus, E.P. Ippen, and J.G. Fujimoto. "Femtosecond Pulse Generation in $Ti:Al_2O_3$ Using Nonlinear Intracavity Elements."

Hultgren, C.T., and E.P. Ippen. "Ultrafast Refractive Index Changes in AlGaAs Diode Lasers."

Fujimoto, J.G. "Femtosecond Lasers and Ultrafast Measurement Techniques."

Wong, N.C. "Squeezed Amplification in a Grain-Saturated Parametric Amplifier."

Conference on Neural Networks for Computing, Snowbird, Utah, April 2-5, 1991.

Wyatt, J.L. "The MIT Vision Chip Project: Analog VLSI Systems for Real-Time Image Acquisition and Early Vision Processing" (poster session).

Design Automation Conference, San Francisco, California, June 17-July 2, 1991.

Devadas, S., K. Keutzer, and S. Malik. "A Synthesis-Based Test Generation and Compaction Algorithm for Multifaults."

McIlrath, M. "Semiconductor Process Representation (SPR) Server Prototyping."

McIlrath, M. "Mini-SPR Prototype Programming Interface."

Device Research Conference, Boulder, Colorado, June 1991.

Eugster, C.C., J.A. del Alamo, and M.J. Rooks. "Planar Field-Effect Coupled Quantum Wires."

Electronic Properties of 2-D Systems Conference, Ninth, Nara, Japan, July 8-12, 1991.

Kumar, A. "Self-Consistent Calculations on Confined Electrons in Three-Dimensional Geometries."

Enrico Fermi International School of Physics, Course CSVIII, Milan, Italy, July 1991.

Prentiss, M.G., N. Bigelow, M.S. Shahriar, P. Hemmer, K. Berggren, J. Mervis, and S. Ezekiel. "Laser Manipulation of Atoms and Ions."

Five Joint Magnetism and Magnetic Materials - Intermag Conference, Pittsburgh, Pennsylvania, June 18-21, 1991.

Berker, A.N. "Absence of Temperature-Driven First-Order Phase Transitions in Systems with Random Bonds."

Hoston, W., and A.N. Berker. "Dimensionality Effects on the Multicritical Phase Diagrams of the Blume-Emery-Griffiths Model with Repulsive Biquadratic Coupling: Mean-Field and Renormalization-Group Studies."

Hoston, W., and A.N. Berker. "New Multicritical Phase Diagrams from the Blume-Emery-Griffiths Model with Repulsive Biquadratic Interactions."

Netz, R.R., and A.N. Berker. "Hard-Spin Mean-Field Theory: Formulation for Ising, XY, and Other Models."

Netz, R.R., and A.N. Berker. "Monte Carlo Mean-Field Theory and Frustrated Systems in Two and Three Dimensions."

Gordon Conference on Atomic Physics, Wolfeboro, New Hampshire, July 1-5, 1991.

Ketterle, W., and D.E. Pritchard. "Trapping Neutral Particles in Static Fields" (poster session).

Ketterle, W., M. Joffe, A. Martin, C. Freeman, and D.E. Pritchard. "Slowing Atoms in a Cavity with Diffuse Laser Light" (poster session).

Gordon Conference on Nonlinear Optics and Lasers, New London, New Hampshire, July 22-26, 1991.

Fujimoto, J.G. "Femtosecond Pulse Generation with APM."

IEEE Acoustics, Speech and Signal Processing Workshop on Applications of Signal Processing to Audio and Acoustics, Mohonk Mountain House, New Paltz, New York, October 20-23, 1991.

Delgutte, B. "Fundamental Issues in Auditory Modeling."

Greenberg, J.E., and P.M. Zurek. "Adaptive Beamformer Performance in Reverberation."

IEEE Computer Society Conference on Computer Vision and Pattern Recognition, Lahaina, Maui, Hawaii, June 3-6, 1991.

Picard, R.W., I.M. Elfadel, and A.P. Pentland. "Markov/Gibbs Texture Modeling: Aura Matrices and Temperature Effects."

IEEE International Conference on Plasma Science, Williamsburg, Virginia, June 3-5, 1991.

Sugiyama, Linda E. "Time Dependent Model for D-^{3}He Fusion Ignition and Burning in a Tokamak."

IEEE International Conference on Robotics and Automation, Sacramento, California, April 1991.

Wyatt Jr., J.L., D.L. Standley, and W. Yang. "The MIT Vision Chip Project: Analog VLSI Systems for Fast Image Acquisition and Early Vision Processing."

IEEE International Symposium on Electromagnetic Compatability, Cherry Hill, New Jersey, August 12-16, 1991.

Lee, C.F., K. Li, S.Y. Poh, R.T. Shin, and J.A. Kong. "Electromagnetic Radiation from a VLSI Package and Heatsink Configuration."

IEEE Microwave Theory and Techniques, Boston, Massachusetts, June 13-14, 1991.

Li, K., M.A. Tassoudji, R.T. Shin, and J.A. Kong. "Simulation of Electromagnetic Phenomena Using a Finite Difference-Time Domain Technique."

IEEE Particle Accelerator Conference, San Francisco, California, May 6-9, 1991.

Conde, M.E., G. Bekefi, and J.S. Wurtele. "A 33 GHz Free Electron Laser Test-Stand for a High Gradient Accelerating Structure."

Integrated Photonics Research Conference, Monterey, California, April 9-11, 1991.

Fujimoto, J.G., and H.A. Haus. "Femtosecond Time Domain Diagnostics of Nonlinear and Linear Waveguide Properties."

Lau, S.D., J.P. Donnelly, C.A. Wang, R.B. Goodman, and R.H. Rediker. "Optical Wavefront Phase Tilt Measurement and Correction Using AlGaAs Integrated Guided-Wave Components."

International A.D. Sakharov Conference on Physics, First, the Lebedev Physical Institute of the USSR Academy of Sciences, Moscow, USSR, May 27-31, 1991.

Coppi, B. "High Energy Plasmas in the Laboratory and in Astrophysics."

International Association for Mathematics and Computers in Simulation World Congress on Computation and Applied Mathematics, Trinity College, Dublin, Ireland, July 22-26, 1991.

Seidel, M.N., and J.L. Wyatt, Jr. "Settling-Time Bounds for Switched-Capacitor Networks."

International Conference on Acoustics, Speech and Signal Processing, 1991, Toronto, Ontario, Canada, May 14-17, 1991.

Cheung, S., and J.S. Lim. "Combined Multi-Resolution (Wideband/Narrowband) Spectrogram."

Preisig, J.C. "A Robust Adaptive Matched Field Processor Based Upon a Minmax Criterion."

Wornell, G.W. "Communication Over Fractal Channels."

International Conference on Computer-Aided Design, Santa Clara, California, November 10-14, 1991.

Lumsdaine, A., M. Reichelt, and J. White. "Conjugate Direction Waveform Methods for Transient Two-Dimensional Simulation of MOS Devices."

Silveira, L.M., J. White, and S. Leeb. "A Modified Envelope-Following Approach to Clocked Analog Circuit Simulation."

Van Aelten, F., J. Allen, and S. Devadas. "Verification of Relations between Synchronous Machines."

International Conference on Coherent and Nonlinear Optics, 14th, Leningrad, USSR, September 24-27, 1991.

Fujimoto, J.G. "Femtosecond Pulse Generation with Additive Pulse Modelocking in Solid State Lasers."

International Conference on Research Trends in Chaotic Dynamics and Transport in Fluids and Plasmas, LaJolla, California, February 18-20, 1991.

Chow, C.C., A.K. Ram, and A. Bers. "Spatio-temporal Chaos in the Nonlinear Three Wave Interaction."

International Electron Devices Meeting, Washington, DC, December 9-11, 1991.

Rahmat, K., J. White, and D.A. Antoniadis. "Computation of Drain and Substrate Currents in Ultra-Short-Channel nMOSFET's Using the Hydrodynamic Model."

International Free Electron Laser Conference, 13th, Santa Fe, New Mexico, August 25-30, 1991.

Conde, M.E., G. Bekefi, and J.S. Wurtele. "A 33 GHz Reversed Field Free Electron Laser."

Jerby, E., E. Agmon, B. Hadas, and M. Bensal. "Traveling Waves Free Electron Laser (TWFEL) Experiment."

Jerby, E., G. Bekefi, and T. Hara. "Macropulse Formation in a Free Electron Laser Oscillator."

International Geoscience and Remote Sensing Symposium, (IGARSS '91), Helsinki University of Technology, Espoo, Finland, June 3-6, 1991.

Kwok, R., Y. Hara, R.G. Atkins, S.H. Yueh, R.T. Shin, and J.A. Kong. "Application of Neural Networks to Sea Ice Classification Using Polarimetric Sar Images."

Le Toan, T., S.V. Nghiem, J.A. Kong, and H.C. Han. "Application of Random Medium Model to Remote Sensing of Vegetation."

International MicroProcess Conference, Kanazawa, Japan, July 15-18, 1991.

Schattenburg, M.L., and H.I. Smith. "X-ray Nanolithography—the Clearest Path to 0.1 and sub-0.15m ULSI."

International Microwave Landing System Progress Forum, Amsterdam, the Netherlands, June 25-26, 1991.

Yang, Y-C.E. "ILS/MLS Frequency Management Assessment."

International Radio Science Union North American Radio Science Meeting, Ottawa, Ontario, Canada, June 24-28, 1991.

Bonanni, P.G., and D.H. Staelin. "Detection and Measurement of Atmospheric Wave Structure Using a Scanning 118-GHz Spectrometer."

International Sherwood Fusion Theory Conference, Seattle, Washington, April 22-24, 1991.

Kupfer, K., A. Bers, and A.K. Ram. "Fast Electron Transport in Current Drive."

Sugiyama, L., B. Coppi, and M. Nassi. "Physics Basis for Compact Ignition Experiments."

International Symposium on Electron, Ion, and Photon Beams, 35th, Seattle, Washington, May 28-31, 1991.

Moel, A., W. Chu, K. Early, Y-C. Ku, E.E. Moon, F. Tsai, H.I. Smith, M.L. Schattenburg, C.D. Fung, F.W. Griffith, and L.E. Haas. "Fabrication and Characterization of High-Flatness Mesa-Etched Silicon Nitride X-ray Masks."

Schattenburg, M.L., K. Li, R.T. Shin, J.A. Kong, and H.I. Smith. "Electromagnetic Calculation of Soft X-ray Diffraction from Nanometer-Scale Gold Structures."

International Symposium on Nanostructures and Mesoscopic Systems, Santa Fe, New Mexico, May 1991.

Altshuler, B.L. "Thermodynamics of Mesoscopic Systems."

International Symposium on Ultrafast Processes in Spectroscopy, Seventh, Bayreuth, Germany, October 7-10, 1991.

Gabetta, G., D. Huang, J. Jacobson, M. Ramaswamy, H.A. Haus, E.P. Ippen, and J.G. Fujimoto "Femtosecond Pulse Generation in Ti:Al_2O_3 Using Nonlinear Intracavity Modulators."

International Workshop on Logic Synthesis, Research Triangle Park, North Carolina, May 7-10, 1991.

Ghosh, A, and S. Devadas. "Implicit Depth-First State Traversal of Sequential Machines."

Van Aelten, F., J. Allen, and S. Devadas. "Verification of Relations Between Synchronous Machines."

Materials Research Society Meeting, Spring, Anaheim, California, April 1991.

Karam, N.H., V. Haven, K. Ismail, F. Legoues, J. Carter, and H.I. Smith. "A New Approach for Low Defect Density GaAs on Patterned Si Substrates by MOCVD."

Materials Research Society Meeting, Boston, Massachusetts, December 1991.

Kunz, R., D.J. Ehrlich, J. Melngailis, and M.W. Horn. "Selective Area Growth of Metal Oxide Films Induced by Patterned Excimer Laser Surface Photolysis."

Microcircuit Engineering 91 International Conference on Microlithography, Rome, Italy, September 17-19, 1991.

Chu, W., S.A. Rishton, M.L. Schattenburg, D.P. Kern, and H.I. Smith. "Fabrication of 50 nm Line-and-Space X-ray Masks in Thick Au Using a 50 keV Electron Beam System."

Chu, W., M.L. Schattenburg, and H.I. Smith. "Low-Stress Gold Electroplating for X-ray Masks."

Early, K., M.L. Schattenburg, D.B. Olster, M.I. Shepard, and H.I. Smith. "Diffraction in X-ray Proximity Printing: Comparing Theory and Experiment for Gratings, Lines, and Spaces."

Microelectronics and Computer Technology Corporation Workshop on Parallel Computing, Dallas, Texas, February 20-21, 1991.

Lumsdaine, A., M. Reichelt, and J. White. "Parallel Circuit Simulation."

Microwave Landing System User Forum, Alaska Region, Anchorage, Alaska, September 20, 1991.

Yang, Y-C. "Project Summary: Instrument Landing System/Microwave Landing System Frequency Management Assessment."

NaseCode VII, Snowbird, Colorado, April 5-11, 1991.

Odeh, F., and J. White. "Multirate A-stability."

National Association of Broadcasters Meeting, Las Vegas, Nevada, April 15-18, 1991.

Lim, J.S. "Progress on HDTV Research at MIT."

National Center for Integrated Photonics Workshop on Phase Array Radar, Arrowhead, California, November 11-12, 1991.

Haus, H.A. "Proposed Approach to the Phased Array Radar Demonstration Project."

Hultgren, C.T., D.J. Dougherty, and E.P. Ippen. "Optical Nonlinearities in GaAs Lasers and Amplifiers."

NATO Advanced Study Institute on Liquid Crystals, Erice, Italy, May 2-12, 1991.

Berker, A.N. "Microscopic Theory of Polar Liquid Crystals and Multiply Reentrant Phase Diagrams."

Netz, R.R., and A.N. Berker. "The Mean-Field Theory for Frustration, Layered Magnets, and Reentrant Liquid Crystals."

NOAA Workshop on Long-Term Upper Stratospheric and Mesospheric Temperature Measurements and Their Importance of Global Change, University of Maryland, June 25, 1991.

Staelin, D.H., and P.W. Rosenkranz. "The Advanced NOAA Instrument Scheduled for the European Platform."

Ocean Acoustics Signal Processing Workshop, Office of Naval Research, Washington, DC, September 6, 1991.

Baggeroer, A.B. "Environmentally Robust Matched Field Processing."

Office of Naval Research/Accelerated Research Initiative Workshop on the Electromagnetic Properties of Sea Ice, University of Washington, Seattle, Washington, December 5-6, 1991.

Kong, J.A. "Electromagnetic Modelling: Inverse."

Optical Society of America, Annual Meeting, San Jose, California, November 3-8, 1991.

Corcoran, C.J., R.H. Rediker, and K. Rauschenbach. "Effects on the Operation of an External-Cavity Laser of Phase Differences Between Multiple Inputs into the Cavity."

Joneckis, L.G., and J.H. Shapiro. "Classical and Quantum Noise Transformations Generated by a Kerr Nonlinearity."

Mecozzi, A., H.A. Haus, and Y. Lai. "Noise of Mode-Locked Lasers."

Moores, J.D., and H.A. Haus. "Intrapulse-Raman-Scattering Soliton Timing Jitter in Ultralong Distance Transmission."

Shapiro, J.H. "Phase-Conjugate Quantum Communication at Zero Error Probability with Finite Average Photon Number."

Wong, N.C. "Precise Optical Frequency Comb Generator Based on Optical Parametric Oscillators."

Wong, N.C. "Gravitational Wave Detection Via an Optical Parametric Oscillator."

Wong, N.C., and D. Lee. "A Tunable Optical Parametric Oscillator for Precision Measurements."

Wong, N.C., K.X. Sun, and J.H. Shapiro. "Squeezed Amplification in a Gain-Saturated Parametric Amplifier."

Progress in Electromagnetics Research Symposium, Cambridge, Massachusetts, July 1-5, 1991.

Lee, H., S.M. Ali, and J.A. Kong. "Hybrid-Mode Analysis of High-Tc Superconducting Planar Transmission Lines."

Rosenkranz, P.W. "Rough-Sea Microwave Emissivities Measured with the SSM/I."

Schattenburg, M.L., K. Li, R.T. Shin, J.A. Kong, and H.I. Smith. "Calculation of Soft X-ray Diffraction from Nanometer-Scale Gold

Structures Using a Finite-Element Time-Domain Method."

Physics Colloquium, Stony Brook, New York, October 15, 1991.

Pritchard, D.E. "Atom Optics and Atom Interferometers."

Santa Cruz Conference on Advanced Research in VLSI, University of California, Santa Cruz, California, March 23-31, 1991.

Ashar, P., S. Devadas, and K. Keutzer. "Testability Properties of Multilevel Logic Networks Derived from Binary Decision Diagrams."

Semiconductor Research Corporation (SRC) Computer Integrated Manufacturing of Integrated Circuits (CIM-IC) Workshop, Raleigh, North Carolina, August 21-23, 1991.

McIlrath, M. "A General Semiconductor Process Modeling Framework."

Society for Neuroscience, New Orleans, Louisiana, November 10-15, 1991.

Srinivasan, M.A., and K. Dandekar. "Role of Mechanics in Cutaneous Mechanoreceptor Response."

Society of Information Display, Anaheim, California, May 6-8, 1991.

Lim, J.S. "ATVA-Progressive System."

Society of Motion Picture and Television Engineers, 25th Annual Conference, Detroit, Michigan, February 1-2, 1991.

Baylon, D.M., and J.S. Lim. "Video Compression and Noise Reduction Using Transform/Subband Coding and Adaptive Amplitude Modulation."

SPIE International Symposium on High Power Lasers, Los Angeles, California, January 20-25, 1991.

Chen, S-C., G. Bekefi, and R. Temkin. "Phase Control of a Long-Pulse Relativistic Magnetron Through Injection Locking."

Fujimoto, J.G., P.A. Schulz, and T.Y. Fan. "Femtosecond Pulse Generation in Solid State Lasers."

SPIE International Symposium on Optical Applied Science and Engineering, San Diego, California, July 20-26, 1991.

Basu, S., M. Muendel, J. Goodberlet, S. Kaushik, and P.L. Hagelstein. "A Search for Gain at 191Å."

Basu, S., P.L. Hagelstein, A. Morganthaler, S. Kaushik, M. Muendel, and J. Goodberlet. "Transient X-ray Laser Schemes at 1μ and at 2μ."

Braud, J.P. "Whispering-Gallery Mirrors for Short-Wavelength Laser Cavities: Shapes and Tolerances."

Braud, J.P. "Polarizing Optics for the Soft X-ray Regime: Whispering-Gallery Mirrors and Multilayer Beamsplitters."

Elfadel, I.M., and A.L. Yuille. "Mean-Field Theory for Grayscale Texture Synthesis Using Markov Random Fields."

Markert, T.H., J.M. Bauer, C.R. Canizares, T. Isobe, S. Nenonen, J. O'Connor, M.L. Schattenburg, K.A. Flanagan, and M.V. Zombeck. "Proportional Counter Windows for the Bragg Crystal Spectrometer on AXAF."

SPIE International Symposium on Optical Engineering and Photonics in Aerospace Sensing, Orlando, Florida, April 1991.

Green, T.J., Jr., J.H. Shapiro, and M.M. Menon. "Target Detection *Performance* Using 3-D Laser Radar Images."

Hakkarainen, J. M., J.J. Little, H-S. Lee, and J.L. Wyatt, Jr. "Interaction of Algorithm and Implementation for Analog VLSI Stereo Vision."

Standley, D., and B.K.P. Horn. "Analog CMOS IC for Object Position and Orientation."

Yang, W. "Analog CCD Processors for Image Filtering."

SPIE Microlithography Symposium, San Jose, California, March 3-8, 1991.

Melngailis, J. "Focused Ion Beam Induced Deposition—A Review."

Statistical Mechanics Meeting, 65th, New Brunswick, New Jersey, May 15-17, 1991.

Hoston, W., and A.N. Berker. "Bicritical and Tetracritical Phase Diagrams of the BEG Model: Dimensionality Effects."

Netz, R.R., and A.N. Berker. "Microscopic Theory of Smectic A and C Phases of Frustrated Liquid Crystals."

Symposium on Applications of Wavelets to Signal Processing, Wright-Patterson Air Force Base, Ohio, March 20-22, 1991.

Wornell, G.W., and A.V. Oppenheim. "Representation, Synthesis, and Processing of Self-Similar Signals."

Symposium on Current Phonetic Research Paradigms: Implications for Speech Motor Control, Stockholm, Sweden, August 12-16, 1991.

Perkell, J.S., M.A. Svirsky, M.L. Matthies, and M.I. Jordan. "Trading Relations Between Tongue-Body Raising and Lip Rounding in Production of the Vowel /u/."

Technology Computer Aided Design/Semiconductor Process Representation Working Group, Palo Alto, California, August 10, 1991.

McIlrath, M. "Report on SPR Prototyping."

McIlrath, M. "TCAD Framework Architectural Issues."

TELECOM - Advanced Television Workshop, Paris, France, May 24-29, 1991.

Lim, J.S. "Research at the MIT Advanced Television Research Program."

Ultrashort Pulse Workshop, Brooks Air Force Base, San Antonio, Texas, December 17-20, 1991.

Izatt, J.A., and J.G. Fujimoto. "Mechanisms and Diagnostics of Ultrashort Pulse Ocular Effects."

VLSI Test Symposium, Atlantic City, New Jersey, April 16, 1991.

Devadas, S., K. Keutzer, and A. Ghosh. "Recent Progress in Synthesis for Testability."

Wisconsin Sematech Center of Excellence Review Committee Meeting, Madison, Wisconsin, October 2-3, 1991.

Melngailis, J. "Focused Ion Beam Lithography for X-ray Mask Making."

Workshop on Compound Semiconductors Materials and Devices (WOCSEMMAD), Ft. Lauderdale, Florida, February 18-20, 1991.

Bahl, S.R., and J.A. del Alamo. "InAlAs/n^+ – InGaAs HFETs: Impact of Dislocations and Channel Quantization."

Workshop on Physics with Penning Traps, Lertorpet, Sweden, June 28-July 2, 1991.

Boyce, K. "Sub-PPB Mass Measurements on Single Ions."

Workshop on Psychophysics of Speech Perception - II, Utrecht, The Netherlands, July 1-5, 1991.

Uchanski, R.M., K.M. Millier, C.M. Reed, and L.D. Braida. "Effects of Token Variability on Resolution for Vowel Sounds."

Workshop on Squeezed States and Uncertainty Relations, College Park, Maryland, March 27-30, 1991.

Bergman, K., and H.A. Haus. "Squeezed Pulsed Light from a Fiber Ring Reflector."

Shapiro, J.H. "Going Through a Quantum Phase."

Shepard, S.R. "On the Measurement of Time for the Quantum Harmonic Oscillator."

A.1.2 Papers To Be Presented

American Physical Society Meeting, Indianapolis, Indiana, March 16-20, 1992.

Aalberts, D.P., and A.N. Berker. "Hard-Spin Mean-Field Theory: Variational Free Energy and First-Order Phase Transitions."

Berker, A.N., and R.R. Netz. "Smectic C Order, In-Plane Domains, and Nematic Reentrance in a Frustrated Microscopic Model of Liquid Crystals."

Netz, R.R. "Symmetry-Breaking Fields in Frustrated Ising Systems on Square and Cubic Lattices."

Netz, R.R. "Multiple Reentrance and New Phases from the Blume-Emery-Griffiths Model in Three Dimensions: Monte Carlo Renormalization-Group Theory."

IEEE International Conference on Acoustics, Speech, and Signal Processing, San Francisco, California, March 23-26, 1992.

Beckmann, P.E., and B.R. Musicus. "A Group-Theoretic Framework for Fault-Tolerant Computation."

Isabelle, S.H., A.V. Oppenheim, and G.W. Wornell. "Effects of Convolution on Chaotic Signals."

Jachner, J., and H. Lee. "Cramer Rao Bounds on Direction Estimates for Closely Spaced Emitters in Multi-Dimensional Applications."

Myers, C., A. Singer, F. Shin, and E. Church. "Modeling Chaotic Systems with Hidden Markov Models."

Oppenheim, A.V., E. Weinstein, K.C. Zangi, M. Feder, and D. Gauger. "Single Sensor Active Noise Cancellation Based on the EM Algorithm."

Oppenheim, A.V., G.W. Wornell, S.H. Isabelle, and K.M. Cuomo. "Signal Processing in the Context of Chaotic Signals."

Preisig, J.C. "Optimal Minmax Estimation and the Development of Minmax Estimation Error Bounds."

Singer, A.C., G.W. Wornell, and A.V. Oppenheim. "Codebook Prediction: A Nonlinear Signal Modeling Paradigm."

IEEE International Conference on Thermodynamics and Statistical Mechanics, Berlin, Germany, August 2-8, 1992.

Berker, A.N. "Critical Behavior Induced by Quenched Disorder."

Netz, R.R., and A.N. Berker. "Smectic C/A_2 Order, Domains, Reentrance in a Microscopic Model of Liquid Crystals."

International Liquid Crystal Conference, 14th, Pisa, Italy, June 21-26, 1992.

Netz, R.R., and A.N. Berker. "Smectic C Order, Nematic Reentrance, Domains, and Smectic A_1 - Smectic A_2 Transitions in a Frustrated Microscopic Model of Liquid Crystals."

Specialist Meeting on Microwave Radiometry and Remote Sensing Applications, Boulder, Colorado, January 14-16, 1992.

Rosenkranz, P.W. "Emission and Absorption of Microwaves by Atmospheric Oxygen and Water Vapor."

Symposium on Frequency Control, 46th, Hershey, Pennsylvania, May 27-29, 1992.

Wong, N.C., and D. Lee. "Optical Parametric Division" (invited talk).

A.1.3 Published Meeting Papers

Alwan, A. "Modelling Speech Perception in Noise: A Case Study of the Place of Articulation Feature." *Proceedings of the 12th International Congress of Phonetic Sciences,* 2:78-81, Aix en Provence, France, August 19-24, 1991.

Annaswamy, A.M., and M.A. Srinivasan. "Adaptive Control for Grasping and Manipulation of Compliant Objects with Compliant Fingerpads." *Proceedings of the American Control Conference,* Boston, Massachusetts, 1991.

Ashar, P., A. Ghosh, and S. Devadas. "Boolean Satisfiability and Equivalence Checking Using General Binary Decision Diagrams." *Proceedings of the International Conference on Computer Design: VLSI in Computers and Processors,* Boston, Massachusetts, October 1991.

Ashar, P., S. Devadas, and K. Keutzer. "Resynthesis of Combinational Logic Circuits for Robust Gate-Delay-Fault Testability." *Proceedings of the International Test Conference,* Nashville, Tennessee, October 1991.

Bahl, S.R., and J.A. del Alamo. "Elimination of Mesa-Sidewall Gate Leakage in InAlAs/InGaAs HFETs by Selective Sidewall Recessing." *Proceedings of the 18th International Symposium on Gallium Arsenide and Related Compounds,* Seattle, Washington, September 9-12, 1991.

Bers, A., and A.K. Ram. "Lower-Hybrid and Fast Alfvén Wave Current Drive—Status of Theory." *Proceedings of the I.A.E.A Technical Meeting on Fast Wave Current Drive in Reactor Scale Tokamaks (Synergy and Complementarity with LHCD and ECRH),* Arles, France, September 23-25, 1991.

Bers, A., V. Fuchs, and C.C. Chow. "Maximizing Absorption in Ion-Cyclotron Heating of Tokamak Plasmas." *Proceedings of the 18th European Physical Society Conference on Controlled Fusion and Plasma Physics,* Berlin, Germany, June 3-7, 1991.

Blum, K.I., D.Y. Noh, A. Mak, K.W. Evans-Lutterodt, J.D. Brock, G.A. Held, and R.J. Birgeneau. "Structure and Phase Transitions of Ge(111) and Si(111) Surfaces at High Temperature." *Proceedings of the International Conference on Surface Scattering,* Bad Honnef, Germany, June 1991.

Cheng, K-T., S. Devadas, and K. Keutzer. "A Partial-Scan Approach to Robust Delay-Fault Test Generation for Sequential Circuits." *Proceedings of the International Test Conference,* Nashville, Tennessee, October 1991.

Chow, C.C., A. Bers, and A.K. Ram. "Spatio-temporal Chaos in the Nonlinear Three Wave Interaction." *Proceedings of the III Potsdam-V Kiev International Workshop on Nonlinear Processes in Physics,* Potsdam, New York, August 1-11, 1991.

Chow, C.C., A. Bers, and A.K. Ram. "Spatio-Temporal Chaos in the Saturation of an Unstable Wavepacket." *Proceedings of the International Sherwood Fusion Conference,* Paper 2D08, Seattle, Washington, April 22-24, 1991.

Chu, A., L. Chu, W. Macropoulos, K. Khair, R. Patel, M. Cordaro, H.J. Lezec, J. Melngailis, and L.J. Mahoney. "Performance and Applications of Novel Oscillators Utilizing Focused Ion Beam Implanted Gunn-Effect Devices." *Proceedings of the 1991 IEEE MTT-S International Microwave Symposium,* Digest 1179, Boston, Massachusetts, June 11-14, 1991.

Covell, M., and J. Richardson. "A New, Efficient Structure for the Short-Time Fourier Transform with an Application in Code-Division Sonar Imaging." *Proceedings of the International Conference on Acoustics, Speech, and Signal Processing,* ICASSP 91, Toronto, Canada, May 14-17, 1991.

Devadas, S., K. Keutzer, and A.S. Krishnakumar. "Design Verification and Reachability Analysis Using Algebraic Manipulation." *Proceedings of the International Conference on Computer Design: VLSI in Computers and Processors,* Boston, Massachusetts, October 1991.

Devadas, S., K. Keutzer, and S. Malik. "Delay Computation in Combinational Logic Circuits: Theory and Algorithms." *Proceedings of the International Conference on Computer-Aided Design,* Santa Clara, California, November 10-14, 1991.

Dron, L. "An Analog Model of Early Visual Processing: Contour and Boundary Detection in the Retina." *Proceedings of the SPIE Intelligent Robots and Computer Vision X,* Boston, Massachusetts, November 14-15, 1991.

Espy-Wilson, C.Y. "Consistency in /r/ Trajectories in American English." *Proceedings of the 12th International Congress of Phonetic Sciences,* 4:370-373, Aix en Provence, France, August 19-24, 1991.

Fleischman, J., S. Ayasli, R.T. Shin, N.C. Chu, H.A. Yueh, and S.V. Nghiem. "Covariance of Phase and Amplitude Fluctuations of Electromagnetic Waves Propagating Through a Random Medium." *Proceedings of the Progress in Electromagnetics Research Symposium,* p. 617, Boston, Massachusetts, July 1-5, 1991.

Floro, J.A., and C.V. Thompson. "Epitaxial Grain Growth and Orientation Metastability in Heteroepitaxial Thin Films." *Proceedings of the Materials Research Society Symposium,* 187:274, Boston, Massachusetts, December 1991.

Frost, H.J., C.V. Thompson, and D.T. Walton. "Abnormal Grain Growth in Thin Films Due to Anisotropy of Free-Surface Energies." *Proceedings of the First International Conference on Grain Growth in Polycrystalline Materials,* Rome, Italy, 1991. Forthcoming.

Han, H.C., J.A. Kong, S.V. Nghiem, and T. LeToan. "Analytical Solution of the Vector Radiative Transfer Equation with Rough Surface Boundary Condition." *Proceedings of the Progress in Electromagnetics Research Symposium,* p. 536, Boston, Massachusetts, July 1-5, 1991.

Hsu, C.C., S.H. Yueh, H.C. Han, R.T. Shin, and J.A. Kong. "Radiative Transfer Modeling of Vegetation Clusters." *Proceedings of the Progress in Electromagnetics Research Symposium,* p. 609, Boston, Massachusetts, July 1-5, 1991.

Kahn, H., and C.V. Thompson. "A Statistical Characterization of Electromigration-Induced Open Failures in 2-Level Metal Structures." *Proceedings of the Materials Research Society Symposium,* 225:15, Boston, Massachusetts, December 1991.

Keith, D.W., and D.E. Pritchard. "Atom Optics." *Proceedings of the NATO Advanced Study Institute on New Frontiers in Quantum Electrodynamics and Quantum Optics,* Istanbul, Turkey, August 14-26, 1989.

Kukula, J., and S. Devadas. "Finite State Machine Decomposition by Transition Pairing." *Proceedings of the International Conference on Computer-Aided Design,* Santa Clara, California, November 10-14, 1991.

Kupfer, K., A. Bers, and A.K. Ram. "Fast Electron Transport During Lower-Hybrid Current Drive." *Proceedings of the 18th European Physical Society Conference on Controlled Fusion and Plasma Physics,* Berlin, Germany, June 3-7, 1991.

Kupfer, K., A. Bers, and A.K. Ram. "Fast Electron Transport in Current Drive." *Proceedings of the International Sherwood Fusion Conference,* Paper 2B05, Seattle, Washington, April 22-24, 1991.

Lee, P.A. "Small Structures: A Laboratory for Studying Strongly Interacting Systems." *Proceedings of the Taniguchi Symposium on Mesoscopic Physics,* Shima, Japan, 1991.

Lee, H-S., and P. Yu. "CMOS Resistive Fuse Circuits." *Proceedings of the Symposium on VLSI Circuits,* pp. 109-110, Oiso, Japan, May 1991.

Li, K., M.A. Tassoudji, R.T. Shin, and J.A. Kong. "Simulation of Electromagnetic Phenomena Using a Finite Difference-Time Domain Technique." *Proceedings of the Seventh Annual Review of Progress in Applied Computational Electromagnetics,* pp. 38-55, Naval Postgraduate School, Monterey, California, March 18-22, 1991.

Liau, V.S., T.W. Stacey, S. Ali, and E. Schloemann. "Tunable Band-Stop Filter Based on Epitaxial Fe Film on GaAs." *Proceedings of the 1991 IEEE MTT-S International Microwave Symposium,* pp. 957-960, Boston, Massachusetts, June 11-14, 1991.

Ma, E., L.A. Clevenger, C.V. Thompson, and K.N. Tu. "Kinetic and Thermodynamic Aspects of Phase Evolution." *Proceedings of the Materials Research Society Symposium,* 187:83, Boston, Massachusetts, December 1991.

Ma, E., C.V. Thompson, and L.A. Clevenger. "A Calorimetric Study of the Kinetics of Al_3Ni Nucleation and Growth During Reactions in Al/Ni Thin Films." *Proceedings of the Materials Research Society Symposium,* 157:455, Boston, Massachusetts, December 1991.

Melngailis, J., P.G. Blauner, A.D. Dubner, J.S. Ro, T. Tao, and C.V. Thompson. "Focused Ion Beam Induced Deposition." *Proceedings of the Second International Symposium on Process Physics and Modeling in Semiconductor Technology,* 91-4:653, Montreal, Quebec, Canada, May 6-11, 1990

Melville, W.K., D.V. Arnold, E. Lamarre, J.A. Kong, R.H. Stewart, and W.C. Keller. "Direct Measurements of EM Bias at Ku and C Bands." *Proceedings of the Progress in Electromagnetics Research Symposium,* p. 168, Boston, Massachusetts, July 1-5, 1991.

Moldoveanu, M.C., and A.K. Jordan. "Theory of Non-Dispersive Electromagnetic Pulses: the Nonlinear Dirac Equation." *Proceedings of the Progress in Electromagnetics Research Symposium,* p. 676, Boston, Massachusetts, July 1-5, 1991.

Perkell, J.S. "Models, Theory and Data in Speech Production." *Proceedings of the 12th International Congress of Phonetic Sciences,* 1:182-191, Aix en Provence, France, August 19-24, 1991.

Preisig, James C. "A Robust Adaptive Matched Field Processor Based Upon a Minmax Criterion." *Proceedings of the International Conference on Acoustics, Speech, and Signal Processing,* ICASSP 91:1349-1352, Toronto, Canada, May 14-17, 1991.

Price, P.J., M. Ostendorf, and S. Shattuck-Hufnagel. "Disambiguating Sentences Using Prosody." *Proceedings of the 12th International Congress of Phonetic Sciences,* 2:418-421, Aix en Provence, France, August 19-24, 1991.

Ram, A.K., A. Bers, V. Fuchs, R.W. Harvey, and M.G. McCoy. "Current Drive by Lower Hybrid Waves in Combination with Fast Alvén Waves." *Proceedings of the International Sherwood Fusion Conference,* Sante Fe, New Mexico, April 6-8, 1992. Forthcoming.

Rappe, A., and J.D. Joannopoulos. "The Design of Convergent and Transferable Ab-Initio Pseudopotentials." *Proceedings of the NATO Advanced Study Institute,* Aussois, France, 1991.

Schattenburg, M.L., and H.I. Smith. "X-ray Nanolithography—the Clearest Path to 0.1 and sub-0.1 μm ULSI." *Proceedings of the 1991 International Symposium on MicroProcess Conference,* Kanazawa, Japan, July 15-18, 1991.

Schattenburg, M.L., K. Li, R.T. Shin, J.A. Kong, D.B. Olster, and H.I. Smith. "Electromagnetic Calculation of Soft X-ray Diffraction from 0.1 μm-Scale Gold Structures." *Proceedings of the 35th International Symposium on Electron, Ion, and Photon Beams,* Paper E84, Seattle, Washington, May 28-31, 1991.

Seidel, M.N., and J.L. Wyatt, Jr. "Settling-Time Bounds for Switched-Capacitor Networks." *Proceedings of the IMACS World Congress on Computation and Applied Mathematics,* pp. 1669-1670, Dublin, Ireland, July 1991.

Shattuck-Hufnagel, S. "Acoustic Correlates of Stress Shift." *Proceedings of the 12th International Congress of Phonetic Sciences,* 4:266-269, Aix en Provence, France, August 19-24, 1991.

Sheen, D.M., S.M. Ali, D.E. Oates, R.S. Withers, and J.A. Kong. "Current Distribution in Superconducting Strip Transmission Lines." *Proceedings of the 1991 IEEE MTT-S International Microwave Symposium,* pp. 161-164, Boston, Massachusetts, June 11-14, 1991.

Smith, H.I., and M.L. Schattenburg. "Proximity X-ray Nanolithography." *Proceedings of the Optical Society of America on Soft X-ray Projection Lithography,* 12:148-149, Monterey, California, April 10-12, 1991.

Standley, D., and B. Horn. "An Object Position and Orientation IC with Embedded Imager." *Proceedings of the IEEE International Solid State Circuits Conference,* pp. 38-38, San Francisco, California, February 13-15, 1991.

Stevens, K.N. "The Contribution of Speech Synthesis to Phonetics: Dennis Klatt's Legacy." *Proceedings of the 12th International Congress of Phonetic Sciences,* 1:28-37, Aix en Provence, France, August 19-24, 1991.

Tassoudji, M.A., C.C. Hsu, Y.E. Yang, R.T. Shin, J.A. Kong, and G. Markey. "Computer-Aided Spectrum Engineering Procedure for Instrument Landing System (ILS) and Microwave Landing System (MLS)." *Proceedings of the Progress in Electromagnetics Research Symposium,* p. 13, Boston, Massachusetts, July 1-5, 1991.

Thompson, C.V. "Experimental and Theoretical Aspects of Grain Growth in Thin Films." *Proceedings of the First International Conference on Grain Growth in Polycrystalline Materials,* Rome, Italy, 1991. Forthcoming.

Thompson, C.V., J.Y. Tsao, and D.J. Srolovitz. "Evolution of Thin Film and Surface Microstructure." *Proceedings of the Materials Research Society Symposium,* 202, Boston, Massachusetts, December 1991.

Thompson, C.V., L.A. Clevenger, R. DeAvillez, E. Ma, and H. Miura. "Kinetics and Thermodynamics of Amorphous Silicide Formation in Metal/Amorphous Multilayer Thin Films." *Proceedings of the Materials Research Society Symposium,* 187:61, Boston, Massachusetts, December 1991.

Van Aelten, F., J. Allen, and S. Devadas. "Verification of Relations Between Synchronous Machines." *Proceedings of the International Conference on Computer-Aided Design,* Santa Clara, California, November 10-14, 1991.

Walton, D.T., H.J. Frost, and C.V. Thompson. "Computer Simulation of Grain Growth in Thin-Film Interconnect Lines." *Proceedings of the Materials Research Society Symposium,* 225:219, Boston, Massachusetts, December 1991.

Walton, D.T., H.J. Frost, and C.V. Thompson. "Modeling of Grain Growth in Thin Film Strips." *Proceedings of the First International Conference on Grain Growth in Polycrystalline Materials,* Rome, Italy, 1991. Forthcoming.

Wilde, L.F., and C.B. Huang. "Acoustic Properties at Fricative-Vowel Boundaries in American English." *Proceedings of the 12th International Congress of Phonetic Sciences,* 5:398-401, Aix en Provence, France, August 19-24, 1991.

Wornell, G.W. "Communication Over Fractal Channels." *Proceedings of the International Conference on Acoustics, Speech, and Signal Processing,* ICASSP 91:1945-1948, Toronto, Canada, May 14-17, 1991.

Yang, Y.E., J.A. Kong, R.T. Shin, B.F. Burke, E.M. Geyer, R.P. Arnold, and E.A. Spitzer. "Spectrum Management for Precision Landing Systems: Instrument Landing Systems (ILS) and Microwave Landing System (MLS)." *Proceedings of the Progress in Electromagnetics Research Symposium,* p. 8, Boston, Massachusetts, July 1-5, 1991.

Yueh, H.A., J.A. Kong, and R.T. Shin. "External Calibration of Polarimetric Radars Using Point and Distributed Targets." *Proceedings of the Third Airborne Synthetic Aperture Radar (AIRSAR) Workshop,* Jet Propulsion Laboratory, Pasadena, California, May 23-24, 1991.

A.2 Journal Articles

A.2.1 Published Journal Articles

Acioli, L.H., M. Ulman, E.P. Ippen, J.G. Fujimoto, H. Kong, B.S. Chen, and M. Cronin-Golomb. "Femtosecond Temporal Encoding in Barium Titanate." *Opt. Lett.* 16(24): 1984-1986 (1991).

Alerhand, O.L., A.N. Berker, J.D. Joannopoulos, D. Vanderbilt, R.J. Hamers, and J.E. Demuth. "Finite-Temperature Phase Diagram of Vicinal Si(100) Surfaces: Alerhand et al. Reply." *Phys. Rev. Lett.* 66(7): 962 (1991).

Alerhand, O., J. Wang, J.D. Joannopoulos, E. Kaxiras, and R. Becker. "Adsorption of As on Stepped Si(100): Resolution of the Sublattice Dilemma." *Phys. Rev. Rapid Comm. B* 44: 6534 (1991).

Alerhand, O., J. Wang, J.D. Joannopoulos, and E. Kaxiras. "Growth of As Overlayers on Vicinal Si(100)." *J. Vac. Sci. Tech. B* 9: 2423 (1991).

Anderson, E.H., V. Boegli, M.L. Schattenburg, D.P. Kern, and H.I. Smith. "Metrology of Electron Beam Lithography Systems Using Holographically Produced Reference Samples." *J. Vac. Sci. Technol. B* 9: 3606-3611 (1991).

Bace, M.M., and J.S. Lim. "A Receiver-Compatible System for Channel Noise Reduction." *IEEE Trans. Circuit Syst. Video Tech.* 1(1): 125-135 (1991).

Bagnato, V., and D. Kleppner. "Bose-Einstein Condensation in Low-Dimensional Traps." *Phys. Rev. A* 44(11): 7439-7441 (1991).

Bagwell, P.F., and A. Kumar. "Evolution of the Quantized Ballistic Conductance with Increasing Disorder in Narrow Wire Arrays." *Bull. Am. Phys. Soc.* 36: 359 (1991).

Bahl, S.R., W.J. Azzam, and J.A. del Alamo. "Orientation Dependence of Mismatched $In_xAl_{1-x}As/In_{0.53}Ga_{0.47}As$ HFETs." *J. Crystal Growth* 111(1-4): 479-483 (1991).

Bahl, S.R., W.J. Azzam, and J.A. del Alamo. "Strained-Insulator $In_xAl_{1-x}As/n^+ - In_{0.53}Ga_{0.47}As$ Heterostructure Field-Effect Transistors." *IEEE Trans. Electron. Devices* 38(9): 1986-1992 (1991).

Basu, S. "Possibility of X-Ray Detection Using Quantum Wells." *IEEE J. Quantum Electron.* 27(9): 2116-2121 (1991).

Beckmann, P.E., and B.R. Musicus. "Fault-Tolerant Round-Robin A/D Converter System." *IEEE Trans. Circuits Syst.* 38(12): 1420-1429 (1991).

Bergman, K., and H.A. Haus. "Squeezing in Fibers with Optical Pulses." *Opt. Lett.* 16(9): 663-665 (1991).

Berker, A.N. "Absence of Temperature-Driven First-Order Phase Transitions in Systems with Random Bonds." *J. Appl. Phys.* 70(10): 5941-5945 (1991).

Bers, A., and A.K. Ram. "Signature of Absolute and Convective Instabilities with Application to Space Plasmas." *Bull. Am. Phys. Soc.* 36: 2462 (1991).

Besing, J.M., C.M. Reed, and K.W. Grant. "Tactual Presentation of Low-Bandwidth Envelope Signals: Benefits to Speechreading." *ASHA* 33: 212 (1991).

Bossi, D.E., W.D. Goodhue, L.M. Johnson, and R.H. Rediker. "Reduced-Confinement GaAlAs Tapered Waveguide Antennas for Enhanced Far-Field Beam Directionality." *IEEE J. Quantum Electron.* 27(3): 687-695 (1991).

Boyce, S.E., R.A. Krakow, and F. Bell-Berti. "Phonological Underspecification and Speech Motor Organisation." *Phonology* 8: 219-236 (1991).

Braida, L.D. "Crossmodal Integration in the Identification of Consonant Segments." *Quart. J. Exper. Psych.* 43A(3): 647-677 (1991).

Braud, J.P., and P.L. Hagelstein. "Whispering-Gallery Laser Resonators. Part I: Diffraction of Whispering-Gallery Modes." *IEEE J. Quantum Electron.* 27(4): 1069-1077 (1991).

Chan, C.H., S.H. Lou, L. Tsang, and J.A. Kong. "Electromagnetic Scattering of Waves by Random Rough Surface: a Finite-Difference Time-Domain Approach." *Microwave Opt. Tech. Lett.* 4(9): 355-359 (1991).

Chiu, T.H., T.Y. Kuo, and C.G. Fonstad. "Growth and Metalization of AlGaAs/GaAs Carbon-Doped HBT's Using Trimethylamine Alane by CBE." *IEEE Electron. Dev. Lett.* EDL-12: 287-289 (1991).

Chow, C.C., A. Bers, and A.K. Ram. "Spatio-temporal Chaos in the Three Wave Interaction." *Bull. Am. Phys. Soc.* 36: 2407 (1991).

Chu, W., H.I. Smith, and M.L. Schattenburg. "Replication of 50-nm-linewidth Device Patterns Using Proximity X-ray Lithography at Large Gaps." *Appl. Phys. Lett.* 59(13): 1641-1643 (1991).

Conde, M.E., and G. Bekefi. "Experimental Study of a 33.3-GHz Free-Electron-Laser Amplifier with a Reversed Axial Guide Magnetic Field." *Phys. Rev. Lett.* 67(22): 3082-3085 (1991).

Coppi, B, and F. Pegoraro. "Symmetries and Global Transport Equations." *Phys. Fluids B* 3(9): 2582-2590 (1991).

Corcoran, C.J., and R.H. Rediker. "Operation of Five Individual Diode Lasers as a Coherent Ensemble by Fiber Coupling into an External Cavity." *Appl. Phys. Lett.* 59(7): 759-761 (1991).

Devadas, S. "Optimizing Interacting Finite State Machines Using Sequential Don't Cares." *IEEE Trans. Comput.-Aided Des.* 10(12): 1473-1484 (1991).

Devadas, S., and A.R. Newton. "Corrections to 'Exact Algorithms for Output Encoding, State Assignment, and Four-Level Boolean Minimization'." *IEEE Trans. Comput.-Aided Des. Integrated Circuits Syst.* 10(11): 1469 (1991).

DiRienzo, A.C., G. Bekefi, C. Chen, and J.S. Wurtele. "Experimental and Theoretical Studies of a 35 GHz Cyclotron Autoresonance Maser Amplifier." *Phys. Fluids B* 3(7): 1755-1765 (1991).

Dubner, A.D., A. Wagner, J. Melngailis, and C.V. Thompson. "The Role of the Ion/Solid Interaction in Ion Beam Induced Deposition of Gold." *J. Appl. Phys.* 70: 665 (1991).

Durlach, N. "Auditory Localization in Teleoperator and Virtual Environment Systems: Ideas, Issues, and Problems." *Perception* 20: 543-554 (1991).

Ehrlich, D.J., and J. Melngailis. "Fast Room-Temperature Growth of SiO_2 Films by Molecular-Layer Dosing." *Appl. Phys. Lett.* 58: 2675-2677 (1991).

Eugster, C.C., T.P.E. Broekaert, J.A. del Alamo, and C.G. Fonstad. "An InAlAs/InAs MODFET." *IEEE Electron. Dev. Lett.* EDL-12: 707-709 (1991).

Feng, S., and P.A. Lee. "Mesoscopic Conductance and Correlations in Laser Speckle Patterns." *Science* 251: 633-639 (1991).

Freyman, R.L., and P.M. Zurek. "Influence of Onset Cues in Lateralization." *J. Acoust. Soc. Am.* 89: 1995 (1991).

Gabetta, G., D. Huang, J. Jacobson, M. Ramaswamy, E.P. Ippen, and J.G. Fujimoto. "Femtosecond Pulse Generation in Ti:Al_2O_3 Using a Microdot Mirror Mode Locker." *Opt. Lett.* 16(22): 1756-1758 (1991).

Gels, M.W., H.I. Smith, A. Argoitia, J. Angus, G.H.M. Ma, J.T. Glass, J. Butler, C.J. Robinson, and R. Pryor. "Large-Area Mosaic Diamond Films Approaching Single-Crystal Quality." *Appl. Phys. Lett.* 58: 2485 (1991).

Ghosh, A., S. Devadas, and A.R. Newton. "Test Generation and Verification for Highly Sequential Circuits." *IEEE Trans. Comput.-Aided Des.* 11(5): 652-667 (1991).

Goossen, K.W., J.E. Cunningham, T.Y. Kuo, W.Y. Jan, and C.G. Fonstad. "Monolayer d-doped Heterojunction Bipolar Transistor Characteristics from 10 to 350 K." *Appl. Phys. Lett.* 59: 682-684 (1991).

Gould, P.L., P.J. Martin, G.A. Ruff, R.E. Stoner, J-L. Picque, and D.E. Pritchard. "Momentum Transfer to Atoms by a Standing Light Wave; Transition from Diffraction to Diffusion." *Phys. Rev. A* 43: 585 (1991).

Grant, K.W., and L.D. Braida. "Evaluating the Articulation Index for Auditory-Visual Input." *J. Acoust. Soc. Am.* 89(6): 2952-2960 (1991).

Grant, K.W., L.D. Braida, and R.J. Renn. "Single-band Envelope Cues as an Aid to Speechreading." *Quart. J. Exper. Psych.* 43A(3): 621-645 (1991).

Green, T.J., Jr., J.H. Shapiro, and M.M. Menon. "Target Detection Performance Using 3-D Laser Radar Images." *SPIE Proc.* 1471: 328-341 (1991).

Griffith, M., G. Langston, M. Heflin, S. Conner, and B. Burke. "The Fourth MIT-Green Bank 5 GHz Survey." *Astrophys. J., Suppl. Ser.* 75: 801-833 (1991).

Habashy, T.M., S.M. Ali, J.A. Kong, and M.D. Grossi. "Dyadic Green's Functions in a Planar

Stratified, Arbitrarily Magnetized Linear Plasma." *Radio Sci.* 26(3): 701-716 (1991).

Hartney, M.A., D.C. Shaver, M.I. Shepard, J. Melngailis, V. Medvedev, and W.P. Robinson. "Surface Imaging of Focused Ion Beam Exposed Resists." *J. Vac. Sci. Technol. B* 9: 3432 (1991).

Hartney, M.A., D.C. Shaver, M.I. Shepard, J.S. Huh, and J. Melngailis. "Silylation of Focused Ion Beam Exposed Resists." *Appl. Phys. Lett.* 59: 485-487 (1991).

Haus, H.A. "Quantum Noise in a Solitonlike Repeater System." *J. Opt. Soc. Am. B* 8(5): 1122-1126 (1991).

Haus, H.A., and E.P. Ippen. "Self-starting of Passively Mode-locked Lasers." *Opt. Lett.* 16(17): 1331-1333 (1991).

Haus, H.A., and W. Huang. "Coupled-Mode Theory." *IEEE Proc.* 79(10): 1505-1518 (1991).

Haus, H.A., J.G. Fujimoto, and E.P. Ippen. "Structures for Additive Pulse Mode Locking." *J. Opt. Soc. Am. B* 8(10): 2068-2076 (1991).

Haus, H.A., K. Bergman, and Y. Lai. "Fiber Gyro with Squeezed Radiation." *J. Opt. Soc. Am. B* 8(9): 1952-1957 (1991).

Haus, H.A., U. Keller, and W.H. Knox. "Theory of Coupled-Cavity Mode Locking with a Resonant Nonlinearity." *J. Opt. Soc. Am. B* 8(6): 1252-1258 (1991).

Haus, H.A., and Y. Lai. "Narrow-Band Distributed Feedback Reflector Design." *J. Lightwave Tech.* 9(6): 754-760 (1991).

Heflin, M.B., M.V. Gorenstein, C.R. Lawrence, and B.F. Burke. "First- and Second-Epoch VLBI Observations of the Gravitational Lens System 2016+112." *Astrophys. J.* 378: 519-536 (1991).

Ho, S-T., P. Kumar, and J.H. Shapiro. "Quantum Theory of Nondegenerate Multiwave Mixing. II. Adiabatic Elimination via Slowly Varying Amplitude Approximation." *Phys. Rev. A* 43(7): 3939-3948 (1991).

Ho, S-T., P. Kumar, and J.H. Shapiro. "Quantum Theory of Nondegenerate Multiwave Mixing. III. Application to Single-Beam Squeezed-State Generation." *J. Opt. Soc. Am. B* 8(1): 37-57 (1991).

Ho, S-T., N.C. Wong, and J.H. Shapiro. "Single-Beam Squeezed-State Generation in Sodium Vapor and its Self-Focusing Limitations." *Opt. Lett.* 16(11): 840-842 (1991).

Hoston, W., and A.N. Berker. "Multicritical Phase Diagrams of the Blume-Emery-Griffiths Model with Repulsive Biquadratic Coupling." *Phys. Rev. Lett.* 67(8): 1027-1030 (1991).

Hoston, W., and A.N. Berker. "Dimensionality Effects on the Multicritical Phase Diagrams of the Blume-Emery-Griffiths Model with Repulsive Biquadratic Coupling: Mean-field and Renormalization-group Studies." *J. Appl. Phys.* 70(10): 6101-6103 (1991).

Hu, Q., and S. Feng. "Feasibility of Far-Infrared Lasers Using Multiple Semiconductor Quantum Wells." *Appl. Phys. Lett.* 59(23): 2923-2925 (1991).

Hu, Q., C.A. Mears, and P.L. Richards. "Millimeter Wave Superconducting Receivers." *IEEE MTT-S Digest* 409 (1991).

Huang, D., E.A. Swanson, C.P. Lin, J.S. Schuman, W.G. Stinson, W. Chang, M.R. Hee, T. Flotte, K. Gregory, C.A. Puliafito, J.G. Fujimoto. "Optical Coherence Tomography." *Sci.* 254: 1178-1181 (1991).

Huang, D., J. Wang, C.P. Lin, C.A. Puliafito, and J.G. Fujimoto. "Micron-Resolution Ranging of Cornea Anterior Chamber by Optical Reflectometry." *Lasers in Surgery and Medicine* 11: 419-425 (1991).

Huh, J.S., M.I. Shepard, and J. Melngailis. "Focused Ion Beam Lithography." *J. Vac. Sci. Technol. B* 9: 173 (1991).

Hultgren, C.T., and E.P. Ippen. "Ultrafast Refractive Index Dynamics in AlGaAs Diode Laser Amplifiers." *Appl. Phys. Lett.* 59(6): 635-637 (1991).

Ismail, K., P.F. Bagwell, T.P. Orlando, D.A. Antoniadis, and H.I. Smith. "Quantum Phenomena in Field-Effect-Controlled Semiconductor Nanostructures." *IEEE Proc.* 79: 1106-1116 (1991).

Ismail, K., F. Legoues, N.H. Karam, J. Carter, and H.I. Smith. "High-Quality GaAs on Sawtooth-Patterned Si Substrates." *Appl. Phys. Lett.* 59(19): 2418-2420 (1991).

Ismail, K., M. Burkhardt, H.I. Smith, N.H. Karam, and P.A. Sekula-Moise. "Patterning and Characterization of Large-Area Quantum Wire

Arrays." *Appl. Phys. Lett.* 58(14): 1539-1541 (1991).

Iu, C-h., G.R. Welch, M.M. Kash, D. Kleppner, D. Delande, and J.C. Gay. "Diamagnetic Rydberg Atom: Confrontation of Calculated and Observed Spectra." *Phys. Rev. Lett.* 66(2): 145-148 (1991).

Jerby, E. "Traveling-Wave Free-Electron Laser." *Phys. Rev. A* 44(1): 703-715 (1991).

Jerby, E., G. Bekefi, and J.S. Wurtele. "Observations of Periodic Intensity Bursts During the Start-up Phase of a Free-Electron-Laser Oscillator." *Phys. Rev. Lett.* 66(16): 2068-2071 (1991).

Jerby, E., G. Bekefi, and J.S. Wurtele. "Experimental and Theoretical Study of Periodic Intensity Bursts in the Start-Up Phase of a Free-Electron Laser Oscillator." *IEEE J. Quantum Electron.* 27(12): 2512-2521 (1991).

Jerby, E., G. Bekefi, and J.S. Wurtele. "Observations of Periodic Intensity Bursts from a Free Electron Laser Oscillator." *Nucl. Instrum. Methods Phys. Res.* A304: 107-110 (1991).

Johnson, A.D., K.J. Maynard, S.P. Daley, Q.Y. Yang, and S.T. Ceyer. "Hydrogen Embedded in Ni: Production by Incident Atomic Hydrogen and Detection by High Resolution Electron Energy Loss." *Phys. Rev. Lett.* 67: 927 (1991).

Kahn, H., and C.V. Thompson. "The Effect of Applied Mechanical Stress on the Electromigration Failure Times of Aluminum Interconnects." *Appl. Phys. Lett.* 56: 1308 (1991).

Karam, N.H., A. Mastrovita, V. Haven, K. Ismail, S. Pennycock, and H.I. Smith. "Patterning and Overgrowth of Nanostructure Quantum Well Wire Arrays by LP-MOVPE." *J. Crystal Growth* 107: 591-597 (1991).

Keane, D.T., P.A. Bancel, G.L. Jordan-Sweet, G.A. Held, A. Mak, and R.J. Birgeneau. "Evidence for Two-Step Disordering of the Au(110) 1 x 2 Reconstructed Surface." *Surf. Sci.* 250: 8 (1991).

Keith, D.W., C.R. Ekstrom, Q.A. Turchette, and D.E. Pritchard. "An Interferometer for Atoms." *Phys. Rev. Lett.* 66(21): 2693-2696 (1991).

Keith, D.W., and M.J. Rooks. "Free-standing Gratings and Lenses for Atom Optics." *J. Vac. Sci. Technol. B* 9: 2846 (1991).

Kinaret, J.M., and P.A. Lee. "Conductance of a Disordered Narrow Wire in a Strong Magnetic Field." *Phys. Rev. B* 43(5): 3847-3855 (1991).

Kleppner, D., C-H. Iu, and G.R. Welch. "Positive Energy Spectroscopy of the Diamagnetic Lithium System." *Comments At. Mol. Phys.* 25(4-6): 301-307 (1991).

Ku, Y-C., L-P. Ng, R. Carpenter, K. Lu, H.I. Smith, L.E. Haas, and I. Plotnik. "In situ Stress Monitoring and Deposition of Zero-Stress W for X-ray Masks." *J. Vac. Sci. Technol. B* 9(6): 3297-3300 (1991).

Kumar, A., and P.F. Bagwell. "Resonant Tunneling in a Quasi-One-Dimensional Wire: Influence of Evanescent Modes." *Phys. Rev. B* 43: 9012-9020 (1991).

Kumar, A., and P.F. Bagwell. "Evolution of the Quantized Ballistic Conductance with Increasing Disorder in Narrow Wire Arrays." *J. Phys. Rev. B* 44: 1747-1753 (1991).

Kuo, T.Y., J.E. Cunningham, K.W. Goosen, A. Ourmazd, W. Jan, C.G. Fonstad, and F. Ren. "Planarized Be δ-doped Heterostructure Bipolar Transistor Fabricated Using Doping Selective Contact and Selective Hole Epitaxy." *J. Appl. Phys.* 30: L262-L265 (1991).

Kupfer, K., and A. Bers. "Fast Electron Transport in Lower-Hybrid Current Drive." *Phys. Fluids B* 3(10): 2783-2795 (1991).

Lai, Y., H.A. Haus, and Y. Yamamoto. "Squeezed Vacuum from Amplitude Squeezed States." *Opt. Lett.* 16(19): 1517-1519 (1991).

Lane, H., J. Perkell, M. Svirsky, and J. Webster. "Changes in Speech Breathing Following Cochlear Implant in Postlingually Deafened Adults." *J. Speech Hear. Res.* 34: 526-533 (1991).

Lau, S.D., J.P. Donnelly, C.A. Wang, R.B. Goodman, and R.H. Rediker. "Optical Phase Difference Measurement and Correction Using AlGaAs Integrated Guided-Wave Components." *IEEE Photonics Tech. Lett.* 3(10): 902-904 (1991).

Lee, P.A., and N. Nagaosa. "Relaxation of Nuclear Spin Due to Long Range Orbital Currents." *Phys. Rev. B* 43: 1223 (1991).

Lezec, H.J., C.R. Musil, J. Melngailis, L.J. Mahoney, and J. Woodhouse. "Dose-Rate Effects in Focused-Ion-Beam Implantation of

Si into GaAs." *J. Vac. Sci. Technol. B* 9: 2709 (1991).

Liu, C.T., D.C. Tsui, M. Shayegan, K. Ismail, D.A. Antoniadis, and H.I. Smith. "Guiding-Center-Drift Resonance of Two-Dimensional Electrons in a Grid-Gate Superlattice Potential." *Appl. Phys. Lett.* 58: 2945-2947 (1991).

Longworth, H.P., and C.V. Thompson. "Abnormal Grain Growth in Aluminum Alloy Thin Films." *J. Appl. Phys.* 69: 3929 (1991).

Lumsdaine, A., J.L. Wyatt, Jr., and I.M. Elfadel. "Nonlinear Analog Networks for Image Smoothing and Segmentation." *J. VLSI Signal Process.* 3: 53-68 (1991).

Ma, E., and C.V. Thompson. "Nucleation and Growth During Reactions in Multilayer Al/Ni Films: The Early Stages of Al_3Ni Formation." *J. Appl. Phys.* 69: 2211 (1991).

Mak, A., K.W. Evans-Lutterodt, K. Blum, D.Y. Noh, J.D. Brock, G.A. Held, and R.J. Birgeneau. "Synchrotron X-ray Diffraction Study of the Disordering of the Ge(111) Surface at High Temperatures." *Phys. Rev. Lett.* 66(15): 2002-2005 (1991).

McCann, P.J., and C.G. Fonstad. "Auger Electron Spectroscopic Analysis of Barium Fluoride Surfaces Exposed to Selenium Vapor." *J. Electron. Mat.* 20(11): 915-920 (1991).

McCann, P.J., and C.G. Fonstad. "Liquid Phase Epitaxial Growth of PbSe on (111) and (100) BaF_2." *J. Cryst. Growth* 114: 687-692 (1991).

McEuen, P.L., E.P. Foxman, U. Meirav, M.A. Kastner, Y. Meir, N.S. Wingreen, and S.J. Wind. "Transport Spectroscopy of a Coulomb Island in the Quantum Hall Regime." *Phys. Rev. Lett.* 66: 1926 (1991).

Meade, R.D., K.D. Brommer, A.M. Rappe, and J.D. Joannopoulos. "Electromagnetic Bloch Waves at the Surface of a Photonic Crystal." *Phys. Rev. B* 44(19): 10961-10964 (1991).

Meade, R.D., K.D. Brommer, A.M. Rappe, and J.D. Joannopoulos. "Photonic Bound States in Periodic Dielectric Materials." *Phys. Rev. B* 44(24): 13772-13774 (1991).

Mears, C.A., Q. Hu, P.L. Richards, A. Worsham, and D.E. Prober. "Quantum Limited Quasiparticle Mixers at 100 GHz." *IEEE Trans. Magn.* MAG-27: 3363 (1991).

Mears, C.A., Q. Hu, and P.L. Richards. "The Effect of the Quantum Susceptance on the Gain of Superconducting Quasiparticle Mixers." *IEEE Trans. Magn.* MAG-27: 3384 (1991).

Mecozzi, A., J.D. Moores, H.A. Haus, and Y. Lai. "Soliton Transmission Control." *Opt. Lett.* 16(23): 1841-1843 (1991).

Meir, Y., N.S. Wingreen, and P.A. Lee. "Transport Through a Strongly Interacting Electron System: Theory of Periodic Conductance Oscillations." *Phys. Rev. Lett.* 66(23): 3048-3051 (1991).

Melngailis, J. "Focused Ion Beam Induced Deposition—A Review." *SPIE Proc.* 1465 (1991).

Mentle, R.E., and J.H. Shapiro. "Track-While-Image in the Presence of Background." *SPIE Proc.* 1471: 342-353 (1991).

Migliuolo, S. "Collisional Viscosity and Finite Ion Larmor Radius Effects on Resistive Internal Kink Modes." *Nucl. Fusion* 31: 365 (1991).

Migliuolo, S., F. Pegoraro, and F. Porcelli. "Stabilization of Collisional Drift-tearing Modes at the Breakdown of the Constant-Psi Approximation." *Phys. Fluids B* 3(6): 1338-1345 (1991).

Miura, H., E. Ma, and C.V. Thompson. "Initial Sequence and Kinetics of Silicide Formation in the Cobalt/Amorphous-Silicon Multilayer Thin Films." *J. Appl. Phys.* 70: 4287 (1991).

Moel, A., W. Chu, K. Early, Y-C. Ku, E.E. Moon, F. Tsai, H.I. Smith, M.L. Schattenburg, C.D. Fung, F.W. Griffith, and L.E. Haas. "Fabrication and Characterization of High-Flatness Mesa-Etched Silicon Nitride X-ray Masks." *J. Vac. Sci. Technol. B* 9(6): 3287-3291 (1991).

Moores, J.D., K. Bergman, H.A. Haus, and E.P. Ippen. "Optical Switching Using Fiber Ring Reflectors." *J. Opt. Soc. Am. B* 8(3): 594-601 (1991).

Moores, J.D., K. Bergman, H.A. Haus, and E.P. Ippen. "Demonstration of Optical Switching by Means of Solitary Wave Collisions in a Fiber Ring Reflector." *Opt. Lett.* 16(3): 138-140 (1991).

Murguia, J.E., M.I. Shepard, J. Melngailis, A.L. Lattes, and S.C. Munroe. "Increase in Silicon CCD Speed with Focused Ion Beam Implanted Channels." *J. Vac. Sci. Technol. B* 9: 2714 (1991).

Nabors, K., and J. White. "FastCap: A Multipole Accelerated 3-D Capacitance Extraction Program." *IEEE Trans. Comput.-Aided Des. Integrated Circuits Syst.* 10(11): 1447-1459 (1991).

Nagaosa, N., and P.A. Lee. "Experimental Consequences of the Uniform Resonating Valence Bond State." *Phys. Rev. B* 43: 1233 (1991).

Nahum, M., Q. Hu, P.L. Richards, N. Newman, and S.A. Sachtjen. "Fabrication and Measurement of a High Tc Superconducting Microbolometer." *IEEE Trans. Magn.* MAG-27: 3081 (1991).

Needels, M., J.D. Joannopoulos, Y. Bar-Yam, S.T. Pantelides, and R.H. Wolfe. "The Enchanting Properties of Oxygen Atoms in Silicon." *Proceedings, Mat. Res. Soc. Symp.* 209: 103-117 (1991).

Needles, M., J.D. Joannopoulos, Y. Bar-Yam, and S.T. Pantelides. "Oxygen Complexes in Silicon." *Phys. Rev. B* 43(5): 4208-4215 (1991).

Netz, R.R., and A.N. Berker. "Hard-spin Mean-field Theory: Formulation for Ising, XY, and Other Models." *J. Appl. Phys.* 70(10): 6074-6076 (1991).

Netz, R.R., and A.N. Berker. "Monte Carlo Mean-Field Theory and Frustrated Systems in Two and Three Dimensions." *Phys. Rev. Lett.* 66(3): 377-380 (1991).

Netz, R.R., and A.N. Berker. "Monte Carlo Mean-Field Theory and Frustrated Systems in Two and Three Dimensions: Netz and Berker Reply." *Phys. Rev. Lett.* 67(13): 1808 (1991).

Nghiem, S.V., M.E. Veysoglu, J.A. Kong, R.T. Shin, K. O'Neill, and A.W. Lohanick. "Polarimetric Passive Remote Sensing of a Periodic Soil Surface: Microwave Measurements and Analysis." *J. Electro. Waves Appl.* 5(9): 997-1005 (1991).

Noh, D.Y., K.I. Blum, M.J. Ramstad, and R.J. Birgeneau. "Long-range Coherence and Macroscopic Phase Separation of Steps on Vicinal Si(111)." *Phys. Rev. B* 44(19): 10969-10972 (1991).

Noh, D.Y., K.I. Blum, M.J. Ramstad, and R.J. Birgeneau. "Long Range Separation of Steps on Vicinal Si(111)." *Phys. Rev. B* 44: 10969 (1991).

Oates, D.E., C. Anderson, D.M. Sheen, and S.M. Ali. "Stripline Resonator Measurements of Z_sVSH_{rf} in $YBa_2Cu_3O_{7-x}$ Thin Films." *IEEE Trans. Microwave Theory Tech.* 39: 1522-1529 (1991).

Pang, X.D., H.Z. Tan, and N.I. Durlach. "Manual Discrimination of Force Using Active Finger Motion." *Percept. Psychophys.* 49(6): 531-540 (1991).

Park, S.L., P.F. Bagwell, A. Yen, D.A. Antoniadis, H.I. Smith, T.P. Orlando, and M.A. Kastner. "Magnetotransport in Multiple Narrow Si Inversion Channels Opened Electrostatically into a Two-Dimensional Electron Gas." *Bull. Am. Phys. Soc.* 36: 360 (1991).

Peake, W.T., and J.J. Rosowski. "Impedance Matching, Optimum Velocity, and Ideal Middle Ears." *Hear. Res.* 53: 1-6 (1991).

Peng, L-H., T.P.E. Broekaert, W-Y. Choi, C.G. Fonstad, and V. Jones. "Defect Activated Infrared Multiphonon Excitation in Iron-doped Semi-insulating Indium Phosphide." *Appl. Phys. Lett.* 59: 564-566 (1991).

Perkell, J.S., E.B. Holmberg, and R.E. Hillman. "A System for Signal Processing and Data Extraction from Aerodynamic, Acoustic and Electroglottographic Signals in the Study of Voice Production." *J. Acoust. Soc. Am.* 89(4): 1777-1781 (1991).

Perkell, J.S., E.B. Holmberg, and R.E. Hillman. "A System for Signal Processing and Data Extraction from Aerodynamic, Acoustic, and Electroglottographic Signals in the Study of Voice Production." *J. Acoust. Soc. Am.* 89(4): 1777-1781 (1991).

Power, M.H., and L.D. Braida. "A Physical Measure of Consistency Among Speech Parameter Vectors: Application to Speech Intelligibility Determination." *J. Acous.. Soc. Am.* 90: 2327 (1991).

Prentiss, M., N. Bigelow, and S. Shahriar. "Forces on Three Level Atoms Including Coherent Population Trapping." *Opt. Lett.* 16: 1695 (1991).

Price, P.J., M. Ostendorf, S. Shattuck-Hufnagel, and C. Fong. "The Use of Prosody in Syntactic Disambiguation." *J. Acoust. Soc. Am.* 90: 1956-1970 (1991).

Pritchard, D.E. "Atom Interferometers." *Opt. Photonics News* (December 1991).

Ram, A.K., and A. Bers. "Propagation and Damping of Mode Converted Ion-Bernstein Waves in Toroidal Plasmas." *Phys. Fluids B* 3(4): 1059-1069 (1991).

Ram, A.K., and A. Bers. "Space-Time Propagation of Electromagnetic Instabilities Across the Magnetic Field in Auroral Regions." *EOS Trans. Am. Geophys. Union* 72 (1991).

Ram, A.K., A. Bers, V. Fuchs, L. Vacca, and M. Shoucri. "Current Drive by Fast Alfvén Waves and in Combination with Lower Hybrid Waves." *Bull. Am. Phys. Soc.* 36: 2339 (1991).

Rankovic, C.M. "An Application of the Articulation Index to Hearing Aid Fitting." *J. Speech Hear. Res.* 34: 391-402 (1991).

Rankovic, C.M., and P.M. Zurek. "Evaluation of Prescriptive Fitting Procedures Using the AI Model." *ASHA* 33: 164 (1991).

Rankovic, C.M., P.M. Zurek, and R.L. Freyman. "Potential Benefits of Adaptive Frequency-Gain Characteristics for Speech Reception in Noise for Hearing-Impaired Individuals." *J. Acoust. Soc. Am.* 90: 2319 (1991).

Rediker, R.H., K.A. Rauschenbach, and R.P. Schloss. "Operation of a Coherent Ensemble of Five Diode Lasers in an External Cavity." *IEEE J. Quantum Electron.* 27(6): 1582-1593 (1991).

Reed, C.M., L.A. Delhorne, N.I. Durlach, and S.D. Fischer. "A Study of the Tactual and Visual Reception of Fingerspelling." *J. Speech Hear. Res.* 33: 786-797 (1991).

Reed, C.M., M.H. Power, N.I. Durlach, L.D. Braida, K.K. Foss, J.A. Reid, and S.R. Dubois. "Development and Testing of Artificial Low-Frequency Speech Codes." *J. Rehabil. Res. Dev.* 28(3): 67-82 (1991).

Rosowski, J.J. "The Effects of External-and Middle-Ear Filtering on Auditory Threshold and Noise-Induced Hearing Loss." *J. Acoust. Soc. Am.* 90(1): 124-135 (1991).

Rosowski, J.J., and A. Graybeal. "What Did Morganucodon Hear?" *Zool. J. Linnean Soc.* 101: 131-168 (1991).

Sarpeshkar, R, J.L. Wyatt, Jr., M.C. Lu, and P.D. Gerber. "Mismatch Sensitivity of a Simultaneously Latched CMOS Sense Amplifier." *IEEE J. Solid-State Circuits* 26(10): 1413-1422 (1991).

Schattenburg, M.L., C.R. Canizares, D. Dewey, K.A. Flanagan, M.A. Hamnett, A.M. Levine, K.S.K. Lum, R. Manikkalingam, T.H. Markert, and H.I. Smith. "Transmission Grating Spectroscopy and the Advanced X-ray Astrophysics Facility." *Opt. Eng.* 30: 1590-1600 (1991).

Schattenburg, M.L., K. Li, R.T. Shin, J.A. Kong, and H.I. Smith. "Electromagnetic Calculation of Soft-X-ray Diffraction from 0.1 μm Gold Structures." *J. Vac. Sci. Technol. B* 9: 3232-3236 (1991).

Schoenlein, R.W., J.G. Fujimoto, G.L. Eesley, and T.W. Capehart. "Femtosecond Relaxation Dynamics of Image-Potential States." *Phys. Rev. B* 43(6): 4688-4698 (1991).

Segal, M., E. Weinstein, and B.R. Musicus. "Estimate-Maximize Algorithms for Multichannel Time Delay and Signal Estimation." *IEEE Trans. Signal Process.* 39(1): 1-16 (1991).

Shapiro, J.H., and S.R. Shepard. "Quantum Phase Measurement: A System-Theory Perspective." *Phys. Rev. A* 43(7): 3795-3818 (1991).

Sheen, D.M., S.M. Ali, D.E. Oates, R.S. Withers, and J.A. Kong. "Current Distribution, Resistance, and Inductance for Superconducting Strip Transmission Lines." *IEEE Trans. Appl. Superconduc.* 1(2): 108-115 (1991).

Shirasaki, M., and H.A. Haus. "Noise Reduction in Quantum Nondemolition Measurement with a Nonlinear Mach-Zehnder Interferometer Using Squeezed Vacuum." *J. Opt. Soc. Am. B* 8(3): 681-684 (1991).

Siegel, P.H., J.E. Oswald, R.G. Dengler, D.M. Sheen, and S.M. Ali. "Measured and Computed Performance of a Microstrip Filter Composed of Semi-insulating GaAs on a Fused Quartz Substrate." *IEEE Microwave Guided Wave Lett.* 1(4) (1991).

Smith, H.I., S.D. Hector, M.L. Schattenburg, and E.H. Anderson. "A New Approach to High Fidelity E-Beam and Ion-Beam Lithography Based on an in situ Global-Fiducial Grid." *J. Vac. Sci. Technol. B* 9(6): 2992-2995 (1991).

Smith, S.P., F. Zarinetchi, and S. Ezekiel. "Narrow-linewidth Stimulated Brillouin Fiber Laser and Applications." *Opt. Lett.* 16(6): 393-395 (1991).

Standley, D. "An Object Position and Orientation IC with Embedded Imager." *IEEE J. Solid-State Circuits* 26(12): 1853-1860 (1991).

Stevens, K.N., and C.A. Bickley. "Constraints Among Parameters Simplify Control of Klatt Formant Synthesizer." *J. Phon.* 19: 161-174 (1991).

Svirsky, M.A., and E.A. Tobey. "Effect of Different Types of Auditory Stimulation on Vowel Formant Frequencies in Multichannel Cochlear Implant Users." *J. Acoust. Soc. Am.* 89: 2895-2904 (1991).

Taherian, M.R., D.J. Yuen, T.M. Habashy, and J.A. Kong. "A Coaxial-Circular Waveguide for Dielectric Measurement." *IEEE Trans. Geosci. Remote Sensing* 29(2): 321-330 (1991).

Tao, T., W. Wilkinson, and J. Melngailis. "Focused Ion Beam Induced Deposition of Platinum for Repair Processes." *J. Vac. Sci. Technol. B* 9(1): 162-164 (1991).

Tsuk, M.J., and J.A. Kong. "A Hybrid Method for the Calculation of the Resistance and Inductance of Transmission Lines with Arbitrary Cross Sections." *IEEE Trans. Microwave Theory Tech.* 39(8): 1338-1347 (1991).

Tulintseff, A.N., S.M. Ali, and J.A. Kong. "Input Impedance of a Probe-Fed Stacked Circular Microstrip Antenna." *IEEE Trans. Antenna Propag.* 39(3): 381-390 (1991).

Uchanski, R.M., K.M. Millier, D.E. Ronan, C.M. Reed, and L.D. Braida. "Effects of Token Variability on Resolution for Vowel Sounds." *J. Acoust. Soc. Am.* 90: 2254 (1991).

Veysoglu, M.E., H.A. Yueh, R.T. Shin, and J.A. Kong. "Polarimetric Passive Remote Sensing of Periodic Surfaces." *J. Electro. Waves Appl.* 5(3): 267-280 (1991).

Vlcek, J.C., and C.G. Fonstad. "Multiply-graded InGaAlAs Heterojunction Bipolar Transistors." *Electron. Lett.* 27: 1213-1215 (1991).

Vlcek, J.C., and C.G. Fonstad. "Precise Computer Control of the MBE Process—Application of Graded InGaAlAs/InP Alloys." *J. Cryst. Growth* 111: 56-60 (1991).

Wilson, B.S., C.C. Finley, D.T. Lawson, R.D. Wolford, D.K. Eddington, and W.M. Rabinowitz. "Better Speech Recognition with Cochlear Implants." *Nature* 352: 236-238 (1991).

Wong, N.C. "Squeezed Amplification in a Nondegenerate Parametric Amplifier." *Opt. Lett.* 16(21): 1698-1700 (1991).

Yen, A., R.A. Ghanbari, Y-C. Ku, W. Chu, M.L. Schattenburg, J.M. Carter, and H.I. Smith. "X-ray Masks with Large-Area 100 nm Period Gratings for Quantum-Effect Device Applications." *Microelectron. Eng.* 13: 271-274 (1991).

Yueh, S.H., and J.A. Kong. "Analysis of Diffraction from Chiral Gratings." *J. Electro. Waves Appl.* 5(7): 701-714 (1991).

Yueh, S.H., J.A. Kong, J.K. Jao, R.T. Shin, H.A. Zebker, and T. LeToan. "K-Distribution and Multi-Frequency Polarmetric Terrain Radar Clutter." *J. Electro. Waves Appl.* 5(1): 1-15 (1991).

Zarinetchi, F., S.P. Smith, and S. Ezekiel. "Stimulated Brillouin Fiber-Optic Laser Gyroscope." *Opt. Lett.* 16(4): 229-231 (1991).

Zitkovsky, I.D., Q. Hu, T.P. Orlando, J. Melngailis, and M. Shepard. "Fabrication of High Tc Superconducting Weaklinks Using Focused Ion Beams." *Appl. Phys. Lett.* 59: 727 (1991).

Zurek, P.M. "Interference Reduction for the Hearing Impaired." *J. Acoust. Soc. Am.* 89: 1957 (1991).

Zurek, P.M. "Probability Distributions of Interaural Phase and Level Differences in Binaural Detection Stimuli." *J. Acoust. Soc. Am.* 90(4): 1927-1932 (1991).

A.2.2 Journal Articles Accepted for Publication

Arias, T.A., M.C. Payne, and J.D. Joannopoulos. "Ab-initio Molecular Dynamics Techniques Extended to Large-Length-Scale Systems." *Phys. Rev. B.*

Arias, T.A., M.C. Payne, and J.D. Joannopoulos. "Precise and Efficient Ab-initio Molecular Dynamics." *Phys. Rev. B.*

Ashar, P., A. Ghosh, and S. Devadas. "Boolean Satisfiability and Equivalence Checking Using General Binary Decision Diagrams." *Integrat. VLSI J.*

Basu, S., M. Muendel, J. Goodberlet, S. Kaushik, and P.L. Hagelstein. "A Search for Gain at 191 Å." *SPIE-Int. Soc. Opt. Eng.*

Bekefi, G. "Double Stream Cyclotron Maser." *SPIE Proc.*

Braud, J.P., and P.L. Hagelstein. "Whispering-Gallery Laser Resonators. Part II: Analysis of Mirrors with Non-Uniform Curvature." *IEEE J. Quantum Electron.*

Broekaert, T.P.E., and C.G. Fonstad. "AlAs Etch-Stop Layers for InGaAlAs/InP Heterostructure Devices and Circuits." *IEEE Trans. Electron. Dev.*

Bryan, M.J., S. Devadas, and K. Keutzer. "Necessary and Sufficient Conditions for Robust Stuck-Open Fault Testability in Multilevel Networks." *IEEE Trans. Comput.-Aided Des.*

Burns, G.F., and C.G. Fonstad. "Monolithic Fabrication of Strain-Free (Al,Ga)As Heterostructure Lasers on Silicon Substrates." *IEEE Photonics Tech. Lett.*

Chamon, C. de C., C.K. Sun, H.A. Haus, and J.G. Fujimoto. "Femtosecond Time Division Interferometry Technique for Measuring the Tensor Components of $X^{(3)}$." *Appl. Phys. Lett.*

Chu, W., S.A. Rishton, M.L. Schattenburg, D.P. Kern, and H.I. Smith. "Fabrication of 50 nm Line-and-Space X-ray Masks in Thick Au Using a 50 keV Electron Beam System." *J. Vacuum Sci. Tech. B.*

Cobra, D.T., A.V. Oppenheim, and J.S. Jaffe. "Geometric Distortions in Side-Scan Sonar Images: A Procedure for Their Estimation and Correction." *IEEE J. Oceanic Eng.*

Conde, M.E., and G. Bekefi. "High Efficiency 33.3 GHz Free Electron Laser Amplifier with a Reversed Axial Guide Magnetic Field." *Nucl. Instrum. Methods A.*

Conde, M.E., and G. Bekefi. "Experimental Study of a 33.3 GHz Free Electron Laser Amplifier with a Reversed Axial Guide Magnetic Field." *SPIE Proc.*

Cornell, E.A., K.R. Boyce, D.L.K. Fygenson, and D.E. Pritchard. "Two Ions in a Penning Trap: Implications for Precision Mass Spectroscopy." *Phys. Rev. A.*

Dal Pino, A., Jr., M. Needels, and J.D. Joannopoulos. "Oxygen Induced Broken-Bond Defect in Silicon." *Phys. Rev. B.*

Devadas, S., and K. Keutzer. "Validatable Nonrobust Delay-Fault Testable Circuits Via Logic Synthesis." *IEEE Trans. Comput.-Aided Des.*

Dynes, S.B.C., and B. Delgutte. "Phase Locking of Auditory-nerve Discharges to Sinusoidal Electric Stimulation of the Cochlea." *Hear. Res.*

Evans, P.V., D.A. Smith, and C.V. Thompson. "Absence of Electrical Activity at High Angle Grain Boundaries in Zone-Melt-Recrystallised Silicon-on-Insulator Films." *Appl. Phys. Lett.*

Friedland, L., and A. Bers. "Hermitian Description of Interacting Inhomogeneous Electron Beams." *Phys. Fluids B.*

Frost, H.J., C.V. Thompson, and D.T. Walton. "Simulation of Thin Film Grain Structures: II. Abnormal Grain Growth." *Acta Metall. Mat.*

Ghosh, A., S. Devadas, and A.R. Newton. "Heuristic Minimization of Boolean Relations Using Testing Techniques." *IEEE Trans. Comput.-Aided Des.*

Ghosh, A., S. Devadas, and A.R. Newton. "Sequential Test Generation and Synthesis for Testability at the Register-Transfer and Logic Levels." *IEEE Trans. Comput.-Aided Des.*

Green, T.J., Jr., and J.H. Shapiro. "Maximum-Likelihood Laser Radar Range Profiling with the Estimation-Maximization Algorithm." *Appl. Opt.*

Greenberg, J.E., and P.M. Zurek. "Evaluation of an Adaptive Beamforming Method for Hearing Aids." *J. Acoust. Soc. Am.*

Haus, H.A., and Y. Lai. "Theory of Cascaded Quarter Wave Shifted Distributed Feedback Resonators." *IEEE J. Quantum Electron.*

Hemmer, P., M. Prentiss, and S. Shahriar. "Optical Force on the Raman Dark State in Two Standing Waves." *Opt. Commun.*

Jiran, E., and C.V. Thompson. "Capillary Instabilities in Thin Continuous Films." *Thin Solid Films.*

Lee, D., and N.C. Wong. "Tunable Optical Frequency Division Using a Phase Locked Optical Parametric Oscillator." *Opt. Lett.*

Longworth, H.P., and C.V. Thompson. "An Experimental Study of Electromigration in Bicrystal Al Lines." *Appl. Phys. Lett.*

Maynard, K.J., A.D. Johnson, S.P. Daley, and S.T. Ceyer. "A New Mechanism for Absorption: Collision Induced Absorption." *J. Chem. Soc.*

Meskoob, B., S. Prasad, M-K. Vai, J.C. Vlcek, H. Sato, and C.G. Fonstad. "Bias-dependence of the Intrinsic Element Values of InGaAs/InAlAs/InP Inverted Heterojunction Bipolar Transistor." *IEEE Trans. Microwave Theory Tech.*

Muendel, M.H., and P.L. Hagelstein. "Four-Wave Frequency Conversion of Coherent Soft X-rays in a Plasma." *Phys. Rev. A.*

Oppenheim, A.V., E. Weinstein, K.C. Zangi, M. Feder, and D. Gauger. "Single-Sensor Active Noise Cancellation Based on the EM Algorithm." *IEEE Trans. Signal Process.*

Peake, W.T., J.J. Rosowski, and T.J. Lynch III. "Middle-ear Transmission: Acoustic Versus Ossicular Coupling in Cat and Human." *Hear. Res.*

Rabinowitz, W.M., D.K. Eddington, L.A. Delhorne, and P.A. Cuneo. "Relations Among Different Measures of Speech Reception in Subjects Using a Cochlear Implant." *J. Acoust. Soc. Am.*

Rappe, A., J.D. Joannopoulos, and P. Bash. "A Test of the Planewaves for the Study of Molecules from First Principles." *J. Am. Chem. Soc.*

Reed, C.M., W.M. Rabinowitz, N.I. Durlach, L.A. Delhorne, L.D. Braida, J.C. Pemberton, B.D. Mulcahey, and D.L. Washington. "Analytic Study of the Tadoma Method: Improving Performance Through the Use of Supplementary Tactual Displays." *J. Speech Hear. Res.*

Rosenkranz, P.W. "Rough-Sea Microwave Emissivities Measured with the SSM/I." *IEEE Trans. Geosci. Remote Sensing.*

Smet, J.H., T.P.E. Broekaert, and C.G. Fonstad. "Peak-to-valley Current Ratios as High as 50:1 at Room Temperature in Pseudomorphic $In_{0.53}Ga_{0.47}As/AlAs/InAs$ Resonant Tunneling Diodes." *J. Appl. Phys.*

Walton, D.T., H.J. Frost, and C.V. Thompson. "The Development of Bamboo and Near-Bamboo Microstructures in Thin Film Strips." *Appl. Phys. Lett.*

Weinstein, E., M. Feder, and A.V. Oppenheim. "Multi-Channel Signal Separation Based on Decorrelation." *IEEE Trans. Signal Process.*

Wong, N.C. "Gravity-Wave Detection Via an Optical Parametric Oscillator" *Phys. Rev. A.*

Woods, W.S., A. Kulkarni, H.S. Colburn, A. Rigopulos, S.D. Pang, N.I. Durlach, and E.M. Wenzel. "On the Externalization of Auditory Images." *Presence.*

Wornell, G.W., and A.V. Oppenheim. "Estimation of Fractal Signals from Noisy Measurements Using Wavelets." *IEEE Trans. Signal Process.*

Yen, A., E.H. Anderson, R.A. Ghanbari, M.L. Schattenburg, and H.I. Smith. "An Achromatic Holographic Configuration for 100 nm Period Lithography." *Appl. Opt.*

Yen, A., M.L. Schattenburg, and H.I. Smith. "A Proposed Method for Fabricating 50 nm-period Gratings by Achromatic Holographic Lithography." *Appl. Opt.*

Yu, P.C., S.J. Decker, H-S. Lee, C.G. Sodini, and J.L. Wyatt, Jr. "CMOS Resistive Fuses for Image Smoothing and Segmentation." *IEEE J. Solid-State Circuits.*

Zhao, Y., D.C. Tsui, M. Santos, M. Shayegan, R.A. Ghanbari, D.A. Antoniadis, and H.I. Smith. "Magneto-optical Absorption in a Two Dimensional Electron Grid." *Appl. Phys. Lett.*

A.2.3 Journal Articles Submitted for Publication

Bagwell, P.F., and A. Kumar. "Comment on Effects of Channel Opening and Disorder on the Conductance of Narrow Wires." *Phys. Rev. B.*

Boning, D.S., M.B. McIlrath, P. Penfield, and E. Sachs. "A General Semiconductor Process Modeling Framework." *IEEE Trans. Semicond. Manuf.*

Coronado, C.A., E. Ho, L.A. Kolodziejski, and C.A. Huber. "Photo-Assisted Molecular Beam Epitaxy of ZnSe." *Appl. Phys. Lett.*

Dron, L. "The Multi-Scale Veto Model: A Two-Stage Analog Network for Edge Detection and Image Reconstruction." *Int. J. Comput. Vision.*

Early, K., G.E. Rittenhouse, J.M. Graybeal, and H.I. Smith. "Sub-100- and Sub-10-nm-thick Membranes Anisotropically Etched in (110) Silicon." *Appl. Phys. Lett.*

Eddington, D.K., G. Girzon, and P.A. Cuneo. "An Electroanatomical Model of Intracochlear Electrical Stimulation II: Tests of Model Predictions for Monopolar Electrodes." *Hear. Res.*

Elfadel, I.M., and R.W. Picard. "On A Unifying Neighborhood-Based Framework for Morphological Analysis and Co-Occurrence Methods." *IEEE Trans. Pattern Anal. Mach. Intell.*

Girzon, G., and D.K. Eddington. "An Electroanatomical Model of Intracochlear Electrical Stimulation I: Formulation, Solution and Predictions for Monopolar Electrodes." *Hear. Res.*

Helmerson, K., A. Martin, and D.E. Pritchard. "Laser and rf Spectroscopy of Magnetically Trapped Neutral Atoms." *J. Opt. Soc. Am. B.*

Holmberg, E., R. Hillman, J. Perkell, and C. Gress. "Relationships Between SPL and Aerodynamic and Acoustic Measures of Voice Production: Inter- and Intra-speaker Variation." *J. Speech Hear. Res.*

Ketterle, W., and D.E. Pritchard. "Trapping Ground State Atoms in Static Fields." *Appl. Phys. B.*

Ketterle, W., A. Martin, M. Joffe, and D.E. Pritchard. "Slowing Atoms with Diffuse Laser Light." *Phys. Rev. Lett.*

Kobler, J.B., J.J. Guinan, Jr., S.R. Vacher, and B.E. Norris. "Acoustic-Reflex Frequency Selectivity in Single Stapedius Motoneurons of the Cat." *J. Neurophysiol.*

Lattes, A.L., S.C. Munroe, M.M. Seaver, J.E. Murguia, and J. Melngailis. "Improved Drift in Two-Phase, Long-Channel, Shallow-Buried-Channel CCD's with Longitudinally Nonuniform Storage-Gate Implants." *IEEE Trans. Electron Devices.*

Oppenheim, A.V., E. Weinstein, K.C. Zangi, M. Feder, and D. Gauger. "Single-Sensor Active Noise Cancellation Based on the EM Algorithm." *IEEE Trans. Signal Process.*

Perkell, J., M. Svirsky, M. Matthies, and M. Jordan. "Trading Relations Between Tongue-body Raising and Lip Rounding in Production of the Vowel /u/." *PERILUS,* the working papers of the Department of Phonetics, Institute of Linquistics, Stockholm.

Perkell, J., and M. Matthies. "Temporal Measures of Anticipatory Labial Coarticulation for the Vowel /u/: Within- and Cross-Subject Variability." *J. Acoust. Soc. Am.*

Perkell, J., H. Lane, M. Svirsky, and J. Webster. "Speech of Cochlear Implant Patients: A Longitudinal Study of Vowel Production." *J. Acoust. Soc. Am.*

Picard, R.W., and I.M. Elfadel. "Texture Modeling: Markov/Gibbs Random Fields, Co-Occurrence, and Boundary Length Optimization." *IEEE Trans. Pattern Anal. Mach. Intell.*

Picard, R.W., and I.M. Elfadel. "On the Structure of Aura Matrices for the Markov/Gibbs Texture Model." *J. Math. Imag. Vision.*

Ravicz, M.E., J.J. Rosowski, and H.F. Voigt. "Sound-power Collection by the Auditory Periphery of the Mongolian Gerbil Meriones Unguiculatus: I. Middle-ear Input Impedance." *J. Acoust. Soc. Am.*

Shattuck-Hufnagel, S. "The Role of Word and Syllable Structure in Phonological Encoding in English." *Cognition.*

Stevens, K.N., S.E. Blumstein, L. Glicksman, M. Burton, and K. Kurowski. "Acoustic and Perceptual Characteristics of Voicing in Fricatives and Fricative Clusters." *J. Acoust. Soc. Am.*

Svirsky, M., H. Lane, J. Perkell, and J. Webster. "Effects of Short-Term Auditory Deprivation on Speech Production in Adult Cochlear Implant Users." *J. Acoust. Soc. Am.*

Turchette, Q.A., D.E. Pritchard, and D.W. Keith. "Numerical Model of a Multiple Grating Interferometer." *J. Opt. Soc. Am. B.*

Umminger, C.B., and C.G. Sodini. "Switched Capacitor Networks for Monolithic Image Processing Systems." *IEEE Trans. Circuits Syst.*

Wightman, C., S. Shattuck-Hufnagel, M. Ostendorf, and P.J. Price. "Segmental Durations in the Vicinity of Prosodic Phrase Boundaries." *J. Acoust. Soc. Am.*

Wong, N.C. "Proposal for a 10 THz, Precision Optical Frequency Comb Generator." *Electron. Lett.*

Wyatt, J.L., Jr., C. Keast, M. Seidel, D. Standley, B. Horn, T. Knight, C. Sodini, H-S. Lee, and T. Poggio. "Analog VLSI Systems for Image Acquisition and Fast Early Vision Processing." *Int. J. Comput. Vision.*

Yen, A., M.L. Schattenburg, H.I. Smith, and G.N. Taylor. "An Anti-Reflective Coating for Use with PMMA at 193 nm." *J. Electrochem. Soc.*

A.3 Books/Chapters in Books

Berker, A.N. "Absence of Temperature-Driven First-Order Phase Transitions in Systems with Random Bonds." In *Science and Technology of Nonostructured Magnetic Materials,* pp. 411-417. Eds. G.C. Hadjipanayis and G.A. Prinz. New York: Plenum Press, 1991.

Bickley, C.A. "Vocal-fold Vibration in a Computer Model of a Larynx." In *Vocal Fold Physiology,* pp. 37-46. Eds. J. Gauffin and B. Hammarberg. San Diego: Singular, 1991.

Chow, C.C., A. Bers, and A.K. Ram. "The Three Wave Interaction and Spatiotemporal Chaos." In *Physics of Space Plasmas (1991),* SPI Conference Proceedings and Reprint Series. Forthcoming.

Coppi, B. "Isotropic Effect in Plasma Confinement." In *Plasma Physics and Controlled Nuclear Fusion Research 1990,* 2: 413. Vienna: I.A.E.A, 1991.

Delgutte, B., and P. Cariani. "Coding of the Pitch of Harmonic and Inharmonic Complex Tones in the Interspike Intervals of Auditory-nerve Fibers." In *Audition, Speech, and Language.* Ed. M.E.H. Schouten. Berlin: Moulton-de Gruyter. Forthcoming.

Halle, M., and K.N. Stevens. "Knowledge of Language and the Sounds of Speech." In *Music, Language, Speech and Brain,* pp. 1-19. Eds. J. Sundberg, L. Nord, and R. Carlson. Basingstoke, Hampshire: Macmillan Press, 1991.

Horn, B.K.P. "Parallel Networks for Machine Vision." In *Research Directions in Computer Science: An MIT Perspective.* Eds. A. Meyer, G.V. Guttag, R.L. Rivest, and P. Szolovits. Cambridge, Massachusetts: MIT Press, 1991.

LaMotte, R.H., and M.A. Srinivasan. "Surface Microgeometry: Neural Encoding and Perception." In *Information Processing in the Somatosensory System.* Eds. O. Franzen and J. Westman. Wenner-Gren International Symposium Series. New York: Macmillan Press, 1991.

Lumsdaine, A., J.L. Wyatt, Jr., and I.M. Elfadel. "Nonlinear Analog Networks for Image Smoothing and Segmentation." In *Parallel Processing on VLSI Arrays.* Ed. J.A. Nossek. Norwell, Massachusetts: Kluwer Academic Publishers, 1991.

Melngailis, J. "Ion Lithography and Focused Ion Beam Implantation." In *Handbook of VLSI Lithography.* Eds. W.B. Glendinning and J.N. Helbert. New York: Noyes Publishers, 1991.

Pritchard, D.E. "Atom Optics." In *Atomic Physics 12,* pp. 165-170. Eds. J.C. Zorn, R.R. Lewis, and M. Weiss. New York: American Journal of Physics, 1991.

Ram, A.K., and A. Bers. "Absolute Versus Convective Analysis of Instabilities in Space Plasmas." In *Physics of Space Plasmas (1990),* SPI Conference Proceedings and Reprint Series, Number 10. Eds. T. Chang, G.B. Crew, and J.R. Jasperse. Cambridge, Massachusetts: Scientific Publishers, 1991.

Rappe, A.M., and J.D. Joannopoulos. "The Design of Convergent and Transferable AB Initio Pseudopotentials." In *Computer Simulated Material Science,* pp. 409-422. Eds. M. Meyer and V. Pontikis. Dordrecht, the Netherlands: Kluwer Academic Publishers, 1991.

Reed, C.M., N.I. Durlach, and L.A. Delhorne. "Natural Methods of Tactual Communication." In *Tactile Aids for the Hearing Impaired.* Ed. I.R. Summers. New York: Taylor and Francis. Forthcoming.

Rosowski, J.J. "Hearing in Transitional Mammals: Predictions from the Middle-ear Anatomy and Hearing Capabilities of Extant Mammals." In *The Evolutionary Biology of Hearing,* pp. 625-631. Eds. D.B. Webster, A.N. Popper, and R.R. Ray. New York: Springer-Verlag, 1991.

Shahriar, S., P. Hemmer, N. Bigelow, and M. Prentiss. "Forces on Three Level Atoms Including Trapped State Contribution." In *Quantum Electronics and Laser Science,* Technical Digest Series, p. 186. Washington, DC: Opt. Soc. Am., 1991.

Smith, H.I., and M.L. Schattenburg. "Lithography for Manufacturing at 0.25 Micrometer and Below." In *Semiconductor Materials and Processing Technology.* Ed. J.M. Poate. Dordrecht, the Netherlands: Kluwer Academic Publishers, 1992.

Srinivasan, M.A. "Tactual Interfaces: The Human Perceiver." In *Human-Machine Interfaces for Teleoperators and Virtual Environments.* Eds. N.I. Durlach, T.B. Sheridan, and S.R. Ellis. NASA Conference Publication 10071, 1991.

Srinivasan, M.A., and R.H. LaMotte. "Encoding of Shape in the Responses of Cutaneous Mecha-

noreceptors." *Information Processing in the Somatosensory System.* Eds. O. Franzen and J. Westman. Wenner-Gren International Symposium Series. New York: Macmillan Press, 1991.

Srinivasan, M.A., and R.H. LaMotte. "Tactile Discrimination and Representation of Texture, Shape, and Softness." In *Human-Machine Interfaces for Teleoperators and Virtual Environments.* Eds. N.I. Durlach, T.B. Sheridan, and S.R. Ellis. NASA Conference Publication 10071, 1991.

Stevens, K.N. "Vocal-Fold Vibration for Obstruent Consonants." In *Vocal Fold Physiology: Acoustic, Perceptual, and Physiological Aspects of Voice Mechanisms,* pp. 29-36. Eds. J. Gauffin and B. Hammarberg. San Diego, California: Singular Publishing Group, 1991.

Stevens, K.N. "Some Factors Influencing the Precision Required for Articulatory Targets: Comments on Keating's Paper." In *Papers in Laboratory Phonology I,* pp. 471-475. Eds. J.C. Kingston and M.E. Beckman. Cambridge: Cambridge University Press, 1991.

Stevens, K.N. "Speech Synthesis Methods: Homage to Dennis Klatt." In *Talking Machines: Theories, Models, and Applications.* Eds. G. Bailly and C. Benoit. New York: Elsevier. Forthcoming.

Stevens, K.N. "Models of Speech Production." In *Handbook of Acoustics.* Ed. M. Crocker. New York: Wiley. Forthcoming.

Stevens, K.N. "Phonetic Evidence for Hierarchies of Features." In *LabPhon3.* Ed. P. Keating. Los Angeles: University of California. Forthcoming.

Wang, J., M. Needels, and J.D. Joannopoulos. "Surface and Fracture Energies in GaAs." In *Surface Physics and Related Topics,* p. 314. Teaneck, New Jersey: World Scientific Publishers, 1991.

A.4 RLE Publications

RLE publications may be obtained by writing the Communications Office, Building 36-412, Research Laboratory of Electronics, Massachusetts Institute of Technology, Cambridge, Massachusetts 02139-4307, at the listed cost.

Prepayment in the form of a check or money order in U.S. dollars payable to MIT RLE is required. Please allow six to eight weeks for foreign surface mail. For foreign airmail, include an additional $4.00 for each report ordered.

RLE 45th Anniversary Brochure. MIT, 1991. 72 pp. $6.50.

RLE currents 4(2): (1991). "The MIT Radiation Laboratory: RLE's Microwave Heritage." 32 pp. No charge.

RLE currents 5(1): (1991). "Pathways to the Future at RLE." 16 pp. No charge.

RLE Progress Report No. 133: January - December 1990. MIT, 1991. 390 pp. No charge.

RLE Speech Communication Group "Working Papers." Vol. 7. MIT, 1991. No charge.

Early, K.R. *Experimental Characteristics and Physical Modeling of Resolution Limits in Proximity Printing X-ray Lithography.* RLE TR-565. MIT, 1991. $29.00.

Huang, C.B. *An Acoustic and Perceptual Study of Vowel Formant Trajectories in American English.* RLE TR-563. MIT, 1991. $16.00.

Musicus, B.R., and S. Prasanna. *OKI Advanced Array Processor (AAP) Hardware Description.* RLE TR-562. MIT, 1991. $14.00.

Tsai, F.S. *Characterization of Mechanical and Optical Properties of X-ray Mask Membranes.* RLE TR-564. MIT, 1991. $11.00.

Wornell, G.W. *Synthesis, Analysis, and Processing of Fractal Signals.* RLE TR-566. MIT, 1991. $20.00.

A.5 RLE Theses

Theses are available from the Microreproduction Laboratory, Building 14-0551, Massachusetts Institute of Technology, Cambridge, Massachusetts 02139-4307. Write for individual prices.

Barwick, D.S. *A Study on Fiber-Coupled, External Cavity, Semiconductor Lasers.* S.M. thesis, Dept. of Electr. Eng. and Comput. Sci., MIT, 1991.

Binder, B.T. *Laser Radar Tomography: The Effects of Speckle.* Ph.D. diss., Dept. of Electr. Eng. and Comput. Sci., MIT, 1991.

Bonanni, P.G. *Atmospheric Wave Detection and Parameter Estimation Using Passive Measurements of Thermal Emission Near 118 GHz.* Ph.D. diss., Dept. of Electr. Eng. and Comput. Sci., MIT, 1991.

Chen, J.C. *Theory of Passively Mode-locked Lasers with Dynamic Gain Saturation.* S.M. thesis, Dept. of Electr. Eng. and Comput. Sci., MIT, 1991.

Chiarchiaro, W.J., II. *54-GHz Radiometer for Profiling the Temperature of the Atmosphere.* S.M. thesis, Dept. of Electr. Eng. and Comput. Sci., MIT, 1991.

Chow, C.C. *Spatiotemporal Chaos in the Nonlinear Three Wave Interaction.* Ph.D. diss., Dept. of Physics, MIT, 1991.

Connell, M.W. *Spectral Distortion of Picosecond Pulses in AlGaAs Diode Laser Amplifiers.* S.B. thesis, Dept. of Electr. Eng. and Comput. Sci., MIT, 1991.

Decker, S.J. *A Resistive Fuse for Image Segmentation and Smoothing.* S.M. thesis, Dept. of Electr. Eng. and Comput. Sci., MIT, 1991.

Delisle, J.T. *Three-Dimensional Profiling Using Depth of Focus.* S.M. thesis, Dept. of Electr. Eng. and Comput. Sci., MIT, 1991.

Dominguez, J. *Effortless Internal Camera Calibration Using the Images of Spheres.* S.B. thesis, Dept. of Electr. Eng. and Comput. Sci., MIT, 1991.

Early, K.R. *Experimental Characterization and Physical Modeling of Resolution Limits in Proximity Printing X-Ray Lithography.* Ph.D. diss., Dept. of Electr. Eng. and Comput. Sci., MIT, 1991.

Freeman, C.G. *Diffuse Slowing of a Beam of Neutral Sodium Atoms.* S.B. thesis, Dept. of Physics, MIT, 1991.

Goh, M.Y. *Radiometric Stability of the Far Infrared Absolute Spectrophotometer (FIRAS).* S.M. thesis, Dept. of Physics, MIT, 1991.

Hara, Y. *Application of Neural Networks to Radar Image Classification.* S.M. thesis, Dept. of Electr. Eng. and Comput. Sci., MIT, 1991.

Hedgcock, J.M. *Development and Testing of a System to Evaluate Manual Tracking Ability.* S.B. thesis, Dept. of Electr. Eng. and Comput. Sci., MIT, 1991.

Helmerson, K. *Laser Cooling and Spectroscopy of Magnetically Trapped Atoms.* Ph.D. diss., Dept. of Physics, MIT, 1991.

Hoston, W.C., Jr. *Multicritical Phase Diagrams of the Blume-Emery-Griffiths Model with Repulsive Biquadratic Coupling: Mean-Field and Renormalization-Group Studies.* S.M. thesis, Dept. of Physics, MIT, 1991.

Huang, C.B. *An Acoustic and Perceptual Study of Vowel Formant Trajectories in American English.* Ph.D. diss., Dept. of Electr. Eng. and Comput. Sci., MIT, 1991.

Iu, C-H. *Energy Level Structure of Atoms in Magnetic Fields.* Ph.D. diss., Dept. of Physics, MIT, 1991.

Johnson, A.D. *Dynamics of Hydrogen Absorption into the Ni(111) Bulk: Spectroscopic Identification and Chemistry of Subsurface Hydrogen.* Ph.D. diss., Dept. of Chem., MIT, 1991.

Keith, D.W. *An Interferometer for Atoms.* Ph.D. diss., Dept. of Physics, MIT, 1991.

Knecht, W. *A Nonlinear Extension of a Beamformer for Multi-Microphone Speech Processing.* S.M. thesis., Dept. of Physics, MIT, 1991.

Ko, W-Y. *Graphical Framework for Computer-Aided Fabrication Environment's Process Flow Representation.* S.M. thesis, Dept. of Electr. Eng. and Comput. Sci., MIT, 1991.

Ku, Y-C. *Fabrication of Distortion Free X-ray Masks Using Low Stress Tungsten.* Ph.D. diss., Dept. of Electr. Eng. and Comput. Sci., MIT, 1991.

Kuo, T.Y. *Delta-Doped Heterojunction Bipolar Transistors.* Ph.D. diss., Dept. of Electr. Eng. and Comput. Sci., MIT, 1991.

Lehár, J. *The Time Delay in the Double Quasar 0957+561 and a Search for Gravitational Lenses.* Ph.D. diss., Dept. of Physics, MIT, 1991.

Leong, K.W. *Intensity Quantum Noise Reduction with an Above-Threshold Optical Parametric Oscillator.* Ph.D. diss., Dept. of Electr. Eng. and Comput. Sci., MIT, 1991.

Liu, Y-C. *Coplanar-Spherical-Particle Coarsening in Discontinuous Ultrathin Polycrystaline Gold Films on Amorphous Silicon-Nitride Substrates.* Ph.D. diss., Dept. of Mater. Sci. and Eng., MIT, 1991.

McQuirk, I.S. *Direct Methods for Estimating the Focus of Expansion in Analog VLSI.* S.M. thesis, Dept. of Electr. Eng. and Comput. Sci., MIT, 1991.

Mitchell, D.R. *The Onset of Chaos for a Semi-Classical Alkali Atom in a Uniform Electric Field.* S.B. thesis, Dept. of Physics, MIT, 1991.

Murguia, J.E. *The Application of Focused Ion Beam Implantation to the Design and Fabrication of MOS Devices.* Ph.D. diss., Dept. of Electr. Eng. and Comput. Sci., MIT, 1991.

Netz, R.R. *Frustration in Magnetic, Liquid Crystal, and Surface Systems: Monte Carlo Mean-Field Theory.* S.M. thesis, Dept. of Physics, MIT, 1991.

Nghiem, S.V. *Electromagnetic Wave Models for Polarimetric Remote Sensing of Geophysical Media.* Ph.D. diss., Dept. of Electr. Eng. and Comput. Sci., MIT, 1991.

Ogno, A. *The History of Tactile Aids for the Deaf: A Case Study of Audiological Engineering Corporation.* S.B. thesis, Dept. of Mech. Eng., MIT, 1991.

Picard, R.W. *Texture Modeling: Temperature Effects on Markov/Gibbs Random Fields.* Sc.D. diss., Dept. of Electr. Eng. and Comput. Sci., MIT, 1991.

Prasanna, G.N.S. *Structure Driven Multiprocessor Compilation of Numeric Problems.* Ph.D. diss., Dept. of Electr. Eng. and Comput. Sci., MIT, 1991.

Quirch, J-A. *Development of a Millimeter Wavelength Circularly Polarized Antenna.* S.B. thesis, Dept. of Electr. Eng. and Comput. Sci., MIT, 1991.

Reisman, C.A. *Envelope Modulation Spectra of Bandpass Filtered Speech.* S.B. thesis, Dept. of Electr. Eng. and Comput. Sci., MIT, 1991.

Ro, J-S. *Microstructure and Mechanism of Gold Films Grown by Ion Beam Induced Deposition.* Ph.D. diss., Dept. of Mater. Sci. and Eng., MIT, 1991.

Sheen, D.M. *Numerical Modeling of Microstrip Circuits and Antennas.* Ph.D. diss., Dept. of Electr. Eng. and Comput. Sci., MIT, 1991.

Standley, D.L. *Analog VLSI Implementation of Smart Vision Sensors: Stability Theory and an Experimental Design.* Ph.D. diss., Dept. of Electr. Eng. and Comput. Sci., MIT, 1991.

Tsai, F.S. *Characterization of Mechanical and Optical Properties of X-Ray Mask Membranes.* S.B. thesis, Dept. of Electr. Eng. and Comput. Sci., MIT, 1991.

Turchette, Q.A. *Numerical Model of a Three Grating Interferometer for Atoms.* S.B. thesis, Dept. of Physics, MIT, 1991.

Vlcek, J.C. *Molecular Beam Epitaxial Growth and Applications of Graded Bandgap in GaAlAs Semiconducting Alloys.* Ph.D. diss., Dept. of Electr. Eng. and Comput. Sci., MIT, 1991.

Walrod, D.B. *Third Order Optical Nonlinearities in Semiconductor Superlattices.* Ph.D. diss., Dept. of Physics, MIT, 1991.

Wornell, G.W. *Synthesis, Analysis, and Processing of Fractal Signals.* Ph.D. diss., Dept. of Electr. Eng. and Comput. Sci., MIT, 1991.

Yen, A. *Fabrication of Large-Area 100 nm-Period Gratings Using Achromatic Holographic Lithography.* Ph.D. diss., Dept. of Electr. Eng. and Comput. Sci., MIT, 1991.

A.6 Miscellaneous

Basu, B., and B. Coppi. *Electromagnetic Modes Driven by Streaming Proton Populations.* RLE PTP Report 91/6, MIT, 1991.

Bers, A., V. Fuchs, and C.C. Chow. "Maximizing Absorption in Ion-Cyclotron Heating of Tokamak Plasmas." *Plasma Fusion Center Report* PFC/JA-91-10. MIT, 1991.

Coppi, B. *Levels of Protection Against the Onset of Internal Oscillations in the Ignitor Experiment.* RLE PTP Report 91/3, MIT, 1991.

Coppi, B., and M. Nassi. *Comments on the Ignitor and the BPX (CIT) Concepts.* RLE PTP Report 91/5, MIT, 1991.

Kupfer, K., and A. Bers. "Fast Electron Transport in Lower-Hybrid Current Drive." *Plasma Fusion Center Report* PFC/JA-91-13. MIT, 1991.

Kupfer, K., A. Bers, and A.K. Ram. "Fast Electron Transport During Lower-Hybrid Current Drive." *Plasma Fusion Center Report* PFC/JA-91-9. MIT, 1991.

Migliuolo, S. *Ion Temperature Gradient Driven Impurity Modes.* RLE PTP Report 91/12, MIT, 1991.

Migliuolo, S. *Theory of Resistive and Ideal Internal Kinks.* RLE PTP Report 91/1, MIT, 1991.

Ram, A.K., and A. Bers. "Comments on Absolute and Convective Instabilities." *Plasma Fusion Center Report* PFC/JA-91-8. MIT, 1991.

Ram, A.K., and A. Bers. "Absolute Versus Convective Analysis of Instabilities in Space Plasmas." *Plasma Fusion Center Report* PFC/JA-91-4. MIT, 1991.

Riconda, C. *Emission, Propagation and Absorption of Synchrotron Radiation in Nonhomogeneous Plasmas.* RLE PTP Report 91/8, MIT, 1991.

Srinivasan, M.A., and K. Dandekar. *Role of Mechanics in Cuteneous Mechanoreceptor Response.* Society for Neuroscience Abstracts, 1991.

Appendix B. Current RLE Personnel

Director: Jonathan Allen
Associate Director: Daniel Kleppner

Professors

Jonathan Allen
Boris Altshuler
Dimitri A. Antoniadis
Arthur B. Baggeroer
George Bekefi
A. Nihat Berker
Abraham Bers
Robert J. Birgeneau
Amar G. Bose
Louis D. Braida
Bernard E. Burke
Sylvia T. Ceyer
Sow-Hsin Chen
Bruno Coppi
Shaoul Ezekiel
Clifton G. Fonstad, Jr.
Lawrence S. Frishkopf
Hermann A. Haus
Albert Hill[1]
Erich P. Ippen
John D. Joannopoulos
Marc A. Kastner
Nelson Y.-S. Kiang
John G. King
Daniel Kleppner
Jin A. Kong
Patrick A. Lee
Jerome Y. Lettvin[1]
Jae S. Lim
Alan V. Oppenheim
William T. Peake
Miklos Porkolab
David E. Pritchard
William F. Schreiber
Campbell L. Searle
Jeffrey H. Shapiro
William M. Siebert
Henry I. Smith
David H. Staelin
Kenneth N. Stevens
Julius A. Stratton[1]
Donald E. Troxel
Thomas F. Weiss
Jerome B. Wiesner[1]
John L. Wyatt, Jr.
Henry J. Zimmermann[1]

Associate Professors

Jesus A. del Alamo
Srinivas Devadas
James G. Fujimoto
Peter L. Hagelstein
Leslie A. Kolodziejski
Jacob K. White

Assistant Professors

John M. Graybeal
Jacqueline N. Hewitt
Qing Hu
Simon G.J. Mochrie
Gregory W. Wornell
Jonathan S. Wurtele

Senior Research Scientists

Nathaniel I. Durlach
John Melngailis
Joseph S. Perkell
Robert H. Rediker

Principal Research Scientists

Donald K. Eddington
John J. Guinan, Jr.
William M. Rabinowitz
Charlotte M. Reed
Philip W. Rosenkranz
Patrick M. Zurek

---

[1] Professor Emeritus.

Research Scientists and Research Specialists

Sami M. Ali
Giovanni Aliberti
John W. Barrett
Santanu Basu
James M. Carter
Bertrand Delgutte
Lorraine A. Delhorne
Ronald C. Englade
David W. Foss
Dennis M. Freeman
Qizheng Gu
Seth M. Hall
Thomas J. Lohman
Ivan Mastovsky
Melanie L. Matthies
Michael B. McIlrath
Dennis P. McNabb
Stefano Migliuolo
Xiao Dong Pang
Abhay K. Ram
John J. Rosowski
Stefanie Shattuck-Hufnagel
Mandayam A. Srinivasan
Linda E. Sugiyama
Mario A. Svirsky
Hong Z. Tan
Ngai Chuen Wong
Ying-Ching E. Yang

Administrative Staff

Donald F. Duffy
Virginia R. Lauricella
Barbara J. Passero
John S. Peck
Gerrard F. Power
William H. Smith
Vicky-Lynn Taylor
Donna Maria Ticchi

Support and Technical Staff

Mary C. Aldridge
Janice L. Balzer
Felicia G. Brady
Margery E. Brothers
Manuel Cabral, Jr.
Donald A. Clements
John F. Cook
Carol A. Costa
Ann K. Dix
Francis M. Doughty
Laura B. Doughty
Dorothy A. Fleischer
Kerry L. Gafney
Deborah A. Gage
Donna L. Gale
Mary S. Greene
Debra L. Harring
Maureen C. Howard
Wendy E. Hunter
Barbara A. King
Cynthia Y. Kopf
Kit-Wah F. Lai
Lisbeth N. Lauritzen
Cindy LeBlanc
David S. Lee
Catherine Lorusso
Eleanora M. Luongo
Rita C. McKinnon
Gina L.B. Milton
Mark K. Mondol
Susan E. Nelson
Donald K. North
Robert H. Priest
Brian E. Ray
Bruce A. Russell
Maxine P. Samuels
Clare F. Smith
Arlene E. Wint
Mary J. Ziegler

Postdoctoral Fellows and Associates

Ashraf S. Alkhairy
Robert C. Armstrong
Alice M. Berglund
Peter A. Cariani
Arnaldo Dal Pino
Susan L. Goldman
Wolfgang Ketterle
Yulin Li
Alexander Martin
Robert D. Meade
David P. Pullman
Sunil Puria
Christine M. Rankovic
Barrett Rogers
Selim M. Shahriar
Rosalie M. Uchanski
Filip Van Aelten
Xin Xu
Xinglong Yan
Yi Yuan

Research Assistants

Charles C. Abnet
Michael Ames
John G. Apostolopoulos
David V. Arnold
Neer R. Asherie
William W. Au
Babak Ayazifar
Ali J. Azarbayejani
Ziad J. Azzam
Sandeep Bahl
Kelly S. Bai
Donald G. Baltus
Keren Bergman
Kevin R. Boyce
John P. Braud
Louis R. Brothers
Martin Burkhardt
Pin-P. Chang
Elaine Y. Chen
Grace H. Chen
Jerry C. Chen
Jyh-Shing Chen
Marilyn Y. Chen
Tak K. Cheng
Shiufun Cheung
Tony Chiang
Kyeongjae Cho
Woo-Young Choi
William Chu
Isaac L. Chuang
Jeffrey A. Colborn
Manoel E. Conde
Samuel R. Conner
Christopher J. Corcoran
Christopher A. Coronado
Michael W. Courtney
Pierre Coutu
Jay Damask
Kristin Dana
Kiran B. Dandekar
Daniel J. DiLorenzo
David J. Dougherty
Paul Duchnowski
Scott b Dynes
Christopher R. Ekstrom
Ibrahim M. Elfadel
John D. Ellithorpe
Darin R. Ernst
Paul W. Fieguth
Siegfried B. Fleischer
Andre B. Fletcher
Joseph A. Frisbie
Alex W. Fung
Eric M. Fuchs
Boris Golubovic
James G. Goodberlet
Mark E. Griffith
Nitin Gupta
Rajesh K. Gupta
Troy D. Hammond
Hsiu C. Han
John C. Hardwick
Scott D. Hector
Michael R. Hee
Eason Ho
Michael S. Ho
Jeffrey R. Holley
David M. Horowitz
Chih-Chien Hsu
Wen Hu
David Huang
Gregory T. Huang
Charles T. Hultgren
Janice M. Huxley
Brian R. Jacobson
Joseph M. Jacobson
Hong Jiao
Michael A. Joffe
Joel T. Johnson
Mark A. Johnson
Mattan Kamon
Charles A. Katz
Farzana I. Khatri
Songmin Kim
Jari M. Kinaret
Cheung-Wei Lam
Dicky Lee
Laurence H. Lee
Gadi Lenz
Stan Y. Liao
Sharlene A. Liu
Jennifer A. Lloyd
Robert I. Lutwak
Gregory R. Martin
Paul S. Martin
Marc O. Mewes
Alberto M. Moel
Michael C. Moldoveanu
Peter A. Monta
John D. Moores
Martin Muendel
Keith S. Nabors
Shujaet Nadeem
Vasant Natarajan
Phillip T. Nee
Julien J. Nicolas
James M. Njeru
John H. Oates
Michael P. O'Connell
Scott N. Paine
Lily Y. Pang
Lisa A. Pickelsimer
Kelly L. Poort
Matthew H. Power
Khalid Rahmat
Malini Ramaswamy
Mark W. Reichelt
Michael J. Schwartz
Amelia H. Shen
Gennady Shvets
Luis M. Silveira
Andrew C. Singer
Jurgen H. Smet
Stephen P. Smith
Jared P. Squire
Robert W. Stadler
Gideon P. Stein
Richard E. Stoner
Chi-Kuang Sun
Ke-Xun Sun
Kohichi R. Tamura
Mohammad A. Tassoudji
Anthony A. Triolo
Michael J. Tsuk
Morrison Ulman
Luigi Vacca
Jesus Noel Villasenor
Pavel S. Volfbeyn
Jing Wang
Li-Fang Wang
Lorin F. Wilde
Timothy A. Wilson
Vincent V. Wong
Albert R. Woo
Rolf A. Wyss
Jiqing Xia
Chang D. Yoo
Kambiz C. Zangi
Farhad Zarinetchi

Teaching Assistants

Saurav Bhatta
John R. Buck
Naomi Chesler
Kevin G. Christian
Shepard S. Doeleman
Anthony E. English
Ibrahim A. Hajjahmad
Kyle K. Iwai
Sumanth Kaushik
Darren L. Leigh
Christian R. Musil
Hanalabos Papadopoulos
Michael O. Polley
Stephen F. Scherock
Scott R. Shepard
Lon E. Sunshine
Murat E. Veysoglu
Susie J. Wee
Taylen J. Wong
Kenneth W. Yee

Graduate Students

Tomas A. Arias
Robert G. Atkins
Ian M. Avruch
Kerry L. Beach
Karl K. Berggren
Bruce L. Carvalho
Palmyra E. Catravas
Claudio L. Cesar
Hwa-Ping Chang
Michael S. Chapman
Irfan U. Chaudhary
Yiu Y. Chu
Kevin M. Cuomo
Charles Q. Davis
Kendall Davis
Anthony D. Della Ratta
Frank DiFilippo
Andy B. Dobrzeniecki
Christopher R. Doerr
Kamyar Eshghi
Jerrold A. Floro
Ethan B. Foxman
Steven G. Frain
Eric J. Gaidos
Edouard A. Garcia
Reza A. Ghanbari
Julie E. Greenberg
Rogeve Gulati
Katherine L. Hall
Helen M. Hanson
John F. Heanue
Olivier Herbelot
Lori K. Herold
Bruce N. Ingle
Steven H. Isabelle
Erik B. Iverson
Mark K. Jablonski
Jacek Jachner
Donna-Jean Kaiser
Chwen-yuen Ku
Volkan C. Kubali
Warren M. Lam
Daniel D. Lee
Eddie F. Lee
Henri J. Lezec
Kevin Li
Harold H. Lim
Yong Liu
Joseph A. Maxwell
Michael M. McCue
Ignacio S. McQuirk
Ann W. Morgenthaler
Malini V. Narayanan
Aradhana Narula
Lynn E. Nelson
Sourabh Niyogi
Janet L. Pan
Gregory E. Penn
Brian M. Perreault
Andrew M. Rappe
Michael D. Richard
Todd H. Rider
Jon C. Sandberg
Steven D. Schultz
Hugh E. Secker-Walker
Mark N. Seidel
Barbara G. Shinn
Chung-Hao Shue
Ricardo Telichevesky
Christopher B. Umminger
Bernadette Upshaw
Kathleen E. Wage
Xinglong Yan
Julius J. Yang
Peter T. Yu

Undergraduate Students

Mustafa K. Ahmed
Carlos A. Aneses
John E. Berberian
Michele M. Bierbaum
Upanishad K. Chakrabarti
Venkatesh R. Chari
Belinda Cheng
Jonathan C. Doan
Mauricio A. Escobar
Othan Estrada
David M. Fanning
Juan Ferrera
Darlene J. Ford
Eliza Fulton
Curtis A. Gabrielson
Rajashi Ghosh
Daniel I. Goldman
Danielle C. Goodman
Andrew H. Grant
James A. Grimm
Daniel F. Gruhl
Akikazu Hashimoto
Todd A. Hay
Surendranauth Hiraman
Erica T. Kashambuzi
Jerome S. Khohayting
Andrew E. Lan
Huy X. Le
Chee-Heng Lee
Huiying Li
Michael H. Lim
Matthew J. Marjanovic
Terrence L. Marshall
Meredith M. McKenzie
Michael S. Mermelstein
Mark D. Messier
Euclid E. Moon
Lee P. Ng
Lynn E. Niles
Daniel B. Olster
Sang H. Park
Thomas J. Paul
Eliot J. Quataert
Kenneth N. Ricci
Diane E. Ronan
Brian A. Rubin
Rohit Sakhuja
Alexis P. Silitch
David L. Sisson
Joie Sun
Roderick D. Tranum

Evren R. Unver
Scott R. Velazquez
Latha Venkataraman
Monika K. Walczak
Janet Wang
Michele A. Wang
Thomas R. Westcott
Eric A. Woods
Peter S. Yesley
Noah D. Zamdmer

Visiting Scientists

Lucio H. Acioli
Sunny Y.C. Auyang
Yuji Awano
Vladimir Barsukov
Corine A. Bickley
Franco Carpignano
Paolo Detragiache
Theodore W. Ducas
Kaigham J. Gabriel
Bernard Gold
Ehud Heyman
Yuzo Hirayama
Pallavi Jha
Lance G. Joneckis
Arthur K. Jordan
Franz X. Kaertner
Che Y. Kim
Jack Kotik
Giovanni Lapenta
Jaejin Lee
Antonio Mecozzi
Cesar F. Meirelles
Christopher B. Moore
Phylis Morrison
Guilia A. Nassi
Marco Nassi
Kevin O'Neill
Karen L. Payton
Caterina Riconda
Stanley J. Rosenthal
Hannes J. Schmiedmayer
Yun Shao
Masataka Shirasaki
Fabrice Vallee
Min Wei
Rongqing Xu
Masanori Yamaguchi
Leonid E. Zakharov

Research Affiliates

John S. Barlow
Herbert J. Bernstein
Giuseppe Bertin
Suzanne Boyce
Frank S. Cardarelli
Steven Colburn
Carol Y. Espy-Wilson
Ignacio Garcia-Otero
Gad Geiger
Richard S. Goldhor
Kenneth W. Grant
Robert D. Hall
Philip R. Hemmer
Robert E. Hillman
Eva B. Holmberg
Caroline B. Huang
Yoshiko Ito
Joseph A. Jarrell
John D. Kierstead
Janet D. Koehnke
Harlan Lane
Charles P. Lin
Neil A. Macmillan
John I. Makhoul
Sharon Y. Manuel
Bruce R. Musicus
Mark R. Nilsen
Leonard L. Picard
Soon Y. Poh
James C. Preisig
Mara G. Prentiss
Stephen A. Raymond
Carol C. Ringo
Joseph F. Rizzo
Jay T. Rubinstein
Robert T. Shin
Richard J. Solomon
Frank J. Stefanov-Wagner
David A. Steffens
Kenneth P. Wacks
Jane W. Webster
Ehud Weinstein
David R. Williams
Meng Yu Zhu

In Memoriam

Professor Emeritus Alan H. Barrett (1927 - 1991)



Nobel laureate Dr. Norman F. Ramsey, Jr. of Harvard University and MIT President Dr. Charles M. Vest rendezvous with RLE's Director Jonathan Allen.



RLE Directors Emeriti Jerome B. Wiesner (left) and Albert G. Hill (center) confer with Robert V. Pound. All three were with RadLab's Group 53 (Radio Frequency).



Institute Professor Emeritus Walter A. Rosenblith catches up with Professor Daniel Kleppner, RLE Associate Director.

Celebrating Milestones

In 1991, two distinguished anniversaries were celebrated: the MIT Radiation Laboratory's 50th and RLE's 45th. The Research Laboratory of Electronics, which was established in 1946, grew out of MIT's wartime Radiation Laboratory (1940-45). Two special events were held to honor the milestones shared by these laboratories. (Photos by John Cook)



Former RLE RadLab editor Dr. Helen L. Thomas with Professor and RLE Director Emeritus Henry J. Zimmerman.



Former RadLab/RLE staffers Frank J. O'Brien and D. Cosmo Papa renew acquaintances.

Appendix C. Milestones

C.1 New Faculty and Staff

Dr. Boris L. Altshuler, Associate Professor of Physics, joined RLE's Surfaces and Interfaces Group.

Dr. Gregory W. Wornell (SM '87, PhD '91), was appointed to Assistant Professor in the the Department of Electrical Engineering and Computer Science. Professor Wornell is a faculty member in RLE's Digital Signal Processing Group.

Dr. Santanu Basu was appointed Research Scientist in RLE's Optics and Devices Group.

Dr. Mario A. Svirsky was appointed Research Scientist in RLE's Speech Communication Group.

Dr. Ying-Ching Eric Yang (SM '85, PhD '89), was appointed Research Scientist in RLE's Center for Electromagnetic Theory and Applications.

C.2 Retirements

Dr. Peter A. Wolff, Professor of Physics and Director Emeritus of both RLE (1967-81) and MIT's Francis Bitter National Magnet Laboratory (1981-86), announced his retirement after 21 years at MIT. Professor Wolff was with RLE's Optics and Devices Group.

C.3 Promotions

Dr. Jesús A. del Alamo, ITT Career Development Professor, was promoted to Associate Professor without tenure in the Department of Electrical Engineering and Computer Science. Professor del Alamo is a faculty member in RLE's Materials and Fabrication Group.

Dr. J. David Litster, Director Emeritus of MIT's Francis Bitter National Magnet Laboratory and former RLE faculty member, was promoted to Vice President and Dean for Research at MIT.

Dr. Jacob White (BS '80), Assistant Professor of Electrical Engineering and Computer Science, was promoted to Associate Professor without tenure in that Department. Professor White is a faculty member in RLE's Circuits and Systems Group.

Dr. John Melngailis was promoted from Principal Research Scientist to Senior Research Scientist in RLE's Materials and Fabrication Group.

C.4 Chair Appointments

A faculty member of RLE's Digital Signal Processing Group, ***Dr. Arthur B. Baggeroer*** (EE '65, SM '65, ScD '68) was appointed Ford Professor of Engineering, which recognizes outstanding senior faculty in the School of Engineering.

Dr. Sylvia T. Ceyer, Professor of Chemistry and faculty member in RLE's Surfaces and Interfaces Group, was named recipient of the first William M. Keck Foundation Professorship in the field of energy.

Dr. Qing Hu, faculty member in RLE's Optics and Devices Group, was appointed Kokusai Denshin Denwa (KDD) Career Development Professor in Communications and Technology for a two-year period beginning September 1, 1991.

Dr. Leslie A. Kolodziejski was appointed Karl Van Tassel Career Development Professor for a two-year period beginning September 1, 1991. Professor Kolodziejski is a faculty member in the Materials and Fabrication Group at RLE.

C.5 Awards and Honors

RLE celebrated its ***45th anniversary*** with a festive gathering of faculty, staff, students and friends at the MIT Museum on October 28, 1991.

The MIT Physics Department celebrated the 90th birthday of ***Professor Emeritus William P. Allis*** (BS '23, MS '24) on November 15, 1991.

Dr. Abraham Bers (SM '55, ScD '59), Professor of Electrical Engineering and Computer Science, was elected Vice Chairman of the Division of Plasma Physics of the American Physical Society. Professor Bers is a faculty member in RLE's Plasma Physics Group.

Dr. Robert J. Birgeneau, Head of MIT's Physics Department and Cecil and Ida Green Professor of Physics, was appointed Dean of MIT's School of Science effective July 1, 1991. Professor Birgeneau is a faculty member in RLE's Surfaces and Interfaces Group.

Dr. Amar Bose (SB '51, SM '52, PhD '56), Professor of Electrical Engineering and Computer

Science, was elected Fellow to the American Academy of Arts and Sciences in May 1991.

A faculty member in RLE's Plasma Physics Group, ***Dr. Bruno Coppi***, Professor of Physics, received the annual Leadership Award from Fusion Power Associates of Gaithersburg, Maryland.

Dr. Hermann A. Haus (ScD '54), Institute Professor, was named recipient of the 1991 Education Medal from the Institute of Electrical and Electronic Engineers. Professor Haus is a faculty member in RLE's Optics and Devices Group.

Dr. Daniel Kleppner, Associate Director of RLE and Lester Wolfe Professor of Physics, received the 1991 Julius Edgar Lilienfeld Prize from the American Physical Society. Professor Kleppner is also faculty member in RLE's Atomic, Molecular, and Optical Physics Group.

Dr. Patrick A. Lee (SB '66, PhD '70), William and Emma Rogers Professor of Physics, received the 1991 Buckley Prize in Condensed Matter Physics from the American Physical Society. Professor Lee was also elected Fellow to the American Academy of Arts and Sciences in May 1991. Professor Lee is a faculty member in RLE's Quantum-Effect Devices Group.

Dr. Miklos Porkolab, Professor of Physics and faculty member in RLE's Plasma Physics Group, was appointed Associate Director for Plasma Research at MIT's Plasma Fusion Center.

Dr. David E. Pritchard, Professor of Physics and faculty member in RLE's Atomic, Molecular, and Optical Physics Group, was awarded the 1991 Herbert P. Broida Prize by the American Physical Society.

Dr. William F. Schreiber, Professor Emeritus of Electrical Engineering and Computer Science, received the 1991 Gold Medal of the International Society for Optical Engineering (SPIE). Professor Schreiber was also elected a Fellow of the Society of Motion Picture and Television Engineers.

Dr. Jeffrey H. Shapiro (SB '67, SM '68, EE '69, PhD '70), Associate Department Head and Professor of Electrical Engineering and Computer Science, was elected Fellow of the Optical Society of America. Professor Shapiro is a faculty member in RLE's Optical Communications Group.

Dr. Thomas F. Weiss (SM '59, PhD '63), Professor of Electrical and Bioengineering and faculty member in RLE's Auditory Physiology Group, was appointed to the Academic Computing Council.

A faculty member in RLE's Circuits and Systems Group, ***Dr. John L. Wyatt, Jr.*** (SB '68), Professor of Electrical Engineering and Computer Science, was named the first Adler Scholar by the Department of Electrical Engineering and Computer Science.

Dr. Jesús A. del Alamo, ITT Career Development Professor and faculty member in RLE's Materials and Fabrication Group, was awarded a 1991 Presidential Young Investigator Award by the National Science Foundation.

Dr. Jacqueline N. Hewitt (PhD '86), Assistant Professor of Physics and faculty member in RLE's Radio Astronomy Group, was awarded a 1991 Presidential Young Investigator Award by the National Science Foundation.

Mr. John W. Barrett, a member of the Sponsored Research Technical Staff in RLE's Radio Astronomy Group, completed 40 years of service with the Laboratory.

Dr. Harlan Lane, a Research Affiliate in RLE's Speech Communication Group, was awarded a five-year MacArthur Foundation fellowship.

Dr. Ying-Ching Eric Yang (SM '85, PhD '89), Research Scientist in RLE's Center for Electromagnetic Theory and Applications, was selected as the 1990 Henry G. Booker Fellow of the International Union of Radio Scientists (URSI).

Appendix D. RLE Research Support Index

3M Company 33-34
Adams-Russell Electronics, Inc. 279
Alfred P. Sloan Foundation 229
Ampex 277-284
Advanced Television Research Program 277-284
American Broadcasting Corporation 277-284
Analog Devices, Inc. 239-241
AT&T Bell Laboratories 17
AT&T Foundation 33-34, 269-270
C.J. LeBel Foundation 291-301
Canada, Natural Sciences and Engineering Research Council 274
Defense Advanced Research Projects Agency (DARPA) 7-12, 17, 33-38, 47-49, 117-121, 214-217, 241-249, 261-262, 267-275
Dennis Klatt Memorial Fund 291-301
Digital Equipment Corporation 214-217, 252-253
Draper (Charles S.) Laboratory 7-8, 11-13, 19-28, 33-36, 82-83, 151-156, 267
Electronics and Telecommunications Research Institute 13
Federal Bureau of Investigation 254
Fujitsu Laboratories 19-28, 83
General Electric Foundation 272
General Instrument 277-284
GTE Laboratories 10
Hitachi Corporation 43
IBM Corporation 9-10, 43, 66, 214-217, 239-241, 250-259
Johnson and Johnson Corporation 97-99
Joint Services Electronics Program (JSEP) 7-9, 12, 14-15, 19-31, 33-41, 55-59, 61-68, 71-76, 81-82, 85-97, 125-134,137-145, 167-176, 214-217
Kodak Corporation 277-284
Lawrence Livermore National Laboratory 183-185
Leaders for Manufacturing Program 232-233
Lockheed Sanders, Inc. 269-270, 272-274
Maryland Procurement Office 109-111
Micrion 50-51
MIT Lincoln Laboratory 82-83
MIT-Woods Hole Oceanographic Institution Joint Program 267-268, 271-272
Motorola Corporation 277-284
NCIPT 7-12
National Aeronautics and Space Administration 74-75, 117-118, 187-188, 217-221, 229, 231-232
National Broadcasting Corporation 277-284
National Center for Integrated Photonics 83-86
National Institutes of Health 291-301, 305-312, 314-316, 321-328
National Institute of Standards and Technology 111-112
National Science Foundation 9-10, 13-17, 33-38 40, 42-43, 49-50, 57-59, 63-65, 70-71, 75-76, 83-86, 88-97, 109-111, 118-119, 134, 163-169, 174-176, 179-185, 188, 225-229, 241-249, 251-254, 272-273, 279-281, 291-301
Packard (David and Lucille) Foundation 229-230
Public Broadcasting System 277-284
Rockwell Corporation 267
Schlumberger-Doll Research 214-217
SEMATECH 50-51
Semiconductor Research Corporation 40-41, 65-66
SM Systems and Research, Inc. 230-231
Spire Corporation 76
Tektronix Corporation 277-284
Texas Instruments 19-28
TRW Systems 13-14
U.S. Air Force - Electronic Systems Division 157-161, 281-282
U.S. Air Force - Office of Scientific Research 66-69, 71-72, 81-82, 85-97, 114-115, 179-183, 269-271, 274-275, 281-282, 312-313
U.S. Army - Corps of Engineers 219-221
U.S. Army - Harry Diamond Laboratories 179-183
U.S. Army Research Office 15, 43-44, 50, 111-114, 170-172
U.S. Department of Energy 100-105, 179-187, 190-207
U.S. Department of Transportation 211-214
U.S. Navy - Naval Research Laboratory 50-51, 65
U.S. Navy - Office of Naval Research 34-36, 88-95, 97-99, 114, 157-160, 163-166, 170-174, 179-183, 214-217, 219-221, 250-259, 265-275, 280-282, 313-314, 316
U.S.-Israel Binational Science Foundation 188
Vertical Arrays for the Heard Island Experiment 266
Vitesse Semiconductor 9-10
Whitaker Health Sciences Fund 321-328
Zenith Corporation 277-284

Project Staff and Subject Index

Project Staff and Subject Index

A

Aalberts, Daniel P. 125, 126
Abernathy, Douglas L. 143
Acioli, Lucio H. 81, 91
Advanced Microwave Sounding Unit 230, 231
Advanced Television Research Program 277–284
Aggarwal, Rajni J. 7, 15
Agrawal, Shyam S. 291
Ahmed, Mustafa K. 179, 183
Alcator 190
Aldridge, Mary C. 81
Ali, Sami M. 211, 239, 252
Aliberti, Giovanni 265
Alkhairy, Ashraf S. 225, 232
Allen, Jonathan 239–260, 291
Allis, William P. 375
Altshuler, Boris L. 55–56, 375
Alwan, Abeer A. 291
Analog Processing
  Wavefront Correction 114
Ananthapadmanabha, Tirupattur V. 291
Ananthraman, Santosh 305
Antoniadis, Dimitri A. 33, 34, 47, 48, 57, 63, 66, 68, 71, 72, 239, 251
Apostolopoulos, John G. 277, 278
Arecibo Observatory 227
Arias, Tomas A. 137
Ariel, Imadiel 55, 61
Armstrong, Robert C. 239
Arnold, David V. 211, 217, 219
Asherie, Neer 179
Astrophysics 74
Atkins, Robert G. 211, 214, 217, 219
Atom-Beam Interferometry 63, 74
Atomic Physics 102, 163–175
Atomic Spectroscopy 101
Atoms
  Diffraction of 170
  Structure in Magnetic Fields 163
AT&T Bell Laboratories 117
Au, William W. 211, 217, 219
Auditory Physiology 321–328
Auditory System 328
  Otoacoustic Emissions 326
  Signal Transmission 321–328
Awano, Yuji 19
Ayazifar, Babak 277, 278
Azzam, Ziad 33

B

Bace, Matthew M. 277, 279
Bach, Susan E. 305
Baggeroer, Arthur B. 265, 375
Bahl, Sandeep R. 19
Bai, Kelly S. 239, 254
Ballentine, Craig 39, 43
Baltus, Donald G. 239
Balzer, Janice L. 321
Barrett, John W. 211, 225, 230, 231, 232, 376
Barsukov, Vladimir M. 291
Barwick, D. Shane 109, 114
Basu, Santanu 81, 101, 103, 375
Baylon, David M. 277, 279
Beach, Kerry L. 291
Beckmann, Paul E. 265, 267
Bekefi, George 179, 180–183
Belk, Paul A. 57
Bennett, Brian R. 19
Berberian, John E. 163, 170
Berglund, Alice M. 321
Bergman, Keren 81, 83
Berker, A. Nihat 125–128
Berkovits, Richard 55
Bers, Abraham 179, 183–189, 375
Besing, Joan M. 305
Betti, Riccardo 179, 190
Bhatta, Saurav Dev 265, 267
Bickley, Corine A. 291
Bierbaum, Michele M. 81, 100
Binder, Bradley T. 109, 112
Biomechanics
  Skin 314, 316
Birgeneau, Robert J. 129–131, 143, 375
Blum, Kenneth I. 129, 143
Bogomolov, Sergei 39, 43
Bonet i Alsina, M. Eulalia 331
Bose, Amar 375
Bossi, Donald E. 115
Boyce, Kevin R. 163, 174
Boyce, Suzanne E. 291
Brady, Felicia G. 179, 180
Braida, Louis D. 305, 308
Brandstein, Michael S. 277, 280
Braud, John Paul 81, 103
Brillouin Scattering 153
Bristowe, Paul D. 39, 42, 75
Broekaert, Thomas P.E. 7, 14, 15
Brookhaven National Laboratory 129
Brothers, L. Reginald 109, 111
Brothers, Margery E. 211

Buck, John R. 265, 268
Burke, Bernard F. 225–228
Burkhardt, Martin 63, 68, 71
Burns, Geoffrey F. 7, 9

C

Cain, Gerald R. 133
California Institute of Technology
  Jet Propulsion Laboratory 220, 221
Canizares, Claude R. 74
Carel, Roland 39, 42, 75
Cariani, Peter A. 321, 324
Carlisle, Ellen 321
Carter, James M. 63, 72, 74
Catravas, Palmyra E. 179, 180
Catunda, Tomaz 163
Ceyer, Sylvia T. 7, 17, 133–135, 375
Chalcopyrite 126
Chalom, Edmund 225
Chamon, Claudio D.C. 95
Chang, Hwa-Ping 291
Chang, Pin P. 163, 167
Channel Dropping Filter 72
Chaos 269, 271, 272
Chari, Venkatesh R. 291
Chaudhary, Irfan U. 81, 105
Chemical Beam Epitaxy 33
Chen, Belinda 305
Chen, Chiping 179, 180
Chen, George C. 33
Chen, Grace H. 225, 229
Chen, Jerry C. 81
Chen, Jyh-Shing 305, 316
Chen, Marilyn R. 291
Chen, Shien-Chi 179, 180
Cheng, Lisa Lai Shen 332
Cheng, Tak K. 86, 87
Cheung, Shiufun 277, 280
Chiang, Tony P. 47, 50
Cho, Kyeongjae 137
Choi, Woo-Young 7, 11, 12, 13, 14, 72
Chomsky, Noam A. 331–337
Chou, Mike T. 63, 72
Chow, Carson C. 179, 183
Christian, Kevin G. 225, 232
Chu, Alex 48
Chu, Larry 48
Chu, William 47, 63, 68, 70, 72
Chuang, Isaac L. 81, 105
Chung, Daniel J.H. 179, 180
Chung, James 48, 66
CMOS 242
Cochlear Implant Laboratory
  See Massachusetts Eye and Ear Infirmary (MEEI)
Cochlear Implants 308
Colborn, Jeffrey A. 179, 204
Cold Fusion 105
Communications
  See Optical Communication
  See Sensory Communication
  See Speech Communication
  See Telecommunications
Computer Vision 241–250
  Hardware 241
  Image Processing 241
Computer-Aided Design 239–260
Conde, Manoel E. 179, 180
Conner, Samuel R. 225
Cooperman, Steven S. 39, 63
Coppi, Bruno 179, 190–203, 376
Corcoran, Christopher J. 109, 114
Cornell University
  National Nanofabrication Facility 171
Coronado, Christopher A. 33
Costa, Carol A. 163
Coulomb Blockade 61, 66
Courtney, Michael W. 163
Coutu, Pierre 211, 217, 219
Cuneo, Patricia A. 321
Cuomo, Kevin M. 265, 269
CVI Incorporated 90

D

Dal Pino, Arnaldo 137
Daley, Sean P. 133, 134
Dally, William 253
Damask, Jay N. 33, 72, 81, 84
Dana, Kristin J. 321, 323
Dandekar, Kiran B. 305, 314
Davis, Charles Q. 321, 323
Davis, Kendall 163, 172
Decker, Steven J. 239, 241, 246
Dehmelt, Hans 175
del Alamo, Jesús A. 19, 68, 70, 118, 375, 376
Delcroix, Jean-Loup 179, 183
Delgutte, Bertrand 321, 324, 325
Delhorne, Lorraine A. 305, 308, 311, 313
Delisle, John T. 225, 232
Della Ratta, Anthony D. 39, 43, 47, 51
Demirdache, Hamida K. 332
Devadas, Srinivas 239, 254–260
DiFilippo, Frank 163, 174
Digital Signal Processing 265–275
Distributed-Feedback Laser 72
Dix, Ann K. 305
Doan, Jonathan C. 179, 180
Doerr, Christopher R. 81, 83

Dolphins
Communication 232
Donoghue, John J. 151
Donovan, Kelley S. 7, 19, 33
Dougherty, David J. 81, 86
Doughty, Francis M. 261
Doughty, Laura B. 179
Dron, Lisa G. 239, 241, 248
Dubner, Andrew D. 39, 43
Ducas, Theodore W. 163, 167
Duchnowski, Paul 305
Durlach, Nathaniel I. 305, 307, 309, 311, 313
Dynes, Scott B.C. 321, 325

E

E-Beam Lithography 65
Ear 321—328
See also Hearing
Cochlear Implants 308
Evolution 321
Middle Ear 321
Muscles 326
Stapedius 326
Early, Kathleen R. 63
Eaton-Peabody Laboratory for Auditory Physiology 321
Eddington, Donald K. 305, 308, 309, 321, 327
Ehrenrich, Victor 16
Ehsani, Farzad 321, 323
Einstein Rings 226
Ekstrom, Christopher R. 163, 170
Electron Irradiation Beams 179
Electron Transport 104
Electron Waveguide 70
Electronic Conduction Models 126
Electronic Devices
Semiconductors 57
Si MOSFETs 57
Superconductors 117
Electronic Materials
Field-Effect Transistors 19
Heterostructures 19
InGaAs 19
InP 19
Quantum Heterostructures 7
Semiconductors 33, 63
Submicron Structures 63
Superconductors 29
Thin Films 39
Microstructural Evolution 39
Elfadel, Ibrahim M. 239, 241
Ellithorpe, John D. 225, 229
Elman, B. 10
Englade, Ronald C. 179, 190
Epitaxy 75
Crystal Growth 137
Ernst, Darin 179, 190
Eshghi, Kamyar 239, 241
Espy-Wilson, Carol Y. 291
Etchin, Sergey 47, 48, 49, 50
Eugster, Cristopher C. 63, 70, 118
Ezekiel, Shaoul 151—161

F

Faas, Michael 55
Failla, Anton 7, 9
Falicov, Alexis 125
Fang, Hao 63, 66
Ferrera, Juan 63, 65
Fiber Optics
Gyroscopes 151, 153
Fieguth, Paul W. 225, 232
FIR Absorption 71
Fitzgerald, Edward W. 179, 204
Fleischer, Dorothy A. 239
Fleischer, Siegfried B. 86, 87
Fleming, Robert C. 63, 74, 75
Fletcher, André B. 225
Floro, Jerrold A. 39, 42, 63, 75
Focal-Plane Detector Arrays 117
Focused Ion Beams 47—52
Fonstad, Clifton G., Jr. 7—18, 72, 84, 120
Foxman, Ethan B. 57
Fractals 270, 274
Freeman, Charles G. 163, 172
Freeman, Dennis M. 321, 323
Freyman, Richard L. 305
Friedland, Lazar 179, 183
Frisbie, Joseph A. 305
Frishkopf, Lawrence S. 321, 323
Frost, Harold J. 39, 40, 42
Frustration 126
Fuchs, Eric M. 305, 313
Fuchs, Vladimir 179, 183
Fujimoto, James G. 7, 81, 88—99
Fusion 190

G

GaAs Epitaxy 76
Gabetta, Guiseppe 81, 88
Gafney, Kerry L. 179
Gage, Deborah A. 265
Gaidos, Eric J. 225
Gale, Donna L. 81

Gantela, Swaroop 305
Garcia, Edouard A. 117, 120
Gas Source Molecular Beam Epitaxy 33
Ghanbari, Reza A. 63, 68, 71
Ghosh, Abhijit 258
Ghosh, Rajashi 305
Goldhor, Richard S. 291
Goldman, Susan L. 305
Golubovic, Boris 109, 115
Goodberlet, James G. 81, 101
Grant, Andrew H. 305
Grant, Kenneth W. 305
Gravitational Lenses 229
Graybeal, John M. 29–31, 73
Green, Thomas J., Jr. 109, 112
Greenberg, Julie E. 305, 307
Griffith, Mark R. 225, 227
Grimm, James A. 163, 174
Gu, Qizheng 211
Guinan, John J., Jr. 321, 326
Gulati, Rogeve 305
Gunn Diodes 47, 48
Gupta, Rajesh K. 117, 119
Gyroscopes
  Fiberoptic 151, 153
  Laser 151, 153

H

Hagelstein, Peter L. 81, 99–107
Hailes, Darby A. 305
Hajjahmad, Ibrahim A. 277, 281
Hakkarainen, Mikko 239, 241, 244
Hall, Katherine L. 81, 85
Hall, Seth M. 291, 305
Halle, Morris 291, 331–337
Hammond, Troy D. 163, 170
Han, Hsiu C. 211, 214, 217, 219
Hanson, Helen M. 291
Hara, Toru 179, 180
Hara, Yoshihisa 211, 219
Hardwick, John C. 277, 281
Harring, Debra L. 277
Harris, John G. 239, 241
Hartney, Mark A. 50
Haus, Hermann A. 7, 11, 33, 34, 72, 81–85, 88, 95, 376
Hearing 305–318, 321–328
  See also Ear
  Binaural 309, 310
  Cochlear Implants 327
Hearing Aids 305, 307
  Cochlear Prostheses 308
Hearing-Impaired Individuals 292, 296, 299, 305–318, 321–328
Hearing-Impaired Individuals *(continued)*
  Tactile Aids 305, 311
Hector, Scott D. 63
Hedgcock, John M. 305
Hee, Michael R. 81, 97
Heflin, Michael B. 225
Held, Richard M. 305, 313
Helmerson, Kristian 163, 172
Hemmer, Philip R. 151
Herold, Lori K. 225
Heron, Peter C. 39
Herrman, Frederick P. 239, 241
Heterodyne Receivers 117
Hewitt, Jacqueline N. 225, 229–230, 376
Heytens, Michael L. 261
High-Definition Television (HDTV) 277–284, 285–286
High-Tc Superconducting Josephson Devices 119
Hillman, Robert E. 291
Ho, Easen 33
Ho, Michael S. 225, 230
Hoffman, Mika C. 333
Hogarty, Sean T. 211, 213
Holden, Timothy A. 298
Holley, Jeffrey R. 163, 167
Holmberg, Eva B. 291
Holographic Lithography 63
Hon, Stephen Y. 81
Hong, Albert G. 305
Hopps, J.H. 12
Horn, Berthold K.P. 239, 241, 242, 245, 248
Horowitz, Paul 227
Hoshino, Isako 7, 17
Hoston, William C., Jr. 125, 126
Hot Electrons 66
Hou, Mary A. 305
Hsu, Chih-Chien 211, 213, 217, 219
Hu, Hang 63, 66
Hu, Qing 15, 117–122, 375
Hu, Wenian 179, 180
Huang, Caroline 291
Huang, David 81, 88, 91, 97
Huang, Gregory T. 211
Huber, Carmen 33
Huffman, Marie K. 291
Hultgren, Charles T. 81, 86
Human-Machine Interfaces 312
Hung, Tsen-Yu 103
Hunter, Wendy E. 225
Hurricane Bob 232
Huxley, Janice M. 81, 82

I

Iatridou, Sabine 333
IBM Corporation 117
  Thomas J. Watson Research Center 63
II-VI Semiconductors 33
Image Processing 265–275
Induced Stochasticity and Chaos 183
Inglefield, Heather E. 39, 43
Institute for Telecommunication Sciences 230
Integrated Circuits 39, 63
  Circuit Design 261
  Computer-Aided Design 239–260
  Computer-Aided Fabrication 261
  Custom 239–260
    Fault Tolerance 254
    Reliability 239–260
  Process Flow Representation 261
  VLSI 7, 9
Interferometry
  Atom Wave 170
Ion
  Focused Ion Beams 47–52
Ippen, Erich P. 7, 81–88, 91
Isabelle, Steven H. 265, 269
Ismail, Khalid 63, 76
Ison, Anna 291
Iu, Chun-ho 163
Iwai, Kyle K. 261
Izatt, Joseph A. 81, 97

J

Jablonski, Mark K. 179, 183
Jachner, Jacek 265, 270
Jackson, Michel T. 291
Jacobson, Brian R. 117
Jacobson, Joseph M. 81, 88
Jerby, Eli 179, 180
Jha, Pallavi 179, 180
Jiao, Hong 163
Joannopoulos, John D. 137–142
Joffe, Michael A. 163, 172
Johnson, Andrew D. 134
Johnson, Joel T. 211, 217, 219
Johnson, Mark A. 291
Joneckis, Lance G. 109
Jones, R. Victor 16
Joo, Young-Chang 39, 41
Jordan, Arthur 211
Josephson Junctions 29

K

Kahn, Harold 39, 40, 63
Kamon, Mattan 239, 254
Karam, Nassar 76
Kärtner, Franz X. 81, 83
Kashani, Abbas 261
Kastner, Marc A. 57–59, 61, 66
Katz, Charles A. 225, 229
Kaushik, Sumanth 81, 105
Kazior, Thomas 49
Kearns, Katherine Susan 333
Keast, Craig L. 239, 241, 243
Keith, David W. 163, 170
Ketterle, Wolfgang 163, 172
Keutzer, Kurt 255, 258
Keyser, Samuel J. 291
Khatri, Farzana I. 81
Khohayting, Jerome S. 211
Kiang, Nelson Y.S. 321
Kierstead, John D. 151
Kim, Che Y. 211
Kim, M. 13
Kim, Songmin 239, 252
Kim, Sue O. 291
Kinaret, Jari M. 61
King, Barbara A. 109
Kleppner, Daniel 163–170, 376
Klipple, Elizabeth Mary 334
Knecht, Wolfgang G. 305, 307
Knowlton, Brett D. 39, 41
Ko, Weng-Yew 261
Kobler, James B. 326
Koehnke, Janet D. 305
Kolodziejski, Leslie A. 33–38, 72, 375
Kong, Jin Au 211–222
Kopf, Cynthia Y. 81
Kotik, Jack 305
Ku, Yao-Ching 63, 65
Kukula, James H. 239, 254
Kumar, Arvind 63, 66
Kupfer, Kenneth C. 179, 183

L

Lahiri, Utpal 335
Lai, Kit-Wah F. 211
Lai, Yinchieh 81, 82
Lam, Cheung-Wei 211, 214
Lam, Warren M. 265, 270
Lan, Andrew E. 117
Lane, Harlan 291, 376
Larson, Sarah L. 211
Laser Gyroscopes 151–156

Laser Physics
Theory 102
Laser Plasma 101
Laser-assisted Epitaxy 36
Lasers 151—161
Additive Pulse Modelocking 88
Diode 114
Femtosecond Pulses 88
Free Electron 179—183
Medical 97
Semiconductor
Arrays 114
External Cavity 114
X-Ray 100, 101, 103
Lashmore-Davies, Christopher 179, 183
Lattice-Nuclear Interactions 105
Lau, Suzanne D. 109, 115
Lauritzen, Lisbeth N. 81
Law, Paul S. 335
Le, Huy X. 117
Leary, Michael H. 19
LeBlanc, Cindy 277
Leder, Harry 336
Lee, David S. 33
Lee, Dicky 109, 111
Lee, Eddie F. 277, 282
Lee, Hae-Seung 239, 241, 244, 245
Lee, Hongsing 211, 214
Lee, Jae-Jin 7, 13
Lee, Patrick A. 61—62, 376
Leeb, Steve 239, 251
Lehár, Joseph 225
Leigh, Darren L. 225, 232
Lenz, Gadi 81, 85
Levy, Ady 63
Lezec, Henri J. 47, 48
Li, Kevin 211
Li, Yulin 133
Liao, Kenneth S. 47, 48
Liao, Stan Y. 239, 254
Liebe, H.J. 230
Lieu, Anh 211
Lim, Harold H. 211, 217, 219
Lim, Jae S. 277—284
Lim, Michael H.Y. 63, 305
Lin, Charles P. 81, 97
Lin, Wei Ming-Yu 211
Linguistics 331—337
Lithography
Focused Ion Beams 47, 50
Litster, J. David 375
Liu, Ya-Chin 39, 63
Liu, Yong 211, 213
Lloyd, Jennifer A. 239, 251
Locke, John 291
Lohman, Thomas J. 261
Longworth, Hai P. 39, 41, 63
Lorusso, Catherine 179
Lumsdaine, Andrew 239, 246, 250, 253
Luongo, Eleanora M. 305
Lutwak, Robert P. 163, 167
Lyubomirsky, Ilya 211, 214

M

Ma, En 39, 43
Ma, Sandra Y. 305
Macmillan, Neil A. 305
Magnetic Fields
Atomic Structure in 163
Magnons 126
Mahoney, Leonard J. 48
Makhoul, John I. 291
Malik, Sharad 255
Manuel, Sharon Y. 291
Manufacturing Processes 232
Marjanovic, Matthew J. 163, 174
Martin, Alexander 163, 172
Martin, David R. 239, 241
Martin, Gregory R. 305
Martin, Paul S. 7, 11, 84
Martinez, Donna R. 47, 63
Martinez, Wilberto 261
Massachusetts Eye and Ear Infirmary (MEEI)
Cochlear Implant Laboratory 321
Eaton-Peabody Laboratory for Auditory Physiology 321
Massachusetts General Hospital
Wellman Laboratories of Photomedicine 97
Mastovsky, Ivan 179, 180
Matthies, Melanie L. 291
Mayfield, Laura 291
McCabe, Margaret M. 151
McCue, Michael P. 321, 326
McEuen, Paul L. 57
McIlrath, Michael B. 261
McQuirk, Ignacio S. 239, 241, 245
Meade, Robert D. 137
Mecozzi, Antonio 81, 82
Meir, Yigal 61
Melcher, Jennifer R. 321
Melngailis, John 39, 43, 47—52, 375
Mentle, Robert E. 109, 112
Merchant, S.N. 322
Meskoob, B. 13
Metalorganic Molecular Beam Epitaxy 34
Mewes, Marc-Oliver 163, 170
Meyerson, Bernard S. 29, 73
Microfabrication 63
Microwave Temperature Sounder 232

Migliuolo, Stefano 179, 190
Mikkleson, J. 9, 10
Millimeter Waves 117
Min, Wei 305, 313
MIT Center for Electromagnetic Theory and Applications 211
MIT Lincoln Laboratory 50, 94, 327
  Laser Radar Measurements Group 113
  Optical Communications Group 98
  Opto-Radar Systems Group 113
MIT Plasma Fusion Center 206
MIT Submicron Structures Laboratory 63
Mitchell, David 163
Miura, Hideo 39, 43
Mizuno, Takahide 179, 180
Mochrie, Simon G.J. 129, 143—145
Moel, Alberto M. 63, 70
Moldoveanu, Michael C. 179, 183, 211, 214
Mondol, Mark K. 63, 65
Monta, Peter A. 277, 282
Moolji, Akbar A. 19
Moon, Euclid E. 63, 70
Moores, John D. 81, 82
Morgenthaler, Ann W. 81, 104
Morshidi, Wan 163, 172
MOSFET 66
Muendel, Martin H. 81, 100
Munguia, Pablo 63
Musicus, Bruce R. 265, 267
Musil, Christian R. 47, 48

N

Nabors, Keith S. 239, 252
Naganuma, Kazunori 81, 85
Nam, Jean O. 211
Nanto, Hidehito 33
Narula, Aradhana 277, 282
Nassi, Giulia Arman 291
Nassi, Marco 179, 190
Natarajan, Vasant 163, 174
National Synchrotron Light Source 129, 143
Nd:Glass 100
Nee, Phillip T. 109, 111
Nelson, Lynn E. 81, 82
Nelson, Susan E. 239
Nenonen, Seppo 63, 75
Netz, Roland R. 125, 126
New England Medical Center
  New England Eye Center 97
Ng, Lee-Peng 63, 65, 163
Nghiem, Son V. 211, 217, 219
Nicolas, Julien J. 277, 283
Njeru, James M. 265, 271
Noh, Do-Young 129
Noise
  Chaotic Signals 275
  in Fiber Optic Systems 109
Nonlinear Waves in Plasmas 183
North, D. Keith 291
Nuttall, William J. 129

O

Oates, John H. 211, 214
Ocean Acoustics 265
Odoardi, Angela R. 7, 19, 33
Ogno, Alexa 305
Olster, Daniel B. 63, 74
Oppenheim, Alan V. 265—275
Optical Communication 109—115
  Devices 7—18
  Squeezed States 109
Optical Devices 34
Optics 79—88, 107
  See also Optical Communication
  Guided-Wave 95
  Integrated 114
  Photosensitive Materials 91
Orlando, Terry P. 66, 68, 71
O'Handley, Robert C. 39, 43
O'Neill, Kevin 211

P

Paine, Scott N. 163, 167
Pan, Janet L. 81
Pang, Xiao Dong 305, 307, 313
Papadopoulos, Haralabos C. 271
Park, Jong Tae 7
Park, Sang H. 33
Parkes-MIT-NRAO (PMN) Southern Hemisphere Survey 227
Patel, Prashun R. 305
Payton, Karen L. 305
Peake, William T. 321
Pedersen, Torstein 291
Peng, Lung-Han 7, 16
Penn, Greg 179
Perilli, Richard R. 7
Perkell, Joseph S. 291
Persistent Current 55
Peterson, Patrick M. 305
Petro, Michael C. 225
Phase Transitions 126, 129
Pheiffer, Brian K. 109, 115
Photo-assisted Epitaxy 36

Photon-assisted Quantum Transport 118
Physiological Acoustics 321–328
Pickelsimer, Lisa A. 239
Plasma Collective Modes 198–203
Plasma Ignition 190
  Confinement 194
Plasma Physics 179–207
  RF Heating and Current Drive 183
  Thermonuclear Plasmas 190
  Tokamaks 190
Plasma Theory 104
PMOS 66
Poggio, Tomaso 239, 241, 242
Poh, Soon Y. 211
Polley, Michael O. 285
Porkolab, Miklos 179, 204–207, 376
Porter, Jean P. 63
Power, Matthew H. 305
Prasad, Sheila 7, 13
Preisig, James C. 265, 272
Prentiss, Mara G. 151
Princeton University 255
Pritchard, David E. 163, 170–175, 376
Pullman, David P. 133
Puria, Sunil 321, 322

Q

Quantum Dot 55, 61, 71
Quantum Hall Effect 61
Quantum Spin Systems 125, 126
Quantum Studies
  Optics 109
Quantum Wires 68
Quirch, Jo-Ana 225

R

Rabinowitz, William M. 305, 307, 308, 311, 313, 321, 327
Radar
  Infrared 112
  Synthetic Aperture 219
Radiation
  Interaction with Matter 157–161
Radio Astronomy 225–233
Rahmat, Khalid 239, 251
Rajan, S.D. 267
Ram, Abhay K. 179, 183
Ramaswamy, Malini 81, 88
Ramsey, Norman 175
Ramstad, Monte J. 129
Rankovic, Christine M. 305
Rappe, Andrew M. 137
Raytheon Corporation 49
Rediker, Robert H. 109, 114–115
Reed, Charlotte M. 305, 311
Reichelt, Mark W. 239, 250, 253
Reisman, Charles A. 305
Resonant Tunneling 61, 72
  Device 29
Richard, Michael D. 265, 272
Richey, Michael T. 305, 311
Rigopulos, Alexander P. 305
Ringo, Carol C. 291
Rittenhouse, George E. 29, 63, 73
Ro, Jaesang 39, 43, 47, 50
Rogers, Barrett 179
Roman, Barbara A. 211, 213
Ronan, Diane E. 305
Rosenkranz, Philip W. 225, 230, 231, 232
Rosowski, John J. 321, 322
Royter, Yakov 7, 11, 12
Rubin, Brian A. 305
Rubinstein, Jay T. 321, 327

S

Saddy, James Douglas 337
Salvucci, Elizabeth M. 129
Sandhu, Sumeet 305
Sawin, Herbert H. 17
Schattenburg, Mark L. 63, 65, 70, 74, 75
Scherock, Stephen F. 265, 273
Schiedmeyer, H. Joerg 163, 170
Schmidt, Martin A. 254
Schreiber, William F. 285–286, 376
Schultz, Steven D. 179, 183
Schwartz, Michael J. 225, 231, 232
Sciutto, Giampiero 277
Seidel, Mark N. 239, 241, 244
Semiconductor Alloys 126
Semiconductor Materials
  Chemical Beam Epitaxy 33
Semiconductors 57
  Compound 19
  Etching 133
  Surface Analysis 125, 129, 137–142, 143
  Surface Chemistry 133
Sensory Communication 305–318
Senturia, Stephen D. 239, 254
Shahriar, M. Selim 151
Shao, Michael 225
Shapiro, Jeffrey H. 109–114, 376
Shattuck-Hufnagel, Stephanie R. 291
Shaver, D.C. 50
Shayegan, M. 71

Sheen, David M. 211, 214
Shen, Amelia H. 239, 254
Shenoy, Krishna V. 7, 9, 10
Shepard, Mark I. 47
Shepard, Scott R. 109
Shimase, Akira 47, 48
Shin, Robert T. 211, 213, 217, 219
Shinn-Cunningham, Barbara G. 305, 313
Shirasaki, Masataka 81, 83
Shue, Chung-Hao 33
Shvets, Gennady 179, 180
Siebert, William M. 321
Signal Processing 7, 232, 265—275, 277—284, 327
Silber, Ronnie 291
Silveira, Luis M. 239, 246, 251, 253
Singer, Andrew C. 265, 274
Singer, Richard A. 7, 8
Single Electron Transistors 57
Skinner, Margaret W. 298
Slab Amplifier 100
Smet, Jurgen H. 7, 15, 16, 117, 120
Smith, Clare F. 225
Smith, Henry I. 29, 33, 34, 50, 57, 63—78, 84
Smith, Stephen P. 151
Snitzer, Elias 151
Sodini, Charles G. 239, 241, 243, 246
Solid-State Far-infrared (THz) Lasers 120
Sosonkina, Jane 47, 51
Spectroscopy
  Millimeter Wave 167
Speech Communication 291—301, 311
Speech Perception 292
Speech Physiology 291
Speech Processing 291
  Spectrograms 280
  Vocoders 280, 281
Speech Production 292, 295
  German language 295
  Hearing-Impaired Individuals 299
Speech Reception 305—318
Spiesberger, John L. 271
Squire, Jared P. 179, 204
Srinivasan, Mandayam A. 305, 311, 313, 314, 316
Stadler, Robert W. 305, 307
Staelin, David H. 225, 230—233
Standley, David L. 239, 241
Stannite 126
Stanton, C.J. 94
Stefanov-Wagner, Frank J. 321
Steffens, David A. 321
Stellmach, Timothy J. 305
Stevens, Kenneth N. 291—301
Stollerman, Anne 133
Stoner, Richard E. 179, 180
Structural Analysis
  Synchrotron Radiation 143
Su, Lisa T-F. 63, 66
Sugiyama, Linda E. 179, 190
Sun, Chi-Kuang 95
Sun, Ke-Xun 109
Sunshine, Lon E. 277, 279, 283
Superconducting Devices 29, 73
  Intersubband Transitions 117
  Resonant-tunneling Device 29
Superconductors 29, 117
Surface Superlattice 68
Surfaces
  Structural Analysis 129
  Surface Chemistry 133
Svirsky, Mario A. 291, 375
Synopsys, Inc. 255
Szafer, Aaron 55

T

Tactile Sense 315
Tamura, Kohichi R. 81, 82
Tan, Hong Z. 305, 311
Tassel, Karl Van 33
Tassoudji, M. Ali 211, 213, 219
Taylor, Colin J. 179, 180
Telecommunications 19
Television
  High-Definition 277—284, 285—286
Telichevsky, Ricard 239, 253
Thin Films 39, 129
Thompson, Carl V. 39—45, 47, 50, 75
Thompson, Clay M. 239, 241
Tierney, Joseph 327
Ting, Leon L. 305
Tokamaks 190
  Versator II 204—207
Traill, Anthony 291
Transistors
  Single Electron 57
Trautman, Theodore R. 133, 134
Troxel, Donald E. 261
Tsai, Flora S. 63, 65
Tsui, Daniel 71
Tufts University 91
Turchette, Quentin A. 163, 170
Tuyo, Michael T. 305

U

Uchanski, Rosalie M. 305
Uda, Takauki 39, 43

Ulman, Morrison 81, 91
Umminger, Christopher B. 239, 241, 246
Underwater Acoustics 265, 266
Upshaw, Bernadette 291
Utz, Arthur L. 133, 134

V

Vacca, Luigi 179, 183
Van Aelten, Filip J. 239, 254
Velazquez, Scott R. 117, 119
Veysoglu, Murat E. 211, 217, 219
Video Detectors 117
Vignaud, Dominique 47, 48
Villasenor, Jesus Noel 179, 204
Visible Light Emitters 34
Vision Chip Designs 242
VLA 227
Vlcek, James C. 7, 13
VLSI 239, 244
  Analog 241
Volfbeyn, Pavel P. 179, 180

W

Wage, Kathleen E. 265
Wagner, A. 39, 43
Walton, Derek T. 39, 40, 42
Wang, Albert 255
Wang, Jing 137
Wang, Li-Fang 211
Washington University School of Medicine 298
Webster, Jane 291
Wee, Susie J. 285
Weinstein, Ehud 265, 268
Weiss, Thomas F. 321–328, 376
Whisper-Gallery Mirrors 103
White, Jacob 239, 250–254, 258, 375
Wilde, Lorin F. 291
Williams, David 291
Williams, Monnica J. 291
Wind, Shalom 57
Wingree, Ned S. 61
Wint, Arlene E. 291
Wisconsin, University. Center for X-Ray Lithography 50
Wolff, Peter A. 375
Wong, Ngai C. 109–114
Wong, Taylen J. 265
Wong, Vincent V. 63, 72, 84
Wood, Sasha K. 179, 180
Wornell, Gregory W. 265, 270, 271, 274, 375
Wright, Alan 225, 227
Wurtele, Jonathan S. 179, 180
Wyatt, John L., Jr. 239, 241–250, 376
Wyss, Rolf A. 117, 118

X

X-Ray Lasers 100, 101, 103
X-Ray Lithography 63
X-Ray Mask 65
X-Ray Scattering 143
X-Ray Spectroscopy 74
X-Ray Window 75
Xia, Jiqing 211, 214
Xu, Xin 47, 51

Y

Yamaguchi, Masanori 211
Yang, Julius J. 133
Yang, Ying-Ching E. 211, 213, 219, 375, 376
Yee, Kenneth 63, 76
Yen, Anthony 63
Yesley, Peter S. 163, 172
Yoo, Chang Dong 277, 284
Yu, Paul C. 239, 241
Yu, Peter T. 109
Yuan, Yi 211, 213
Yueh, Herng A. 211, 217, 219
Yuksel, Ayca 33
Yunus, Sabah 63, 65

Z

Zakharov, Leonid E. 179, 190
Zamdmer, Noah D. 117
Zangi, Kambiz C. 265, 275
Zarinetchi, Farhad 151
Zhao, Yang 63, 71
Zhu, Meng Y. 321
Zincblende 126
Zissman, Marc 327
ZnSe 34
Zue, Victor W. 305
Zurek, Patrick M. 305, 307, 309, 310

RESEARCH LABORATORY of ELECTRONICS
MASSACHUSETTS INSTITUTE OF TECHNOLOGY
CAMBRIDGE, MASSACHUSETTS 02139

RLE Publications Update
January — June 1992

This list includes many of the journal articles, conference papers, chapters in books, theses, and RLE technical reports published by the various research groups within RLE during the period January through June 1992. • Publications listed in the General Interest section as well as technical reports distributed throughout this *Update* are available from the RLE Communications Office. Please use the order form on the last page. • Theses and dissertations are available from the MIT Microreproduction Laboratory, Room 14-0551, Cambridge, Massachusetts 02139-4307. • Other publications may be requested directly from the authors listed.

General Interest

RLE Brochure. Research Laboratory of Electronics, MIT, 1991. 72 pp. $6.50.

RLE Progress Report No. 134: January - December 1991. Research Laboratory of Electronics, MIT, 1992. 400 pp. No charge.

RLE Technical Reports, 1946-1991. Research Laboratory of Electronics, MIT, 1991. 26 pp. $4.00.

Advanced Television and Signal Processing

"Combined Multiresolution (Wide-Band/Narrow-Band) Spectrogram," by S. Cheung and J.S. Lim. *IEEE Trans. Signal Process.* 40(4): 975-977 (1992).

"Design of an HDTV System," by J.S. Lim. Paper presented at the DARPA Meeting, Washington, D.C., January 14-16, 1992. *Error Concealment Techniques for an All-Digital HDTV System*, by A. Narula. S.M. thesis. Department of Electrical Engineering and Computer Science, MIT, 1992.

"Pel-Adaptive Model-Based Interpolation of Spatially Subsampled Images," by B. Ayazifar and J.S. Lim. Paper presented at the IEEE International Conference on Acoustics, Speech, and Signal Processing, San Francisco, California, March 23-26, 1992.

Atomic, Molecular, and Optical Physics

"Laser and rf Spectroscopy of Magnetically Trapped Neutral Atoms," by K. Helmerson, A. Martin, and D.E. Pritchard. *J. Opt. Soc. Am. B* 9(4): 483-492 (1992).

Measurement of the Rydberg Frequency Using Circular Rydberg States of Atomic Hydrogen, by P.P. Chang. Ph.D. diss. Department of Physics, MIT, 1992.

"Two Ions in a Penning Trap: Implications for Precision Mass Spectroscopy," by E.A. Cornell, K.R. Boyce, D.L.K. Fygenson, and D.E. Pritchard. *Phys. Rev. A.* 45(5): 3049-3059 (1992).

Auditory Physiology

"The Acoustic Input Impedance of the Stapes and Cochlea in Human Temporal Bones," by S.N. Merchant, M.E. Ravicz, and J.J. Rosowski. Poster presented at the Association for Research in Otolaryngology Meeting, 15th, St. Petersburg, Florida, February 2-6, 1992.

"Middle-ear Transmission: Acoustic Versus Ossicular Coupling in Cat and Human" by W.T. Peake, J.J. Rosowski, and T.J. Lynch III. *Hear. Res.* 57: 245-268 (1992).

Circuits and Systems

"Analog VLSI for Robot Vision," by J.L. Wyatt, Jr. Paper presented at the DARPA Semi-annual Contractors Meeting, Salt Lake City, Utah, January 6-7, 1992.

"Analog VLSI for Robot Vision," by J.L. Wyatt, Jr. Paper presented at the DARPA Workshop on Computational Sensors, Philadelphia, Pennsylvania, May 11-12, 1992.

Automatic Procedures for the Behaviorial Vertification of Digital Designs, by F. Van Aelten. Ph.D. diss. Department of Electrical Engineering and Computer Science, MIT, 1992.

"Compositional Verification of Systems with Synchronous Globally Timed Control," by F. Van Aelten, J. Allen, and S. Devadas. Paper presented at the MIT/Brown Conference on Advanced Research in VLSI and Parallel Systems, Providence, Rhode Island, March 25-27, 1992.

"Event Suppression: Improving the Efficiency of Timing Simulation for Synchronous Digital Circuits," by S. Devadas, K. Keutzer, S. Malik, and A. Wang. Paper presented at the MIT/Brown Conference on Advanced Research in VLSI and Parallel Systems, Providence, Rhode Island, March 25-27, 1992.

A Formal Approach to Incremental Consistency Maintenance in Multirepresentation VLSI Databases, by R.C. Armstrong. Ph.D. diss. Department of Electrical Engineering and Computer Science, MIT, 1992.

Theoretical and Practical Aspects of Parallel Numerical Algorithms for Initial Value Problems, with Applications, by A. Lumsdaine. Ph.D. diss. Department of Electrical Engineering and Computer Science, MIT, 1992.

"VLSI Computer-Aided Design," *RLE currents* 5(2): (1992). 24 pp. No charge.

Digital Signal Processing

Adaptive Matched Field Processing in an Uncertain Propagation Environment, by J.C. Preisig. RLE TR No. 567. Research Laboratory of Electronics, MIT, 1992. 173 pp. $17.00.

Adaptive Matched Field Processing in an Uncertain Propagation Environment, by J.C. Preisig. Ph.D. diss. Department of Electrical Engineering and Computer Science, MIT, 1992.

"Codebook Prediction: A Nonlinear Signal Modeling Paradigm," by A.C. Singer, G.W. Wornell, and A.V. Oppenheim. Paper presented at the IEEE International Conference on Acoustics, Speech, and Signal Processing, San Francisco, California, March 23-26, 1992.

"Computer-Aided Algorithm Design and Rearrangement," by M.M. Covell, C.S. Myers, and A.V. Oppenheim. In *Symbolic and Knowledge-Based Signal Processing*. Eds. A.V. Oppenheim and S.H. Nawab. Englewood Cliffs, New Jersey: Prentice-Hall, 1992.

"Cramer Rao Bounds on Direction Estimates for Closely Spaced Emitters in Multi-Dimensional Applications," by J. Jachner and H. Lee. Paper presented at the IEEE International Conference on Acoustics, Speech, and Signal Processing, San Francisco, California, March 23-26, 1992.

"Effects of Convolution on Chaotic Signals," by S.H. Isabelle, A.V. Oppenheim, and G.W. Wornell. Paper presented at the IEEE International Conference on Acoustics, Speech, and Signal Processing, San Francisco, California, March 23-26, 1992.

"A Group-Theoretic Framework for Fault-Tolerant Computation," by P.E. Beckmann, and B.R. Musicus. Paper presented at the IEEE International Conference on Acous-

tics, Speech, and Signal Processing, San Francisco, California, March 23-26, 1992.

"Modelling Chaotic Systems with Hidden Markov Models," by C. Myers, A.C. Singer, F. Shin, and E. Church. Paper presented at the IEEE International Conference on Acoustics, Speech, and Signal Processing, San Francisco, California, March 23-26, 1992.

Multi-Channel Signal Separation Based on Decorrelation, by E. Weinstein, M. Feder, and A.V. Oppenheim. RLE TR No. 573. Research Laboratory of Electronics, MIT, 1992. 25 pp. $9.00.

"Optimal Minmax Estimation and the Development of Minmax Estimation Error Bounds," by J.C. Preisig. Paper presented at the IEEE International Conference on Acoustics, Speech, and Signal Processing, San Francisco, California, March 23-26, 1992.

Probablistic State Estimation with Discrete-Time Chaotic Systems, by M.D. Richard. RLE TR No. 571. Research Laboratory of Electronics, MIT, 1992. 90 pp. $12.00.

"Signal Processing in the Context of Chaotic Signals," by A.V. Oppenheim, G.W. Wornell, S.H. Isabelle, and K.M. Cuomo. Paper presented at the IEEE International Conference on Acoustics, Speech, and Signal Processing, San Francisco, California, March 23-26, 1992.

"Single Sensor Active Noise Cancellation Based on the EM Algorithm," by A.V. Oppenheim, E. Weinstein, K.C. Zangi, M. Feder, and D. Gauger. Paper presented at the IEEE International Conference on Acoustics, Speech, and Signal Processing, San Francisco, California, March 23-26, 1992.

Spread Spectrum Modulation and Signal Masking Using Synchronized Chaotic Systems, by K.M. Cuomo, A.V. Oppenheim, and S.H. Isabelle. RLE TR No. 570. Research Laboratory of Electronics, MIT, 1992. 39 pp. $10.00.

"Wavelet-Based Representations for a Class of Self-Similar Signals with Application to Fractal Modulation," by G.W. Wornell and A.V. Oppenheim. *IEEE Trans. Info. Theory* 38(2): 785-800 (1992).

"Wavelets, Self-Similar Signals, and Fractal Modulation," by A.V. Oppenheim and G.W. Wornell. Talk presented at the Conference on the Role of Wavelets in Signal Processing Applications, Wright-Patterson Air Force Base, Ohio, March 11-13, 1992.

Electromagnetics

Broadband Impedance Matching Networks for Bandwidth Enhancement of Microstrip Radiators, by G.W. Eswein. S.M. thesis. Department of Electrical Engineering and Computer Science, MIT, 1992.

Electromagnetic Inverse Methods and Applications for Inhomogeneous Media Probing and Synthesis, by J.J. Xia. Ph.D. diss. Department of Electrical Engineering and Computer Science, MIT, 1992.

"Electromagnetic Inverse Scattering in Remote Sensing," by J.J. Xia and J.A. Kong. Paper presented at the Optical Society of America Topical Meeting, New Orleans, Louisiana, April 13-15, 1992.

Electromagnetic Wave Phenomena in Inhomogeneous and Anisotrophic Media, by H.C. Han. Ph.D. diss. Department of Electrical Engineering and Computer Science, MIT, 1992.

"The Renormalized STIE Approach Applied to Inversion of Soil Moisture Profiles," by J.J. Xia, T.M. Habashy, R.T. Shin, and J.A. Kong. Paper presented at the National Radio Science Meeting, Boulder, Colorado, January 7-10, 1992.

"Theoretical Modeling for Passive Microwave Remote Sensing of Earth Terrain (abstract)," by J.A. Kong. Paper presented at the Specialist Meeting on Microwave Radiometry and Remote Sensing Applications, Boulder, Colorado, January 14-16, 1992.

Materials and Fabrication

Characterization of InGaAlAs Resonant Tunneling Transistors, by T.P.E. Broekaert. Ph.D. diss. Department of Electrical Engineering and Computer Science, MIT, 1992.

"Elimination of Mesa-Sidewall Gate Leakage in InAlAs/InGaAs Heterostructures by Selective Sidewall Recessing," by S.R. Bahl and J.A. del Alamo. *IEEE Electron Device Lett.* 13(4): 195-197 (1992).

"Integrating Optical Devices with VLSI Electronics," by C.G. Fonstad, Jr. Paper presented at the Workshop on Compound Semiconductor Microwave Materials and Analog Devices, San Antonio, Texas, February 17-19, 1992.

"Laser-Assisted Growth of ZnSe by Metalorganic Molecular Beam Epitaxy," by C.A. Coronado, E. Ho, L.A. Kolodziejski, and C.A. Huber. Paper presented at the Materials Research Society Symposium, San Francisco, California, April 27-May 1, 1992.

"Quantum-Wave Tunnel Barrior n-n-n Transistors," by C.G. Fonstad, Jr. Paper presented at the Workshop on Compound Semiconductor Microwave Materials and Analog Devices, San Antonio, Texas, February 17-19, 1992.

Optical Communications

"Gravity-Wave Detection Via an Optical Parametric Oscillator," by N.C. Wong. *Phys. Rev. A.* 45(5): 3176-3183 (1992).

Integrated AlGaAs Reduced-Confinement Tapered Waveguide Antennas, by B.K. Pheiffer. S.M. thesis. Department of Electrical Engineering and Computer Science, MIT, 1992.

Operation of Five Individual Laser Diodes as a Coherent Ensemble by Fiber Coupling into an External Cavity, by C.J. Corcoran. Ph.D. diss. Department of Electrical Engineering and Computer Science, MIT, 1992.

"Optical Parametric Division," by N.C. Wong and D. Lee. Paper presented at the 46th Annual Symposium on Frequency Control, Hershey, Pennsylvania, May 27-29, 1992.

Optical Phase Difference Measurement and Correction Using AlGaAs Guided-Wave Components, by S.D. Lau. Ph.D. diss. Department of Electrical Engineering and Computer Science, MIT, 1992.

"Quantum Phase Measurements with Infinite Peak-Likelihood and Zero Phase Information," by Z. Hradil and J.H. Shapiro. *Quantum Opt.* 4: 31-37 (1992).

Three-Dimensional Object Recognition Using Laser Radar, by T.J. Green, Jr. Ph.D. diss. Department of Electrical Engineering and Computer Science, MIT, 1992.

"Tunable Optical Frequency Division," by N.C. Wong, D. Lee, and L.R. Brothers. Paper presented at the International Quantum Electronics Conference, Vienna, June 1992.

"Tunable Optical Frequency Division Using a Phase Locked Optical Parametric Oscillator," by D. Lee and N.C. Wong. *Opt. Lett.* 17(1): 13-15 (1992).

Optics and Devices

"Beating the Shot-Noise Limit with Squeezed Light," by H.A. Haus and K. Bergman. Paper presented at the Department of Defense Fiber Optic Conference, McLean, Virginia, March 23, 1992.

"Femtosecond Time Division Interferometry Technique for Measuring the Tensor Components of X(3)," by C. Chamon, C.K. Sun, H.A. Haus, and J.G. Fujimoto. *Appl. Phys. Lett.* 60(5): 533-535 (1992).

"Femtosecond Time Domain Measurements of Group Velocity Dispersion in Diode Lasers at 1.5 μm," by K.L. Hall, G. Lenz, and E.P. Ippen. *J. Lightwave Technol.* 10(5): 616-619 (1992)

"Investigations of Whisper Gallery Mirrors for Extreme Ultraviolet (EUV) and Soft X-rays," by T-Y. Hung and P.L. Hagelstein. *IEEE J. Quantum Electron.* 28(5): 1376-1383 (1992).

"Modulation and Filtering Control of Soliton Transmission," by A. Mecozzi, J.D. Moores, H.A. Haus, and Y. Lai. Paper presented at the Optical Fiber Communication Conference, San Jose, California, February 2-7, 1992.

"Narrow-Band Optical Channel-Dropping Filter," by H.A. Haus and Y. Lai. *J. Lightwave Technol.* 10(1): 57-62 (1992).

Noise Measurements of Modelocked Laser Pulses, by S. Hon. B.S. thesis. Department of Electrical Engineering and Computer Science, MIT, 1992.

"Photon-Assisted Transport through Quantum Point Contacts," by Q. Hu, R.A. Wyss, C.C. Eugster, and J.A. del Alamo. Paper presented at the American Physical Society, Indianapolis, Indiana, March 16-20, 1992.

"Self-Focusing Induced Saturable Loss for Laser Modelocking," by D. Huang, M. Ulman, L.H. Acioli, H.A. Haus, and J.G. Fujimoto. *Opt. Lett.* 17(7): 511-513 (1992).

"Theory of Cascaded Quarter Wave Shifted Distributed Feedback Resonators," by H.A. Haus and Y. Lai. *IEEE J. Quantum Electron.* 28(1): 205-213 (1992).

"Ultrafast Waveguide Optics," by E.P. Ippen. Plenary talk presented at the Optical Society of America Topical Meeting, New Orleans, Louisiana, April 13-15, 1992.

"Ultra-Long Distance Wavelength-Division-Multiplexed Soliton Transmission Using Inhomogeneously Broadened Fiber Amplifiers," by J.D. Moores. *J. Lightwave Technol.* 10(4): 482-487 (1992).

Ultrashort Pulse Generation and Applications in Optical Fibers, by J.M. Huxley. Ph.D. diss. Department of Electrical Engineering and Computer Science, MIT, 1992.

"Wavelength-Division (DE) Multiplexing Using Cascaded DFB Filters," by J.N. Damask and H.A. Haus. Paper presented at the Optical Fiber Communication Conference, San Jose, California, February 2-7, 1992.

Whispering-Gallery Mirrors and Laser Cavities for Soft X-rays and the Extreme Ultraviolet, by J.P. Braud. Ph.D. diss. Department of Electrical Engineering and Computer Science, MIT, 1992.

Plasma Physics

Change of Confinement Properties and Transition from Absolute to Non-Normal Mode Microinstabilities, by B. Basu and B. Coppi. PTP Report 92/1. Research Laboratory of Electronics, MIT, 1992.

"Comments on Absolute and Convective Instabilities," by A.K. Ram and A. Bers. *Geophys. Res. Lett.* 19(2): 143-145 (1992).

"Current Drive by Lower Hybrid Waves in Combination with Fast Alfven Waves," by A.K. Ram, A. Bers, V. Fuchs, R.W. Harvey, and M.G. McCoy. Paper presented at the International Sherwood Fusion Theory Conference, Santa Fe, New Mexico, April 6-8, 1992.

"Design Studies of a 3.3-GHz Relativistic Klystron Amplifier," by C. Chen, P. Catravas, and G. Bekefi. Paper presented at the SPIE International Society for Optical Engineering, Los Angeles, California, January 19-24, 1992.

"Double Stream Cyclotron Maser," by G. Bekefi. *SPIE Proc.* 1629: 130-143 (1992).

"Double Stream Cyclotron Maser," by G. Bekefi, A. Bers, and A. Ram. Paper presented at the SPIE International Society for Optical Engineering, Los Angeles, California, January 19-24, 1992.

Energy and Current Transport: Symmetry Breaking and Degradation, by B. Coppi and F. Pegoraro. PTP Report 92/3.

Research Laboratory of Electronics, MIT, 1992.

"Experimental Study of a 33.3 GHz Free-Electron Laser Amplifier with a Reversed Axial Guide Magnetic Field," by M.E. Conde and G. Bekefi. *SPIE Proc.* Vol. 1629: Intense Microwave and Particle Beams III 1629: 153-158 (1992).

Fast Nonlinear Exponential m=1 Reconnection in Tokamaks, by L. Zakharov and B. Rogers. PTP Report 92/4. Research Laboratory of Electronics, MIT, 1992.

"Free Boundary Current Ramp and Current Profile Control in a D-T Ignition Experiment," by L.E. Sugiyama and M. Nassi. *Nuclear Fusion* 32(3): 387-404 (1992).

"Physics Basis for Compact Ignition Experiments," by B. Coppi, M. Nassi, and L.E. Sugiyama. *Phys. Scr.* 45: 112-132 (1992).

"Physics Principles of Ignition Experiments," by B. Coppi, M. Nassi, and L. Sugiyama. Paper presented at the International Sherwood Fusion Theory Conference, Santa Fe, New Mexico, April 6-8, 1992.

"A Three Dimensional, Toroidal Two Fluid Model with Hot Particles," by L.E. Sugiyama and W. Park. Paper presented at the International Sherwood Fusion Theory Conference, Santa Fe, New Mexico, April 6-8, 1992.

Theory of Resistive and Ideal Internal Kinks, by S. Migliuolo. RLE TR No. 568. Research Laboratory of Electronics, MIT, 1992. 83 pp. $15.00.

Two-Fluid MHD Description of the Internal Kink Mode in Tokamaks, by L. Zakharov, B. Rogers, and B. Coppi. PTP Report 92/2. Research Laboratory of Electronics, MIT, 1992.

Quantum-Effect Devices

"An Anti-Reflection Coating for Use with PMMA at 193 nm," by A. Yen, H.I. Smith, M.L. Schattenburg, and G.N. Taylor. *J. Electrochem. Soc.* 139(2): 616-619 (1992).

"Fabrication of 50 nm Line-and-Space X-ray Masks in Thick Au Using a 50 keV Electron Beam System," by W. Chu, H.I. Smith, S.A. Rishton, D.P. Kern, and M.L. Schattenburg. *J. Vacuum Sci. Tech. B.* 10(1): 118-121 (1992).

Radio Astronomy

"Emission and Absorption of Microwaves by Atmospheric Oxygen and Water Vapor," by P.W. Rosenkranz. Paper presented at the Specialist Meeting on Microwave Radiometry and Remote Sensing Applications, Boulder, Colorado, January 14-16, 1992.

"Passive Microwave Observations of Atmospheric Parameters from Space," by D.H. Staelin. Paper presented at the Specialist Meeting on Microwave Radiometry and Remote Sensing Applications, Boulder, Colorado, January 14-16, 1992.

"The Radio Time Delay in the Double Quasar 0957+561," by J. Lehar, J.N. Hewitt, D.H. Roberts, and B.F. Burke. *Astrophys. J.* 384: 453-466 (1992).

"Reconciling the Image Brightness Ratios in the Gravitational Lens System 0957+561," by S.R. Conner, J. Lehar, and B.F. Burke. *Astrophys. J.* 387: L61-L64 (1992).

Sensory Communication

"Analytic Study of the Tadoma Method: Improving Performance Through the Use of Supplementary Tactual Displays," by C.M. Reed, W.M. Rabinowitz, N.I. Durlach, L.A. Delhorne, L.D. Braida, J.C. Pemberton, B.D. Mulcahey, and D.L. Washington. *J. Speech Hear. Res.* 35: 450-465 (1992).

"Evaluation of an Adaptive Beamforming Method for Hearing Aids," by J.E. Greenberg and P.M. Zurek. *J. Acoust. Soc. Am.* 91(3): 1662-1676 (1992).

"Potential Benefits of Adaptive Frequency-gain Characteristics for Speech Reception in Noise," by C.M. Rankovic, R.L. Freyman, and P.M. Zurek. *J. Acoust. Soc. Am.* 91(1): 354-362 (1992).

Speech Communication

"Acoustic and Perceptual Characteristics of Voicing in Fricatives and Fricative Clusters," by K.N. Stevens, S.E. Blumstein, L. Glicksman, M. Burton, and K. Kurowski. *J. Acoust. Soc. Am.* 91(5): 2979-3000 (1992).

Modeling Speech Perception in Noise: The Stop Consonants as a Case Study, by A. A.H. Alwan. Ph.D. diss. Department of Electrical Engineering and Computer Science, MIT, 1992.

Modeling Speech Perception in Noise: The Stop Consonants as a Case Study, by A. A.H. Alwan. RLE TR No. 569. Research Laboratory of Electronics, MIT, 1992. 133 pp. $16.00.

"Temporal Measures of Anticipatory Labial Coarticulation for the Vowel /u/: Within- and Cross-subject Variability," by J.S. Perkell and M.L. Matthies. *J. Acoust. Soc. Am.* 91(5): 2911-2925 (1992).

Three-Dimensional Reconstruction of the Tectorial Membrane: an Image Processing Method Using Nomarski Differential Interference Contrast Microscopy, by K.J. Dana. Ph.D. diss. Department of Electrical Engineering and Computer Science, MIT, 1992.

Surfaces and Interfaces

"Ab Initio Statistical Mechanics of Structural Phase Transitions," by K.M. Rabe and J.D. Joannopoulos. In *Electronic Phase Transitions*, Eds. W. Hanke and Y.V. Kopaev, pp. 135-175. The Netherlands: Elsevier Science Publishers, 1992.

"Ab Initio Molecular-Dynamics Techniques Extended to Large-Length-Scale Systems," by T.A. Arias, M.C. Payne, and J.D. Joannopoulos. *Phys. Rev. B.* 45(4): 1538-1549 (1992).

"Ab-Initio Theory of the Si(111)-(7x7) Surface Reconstruction—A Challenge for Massively Parallel Computation," by K.D. Brommer, M. Needels, B.E. Larson, and J.D. Joannopoulos. *Phys. Rev. Lett.* 68(9): 1355-1358 (1992).

"The Enchanting Properties of Oxygen Atoms in Silicon," by J.D. Joannopoulos. Talk presented at the American Physical Society Meeting, Indianapolis, Indiana, March 16-20, 1992.

"Localization, Defects and Surfaces of Photonic Crystals," by R.D. Meade, K.D. Brommer, J.D. Joannopoulos, and A.M. Rappe. Paper presented at the American Physical Society Meeting, Indianapolis, Indiana, March 16-20, 1992.

"Oxygen Induced Broken-Bond Defect in Silicon," by A. Dal Pino, Jr., M. Needels, and J.D. Joannopoulos. *Phys. Rev. B.* 45(7): 3304-3308 (1992).

"Smectic-C Order, In-Plane Domains, and Nematic Reentrance in a Microscopic Model of Liquid Crystals," by R.R. Netz and A.N. Berker. *Phys. Rev. Lett.* 68(3): 333-336 (1992).

Miscellaneous

Design and Implementation of a Parallel Persistent Object System, by M.L. Heytens. Ph.D. diss. Department of Electrical Engineering and Computer Science, MIT, 1992.

A New Approach to Parameter Optimization of Products and Manufacturing Processes, by A.S. Alkhairy. RLE TR No. 572. Research Laboratory of Electronics, MIT, due June 1992. Price to be announced.

Publications Order Form

Research Laboratory of Electronics
Document Room 36-412
Massachusetts Institute of Technology
Cambridge, MA 02139-4307 USA
Tel. (617) 253-2566
Fax. (617) 258-7864

Please send me the following publications. I enclose a check for the correct amount of U.S. dollars made payable to the MIT Research Laboratory of Electronics. Prices listed include third class postage and handling charges. For foreign surface mail please allow 6-8 weeks for delivery. To have reports sent first class within the U.S.A. or Canada, or via air mail, add the amount indicated below for each publication.

To have your name added to our mailing list, please check here: ☐

Name: _____

Address: _____

_____

_____

Number of Copies	Report Number	Title/Author		Unit Price	Price
For shipping via first class/air mail:			U.S.A., Canada add $1.00/copy		
			Europe add $4.00/copy		
			Asia & Africa add $6.00/copy		
				TOTAL	

RLE currents

Volume 5, Number 2 • Spring 1992

The Research Laboratory of Electronics at the Massachusetts Institute of Technology

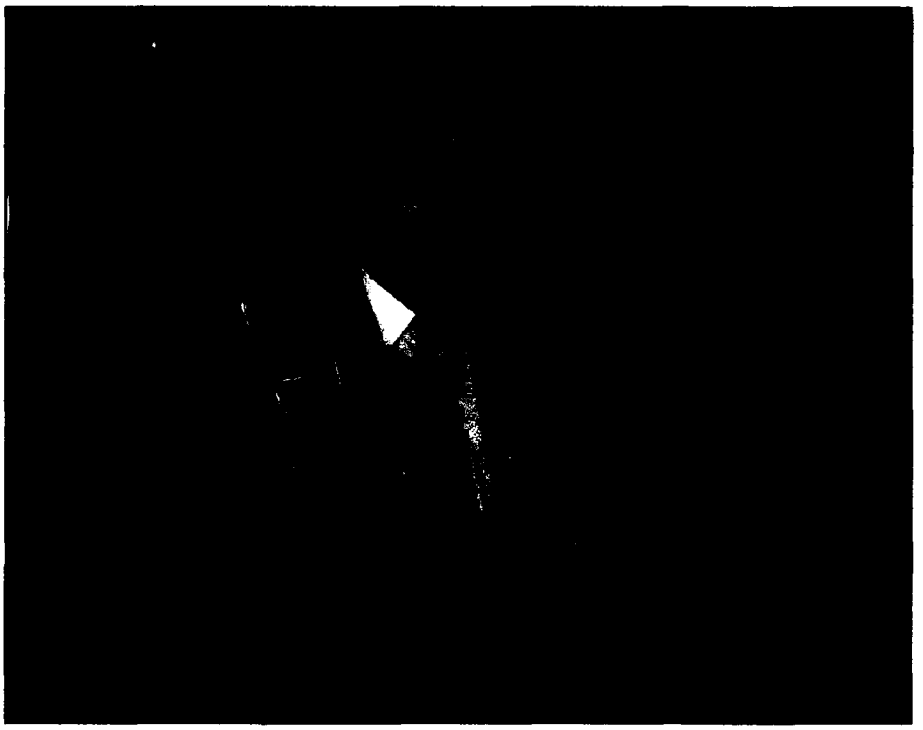
Chipping Away at VLSI COMPUTER-AIDED DESIGN

In search of enlightenment, medieval theologians posed the question, "How many angels can dance on the head of a pin?" Today, faced with a similar but more mundane paradox, computer experts seek an answer to the question, "How many transistors can fit on a microchip?" As semiconductor materials and processing technologies have advanced, electronic components have become smaller, circuit arrays denser, microchips larger, and their functions faster and more complex. Scientists and engineers must now tame the rapid pace of this challenging technology by devising new design methods for integrated circuits that are quick, reliable, and economical.

Computer scientists, electrical engineers, mathematicians, materials scientists, and physicists are all engaged in the highly interdisciplinary field of integrated circuit design. Their investigations are driven, in part, by the quest for faster, more accurate, and more powerful digital computers. Conversely, these high-performance computers are the vehicles that transport researchers into still deeper and more fascinating areas of exploration.

It is simple to design a circuit that contains a few transistors, but the design of an entire system that uses thousands of transistors involves many designers who may work on different parts or stages of the design simultaneously. To be successful, a design team must possess an understanding of each level of design. Rarely does one person possess expertise at all levels, nor is the entire process achieved solely by human means. Without modern computer-

(continued on page 2)



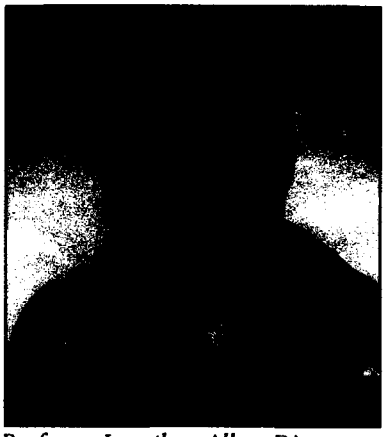
An integrated circuit mask layout of the Intel 386 microprocessor (magnified 200 times) provides a backdrop for Professor Jonathan Allen. This computer-generated plot of the 386 chip, which contains 275,000 transistors, was part of a recent display at the MIT Museum, "Information Art: Diagramming Microchips." (Photo by John F. Cook)

Director's Message

The onslaught of VLSI technology has brought a vast new set of possibilities to compact, high-functionality, low-cost applications. Tens of millions of transistors can be fabricated on a single integrated circuit chip, but the design of these systems remains a huge challenge.

RLE's Circuits and Systems Group is developing new design methodologies and building novel chips to serve these increasingly aggressive applications. Techniques for logic synthesis, design for testability, high-accuracy circuit extraction, device and circuit simulation, highly parallel design architectures, consistent design frameworks, functional verification, and the realization of fast parallel systems are the main foci of this research. The common thread for these diverse projects is the need to characterize and optimize multiple views of a single design at several levels of abstraction, ranging from a high-level functional view to the geometrical mask specification needed for fabrication.

Many design techniques dwell at a single level of representation, but others provide transformations between these levels while maintaining their consistent relation. The need to break down the complexity of these large target systems is addressed through the techniques of structural partitioning, as well as the suppression of detail provided by the increased emphasis on higher level abstractions. Nevertheless, when performance is critical (and it usually is), there is no substitute for fine-grained manipulation of physically related models, and RLE's group has provided many algorithms aimed at the pursuit of high performance.



Professor Jonathan Allen, Director Research Laboratory of Electronics

The emerging trend of computer-aided design research is to provide the means to design (in all aspects) highly optimized, reliable systems that don't have to be iteratively fabricated to achieve design goals. As this research progresses, general techniques of design representation and evolution, optimization, and verification are becoming apparent. So, it will be no surprise to see this group provide new design methodologies for many other physical substrates, such as biological materials and micromechanical systems. Thus, design synthesis is becoming a generic discipline that will bring many technologies into highly useful systems.

VLSI COMPUTER-AIDED DESIGN

(continued)

aided design techniques, today's microchip designs would be impossible to create. This article is an overview of integrated circuit design and a look at RLE's research activities in this field.

Smaller and Smaller

Integration refers to the number of transistors placed on a single microchip. It reduces cost through economies of scale and improves circuit reliability at the chip level rather than at the circuit board level. Integration has mushroomed from small-scale integration (SSI) with about 4,000 transistors on chip, to very large-scale integration (VLSI), with hundreds of thousands of electronic devices on chip. In VLSI, the chip itself has become an integrated system containing approximately a million transistors and thousands of other components. VLSI systems have attained device dimensions smaller than the wavelength of visible light, and novel high-resolution lithographic techniques are used to fabricate these highly complex circuits (see ***currents***, December 1988). Other rapidly emerging integration technologies include ULSIC (ultra-large-scale integrated circuit), which seeks to pack more than 4 million transistors on one chip with linewidths (the traces that conduct current) measuring 1 micron or less, and VHSIC (very high-speed integrated circuit), with a goal of tens of millions of transistors on a chip.

Tracing the Electronic Circuit

Electron or vacuum tubes were introduced in 1904 with Sir John Ambrose

RLE *currents*

RLE ***currents*** is a biannual publication of the Research Laboratory of Electronics at the Massachusetts Institute of Technology.

Jonathan Allen. . . . . Editor-in-Chief
John F. Cook. . . . . Photography
Everett Design . . . . . Design
Dorothy A. Fleischer . . . . . Staff Writer and Editor
Barbara Passero. . . . . Production and Circulation
Donna Maria Ticchi. . . . . Managing Editor
Henry J. Zimmermann . . . . . Advice and Perspective

The staff of ***currents*** would like to thank Professor John L. Wyatt, Jr. for his contributions to this issue.

Inquiries may be addressed to RLE ***currents***, 36-412, Research Laboratory of Electronics, Massachusetts Institute of Technology, 77 Massachusetts Avenue, Cambridge, MA 02139-4307.

(ISSN 1040-2012)

RLE

© 1992. Massachusetts Institute of Technology. All rights reserved worldwide.

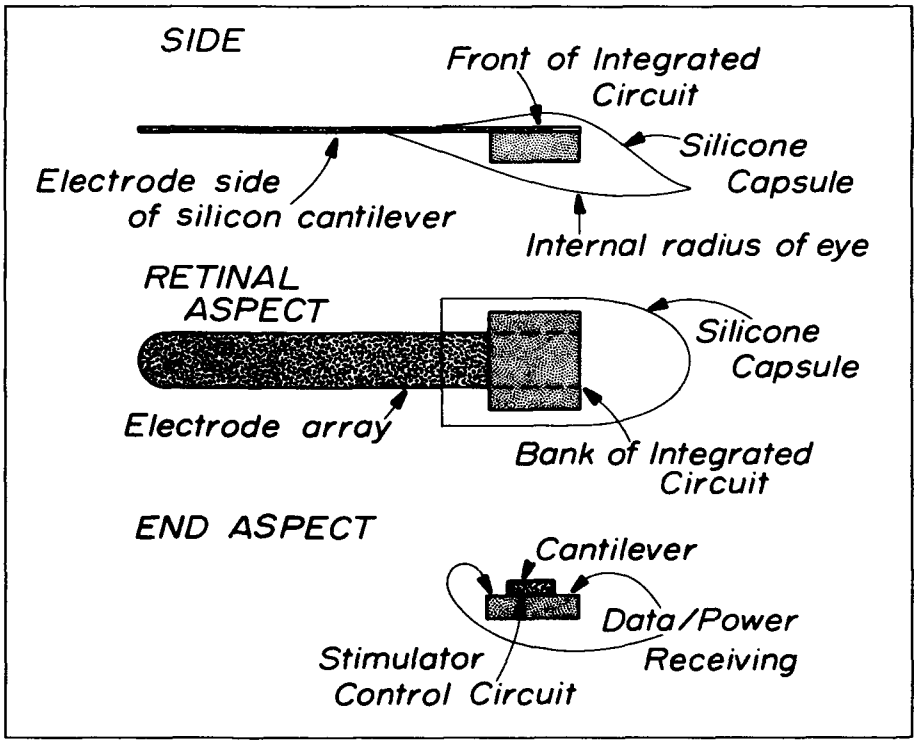
Fleming's invention of the diode tube, a "valve" that could control or rectify alternating current. Later that year, American inventor Lee DeForest discovered the triode tube, which not only controlled current flow, but also functioned as an electronic switch. In 1945, vacuum tubes were used in the first operational electronic computer, the ENIAC (Electronic Numerical Integrator and Calculator). It filled an entire room at the University of Pennsylvania, weighed 60,000 pounds, and used 18,000 vacuum tubes to perform computations. Unfortunately, because the vacuum tubes generated high temperatures (400° F) and consumed enormous amounts of energy, they needed to be constantly replaced.

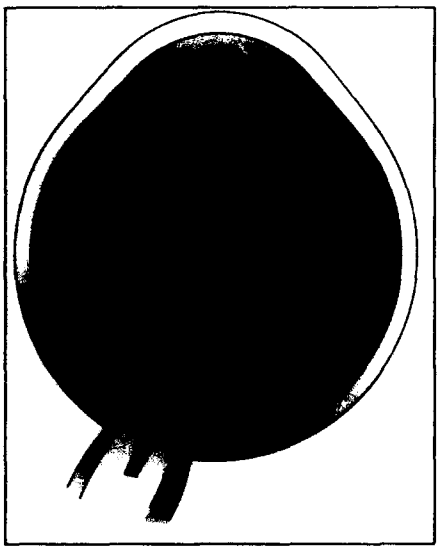
The age of microelectronics arrived in 1947 with the invention of the transistor. Bell Telephone Laboratory physicists John Bardeen and Walter H. Brattain designed the point contact transistor using two wires positioned on a germanium crystal. Later that year, fellow Bell physicist William B. Shockley invented the junction or bipolar transistor. An improvement on the point contact transistor, the bipolar transistor had no wires to align and exploited the conducting properties of silicon, another semiconducting element less temperature-sensitive than germanium. Because only the charge carriers move in the semiconductor's crystal lattice, transistors became known as solid-state devices. An improvement over vacuum tubes, they consumed much less power, generated little heat, and could be bat-

(continued on page 4)



Professor John L. Wyatt, Jr. is part of a research team that is attempting to design an implantable silicon chip that will restore vision to patients with diseases of the outer retina. (Photo by John F. Cook)





An artist's rendition (above) of the implantable silicon retina microchip and its electrode array on the retinal surface currently being developed by Professor John L. Wyatt, Jr. and his collaborators. The chip will be surgically implanted adjacent to the retina. Light will pass through the lens of the eye and focus on the chip. Electrical pulses will then be transmitted to the retina through an on-chip array of stimulating electrodes. The pulses will directly stimulate the optic nerve or ganglion cells in the retina, causing them to fire as if they were stimulated by healthy photoreceptors. (At left) A cross section of the eye that shows the planned position of the chip as it is implanted adjacent to the retina.

tery powered. Transistors were first used commercially in Raytheon hearing aids and Texas Instruments portable radios. These discoveries earned Bardeen, Brattain, and Shockley the 1956 Nobel Prize in physics.

These first transistors had fragile wires that connected them to a circuit board, and were prone to breaking off. In 1957, attempting to fix this problem, scientists at Fairchild Semiconductor devised the first integrated circuit by placing all transistor components on and in a single layer of semiconductor material called a *substrate*. The first working integrated circuit (made of germanium) was announced by Jack Kilby of Texas Instruments in 1957. Later that year, Fairchild scientists designed a silicon integrated circuit using the *planar process*, where all circuit activity occurred on a few related planes in the integrated circuit, thus making it more efficient and easier to produce. The planar process became the standard for the manufacture of all integrated circuits.

In 1957, when the Soviet satellite Sputnik was launched, the space race began. The U.S. government invested heavily in the microelectronics industry, and the fierce competition between Americans and Soviets fueled the rapid pace of research. In 1959, a single chip contained only one device component, but by 1970 it contained 30,000 components. Microelectronics is a cornerstone in the American space program, and proved vital to its success during the '60s.

The "computer on a chip" was realized in 1971 with the invention of the microprocessor by Marcian "Ted" Hoff of Intel. It differed from earlier integrated circuits because it combined all computer operations on one microchip. In a space no larger than the head of a nail, the microprocessor incorporated a central processing unit (CPU), memory, controllers, buffers, input, and output. One microprocessor consumes $1/1{,}000{,}000$ the power and costs $1/30{,}000$ the price of the ENIAC, and it performs 200 times faster. Compared to other simple computer logic chips whose functions are hard-wired in an integrated circuit, a microprocessor's operations can be changed by simply altering its program. Microprocessors have opened the way for smaller, programmable appliances and equipment capable of robotics and precise measurements. Without them, personal computers and their smaller relatives would not be possible.

Elements of a System

Integrated circuits eliminated the many discrete electronic components that make up a hard-wired circuit (including resistors, inductors, and capacitors). Instead, semiconductor materials such as silicon and germanium now do the work of these individual components. Because they are smaller, more reliable, cost less, and perform better than conventional circuits, semiconductor integrated circuits are now the basic components of today's electronic systems.

Extremely pure silicon is used as a base semiconductor material for integrated circuits. By *doping* (combining) silicon with phosphorus, the silicon acquires excess electrons and is called *n-type* silicon. Doped with boron, the silicon has a lack of electrons and is called *p-type* silicon. When p-type and n-type are juxtaposed, electrons and holes (arising from the incomplete bonds) flow under the influence of an applied voltage. Since current can flow only from p-type to n-type material, it functions as a one-way switch called a *semiconductor diode* (similar to DeForest's earlier vacuum tube diode). The semiconductor diode is the foundation of the bipolar transistor used in high-speed computer applications. Here, a sandwich of n- and p-type materials is formed that acts as both a switch and an amplifier (similar to Shockley's earlier junction transistor). In order to perform logical functions, the silicon materials are combined on one surface (side by side or stacked) and etched into well-defined areas in the planar process. This method provides pathways along which the electrons move.

There are several classes of circuits, formed by a variety of fabrication techniques and used in many different applications. The two major classes are analog and digital circuits. Analog circuits react continuously to input, as in a temperature sensor. Conversely, digital circuits are two-state devices (on/off) and handle inputs in the form of binary digits or *bits* (0/1). Hybrid analog/digital chips contain both types of circuits; for example, an analog sensor whose data is converted to a digital read-out.

Gate circuits perform fundamental logic operations by selecting and transmitting part of the input signal while blocking out the rest (*e.g.*, one of every ten pulses). *Logic* circuits (including gate circuits, but not vice versa) are made by connecting two or more logic gates, and address only the presence or absence of signals, not their shape. By combining various logic functions, circuit designers can provide digital chips with different operations.

Circuit or chip designs can be standard, semi-custom, or custom. Standard chips use the manufacturer's design and are the least expensive to fabricate because of economies of scale. Semi-custom chips follow a standard design, but use two techniques to customize applications: by manipulating the logic function of the logic gates in the gate arrays and determining which gates will be connected or active, or by adding an extra layer of metal interconnect for more functions. Custom circuits follow a proprietary design and layout and are made for a highly specific application. Custom chips are costly and the most time consuming to design and manufacture.

Other major classes of semiconductor circuit include metal-oxide semiconductor field-effect transistors or MOSFETS. They are grouped by their fabrication process: complementary MOS (CMOS), p-type MOS (PMOS), and n-type MOS (NMOS). These circuits operate on low power and produce less heat than bipolar devices.

The Automated Approach to Microelectronic System Design

In automating the design process, there are several levels at which designers operate. The entire design process can be viewed as a sequence of transformations at and between various design levels. A structured design method builds in consistency between the *behavioral, structural,* and *physical* representations present at all levels in the process. This structured approach helps to simplify the design and reduce errors. One method of structured design is *abstraction,* where simplified models represent the actual objects and their functions. Abstraction helps to suppress detailed information and gives structure to a problem, thus making it easier to solve. In complex systems, several levels of hierarchical abstraction may be necessary to describe an object. Hierarchy helps to divide the circuit into multiple levels and reduce design complexity. Levels of abstraction in the design process include:

Functional design, where the designer determines the input and output behavior of major components in a system

and their role in solving a specific problem. At this level, the designer uses a high-level description language to develop a behavior representation (for example, a circuit's function) or the system's architecture.

System architecture, where individual functions of each system component are decomposed into blocks of various register subsystems to indicate parallelism. At this level, it must be determined whether or not the intended system can meet specific performance objectives, given the architecture and technology used. If not, alternatives must be explored.

Logic design, which defines the logic structure that will implement the functional design. Structural representations are either a textual or schematic description, and analysis is made by simulations at the gate or register levels.

Circuit design, where the designer addresses the currents and voltages that will operate in a system. By using components developed in the logic design phase, and keeping in mind the system's overall design, the designer builds the system's transistor circuits. Using automatic synthesis tools, the transistors are properly sized to meet signal delay requirements. Circuit and timing simulations analyze the design, and timing verification tools check signal delay specifications.

Physical design, where the designer determines how a system will actually be constructed. The behavioral and structural representations of earlier design stages are translated into geometric representations used to manufacture the system. Automatic synthesis, analysis, and verification tools are used to transform the earlier circuit design into a mask specification layout that is used in chip fabrication.

Other techniques in structured design include *regularity*, which reduces complexity through the use of iteration, and *standardization*.

Computer-Aided Design in VLSI

Interactive graphic workstations enable the user to create detailed visual information while communicating with a powerful, automated system. Computer-aided design (CAD) is used for geometric modeling, analysis, testing, drafting, and documentation. It is also applied to engineering (automated design, simulation analysis, process and tool design) and manufacturing (numerical control, robotics, processing planning, and factory management).

Because highly complex microprocessor designs have become too difficult to draft manually, circuit designers use computer-aided design methods to lay them out. Within the last 15 years, integrated circuit design has progressed from an entirely manual process to one that is substantially automated. Powerful CAD workstations perform many time-consuming, repetitive tasks while permitting designers and engineers to focus on analysis and creativity. A CAD workstation can display all or part of a circuit diagram to verify a correct design, change the function of a logic device, calculate how a microprocessor will work while its design is in progress, and store room-sized diagrams.

CAD software tools assist the development of techniques and algorithms. There are currently four types of CAD tools that support the physical design of an integrated circuit. The first is the *geometric* approach, where a commercially available interactive graphic system is used by the designer to create the exact shape of a structure on an integrated circuit mask. In the *symbolic* approach, details are hidden and the designer works with symbols that the CAD system converts to exact geometries. In the *cell-based* approach, individual function cells and performance data can be completely characterized and their specifications stored in a computerized cell library. As the library grows, the building of block diagrams and their subsequent conversion into mask layouts for chip fabrication becomes more efficient. Finally, in the *procedural* method, cells are automatically placed in a complete integrated circuit layout that uses a procedural language to describe their placement and interconnections. The trend in CAD tools has been towards *delayed binding*. This means deferring decisions on a circuit's components and functions as late as possible in the design to afford the designer more flexibility in the process.

CAD tests a circuit design by simulating it, rather than constructing expensive breadboarding or hardware. Previously, in hardware testing, costly errors often did not appear until the chip was already fabricated. Through the use of CAD, a circuit's timing can be tested separately from its logic functions, and corrections can be made less expensively at the design stage.

Levels of Representation in the Design Process

Throughout the integrated circuit design process, several different views or representations show various aspects of the system. These are the behavioral, structural, and physical representations.

Behavioral Specification

At the beginning of the design process, the designer develops a behavioral description of a circuit's function and determines which algorithms will be coded to perform this particular function. The behavioral description is then simulated by compiling and executing a functional language program or by using a behavioral simulator with its own language.

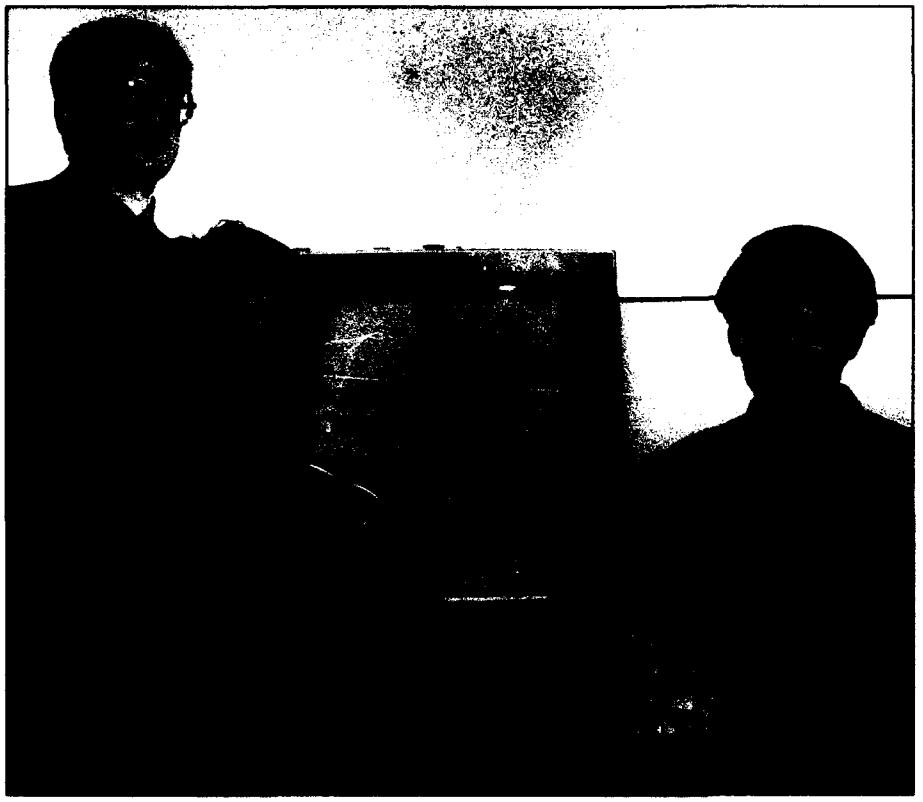
Once simulated, the behavioral description is translated into a structural or circuit description. Structural representations, such as block diagrams and schematic drawings, show the composition of circuit elements in terms of components and their interconnections. In its simplest form, a structural description is a *net list*, which represents the interconnections of cells and logic gates in a design. The net list shows topological connections but not the geometry of cell locations on a chip.

High-Level Synthesis

High-level or system-level synthesis involves the *partitioning* or specification of various subsystems. This "divide and conquer" approach helps to manage complexity and imposes more structure on a design. It is usually done manually for designs that do not require any design exploration. Partitioning is associated with the development of a system concept and the definition of a realizable architecture and its requirements.

Architectural exploration is performed during high-level synthesis and involves the mapping of variables to registers or signals, operators to functional units, and control structures to controller operations. The goal of architectural exploration is to find the optimal implementation of a circuit. It entails a heuristic or exhaustive search of the design space to explore the different ways in which the design can be implemented.

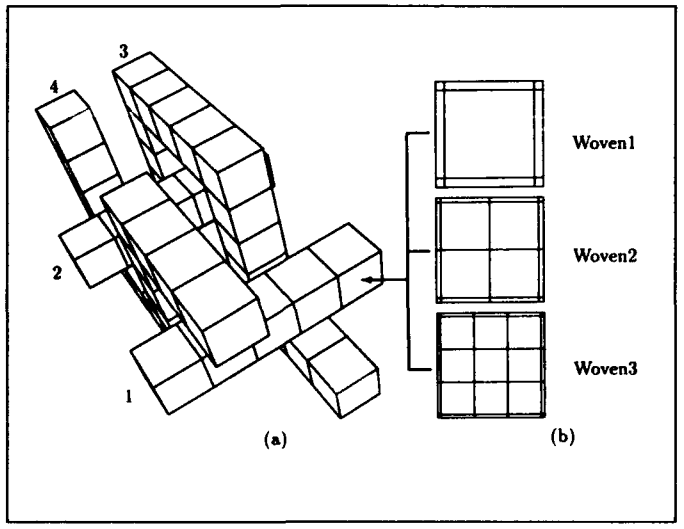
(continued on page 6)



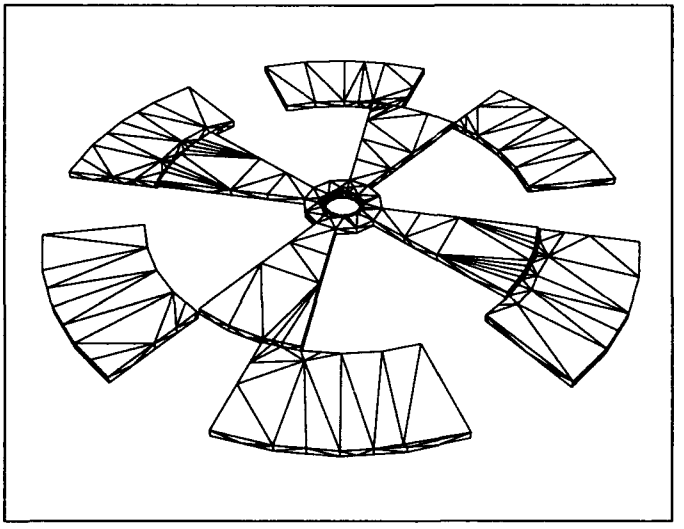
Professor Jacob K. White and graduate students Songmin Kim and Keith S. Nabors demonstrate the types of three-dimensional integrated circuit and packaging structures that can be routinely analyzed by FASTCAP, a very fast capacitance extraction program developed at MIT. Using a computer-aided design workstation, FASTCAP can quickly and accurately analyze complex structures. It uses a novel multipole-accelerated, preconditioned iterative method to compute surface charge densities. FASTCAP's capabilities are being extended to perform three-dimensional inductance extraction and transient interconnect analysis. (Photo by John F. Cook)

Tasks include: ***resource allocation***, the selection of the type and number of functional units; ***scheduling***, the assignment of time slots to the components' operations; and ***resource assignment***, the assignment of operations to specific functional components. The allocation of more resources results in a more parallel system with greater performance, but with a higher hardware cost and larger chip area. This is known as a trade-off between time and area. System-level synthesis produces a description of the data path and controllers.

The next step is ***register transfer-level synthesis***, where a functional or register transfer-level model describes the implementation of the data path and controller. Data path optimization is aimed at better resource allocation and assignment for both timing and area. Tasks in data path optimization include ***resynthesis*** for a variety of block implementations and ***register relocation*** to achieve structural modifications. The controller, which generates control variables for registers and memory units, is transformed from its abstract description to a ***finite-state system***. In this transformation, controller architecture is selected, states are assigned, inputs and outputs are encoded, and the controller



An illustration of a woven bus interconnect problem in an integrated circuit that was solved by Professor Jacob White and his students using the FASTCAP program. Successively finer panelings of a bus' surface are shown in (b), which represent a set of nested discretizations used to perform numerical simulation. The FASTCAP program, developed at MIT, can compute the surface charge densities on these structures and can solve problems involving the discretizations of thousands of panels in only a few minutes on a scientific workstation.



Growing research and commercial activity in silicon integrated circuit-based micromechanical structures has piqued interest in computer-aided design tools for this field. At RLE, Professor Jacob K. White and his collaborators are developing a MicroElectro-Mechanical Computer-Aided Design system (MEMCAD) to assist designers in performing realistic simulations for structures such as microsensors and micromotors. The MEMCAD system was used to perform electrostatic force analysis on this solid model of a micromotor.

is decomposed into smaller, interacting finite-state machines (sequential circuits with a finite number of possible states). Register transfer-level synthesis produces a system that is decomposed into blocks of *combinational logic*, where outputs are entirely dependent upon inputs, and *sequential storage components*, where inputs plus the state of memory elements in the circuit determine the outputs.

Results from the register transfer-level synthesis are optimized and mapped to a gate-level hardware structure or a schematic in logic-level synthesis, where the system is described as an interconnection of switching elements or gates. At this level, the goal is to minimize logic in both path delay and area, and to ensure the logical correctness of the design to implement the various blocks. If the system utilizes a two-level logic architecture, the results are sent to a PLA generator. If the architecture uses multi-level logic, then *technology mapping* is used.

Technology mapping uses the network of technology-independent abstract logic gates developed in logical-level synthesis and maps them to elements of a specific semi-custom cell library. Thus, technology data is added to the earlier structural description and results in an abstract hardware network. The different methods of technology mapping produce a variety of area and delay values. Issues involved in technology mapping include whether or not it should be the first or last synthesis design step, and which technology should be selected. As synthesis moves to higher levels of abstraction, technology mapping moves into the earlier stages of design. It is important that the mapping of an abstract, technology-independent circuit to a specific target architecture meet *testability* requirements. These requirements are related to *design for testability*, where the goals are controllability (control of circuit nodes so they can be tested) and observability (the ability to observe faults).

Physical Design

The physical design stage transforms circuit design specifications into physical mask representations used to manufacture the electronic circuit. The designer must follow strict geometric design rules associated with the constraints of the fabrication process. These include requirements for minimum feature sizes of the various components, as well as the spacings and connections between them. Failure to follow these rules can make the chip inoperable, unreliable, or unmanufacturable.

Today's computer-aided design methods speed the process of physical design by automatically translating specifications from the chip's behavioral or structural description to its physical layout. The designer uses automatic layout techniques to quickly map the structural representation into a circuit's physical representation. Although these techniques result in a more error-free layout, the layout itself may not be as efficient or creative as one produced by a human designer. The designer must also be concerned with both the placement of components and their interconnections.

This phase of design begins with a physical representation or floorplan that consists of geometric coordinates for the circuit elements and interconnection. The designer uses the floorplan to determine actual structures as they relate to the circuit's logic functions, to estimate the size and position of major blocks in the system, and to check timing paths. From this floorplan, a symbolic layout with predefined cells is constructed.

A *mask layout* is generated from this symbolic layout and consists of two-dimensional patterns (rectangles) to represent the different mask patterns used in circuit fabrication. A *layout editor* is used to draw the graphical shapes that define the mask layout. The editor does not check these shapes, so testing must be done to ensure their correctness. Symbolic layout editors can be used to limit the shapes available to the designer, thus minimizing layout errors, but at a cost trade-off in layout density.

In the procedural or program-driven synthesis method, computer programming techniques such as conditionals, loops, variables, and procedure calls are used to create graphical objects. Compactors (or compaction algorithms) can also be used to automate a circuit's geometric design by moving its components and wires to optimize space.

During the synthesis phase of physical design, tools for *automatic placement* (to position components on a layout surface) and *routing* (to interconnect components with wiring) create new or improved layouts from earlier structural representations. These include:

A placer, which maps the cells to predefined physical gates. By optimizing details from a net list description, such as the total length of wire used to connect the cells, it assigns those gates to locations on the chip.

Various *routing algorithms* that can be chosen to generate the wires connecting the cells. Channel routers simultaneously route all wires in rectangular areas. A maze router routes wires individually on a grid, taking into account barriers or blockages.

A *programmable logic array* (PLA) produced by a PLA generator program. From a set of Boolean functions, arbitrary two-level logic is transformed into a geometric structure. A logic or PLA optimizer minimizes the logic in a PLA to reduce its area without changing its function.

A *silicon compiler* that builds a physical description or layout of a chip from its behavioral description. The designer specifies a design structure, then the circuit's parameters (functional, electrical, and geometrical) are processed by corresponding module compilers. All relevant design rules are stored in a *technology file* to check the circuit. Timing and logic models are also generated for each component in the circuit. The system then uses placement and routing or PLAs to form a chip composite. A package editor supplies packaging information for the fabrication process, and a simulator can then test the chip.

Simulation

Simulation ensures that the chosen design is the one needed to perform all the desired functions. It also determines the circuit's operating speed and checks any delays or faults that might be present. The determination of accurate circuit timing during simulation is a trade-off in terms of determining the optimal performance of the circuit. Computer-aided design tools can be used to simulate performance at all levels of representation. A variety of simulators for behavior, logic, and transistor switch-level timing include *gate-level* or *logic simulators* for logic gates, *transistor* or *switch simulators*, and highly accurate *circuit simulators*. *Timing simulators* are gate-level or transistor simulators for accurate timing. *Mixed-mode simulators* allow a combination of simulation

(continued on page 8)

modes. A *timing analyzer* can be used to estimate path delays without simulation.

Analysis, Verification, and Testing

Analysis, verification, and concern for testing procedures are found within all levels of design—from a system's behavioral specification through its physical design.

Analysis

Because fabrication of an integrated circuit is time consuming and expensive, chip analysis and verification is essential before it is manufactured. Analysis operations evaluate the consistency or correctness of a chip's behavioral, structural, and physical design representations. A variety of tools are used to check errors:

The automated *design rule checker* (DRC) is a reliable method used to check layout geometry to ensure that it follows the design rules.

Circuit extractors analyze the layout, then extract a net list of transistors, thus converting a physical description back to a structural description. The structural circuit description can then be simulated with a switch or circuit simulator. Programs to verify the extracted net list include: a *network comparison program,* which compares the net list from the circuit design phase to the extracted net list from physical design; and an *electrical rules checker* (ERC), which checks the electrical properties of a circuit. *Parameter extractors* can determine electrical parameters from layout information for timing simulation.

Verification

Verification is the final phase of design. It is a formal process to demonstrate the equivalence of two design representations under all specified conditions. One example is to compare a schematic diagram and a physical layout that has been synthesized from that schematic. In many cases, formal verification techniques are preferred over simulation because it results in a reliable mathematical proof rather than the experimental results of test case simulation.

Testing

Testing has come to the forefront in VLSI, whereas in previous years it was considered a secondary concern to the overall design process. Testing involves checking the completed integrated circuit to see if it was manufactured correctly and to determine if the final design is the one that the designer had intended to build. Testing simulates operating conditions and detects faults at the circuit level which may affect performance. A set of *test vectors* are developed in a test language to detect a circuit's input and output behavior. *Test generators* can automatically develop a set of tests for a particular circuit, although they require some restrictions on the design. *Fault simulators* grade tests by simulating a circuit, assuming a fault, and verifying that the test vectors propagate the differences as a result of that fault as seen in the outputs. The most common fault model found in integrated circuits are *stuck-at faults,* where a node is stuck in the on or off position. The percentage of faults detected indicates the quality of the test. Testing indicates the *yield,* or number of functioning chips, and the test engineer may recommend design improvements to correct the observed defects.

VLSI Computer-Aided Design in RLE

RLE research activities in VLSI technology range from crystal growth for semiconductor materials to new photolithographic fabrication processes. Additional research involves device physics and the design of computational algorithms. The ongoing investigations in RLE's Circuits and Systems Group seek to provide the means for designing custom integrated circuits quickly, correctly, and economically.

Professor Jonathan Allen's research is concerned with performance-directed synthesis of VLSI systems. He and his students explore the development of new CAD tools that can serve as an integrated framework for design exploration while providing high-performance circuit optimization and consistently aligned representations at all levels of the design process.

A current project focuses on basic methodologies for very high-speed clocking strategies. Using CMOS technology, a new circuit style called *true single-phase clocking* enables clock speeds of several hundred megahertz. The cause for this high-speed performance is now under study. The circuit is expected to be used in a wide variety of applications and provide an important capability to performance-directed synthesis. Further studies also seek to provide a systematic design methodology for this new class of circuits.

Another system under study will permit comprehensive architectural design exploration while predicting the speed performance of a proposed design. This work involves the systematic exploration of signal processing algorithms and architectural alternatives, then extending the results to the layout level. The project has already contributed highly optimized array architectures for digital signal processing systems.

An innovative VLSI design database is being developed that will supply automatic consistency maintenance between several design representations. The goal of this work is a database design that will automatically, incrementally, and continuously provide for consistent alignment of all levels of design abstraction. The project is now being extended to include other design modules, the introduction of new schema compilers, and the extension of its basic methodology to functional representations.

Other important research in Professor Allen's group concerns the development of new techniques to concisely represent waveform transition effects in integrated circuits. These techniques were combined with macromodeling techniques to accurately characterize integrated circuit systems. Also, grammatical techniques that verify the correctness of circuit style were extended to semantic tests that check for device size, charge sharing, and other electrical phenomena not easily represented in grammatical form.

Professor John L. Wyatt, Jr. and his collaborators are building VLSI chips for machine vision, and have produced three camera processor chips that operate at over 1,000 frames per second. The goal of this research, known as the MIT Vision Chip Project, is to design and build a very powerful, fast, and compact early vision system that can operate in real time.

Early vision refers to a set of processes that recover the physical properties of three-dimensional objects from a two-dimensional array of image intensity data. Early vision systems process raw visual data such as the fine details of texture and spatial gradients or temporal changes in incident light intensity. The

system produces a simplified representation of an image in which features such as boundaries and information on depth and velocity have been extracted. Its results are passed to a higher level system that can perform object recognition, scene analysis, or robot navigation.

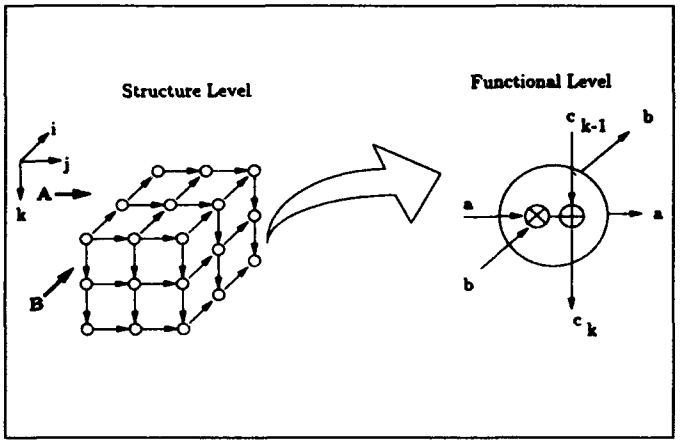
Investigators chose to design an analog early vision system because it is simpler, faster, and uses less space than digital circuitry. Tasks involve hardware development for existing algorithms and modifying other algorithms to match the hardware's specific requirements. The project has brought together several investigators with a broad range of expertise in CMOS and charge coupled device (CCD) technology, innovative circuit and system design, robotic algorithms, physiology, nonlinear circuit theory, parallel computation, and fabrication technology. Many of the system's chips are custom made and require custom fabrication at MIT's Microsystems Technology Laboratories.

In a highly experimental project, Professor Wyatt is also part of a second team that is attempting to design and construct a silicon retinal implant chip for the blind. The retina is a delicate and complex tissue (it is considered part of

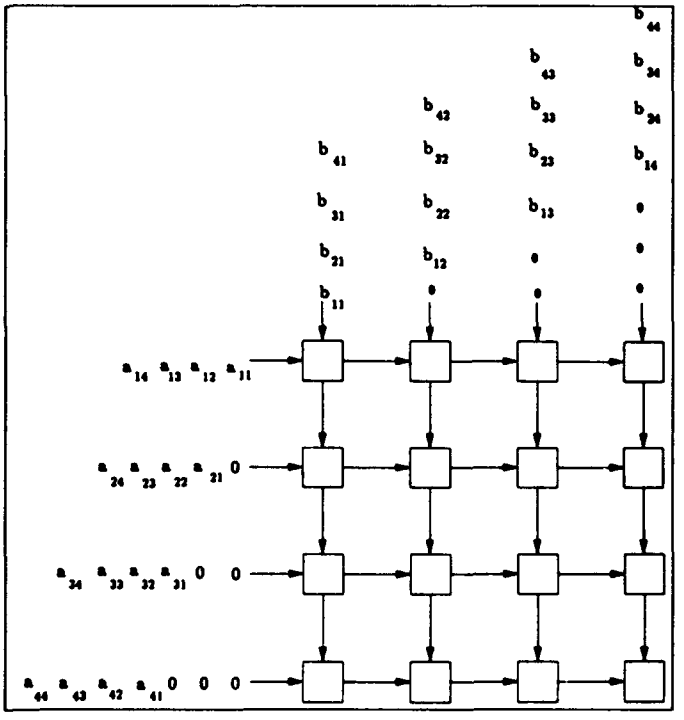
(continued on page 10)



In an abstract cubist environment, Professor Srinivas Devadas (center) and graduate students Stan Y. Liao (left) and Filip J. Van Aelten study verification procedures to ensure digital circuit designs are consistent with signal flow graphs. A signal flow graph is an abstract representation of a specific computation that is to be performed. Stan holds a model cube that illustrates a typical signal flow graph to which array-based processors must conform. The computer monitor displays a signal flow graph and the microcoded processor that implements it. (Photo by John F. Cook)



A



B

These figures illustrate a simple specification/implementation pair for matrix multiplication used by Professor Srinivas Devadas and his students. The specification (A) is a three-dimensional signal flow graph where every node performs a multiplication and an addition. Deriving an implementation from this specification involves the tasks of hardware allocation and scheduling. The resulting implementation (B) is a two-dimensional array processor. The verification task is to check if the input/output behaviors of both the specification and the implementation are in a certain formal relation.

the brain), and vision loss is usually permanent. Some patients can be helped with special low-vision glasses, but there is currently no medical treatment available to repair retinal damage. The team (which includes investigators from the Massachusetts Eye and Ear Infirmary, Massachusetts General Hospital, Lincoln Laboratory, and RLE) is designing a prosthesis that may help restore vision to these patients, especially those suffering from macular degeneration and retinitis pigmentosa.

The prosthesis will be a two-sided silicon microchip implanted adjacent to the retina. Light passing through the eye's lens will be focused on a photoreceptor array located on the chip, and electrical impulses will be sent to the retina through an array of stimulating electrodes also on the chip. Healthy optic nerve cells in the retina will be stimulated by the pulses, causing them to fire. Because this research is in its early stages, there are still many issues to be addressed, such as how to design and mount the device properly so there is no discomfort or further damage to the retina, yet close enough to ensure sufficient electrical stimulation. Questions also must be answered about the toxicity of the device and the effects of electrical stimulation on the retina.

Professor Jacob K. White and his students perform numerical analysis for circuit and device simulation. They also investigate parallel computation and the interactions between numerical algorithms and computer architecture.

His group's research has contributed to circuit and device simulation using *waveform relaxation* techniques. Waveform relaxation is an iterative method used to analyze nonlinear dynamical systems in the time domain. At each iteration, the method decomposes the system into several dynamical subsystems. Each subsystem is analyzed for the entire given time interval. The efficiency of these methods has been improved for circuit simulation and, recently, the techniques were accelerated to reduce relaxation iterations by almost an order of magnitude. These algorithms may be effective in solving a broad range of time-dependent partial differential equations, such as those in fluid mechanics, and may lead to very efficient parallel simulation algorithms.

Another project addresses simulation algorithms for clocked analog circuits, where frequency and time-domain techniques are combined to analyze switching circuits. Algorithms have been developed to simulate switched capacitor filters and switching power converters. These methods are based on accurately simulating selected cycles of a high-frequency clock with a standard discretization method and then combining the selected cycles by computing the low-frequency behavior with either a truncated Fourier series for steady-state calculations or low-order polynomials for transient calculations. By accurately computing the solution over a few selected cycles, an accurate long-time solution can be attained. This is known as an *envelope-following algorithm.*

Approaches to more accurately compute the electric fields in MOS devices are also being explored. Numerical techniques to solve the energy balance equation for electron temperatures were proven and used to predict substrate currents in MOS devices. A method was derived that uses a two-dimensional simulator developed by the group. The predicted results matched the measured data on devices with channel lengths as short as 0.16 micron. Monte Carlo techniques are also being evaluated for device simulation on massively parallel computers. Monte Carlo simulation methods approximate the behavior of a system by performing a single computation many times using a random-number input, then examining the statistical distribution of the results to help make a design decision. Monte Carlo methods are used when a problem is too complex for a closed-form mathematical solution. These techniques are now being used in transient calculations with self-consistent electric fields.

A program has been devised to provide three-dimensional capacitance extraction in linear time. It is based on a novel adaptive multipole algorithm that is three orders of magnitude faster than standard techniques. The program, FASTCAP, has been generalized to cover a broad class of applications including the computation of torque by micromotor designers. Recent improvements to FASTCAP have resulted in performance faster than standard boundary-element-based programs and have achieved more accurate results for complex problems while retaining the linear time complexity of the basic algorithm.

The group is also taking an applications-oriented approach to parallel numerical algorithms in circuit and device simulation. Application programs and techniques are being developed for both massively parallel single and multiple instruction, multiple data machines. In addition, they are seeking to understand the fundamental aspects of the interaction between architecture and certain numerical algorithms.

Also underway is a project to develop a microelectromechanical CAD system that will enable microsensor designers to easily perform realistic simulations. The system currently performs electromechanical analyses; for example, calculating capacitance versus pressure for a square diaphragm deformed by differential pressure.

Professor White has used his numerical analysis techniques to assist other RLE investigators. In the Auditory Physiology Group, two-dimensional steady-state fluid calculations were carried out for cochlear hydrodynamics. In the Electromagnetics Group, these techniques helped to solve inductance calculations and problems involving transmission lines with nonlinear loads. Simlab, an interactive and easily modified circuit simulator, was developed for the MIT Vision Chip Project. It is used to investigate simulation techniques for circuits in early vision research.

Professor Srinivas Devadas and his group explore all aspects of computer-aided design for integrated circuits and systems, including the development of new techniques to perform automated logic synthesis, design verification, and VLSI system testing. He and his students devise logic optimization methods that consider not only area, performance, and power consumption, but also the testability of a designed circuit. The group also develops verification methods for the behavioral, logic, and circuit levels, and devises efficient test generation methods at the logic level that can easily test fabricated integrated circuits. This research involves developing new algorithms, proving theoretical results from these algorithms, and demonstrating their effectiveness by creating software programs that solve practical problems.

Professor Devadas and his students have developed a method to precisely and efficiently compute logic circuit delay using timed test generation. They are also working on an analysis of statistical delay to accurately predict the percentage of fabricated integrated circuit chips

that will meet a desired performance goal. The group has also formulated a calculus of event simulation and has applied it to different models of timing behavior so the number of events that need to be evaluated in a circuit simulation can be reduced. Using conventional stuck-at-fault testing techniques, they have developed a unique delay computation algorithm for all functioning circuit delay paths.

Another project employs string function theory to develop an efficient and formal methodology that will verify logic implementations when compared to behavioral specification. New definitions of behavioral equivalence (for example, equivalence relations between serial, parallel, and pipelined implementations of behavioral specifications) were established that use this string function theory. This research may produce a string function theory and formalism for behavioral synthesis.

The group studies new approaches to determine encoding problems associated with state assignment and finite-state machine decomposition. The goal of this research is to obtain logic-level implementations that are minimal in area and delay. The prime-factorization-based encoding of N-state counters has proven to be a successful approach. Decomposition-based methods have been used for state assignment to solve the encoding problem in general finite-state machines. The group also investigates the use of re-encoding techniques for sequential circuit optimization.

Professor Devadas and his collaborators have furthered the concept of VLSI synthesis and testing for testability. Theoretically, this approach has resulted in rigorous and formal characterizations of logic circuits. It has also provided methods for automatic synthesis to enable the design of VLSI circuits with unprecedented levels of testability (guaranteed 100% testability for delay faults; a fault model more comprehensive than customary stuck-at fault models). This research focuses on test generation under stuck-at and delay fault models for non-scan VLSI circuits, and synthesis for sequential testability.

Professor Devadas has developed several algorithms for fundamental logic synthesis problems and efficient formal verification methods. His work has resulted in a prototype system for CAD algorithms. One technique has led to the synthesis of a large speech recognition chip that is possibly the most testable circuit ever automatically synthesized and designed. The circuit contains approximately 25,000 transistors and is fully testable under the most comprehensive fault model currently known, the robust path delay model.

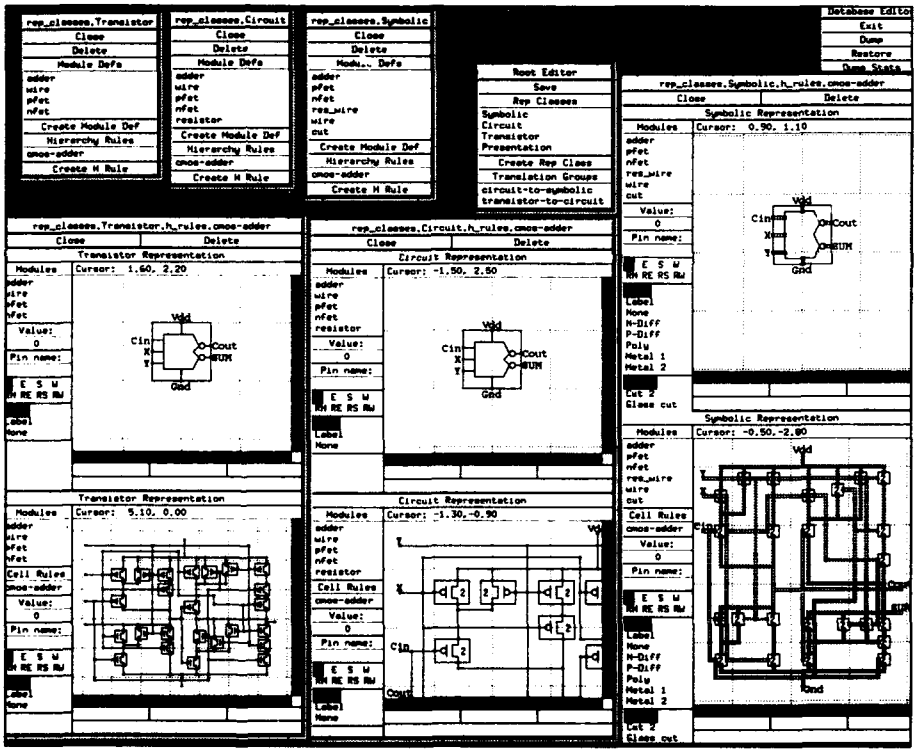
Other research activities in his group include the automated synthesis of circuits for low-power consumption and the development of built-in self-test techniques for the random pattern testability of a circuit design.

Future Directions in VLSI

It may one day be possible to automatically design reliable and economical VLSI systems from the algorithmic level through the fabrication of a circuit. To realize this potential, advances in CAD tools for VLSI must keep pace with the capabilities of fabrication technology.

The development of highly advanced CAD tools will not only result in high-performance computers and electronic devices, but the methods used to implement these tools may also be extended to a wide range of other disciplines such as computational biology, biochemistry, and artificial intelligence. An example is the current problem of matching DNA strings in biochemistry. This is a difficult, discrete combinatorial optimization problem that is also found in integrated circuit computer-aided design.

by Dorothy A. Fleischer



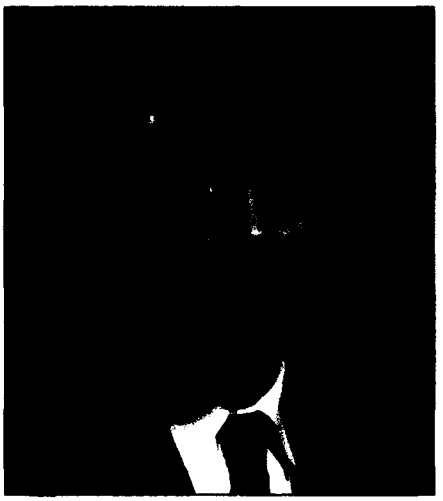
A prototype database manager used to design full-custom VLSI systems was recently developed by graduate student Robert C. Armstrong in Professor Jonathan Allen's group. The database manager, called FICOM (Framework for Incremental Consistency Maintenance), simultaneously displays the various design views of an integrated circuit (including its architectural form, logic diagram, circuit schematic, and mask layout geometry) and helps to maintain a consistent relation of all the views so that they correspond to the same circuit implementation. In this example, FICOM is used to design a full adder module. The three levels of abstraction are shown from left to right (transistor view, circuit schematic, and symbolic layout). The top row shows the module block views and the bottom row shows the module contents. FICOM vertically displays the circuit's structural hierarchy, while consistent views are displayed horizontally in an interrelated fashion. Changes made by the designer in one view are automatically translated to changes in other related views. This retains the overall consistency and well-formedness of a circuit's design.

FACULTY PROFILE:
John L. Wyatt, Jr.

You would be correct to say that Professor John L. Wyatt, Jr. is a man of vision. Currently, he is a member of two interdisciplinary research teams, the MIT Vision Chip Project which is exploring early vision, and another collaboration developing the design of an implantable retina microchip.

Professor Wyatt was born in Memphis, Tennessee, in 1946. He attended MIT (BSEE '68), Princeton University (MSEE '70), and the University of California/Berkeley (PhD '79). His early professional experience included stints as a design engineer with the U.S. Public Health Service from 1969 to 1971, and as a postdoctoral associate with the Medical College of Virginia from 1978 to 1979. Following his postdoctoral research, Professor Wyatt returned to MIT in 1979 as an assistant professor in the Electrical Engineering and Computer Science Department, and joined RLE's Communication Biophysics Group. He was promoted to associate professor in 1984, and to full professor in 1990. MIT's Department of Electrical Engineering and Computer Science named him the first Adler Scholar in 1990. The scholarship enabled Professor Wyatt to relinquish his teaching responsibilities for one semester to take a class in machine vision.

Professor Wyatt's broad range of knowledge encompasses areas of mathematics, engineering, neurophysiology, thermodynamics, biochemical transport, and VLSI design and simulation. His current research activities in RLE's Circuits and Systems Group focus on the dynamics of nonlinear circuits and systems, machine vision algorithms and analog VLSI for machine vision, and retinal stimulation using a microchip.



Professor John L. Wyatt, Jr. (Photo by John F. Cook)

• *What sparked your interest in science and engineering?*

Originally, I started out as a junior chemist at age five. My childhood love was explosives. I made homemade gunpowder with a coffee grinder, which is great for grinding charcoal very fine, and made brightly colored bombs. The druggist around the corner gladly sold me potassium nitrate and flowers of sulfur, and I quickly branched out into many other kinds of explosives—zinc dust and sulfur, potassium perchlorate and sugar. I terrified my parents. Once, when I wasn't able to go to school, the kids asked, "Where's Jack, did he blow himself up?"

In grade school and junior high, I transmitted illegally on television frequencies and messed up all the televisions in the neighborhood. By the time I was in seventh grade, I was making homemade radios, even though I didn't understand them very well. I had a 250-foot antenna stretched from one backyard to another and picked up the Voice of the Andes from Quito, Ecuador. I never did get a ham license because I got bored learning Morse code.

During summers in high school, I attended classes at an industrially oriented high school taught by an excellent teacher, Hugh Phillips. He had a plaque that read "Father of Nicaraguan Radio." Apparently, he had put together their radio system. He taught high school kids who were interested in vacuum tube analysis and design to get their commercial radio engineers' license. In his class, we didn't learn mathematical theory because we hadn't learned calculus yet, but we did learn to design conventional circuits. Our final exam at the end of the second summer had no written material except a parts catalog. We were to build a five-tube superheterodyne AM receiver with whatever we wanted from the catalog. By the end of the class, we didn't just know about circuits, we had acquired the competence to build them ourselves. I was lucky to take the class because it helped determine my direction. I found my interest in electronics to be more compelling than my formal liberal arts education. The classes at my private school only taught me to do what many other people could do, whereas the technical high school prepared me to do things for my future, and I could do them myself.

• *You had a good idea of where you were going quite early on.*

In high school, my ambition was to go to Italy, get a job until I learned the language, and join the Ferrari mechanics program. I had raced go-carts in National Carting Association races with friends, and I was a good two-cycle engine mechanic. College seemed too boring and conformist. I wanted to become a good race mechanic, and Ferrari seemed like the place to go. So, I didn't apply to college, but my dad applied for me. He told me that I could be a perfectly good Ferrari race mechanic with an MIT degree, that it wouldn't hinder me at all.

It didn't matter too much to me when I was accepted to MIT, but it was sheer excitement when I moved to Boston. It took away the last vestiges of juvenile delinquency. People here didn't tell me how I had to be, that I had to be like them, or that I had to see it their way. They had a lot to teach and they were going to tell me how it all worked. People at MIT complain that this place is not a hand-holding, protective community. There may be some validity to that, but I found it liberating. If it had been very protective, I would never have felt that I was on my own. It was an intellectually sharp community, and how I handled my life was entirely up to me. I wanted the intellectual wizards to guide me and say here it is; people like Art Mattuck in math and Tony French in physics. But,

after two years at MIT, despite all its wonder, I was burned out. I took my junior year in Germany, learned the language, went skiing, and studied comparative literature and philosophy. That gave me a wonderful junior year and brought me back to MIT rejuvenated.

• ***What happened after MIT?***

I wanted to do a second bachelor's in math, but the draft board said no. I was attending graduate school at Princeton in electrical engineering and I was given time to complete my spring semester in 1969. I filed as a conscientious objector who was willing to take care of the wounded. That meant they would have sent me to Vietnam where I would have gone into combat without a gun. I didn't think of the practical consequences of my decision; I just checked off that particular box on my draft form because that's how I felt ethically. The U.S. has five armed services and two other uniformed services that are not armed—the Public Health Service and the Coast and Geodetic Survey. I was lucky to get a job at the Public Health Service in Maryland.

My two years there yielded my first patent. It was for a cheap, reliable radiation measurement instrument. I was able to devote full time to a real design project, and it reaffirmed my love for circuits. The instrument I designed used discrete components and was supposed to work down to one femtoampere (10^{-15} amperes). Unfortunately, it made a great seismograph. It would go off scale when trucks came down the highway over a quarter-mile away. I could stand across the lab, make a sharp move with my hands in the air, and drive it off scale. It was the most sensitive, if least accurate, seismograph I'd ever seen. The instrument worked this way for about a month, and then it hit me. I had built everything on high-quality ceramic standoff insulators so there would be no current leakage. I recalled something that I had read in the *Boys' First Book of Electricity* in the third grade—ceramics are piezoelectric! I had forgotten it and no one around there knew. The ceramics generated electricity every time there was the smallest movement. So, I put everything on Teflon insulators and the problems went away. It made me think that circuits were wonderful and magical, and it made me feel competent to be able to solve problems with them.

Eventually, the instrument was developed further and we applied for a patent on the whole system. It is widely used in Europe for low-level x-ray emission monitoring. Of course, I signed away my royalty rights to the government. In a way, it was nice that it was a government job. The time schedule was flexible, there wasn't a profit margin, and I was given more to do than if I had worked at IBM. There's something good about government work, even though the standards are lower and there's less super-quality talent. For young people who want a bigger piece of the pie than they can get in industry, all they have to do there is ask for it.

• ***Did you have a mentor?***

Although I never met him personally, Norbert Wiener was my first mentor. I read his books, and what I understood excited me, because he thought about systems and how they worked on a large scale. He covered statistical mechanics, neurophysiology, and control theory, and tied them together to see what they had in common. Back then, I didn't understand the math very well, but his broad, technical inquiries were wonderful.

The first three mentors whom I knew personally served on my thesis committee at Berkeley—Professors Charlie Desoer, Leon Chua, and George Oster. Charlie was excellent at circuits and feedback systems, especially nonlinear ones. He created an atmosphere in which deep thinking in systems was encouraged. He also provided the glue for many faculty and grad students in a culture that reached out to others in biology, circuits, and economics. It was easier to talk to him than many other system theorists because he didn't demand that you translate a question into mathematicalese. This required him to know the engineering descriptions apart from the math, and to be willing to take the burden of translation off the student's shoulders. Charlie was also a great apostle of clarity. When you thought you had something basically right, he would consider that merely foreground—NOW we start. Leon was excellent at making nonlinear circuits and thinking deeply about their weird behavior. He helped to create a vocabulary and an environment for that, and he provided me with enormous encouragement to publish. Just as Charlie and Leon were into the mathematical parts of a problem and understanding the dynamics of nonlinear systems, George was wonderful in biology and modeling. He created the field of network thermodynamics, where he used nonlinear circuit theory to model complicated, interactive thermodynamic systems. Thermodynamics was originally developed to study things that are thermal yet simple, like a steam engine. If you want to model something complicated, like a human cell, you need a discipline like circuit theory. Circuit theory is great in helping you understand complicated things as an interconnection of simple components. There was a need to model complicated, interactive systems in cells, but no one had done it, and George went a long way in that direction.

• ***You spent seven years completing your doctorate at Berkeley.***

If you had mathematical interests in the behavior of circuits and systems, even biological systems, it was a wonderful time to be at Berkeley. It was cheap back then, and probably still is. I think tuition was $350 a quarter. So, one could afford to learn things deeply. Many of us spent years working through real analysis courses as a side interest, but our own work was either engineering or biology. Rather than taking the attitude, "I've got to get out of here, so I'll learn the minimum aside from my discipline," you could say, "I'll devote eighteen months to getting real analysis under control, then take a couple of more courses a quarter for four consecutive quarters." I went there with a master's degree, and took more than twice the course load required for a doctorate for students who arrived there with a bachelor's. I did all the pre-med requirements except second-quarter organic chemistry and genetics. I did everything for a master's in math, except the thesis. At that point, I was tired of graduate school, so I wrote up my dissertation and bought a one-way ticket to Cairo, Egypt. Luckily, I brought along enough traveler's checks to make it back four months later.

• ***Were you still considering a career in medicine?***

I probably should have gone to med school, but after Berkeley, I was tired. I just couldn't think of putting aside the previous five years of research for another eight years while I did an MD, an internship, and a residency. I had worked in Highland Hospital in Oakland as a volunteer. Ultimately, I found it overwhelming to deal with the patients who came in from knifings and gun fights. I couldn't see fixing it, nor could I see an end to it. It was also terrible to be with people in areas where they were so afraid. I wasn't drawn into doing that for forty more years when I couldn't change it. My dad was a doctor in internal medicine, and his dad before him was a physician. My dad was also knowledgeable in cardiology and he was one of Tennessee's leading experts in tropical diseases, having served four years in the army in Panama. He was more involved with people than I am, and very empathetic. I can inspire people intellectually, but I'm not as good at understanding their deep, personal fears. Probably, I would have been a research MD rather than a clinician.

Following Berkeley, I did a postdoc at the Medical College of Virginia with Professor Don Mikulecky, who modeled membrane transport in cells. I had reviewed his papers as a grad student and I liked his work, so I called him up. He invited me for a postdoc and I worked one year in the department of physiology. Eventually, I realized that I wanted a regular job. When I looked around, there were only a few intellectually good organizations that were in interesting places. It came down to Columbia and MIT. I came within minutes of going to Columbia, but MIT called just in time, and I accepted an assistant professor position.

• ***After returning to MIT in 1979, you worked with Professor William Siebert in RLE's Biophysics Group.***

Bill Siebert was my mentor at that time. He helped me find my way around MIT and to understand how things worked here. We had a joint interest in thermodynamics and its analytic basis in terms of circuit theory and random stochastic processes. He and I still share interests in signal processing, thermodynamics, and biological modeling. He worked with me to supervise Han-Ngee Tan's 1984 dissertation. We used circuit theory and random processes to understand how electrical circuits driven by thermal noise behaved like other thermodynamic systems. It's usually understood in a macroscopic way, like steam and power, but we were interested in the microscopic level, and came up with new results and a good paper. We found an extension of the second law of thermodynamics to the frequency domain representation of random noise. It didn't require the noise to be thermal, and that was new. Then, we set up an analytic framework which allowed us to produce a thermodynamic description of noise in nonlinear circuits. The description worked and made sense, not only away from equilibrium (where most of thermodynamics fails), but also away from steady state. It was hard to get answers in closed form, but the equations were exactly right even during violent transients. That was such a relief compared to classical thermodynamics where, once things became nonequilibrium or nonsteady state, the concepts failed. In our treatment, they didn't fail.

• ***How did you become interested in nonlinear theory?***

I was tired of linearity, Fourier transforms, and all the tools used by electrical engineers. It seemed like a spent language with overused verbiage. That's not quite true since there still is new and interesting work to do in linear systems, but much of what electrical engineers do is not interesting. In nonlinear theory, none of the verbiage works, so you need to start fresh. The tools are few, the problems hard, and you aren't using up the language created by others. Nonlinear systems have interesting phenomena—they can serve as storage media, they can oscillate, they can go chaotic, they can blow off into infinity, and they can have multiple and different oscillations depending on where you start. Also, many biology problems are nonlinear. It isn't a question of what you prefer, it's a question of how the system acts. If you linearize it, you miss the problem.

• ***What attracted you to research in machine and human vision?***

Initially, I did a bachelor's project in neurophysiology at MIT with Murray Eden. Then, at Berkeley, I began my doctoral work with Frank Werblin, who was a bioengineering professor in the electrical engineering department. He worked on intracellular microelectrode recording in the retina. Although I wasn't the world's best experimentalist, I was left with an interest in how cells in the eye can process information and with a respect for how hard it is to do these experiments. In postdoc research, I used circuit models to represent transport phenomena in cell membranes, but there was nothing neural or visual about it.

After I returned to MIT in 1979, the field of neural networks or artificial neural systems began to arise. I took a leave of absence for one semester to study neural nets at Lincoln Lab and Caltech. Carver Mead's neural nets work at Caltech interested me. He used circuits loosely modeled on the behavior of the nervous system, to do information processing. They were building chips to do vision, and his artificial retina designs inspired me. He had come to MIT to give a talk, and I had approached him afterwards to tell him that's exactly how we ought to be using silicon. I had it in my mind, from my work with Frank Werblin, that silicon should be used to make retinas and arrays that responded to light and did on-chip processing. All the digital research with silicon seemed to be in a completely different spirit from that. Carver had the knowledge and the revolutionary desire to do something different. After working at Lincoln, I visited Carver's group at Caltech for two months and returned to Lincoln to teach what Carver was doing.

I was inspired by Carver's group, and I felt we needed to do that kind of work at MIT. His shouldn't be the only group working on analog VLSI for vision. So, that's why I started the vision chip project. In analog microchip design, we have better talent than the Caltech group—Harry Lee and Charlie Sodini—and we have our own fabrication facility. Charlie is our fab expert and Harry is our circuit design expert, and they know enough about each other's area. I began to talk to other people

at MIT, like Tommy Poggio and Berthold Horn, and we began work on the MIT Vision Chip Project.

Our approach differs from Carver's. His is based on the nervous system. We simply build analog systems. Carver is inspired to learn analog circuit design that copies the nervous system, and we're inspired to use analog circuits for new engineering applications of vision. Carver also does continuous-time CMOS circuits in subthreshold modes. This involves very tiny currents where the transistors work exponentially. We don't operate there, partly because those systems run slow, and partly because transistor matching is so poor. Also, we do things utterly unlike what Carver does, like charge coupled devices (CCDs). We aim for engineering performance. In the long term, he does too, but we're not interested so much in the nervous system. At MIT, there are no experts in analog circuit design *and* neurophysiology, so we have to build the project around the people we have, how they think, and what they like to do.

The vision chip project has worked out well. We've designed and built very fast chips; 1,000 frames per second is normal in our work. We believe we can design analog chips that work at speeds about two orders of magnitude higher than digital, with power two orders of magnitude lower than digital, and cheaper than digital because the chips are smaller when manufactured in quantity. At the same time, they're special purpose and not programmable like a digital chip. One of our doctoral students has designed a chip that does on-chip filtering and produces an image that looks like an edge map. The chip is an ordinary CCD camera with on-chip processing at 1,000 frames per second. Another student has designed a camera chip that determines the position of a bright object and its orientation within a scene at 5,000 frames per second. That's a single-chip system. Yet another student has designed a CCD system that simplifies images by preserving the edges but smoothing out the gray areas. We have other single-chip systems that are being tested or designed, as well as other chips that test particular technologies, but they're not complete systems on a single chip.



Professor John L. Wyatt, Jr. (seated) compares notes with graduate students (from left): Mark N. Seidel, Malini V. Narayanan, and Paul R. Pilotte. (Photo by John F. Cook)

• ***Does the vision chip project have any application to artificial intelligence?***

Our work doesn't relate to traditional artificial intelligence, which works with *highly processed* data that already make logical sense. We work with *raw* data that describe the world and determine how we can make sense of that data. We model the eyes and the early visual parts of the brain that find edges, determine motion, and find form. The applications we have in mind for the vision chip project are automatic manufacturing and vehicle navigation, where it is important to quickly sense objects visually—fast enough to guide a robot arm that's doing a quick job.

• ***What is involved in your other project, the implantable retina chip?***

The group of people I work with includes Dr. Dave Edell (a principal research scientist from the Harvard-MIT Division of Health, Sciences, and Technology), who consults for Lincoln Lab, and Dr. Joe Rizzo, MD (an ophthalmologist and neurologist from the Massachusetts Eye and Ear Infirmary). For many years, Joe has worked on retinal transplants in animals. The hope is that someday this procedure can be used to restore the function of damaged retinas in humans. It's technically successful, but there's currently no hope for connecting a transplanted retina to the brain. Joe thought there may be some way to assist a damaged retina electronically. He asked if we could design a chip to place in the eye, and I told him probably not. How do you get power into the chip without wires hanging out and risking infection? How can you put anything up against the retina without wrecking it? The retina has the mechanical consistency of a single layer of wet tissue paper, and it doesn't want you to mess with it. Furthermore, it's not firmly attached to the back of the eye. So, it's a difficult place to work.

Fortunately, the retina is built backwards in the eye and it's all very transparent. The receptor cells are on the retina's edge farthest from the lens, and the output or ganglion cells are nearest the lens. There are two illnesses in which the receptor cells die, but the output cells apparently continue to work—retinitis pigmentosa and macular degeneration. Approximately 10 million people in the U.S. suffer from these two forms of blindness and more than 400,000 are legally blind. Since the output cells continue to function in both illnesses, it's theoretically possible to drive them with an implantable microchip with an array of electrodes. Human cells can be driven electrically. We don't have to penetrate the cells with electrodes, all we have to do is put an electrode near them (closer than 50 microns) and pulse the electrode with voltage at the right polarity. The cells will fire as if they were driven through synapses in a healthy retina.

It is amazing how good modern integrated circuit technology is. The diameter of ganglion cell bodies in a human is about 30 microns. With modern commercial fabrication, we can produce individual features, such as the width of a piece of wire, as small as 0.6 micron. So, a cell in the eye is about fifty times bigger than a structure made with commer-

cially available chip technology. It is possible to cover a single human cell with lots of these fabricated structures. Our goal is to make an electrode array, using new techniques to stimulate the ganglion cells, that can gently sit on the retina and provide some degree of vision.

There are many difficulties. First, the retina is extremely pressure-sensitive. Pressure as little as 10 millimeters of mercury can produce blindness, and that's pressure mediated gently through a fluid. You could imagine putting a brick of a microchip up against the retina and somehow attaching it. The retina would not like it any more than you would like being caressed by a bulldozer! We must find ways to gently attach the array so it doesn't sit like a concrete block on the retina. There are also chemical forms of toxicity. If we were to insert very small quantities of copper or iron in the eye, the retina would be completely destroyed. In addition, the electrical driving process produces electrochemical products that can well be toxic. So, we have mechanical toxicity from the pressure, chemical toxicity from the substances placed in the eye, and electrochemical toxicity from the driving process. Plus, there's surgical damage simply from entering the eye and the possibility of rejection. Those issues alone make it a difficult problem.

Right now, I don't know the likelihood of the project's success. But since it can help such a large population, I think we must take the risk. Either it won't work at all, or it will work after a prodigious effort. It may not provide good vision any time soon, but the difference between total blindness and the ability to see one's way around just a bit is very important.

• What is the biggest obstacle to your research?

My biggest obstacle is that I'm primarily involved in practical projects when my own research is theoretical. So, I've created a situation for myself where I'm a fish out of water. The vision chip project is largely about design, building, and testing chips, although there are some theoretical notions about using linear-nonlinear resistive grids as parallel image processing machines. Similarly, the retina chip project has no theory in it right now. It's all biological experimentation. The up side is that I saw these things which needed doing, and I put together the groups to do them. These two projects are important because they bring people together in interesting, worthwhile lines of work; people who wouldn't necessarily know each other. The down side is that I spend a large amount of time administering and supervising other peoples' research.

In general, the biggest obstacle to any research is time. It seems there's a trend at U.S. colleges and universities to turn researchers into research supervisors. The trend is to take people who are good at research, tenure them on the basis of their contributions (to a significant extent in research), and then cease to reward them for doing the research. Instead, they are rewarded for doing administrative work, bringing in funds, or starting new directions. There are the basics—teaching, acquiring funds, finding graduate students, and sitting on exam committees. By the time all that's done, plus administering and reporting on a project, you've already done a moderately demanding year of work. So, doing your own research is a luxury. I think that's the biggest problem for a university professor. Some people quit and don't do research, others administer research but don't do it themselves. One can get absorbed by the administrative activities within an academic department, especially a large one, because the amount of administrative work grows more rapidly than the size of the department.

• How do you see your role as a teacher?

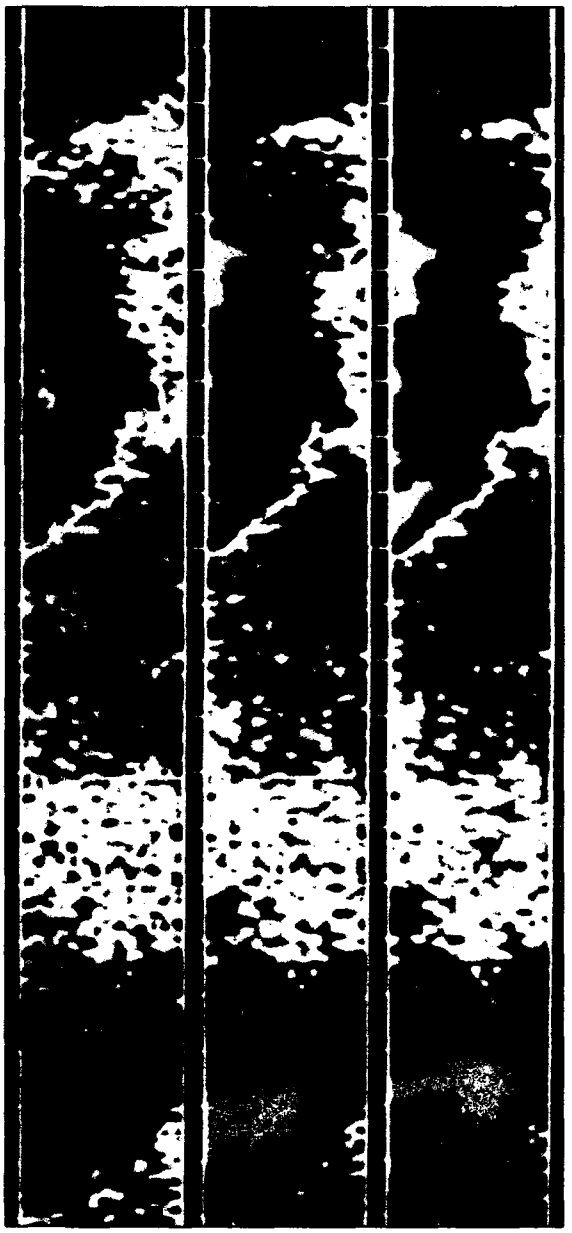
I view the job of a teacher as one of clarifying, at least for graduate courses. That means telling the story in a rough way to get the intuition across, then telling the story again in a precise way to get the math right, and finally tying them together. I try to teach things I don't know very well, though I avoid things that I'm utterly unqualified to teach. Right now, I'm teaching a course on estimation and random processes. I haven't thought about that material in almost two decades. So, preparing to teach it is a real learning experience for me. If you've got to teach, why not make it a learning experience!

• What is the future for VLSI?

The most important thing that has happened in VLSI is the incredible, highly developed fabrication technology, where billions of dollars have been spent to optimize it. The technology is potentially good in many applications, particularly where electricity plays either a small role or no role at all—the microfabrication of accelerometers, small actuators, electric motors and pumps; and in on-chip chemistry applications, such as electrophoresis, which is used to separate out chemical compounds. The application of chips to other things that handle analog data is one of the most interesting things going on—on-chip chemical actuators; sensors for temperature, mechanical pressure, and acceleration; and motors that can move gases around. There are chips with arrays of tiny, electrically controlled mirrors that can reflect light and produce a display. In principle, they can modulate images from space and overcome the effects of atmospheric motion.

As I mentioned before, in the implantable retina chip project, it's amazing that the ganglion cells are about 30 microns in diameter, and the objects that can be fabricated in the modern commercial process are on the order of 0.6 micron in diameter. These feature sizes are already below the biological scale of most human cells. Using this technology to interface to the nervous system is extremely interesting. The digital handling of information on-chip is a well-developed activity, but using analog technology to interface with physical and biological media, and to do chemistry on chip is a new and exciting process. A company in California uses this technology to grow proteins in a 100x100 array of cells—10,000 different ones on a single chip—with no electricity involved at all. They start to grow the cells and cover a fraction of them. Then, they grow a certain amino acid on the uncovered cells. By programming which cells are covered, they can grow 10,000 different proteins at once and know exactly what each one is. If they want to assay something for a response to a certain antigen, they can do all 10,000 tests at once. This may be of more revolutionary importance in terms of technology than what's been done electrically on a chip.

What About Bob?



High-resolution passive microwave images of Block Island, Rhode Island, as it lies below the storm clouds of Hurricane Bob. The solid-colored semicircle on the upper left of each recording shows clouds normally associated with a hurricane. From left to right, the three magnetic tape strips show data at descending levels of altitude. Changes in temperature are indicated by different colors, and the eye of the storm appears to be warmer than its surrounding area by several degrees. The activity shown on the lower left is a band of rain associated with the storm.

The gray skies and heavy subtropical air over NASA's airfield on Wallops Island, Virginia, testified to the approach of Hurricane Bob on the morning of August 19, 1991. One week earlier, scientists from laboratories across the country had assembled to gather data on convection and precipitation, and the electrification of thunderstorms.

Participants from RLE's Radio Astronomy Group were Principal Research Scientist Dr. Philip W. Rosenkranz, Sponsored Research Staff John W. "Jack" Barrett, and graduate student Michael J. Schwartz. The trio conducts experiments in microwave atmospheric sensing with Dr. David H. Staelin, Assistant Director of Lincoln Laboratory and Professor of Electrical Engineering and Computer Science. Using high-altitude research aircraft and meteorological satellites, they collect data on atmospheric water vapor, ozone, temperature, and surface conditions on Earth.

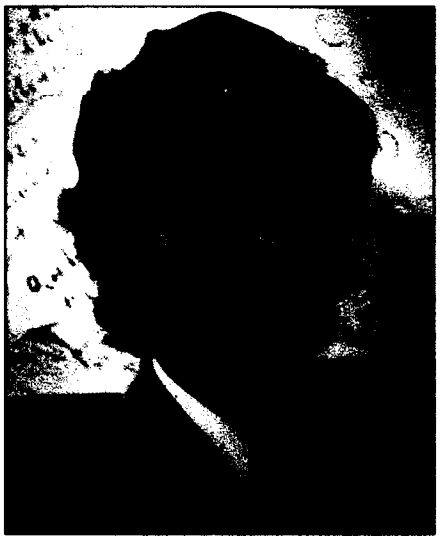
On the morning of the storm, Jack Barrett and Mike Schwartz were hoping to gather additional data with RLE equipment aboard the high-altitude ER-2 aircraft. The plane has flown earlier research missions over thunderstorms south of Cape Hatteras, North Carolina. Since the plane's wingspan was so large, it was now grounded in the face of the impending hurricane. This was not the kind of aircraft suited for windy take-offs and landings.

Later that morning, conditions changed, and clearing skies indicated that Bob's path would miss Wallops Island. The ER-2 quickly took to the skies and caught up with Bob just before it slammed into New England. Hurricanes are normally viewed from space satellite images, and the RLE team did not suspect that Bob would make such an excellent subject for their high-resolution microwave sensing experiment. Their passive microwave methods proved advantageous because they could receive signals from within and below cloud cover; other techniques would not have penetrated the cloud tops. The microwave instrumentation on board the ER-2 was built at RLE and consisted of a series of receivers sensitive to the 5- and 3-millimeter oxygen bands in the atmosphere. RLE's successful, high-flying mission produced the first high-resolution passive microwave images of a hurricane's center from several kilometers distance, and recorded temperatures at eight different altitude levels.

The RLE Radio Astronomy Group is currently analyzing the data collected from Wallops Island. Aside from the terrible coastal damage left by the storm, their microwave images are all that remain of Hurricane Bob, and represent a bench mark for others to challenge.

by John F. Cook

circuit breakers



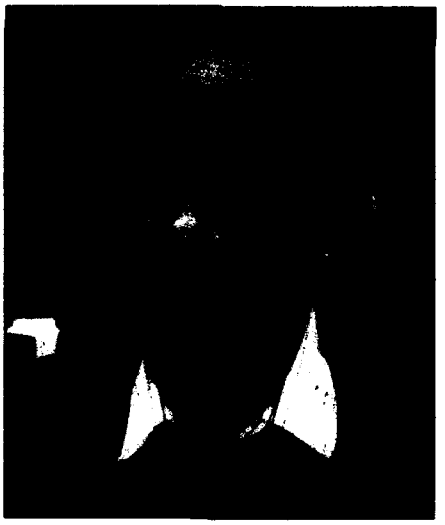
Dr. Srinivas Devadas will be promoted to Associate Professor of Electrical Engineering and Computer Science, effective July 1, 1992. Professor Devadas, a graduate of the Indian Institute of Technology (B. Tech. '85) and the University of California, Berkeley (MS '86, PhD '88), joined the MIT faculty as an assistant professor in 1988. He held the Analog Devices Career Development Professorship from 1989 to 1991. As a faculty member in RLE's Circuits and Systems Group, Professor Devadas explores the synthesis and testing of VLSI circuits and systems, particularly in the areas of test generation and logic synthesis. He has made significant contributions to data path synthesis and logic synthesis and verification. *Photo by John F. Cook.*

Dr. Leslie A. Kolodziejski, Karl Van Tassel Career Development Assistant Professor, will be promoted to Associate Professor of Electrical Engineering and Computer Science, effective July 1, 1992. Professor Kolodziejski came to MIT as an assistant professor in 1988 from the faculty of Purdue University (BS '83, MS '84, PhD '86). As a member of RLE's Materials and Fabrication Group, she conducts research in materials growth for electronic and optical applications. Her research focuses on the growth of II-VI and III-V materials using chemical beam epitaxy techniques. She also holds a

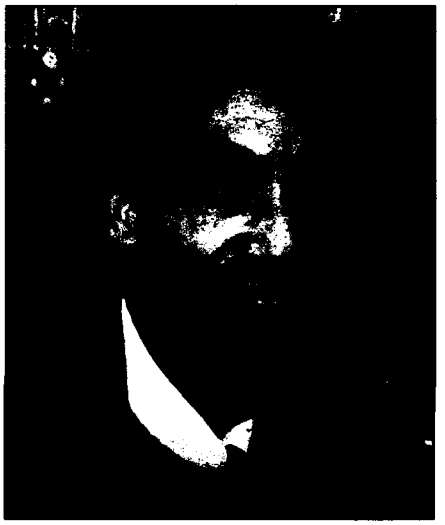


Dr. Leslie A. Kolodziejski

Presidential Young Investigator Award (1987-92) from the National Science Foundation. *Photo by John F. Cook.*



Dr. John J. Guinan, Jr. (SB 63, SM 64, PhD 68), Principal Research Scientist in RLE's Auditory Physiology Group, was appointed Associate Director of the Eaton-Peabody Laboratory at the Massachusetts Eye and Ear Infirmary, effective January 28, 1992. Dr. Guinan has been affiliated with RLE since 1963, and conducts experimental research on the mammalian efferent system, which the central nervous system uses to control incoming messages from the ear to the brain. His research has furthered understanding of the processes involved in hearing, particularly how the central nervous system responds to sound, and has demonstrated that the concepts associated with man-made engineering systems can be applied to the study of the nervous system. Dr. Guinan is a member of the American Association for the Advancement of Science, the Federation of American Scientists, the Acoustical Society of America, and the Society for Neuroscience. *Photo by John F. Cook.*



Mr. Qizheng Gu was appointed Research Scientist in RLE's Center for Electromagnetic Theory and Applications, effective February 1, 1992. As a visiting scientist in RLE since 1983, Mr. Gu has conducted research in electromagnetic interference modeling of receivers for precision aircraft landing systems and the theoretical analysis of transient signal propagation and interference in high-speed integrated circuits. From 1962 to 1983, he was senior engineer and deputy director of the Research Department at Shanghai Xinhua Radio Factory. He has also served as professor and deputy director of the Research Laboratory of Electrical Engineering at Shanghai's Research Institute of Mechanical and Electrical Engineering since 1987. Mr. Gu graduated from Fudan University in Shanghai in 1960. Since 1978, he has received four Awards of Important Science and Technology Achievements from the People's Republic of China. *Photo by John F. Cook.*

alumni notes

Corine A. Bickley (PhD '87), Visiting Scientist in RLE's Speech Communication Group and Lecturer at MIT's Writing Program, teamed up with undergraduate Thomas R. Westcott ('93) of RLE's Sensory Communication Group to teach an American Sign Language seminar at MIT. The seminar not only included sign language instruction, but also addressed the sociological issues of deafness and technological advances in aids for the deaf.

William T. Dyall (SM '48) is keeping the staff of ***currents*** on its toes. As a member of the Society for the Preservation of English Language and Literature (SPELL), he has become ***currents'*** unofficial "goofreader." Mr. Dyall is retired from Sierra International and lives in Los Altos, California.

Raymond M. Redheffer (SB '43, SM '47, PhD '48), retired Professor of Mathematics at UCLA, writes from his home in Los Angeles. In November 1991, Dr. Redheffer received an honorary doctorate in mathematics from Karlsruhe University in Germany, the first conferred in 31 years. Dr. Redheffer was a member of the MIT Radiation Laboratory (1942-46) and RLE's antenna group (1946-48).

According to *The Boston Globe* of February 7, 1992, ***Robert J. Shillman*** (SM '72, PhD '74), "colorful entrepreneur and president of Cognex Corporation of Needham, rented out the JFK Library last night to hand out $500,000 in bonuses to 130 employees. A George Bush impersonator was on the program for added levity."

Thomas E. Stern (SB/SM '53, ScD '56), Dicker Professor and Chairman of Columbia University's Department of Electrical Engineering, recalls many familiar names and faces that appeared in the fall 1991 issue of ***currents***. Since 1985, he has served as Technical Director of Columbia University's Center for Telecommunications Research, and conducts research in optical communication networks. Columbia's Electrical Engineering Department will celebrate its centennial this year, and Dr. Stern writes, "That's one of the things that put me in the mood to reminisce."

Both ***Stewart D. Personick*** (SM '68, EE '69, ScD '70) and ***Charles L. Seitz*** (SB '65, SM '67, PhD '71) were elected to the National Academy of Engineering. Dr. Personick is Assistant Vice President of Bell Communications Research, Inc. in Morristown, New Jersey, and Dr. Seitz is on the computer science faculty at the California Institute of Technology in Pasadena, California. They joined thirteen other MIT alumni and two MIT faculty members who were recently elected to the academy, one of the highest professional honors for an engineer.

RLE congratulates the following alumni for awards recently presented by the Institute of Electrical and Electronic Engineers:

C. Gordon Bell (ScD '53), a computer industry consultant, received the 1992 John von Neumann Medal.

John H. Cafarella (SM/EE '73, ScD '75), partner in Micrilor, Inc. of Wakefield, Massachusetts, was elected to Fellow in the IEEE Signal Processing Society.

G. David Forney, Jr. (SM '63, ScD '65), Vice President at Motorola Codex Corporation in Mansfield, Massachusetts, was awarded the 1992 Edison Medal. The medal is presented for a career of meritorious achievement in electrical science or engineering.

Thomas S. Huang (SM '60, ScD '63), Professor of Electrical Engineering at the University of Illinois/Champaign-Urbana, was honored by the IEEE Signal Processing Society with its 1991 Society Award for contributions and leadership in the areas of image and multidimensional signal processing.

James L. Massey (SM '60, PhD '62), Professor of Digital Systems Engineering at the Swiss Federal Technical University in Zurich, Switzerland, received the 1992 Alexander Graham Bell Medal. The medal is awarded for exceptional contributions to the advancement of telecommunications.

Ronald W. Schafer (PhD '68), Institute Professor at the Georgia Institute of Technology, was named recipient of the 1992 Education Medal. He was cited for excellence in curriculum development, teaching, and textbooks in digital signal processing and digital speech processing. Dr. Schafer joins other distinguished RLE alumni as previous Education Medal winners: Institute Professor Hermann A. Haus (ScD '54) in 1991, Professor Alan V. Oppenheim (SB/SM '61, ScD '64) in 1988, and Professor Emeritus Robert M. Fano (SB '41, ScD '47) in 1977.

UPDATE

Publications

RLE has recently published the following technical reports:

Adaptive Matched Field Processing in an Uncertain Propagation Environment, by James C. Preisig. RLE TR No. 567. January 1992. 173 pp. $17.00.

Theory of Resistive and Ideal Internal Kinks, by Stefano Migliuolo. RLE TR No. 568. February 1992. 83 pp. $15.00.

Modeling Speech Perception in Noise: The Stop Consonants as a Case Study, by Abeer A.H. Alwan. RLE TR No. 569. February 1992. 133 pp. $16.00.

Spread Spectrum Modulation and Signal Masking Using Synchronized Chaotic Systems, by Kevin M. Cuomo, Alan V. Oppenheim, and Steven H. Isabelle. RLE TR No. 570. February 1992. 39 pp. $10.00.

Probabilistic State Estimation with Discrete-Time Chaotic Systems, by Michael D. Richard. RLE TR No. 571. March 1992. 90 pp. $12.00.

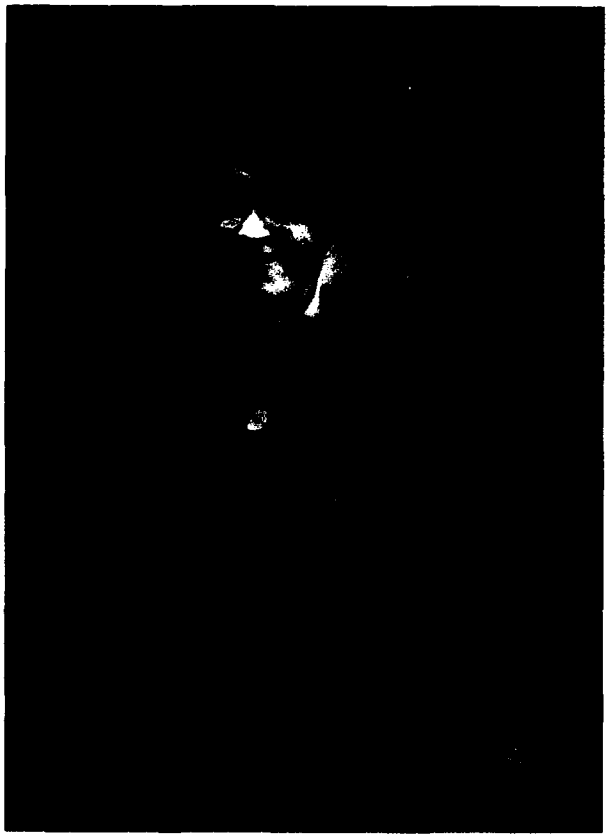
A New Approach to Parameter Optimization of Products and Manufacturing Processes, by Ashraf S. Alkhairy, RLE TR No. 572. Price to be announced. Available in September 1992.

In addition, ***RLE Progress Report No. 134,*** which covers the period January through December 1991, provides extensive information about the research objectives and projects of RLE's research groups. It also lists faculty, staff, and students who participated in each research project, in addition to current RLE personnel, and identifies funding sources. The ***Progress Report*** is available for $5.00 (to U.S. addresses) and $9.00 (to foreign addresses) to cover postage and handling.

Ordering information is on back cover.

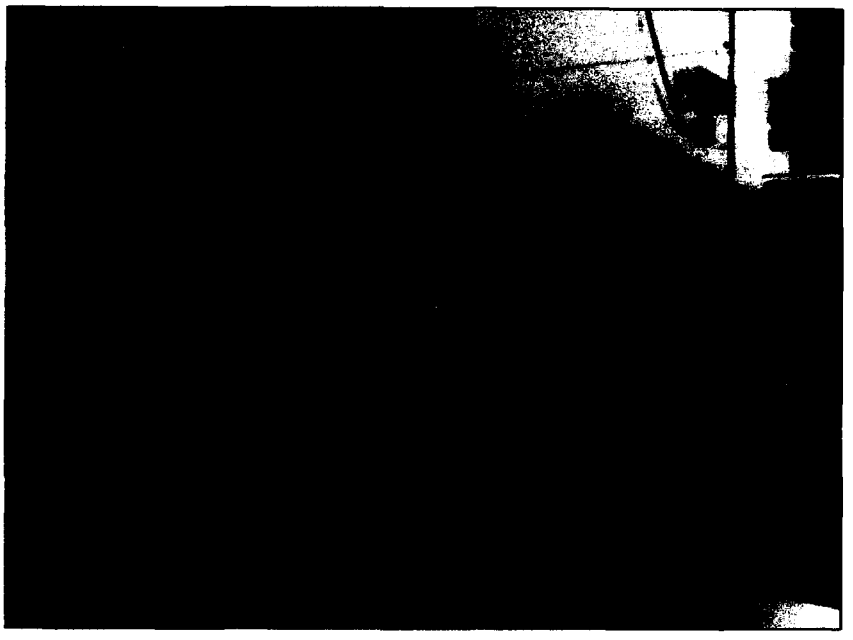
History of VLSI Computer-Aided Design at RLE

"Although there was a great deal of activity in RLE in the early 1960s in characterizing semiconductor devices and circuits, MIT did not participate strongly in the early development of integrated circuits as opposed to the study of discrete devices. In 1978, however, Professors Jonathan Allen and Paul Penfield recognized that important new design techniques, focused on MOS (Metal-Oxide-Semiconductor) circuits, had opened up the possibility of designing large circuits at a system level with impressive performance. Building on a semester visit by Ms. Lynn Conway of the Xerox Palo Alto Research Center, a robust new activity in integrated-circuit design built up, spanning interests all the way from the device level to large complex computing systems. The emphasis in RLE has been on the building of a number of software design tools, many of which are used extensively in industry, and on the development of new circuit-analysis techniques and high-performance architectures for digital signal processing."—A Century of Electrical Engineering and Computer Science at MIT, 1882-1982 *by Karl L. Wildes and Nilo A. Lindgren*



1954

Professors Henry J. Zimmermann, Samuel J. Mason, and Richard B. Adler were part of a group in RLE that investigated the fundamental principles of transistor circuit design and their practical application in communication engineering. The study of noise in semiconductors was also related to this research. Professor Zimmermann is shown here in a 1975 photo. (Photo by Ivan Massar/Black Star)



1962

MIT doctoral student Ivan E. Sutherland (PhD '63) developed Sketchpad, an interactive computer graphics program that was implemented on Lincoln Laboratory's TX-2 computer. By the mid-'60s, major American corporations were conducting research on interactive computer graphics. (Photo courtesy of Lincoln Laboratory)

1950s/1960s

Professor Richard D. Adler was a member of RLE since its inception in 1946. From 1951 to 1953, he was the leader of Lincoln Laboratory's first solid-state and transistor group. Along with Professors Samuel J. Mason, Carl R. Hurtig, and Walter E. Morrow, Jr., he pioneered the development of a new nonlinear circuit model for point-contact transistors. From 1960 to 1968, he served as technical director of the Semiconductor Electronics Education Committee (SEEC), an international university- and industry-sponsored educational development effort. The SEEC successfully introduced solid-state electronics into university curricula by producing seven textbooks, pedagogical lab experiments, and four educational films on the subject. Other members of the SEEC included Professors Campbell L. Searle, Paul E. Gray, Arthur C. Smith, and Richard D. Thornton. Professor Adler is shown lecturing in a 1963 photo (courtesy MIT Museum) and Professor Thornton examines a component in a 1975 photo (Ivan Massar/Black Star).







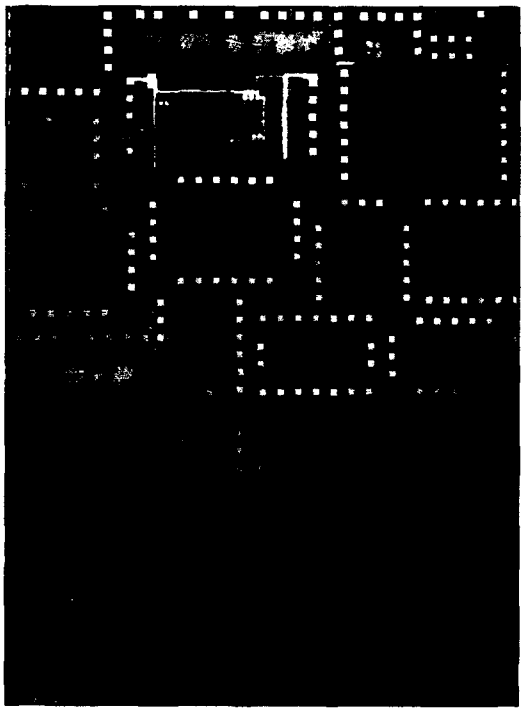
Winter 1978

In January 1978, about 25 MIT faculty members and scientists participated in an intensive LSI design workshop. The challenge was for the workshop participants to become the foundation of MIT's new thrust into integrated circuit design. Just as the avalanche of new information concluded, the workshop was commemorated by New England's blizzard of 1978, which closed MIT for a week and gave the attendees some time to reflect and complete their take-home final exam. (Photo by Stephen L. Finberg '77)



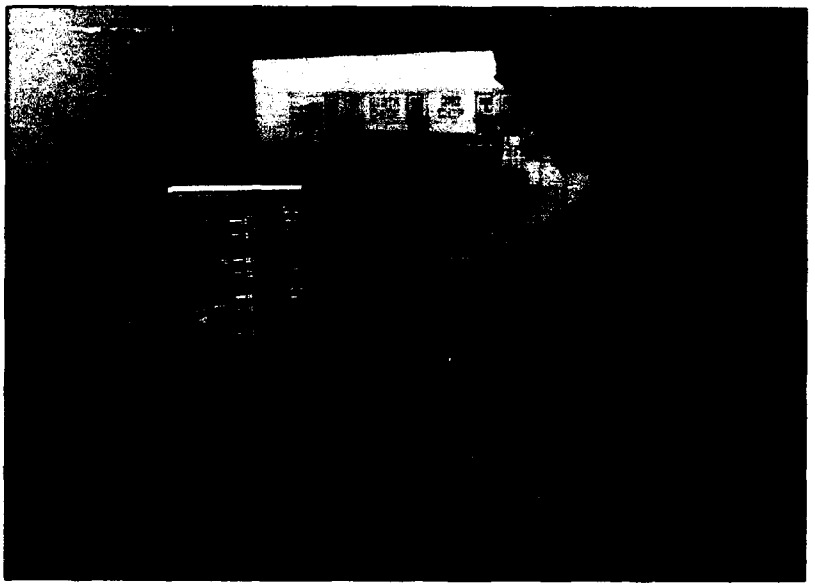
Fall 1978

Visiting Associate Professor Lynn A. Conway introduced MIT students to their first VLSI design course in the fall of 1978. As a researcher from Xerox Palo Alto Research Center, she had collaborated with Professor Carver Mead from the California Institute of Technology on a landmark system-oriented approach to VLSI design. Thirty students enrolled in the new course, which was based on this approach. Professor Conway is now the Assistant Dean of Engineering at the University of Michigan at Ann Arbor. (Photo courtesy of Lynn A. Conway)



Fall 1978

The 1978 MIT Multiproject Chip was the most ambitious multiproject chip to date. Designs were produced by students from Professor Lynn Conway's VLSI design course. This endeavor guided the more extensive multi-university multiproject chip set (MPC79), which involved 124 designers from eight universities. (Photo courtesy of Paul L. Penfield, Jr.)



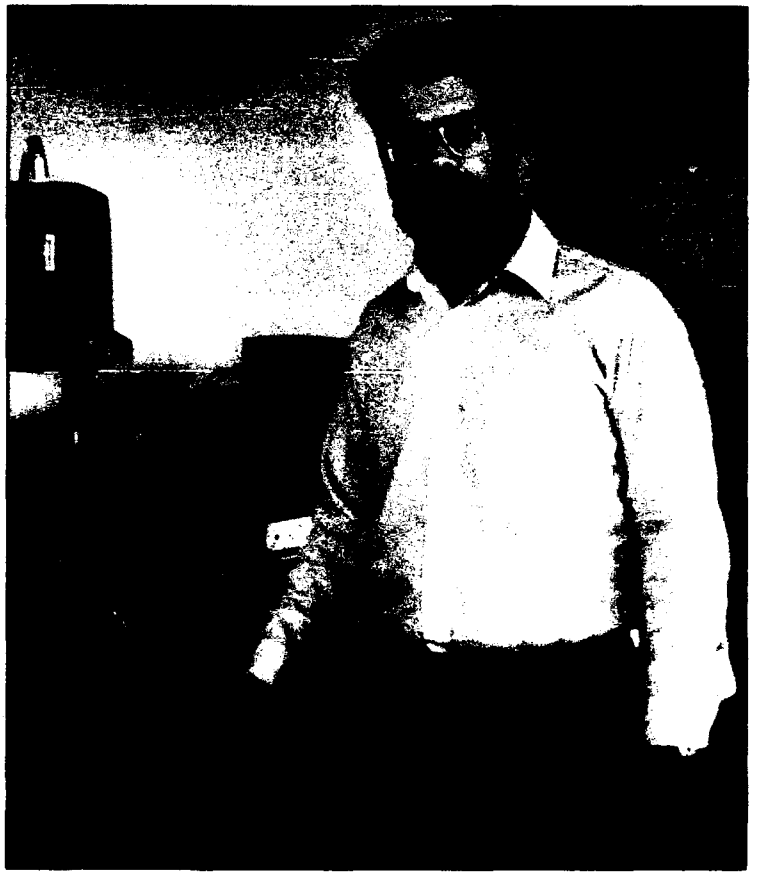
1983

Professor Jonathan Allen and graduate student Larry D. Seiler inspect the design of a system for high-speed design rule checking that uses four custom integrated circuits in a novel architecture. The design rule checker was used in Professor Allen's VLSI design course, which continued the curriculum brought to MIT by Professor Lynn Conway. (Photo by John F. Cook)



1984

The features of a CMOS chip developed at AT&T Bell Laboratories are examined by (from left) Dr. Michael K. Maul of Bell Labs, Dr. J. Peter Bartl of MIT's Industrial Liaison Program, Dr. W. Dexter Johnston and Mr. Victor A. Vyssotsky of Bell Labs, and Professor Paul L. Penfield, Jr., Director of MIT's Microsystems Technology Laboratories. The same fabrication process used to manufacture this chip would later be used to produce a chip designed by Professor Lance A. Glasser of RLE. (Photo courtesy of MIT Museum)



1985

As a principal investigator in RLE's Circuit and Systems Group, Professor Lance A. Glasser studied integrated circuit design and its application in digital VLSI systems, such as massively parallel multiprocessors. His important contributions include research in waveform bounding, a novel ultraviolet write-enable programmable read-only memory (PROM) circuit, and a book which he co-authored, The Design and Analysis of VLSI Circuits. *Currently, he is with the Defense Advanced Research Projects Agency in Arlington, Virginia. (Photo by John F. Cook)*

UPDATE

Industrial Connections

RLE actively promotes innovative relationships between the laboratory and business organizations through RLE Collegium membership, research projects, and special partnerships. The goal is to increase communication between RLE researchers and industrial professionals in electronics and related fields.



Working with Professor David H. Staelin (right), Dr. Ashraf S. Alkhairy has developed a novel approach to manufacturing. Dr. Alkhairy's method is a mathematically rigorous approach used to compute system parameters that can optimize quality in product and manufacturing process development. The number of experiments needed to implement the approach can be an order of magnitude smaller than those required by other methods. Since June 1991, it has been in use at Hewlett-Packard's Avondale, Pennsylvania facility, which produces chromatographic columns, and at their San Diego, California operation since November 1991. This system is expected to save up to $3 million for the two Hewlett-Packard sites over a three-year period. Dr. Alkhairy is currently a postdoctoral associate in RLE, and his research in this area is documented in his doctoral thesis, which will soon be available as RLE Technical Report No. 572. (Photo by John F. Cook)

RLE Collegium

The RLE Collegium was founded in 1987, and the annual membership fee is $20,000. Members of MIT's Industrial Liaison Program can elect to apply a portion of their ILP membership fee to the RLE Collegium. Collegium members have the opportunity to develop close affiliations with the laboratory's research staff, and can quickly access emerging results and scientific directions. Collegium benefits include access to a wide range of publications, seminars, and laboratory visits. For more information on the RLE Collegium, please contact RLE Headquarters or the Industrial Liaison Program at MIT.

Daimler-Benz and McDonnell Douglas Join RLE Collegium

Daimler-Benz of Stuttgart, Germany, renowned for its Mercedes-Benz vehicle division, has joined the RLE Collegium. In 1886, Gottlieb Daimler and Karl Benz produced their first motor cars, and the two companies merged in 1926. Today, Daimler-Benz is positioning itself to become an international force in high-technology development. It has recently acquired the AEG electronics company and formed two new divisions—Deutsche Aerospace and Daimler-Benz Inter-Services. Much like RLE, Daimler-Benz is active in a broad spectrum of research including information technology, new materials and production processes, and artificial intelligence.

The McDonnell Douglas Corporation of St. Louis, Missouri, a world leader in avionics and aerospace technology, recently joined the RLE Collegium. The corporation was formed in 1967 through a merger of the McDonnell Company (founded by the late James S. McDonnell, Jr. '25) and the Douglas Aircraft Company (founded by the late Donald W. Douglas '17). McDonnell Douglas is the world's second largest deliverer of commercial aircraft and the largest U.S. military contractor, with the broadest base of products of any other aerospace company in the world. McDonnell Douglas offers a wide range of products and services that includes everything from training and launch systems to the Space Station Freedom.

RLE welcomes inquiries regarding the laboratory's research. To request an RLE ***Progress Report,*** an RLE ***Collegium Prospectus,*** or for more information on other RLE publications, please contact:

Research Laboratory of Electronics
Massachusetts Institute of Technology
77 Massachusetts Avenue
Cambridge, MA 02139-4307
Collegium: (617) 253-2509/2510
Publications: (617) 253-2566
Fax: (617) 258-7864